UNIVERSITY OF CALIFORNIA

Santa Barbara

Probing Covalent Metal-Ligand Bonding in f-Elements: Insights from ^{13}C NMR Spectroscopy

A dissertation submitted in partial satisfaction of the

requirements for the degree Doctor of Philosophy

in Chemistry

by

Osvaldo Ordoñez

Committee in charge:

Professor Trevor W. Hayton, Chair

Professor Peter C. Ford

Professor Nadia G. Léonard

Professor Vojtech Vlcek

September 2024

The dissertation of Osvaldo Ordoñez is approved.

_____

Professor Peter C. Ford

_____

Professor Nadia G. Léonard

_____

Professor Vojtech Vlcek

_____

Professor Trevor W. Hayton, Committee Chair

June 2024

Probing Covalent Metal-Ligand Bonding in f-Elements: Insights from ^{13}C NMR Spectroscopy

Osvaldo Ordoñez

Acknowledgements

I want to express my gratitude to my undergraduate mentor, Prof. R. Daniel Little, for sparking my interest in synthetic chemistry, guiding my development as a scientist, and for inspiring me to pursue graduate school. Dan, thank you for your continuous guidance and support during both my undergraduate and graduate studies. I would like to thank Dr. Marco Lam, my graduate mentor in the Little group, for all the invaluable advice and help you have given me. Similarly, I would like to thank my undergraduate mentor, Prof. Lior Sepunaru, whose unwavering support has been instrumental in shaping my scientific journey. Lior, I am incredibly grateful for your mentorship and encouragement throughout my undergraduate and graduate studies.

I am deeply thankful to Prof. Trevor W. Hayton for his dedicated mentorship over the past 5 years, investing significant time and effort in shaping me into a successful synthetic chemist. Trevor, thank you for your unwavering support and patience, especially in guiding me through my research projects, which has been instrumental in my development as an independent scientist. I also want to thank my thesis committee members, Prof. Peter C. Ford, Prof. Nadia G. Léonard, and Prof. Vojtech Vlcek, for their support and advise throughout my graduate studies. I also extend a special thanks to Dr. Guang Wu, for his indispensable role in my successful learning of X-ray crystallography. I would also like to thank Prof. Jochen Autschbach and Dr. Xiaojuan Yu for their invaluable contribution to the computational work that provided valuable insights for my research projects. Additionally, I want to express my gratitude to Dr. Andrew J. Gaunt, my mentor during my time at Los Alamos National Laboratory, for making my experience truly exceptional. I would like to thank him for mentoring me and providing invaluable advice and support that I will cherish and apply

throughout my entire career. I also would like to thank Dr. Jesse Murillo for his indispensable assistance with my experiments at LANL and for his valuable insights.

To the Hayton group members, each of you has contributed immensely to making this experience delightful and unforgettable. To Dr. Mikiyas Assefa, thank you for your kindness and willingness to always help, especially during my first year as a graduate student and thank you for continuing to assist and help me as I transition to the next phase of my scientific journey. To Dr. Greggory Kent, Dr. Selena Staun, Dr. Alexander Touchton, and Dr. Miguel Baeza Cinco, I deeply appreciate the opportunity to work alongside you and thanks for the invaluable help training me, from learning Schlenk techniques to effectively working in the glovebox. And to my current group members, Phoebe Hertler, Thien Nguyen, Kaushalya Kumarihami, Gigi Godinho, Dylan Tietje-Mckinney, Jordan Brower, and Megan Schuerlein, I have truly valued our time working together and I am deeply grateful for your support over the years.

I want to express my heartfelt gratitude to my family, who supported and encouraged me throughout my undergraduate and graduate studies. I want to give special thanks to my parents, who have gone above and beyond to help me reach success, and whose unconditional love and support made this journey possible. To my fiancée Elsie, thank you for being my unwavering support and encouragement through every step of my scientific journey and for filling my days with endless joy and happiness. I could not have achieved this without you by my side, and I am extremely thankful, I love you 3000!

Vita of Osvaldo Ordoñez

September 2024

EDUCATION

Doctor of Philosophy in **Chemistry** June 2024
University of California, Santa Barbara
Advisor: Prof. Trevor W. Hayton

Bachelor of Science in **Biochemistry** September 2018
University of California, Santa Barbara
Advisor: Prof. R. Daniel Little & Prof. Lior Sepunaru

PROFESSIONAL EMPLOYMENT

University of California, Santa Barbara 2019-2024
Department of Chemistry and Biochemistry
Graduate Student Researcher, Hayton Research Group

Los Alamos National Laboratory 2022-2023
Inorganic, Isotope, and Actinide Chemistry Group
Graduate Student Researcher, Supervisor: Dr. Andrew Gaunt

University of California, Santa Barbara 2018-2018
Department of Chemistry and Biochemistry
Undergraduate Student Researcher, Sepunaru Research Group

University of California, Santa Barbara, 2017-2018
Department of Chemistry and Biochemistry
Undergraduate Student Researcher, Little Research Group

PUBLICATIONS

Ordoñez, O.; Yu, X.; Schuerlein, M. A.; Wu, G.; Autschbach, J.; Hayton, T. W., An Actinide Complex with a Nucleophilic Allenylidene Ligand. *Submitted.*

Ordoñez, O.; Yu, X.; Wu, G.; Autschbach, J.; Hayton, T. W., Quantifying Actinide-Carbon Bond Covalency in a Uranyl-Aryl Complex Utilizing Solution ^{13}C NMR Spectroscopy. *Inorg. Chem.* **2024**, *63*, 9427-9433.

Ordoñez, O.; Kent, G. T.; Schuerlein, M. A.; Wu, G.; Hayton, T. W., Ring-Opening in the Actinide Cyclopropyl Complexes $[Cp3U(2,2\text{-diphenylcyclopropyl})]^{n-}$ (n = 0, 1). *Organometallics*. **2023,** *42*, 2347–2352.

Ordoñez, O.; Yu, X.; Wu, G.; Autschbach, J.; Hayton, T. W., Assessing the 4f Orbital Participation in the Ln-C Bonds of $[Li(THF)_4][Ln(C_6Cl_5)_4]$ (Ln = La, Ce). *Inorg. Chem*. **2022**, *61*, 15138–15143.

Ordoñez, O.; Yu, X.; Wu, G.; Autschbach, J.; Hayton, T. W., Homoleptic Perchlorophenyl "Ate" Complexes of Thorium(IV) and Uranium(IV). *Inorg. Chem*. **2021**, *60*, 12436–12444.

Ordoñez, O.; Yu, X.; Wu, G.; Autschbach, J.; Hayton, T. W., Synthesis and Characterization of two Uranyl-Aryl "Ate" Complexes. *Chem. Eur. J*. **2021**, *27*, 5885–5889.

AWARDS

- Robert H. DeWolfe Distinguished Teaching Fellowship, UCSB DCB 2024
- UC President's Pre-Professoriate Fellowship 2023
- G. T. Seaborg Institute Graduate Research Program Fellowship, LANL 2023
- Graduate Research Mentorship Program Fellowship, UCSB 2022
- Outstanding Service to Department Award, UCSB DCB 2022
- G. T. Seaborg Institute Graduate Research Program Fellowship, LANL 2022
- Innovations in Nuclear Technology R&D Award, NEUP DOE 2021
- Outstanding Service to Department Award, UCSB DCB 2021
- Chair's Fellowship for Research Excellence, UCSB DCB 2021
- Sandra Lamb Memorial Award, UCSB DCM 2021
- Honorable Mention, NSF GRFP 2021
- Edison-McNair Summer Research Fellowship, UCSB 2017
- Edison-McNair GRE Scholar, UCSB 2017

FIELDS OF STUDY

Major Field: Synthetic Inorganic Chemistry

Studies in: Organometallic Lanthanide and Actinide Chemistry

Abstract

Probing Covalent Metal-Ligand Bonding in f-Elements: Insights from ^{13}C NMR Spectroscopy

by

Osvaldo Ordoñez

Reaction of $[UO_2Cl_2(THF)_3]$ with 3 equiv of LiC_6Cl_5 in Et_2O resulted in the formation of the first uranyl aryl complex, $[Li(Et_2O)_2(THF)][UO_2(C_6Cl_5)_3]$ ([Li][**2.1**]) in good yields. Subsequent dissolution of [Li][**2.1**] in THF resulted in conversion to $[Li(THF)_4][UO_2(C_6Cl_5)_3(THF)]$ ([Li][**2.2**]), also in good yields. DFT calculations reveal that the U-C bonds in [Li][**2.1**] and [Li][**2.2**] exhibit appreciable covalency. Additionally, the ^{13}C chemical shifts for their C_{ipso} environments are strongly affected by spin-orbit coupling – a consequence of 5f orbital participation in the U-C bonds.

Reaction of $AnCl_4(DME)_n$ (An = Th, n = 2; U, n = 0) with 5 equiv of LiC_6Cl_5 in Et_2O resulted in the formation of homoleptic actinide-aryl "ate" complexes $[Li(DME)_2(Et_2O)]_2[Li(DME)_2][Th(C_6Cl_5)_5]_3$ ([Li][**3.1**]) and $[Li(Et_2O)_4][U(C_6Cl_5)_5]$ ([Li][**3.2**]). Similarly, reaction of $AnCl_4(DME)_n$ (An = Th, n = 2; U, n = 0) with 3 equiv of LiC_6Cl_5 in Et_2O resulted in formation of heteroleptic actinide-aryl "ate" complexes $[Li(DME)_2(Et_2O)][Li(Et_2O)_2][ThCl_3(C_6Cl_5)_3]$ ([Li][**3.3**]) and $[Li(Et_2O)_3][UCl_2(C_6Cl_5)_3]$ ([Li][**3.4**]). Density functional calculations show that the An-C_{ipso} σ-bonds are considerably

more covalent for the uranium complexes vs. the thorium analogues, in line with past results. Additionally, good agreement between experiment and calculations is obtained for the $^{13}C_{ipso}$ NMR chemical shifts in [Li][**3.1**] and [Li][**3.3**]. The calculations demonstrate a deshielding by ca. 29 ppm from spin-orbit coupling effects originating at Th, which is a direct consequence of 5f orbital participation in the Th-C bonds.

Reaction of $[Ln(NO_3)_3(THF)_4]$ (Ln = La; Ce) with 4 equiv of LiC_6Cl_5 in Et_2O resulted in the formation of the homoleptic lanthanide-aryl "ate" complexes $[Li(THF)_4][La(C_6Cl_5)_4]$ ([Li][**4.1**]) and $[Li(THF)_4][Ce(C_6Cl_5)_4]$ ([Li][**4.2**]). These complexes represent the first isolated homoleptic perchlorophenyl complexes for the lanthanides. In the solid state, both [Li][**4.1**] and [Li][**4.2**] exhibit octa-coordinate lanthanide centers, with four Ln-C σ-bonds and four Cl→Ln dative interactions involving the *ortho*-Cl atoms of the C_6Cl_5 ligands. Despite this apparent steric saturation, both [Li][**4.1**] and [Li][**4.2**] are highly temperature sensitive and quickly decompose in solution at room temperature. Density functional calculations show that the Ln-C_{ipso} donation bonds feature only weak 4f participation (e.g., ~1% 4f weight for [**4.1**]$^-$). Nonetheless, the ^{13}C chemical shift for the C_{ipso} nuclei of [**4.1**]$^-$ includes ca. 8 ppm of deshielding from spin-orbit coupling effects from the 4f (and 5d) participation in its La-C bonds.

Reaction of $[UO_2Cl_2(THF)_2]_2$ with *in situ* generated LiFmes (FmesH = 1,3,5-$(CF_3)_3C_6H_3$) in Et_2O resulted in the formation of the uranyl aryl complexes, $[Li(THF)_3][UO_2(Fmes)_3]$ ($[Li(THF)_3]$[**5.1**]) and $[Li(Et_2O)_3(THF)][UO_2(Fmes)_3]$ ($[Li(Et_2O)_3(THF)]$[**5.1**]), in good to moderate yields after crystallization from hexanes or Et_2O, respectively. Both complexes were characterized by X-ray crystallography and NMR spectroscopy. DFT calculations reveal that the C_{ispo} resonance in [**5.1**]$^-$ exhibits a deshielding of 51 ppm from spin-orbit coupling effects

originating at uranium, which indicates an appreciable covalency in the U-C bonding interaction.

The reaction of [Cp_3AnCl] (An = Th, U) with *in situ* generated 1-lithium-2,2-dipenylcyclopropane results in the formation of [Cp_3An(2,2-diphenylcyclopropyl)] (U = **6.1**, Th = **6.2**), in good yield. Reduction of **6.1** with KC_8, in the presence of 2.2.2-cryptand, results in formation of a rare U(III) alkyl complex, [K(2.2.2-cryptand)][Cp_3U(2,2-diphenylcyclopropyl)] (**6.3**). Thermolysis or photolysis of **6.1** for 10 d in toluene results in isomerization to the U(IV) η^1-allyl complex, [$Cp_3U(\eta^1$-3,3-diphenylallyl)] (**6.4**). Moreover, photolysis of 2 in THF for 9 h at room temperature results in isomerization to the U(III) η^1-allyl complex, [K(2,2,2-cryptand)][$Cp_3U(\eta^1$-3,3-diphenylallyl)] (**6.5**). Both **6.4** and **6.5** were fully characterized. In addition, selective labelling of the C_α positions of **6.1** and **6.3** with deuterium revealed that cyclopropyl ring-opening occurs via distal C-C bond cleavage via a hypothesized η^3-allyl intermediate.

The reaction of [Cp_3Th(3,3-diphenylcyclopropenyl)] with 1 equiv of LDA results in the formation of a thorium allenylidene complex, [$Li(Et_2O)_2$][$Cp_3Th(CCCPh_2)$] ([$Li(Et_2O)_2$][**7.1**]) in good yield. Additionally, deprotonation of [Cp_3Th(3,3-diphenylcyclopropenyl)] with 1 equiv of LDA, in presence of 12-crown-4 or 2.2.2-cryptand, result in the formation of discrete cation/anion pair of thorium allenylidene complexes, [Li(12-crown-4)(THF)][$Cp_3Th(CCCPh_2)$] ([Li(12-crown-4)(THF)][**7.1**]) and [Li(2.2.2-cryptand)][$Cp_3Th(CCCPh_2)$] ([Li(2.2.2-cryptand)][**7.1**]), respectively. Interestingly, complex [$Li(Et_2O)_2$][**7.1**] undergoes dimerization upon standing at room temperature resulting in the formation of [$Cp_2Th(CCCPh_2)]_2$ (**7.2**), via loss of LiCp**.** In addition, the reaction of [$Li(Et_2O)_2$][**7.1**] with MeI results in electrophilic attack at the C_γ carbon atom leading to the

formation of a thorium acetylide complex, [$Cp_3Th(C{\equiv}CC(Me)Ph_2)$] (**7.3**), which can be isolated in 83% yield upon work-up. Reaction of [$Li(Et_2O)_2$][**7.1**] with benzophenone results the formation of 1,1,4,4-tetraphenylbutatriene (**7.4**) in 99% yield, according to integration against an internal standard. Furthermore, density functional theory (DFT) calculations were performed to analyze the bonding in [**7.1**]$^-$ and **7.2** revealing significant electron delocalization across the allenylidene ligand. Additionally, calculations of the ^{13}C NMR chemical shifts for the C_α, C_β, and C_γ environments of the allenylidene ligand were in good agreement with experimental. The calculations reveal modest deshielding induced by spin-orbital effects originating at Th due to the involvement of the 5f orbitals in the Th-C bonds.

The reaction of $AnCl_4(DME)_n$ (An = Th, n = 2; U, n = 0) with 4 equiv of [$Li(TMEDA)_2$][1,2-$S_2C_6H_4$] in THF resulted in the formation of homoleptic actinide thiolate complexes, [$Li(THF)_2]_4$[$Th(1,2\text{-}(S_2)C_6H_4)_4$] (**8.1**) and [$Li(TMEDA)]_4$[$U(1,2\text{-}(S_2)C_6H_4)_4$] (**8.2**), which can be isolated in moderate yields. Additionally, reaction of [$UO_2Cl_2(OPPh_3)_2$] with 2 equiv of KMMP (MMP = methyl-3-mercaptopropionate) in THF results in immediate formation of dark red solution to afford the isolation of [$UO_2(MMP)_2(OPPh_3)_2$] (**8.3**). Furthermore, reaction of [$UO_2Cl_2(OPCy_3)_2$] with 2 equiv of NaMMP in THF result in the formation of [$UO_2(MMP)_2(OPCy_3)_2$] (**8.5**).

Table of Contents

List of Figures

List of Schemes

List of Tables

List of Abbreviations

°	degree
°C	degree Celsius
ε	extinction coefficient
Δ	difference
δ	chemical shift, ppm
η^n	hapticity of order n
κ^n	denticity of order n
μ	micro or denotes bridging atom
ν	stretching frequency, cm^{-1}
Å	angstrom, 10^{-10} m
An	Actinide
av.	average
BDE	bond dissociation energy
br	broad
Bu	butyl
calcd.	calculated
$^{13}C\{^1H\}$	Carbon-13 proton decoupled
ca.	circa
Cp’	1,2,4-^{t}Bu$_3$C$_5$H$_2$
Cp*	η^5-C$_5$Me$_5$
Cp	η^5-C$_5$H$_5$

cm^{-1}	wavenumber
12-crown-4	1,4,7,10-tetraoxacyclododecane
18-crown-6	1,4,7,10,13,16-hexaoxacyclooctadecane
2,2,2-cryptand	4,7,13,16,21,24-hexaoxa-1,10-diazabicyclo[8.8.8]hexacosane
CSM	Continuous Shape Measure
Cy	Cyclohexyl
d	doublet *or* day(s)
d_n	deuterated in *n* positions
DFT	Density Functional Theory
DME	1,2-dimethoxyethane
e^-	electron
eq	equation
EPR	Electron Paramagnetic Resonance
equiv	equivalent
Et	ethyl
Et_2O	diethyl ether
g	gram(s)
GOF	goodness of fit
^1H	Hydrogen-1
h	hour(s)
HOMO	Highest Occupied Molecular Orbital
^iPr	isopropyl
IR	infrared

ITI	Inverse Trans Influence
J	NMR coupling constant
K	Kelvin
L	liter *or* ligand
LDA	Lithium diisopropylamide
$^{7}Li\{^{1}H\}$	Lithium-7 proton decoupled
Ln	lanthanide
M	Molar *or* Mega
m	meter *or* multiplet *or* medium
m	meta
Me	methyl
MeCN	Acetonitrile
min	minute(s)
mL	milliliter(s)
mmol	millimole(s)
MO	Molecular Orbital
mol	mole(s)
NBO	natural bond order
^{n}Bu	n-butyl
NIR	near infrared
NLMO	Natural Localized Molecular Orbital
NMR	nuclear magnetic resonance
o	ortho

p	para
Ph	phenyl
ppm	parts per million
py	pyridine
QTAIM	Quantum Theory of Atoms-in-Molecules
redox	reduction-oxidation
RT	room temperature
s	singlet *or* strong *or* second(s)
sh	shoulder
SOC	Spin orbit coupling
t	triplet
^{t}Bu	*tert*-butyl
THF	tetrahydrofuran
TMEDA	*N,N,N',N'*-tetramethylethylenediamine
tol	toluene
UV	ultraviolet
vis	visible
vs	very strong *or* versus
vw	very weak
w	weak
WBI	Wiberg Bond Index
WFT	Multi-configurational Wavefunction Theory
XAS	X-ray Absorption Spectroscopy

XPS	X-ray Photoelectron Spectroscopy

MAMBA MENTALITY

It’s a constant quest to try to be better today than you were yesterday
and better tomorrow than you were the day before.

-Kobe Bryant

Chapter 1. Introduction

1.1 Bonding and Covalency in f-elements

Spent nuclear fuel (SPF) is predominantly composed of uranium (95.6 %), accompanied by stable fission products (2.9 %), such as lanthanides and transition metals, alongside the minor actinides that result from neutron absorption by uranium and plutonium.[1] Despite constituting only 0.1% of spent nuclear fuel, minor actinides are responsible for a significant portion of its long-term radiotoxicity.[2] Thus, the selective extraction of minor actinides is important to mitigate the hazards with spent nuclear fuel, along with the ability to reprocess and recycle components within the nuclear fuel cycle.[3] However, due to identical oxidation states and similar ionic radii between the actinides (An) and the lanthanides (Ln), the separation of the minor actinides from SNF remains as one of the most difficult separation challenges.[4-7] Previously, the use of soft donor atoms (e.g., S, N) in ligands was shown to distinguish between An(III) and Ln(III) coordination.[8-10] It has been argued that the discrimination in the coordination from soft donor ligands can be explained through differences in M-L covalency.[8, 11-21] Due to the significant interest in the separation of the trivalent actinides from the trivalent lanthanides, it is highly desirable to probe and quantify the participation of the 5f orbitals in metal-ligand bonding.[22-26] However, determining the extent of covalent participation in the actinides poses significant challenges. A convenient way to indicate covalent participation in metal-ligand bonding is the mixing coefficient, λ, which is described by Eq 1.1.[27, 28]

Equation 1.1

$$\lambda = \frac{H_{ML}}{E_M^0 - E_L^0}$$

The Hamiltonian matrix element (H_{ML}) between orbitals describes the overlap between the two orbitals, whereas the E_M^0 and E_L^0 describe the orbital energy of the metal and ligand, respectively. This mixing coefficient suggests that greater covalent participation in metal-ligand bonding can be induced by enhancing orbital overlap. Additionally, decreasing the orbital energy difference between the metal and ligand orbitals also results in higher covalency (Figure 1.1).[27, 28] Evaluating the degree of covalency in f elements metal-ligand bonding is important in understanding periodic trends, alongside determining whether it arises from orbital overlap or orbital energy degeneracy. Furthermore, understanding how the oxidation state of the metal center and the type of ligand influence f orbital participation in metal-ligand bonding is essential. A thorough comprehensive understanding of the chemical bonding and electronic structure of the f elements is important for developing efficient separation techniques in the future.

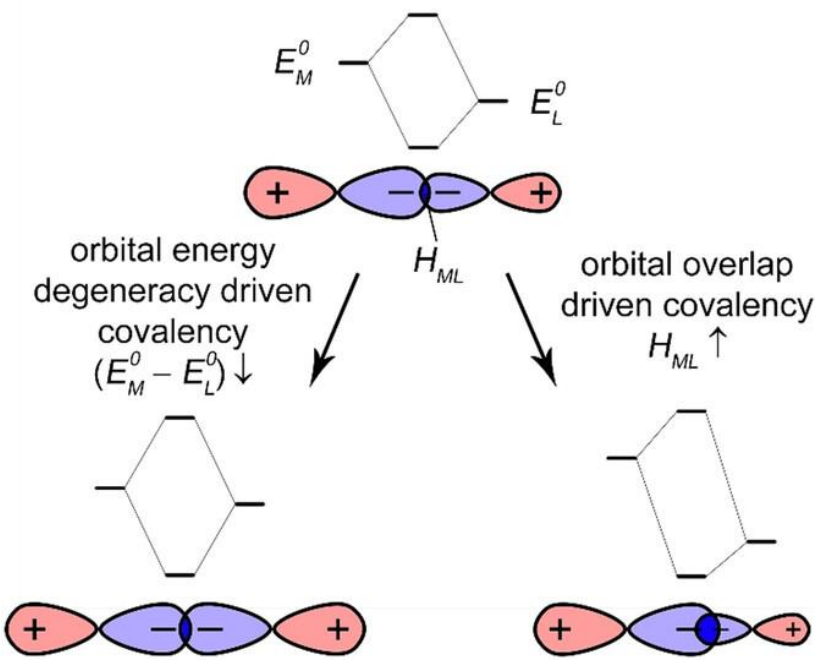

Figure 1.1. Orbital energy degeneracy driven covalency and orbital overlap drive covalency. Taken from ref [28]

Considering accessible oxidation states is important for understanding similarities and differences between the lanthanides and actinides, as they play a role in determining the stability and chemical properties of the f elements. The lanthanides tend to favor the trivalent oxidation state as they represent their most thermodynamically stable states (Table 1.1). However, it has been demonstrated that divalent Ln ions are accessible for all the lanthanides except radioactive promethium.[29] Among them, europium, ytterbium, and samarium have readily accessible +2 oxidation states due to the half-filled shell $4f^7$ of Eu(II), the filled shell $4f^{14}$ of Yb(II), and nearly half-filled shell $4f^6$ of Sm(II).[30, 31] In addition, molecular complexes containing lanthanides in the +4 oxidation states are limited to cerium, praseodymium, and terbium.[32] In contrast, the early actinide exhibit diverse redox chemistry with a wide range of accessible oxidation states. In particular, uranium, neptunium, and plutonium display a diverse range of accessible oxidation states similar to that observed in transition metals. While, the later actinides tend to primarily adopt a trivalent oxidation state, similar to the lanthanides, as their most stable oxidation state.[27] The f-orbital participation in metal-ligand bonding is strongly related to the oxidation state.[27] Notably, as the oxidation states increase, there is a greater degree of covalency within metal ligand bonding.[33-35]

Table 1.1. Oxidation state of the lanthanides and actinides

La	**Ce**	**Pr**	**Nd**	**Pm**	**Sm**	**Eu**	**Gd**	**Tb**	**Dy**	**Ho**	**Ef**	**Tm**	**Yb**	**Lu**
+2	+2	+2	+2		+2	+2	+2	+2	+2	+2	+2	+2	+2	+2
+3	**+3**	**+3**	**+3**	**+3**	**+3**	**+3**	**+3**	**+3**	**+3**	**+3**	**+3**	**+3**	**+3**	**+3**
	+4	+4						+4						
Ac	**Th**	**Pa**	**U**	**Np**	**Pu**	**Am**	**Cm**	**Bk**	**Cf**	**Es**	**Fm**	**Md**	**No**	**Lr**
			+2	+2	+2	+2			+2	+2	+2	+2	**+2**	

+3	+3	+3	+3	+3	+3	**+3**	**+3**	**+3**	**+3**	**+3**	**+3**	**+3**	+3	**+3**
	+4	+4	+4	+4	**+4**	+4	+4	+4	+4					
		+5	+5	**+5**	+5	+5								
			+6	+6	+6	+6								
				+7	+7									

Bold represents the most stable oxidation state.

Within the transition metals, the valence d-orbitals extend into the periphery of the ligand atoms, enabling interactions with the valence orbitals of the ligand atoms to establish covalent bonds.[36, 37] In contrast, the involvement of valence 4f orbitals of lanthanides in chemical bonding is negligible with surrounding atoms. Specifically, the 4f orbitals experience poor shielding from the nucleus, causing them to contract and become more core-like (Figure 1.2).[27, 38] Conversely, in the actinides the 5f and 6d orbital are close in energy and are both capable of contributing in covalent bonds.[39, 40] Although 5f and 6d orbitals have similar energy they differ significantly in the radial distribution. Specifically, the 6d orbitals have sufficient radial distribution and may contribute in metal-ligand bonding. Although, the 5f orbitals are less contracted than the 4f orbitals in the lanthanides, they are significantly less diffused than the 6d orbitals.[40] The 5f orbitals of the later actinides are contracted and primarily adopt a trivalent oxidation state similar to the lanthanides.[27] Interesting, in early actinides the 5f orbitals are less contracted and shielded, primarily due to the relativistic effects causing radial expansion. As a result, the frontier 5f orbitals in the early actinides are more accessible for metal-ligand covalent interactions. Additionally, the radial distribution of the 5f orbitals decreases as you move across the f elements. [41]

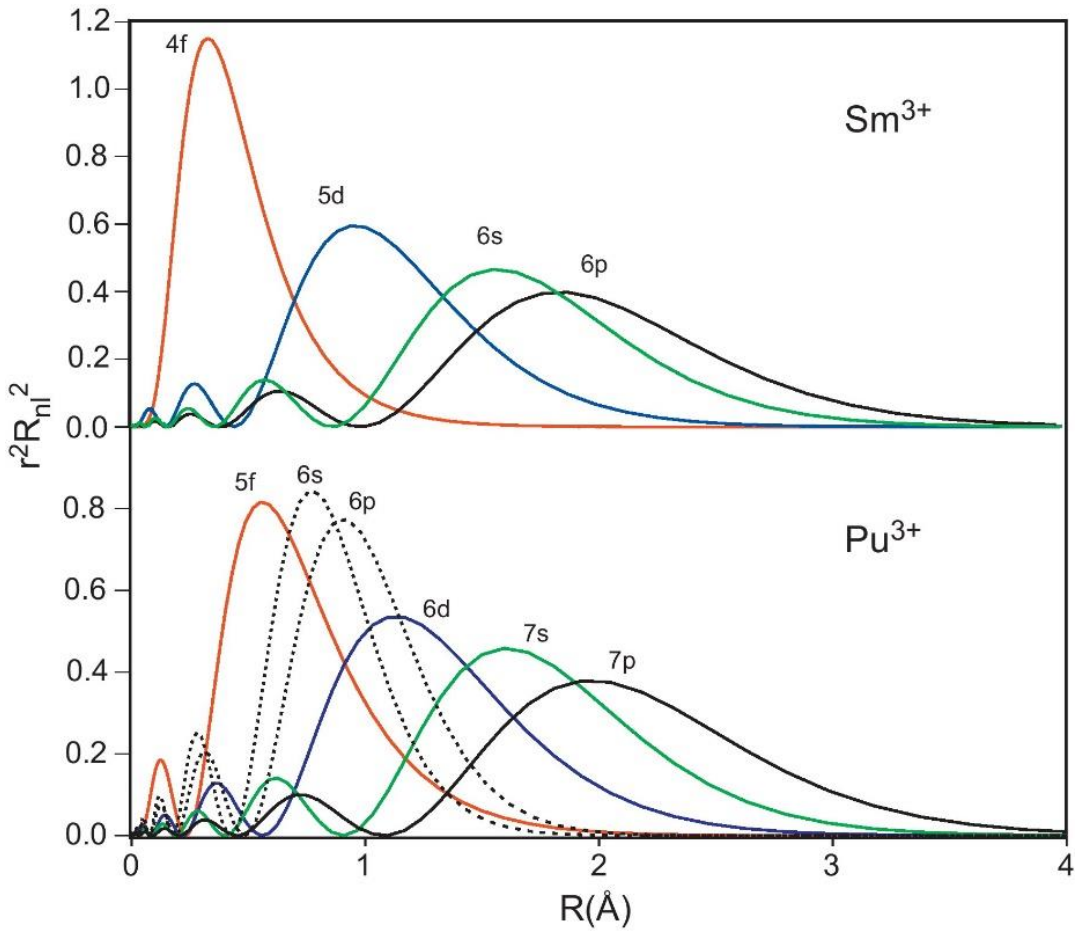

Figure 1.2. Relativistic radial distribution functions for Pu^{3+} and Sm^{3+}. Taken from ref [27].

Furthermore, as we traverse across the actinide series, the energy of the 5f orbitals tends to decrease.[42-44] Specifically, within the early actinides, there is a near-degeneracy between the 5f and 6d orbitals.[45] The near-degeneracy allows accessible occupation of both the 5f and 6d in the ground state configuration. However, around plutonium, the 5f orbitals drop significantly below the 6d orbitals tend to favor exclusive occupation of the 5f orbitals.[46] Notably, as the involvement of the 6d orbitals decrease and the contraction of the 5f orbitals increases within the late actinides, the electronic configuration and chemical behavior start to resemble that observed in the lanthanides (Table 1.2).[47] Interestingly, in the late actinides the lower energy of the 5f orbitals aligns with the 2p orbitals of nitrogen or oxygen, facilitating

stronger covalent interactions.[48] . Studying the trends across the actinides series is important for understanding the involvement of the 5f and 6d orbitals in metal-ligand bond, as these trends involve variations in stable oxidation states, orbital overlap, and energy matching.

Table 1.2. Ground electronic configuration of the lanthanides and actinides.

Lanthanide	***Atomic #***	***Electron Config.***	***Actinide***	***Atomic #***	***Electron Config.***
La	57	$[Xe]5d^16s^2$	Ac	89	$[Rn]6d^17s^2$
Ce	58	$[Xe]4f^15d^16s^2$	Th	90	$[Rn]6d^27s^2$
Pr	59	$[Xe]4f^36s^2$	Pa	91	$[Rn]5f^26d^17s^2$
Nd	60	$[Xe]4f^46s^2$	U	92	$[Rn]5f^36d^17s^2$
Pm	61	$[Xe]4f^56s^2$	Np	93	$[Rn]5f^46d^17s^2$
Sm	62	$[Xe]4f^66s^2$	Pu	94	$[Rn]5f^67s^2$
Eu	63	$[Xe]4f^76s^2$	Am	95	$[Rn]5f^77s^2$
Gd	64	$[Xe]4f^75d^16s^2$	Cm	96	$[Rn]5f^76d^17s^2$
Tb	65	$[Xe]4f^96s^2$	Bk	97	$[Rn]5f^97s^2$
Dy	66	$[Xe]4f^{10}6s^2$	Cf	98	$[Rn]5f^{10}7s^2$
Ho	67	$[Xe]4f^{11}6s^2$	Es	99	$[Rn]5f^{11}7s^2$
Er	68	$[Xe]4f^{12}6s^2$	Fm	100	$[Rn]5f^{12}7s^2$
Tm	69	$[Xe]4f^{13}6s^2$	Md	101	$[Rn]5f^{13}7s^2$
Yb	70	$[Xe]4f^{14}6s^2$	No	102	$[Rn]5f^{14}7s^2$
La	71	$[Xe]4f^{14}5d^16s^2$	Lr	103	$[Rn]5f^{14}6d^17s^2$

1.2 Measuring Covalency with XAS in f elements

There are several spectroscopic techniques and methods developed to directly measure f orbital participation in the metal-ligand bond.[22, 25, 49-65] For example, ligand K-edge X-ray absorption spectroscopy (XAS) is used to evaluate covalency in metal complexes, which

examines bound state transitions that occur on the low energy side of the ligand K-edge. [24, 66-77] This entails the excitation of 1s electron localized on the ligand, into singly occupied or unoccupied acceptor orbitals of the metal complex. Specifically, Cl K-edge XAS and both ground-state and time dependent density function theory (TDDFT) calculations were used to evaluate the relative roles of the valence f and d orbitals in M-Cl bonds for $Cp^*_2MCl_2$ (M = Ti, Zr, Hf, Th, U).[67] Interestingly, the K-edge X-ray absorption spectrum of $Cp^*_2ThCl_2$ does not exhibit pre-edge features (Figure 1.3), however examination of the second and fourth derivative suggest the presence of a weak shoulder that could not be sufficiently resolved to extract meaningful experimental intensities. In contrast, the Cl K-edge X-ray absorption spectrum of the uranium analogue contains three distinct pre-edge features, as confirmed by examination of the second derivative, indicating covalency in the metal-ligand bonding. Additionally, Kozimor and co-workers evaluated An-Cl covalency in a series of actinide hexachloride complexes, $[AnCl_6]^{2-}$ (An = Th, U, Np, Pu) using Cl K-edge X-ray absorption spectroscopy and DFT calculations. The results reveal that participation of 5f orbital increases and 6d orbital decrease across the early actinide(IV) series, indicating that 5f orbital participation was the largest in Pu.[42]

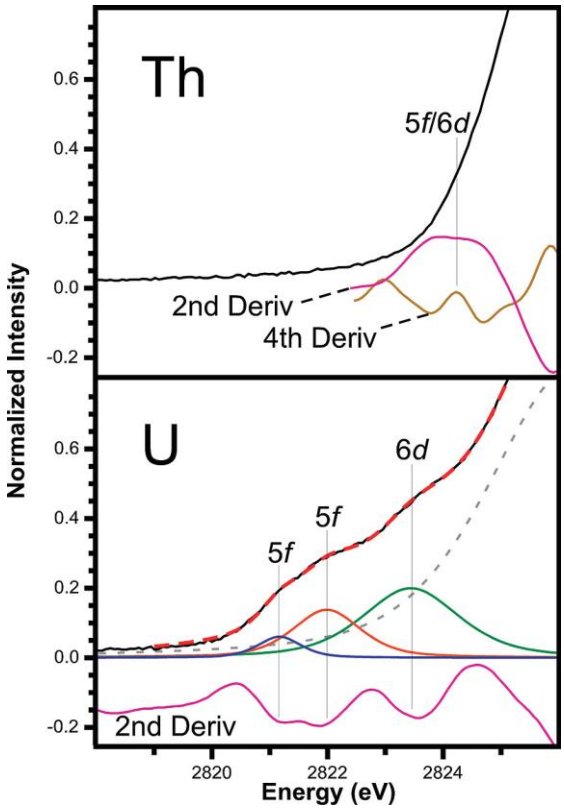

Figure 1.3**.** Cl K-edge X-ray absorption spectrum of $Cp^*_2AnCl_2$ (An = Th, Top; U, Bottom). Taken from ref.[67]

Interestingly, Cl K-edge XAS was used to examine 4f and 5d orbital mixing in the Ln-Cl bonds in a series of highly symmetric O_h-$[LnCl_6]^{x-}$ (Ln = Ce, Nd, Sm, Eu, Gd, x = 3) and $[CeCl_6]^{2-}$.[34] Interestingly, the Cl K-edge XAS spectra for $[CeCl_6]^{2-}$ (formally Ce^{IV}) reveals two clear pre-edge feature, whereas the Cl K-edge XAS spectra for $[CeCl_6]^{3-}$ (formally Ce^{III}) reveals a single pre-edge feature. Specifically, the spectrum for $[CeCl_6]^{2-}$ revealed a pre-edge feature at low energy that arises from Ce 4f orbital mixing with Cl 3p orbitals, however no such transition was observed for $[CeCl_6]^{3-}$ (Figure 1.4). The 4f orbital participation in $[CeCl_6]^{2-}$was rationalized by energy near-degeneracy covalency of Ce 4f and Cl 3p orbital mixing that is promoted by the increase in Ce oxidation. Surprisingly, the 4f orbital participation in $[CeCl_6]^{2-}$ was twice that observed compared to the more diffused for the 5f

orbital in $[UCl_6]^{2-}$, supported by larger Cl 3p-character for Ce^{IV} (9.9(9) %) vs U^{IV} (5.7(6) %). The increase in 4f orbital participation in $[CeCl_6]^{2-}$ was attributed to the lower energy of the Ce 4f orbitals vs U 5f orbitals.

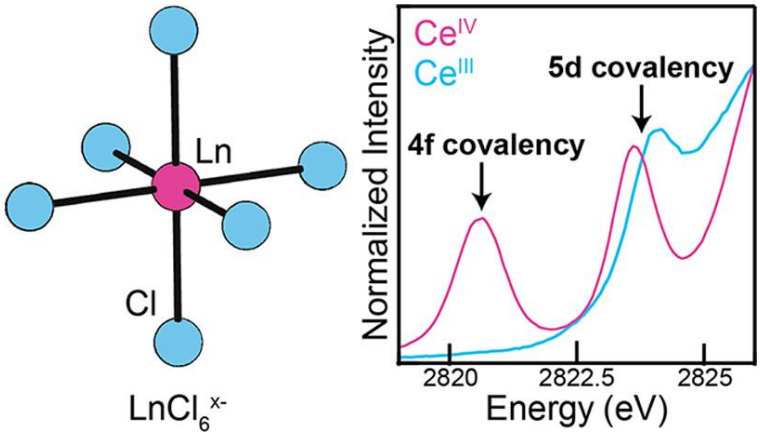

Figure 1.4. Cl K-edge X-ray absorption spectrum for $[CeCl_6]^{2-}$and $[CeCl_6]^{3-}$. Taken from ref.[34]

The understanding of electronic structure and chemical bonding in organometallic actinide chemistry has been notably advanced through the study of actinide sandwich complexes, specifically, actinocenes $[An(C_8H_8)_2]$ (An = Th, Pa, U, Np, Pu).[78-81] Investigations into these complexes revealed evidence of covalent mixing between the ligand and the metal 5f and 6d orbital.[82-90] In this regard, Shuh and co-workers used ligand K-edge XAS to examine 5f covalency in actinocenes (Figure 1.5).[23] Specifically, C K-edge XAS and time-dependent density functional theory was used to evaluate the electron structure of thorocene, $[Th(C_8H_8)_2]$, and uranocene $[U(C_8H_8)_2]$. Computational analysis of the experimental data revealed substantial δ-type mixing of the 5f orbitals with the $C_8H_8^{2-}$ ligands. Interestingly, the mixing increased from Th^{4+} to U^{4+}attributed to the decrease in energy of the 5f orbitals, resulting in closer alignment with the energy to the ligand orbitals.[44, 56] In addition, the C K-edge XAS analysis of the thorocene displayed evidence for significant ϕ-orbital interactions,

whereas the uranocene shows minimal ϕ-type covalency. The C K-edge XAS and time-dependent density functional theory analysis of the actinocenes illustrated that covalent mixing does not uniformly increase across different molecular orbital interactions in the later actinides.

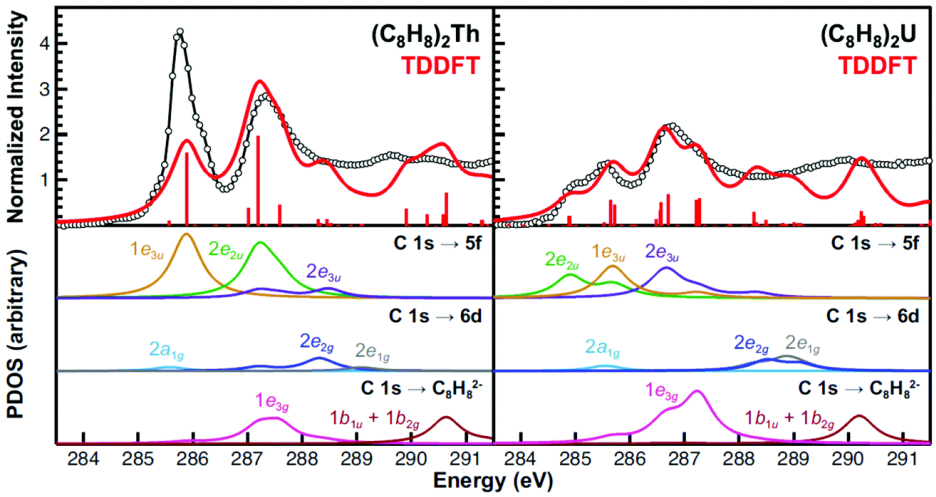

Figure 1.5. C K-edge XAS data obtained for [An(C_8H_8)$_2$] (An = Th, U) (black circles and traces). The TDDFT calculations in the top panes (red). The partial density of states (PDOS) derived from the TDDFT for final states associated with the 5f, 6d, or ligand-based orbitals. Taken from ref.[23]

While XAS has provided significant insight into the nature of the electronic structure and chemical bonding in f elements, it encounters challenges in distinguishing between degeneracy and overlap drive covalency in metal-ligand bonding.[91] Also, XAS is limited in its applicability when studying complexes that contain multiple chemical environments. Additionally, XAS requires synchrotron beam time, restricting the number of studies performed. Consequently, there is a demand for developing affordable and accessible methods to investigate covalency in metal-ligand to further understand the electronic structure and chemical bonding in the f-elements.

1.3 Measuring Covalency with NMR Spectroscopy in f elements

Nuclear magnetic resonance (NMR) spectroscopy is one of the most powerful tools that is readily accessible to investigate the structure, dynamics, and chemical kinetics of chemical systems.[92] Specifically, NMR chemical shifts provide information about the molecular and electronic structure due to the resonant frequency of a particular nuclear environment.[93, 94] More recently, NMR spectroscopy combined with DFT calculations has emerged as a valuable tool to evaluate An-L and Ln-L bonding covalency. Specifically, ^{1}H,[95, 96] ^{13}C,[95, 97-108] ^{15}N,[109-111] ^{19}F,[112-116] ^{31}P,[117] ^{29}Si,[118] ^{77}Se,[119, 120] and ^{125}Te[119] NMR spectroscopy have proven useful to quantify the amount of f and d orbital participation in Ln-L and An-L bonding. Relativistic effects significantly impact NMR chemical shifts in heavy-element complexes. These effects arise from spin-orbit coupling and magnetically induces spin polarization, originating at the heavy atom and extending to the spectator nucleus through a Fermi-contact-type interaction.[121] Therefore, NMR chemical shifts for Ln- or An- bound nuclei are strongly affected by spin-orbit (SO) coupling, a consequence of both f and d orbital involvement in bonding.[122] However, NMR analysis of Ln and An complexes are limited to close-shell $4f^0$ (La^{III}, Ce^{IV}), $4f^{14}$(Lu^{III}), and $5f^0$ (Th^{IV}, Pa^{V}, U^{VI}) electron configurations.

Nonetheless, the use ^{13}C NMR spectroscopy has been applied to evaluate metal ligand bonding in a wide variety of organometallic actinide complexes. For instance, Hayton and Hrobárik report the synthesis and characterization of tetraalkyl-uranyl complex, $[Li(DME)_{1.5}]_2[UO_2(CH_2SiMe_3)_4]$ and homoleptic hexaalkyl-uranium(VI) complex, $[U((CH_2SiMe_3)_6]$.[97, 123] Notably, the methylene ^{13}C chemical resonance of the CH_2SiMe_3 ligand in $[Li(DME)_{1.5}]_2[UO_2(CH_2SiMe_3)_4]$ is significantly deshielded at 242.9 ppm. Additionally, the ^{13}C NMR spectrum of $[U(CH_2SiMe_3)_6]$ displays a resonance at 434.3 ppm,

which is assigned to the methyl carbon atom of the CH_2SiMe_3 ligand. The ^{13}C NMR chemical shifts were calculated revealing SO coupling contributions of 177 ppm in $[Li(DME)_{1.5}]_2[UO_2(CH_2SiMe_3)_4]$ and 348 ppm in $[U(CH_2SiMe_3)_6]$, which are responsible for the large downfield shift observed. The large SO coupling contribution is attributable to the involvement of the 5f (and 6d) subshells in the U-C bonds. The larger deshielding observed in the ^{13}C NMR chemical shift in $[U(CH_2SiMe_3)_6]$ is a consequence of greater participation of the 5f orbitals in the U-C bonds. The examination of ^{13}C chemical shifts through DFT in the both homoleptic and heteroleptic U^{6+} alkyl complexes demonstrate the effect of the 5f orbital involvement resulting in variations in SO coupling contributions.

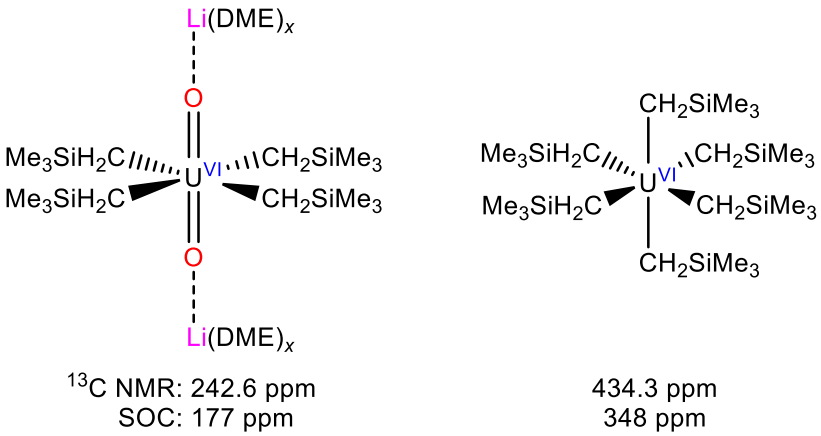

Figure 1.6. ^{13}C chemical shifts and SOC of Actinide Alkyl Complexes. Adapted from ref.[97]

Furthermore, analysis of ^{13}C chemical shifts with DFT calculations has proven useful in a variety of organometallic actinide complexes featuring acetylide ligands. Specifically, Schelter and Hrobárik report the synthesis and characterization of a series of uranium(VI) acetylide complexes, $[U(O)(C{\equiv}C\text{-}C_6H_4\text{-}p\text{-}R)\{N(SiMe_3)_2\}_3]$ (R = NMe_2, OMe, Me, Ph, H, Cl).[100] Interestingly, changing the para substituents on the aryl ring resulted in a difference in the ^{13}C chemical shifts, ranging from 392.1 ppm to 409.7 ppm. The downfield shifts observed in the ^{13}C chemical shifts are attributed to the effect of SO coupling, which arises from

significant U(5f) and C(2s) orbitals in the U-C bonds. Furthermore, DFT calculations indicated that within this series of uranium(VI) acetylide complexes, the U-C bond tended to shortened as electron donating ability of the para substituent increased. Significantly, the U-C bonds exhibit 28-29% total uranium character with 5f orbital contribution of 60-62%. In addition, Hayton and Autschbach examine the ^{13}C chemical shifts in a thorium parent acetylide complex, $[Th(C{\equiv}CH)(NR_2)_3]$ (R = $SiMe_3$), and in a thorium dicarbide complex, $[\{Th(NR_2)_3\}_2(\mu,\eta^1{:}\eta^1\text{-}C_2)]$ (R = $SiMe_3$).[103] The calculated ^{13}C chemical shift for $[Th(C{\equiv}CH)(NR_2)_3]$ is 174.9 ppm (expt. = 176.1 ppm), which includes a 32.2 ppm deshielding contribution due to SO coupling. The calculated ^{13}C chemical shift for $[\{Th(NR_2)_3\}_2(\mu,\eta^1{:}\eta^1\text{-}C_2)]$ is 205.7 ppm (expt. = 202.7 ppm) with a 38.9 ppm deshielding SO coupling contribution. The deshielding contribution due to SO coupling is a direct result of the 5f orbital participation. Specifically, DFT calculations reveal 17% total thorium weight with 5f contributions of 14% in $[Th(C{\equiv}CH)(NR_2)_3]$ and 16% in $[\{Th(NR_2)_3\}_2(\mu,\eta^1{:}\eta^1\text{-}C_2)]$. For comparison, the uranium(VI) acetylide complexes feature more deshielding SO coupling contribution in their ^{13}C chemical resonance attributed to the greater degree if 5f orbital involvement in the An-C bonds.

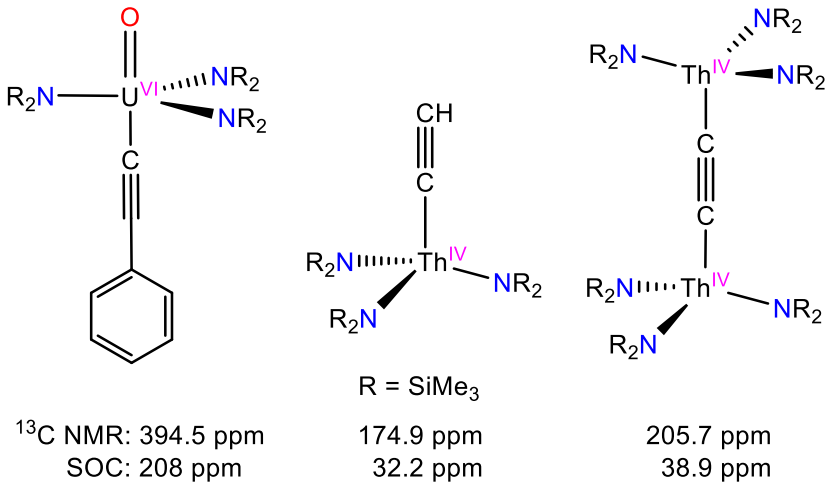

Figure 1.7. ^{13}C chemical shifts and SOC of Actinide Acetylide Complexes. Adapted from refs.[100, 103]

More recently, the evaluation of ^{13}C chemical shifts has been demonstrated in assessing Ln-C bonding. For instance, Schelter and Autschbach report the synthesis and characterization of a cerium(IV) aryl complex, $[Li(THF)_4][Ce^{IV}(\kappa^2\text{-}ortho\text{-oxa})(MBP)_2]$ (*ortho*-oxa = dihydro-dimethyl-2-[4-(trifluoromethyl)phenyl]-oxazolide and MBP^{2-} = 2,2′-methylenebis(6-*tert*-butyl-4-methylphenolate)).[101] Notably, analysis of the ^{13}C chemical shifts revealed a calculated 40 ppm SO-induced shift for the C_{ipso} resonance. This downfield shift observed is attributed to the involvement of the 4f orbitals in the Ce-C bond. Specifically, natural localized molecular orbital analysis (NLMO) shows a 12 % metal contribution to the Ce^{IV}-C_{aryl} bond. Importantly, analysis of the Ce^{IV}-aryl complex represents the first example of quantifying covalency in the lanthanides using NMR spectroscopy, a promising avenue for further investigation.

Additionally, Liddle and co-workers reported the synthesis and characterization of cerium(IV)-diphosphonioalkylidene complexes, $[Ce(BIPM^{TMS})(ODipp)_2]$ ($BIPM^{TMS}$ = $\{C(PPh_2NSiMe_3)_2\}^{2-}$) and $[Ce(BIPM^{TMS})_2]$.[124-126] The solution ^{13}C chemical resonance of the

carbene center in [Ce(BIPM^{TMS})(ODipp)$_2$] is observed at 324.6 ppm and in [Ce(BIPM^{TMS})$_2$] 343.5 ppm. The solid-state ^{13}C NMR spectroscopy reveals a resonance at 322.5 ppm for [Ce(BIPM^{TMS})(ODipp)$_2$] and two resonances at 334.5 ppm and 341.5 ppm for [Ce(BIPM^{TMS})$_2$], which are similar to those observed in solution NMR spectra.[127] The calculated ^{13}C chemical shift for [Ce(BIPM^{TMS})(ODipp)$_2$] is 324.9 ppm and for [Ce(BIPM^{TMS})$_2$] is 341.8 ppm, which are in good agreement with experimental values. These calculated ^{13}C chemical shift reveal considerable amounts of SO coupling contribution of 26.5 ppm in [Ce(BIPM^{TMS})(ODipp)$_2$] and 82.9 ppm in [Ce(BIPM^{TMS})$_2$]. Further analysis of the ^{13}C chemical shift and a natural localized molecular orbital analysis indicates the presence of Ce=C double bond character.

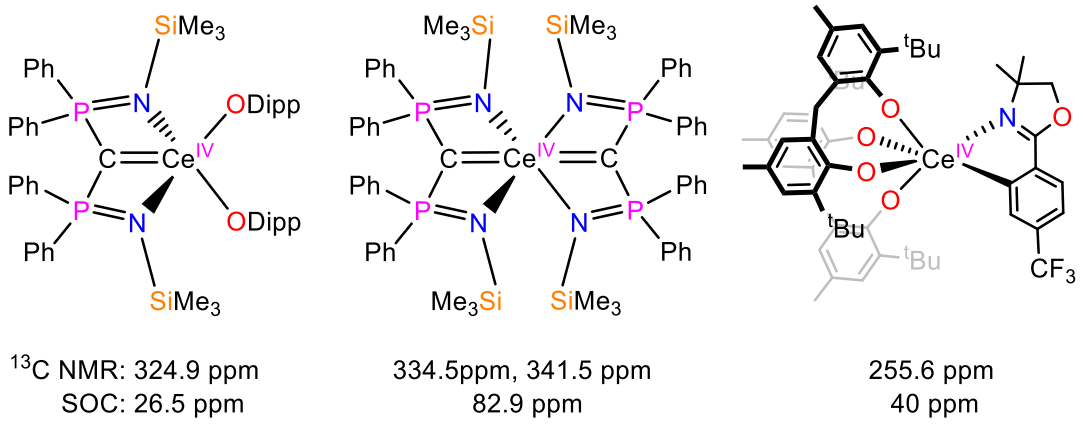

Figure 1.8. ^{13}C chemical shifts and SOC of Cerium Carbene and Aryl Complexes. Adapted from refs.[101, 127]

Importantly, the utilization of NMR spectroscopy as a tool for investigating the electronic structure of actinides requires close collaboration with computational experts. For my thesis work, I have been collaborating with Prof. Jochen Autschbach and Dr. Xiaojuan Yu at the State University of New York Buffalo. They have performed and refined calculations essential for evaluating metal-ligand bonding in f elements. Their invaluable contribution has played a

pivotal role in propelling the application of NMR spectroscopy to gain deeper insights into covalency in f elements, emerging as a prominent method.[102-110, 128-130]

1.4 General Remarks

The overall goal of this research is to gain a better understanding of metal-ligand bonding in f elements. Specifically, through the synthesis, characterization, and analysis of the electronic structure of lanthanide aryl complexes, actinide aryl complexes, actinide cyclopropyl complexes, and actinide allenylidene complexes.

Chapter 2 describes the synthesis and characterization of the first structurally characterized uranyl aryl complexes. The use of perhalogenated aryl ligand results in the generation of stable uranyl aryl complexes. A discussion of a combined ^{13}C NMR spectroscopic and relativistic DFT calculations to further understand the electronic structure and chemical bonding in the uranium-carbon bonds.

Chapter 3 describes the synthesis and characterization of the first homoleptic perhaloaryl complexes of the actinides. Their remarkable thermal stability, which is much greater than other homoleptic actinide aryl complexes is discussed. Additionally, their enhanced thermal stability enabled a detailed spectroscopic and computation analysis, which uncovered moderate amounts of An-C bond covalency in these complexes is discussed.

Chapter 4 describes the synthesis and characterization of the first homoleptic perchloroaryl complexes of the lanthanides. These complexes proved to be highly thermally sensitive; nonetheless, both complexes were characterized by X-ray crystallography and $^{13}C\{^{1}H\}$ NMR spectroscopy, and their electronic structures were examined by relativistic density functional theory (DFT).

Chapter 5 describes the synthesis and characterization of uranyl aryl complexes, an extremely rare example of a uranyl organometallic complex. Their unusual stability is a consequence of the presence of the *ortho*-CF_3 substituents, which impart significant kinetic stability to the U-C bonds is discussed. A discussion of a combined ^{13}C NMR spectroscopic and relativistic DFT computational analysis was used to study the nature of the U-C bonds.

Chapter 6 describes the synthesis and reactivity of the first structurally characterized cyclopropyl complexes of the actinides. Photolysis (or thermolysis) results in cyclopropyl ring-opening, and formation of the η^1-allyl complexes, that represent the first examples of cyclopropyl ring-opening in the actinides is discussed. A discussion of deuterium labelling studies that demonstrate ring-opening occurs via distal C-C bond cleavage, through an unobserved η^3-allyl intermediate.

Chapter 7 describes the conversion of cyclopropenyl to allenylidene by deprotonation via an exogenous base, which is unprecedented and promises the potential of a general route to thorium allenylidene complexes. A discussion of reactivity studies of thorium allenylidene complex towards electrophiles that results in a regioselective electrophilic attack at the C_γ carbon atom leading to the formation of a thorium acetylide complex. These complexes are also explored by a combined ^{13}C NMR spectroscopic and relativistic DFT calculations and a discussion of their electronic structure is given.

Chapter 8 describes the synthesis and characterization of two homoleptic actinide benzene-1,2-dithiolate complexes. These complexes were characterized by X-ray crystallography and NMR spectroscopy. The reactivity of the homoleptic uranium benzene-1,2-dithiolate complex towards $1e^-$ oxidation is discussed. Additionally, the synthesis, characterization, and reactivity of uranyl thiolate complexes is discussed.

1.5 References

(1) Choppin, G.; Liljenzin, J.-O.; Rydberg, J.; Ekberg, C. *Radiochemistry and nuclear chemistry*; Academic Press, 2013.
(2) Madic, C.; Lecomte, M.; Baron, P.; Boullis, B. Separation of long-lived radionuclides from high active nuclear waste. *C. R. Phys.* **2002**, *3*, 797-811.
(3) Bates, E. A.; Driscoll, M. J.; Lester, R. K.; Arnold, B. W. Can deep boreholes solve Americaʹs nuclear waste problem? *Energy Policy* **2014**, *72*, 186-189.
(4) Ionova, G.; Ionov, S.; Rabbe, C.; Hill, C.; Madic, C.; Guillaumont, R.; Modolo, G.; Krupa, J. C. Mechanism of trivalent actinide/lanthanide separation using synergistic mixtures of di(chlorophenyl)dithiophosphinic acid and neutral O-bearing co-extractants. *New J. Chem.* **2001**, *25*, 491-501.
(5) Leoncini, A.; Huskens, J.; Verboom, W. Ligands for f-element extraction used in the nuclear fuel cycle. *Chem. Soc. Rev.* **2017**, *46*, 7229-7273.
(6) Nash, K. L. A Review of the basic chemistry and recent developments in trivalent f-elements separations. *Solvent Extr. Ion Exch.* **1993**, *11*, 729-768.
(7) Veliscek-Carolan, J. Separation of actinides from spent nuclear fuel: A review. *J. Hazard. Mater.* **2016**, *318*, 266-281.
(8) Kolarik, Z.; Müullich, U. Extraction of Am(lll) and Eu(lll) by 2-substituted benzimidazoles. *Solvent Extr. Ion Exch.* **1997**, *15*, 361-379.
(9) Jensen, M. P.; Bond, A. H. Comparison of Covalency in the Complexes of Trivalent Actinide and Lanthanide Cations. *J. Am. Chem. Soc.* **2002**, *124*, 9870-9877.
(10) Watanabe, M.; Mirvaliev, R.; Tachimori, S.; Takeshita, K.; Nakano, Y.; Morikawa, K.; Chikazawa, T.; Mori, R. Selective Extraction of Americium(III) over Macroscopic Concentration of Lanthanides(III) by Synergistic System of TPEN and D2EHPA in 1-Octanol. *Solvent Extr. Ion Exch.* **2004**, *22*, 377-390.
(11) Chandrasekar, A.; Ghanty, T. K. Uncovering Heavy Actinide Covalency: Implications for Minor Actinide Partitioning. *Inorg. Chem.* **2019**, *58*, 3744-3753.
(12) Deblonde, G. J. P.; Ricano, A.; Abergel, R. J. Ultra-selective ligand-driven separation of strategic actinides. *Nat. Commun.* **2019**, *10*, 2438.
(13) Grimes, T. S.; Heathman, C. R.; Jansone-Popova, S.; Ivanov, A. S.; Bryantsev, V. S.; Zalupski, P. R. Exploring Soft Donor Character of the N-2-Pyrazinylmethyl Group by Coordinating Trivalent Actinides and Lanthanides Using Aminopolycarboxylates. *Inorg. Chem.* **2020**, *59*, 138-150.
(14) Ekberg, C.; Fermvik, A.; Retegan, T.; Skarnemark, G.; Foreman, M. R. S.; Hudson, M. J.; Englund, S.; Nilsson, M. An overview and historical look back at the solvent extraction using nitrogen donor ligands to extract and separate An(III) from Ln(III). *Radiochim. Acta* **2008**, *96*, 225-233.
(15) Panak, P. J.; Geist, A. Complexation and Extraction of Trivalent Actinides and Lanthanides by Triazinylpyridine N-Donor Ligands. *Chem. Rev.* **2013**, *113*, 1199-1236.
(16) Geist, A.; Müllich, U.; Magnusson, D.; Kaden, P.; Modolo, G.; Wilden, A.; Zevaco, T. Actinide(III)/Lanthanide(III) Separation Via Selective Aqueous Complexation of Actinides(III) using a Hydrophilic 2,6-Bis(1,2,4-Triazin-3-Yl)-Pyridine in Nitric Acid. *Solvent Extr. Ion Exch.* **2012**, *30*, 433-444.

(17) Weaver, B.; Kappelmann, F. A. Preferential extraction of lanthanides over trivalent actinides by monoacidic organophosphates from carboxylic acids and from mixtures of carboxylic and aminopolyacetic acids. *J. Inorg. Nucl. Chem.* **1968**, *30*, 263-272.
(18) Nash, K. L. The Chemistry of TALSPEAK: A Review of the Science. *Solvent Extr. Ion Exch.* **2015**, *33*, 1-55.
(19) Weaver, B.; Kappelmann, F. *TALSPEAK: a new method of separating americium and curium from the lanthanides by extraction from an aqueous solution of an aminopolyacetic acid complex with a monoacidic organophosphate or phosphonate*; Oak Ridge National Lab.(ORNL), Oak Ridge, TN (United States), 1964.
(20) Klaehn, J. R.; Peterman, D. R.; Harrup, M. K.; Tillotson, R. D.; Luther, T. A.; Law, J. D.; Daniels, L. M. Synthesis of symmetric dithiophosphinic acids for "minor actinide" extraction. *Inorg. Chim. Acta* **2008**, *361*, 2522-2532.
(21) Ionova, G.; Ionov, S.; Rabbe, C.; Hill, C.; Madic, C.; Guillaumont, R.; Krupa, J. C. Mechanism of trivalent actinide/lanthanide separation using bis(2,4,4-trimethylpentyl) dithiophosphinic acid (Cyanex 301) and neutral O-bearing co-extractant synergistic mixtures. *Solvent Extr. Ion Exch.* **2001**, *19*, 391-414.
(22) Seaman, L. A.; Wu, G.; Edelstein, N.; Lukens, W. W.; Magnani, N.; Hayton, T. W. Probing the 5f Orbital Contribution to the Bonding in a U(V) Ketimide Complex. *J. Am. Chem. Soc.* **2012**, *134*, 4931-4940.
(23) Minasian, S. G.; Keith, J. M.; Batista, E. R.; Boland, K. S.; Clark, D. L.; Kozimor, S. A.; Martin, R. L.; Shuh, D. K.; Tyliszczak, T. New evidence for 5f covalency in actinocenes determined from carbon K-edge XAS and electronic structure theory. *Chem. Sci.* **2014**, *5*, 351-359.
(24) Minasian, S. G.; Keith, J. M.; Batista, E. R.; Boland, K. S.; Clark, D. L.; Conradson, S. D.; Kozimor, S. A.; Martin, R. L.; Schwarz, D. E.; Shuh, D. K.; et al. Determining Relative f and d Orbital Contributions to M–Cl Covalency in MCl_6^{2-} (M = Ti, Zr, Hf, U) and $UOCl_5^{-}$ Using Cl K-Edge X-ray Absorption Spectroscopy and Time-Dependent Density Functional Theory. *J. Am. Chem. Soc.* **2012**, *134*, 5586-5597.
(25) Lukens, W. W.; Edelstein, N. M.; Magnani, N.; Hayton, T. W.; Fortier, S.; Seaman, L. A. Quantifying the σ and π Interactions between U(V) f Orbitals and Halide, Alkyl, Alkoxide, Amide and Ketimide Ligands. *J. Am. Chem. Soc.* **2013**, *135*, 10742-10754.
(26) Kozimor, S. A.; Yang, P.; Batista, E. R.; Boland, K. S.; Burns, C. J.; Christensen, C. N.; Clark, D. L.; Conradson, S. D.; Hay, P. J.; Lezama, J. S.; et al. Covalency Trends in Group IV Metallocene Dichlorides. Chlorine K-Edge X-Ray Absorption Spectroscopy and Time Dependent-Density Functional Theory. *Inorg. Chem.* **2008**, *47*, 5365-5371.
(27) Neidig, M. L.; Clark, D. L.; Martin, R. L. Covalency in f-element complexes. *Coord. Chem. Rev.* **2013**, *257*, 394-406.
(28) Pace, K. A.; Klepov, V. V.; Berseneva, A. A.; zur Loye, H.-C. Covalency in Actinide Compounds. *Chem. Eur. J.* **2021**, *27*, 5835-5841.
(29) MacDonald, M. R.; Bates, J. E.; Ziller, J. W.; Furche, F.; Evans, W. J. Completing the Series of +2 Ions for the Lanthanide Elements: Synthesis of Molecular Complexes of Pr^{2+}, Gd^{2+}, Tb^{2+}, and Lu^{2+}. *J. Am. Chem. Soc.* **2013**, *135*, 9857-9868.
(30) Evans, W. J. Perspectives in reductive lanthanide chemistry. *Coord. Chem. Rev.* **2000**, *206-207*, 263-283.

(31) Meyer, G. Small cause – Great effect: What the $4f^{n+1}5d^0 \rightarrow 4f^n5d^1$ configuration crossover does to the chemistry of divalent rare-earth halides and coordination compounds. *J. Solid State Chem.* **2019**, *270*, 324-334.
(32) Gompa, T. P.; Ramanathan, A.; Rice, N. T.; La Pierre, H. S. The chemical and physical properties of tetravalent lanthanides: Pr, Nd, Tb, and Dy. *Dalton Trans.* **2020**, *49*, 15945-15987.
(33) Bagus, P. S.; Nelin, C. J.; Hrovat, D. A.; Ilton, E. S. Covalent bonding in heavy metal oxides. *J. Chem. Phys.* **2017**, *146*, 134706.
(34) Löble, M. W.; Keith, J. M.; Altman, A. B.; Stieber, S. C. E.; Batista, E. R.; Boland, K. S.; Conradson, S. D.; Clark, D. L.; Lezama Pacheco, J.; Kozimor, S. A.; et al. Covalency in Lanthanides. An X-ray Absorption Spectroscopy and Density Functional Theory Study of $LnCl_6^{x-}$ (x = 3, 2). *J. Am. Chem. Soc.* **2015**, *137*, 2506-2523.
(35) Beekmeyer, R.; Kerridge, A. Assessing Covalency in Cerium and Uranium Hexachlorides: A Correlated Wavefunction and Density Functional Theory Study. In *Inorganics*, 2015; Vol. 3, pp 482-499.
(36) Yatsimirskii, K. B. Ranges of oxidation states ford-transition metals in their complex compounds. *Theor. Exp. Chem.* **1997**, *33*, 248-253.
(37) Frenking, G.; Fröhlich, N. The Nature of the Bonding in Transition-Metal Compounds. *Chem. Rev.* **2000**, *100*, 717-774.
(38) Crosswhite, H. M.; Crosswhite, H.; Carnall, W. T.; Paszek, A. P. Spectrum analysis of U^{3+}:$LaCl_3$. *J. Chem. Phys.* **1980**, *72*, 5103-5117.
(39) Worden, E. F.; Blaise, J.; Fred, M.; Trautmann, N.; Wyart, J.-F. Spectra and Electronic Structures of Free Actinide Atoms and Ions. In *The Chemistry of the Actinide and Transactinide Elements*, Morss, L. R., Edelstein, N. M., Fuger, J. Eds.; Springer Netherlands, 2006; pp 1836-1892.
(40) Schreckenbach, G.; Hay, P. J.; Martin, R. L. Density functional calculations on actinide compounds: Survey of recent progress and application to $[UO_2X_4]^{2-}$ (X=F, Cl, OH) and AnF_6 (An=U, Np, Pu). *J. Comput. Chem.* **1999**, *20*, 70-90.
(41) Vitova, T.; Pidchenko, I.; Fellhauer, D.; Bagus, P. S.; Joly, Y.; Pruessmann, T.; Bahl, S.; Gonzalez-Robles, E.; Rothe, J.; Altmaier, M.; et al. The role of the 5f valence orbitals of early actinides in chemical bonding. *Nat. Commun.* **2017**, *8*, 16053.
(42) Su, J.; Batista, E. R.; Boland, K. S.; Bone, S. E.; Bradley, J. A.; Cary, S. K.; Clark, D. L.; Conradson, S. D.; Ditter, A. S.; Kaltsoyannis, N.; et al. Energy-Degeneracy-Driven Covalency in Actinide Bonding. *J. Am. Chem. Soc.* **2018**, *140*, 17977-17984.
(43) Kelley, M. P.; Su, J.; Urban, M.; Luckey, M.; Batista, E. R.; Yang, P.; Shafer, J. C. On the Origin of Covalent Bonding in Heavy Actinides. *J. Am. Chem. Soc.* **2017**, *139*, 9901-9908.
(44) Pepper, M.; Bursten, B. E. The electronic structure of actinide-containing molecules: a challenge to applied quantum chemistry. *Chem. Rev.* **1991**, *91*, 719-741.
(45) Bursten, B. E.; Rhodes, L. F.; Strittmatter, R. J. Bonding in tris(η^5-cyclopentadienyl) actinide complexes. 2. The ground electronic configurations of "base-free" Cp_3An complexes (An = thorium, protactinium, uranium, neptunium, plutonium). *J. Am. Chem. Soc.* **1989**, *111*, 2756-2758.
(46) Kirker, I.; Kaltsoyannis, N. Does covalency really increase across the 5f series? A comparison of molecular orbital, natural population, spin and electron density analyses of $AnCp_3$ (An = Th–Cm; Cp = η^5-C_5H_5). *Dalton Trans.* **2011**, *40*, 124-131.
(47) Kaltsoyannis, N.; Scott, P. R. *The F Elements*; Oxford University Press, 2007.

(48) Wen, X.-D.; Martin, R. L.; Henderson, T. M.; Scuseria, G. E. Density Functional Theory Studies of the Electronic Structure of Solid State Actinide Oxides. *Chem. Rev.* **2013**, *113*, 1063-1096.
(49) Formanuik, A.; Ariciu, A.-M.; Ortu, F.; Beekmeyer, R.; Kerridge, A.; Tuna, F.; McInnes, E. J. L.; Mills, D. P. Actinide covalency measured by pulsed electron paramagnetic resonance spectroscopy. *Nat. Chem.* **2017**, *9*, 578-583.
(50) Boatner, L. A.; Abraham, M. M. Electron paramagnetic resonance from actinide elements. *Rep. Prog. Phys.* **1978**, *41*, 87.
(51) Aminov, L. K.; Kurkin, I. N.; Malkin, B. Z. Superhyperfine structure in the EPR spectra and optical spectra of impurity f ions in dielectric crystals: A review. *Phys. Solid State* **2013**, *55*, 1343-1363.
(52) Gourier, D.; Caurant, D.; Arliguie, T.; Ephritikhine, M. EPR and Angle-Selected ENDOR Study of 5f-Ligand Interactions in the $[U(\eta^7\text{-}C_7H_7)_2]^-$ Anion, an f^1 Analogue of Uranocene. *J. Am. Chem. Soc.* **1998**, *120*, 6084-6092.
(53) Kalvius, G. Mössbauer spectroscopy of actinides: Some applications to solid state chemistry. *J. Less-Common Met.* **1986**, *121*, 353-378.
(54) Brennan, J. G.; Green, J. C.; Redfern, C. M. Covalency in bis([8]annulene)uranium from photoelectron spectroscopy with variable photon energy. *J. Am. Chem. Soc.* **1989**, *111*, 2373-2377.
(55) Clark, J. P.; Green, J. C. An investigation of the electronic structure of bis(η-cyclo-octatetraene)-actinoids by helium-(I) and -(II) photoelectron spetroscopy. *J. Chem. Soc., Dalton Trans.* **1977**, 505-508.
(56) Kerridge, A.; Kaltsoyannis, N. Are the Ground States of the Later Actinocenes Multiconfigurational? All-Electron Spin− Orbit Coupled CASPT2 Calculations on An $(\eta^8\text{-}C_8H_8)_2$ (An= Th, U, Pu, Cm). *J. Phys. Chem. A* **2009**, *113*, 8737-8745.
(57) Nguyen, T. H.; Paul, E. L.; Lukens, W. W.; Hayton, T. W. Evaluating f-Orbital Participation in the U^V═E Multiple Bonds of $[U(E)(NR_2)_3]$ (E = O, $NSiMe_3$, NAd; R = $SiMe_3$). *Inorg. Chem.* **2023**, *62*, 6447-6457.
(58) Schmidt, A.-C.; Heinemann, F. W.; Lukens, W. W., Jr.; Meyer, K. Molecular and Electronic Structure of Dinuclear Uranium Bis-μ-Oxo Complexes with Diamond Core Structural Motifs. *J. Am. Chem. Soc.* **2014**, *136*, 11980-11993.
(59) Graves, C. R.; Vaughn, A. E.; Schelter, E. J.; Scott, B. L.; Thompson, J. D.; Morris, D. E.; Kiplinger, J. L. Probing the Chemistry, Electronic Structure and Redox Energetics in Organometallic Pentavalent Uranium Complexes. *Inorg. Chem.* **2008**, *47*, 11879-11891.
(60) Graves, C. R.; Yang, P.; Kozimor, S. A.; Vaughn, A. E.; Clark, D. L.; Conradson, S. D.; Schelter, E. J.; Scott, B. L.; Thompson, J. D.; Hay, P. J.; et al. Organometallic Uranium(V)−Imido Halide Complexes: From Synthesis to Electronic Structure and Bonding. *J. Am. Chem. Soc.* **2008**, *130*, 5272-5285.
(61) Morris, D. E.; Da Re, R. E.; Jantunen, K. C.; Castro-Rodriguez, I.; Kiplinger, J. L. Trends in Electronic Structure and Redox Energetics for Early-Actinide Pentamethylcyclopentadienyl Complexes. *Organometallics* **2004**, *23*, 5142-5153.
(62) Schelter, E. J.; Yang, P.; Scott, B. L.; Thompson, J. D.; Martin, R. L.; Hay, P. J.; Morris, D. E.; Kiplinger, J. L. Systematic Studies of Early Actinide Complexes: Uranium(IV) Fluoroketimides. *Inorg. Chem.* **2007**, *46*, 7477-7488.

(63) Schelter, E. J.; Yang, P.; Scott, B. L.; Da Re, R. E.; Jantunen, K. C.; Martin, R. L.; Hay, P. J.; Morris, D. E.; Kiplinger, J. L. Systematic Studies of Early Actinide Complexes: Thorium(IV) Fluoroketimides. *J. Am. Chem. Soc.* **2007**, *129*, 5139-5152.
(64) Clark, A. E.; Martin, R. L.; Hay, P. J.; Green, J. C.; Jantunen, K. C.; Kiplinger, J. L. Electronic Structure, Excited States, and Photoelectron Spectra of Uranium, Thorium, and Zirconium Bis(Ketimido) Complexes $(C_5R_5)_2M[-NCPh_2]_2$ (M = Th, U, Zr; R = H, CH_3). *J. Phys. Chem. A* **2005**, *109*, 5481-5491.
(65) Burns, C. J.; Bursten, B. E. Covalency in f-Element Organometallic Complexes: Theory and Experiment. *Comments Inorg. Chem.* **1989**, *9*, 61-93.
(66) Solomon, E. I.; Hedman, B.; Hodgson, K. O.; Dey, A.; Szilagyi, R. K. Ligand K-edge X-ray absorption spectroscopy: covalency of ligand–metal bonds. *Coord. Chem. Rev.* **2005**, *249*, 97-129.
(67) Kozimor, S. A.; Yang, P.; Batista, E. R.; Boland, K. S.; Burns, C. J.; Clark, D. L.; Conradson, S. D.; Martin, R. L.; Wilkerson, M. P.; Wolfsberg, L. E. Trends in Covalency for d- and f-Element Metallocene Dichlorides Identified Using Chlorine K-Edge X-ray Absorption Spectroscopy and Time-Dependent Density Functional Theory. *J. Am. Chem. Soc.* **2009**, *131*, 12125-12136.
(68) Denning, R. G.; Green, J. C.; Hutchings, T. E.; Dallera, C.; Tagliaferri, A.; Giarda, K.; Brookes, N. B.; Braicovich, L. Covalency in the uranyl ion: A polarized x-ray spectroscopic study. *J. Chem. Phys.* **2002**, *117*, 8008-8020.
(69) Fillaux, C.; Den Auwer, C.; Guillaumont, D.; Shuh, D. K.; Tyliszczak, T. Investigation of actinide compounds by coupling X-ray absorption spectroscopy and quantum chemistry. *J. Alloys Compd.* **2007**, *444-445*, 443-446.
(70) Sergentu, D.-C.; Autschbach, J. Covalency in actinide(iv) hexachlorides in relation to the chlorine K-edge X-ray absorption structure. *Chem. Sci.* **2022**, *13*, 3194-3207.
(71) Govind, N.; de Jong, W. A. Simulating Cl K-edge X-ray absorption spectroscopy in MCl_6^{2-} (M = U, Np, Pu) complexes and $UOCl_5^-$ using time-dependent density functional theory. *Theor. Chem. Acc.* **2014**, *133*, 1463.
(72) Kasper, J. M.; Li, X.; Kozimor, S. A.; Batista, E. R.; Yang, P. Relativistic Effects in Modeling the Ligand K-Edge X-ray Absorption Near-Edge Structure of Uranium Complexes. *J. Chem. Theory Comput.* **2022**, *18*, 2171-2179.
(73) Sergentu, D.-C.; Autschbach, J. X-ray absorption spectra of f-element complexes: insight from relativistic multiconfigurational wavefunction theory. *Dalton Trans.* **2022**, *51*, 1754-1764.
(74) Ferrier, M. G.; Stein, Benjamin W.; Bone, S. E.; Cary, S. K.; Ditter, A. S.; Kozimor, S. A.; Lezama Pacheco, J. S.; Mocko, V.; Seidler, G. T. The coordination chemistry of Cm^{III}, Am^{III}, and Ac^{III} in nitrate solutions: an actinide L_3-edge EXAFS study. *Chem. Sci.* **2018**, *9*, 7078-7090.
(75) Ramanantoanina, H.; Kuri, G.; Martin, M.; Bertsch, J. Study of electronic structure in the L-edge spectroscopy of actinide materials: UO_2 as an example. *PCCP* **2019**, *21*, 7789-7801.
(76) Altman, A. B.; Pacold, J. I.; Wang, J.; Lukens, W. W.; Minasian, S. G. Evidence for 5d-σ and 5d-π covalency in lanthanide sesquioxides from oxygen K-edge X-ray absorption spectroscopy. *Dalton Trans.* **2016**, *45*, 9948-9961.
(77) Nitsche, H. Synchrotron X-ray absorption spectroscopy: a new tool for actinide and lanthanide speciation in solids and solution. *J. Alloys Compd.* **1995**, *223*, 274-279.

(78) Starks, D. F.; Parsons, T. C.; Streitwieser, A.; Edelstein, N. Bis(π-cyclooctatetraene)protactinium. *Inorg. Chem.* **1974**, *13*, 1307-1308.
(79) Karraker, D. G.; Stone, J. A.; Jones, E. R., Jr.; Edelstein, N. Bis(cyclooctatetraenyl)neptunium(IV) and bis(cyclooctatetraenyl)plutonium(IV). *J. Am. Chem. Soc.* **1970**, *92*, 4841-4845.
(80) Streitwieser, A., Jr.; Yoshida, N. Di-π-cyclooctatetraenethorium. *J. Am. Chem. Soc.* **1969**, *91*, 7528-7528.
(81) Streitwieser, A., Jr.; Mueller-Westerhoff, U. Bis(cyclooctatetraenyl)uranium (uranocene). A new class of sandwich complexes that utilize atomic f orbitals. *J. Am. Chem. Soc.* **1968**, *90*, 7364-7364.
(82) Rösch, N.; Streitwieser, A. SCF-Xα scattered-wave MO study of thorocene and uranocene. *J. Organomet. Chem.* **1978**, *145*, 195-200.
(83) Pyykkoe, P.; Lohr, L. L., Jr. Relativistically parameterized extended Hueckel calculations. 3. Structure and bonding for some compounds of uranium and other heavy elements. *Inorg. Chem.* **1981**, *20*, 1950-1959.
(84) Levanda, C.; Streitwieser, A., Jr. Synthesis and properties of substituted thorocenes. *Inorg. Chem.* **1981**, *20*, 656-659.
(85) Roesch, N.; Streitwieser, A., Jr. Quasirelativistic SCF-X α scattered-wave study of uranocene, thorocene, and cerocene. *J. Am. Chem. Soc.* **1983**, *105*, 7237-7240.
(86) Rösch, N. Comparison of non-relativistic and quasi-relativistic SCF-Xα scattered-wave calculations of uranocene, thorocene and cerocene. *Inorg. Chim. Acta* **1984**, *94*, 297-299.
(87) Chang, A. H. H.; Pitzer, R. M. Electronic structure and spectra of uranocene. *J. Am. Chem. Soc.* **1989**, *111*, 2500-2507.
(88) Dolg, M.; Fulde, P.; Stoll, H.; Preuss, H.; Chang, A.; Pitzer, R. M. Formally tetravalent cerium and thorium compounds: a configuration interaction study of cerocene $Ce(C_8H_8)_2$ and thorocene $Th(C_8H_8)_2$ using energy-adjusted quasirelativistic ab initio pseudopotentials. *Chem. Phys.* **1995**, *195*, 71-82.
(89) Seyferth, D. Uranocene. The First Member of a New Class of Organometallic Derivatives of the f Elements. *Organometallics* **2004**, *23*, 3562-3583.
(90) Kerridge, A. Oxidation state and covalency in f-element metallocenes (M = Ce, Th, Pu): a combined CASSCF and topological study. *Dalton Trans.* **2013**, *42*, 16428-16436.
(91) Kerridge, A. Quantification of f-element covalency through analysis of the electron density: insights from simulation. *Chem. Commun.* **2017**, *53*, 6685-6695.
(92) Rule, G. S.; Hitchens, T. K. *NMR spectroscopy*; Springer, 2006.
(93) Ramsey, N. F. Magnetic Shielding of Nuclei in Molecules. *Phys. Rev.* **1950**, *78*, 699-703.
(94) Marek, R. ^{15}N NMR Applications. In *Encyclopedia of Spectroscopy and Spectrometry (Second Edition)*, Lindon, J. C. Ed.; Academic Press, 2010; pp 1892-1898.
(95) Greif, A. H.; Hrobárik, P.; Autschbach, J.; Kaupp, M. Giant spin–orbit effects on ^{1}H and ^{13}C NMR shifts for uranium(VI) complexes revisited: role of the exchange–correlation response kernel, bonding analyses, and new predictions. *PCCP* **2016**, *18*, 30462-30474.
(96) Hrobárik, P.; Hrobáriková, V.; Greif, A. H.; Kaupp, M. Giant Spin-Orbit Effects on NMR Shifts in Diamagnetic Actinide Complexes: Guiding the Search of Uranium(VI) Hydride Complexes in the Correct Spectral Range. *Angew. Chem. Int. Ed.* **2012**, *51*, 10884-10888.
(97) Seaman, L. A.; Hrobárik, P.; Schettini, M. F.; Fortier, S.; Kaupp, M.; Hayton, T. W. A Rare Uranyl(VI)–Alkyl Ate Complex $[Li(DME)_{1.5}]_2[UO_2(CH_2SiMe_3)_4]$ and Its Comparison with a Homoleptic Uranium(VI)–Hexaalkyl. *Angew. Chem. Int. Ed.* **2013**, *52*, 3259-3263.

(98) Smiles, D. E.; Wu, G.; Hrobárik, P.; Hayton, T. W. Synthesis, Thermochemistry, Bonding, and ^{13}C NMR Chemical Shift Analysis of a Phosphorano-Stabilized Carbene of Thorium. *Organometallics* **2017**, *36*, 4519-4524.
(99) Rungthanaphatsophon, P.; Huang, P.; Walensky, J. R. Phosphorano-Stabilized Carbene Complexes with Short Thorium(IV)– and Uranium(IV)–Carbon Bonds. *Organometallics* **2018**, *37*, 1884-1891.
(100) Mullane, K. C.; Hrobárik, P.; Cheisson, T.; Manor, B. C.; Carroll, P. J.; Schelter, E. J. ^{13}C NMR Shifts as an Indicator of U–C Bond Covalency in Uranium(VI) Acetylide Complexes: An Experimental and Computational Study. *Inorg. Chem.* **2019**, *58*, 4152-4163.
(101) Panetti, G. B.; Sergentu, D.-C.; Gau, M. R.; Carroll, P. J.; Autschbach, J.; Walsh, P. J.; Schelter, E. J. Isolation and characterization of a covalent Ce^{IV}-Aryl complex with an anomalous ^{13}C chemical shift. *Nat. Commun.* **2021**, *12*, 1713.
(102) Kent, G. T.; Yu, X.; Wu, G.; Autschbach, J.; Hayton, T. W. Synthesis and electronic structure analysis of the actinide allenylidenes, $[\{(NR_2)_3\}An(CCCPh_2)]^-$ (An = U, Th; R = $SiMe_3$). *Chem. Sci.* **2021**, *12*, 14383-14388.
(103) Kent, G. T.; Yu, X.; Pauly, C.; Wu, G.; Autschbach, J.; Hayton, T. W. Synthesis of Parent Acetylide and Dicarbide Complexes of Thorium and Uranium and an Examination of Their Electronic Structures. *Inorg. Chem.* **2021**, *60*, 15413-15420.
(104) Ordoñez, O.; Yu, X.; Wu, G.; Autschbach, J.; Hayton, T. W. Synthesis and Characterization of Two Uranyl-Aryl "Ate" Complexes. *Chem. Eur. J.* **2021**, *27*, 5885-5889.
(105) Ordoñez, O.; Yu, X.; Wu, G.; Autschbach, J.; Hayton, T. W. Quantifying Actinide–Carbon Bond Covalency in a Uranyl–Aryl Complex Utilizing Solution ^{13}C NMR Spectroscopy. *Inorg. Chem.* **2023**.
(106) Ordoñez, O.; Yu, X.; Wu, G.; Autschbach, J.; Hayton, T. W. Homoleptic Perchlorophenyl "Ate" Complexes of Thorium(IV) and Uranium(IV). *Inorg. Chem.* **2021**, *60*, 12436-12444.
(107) Ordoñez, O.; Yu, X.; Wu, G.; Autschbach, J.; Hayton, T. W. Assessing the 4f Orbital Participation in the Ln–C Bonds of $[Li(THF)_4][Ln(C_6Cl_5)_4]$ (Ln = La, Ce). *Inorg. Chem.* **2022**, *61*, 15138-15143.
(108) Kent, G. T.; Yu, X.; Wu, G.; Autschbach, J.; Hayton, T. W. Ring-opening of a thorium cyclopropenyl complex generates a transient thorium-bound carbene. *Chem. Commun.* **2022**, *58*, 6805-6808.
(109) Staun, S. L.; Sergentu, D.-C.; Wu, G.; Autschbach, J.; Hayton, T. W. Use of ^{15}N NMR spectroscopy to probe covalency in a thorium nitride. *Chem. Sci.* **2019**, *10*, 6431-6436.
(110) Sergentu, D.-C.; Kent, G. T.; Staun, S. L.; Yu, X.; Cho, H.; Autschbach, J.; Hayton, T. W. Probing the Electronic Structure of a Thorium Nitride Complex by Solid-State ^{15}N NMR Spectroscopy. *Inorg. Chem.* **2020**, *59*, 10138-10145.
(111) Du, J.; Seed, J. A.; Berryman, V. E. J.; Kaltsoyannis, N.; Adams, R. W.; Lee, D.; Liddle, S. T. Exceptional uranium(VI)-nitride triple bond covalency from ^{15}N nuclear magnetic resonance spectroscopy and quantum chemical analysis. *Nat. Commun.* **2021**, *12*, 5649.
(112) DeVore, M. A., II; Klug, C. A.; Kriz, M. R.; Roy, L. E.; Wellons, M. S. Investigations of Uranyl Fluoride Sesquihydrate ($UO_2F_2 \cdot 1.57H_2O$): Combining ^{19}F Solid-State MAS NMR Spectroscopy and GIPAW Chemical Shift Calculations. *J. Phys. Chem. A* **2018**, *122*, 6873-6878.
(113) Gabuda, S. P.; Falaleeva, L. G.; Gagarinskii, Y. V. Dipolar Broadening of the NMR Spectrum of ^{19}F in UF_4. *Phys. Status Solidi B* **1969**, *33*, 435-438.

(114) Martel, L.; Capelli, E.; Body, M.; Klipfel, M.; Beneš, O.; Maksoud, L.; Raison, P. E.; Suard, E.; Visscher, L.; Bessada, C.; et al. Insight into the Crystalline Structure of ThF_4 with the Combined Use of Neutron Diffraction, ^{19}F Magic-Angle Spinning-NMR, and Density Functional Theory Calculations. *Inorg. Chem.* **2018**, *57*, 15350-15360.
(115) Capan, C.; Dempsey, R. J.; Sinkov, S.; McNamara, B. K.; Cho, H. Probing the Pu^{4+} magnetic moment in PuF_4 with ^{19}F NMR spectroscopy. *Phys. Rev. B* **2016**, *93*, 224409.
(116) Saielli, G.; Bini, R.; Bagno, A. Computational ^{19}F NMR. 1. General features. *Theor. Chem. Acc.* **2012**, *131*, 1140.
(117) Du, J.; Hurd, J.; Seed, J. A.; Balázs, G.; Scheer, M.; Adams, R. W.; Lee, D.; Liddle, S. T. ^{31}P Nuclear Magnetic Resonance Spectroscopy as a Probe of Thorium–Phosphorus Bond Covalency: Correlating Phosphorus Chemical Shift to Metal–Phosphorus Bond Order. *J. Am. Chem. Soc.* **2023**, *145*, 21766-21784.
(118) Réant, B. L. L.; Berryman, V. E. J.; Basford, A. R.; Nodaraki, L. E.; Wooles, A. J.; Tuna, F.; Kaltsoyannis, N.; Mills, D. P.; Liddle, S. T. ^{29}Si NMR Spectroscopy as a Probe of s- and f-Block Metal(II)–Silanide Bond Covalency. *J. Am. Chem. Soc.* **2021**, *143*, 9813-9824.
(119) Smiles, D. E.; Wu, G.; Hrobárik, P.; Hayton, T. W. Use of ^{77}Se and ^{125}Te NMR Spectroscopy to Probe Covalency of the Actinide-Chalcogen Bonding in $[Th(En)\{N(SiMe_3)_2\}_3]^-$ (E = Se, Te; n = 1, 2) and Their Oxo-Uranium(VI) Congeners. *J. Am. Chem. Soc.* **2016**, *138*, 814-825.
(120) Wu, W.; Rehe, D.; Hrobárik, P.; Kornienko, A. Y.; Emge, T. J.; Brennan, J. G. Molecular Thorium Compounds with Dichalcogenide Ligands: Synthesis, Structure, ^{77}Se NMR Study, and Thermolysis. *Inorg. Chem.* **2018**, *57*, 14821-14833.
(121) Kaupp, M. Chapter 9 - Relativistic Effects on NMR Chemical Shifts. In *Theor. Comp. Chem.*, Schwerdtfeger, P. Ed.; Vol. 14; Elsevier, 2004; pp 552-597.
(122) Vícha, J.; Novotný, J.; Komorovsky, S.; Straka, M.; Kaupp, M.; Marek, R. Relativistic Heavy-Neighbor-Atom Effects on NMR Shifts: Concepts and Trends Across the Periodic Table. *Chem. Rev.* **2020**, *120*, 7065-7103.
(123) Fortier, S.; Walensky, J. R.; Wu, G.; Hayton, T. W. High-Valent Uranium Alkyls: Evidence for the Formation of $U^{VI}(CH_2SiMe_3)_6$. *J. Am. Chem. Soc.* **2011**, *133*, 11732-11743.
(124) Gregson, M.; Lu, E.; McMaster, J.; Lewis, W.; Blake, A. J.; Liddle, S. T. A Cerium(IV)–Carbon Multiple Bond. *Angew. Chem. Int. Ed.* **2013**, *52*, 13016-13019.
(125) Gregson, M.; Lu, E.; Tuna, F.; McInnes, E. J. L.; Hennig, C.; Scheinost, A. C.; McMaster, J.; Lewis, W.; Blake, A. J.; Kerridge, A.; Liddle, S. T. Emergence of comparable covalency in isostructural cerium(IV)– and uranium(IV)–carbon multiple bonds. *Chem. Sci.* **2016**, *7*, 3286-3297.
(126) Gregson, M.; Lu, E.; Mills, D. P.; Tuna, F.; McInnes, E. J. L.; Hennig, C.; Scheinost, A. C.; McMaster, J.; Lewis, W.; Blake, A. J.; et al. The inverse-trans-influence in tetravalent lanthanide and actinide bis(carbene) complexes. *Nat. Commun.* **2017**, *8*, 14137.
(127) Baker, C. F.; Seed, J. A.; Adams, R. W.; Lee, D.; Liddle, S. T. $^{13}C_{carbene}$ nuclear magnetic resonance chemical shift analysis confirms Ce^{IV}=C double bonding in cerium(IV)–diphosphonioalkylidene complexes. *Chem. Sci.* **2024**, *15*, 238-249.
(128) Hertler, P. R.; Yu, X.; Brower, J. D.; Nguyen, T.-A. D.; Wu, G.; Autschbach, J.; Hayton, T. W. Exploring Spin-Orbit Effects in a $[Cu_6Tl]^+$ Nanocluster Featuring an Uncommon Tl−H Interaction. *Chem. Eur. J.* **2024**, *30*, e202400390.

(129) Nguyen, T. H.; Yu, X.; Kent, G. T.; Autschbach, J.; Hayton, T. W. U–C Bond Insertion, Ring-Opening, and C–H Activation in a Uranium Bis(diisopropylamino)cyclopropenylidene (BAC) Adduct. *Organometallics* **2023**, *42*, 1005-1012.
(130) Assefa, M. K.; Sergentu, D.-C.; Seaman, L. A.; Wu, G.; Autschbach, J.; Hayton, T. W. Synthesis, Characterization, and Electrochemistry of the Homoleptic f Element Ketimide Complexes $[Li]_2[M(N{=}CtBuPh)_6]$ (M = Ce, Th). *Inorg. Chem.* **2019**, *58*, 12654-12661.

Chapter 2. Synthesis and Characterization of two Uranyl-Aryl "Ate" Complexes

Portions of this work were published in:

Osvaldo Ordoñez, Xiaojuan Yu, Guang Wu, Jochen Autschbach, and Trevor W. Hayton, Synthesis and Characterization of two Uranyl-Aryl "Ate" Complexes. *Chem. Eur. J.* **2021**, 27, 5885–5889

Table of Contents

2.1 Introduction

There are only a handful of uranyl complexes that feature direct uranium-carbon bonds, despite UO_2^{2+} being the most studied fragment in uranium chemistry.[1-4] Remarkably, the first attempt to make an organometallic uranyl complex was over 150 years ago;[5, 6] however, the first structurally characterized uranyl hydrocarbyl complex was only reported by Sarsfield in 2002.[7] Earlier attempts to make uranyl organometallics often failed because of the reducing nature of many alkylating reagents. For example, reaction of $U^{VI}O_2Cl_2$ with 2 equiv of phenyllithium resulted in the formation of $U^{IV}O_2$ and biphenyl.[8, 9] Similarly, reaction of $U^{VI}O_2I_2(THF)_3$ with KCp resulted in reduction to afford the pentavalent uranyl(V) fragment.[10]

In spite of the abovementioned challenges, several strategies have been developed in the last two decades to facilitate the formation of uranyl organometallic complexes.[7, 11-24] For example, Sarsfield and co-workers stabilized the U-C bond in [(BIPMH)UO_2Cl(THF)] (**A**, BIPMH = $HC(PPh_2NSiMe_3)_2$) by utilizing a chelating bis(iminophosphorano)methanide ligand (Scheme 2.1).[7] This strategy was later used in the synthesis of the first uranyl carbene complex, [UO_2(SCS)$(py)_2$] (**B**, SCS = $[C(Ph_2PS)_2]^{2-}$),[21] as well as the first uranyl η^5-pyrrole complex, [Li(THF)][$UO_2(L^{\Delta})$Cl(THF)] (L^{Δ} = $[Me_8$-calix[4]pyrrole$]^{2-}$).[25] Another successful strategy involves formation of the uranyl fragment by oxygen atom transfer to a low-valent uranium cyclopentadienyl precursor.[13, 16] In addition, our research group has utilized "ate" complex formation to stabilize uranyl-carbon bonds by saturation of the uranium coordination sphere, as exemplified by [Li(MeIm)][(UO_2(Ar_2nacnac)$(C_4H_5N_2)_2$] (**C**)[24] and [$Li(DME)_{1.5}]_2[UO_2(CH_2SiMe_3)_4$] (**D**) (

).[23]

Scheme 2.1. Examples of uranyl complex with direct U-C σ bonds. MeIm = 1-methylimidazole, Ar = 2,6-$^{i}Pr_2C_6H_3$.

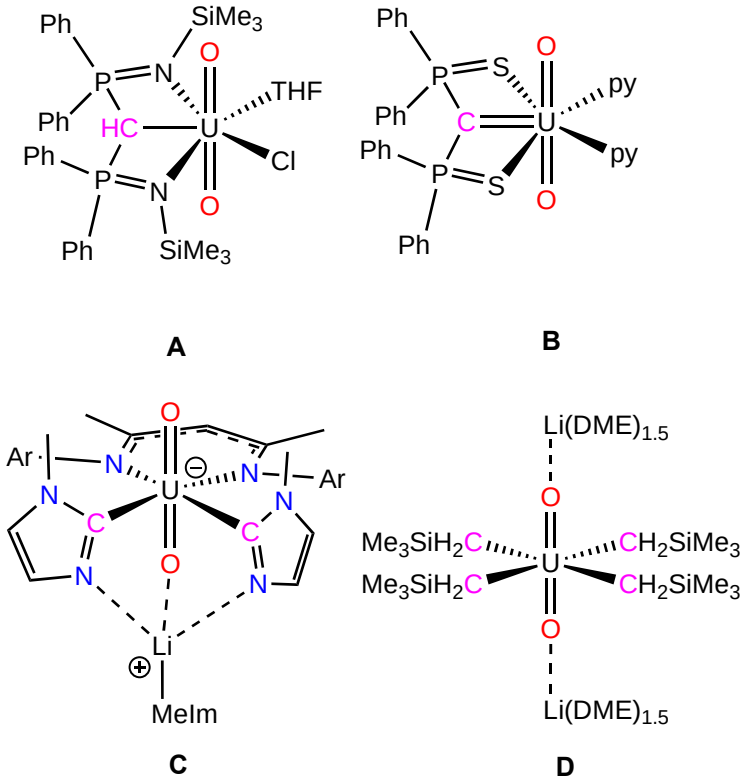

Recognizing that reduction of the uranium center was a major impediment to previous synthetic attempts, I attempted to ligate the percholorophenyl fragment, $[C_6Cl_5]^-$, to uranyl, because it is a much poorer reducing agent than most other alkylating agents, and thus should not as readily reduce the high-valent U^{6+} center in uranyl.[26] Homoleptic and heteroleptic perhalophenyl complexes are known for a wide variety of transition metals,[26-36] yet no reported perhalophenyl complexes are known for actinides, making this a potentially fruitful avenue of investigation. Herein, I describe the synthesis and characterization of the first structurally characterized uranyl aryl complexes, $[Li(Et_2O)_2(THF)][UO_2(C_6Cl_5)_3]$ ([Li][**2.1**]) and $[Li(THF)_4][UO_2(C_6Cl_5)_3(THF)]$ ([Li][**2.2**]). Additionally, analysis of their electronic

structures and ^{13}C NMR spectra by relativistic density functional theory (DFT) calculations, which revealed the degree of participation of the 5f subshell in the uranium-carbon bonds.

2.2 Results and Discussion

2.2.1 Synthesis and Characterization

The preparation of *in situ* generated LiC_6Cl_5 was done according to the literature procedure with slight modifications.[37] A slow addition of a cold (-25 °C) solution of 2.5 M *n*-BuLi in hexanes was added dropwise to a cold (-25 °C) colorless stirring suspension of C_6Cl_6 in Et_2O. Upon addition of *n*-BuLi, the colorless solids dissolved and immediate formation of a golden colored solution. It is important to note that the LiC_6Cl_5 generated *in situ* must be used immediately and extended reaction times lead to the formation of black tacky solids. Subsequent, addition of a cold (-25 °C) solution of 3 equiv of *in situ* generated LiC_6Cl_5[37] to a cold (-25 °C) suspension of $[UO_2Cl_2(THF)_3]$[38] in Et_2O results in immediate formation of an orange solution, concomitant with the deposition of a flocculent brown-orange precipitate. Work-up of this solution, followed by crystallization from Et_2O, affords $[Li(Et_2O)_2(THF)][UO_2(C_6Cl_5)_3]$ ([Li][**2.1**]), which can be isolated as orange plates in 74% yield (Scheme 2.2). Notably, fast addition of LiC_6Cl_5 to suspension of $[UO_2Cl_2(THF)_3]$ resulted in intractable dark brown reaction mixtures. Dissolution of complex [Li][**2.1**] in THF results in an immediate color change to dark amber. Crystallization of this solution affords $[Li(THF)_4][UO_2(C_6Cl_5)_3(THF)]$ ([Li][**2.2**]) as amber plates in 86% isolated yield (Scheme 2.2). Significantly, [Li][**2.1**] and [Li][**2.2**] are first structurally characterized uranyl aryl complexes and are rare examples of crystallographically-authenticated uranyl organometallics.

Both [Li][**2.1**] and [Li][**2.2**] are moisture-sensitive crystalline solids that are soluble in ethereal solvents and benzene, but are insoluble in hexanes. Additionally, both decompose upon dissolution in pyridine. Surprisingly, complex [Li][**2.1**] displays good thermal stability in benzene-d_6 over the course of 24 h, according to $^{13}C\{^1H\}$ NMR spectroscopy (Figure 2.18). In contrast, both [Li][**2.1**] and [Li][**2.2**] completely decompose in THF-d_8 over this time frame (Figure 2.19). Prolonged exposure of [Li][**2.1**] to vacuum also results in significant decomposition, as evidenced by the observation of pentachlorobenzene (C_6Cl_5H) resonances in its $^{13}C\{^1H\}$ spectrum (Figure S15).[39] I surmise that the good thermal stability of [Li][**2.1**] in benzene-d_6 is partly a consequence of poor reducing ability of the $[C_6Cl_5]^-$ ligand; however, the *o*-chloro substitution also likely imparts increased kinetic stabilization relative to non-chlorinated aryl ligands, which can undergo facile *ortho*-CH activation.[40, 41]

Scheme 2.2. Synthesis of $[Li(Et_2O)_2(THF)][UO_2(C_6Cl_5)_3]$ ([Li][**2.1**]) and $[Li(THF)_4][UO_2(C_6Cl_5)_3(THF)]$ ([Li][**2.2**]).

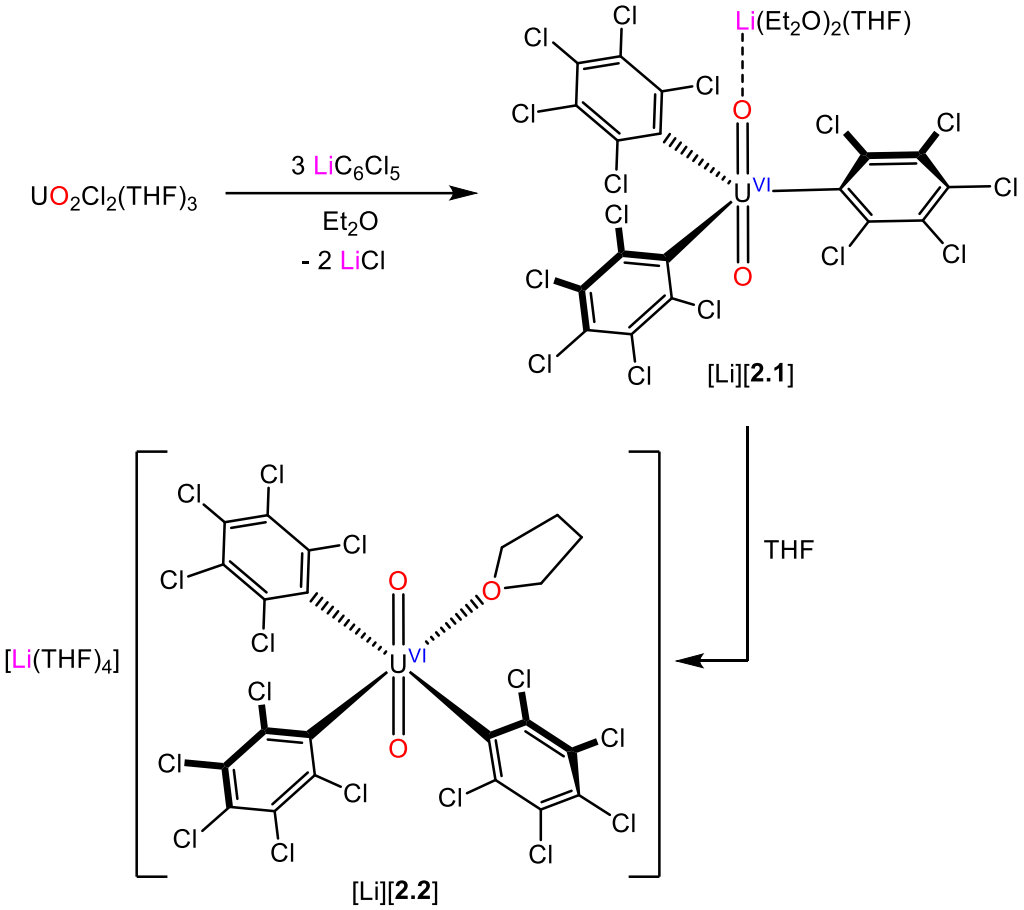

Both [Li][**2.1**] and [Li][**2.2**] (as the THF solvate, [Li][**2.2**]·THF) crystallize in the monoclinic space group $P2_1/n$ (Figure 2.1). The solid-state molecular structure of [Li][**2.1**] reveals a trigonal bipyramidal uranium center, coordinated by two oxygen atoms of the uranyl fragment and three carbon atoms of the pentachlorophenyl ligands. The solid-state molecular structure of [Li][**2.2**]·THF reveals a distorted octahedral uranium center, coordinated by two oxo ligands, three pentachlorophenyl ligands, and one THF ligand. Additionally, an $[Li(Et_2O)_2(THF)]^+$ cation is coordinated to a uranyl oxo ligand in complex [Li][**2.1**]. The O-U-O angles in [Li][**2.1**] (178.7(2)°) and [Li][**2.2**] (173.7(4)°) are typical of the uranyl

fragment.[1, 3] Likewise, the U-O_{yl} bond lengths in [Li][**2.1**] (U1-O1 = 1.750(5), U1-O2 = 1.779(5) Å) and [Li][**2.2**] (U1-O1 = 1.760(8), U1-O2 = 1.765(8) Å) are typical of uranyl(VI) U-O_{yl} distances (1.76-1.79 Å).[1, 3] Curiously, coordination of Li^+ to an oxo ligand in [Li][**2.1**] does not result in any perturbation of the U-O_{yl} bond length, as both U-O_{yl} distances are within error, in contrast to past examples of Lewis acid coordination.[23, 42-44] These data suggest the Li-O_{yl} interaction is relatively weak, a suggestion which is further supported by the Li-O_{yl} bond length (2.043(15) Å), which is longer than typical Li-O_{yl} interactions (1.87(1) Å - 1.94(1) Å).[1, 23, 24, 43, 45] The U-C bond lengths in [Li][**2.1**] (range = 2.471(8) – 2.489(8) Å) are similar to those of other σ-bonded uranium-hydrocarbyl complexes. For example, the U-C distances in **C** are 2.498(6) Å and 2.499(7) Å, whereas those in **D** range from 2.497(6) to 2.481(6) Å.[15, 23, 24] In contrast, the U-C distances in **2.2** (range = 2.552(11) – 2.627(12) Å) are somewhat longer, reflecting its higher coordination number. Finally, the U-C_{ipso}-C_{ortho} angles in [Li][**2.1**] and [Li][**2.2**] show minimal deviation from 120°, excluding the possibility of Cl→U dative interactions in the solid-state.

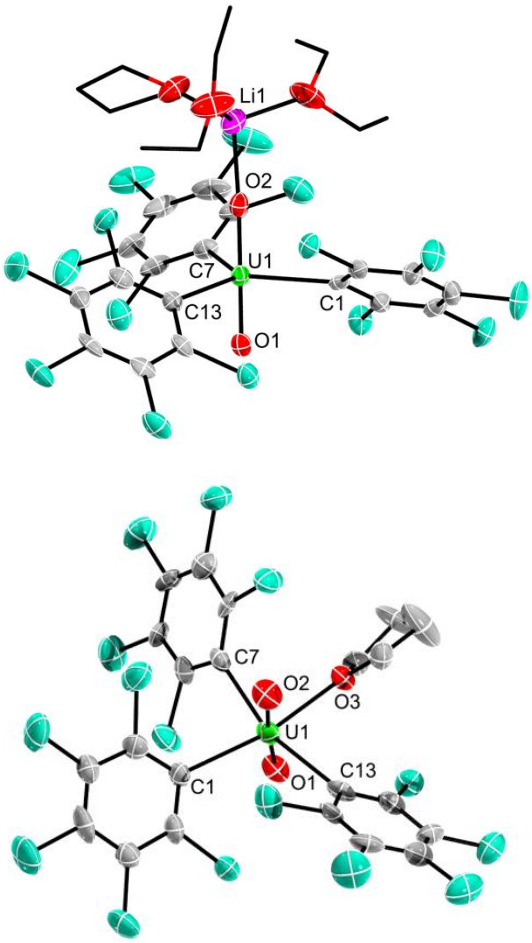

Figure 2.1. Solid-state molecular structure of [Li][**2.1**] (top) and [Li][**2.2**]·THF (bottom) shown with 50% probability ellipsoids. All hydrogen atoms, solvate molecules, and a [Li(THF)4]+ counterion have been omitted for clarity. Selected bond lengths (Å) and angles (°) for 2.1: U1-O1 = 1.750(5), U1-O2 = 1.779(5), U1-C1 = 2.484(7), U1-C7 = 2.471(8), U1-C13 = 2.489(8), O2-Li1 = 2.043(15), O1-U1-O2 = 178.7(2), C1-U1-C7 = 123.5(3), C7-U1-C13 = 119.0(3), C13-U1-C1 = 117.4(2). 2.1·THF: U1-O1 = 1.760(8), U1-O2 = 1.765(8), U1-O3 = 2.424(7), U1-C1 = 2.627(12), U1-C13 = 2.563(12), U1-C7 = 2.552(11), O1-U1-O2 = 173.7(4), C1-U1-C7 = 91.2(4), C7-U1-C13 = 106.6(4), C13-U1-O3 = 83.6(3), O3-U1-C1 = 78.7(3).

The $^{13}C\{^{1}H\}$ NMR spectrum of [Li][**2.1**] in benzene-d_6 features a resonance at 236.7 ppm (Figure 2.2), attributable to the *ipso* carbon of the pentachlorophenyl ligand, as well as resonances at 138.0, 134.2, and 132.4 ppm, assignable to the *ortho*, *meta*, and *para* resonances of the pentachlorophenyl ligand, respectively. Its $^{7}Li\{^{1}H\}$ NMR spectrum in benzene-d_6 features a sharp resonance at –3.34 ppm (Figure 2.6). The $^{13}C\{^{1}H\}$ NMR spectrum of [Li][**2.2**] in THF-d_8 features a resonance at 239.4 ppm (Figure 2.13), attributable to the *ipso* carbon of the pentachlorophenyl ligand, as well as resonances at 139.4, 133.6, and 130.5 ppm, assignable to the *ortho*, *meta*, and *para* carbons of the pentachlorophenyl ligand, respectively. The observation of only one aryl environment in this spectrum is evidence of reversible THF binding at a faster rate that the NMR time scale. Its $^{7}Li\{^{1}H\}$ NMR spectrum in THF-d_8 features a sharp resonance at –0.87 ppm (Figure 2.12). Curiously, the $^{13}C\{^{1}H\}$ NMR spectrum of [Li][**2.2**] in benzene-d_6 is nearly identical to that of [Li][**2.1**] in benzene-d_6, which is suggestive of dissociation of THF and reformation of [Li][**2.1**] in this solvent. Not surprisingly, the $^{13}C\{^{1}H\}$ NMR spectrum of [Li][**2.1**] in THF-d_8 features a similar C_{ispo} chemical shift as that of [Li][**2.2**] in the same solvent.

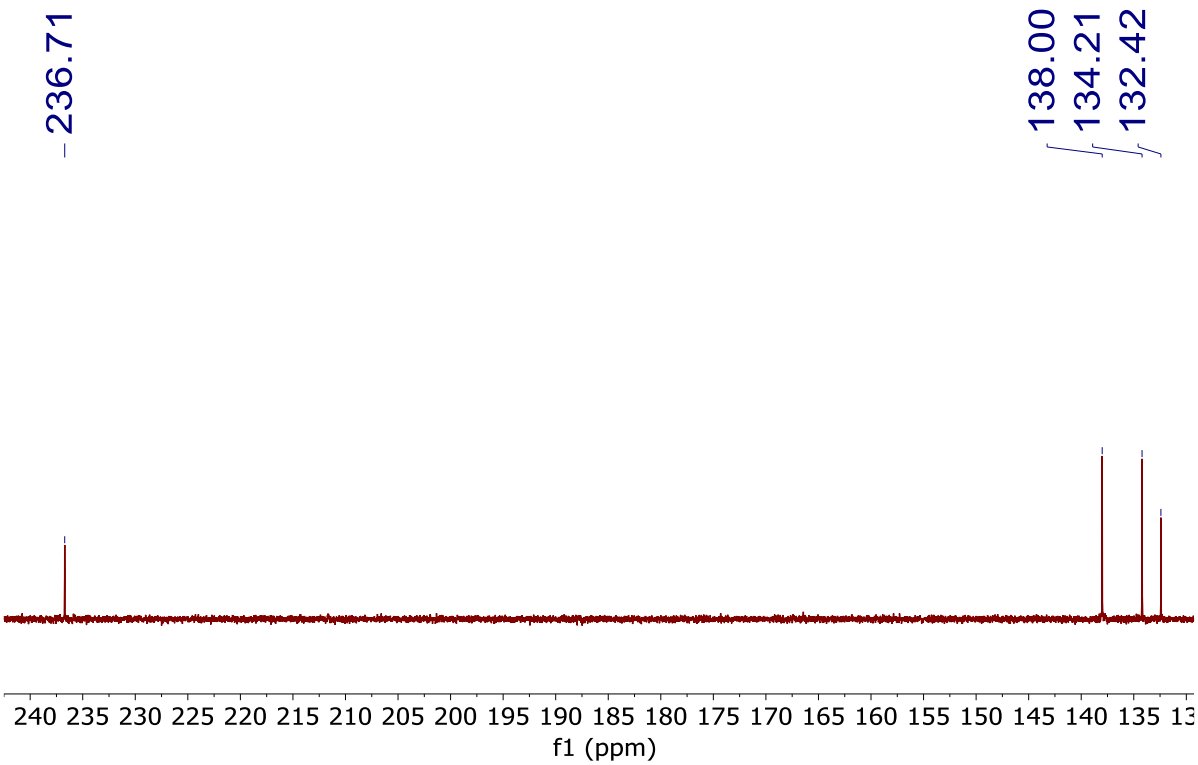

Figure 2.2. $^{13}C\{^{1}H\}$ NMR spectrum of [Li][**2.1**] in benzene-d_6.

Addition of a cold (-25 °C) solution of 3 equiv of LiC_6Cl_5[37] to a cold (-25 °C) suspension of yellow suspension of ^{18}O-labelled $[UO_2Cl_2(THF)_3]$[46] in Et_2O results in an immediate color change to bright orange, concomitant with the deposition of a flocculent brown precipitate. After 5 min of stirring at room temperature, work-up of this solution, followed by crystallization from Et_2O, affords $[Li(Et_2O)_2(THF)][U^{18}O_2(C_6Cl_5)_3]$ ([Li][**2.1-^{18}O**]), which can be isolated as orange plates in 73 % yield (Scheme 2.3). Dissolution of complex [Li][**2.1-^{18}O**] in THF results in an immediate color change to dark amber. Work-up of this solution, followed by crystallization from THF affords $[Li(THF)_4][U^{18}O_2(C_6Cl_5)_3(THF)]$ ([Li][**2.2-^{18}O**]) as amber plates in 65% isolated yield.

Scheme 2.3. Synthesis of [Li][**2.1-^{18}O**] and [Li][**2.2-^{18}O**].

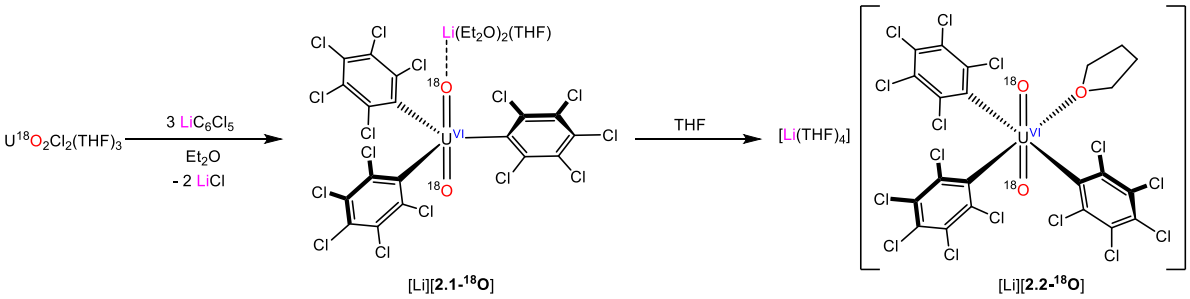

I also characterized [Li][**2.1**] and [Li][**2.2**] along with their ^{18}O-labelled analogues, [Li][**2.1-^{18}O**] and [Li][**2.2-^{18}O**], by IR and Raman spectroscopies. Unfortunately, the U=O ν_{asym} modes for neither [Li][**2.1**] nor [Li][**2.2**] could be identified in their IR spectra, even with the assistance of isotopic labelling, likely because these modes are buried under ligand vibrations. However, the Raman spectrum of [Li][**2.1**] exhibits a strong absorption at 834 cm^{-1}, which I have assigned to the U=O ν_{sym} mode. This vibration redshifts to 787 cm^{-1} in the Raman spectrum of [Li][**2.1-^{18}O**] (Figure 2.3). The magnitude of this shift (48 cm^{-1}) is similar to those observed previously upon ^{18}O labelling,[15] further confirming our assignment. I also attempted to record Raman spectra for [Li][**2.2**] and [Li][**2.2-^{18}O**] but were thwarted by sample decomposition. The ν_{sym} value for [Li][**2.1**] is comparable to those measured for other uranyl organometallics.[47] For example, the U=O ν_{sym} modes for [$UO_2Cl(\kappa^3$-$E(Ph_2PNSiMe_3)_2)(THF)$] are 829 cm^{-1} (E = N) and 825 cm^{-1} (E = CH), respectively,[20, 47] suggesting that the three equatorial ligand sets have comparable donor abilities.

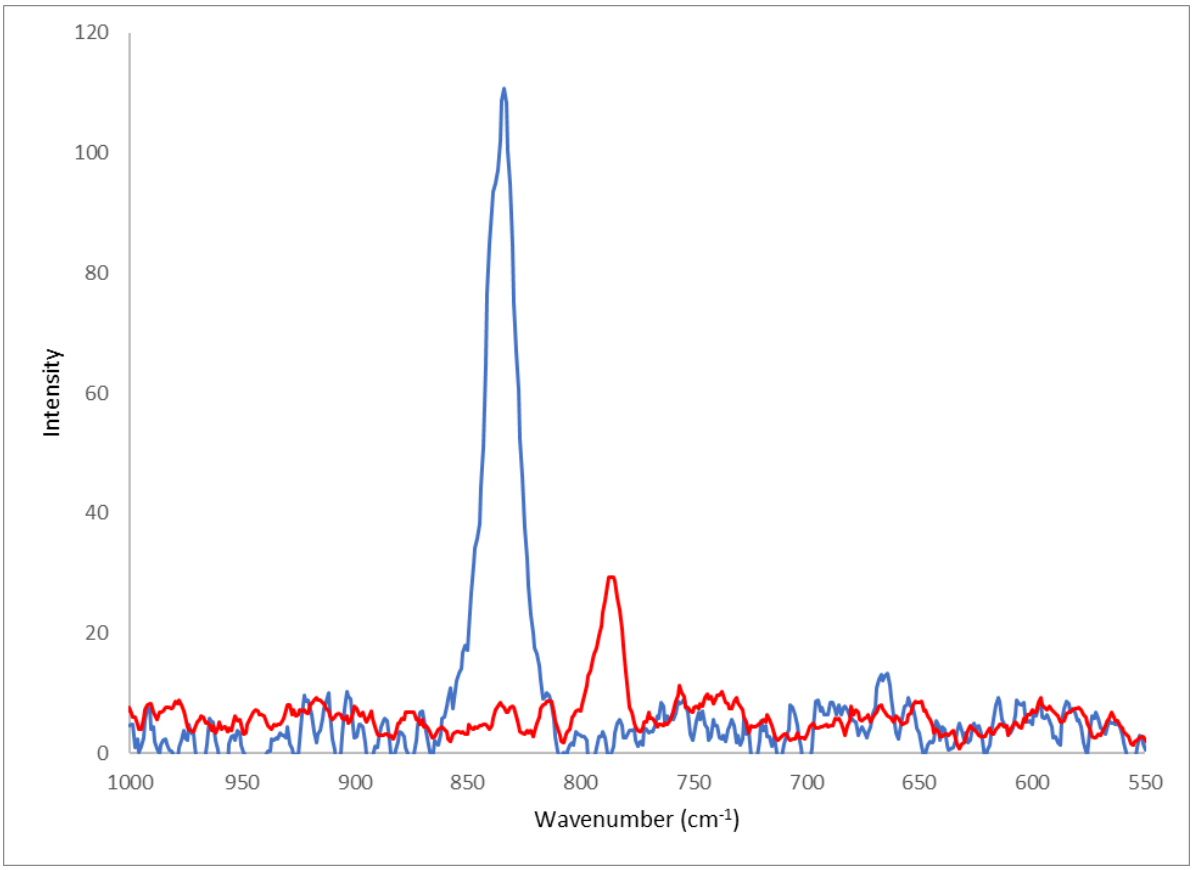

Figure 2.3. Overlay of partial Raman spectra of [Li][**2.1**-^{18}**O**] (red) and [Li][**2.1**] (blue).

2.2.2 Computational Analysis

To gain a detailed understanding of the electronic structure and chemical bonding in [Li][**2.1**] and [Li][**2.2**], Dr. Xiaojuan Yu and Prof. Jochen Autschbach at the State University of New York at Buffalo carried out relativistic DFT calculations on the anionic components of these compounds, [**2.1**]$^-$ and [**2.2**]$^-$ respectively. Complete computational details for these calculations are given in the 2.4.8 Computational Data Details. For both complexes, the optimized average U-O and U-C_{ispo} distances are within 0.04 Å and 0.02 Å, respectively, of those measured in the solid state. This good agreement indicates that the optimized structures are reliable, especially with regard to the U-C_{ispo} distance. According to NLMO (natural

localized molecular orbital) analyses (Figure 2.4 and Table 2.2), [**2.1**]$^-$ and [**2.2**]$^-$ display very similar characteristics for the U-C_{ipso} interactions, which are represented by two-center two-electron σ(U-C_{ispo}) bonds ranging from 22 to 20% uranium character and Wiberg bond orders of 0.67 and 0.60, respectively. The U 5f contributions in these 2c-2e orbitals range from 28% in [**2.1**]$^-$ to 42% in [**2.2**]$^-$, whereas the 6d contributions are larger, ranging from 59% in [**2.1**]$^-$ to 46% in [**2.2**]$^-$. Not surprisingly, the covalent character of the U-O(THF) interaction in [**2.2**]$^-$ is much lower, with minor σ and π contributions via donation bonding and a Wiberg bond order of 0.39. For comparison, the uranyl alkyl complex, $[Li(DME)_{1.5}]_2[UO_2(CH_2SiMe_3)_4]$ (**D**), features similar %U character in its U-C bonds (22%), but greater 5f character and lower 6d character (53% 5f vs. 34% 6d).[23]

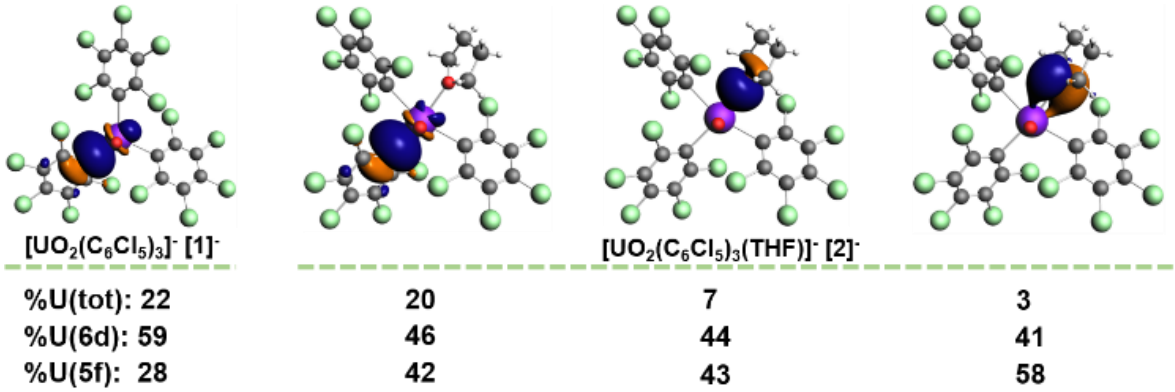

Figure 2.4. Representative U-L bonding NLMOs in [**2.1**]$^-$ and [**2.2**]$^-$. Weight-% metal character and 6d vs. 5f contribution at the metal averaged over equivalent NLMOs. (Isosurface values ±0.03 a.u. Color code for atoms: U purple, O red, Cl seafoam green, C dark gray.)

The ^{13}C NMR chemical shifts for both complexes were calculated without and with effects from SO coupling,[48, 49] using a PBE-based hybrid with 40% (and 25%, see 2.4.8 Computational Data Details) exact exchange. This type of calculation has previously provided

accurate ^{13}C NMR shifts in actinide compounds.[23, 50-52] The averaged calculated C_{ipso} chemical shift for [**2.1**]$^-$ is 242 ppm, in good agreement with the measured value (237 ppm) given that the calculations necessarily use approximations. SO coupling is responsible for a 62 ppm downfield contribution in this shift, due to the involvement of the 5f (and 6d) subshells in the U-C_{ipso} bonds. For [**2.2**]$^-$, the calculated chemical shift of the C_{ipso} environment *trans* to THF is 246 ppm, including 68 ppm due to SO effects, whereas the calculated average chemical shift of the C_{ipso} environments *cis* to THF is 261 ppm. Per the bonding breakdown in Figure 2, there is a cancellation of opposite trends due to the added U-O(THF) interaction in [**2.2**]$^-$: The overall uranium weight in σ(U-C_{ispo}) is slightly lower for the *trans* C_{ipso} environment, but the 5f percentage is higher. The latter is likely responsible for the larger SO shift observed for this environment vs. the SO shift observed for [**2.1**]$^-$. For comparison, the SO contribution to the ^{13}C chemical shift in **D** was calculated to be much larger (177 ppm),[23] which can be rationalized by the larger 5f contribution to its U-C bonds vs. those found for [**2.1**]$^-$ and [**2.2**]$^-$. Significantly, this comparison nicely showcases the exquisite sensitivity of ^{13}C chemical shifts to the 5f participation in An-C bonding.[23, 50, 53, 54]

2.3 Summary

In summary, I prepared and characterized the first structurally-authenticated uranyl-aryl complexes, $[Li(Et_2O)_2(THF)][UO_2(C_6Cl_5)_3]$ ([Li][**2.1**]) and $[Li(THF)_4][UO_2(C_6Cl_5)_3(THF)]$ ([Li][**2.2**]), and have confirmed their formulations by X-ray crystallography. A combined ^{13}C NMR spectroscopic and DFT computational analysis reveals that the U-C bonds in [Li][**2.1**] and [Li][**2.2**] feature appreciable amounts of covalency with high levels of 5f participation. Moreover, complex [Li][**2.2**] exhibits good thermal stability in arene solvents, which I believe is a function of the poor reducing ability of the $[C_6Cl_5]^-$ ligand, coupled with the *o*-chloro

substitution. The surprisingly good thermal stability suggests that perhalogenated aryl ligands could be broadly useful for the generation of stable actinide aryl complexes, a class of materials that offers many insights into actinide electronic structure and provides excellent benchmarking opportunity for high level quantum chemical calculations.[54, 55]

2.4 Experimental

2.4.1 General Procedures

General. All reactions and subsequent manipulations were performed under anaerobic and anhydrous conditions under an atmosphere of dinitrogen. Hexanes, diethyl ether (Et_2O), and toluene were dried using a Vacuum Atmospheres DRI-SOLV Solvent Purification system and stored over 3Å sieves for 24 h prior to use. Tetrahydrofuran (THF) was distilled over Na/benzophenone and stored over activated 3 Å molecular sieves for 24 h prior to use. Benzene-d_6 and thf-d_8 were dried over 3Å molecular sieves for 24 h prior to use. LiC_6Cl_5,[37] $[UO_2Cl_2(THF)_3]$,[38] and ^{18}O-labelled $[UO_2Cl_2(THF)_3]$[46] were synthesized according to the previously reported procedures. All other reagents were purchased from commercial suppliers and used as received.

^{1}H, ^{13}C{^{1}H}, and ^{7}Li{^{1}H} NMR spectra were recorded on an Agilent Technologies 400-MR DD2 400 MHz spectrometer or a Bruker AVANCE NEO 500 MHz spectrometer. ^{1}H and ^{13}C{^{1}H} NMR spectra were referenced to external tetramethylsilane (TMS) using the residual protio solvent peaks as internal standards. ^{7}Li{^{1}H} NMR spectra are referenced indirectly with the ^{1}H chemical shift of TMS at 0 ppm, according to IUPAC standard.[56, 57] IR spectra were recorded on a Nicolet 6700 FT-IR spectrometer. Raman spectra were recorded on a JY Horiba Labram-Aramis Raman microscope with a 633 nm laser. The sample was placed on a glass microscope slide and enclosed with a coverslip that was held in place by a bead of silicone

grease. Elemental analyses were performed by the Microanalytical Laboratory at the University of California (Berkeley, CA).

2.4.2 Synthesis of [LiC_6Cl_6]

The synthesis of LiC_6Cl_5 was done according to the literature procedure with slight modifications.[37] A cold solution (–25 °C) of 2.5 M *n*-BuLi in hexanes (0.2 mL, 0.50 mmol) was added dropwise to a cold, stirring suspension (–25 °C) of C_6Cl_6 (142.4 mg, 0.50 mmol) in Et_2O (2 mL). Upon addition of *n*-BuLi, the solids dissolved and solution became a golden color. The resulting LiC_6Cl_5 solution was used as is, and assumed to be 0.25 M. The $^7Li\{^1H\}$ NMR spectrum of LiC_6Cl_5 in benzene-d_6 displays a single resonance at 0.89 ppm.

2.4.3 Synthesis of [$Li(Et_2O)_2(THF)$][$UO_2(C_6Cl_5)_3$] ([Li][2.1])

A cold (-25 °C) solution of LiC_6Cl_5 (2 mL in Et_2O, 0.50 mmol, 0.25 M) was added to a cold (-25 °C), yellow suspension of [$UO_2Cl_2(THF)_3$] (93 mg, 0.17 mmol) in Et_2O (2 mL). This resulted in an immediate color change to bright orange concomitant with the deposition of a flocculent brown-orange precipitate. After 5 min, the reaction mixture was filtered through a Celite column (0.5 cm × 5 cm) supported on glass wool to afford a clear, orange filtrate. The volume of the filtrate was reduced to 2 mL *in vacuo*, hexanes (5 mL) was layered onto the solution, and the sample was stored at –25 °C for 24 h, which resulted in the deposition of orange plates. The solid was isolated by decanting the supernatant and then dried *in vacuo* (153 mg, 74 % yield). Anal. Calcd for $C_{30}H_{28}LiO_5Cl_{15}U$: C, 28.93; H, 2.27. Found: C, 28.55; H, 2.07. ^1H NMR (500 MHz, 25 °C, benzene-d_6): δ 3.13 (br m, 8H, OCH_2CH_3), 2.85 (br s, 4H, OCH_2CH_2), 1.02 (br s, 4H, OCH_2CH_2), 0.95 (br t, 12H, OCH_2CH_3). ^1H NMR (500 MHz, 25 °C, THF-d_8): δ 3.62 (br m, 4H, OCH_2CH_2), 3.38 (q, 8H, OCH_2CH_3), 1.77 (br

m, 4H, OCH_2CH_2), 1.11 (br t, 12H, OCH_2CH_3). $^{13}C\{^1H\}$ NMR (500 MHz, 25 °C, benzene-d_6): δ 236.71 (*i*-C), 138.00 (*o*-C), 134.21 (*m*-C), 132.42 (*p*-C), 68.05 (OCH_2CH_2), 65.63 (OCH_2CH_3), 25.05 (OCH_2CH_2), 15.05 (OCH_2CH_3). $^{13}C\{^1H\}$ NMR (500 MHz, 25 °C, THF-d_8): δ 239.35 (*i*-C), 139.39 (*o*-C), 133.62 (*m*-C), 130.48 (*p*-C). $^{7}Li\{^1H\}$ NMR (400 MHz, 25 °C, benzene-d_6): δ -3.34 (s). $^{7}Li\{^1H\}$ NMR (400 MHz, 25 °C, THF-d_8): δ -0.47 (br s). IR (KBr pellet, cm^{-1}): 1729 (w), 1637 (w), 1556 (w), 1544 (w), 1523 (m), 1508 (w), 1458 (w), 1444 (w), 1421 (vw), 1396 (s), 1334 (s), 1313 (m), 1284 (m), 1261 (w), 1226 (m), 1184 (w), 1170 (s), 1141 (w), 1112 (w), 1087 (m), 1062 (m), 1043 (m), 1002 (w), 923 (m), 891 (w), 865 (m), 823 (s), 796 (w), 782 (w), 702 (w), 684 (m), 663 (w) 580 (vw), 563 (w), 526 (w), 459 (w), 418 (w), 408 (w). Raman (cm^{-1}): 834 (s).

2.4.4 Synthesis of $[Li(THF)_4][UO_2(C_6Cl_5)_3(THF)]$ ([Li][2.1])

Method A: Dissolution of [Li][**2.1**] (173 mg, 0.14 mmol) in THF (2 mL) resulted in an immediate color change to a dark amber. The amber solution was filtered through a Celite column (0.5 cm × 5 cm) supported on glass wool, affording a clear, dark amber filtrate. The volume of the filtrate was reduced to 2 mL *in vacuo*, hexanes (5 mL) was layered onto the solution, and the sample was stored at –25 °C for 24 h, which resulted in the deposition of amber plates. The solid was isolated by decanting the supernatant and then dried briefly *in vacuo* (166 mg, 86 % yield). Anal. Calcd for $C_{38}H_{40}LiO_7Cl_{15}U$: C, 32.94; H, 2.91 Found: C, 31.51; H, 2.45. ^1H NMR (500 MHz, 25 °C, benzene-d_6): δ 3.44 (br s, 20H, OCH_2CH_2), (1.35 (br s, 20H, OCH_2CH_2). ^1H NMR (500 MHz, 25 °C, THF-d_8): δ 3.62 (br m, 20H, OCH_2CH_2), 1.78 (br m, 20H, OCH_2CH_2). $^{13}C\{^1H\}$ NMR (500 MHz, 25 °C, benzene-d_6): δ 235.89 (*i*-C), 138.23 (*o*-C), 134.04 (*m*-C), 132.20 (*p*-C), 67.85 (OCH_2CH_2), 25.68 (OCH_2CH_2). $^{13}C\{^1H\}$ NMR (500 MHz, 25 °C, THF-d_8): δ 239.42 (*i*-C), 139.39 (*o*-C), 133.62 (*m*-C), 130.49 (*p*-C),

68.39 (O*C*$H_2$$CH_2$), 27.31 (OCH$_2$*C*H$_2$). ^{7}Li{^{1}H} NMR (400 MHz, 25 °C, benzene-*d*$_6$): δ -3.57 (s). ^{7}Li{^{1}H} NMR (400 MHz, 25 °C, THF-*d*$_8$): δ -0.87 (br s). IR (KBr pellet, cm^{-1}): 1729 (w), 1637 (w), 1556 (w), 1544 (w), 1523 (w), 1508 (w), 1500 (w), 1459 (w), 1448 (w), 1421 (vw), 1398 (s), 1334 (s), 1311 (m), 1284 (m), 1226 (w), 1170 (s), 1139 (w), 1122 (vw), 1106 (vw), 1087 (m), 1060 (m), 1043 (s), 1018 (w), 948 (vw), 931 (s), 887 (w), 865 (w), 821 (m), 777 (vw), 701 (w), 684 (s), 661 (s), 576 (vw), 563 (w), 526 (w).

Method B: A cold (-25 °C) solution of LiC_6Cl_5 (2 mL in Et_2O, 0.50 mmol, 0.25 M) was added to a cold (-25 °C), stirring, yellow suspension of $[UO_2Cl_2(THF)_2]_2$ (81 mg, 0.17 mmol) in Et_2O (2 mL). This resulted in an immediate color change to bright orange, concomitant with the deposition of a flocculent brown-orange precipitate. After 5 min of stirring, the reaction mixture was filtered through a Celite column (0.5 cm × 5 cm) supported on glass wool to afford a clear, orange filtrate. The volatiles were removed *in vacuo* and the resulting orange oil was extracted into THF (2 mL) to generate a dark amber solution, which was filtered through a Celite column (0.5 cm × 5 cm) supported on glass wool. Hexanes (5 mL) was layered onto the clear amber filtrate, and the sample was stored at –25 °C for 24 h, which resulted in the deposition of amber plates. The solid was isolated by decanting the supernatant and then dried briefly *in vacuo* (118 mg, 51% yield).

2.4.5 Synthesis of [Li(Et$_2$O)$_2$(THF)][U^{18}O$_2$(C$_6$Cl$_5$)$_3$] ([Li][2.1-^{18}O])

A cold (-25 °C) solution of LiC_6Cl_5 (2 mL in Et_2O, 0.50 mmol, 2.5 M) was added to a cold (-25 °C), stirring yellow suspension of ^{18}O-labelled $[UO_2Cl_2(THF)_3]$ (94 mg, 0.17 mmol) in Et_2O (2 mL). This resulted in an immediate color change to bright orange, concomitant with the deposition of a flocculent brown precipitate. After 5 min of stirring, the reaction mixture was filtered through a Celite column (0.5 cm × 5 cm) supported on glass wool to afford a

clear, orange filtrate. The volume of the filtrate was reduced to 2 mL *in vacuo*, hexanes (5 mL) was layered onto the solution, and the sample was stored at –25 °C for 24 h, which resulted in the deposition of orange plates. The solid was isolated by decanting the supernatant and then dried *in vacuo* (152 mg, 73 % yield). IR (KBr pellet, cm^{-1}): 1729 (w), 1637 (w), 1556 (w), 1540 (w), 1523 (m), 1508 (s), 1459 (m), 1446 (m), 1421 (vw), 1398 (s), 1334 (m), 1313 (m), 1286 (m), 1261 (m), 1228 (m), 1184 (m), 1170 (s), 1141 (m), 1112 (w), 1089 (m), 1061 (m), 1039 (m), 1005 (m), 973 (vw), 946 (vw), 914 (s), 887 (m), 874 (m), 837 (vw), 825 (m), 783 (m), 700 (w), 684 (s), 661 (s), 594 (vw), 580 (vw), 563 (w), 526 (w), 472 (vw), 445 (w), 428 (w), 420 (w), 408 (w). Raman (cm^{-1}): 787 (w).

2.4.6 Synthesis of $[Li(THF)_4][U^{18}O_2(C_6Cl_5)_3(THF)]$ ([Li][2.2-^{18}O])

Dissolution of complex [Li][**2.1-^{18}O**] (58 mg, 0.05 mmol) in THF (1 mL) resulted in an immediate color change to amber. The amber solution was filtered through a Celite column (0.5 cm × 5 cm) supported on glass wool to afford a clear, amber filtrate. The volume of the filtrate was reduced to 1 mL *in vacuo*, hexanes (4 mL) was layered onto the solution, and the sample was stored at –25 °C for 24 h, which resulted in the deposition of amber plates. The solid was isolated by decanting the supernatant and then dried briefly *in vacuo* (42 mg, 65% yield). IR (KBr pellet, cm^{-1}): 1729 (w), 1637 (w), 1556 (w), 1544 (w), 1523 (w), 1500 (w), 1459 (w), 1448 (w), 1421 (vw), 1396 (s), 1334 (s), 1311 (s), 1284 (s), 1226 (w), 1170 (m), 1138 (w), 1122 (vw), 1105 (vw), 1087 (m), 1052 (s), 1043 (s), 1018 (m), 914 (m), 887 (s), 866 (s), 821 (s), 700 (w), 685 (s), 661 (s), 576 (vw), 563 (w), 526 (w).

2.4.7 X-Ray Crystallography

Data for all complexes were collected on a Bruker KAPPA APEX II diffractometer equipped with an APEX II CCD detector using a TRIUMPH monochromator with a Mo Kα X-ray source (α = 0.71073 Å). The crystals were mounted on a cryoloop under Paratone-N oil, and all data were collected at 100(2) K using an Oxford nitrogen gas cryostream. Data were collected using ω scans with 0.5° frame widths. Frame exposures of 10 seconds were used for both [Li][**2.1**] and [Li][**2.2**]·THF. Data collection and cell parameter determination were conducted using the SMART program.[58] Integration of the data frames and final cell parameter refinement were performed using SAINT software.[59] Absorption correction of the data was carried out using the multi-scan method SADABS.[60] Subsequent calculations were carried out using SHELXTL.[61] Structure determination was done using direct or Patterson methods and difference Fourier techniques. All hydrogen atom positions were idealized and rode on the atom of attachment. Structure solution and refinement were performed using SHELXTL.[61] Graphics, and creation of publication materials were performed using Diamond.[62]

For complex [Li][**2.1**], carbon atoms of one Et_2O solvate exhibited positional disorder, which was addressed by constraining the affected atoms with SADI and EADP commands. The carbon atoms of the disordered Et_2O ligand were refined isotropically. Further crystallographic details of complexes [Li][**2.1**] and [Li][**2.2**]·THF can be found in Tables S3. Complexes [Li][**2.1**] and [Li][**2.2**]·THF have been deposited in the Cambridge Structural Database ([Li][**2.1**]: CCDC 2042503; [Li][**2.2**]·THF: CCDC 2042504).

Table 2.1. X-ray crystallographic data for complexes [Li][**2.1**] and [Li][**2.2**]·THF.

	[Li][**2.1**]	[Li][**2.2**]·THF
Formula	$C_{30}H_{28}LiO_5Cl_{15}U$	$C_{42}H_{48}LiO_8Cl_{15}U$
Crystal Habit, Color	Plate, Orange	Plate, Amber
Crystal Size (mm)	0.2 × 0.1 × 0.05	0.2 × 0.1 × 0.05
MW (g/mol)	1245.24	1457.52
crystal system	Monoclinic	Monoclinic
space group	$P2_1/n$	$P2_1/n$
a (Å)	11.067(3)	12.484(5)
b (Å)	24.272(7)	22.571(8)
c (Å)	16.186(4)	19.556(7)
α (°)	90.00	90.00
β (°)	99.773(5)	104.162(8)
γ (°)	90.00	90.00
V (Å^3)	4285(2)	5343(3)
Z	4	4
T (K)	118(2)	110(2)
λ (Å)	0.71073	0.71073
GOF	1.015	0.912
Density (calcd) (Mg/m^3)	1.930	1.812
Absorption coefficient (mm^{-1})	4.761	3.836
F_{000}	2392	2856
Total no Reflections	7231	10627
Unique Reflections	7231	10627
Final R indices*	R_1 = 0.0436 wR_2 = 0.1064	R_1 = 0.0708 wR_2 = 0.1812
Largest Diff. peak and hole (e$^-$ A^{-3})	1.330, -0.981	1.541, -0.992

*For [I>2σ(I)]

2.4.8 Computational Data Details

Geometries were fully optimized with the Amsterdam Density Functional (ADF) suite (version 2017)[63] using the BP86[64] functional, the scalar relativistic (SR) all-electron Zeroth-Order Regular Approximation[65] (ZORA), and the Slater-type atomic orbital (STO) basis sets of triple-ζ doubly polarized (TZ2P)[66] quality for all atoms. An atom-pairwise correction for dispersion forces were considered via Grimme's D3 model augmented with the Becke-Johnson (BJ) damping.[67] The conductor-like screening model (COSMO) was used to describe solvent effects.[68] Nuclear magnetic shielding constants for both [**2.1**]$^-$ and [**2.2**]$^-$ were calculated at the DFT/ZORA-SR and DFT/spin-orbit (SO) ZORA levels of theory with the TZ2P basis. The computations of the NMR shielding tensors[69] employed the hybrid PBE0[49] exchange-correlation functional with 25% (standard) and 40% exact-exchange and the response of the XC functional (fXC option). The ^{13}C shifts δ_i are calculated via $\delta_i = \sigma_{benz} - \sigma_i + \delta_{benz}$. Where σ_i is the calculated shielding of the carbon nucleus of interest, σ_{benz} and δ_{benz} are the calculated carbon shielding and the experimental chemical shift of benzene (128.8 ppm),[70] respectively. Note that in the present work the choice of a secondary reference instead of TMS hardly made a difference. To quantify the compositions of the chemical bonds, natural localized molecular orbital (NLMO) analyses were carried out with the NBO program, version 6.0, as interfaced with ADF.[71]

Table 2.2. % compositions of the U-L bonding NLMOs in [**2.1**]$^-$ and [**2.2**]$^-$.

Complex	Orbital	Tolal L	2s	2p	Total U	7s	7p	6d	5f
[**2.1**]$^-$	σ(U-C)	72	28	72	22	12	0	59	28
[**2.2**]$^-$	σ(U-C) (*trans* to THF)	73	30	70	20	13	0	46	42
	σ(U-O)	91	45	55	7	13	0	44	43
	π(U-O)	94	0	100	3	0	1	41	58

Table 2.3. Calculated carbon shielding (σ) and chemical shift (δ) for [**2.1**]$^-$ and [**2.2**]$^-$.

Compounds	**Method**	**Label**	**σ_{calc} (ppm)**	**δ_{calc} (ppm)**	**δ_{expt} (ppm)**
Benzene	PBE0/SO-PBE0 (HF=25%)	C	51.7 / 52.5	-	128.8[15]
	PBE0/SO-PBE0 (HF=40%)	C	52.9 / 53.7	-	128.8[15]
[**2.1**]$^-$	PBE0/SO-PBE0 (HF=25%)	C_{ipso}	–2.4 / –66.2	182.9 / 247.5	236.7 (This work)
	PBE0/SO-PBE0 (HF=40%)	C_{ipso}	1.7 / –59.9	180.0 / 242.4	236.7 (This work)
[**2.2**]$^-$	PBE0/SO-PBE0 (HF=25%)	C_{ipso} (*trans* to THF)	0.2 / –76.7	180.3 / 258.0	239.4 (This work)
	PBE0/SO-PBE0 (HF=40%)	C_{ipso} (*trans* to THF)	3.6 / –63.4	178.1 / 245.9	239.4 (This work)
	PBE0/SO-PBE0 (HF=25%)	C_{ipso} (*cis* to THF)	–3.3 / –99.0	183.8 / 280.3	-
	PBE0/SO-PBE0 (HF=40%)	C_{ipso} (*cis* to THF)	0.0 / –78.6	181.7 / 261.1	-

2.5 Appendix

2.5.1 NMR Spectra

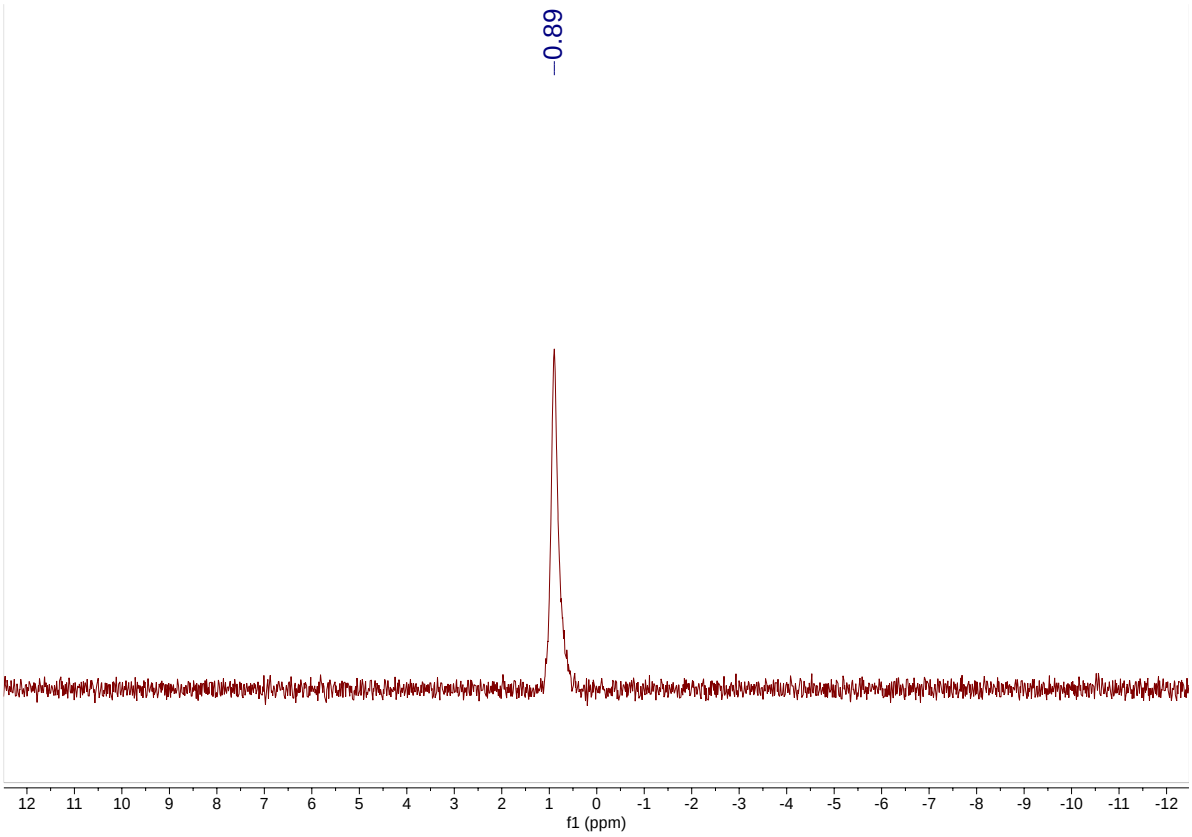

Figure 2.5. $^{7}Li\{^{1}H\}$ NMR spectrum of LiC_6Cl_5 in benzene-d_6.

Experimental details: An aliquot (1 mL) of the 0.25 M LiC_6Cl_5 stock solution was transferred to a 20 ml vial, and the volatiles were removed *in vacuo*. The resulting golden oil was dissolved in benzene-d_6 (0.5 mL), and a $^{7}Li\{^{1}H\}$ NMR spectrum was recorded.

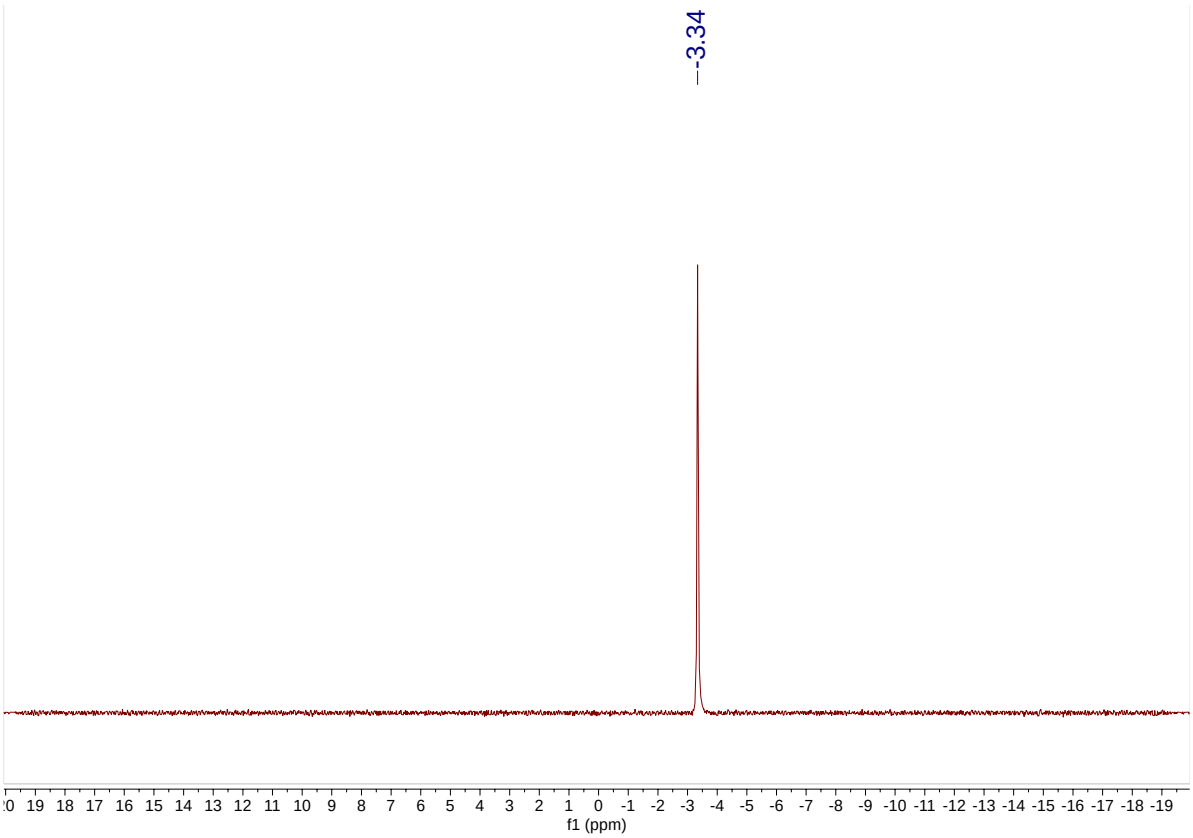

Figure 2.6. $^{7}Li\{^{1}H\}$ NMR spectrum of [Li][**2.1**] in benzene-d_6.

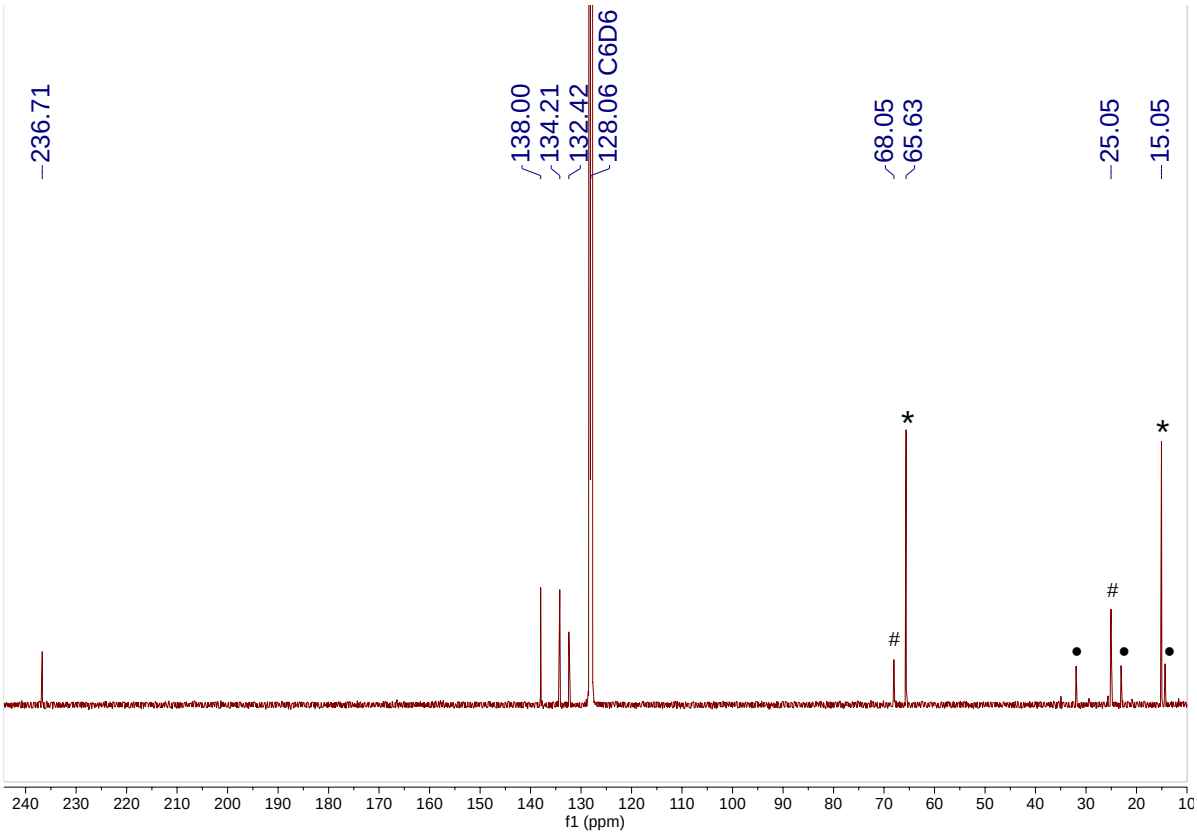

Figure 2.7. $^{13}C\{^{1}H\}$ NMR spectrum of [Li][**2.1**] in benzene-d_6. (*) indicates the presence of Et_2O, (#) indicates the presence of THF, and (•) indicates the presence of *n*-hexane.

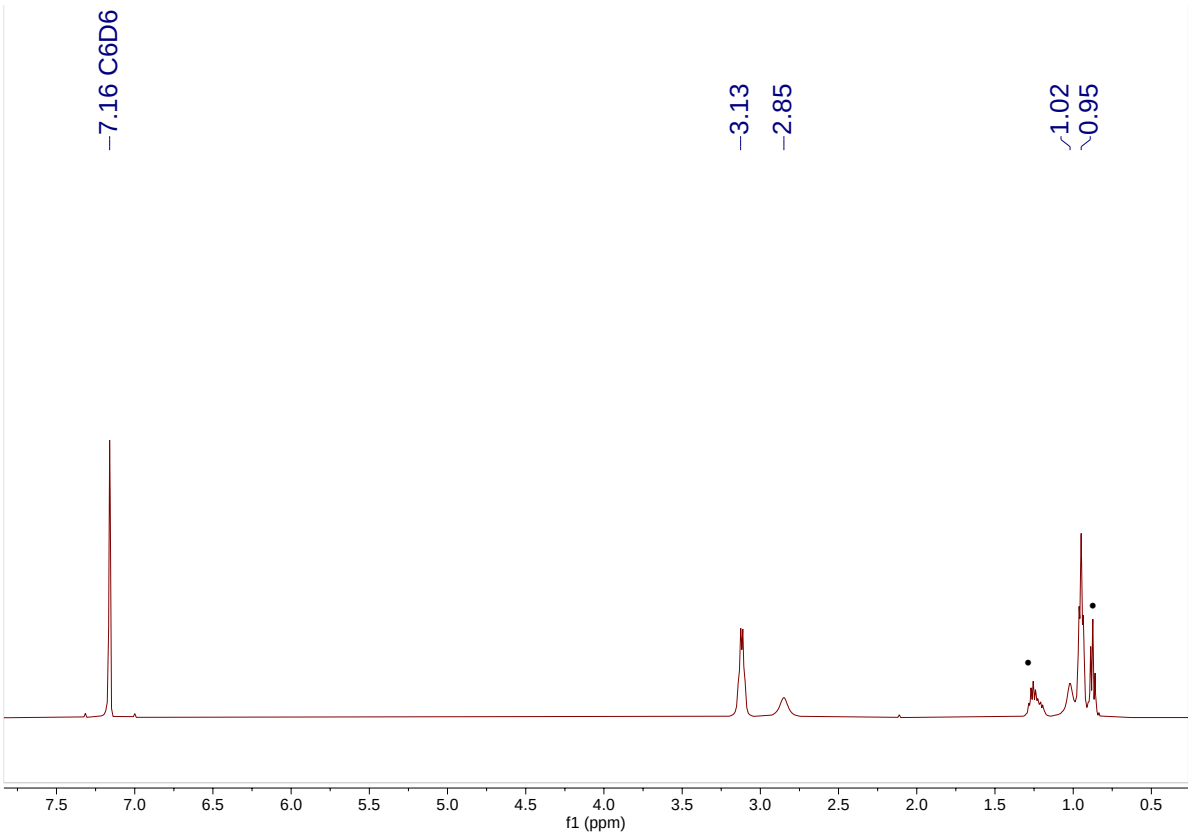

Figure 2.8. ^{1}H NMR spectrum of [Li][**2.1**] in benzene-d_6. (•) indicates the presence of n-hexane and n-pentane.

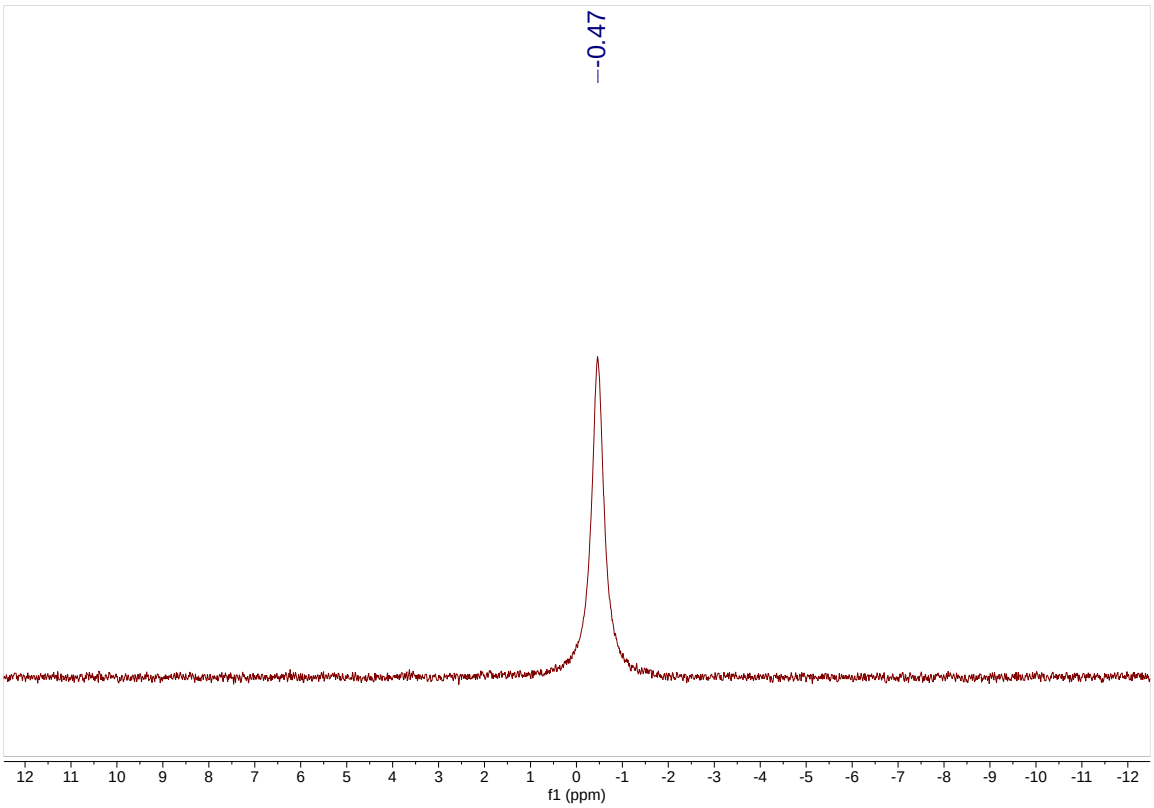

Figure 2.9. $^{7}Li\{^{1}H\}$ NMR spectrum of [Li][**2.1**] in THF-d_8.

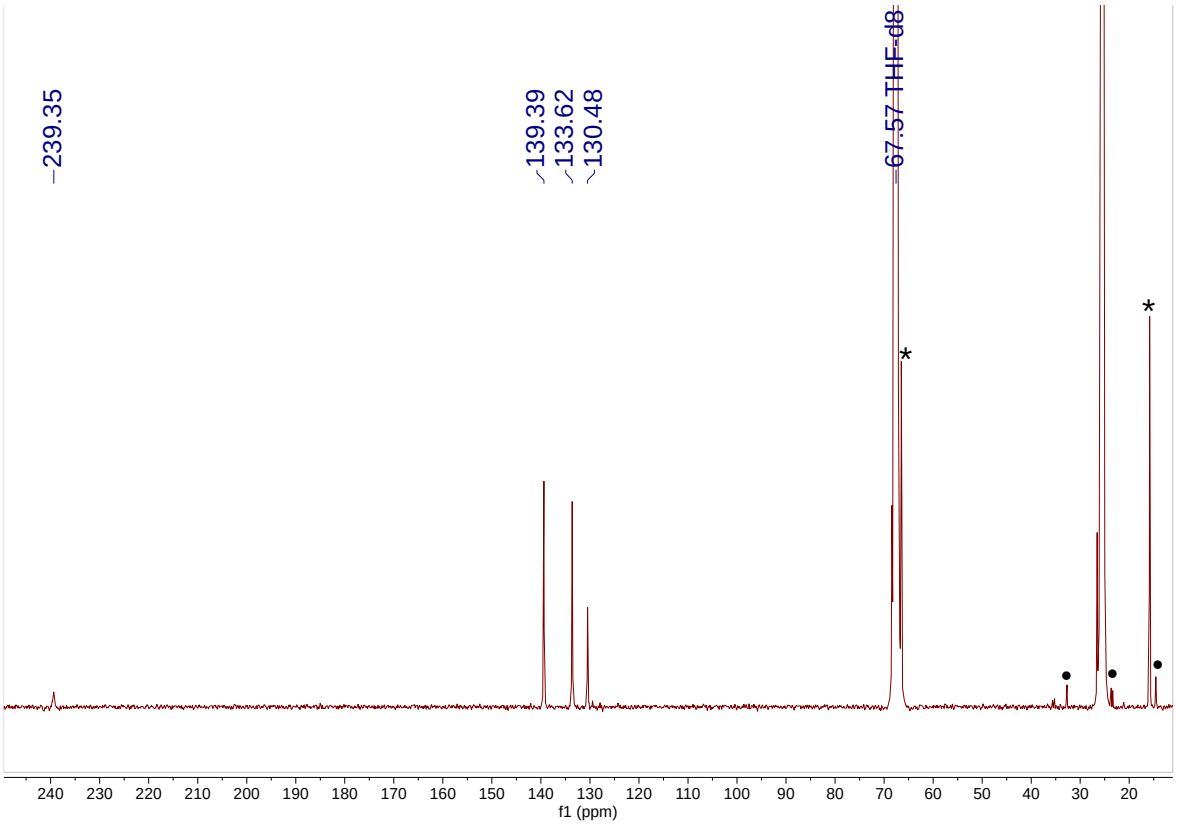

Figure 2.10. $^{13}C\{^{1}H\}$ NMR spectrum of [Li][**2.1**] in THF-d_8. (*) indicates the presence of Et_2O and (•) indicates the presence of *n*-hexane.

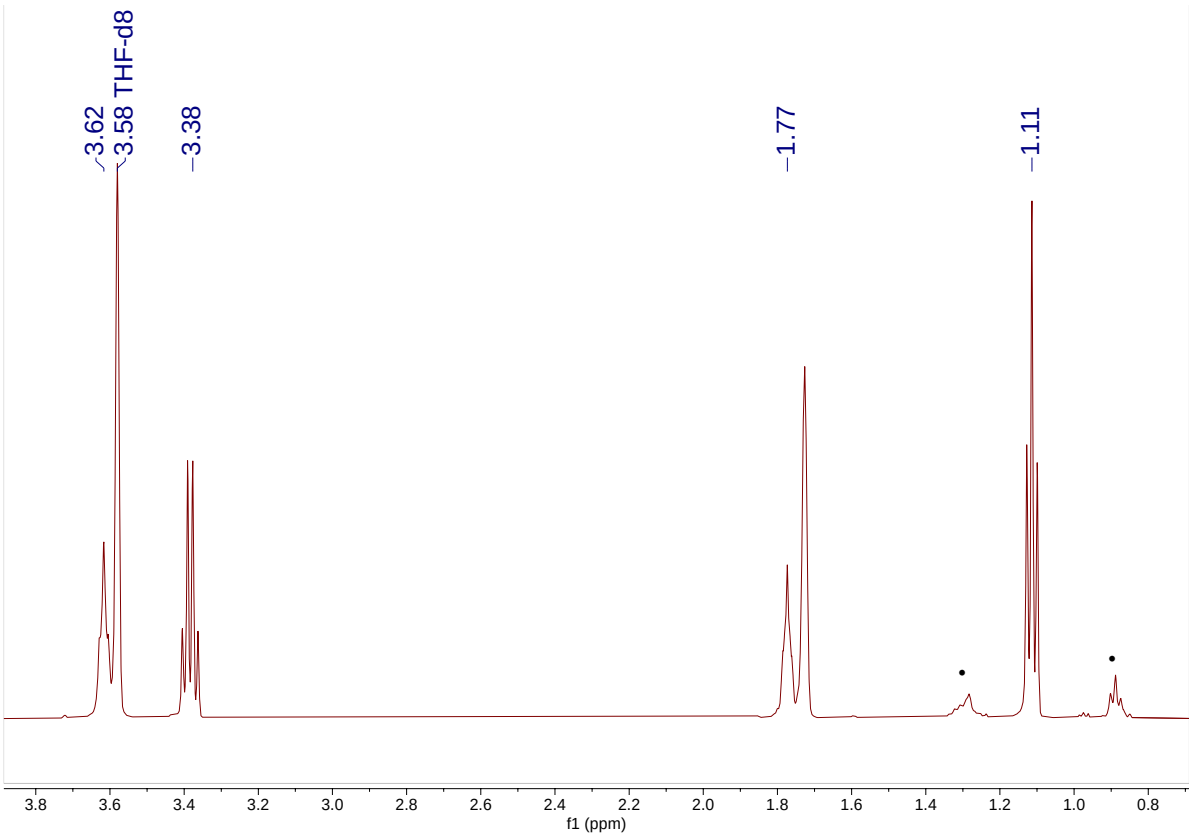

Figure 2.11. ^{1}H NMR spectrum of [Li][**2.1**] in THF-d_8. (•) indicates the presence of *n*-hexane.

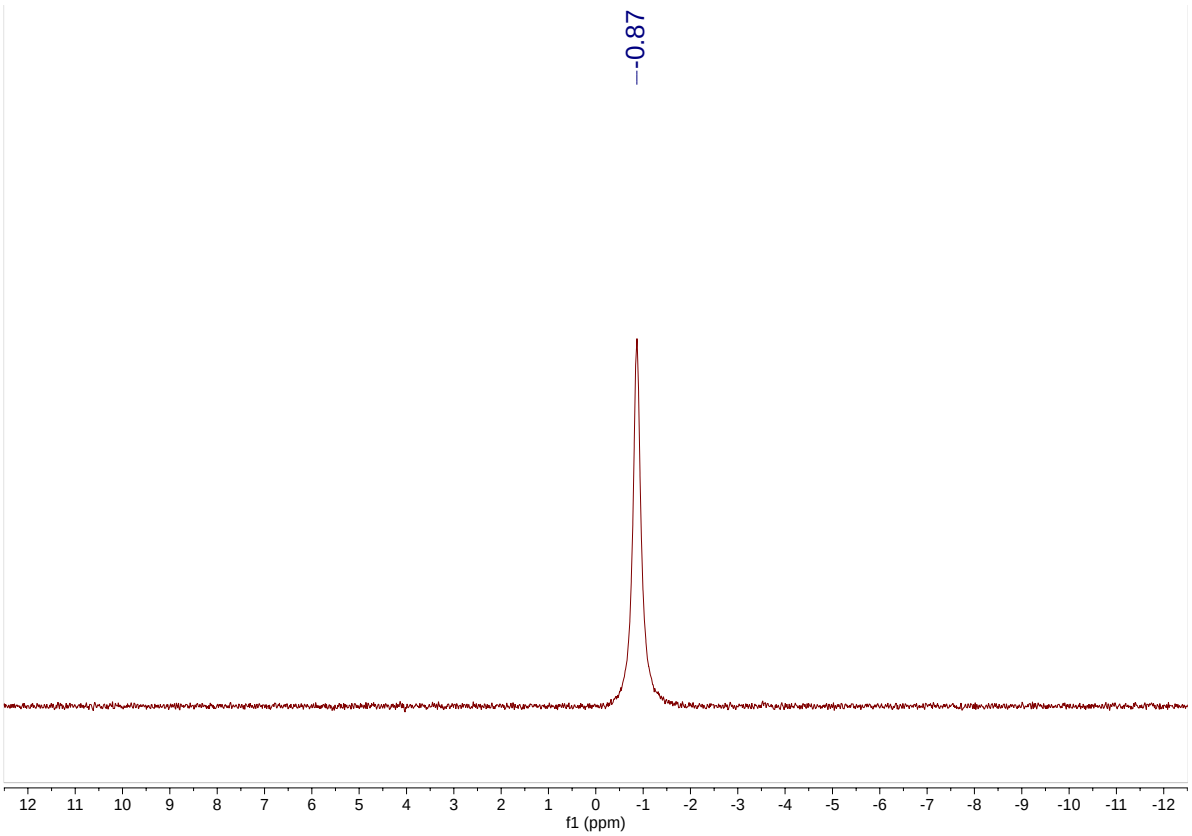

Figure 2.12. $^{7}Li\{^{1}H\}$ NMR spectrum of [Li][**2.2**] in THF-d_8.

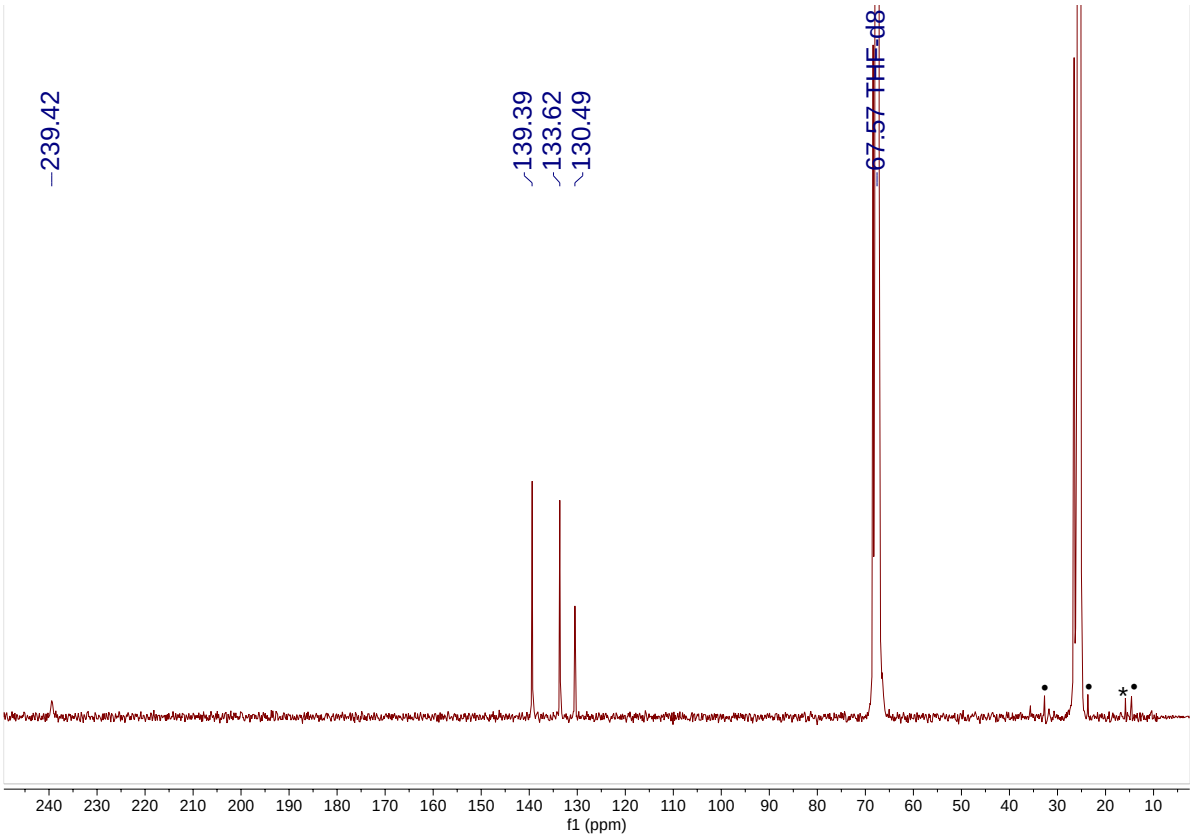

Figure 2.13. $^{13}C\{^{1}H\}$ NMR spectrum of [Li][**2.2**] in THF-d8. (•) indicates the presence of n-hexane.

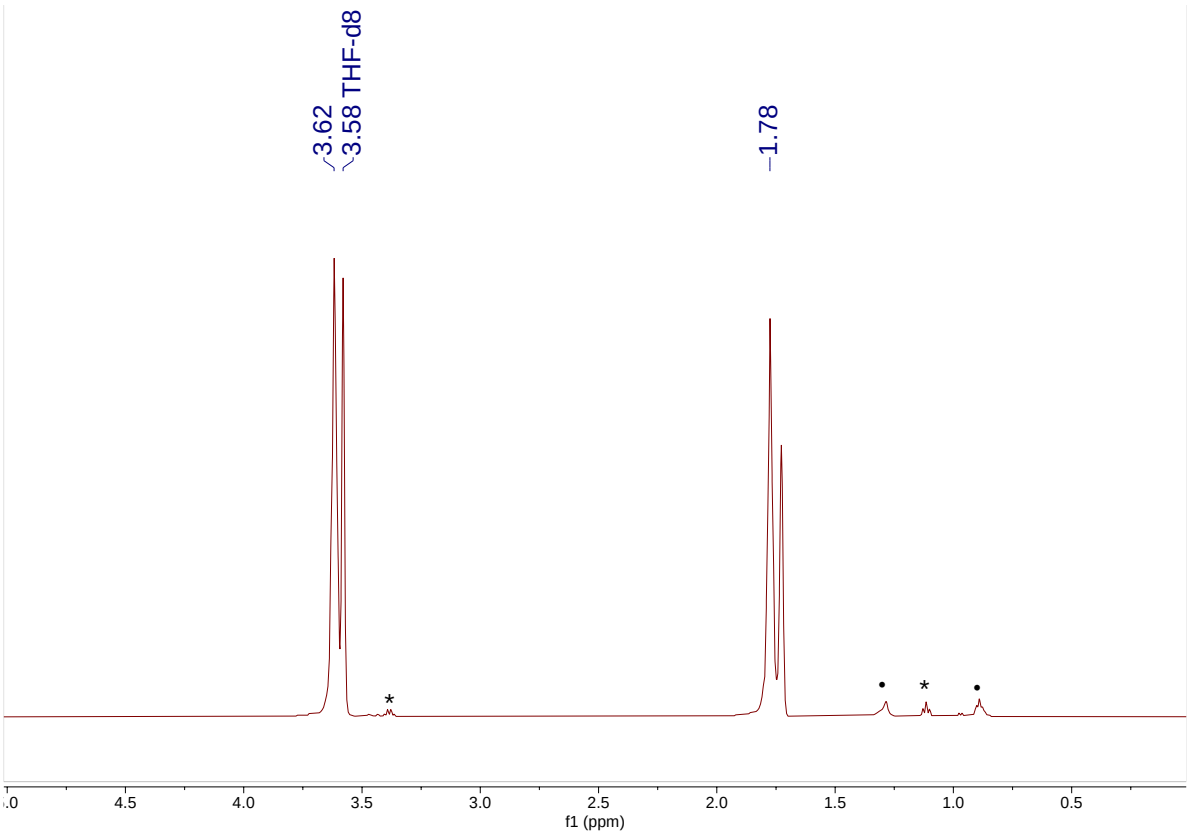

Figure 2.14. ^{1}H NMR spectrum of [Li][**2.2**] in THF-d_8. (*) indicates the presence of diethyl ether. (•) indicates the presence of *n*-hexane.

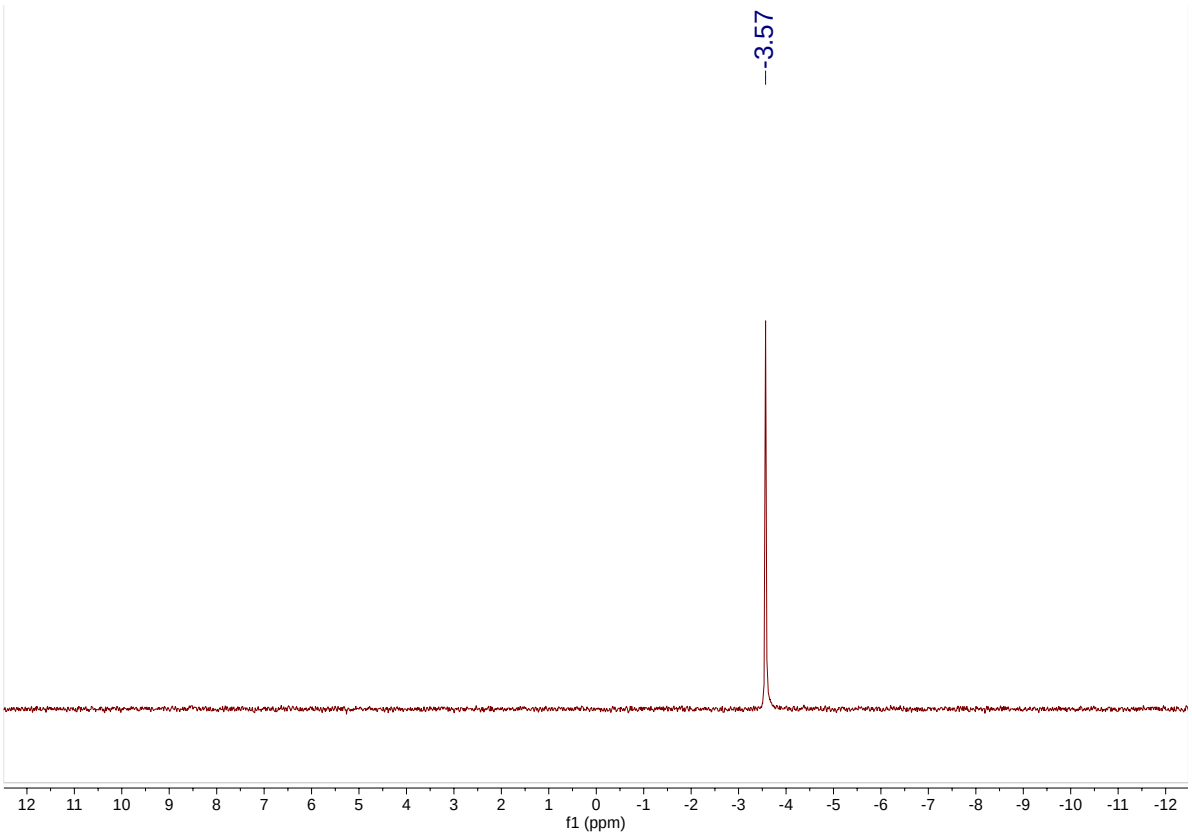

Figure 2.15. $^{7}Li\{^{1}H\}$ NMR spectrum of [Li][**2.2**] in benzene-d_6.

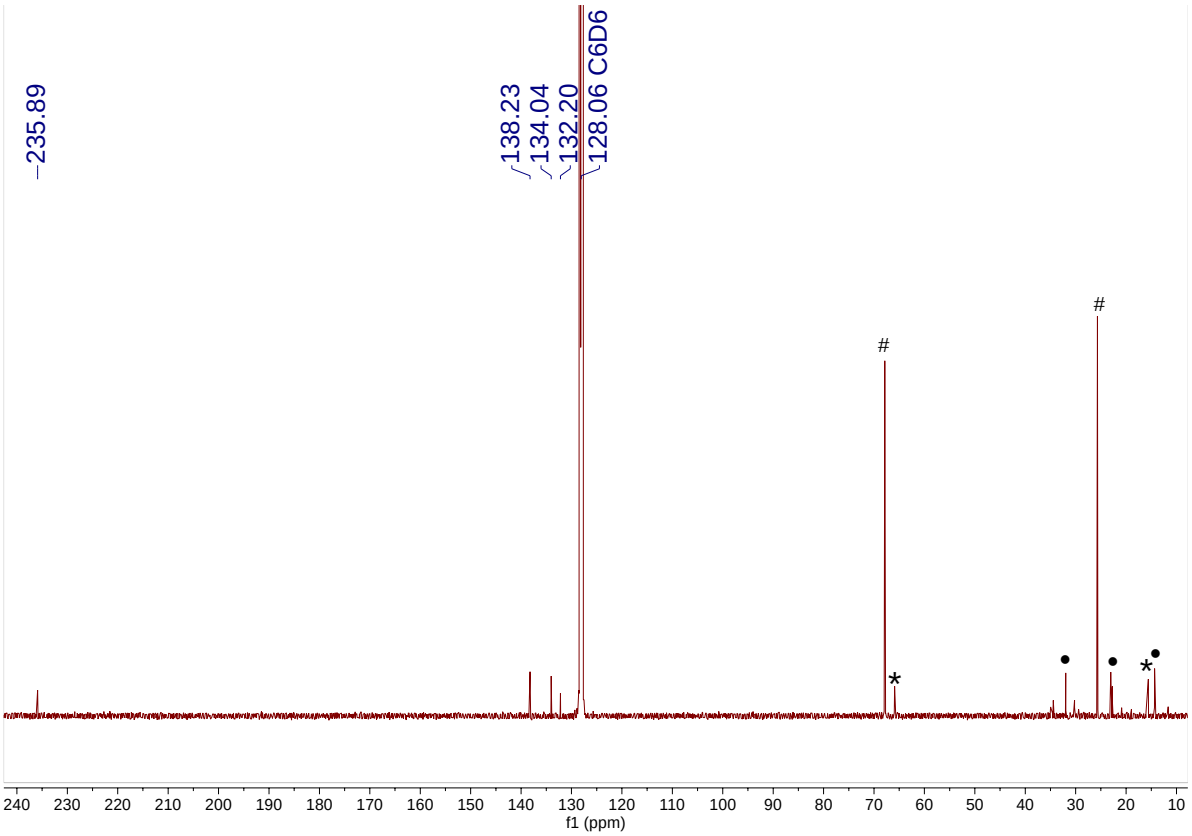

Figure 2.16. $^{13}C\{^{1}H\}$ NMR spectrum of [Li][**2.2**] in benzene-d_6. (*) indicates the presence of Et_2O, (#) indicates the presence of THF, and (•) indicates the presence of *n*-hexane.

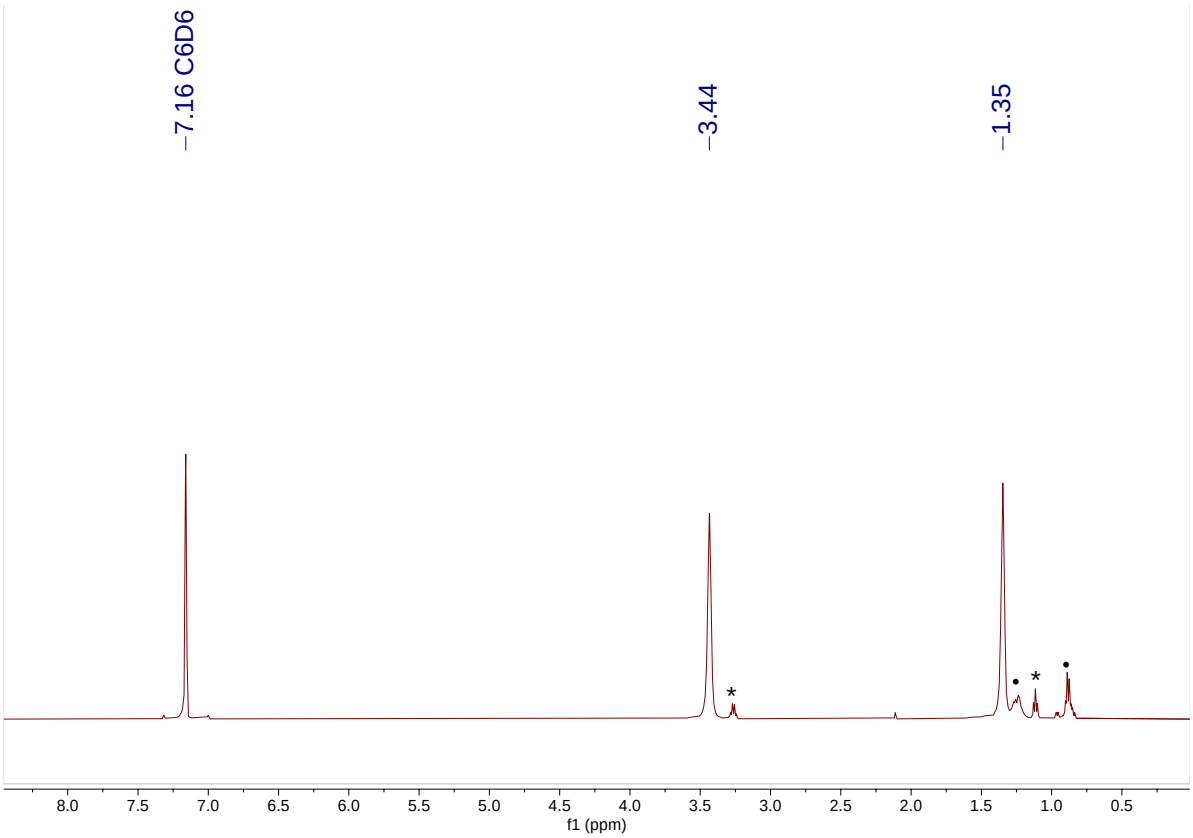

Figure 2.17. ^{1}H NMR spectrum of [Li][**2.2**] in benzene-d_6. (*) indicates the presence of diethyl ether. (•) indicates the presence of n-hexane.

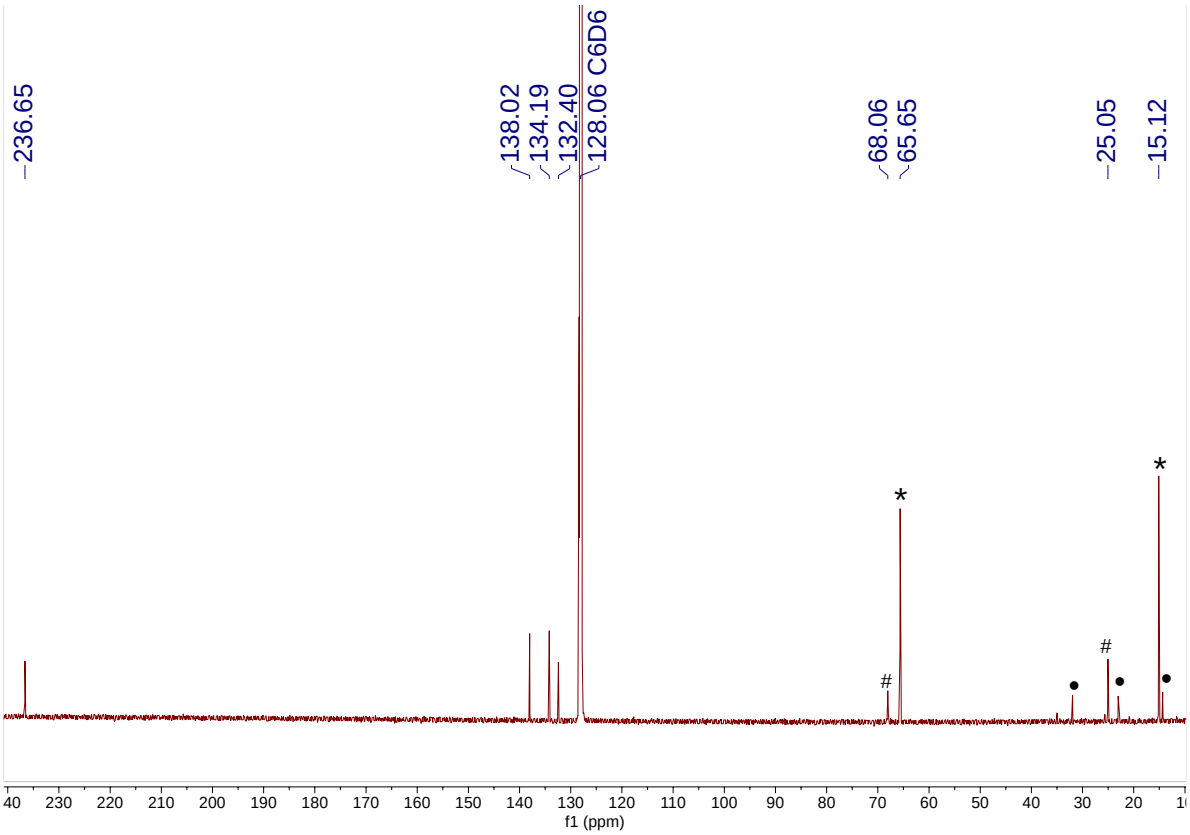

Figure 2.18. $^{13}C\{^{1}H\}$ NMR spectrum of [Li][**2.1**] in benzene-d_6 after standing in solution for 24 h. (*) indicates the presence of Et_2O, (#) indicates the presence of THF, and (•) indicates the presence of *n*-hexane.

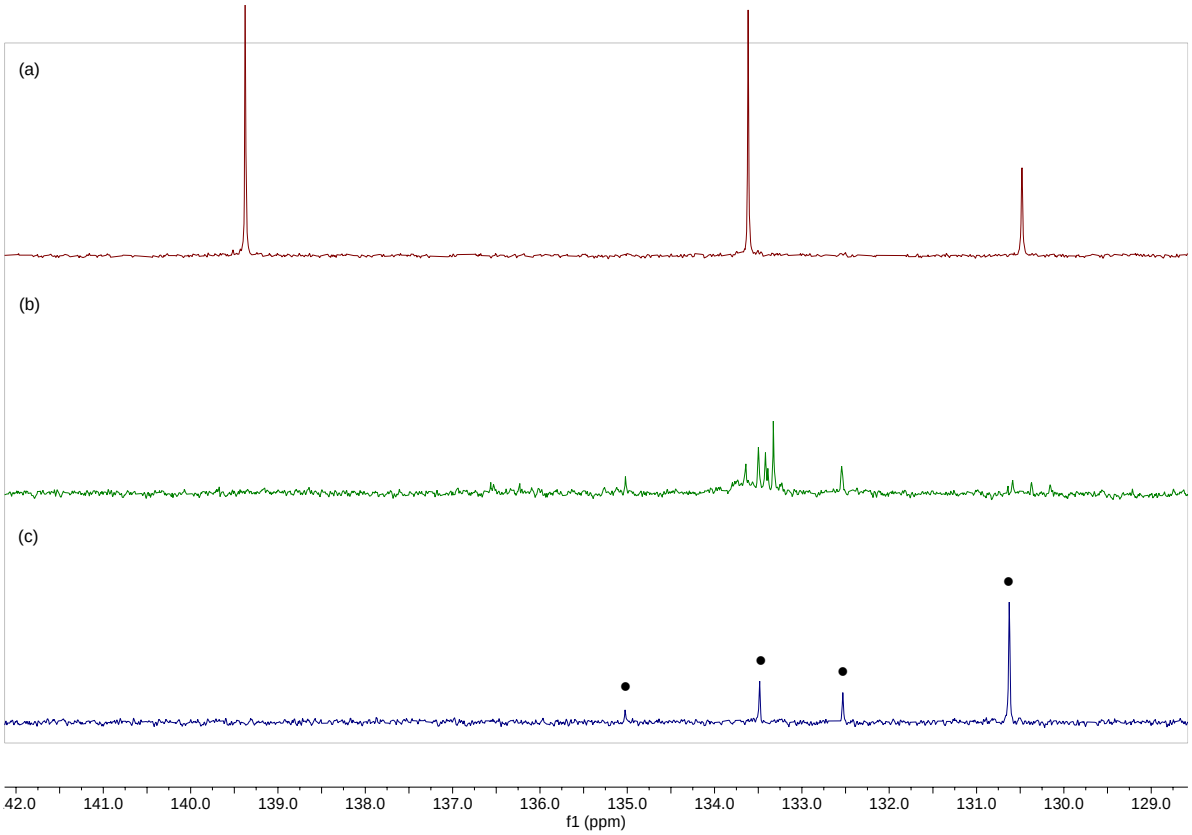

Figure 2.19. (a) Partial $^{13}C\{^{1}H\}$ NMR spectrum of [Li][**2.2**] in THF-d_8. (b) Partial $^{13}C\{^{1}H\}$ NMR spectrum of [Li][**2.2**] in THF-d_8 after standing for 24 h in solution. (c) Partial $^{13}C\{^{1}H\}$ NMR spectrum in THF-d_8 of a crystalline sample of [Li][**2.2**] that was exposed to vacuum for 45 min. (•) indicates the presence of C_6Cl_5H.[39]

2.5.2 IR Spectra

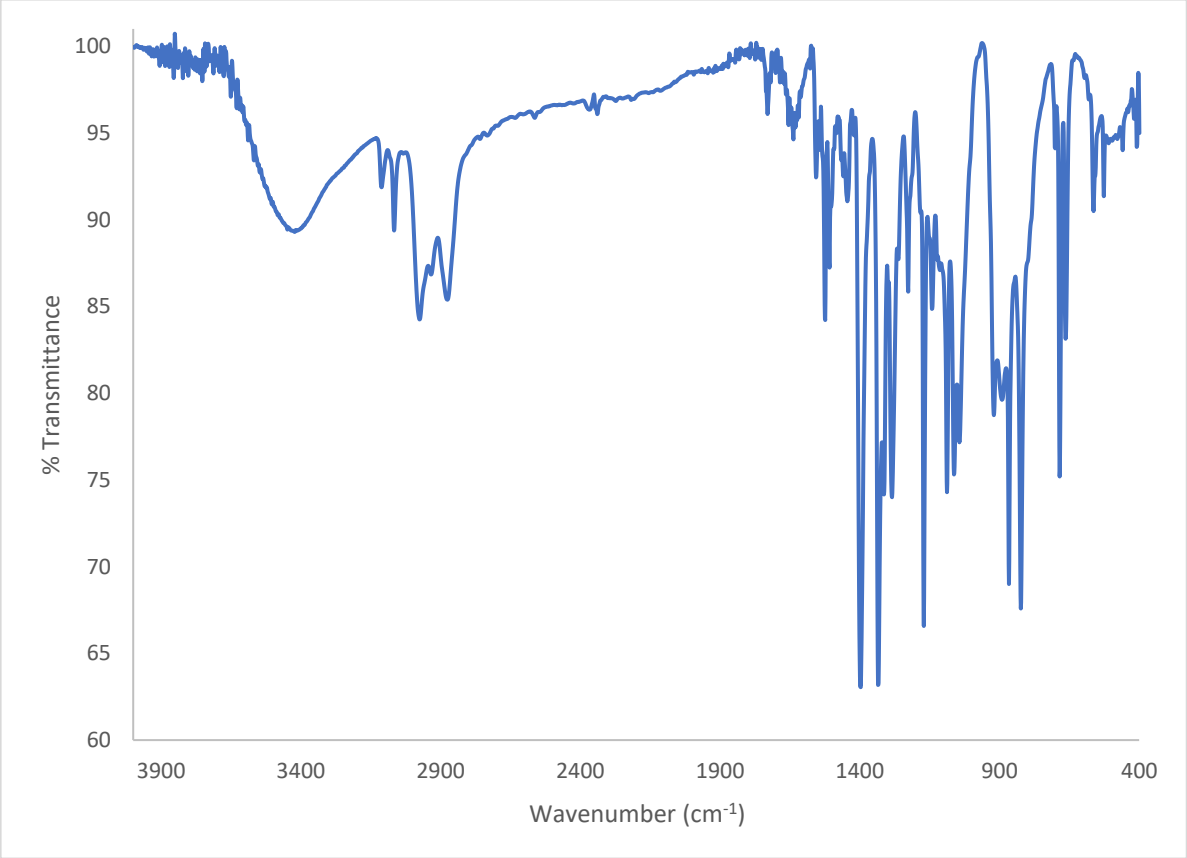

Figure 2.20. IR spectrum of [Li][**2.1**] (KBr pellet).

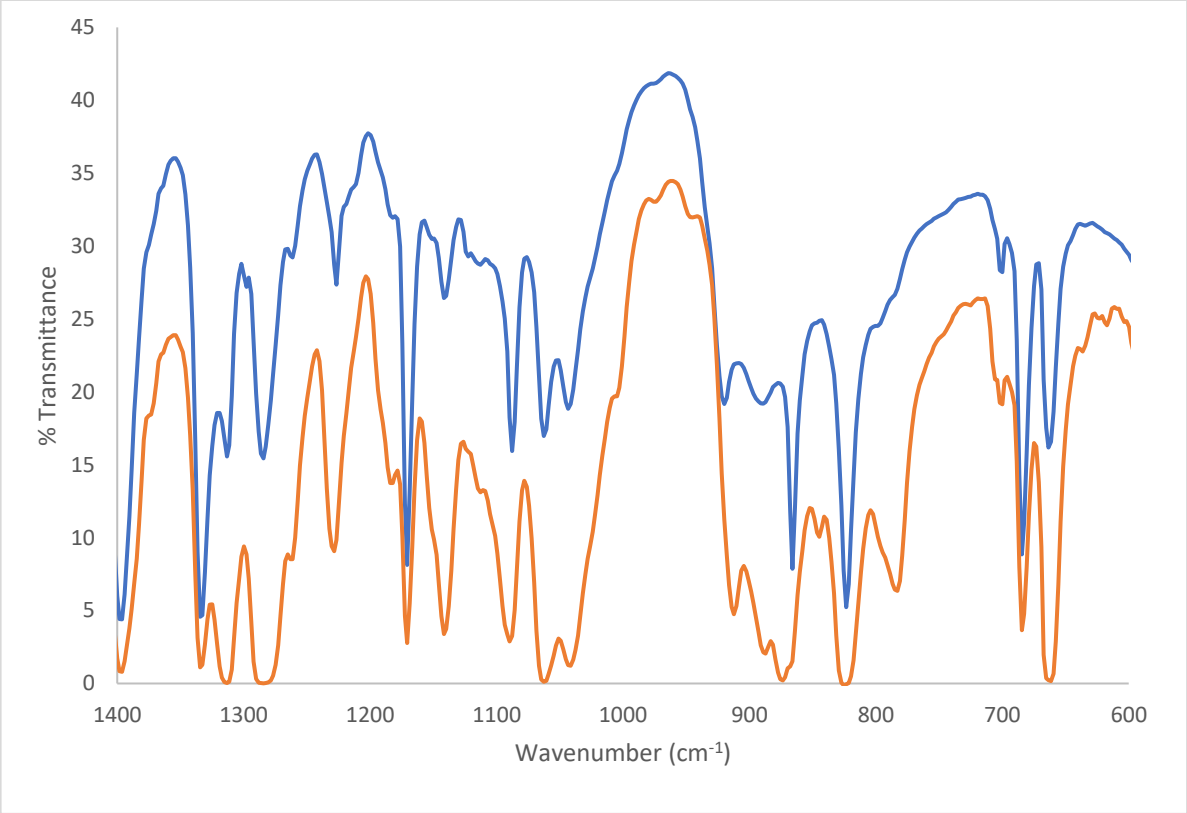

Figure 2.21. Overlay of partial IR spectrum of [Li][**2.1**-^{18}**O**] (KBr pellet) (orange) and [Li][**2.1**] (KBr pellet) (blue).

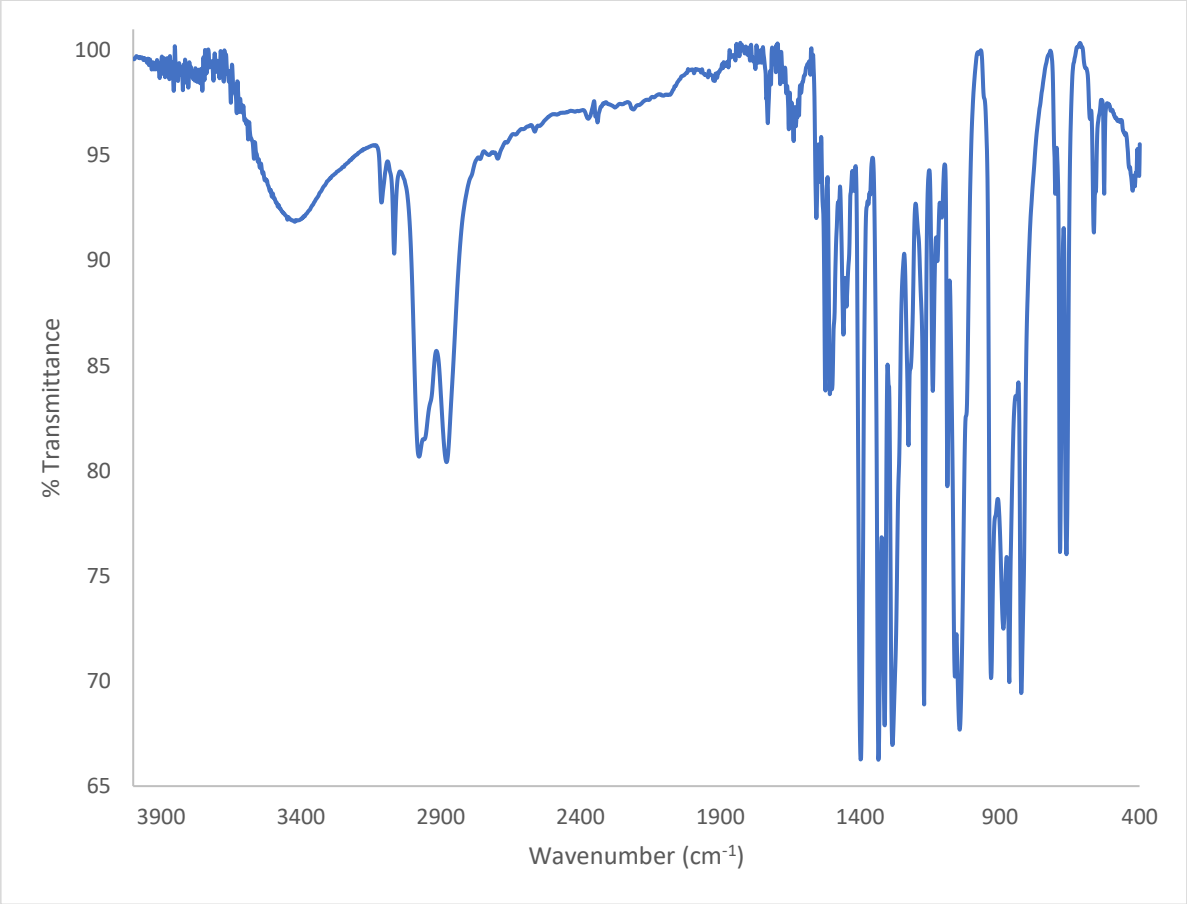

Figure 2.22. IR spectrum of [Li][**2.2**]·THF (KBr pellet).

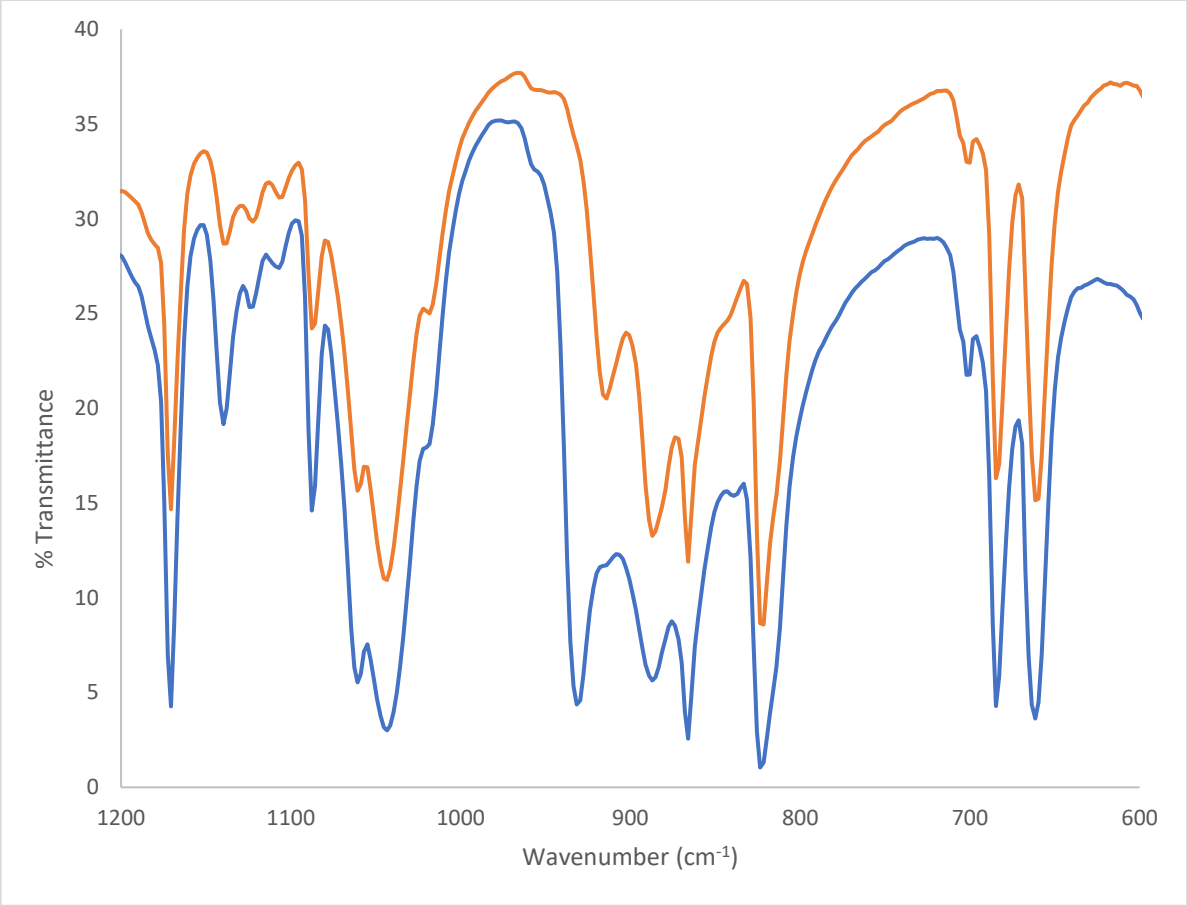

Figure 2.23. Overlay of partial IR spectra of [Li][**2.2**-^{18}**O**] (KBr pellet) (orange) and [Li][**2.2**] (blue).

2.6 References

(1) Fortier, S.; Hayton, T. W. Oxo ligand functionalization in the uranyl ion (UO_2^{2+}). *Coord. Chem. Rev.* **2010**, *254*, 197-214.
(2) Jones, M. B.; Gaunt, A. J. Recent Developments in Synthesis and Structural Chemistry of Nonaqueous Actinide Complexes. *Chem. Rev.* **2013**, *113*, 1137-1198.
(3) Edelstein, N. M.; Fuger, J.; Morss, L. R. *The chemistry of the actinide and transactinide elements*; Springer, 2006.
(4) Baker, R. J. New Reactivity of the Uranyl(VI) Ion. *Chem. Eur. J.* **2012**, *18*, 16258-16271.
(5) Sand, J.; Singer, F. Stickoxyd und das Grignardsche Reagens. *Justus Liebigs Ann. Chem.* **1903**, *329*, 190-194.
(6) Hallwachs, W.; Schafarik, A. Ueber die Verbindungen der Erdmetalle mit organischen Radicalen. *Justus Liebigs Ann. Chem.* **1859**, *109*, 206-209.
(7) Sarsfield, M. J.; Helliwell, M.; Collison, D. The first uranyl–methine carbon bond; a complex with out-of-plane uranyl equatorial coordination. *Chem. Commun.* **2002**, 2264-2265.
(8) Seyam, A. M. Observations on the reaction of uranium tetrachloride and dichlorodioxouranium(VI) with lithium alkyls. *Inorg. Chim. Acta* **1985**, *110*, 123-126.
(9) Seyam, A. M. Thermal studies of 'dialkyldioxouranium(VI)'. *Inorg. Chim. Acta* **1982**, *58*, 71-74.
(10) Berthet, J.-C.; Siffredi, G.; Thuéry, P.; Ephritikhine, M. Easy access to stable pentavalent uranyl complexes. *Chem. Commun.* **2006**, 3184-3186.
(11) Arnold, P. L.; Casely, I. J.; Turner, Z. R.; Carmichael, C. D. Functionalised Saturated-Backbone Carbene Ligands: Yttrium and Uranyl Alkoxy–Carbene Complexes and Bicyclic Carbene–Alcohol Adducts. *Chem. Eur. J.* **2008**, *14*, 10415-10422.
(12) Berthet, J.-C.; Thuéry, P.; Ephritikhine, M. The first actinyl cyanide. *Chem. Commun.* **2007**, 604-606.
(13) Kiernicki, J. J.; Cladis, D. P.; Fanwick, P. E.; Zeller, M.; Bart, S. C. Synthesis, Characterization, and Stoichiometric U–O Bond Scission in Uranyl Species Supported by Pyridine(diimine) Ligand Radicals. *J. Am. Chem. Soc.* **2015**, *137*, 11115-11125.
(14) Lu, E.; Cooper, O. J.; McMaster, J.; Tuna, F.; McInnes, E. J. L.; Lewis, W.; Blake, A. J.; Liddle, S. T. Synthesis, Characterization, and Reactivity of a Uranium(VI) Carbene Imido Oxo Complex. *Angew. Chem., Int. Ed.* **2014**, *53*, 6696-6700.
(15) Maity, A. K.; Ward, R. J.; Rupasinghe, D. M. R. Y. P.; Zeller, M.; Walensky, J. R.; Bart, S. C. Organometallic Uranyl Complexes Featuring a Carbodicarbene Ligand. *Organometallics* **2020**, *39*, 783-787.
(16) Maynadié, J.; Berthet, J.-C.; Thuéry, P.; Ephritikhine, M. The first cyclopentadienyl complex of uranyl. *Chem. Commun.* **2007**, 486-488.
(17) Mills, D. P.; Cooper, O. J.; Tuna, F.; McInnes, E. J. L.; Davies, E. S.; McMaster, J.; Moro, F.; Lewis, W.; Blake, A. J.; Liddle, S. T. Synthesis of a Uranium(VI)-Carbene: Reductive Formation of Uranyl(V)-Methanides, Oxidative Preparation of a $[R_2C{=}U{=}O]^{2+}$ Analogue of the $[O{=}U{=}O]^{2+}$ Uranyl Ion (R = $Ph_2PNSiMe_3$), and Comparison of the Nature of $U^{IV}{=}C$, $U^{V}{=}C$, and $U^{VI}{=}C$ Double Bonds. *J. Am. Chem. Soc.* **2012**, *134*, 10047-10054.
(18) Mungur, S. A.; Liddle, S. T.; Wilson, C.; Sarsfield, M. J.; Arnold, P. L. Bent metal carbene geometries in amido N-heterocyclic carbene complexes. *Chem. Commun.* **2004**, 2738-2739.

(19) Sarsfield, M. J.; Helliwell, M.; Raftery, J. Distorted Equatorial Coordination Environments and Weakening of UO Bonds in Uranyl Complexes Containing NCN and NPN Ligands. *Inorg. Chem.* **2004**, *43*, 3170-3179.
(20) Sarsfield, M. J.; Steele, H.; Helliwell, M.; Teat, S. J. Uranyl bis-iminophosphorane complexes with in- and out-of-plane equatorial coordination. *Dalton Trans.* **2003**, 3443-3449.
(21) Tourneux, J.-C.; Berthet, J.-C.; Cantat, T.; Thuéry, P.; Mézailles, N.; Ephritikhine, M. Exploring the Uranyl Organometallic Chemistry: From Single to Double Uranium−Carbon Bonds. *J. Am. Chem. Soc.* **2011**, *133*, 6162-6165.
(22) Oldham Jr, W. J.; Oldham, S. M.; Scott, B. L.; Abney, K. D.; Smith, W. H.; Costa, D. A. Synthesis and structure of N-heterocyclic carbene complexes of uranyl dichloride. *Chem. Commun.* **2001**, 1348-1349.
(23) Seaman, L. A.; Hrobárik, P.; Schettini, M. F.; Fortier, S.; Kaupp, M.; Hayton, T. W. A Rare Uranyl(VI)–Alkyl Ate Complex $[Li(DME)_{1.5}]_2[UO_2(CH_2SiMe_3)_4]$ and Its Comparison with a Homoleptic Uranium(VI)–Hexaalkyl. *Angew. Chem., Int. Ed.* **2013**, *52*, 3259-3263.
(24) Schettini, M. F.; Wu, G.; Hayton, T. W. Synthesis and reactivity of a uranyl-imidazolyl complex. *Chem. Commun.* **2012**, *48*, 1484-1486.
(25) Kent, G. T.; Murillo, J.; Wu, G.; Fortier, S.; Hayton, T. W. Coordination of Uranyl to the Redox-Active Calix[4]pyrrole Ligand. *Inorg. Chem.* **2020**, *59*, 8629-8634.
(26) García-Monforte, M. A.; Alonso, P. J.; Forniés, J.; Menjón, B. New advances in homoleptic organotransition-metal compounds: The case of perhalophenyl ligands. *Dalton Trans.* **2007**, 3347-3359.
(27) Alonso, P. J.; Forniés, J.; García-Monforte, M. A.; Martín, A.; Menjón, B. New Homoleptic Organometallic Derivatives of Vanadium(III) and Vanadium(IV): Synthesis, Characterization, and Study of Their Electrochemical Behaviour. *Chem. Eur. J.* **2005**, *11*, 4713-4724.
(28) Alonso, P. J.; Arauzo, A. B.; Forniés, J.; García-Monforte, M. A.; Martín, A.; Menjón, B.; Martínez, J. I.; Rillo, C.; Sáiz-Garitaonandia, J. J. A Square-Planar Organoiron(III) Compound with a Spin-Admixed State. *Angew. Chem., Int. Ed.* **2006**, *45*, 6707-6711.
(29) Alonso, P. J.; Forniés, J.; García-Monforte, M. A.; Martín, A.; Menjón, B.; Rillo, C. A New Series of Homoleptic, Paramagnetic Organochromium Derivatives: Synthesis, Characterization, and Study of Their Magnetic Properties. *Chem. Eur. J.* **2002**, *8*, 4056-4065.
(30) J. Alonso, P.; R. Falvello, L.; Forniés, J. Synthesis and first structural characterisation of a homoleptic tetraorganochromate(III) salt. *Chem. Commun.* **1998**, 1721-1722.
(31) Alonso, P. J.; Forniés, J.; García-Monforte, M. A.; Martín, A.; Menjón, B. The first structurally characterised homoleptic organovanadium(III) compound. *Chem. Commun.* **2001**, 2138-2139.
(32) Alonso, P. J.; Forniés, J.; García-Monforte, M. A.; Martín, A.; Menjón, B. The first structurally characterised homoleptic σ-organotitanium(III) compound. *Chem. Commun.* **2002**, 728-729.
(33) Garcia, M. P.; Jimenez, M. V.; Oro, L. A.; Lahoz, F. J.; Tiripicchio, M. C.; Tiripicchio, A. A homoleptic mononuclear iridium(II) organometallic complex: synthesis and x-ray structure of $[Ir(C_6Cl_5)_4]_2$. *Organometallics* **1993**, *12*, 4660-4663.
(34) P. García, M.; Victoria Jiménez, M.; J. Lahoz, F.; A. López, J.; A. Oro, L. Synthesis of the homoleptic rhodium(III) complex $[Rh(C_6Cl_5)_3]$. Molecular structures of $[Rh(C_6Cl_5)_3]$ and $[Rh(C_6Cl_4–C_6Cl_4)(C_6Cl_5)(SC_4H_8)_2]$. *J. Chem. Soc. Dalton Trans.* **1998**, 4211-4214.

(35) Fornies, J.; Menjon, B.; Sanz-Carrillo, R. M.; Tomas, M.; Connelly, N. G.; Crossley, J. G.; Orpen, A. G. Synthesis and Structural Characterization of the First Isolated Homoleptic Organoplatinum(IV) Compound: [$Pt(C_6Cl_5)_4$]. *J. Am. Chem. Soc.* **1995**, *117*, 4295-4304.
(36) Ara, I.; Forniés, J.; García-Monforte, M. A.; Martín, A.; Menjón, B. Synthesis and Characterization of Pentachlorophenyl–Metal Derivatives with d^0 and d^{10} Electron Configurations. *Chem. Eur. J.* **2004**, *10*, 4186-4197.
(37) Rausch, M. D.; Tibbetts, F. E.; Gordon, H. B. Perhaloaryl-metal chemistry: II. Pentachlorophenyllithium. *J. Organomet. Chem.* **1966**, *5*, 493-500.
(38) Wilkerson, M. P.; Burns, C. J.; Paine, R. T.; Scott, B. L. Synthesis and Crystal Structure of $UO_2Cl_2(THF)_3$: A Simple Preparation of an Anhydrous Uranyl Reagent. *Inorg. Chem.* **1999**, *38*, 4156-4158.
(39) Takeuchi, Y.; Furuyama, H.; Fukushi, S.; Fujiwara, S. Carbon-13 nuclear magnetic resonance spectra of polychloro- and polybromo-benzenes. *J. Chem. Soc., Perkin Trans. 2* **1985**, 175-177.
(40) Seaman, L. A.; Pedrick, E. A.; Tsuchiya, T.; Wu, G.; Jakubikova, E.; Hayton, T. W. Comparison of the Reactivity of 2-Li-$C_6H_4CH_2NMe_2$ with MCl_4 (M=Th, U): Isolation of a Thorium Aryl Complex or a Uranium Benzyne Complex. *Angew. Chem., Int. Ed.* **2013**, *52*, 10589-10592.
(41) Pedrick, E. A.; Seaman, L. A.; Scott, J. C.; Griego, L.; Wu, G.; Hayton, T. W. Synthesis and Reactivity of a U(IV) Dibenzyne Complex. *Organometallics* **2016**, *35*, 494-502.
(42) Seaman, L. A.; Pedrick, E. A.; Wu, G.; Hayton, T. W. Promoting oxo functionalization in the uranyl ion by ligation to ketimides. *J. Organomet. Chem.* **2018**, *857*, 34-37.
(43) Seaman, L. A.; Schnaars, D. D.; Wu, G.; Hayton, T. W. Isolation of a uranyl amide by "ate" complex formation. *Dalton Trans.* **2010**, *39*, 6635-6637.
(44) Cowie, B. E.; Purkis, J. M.; Austin, J.; Love, J. B.; Arnold, P. L. Thermal and Photochemical Reduction and Functionalization Chemistry of the Uranyl Dication, $[U^{VI}O_2]^{2+}$. *Chem. Rev.* **2019**, *119*, 10595-10637.
(45) Danis, J. A.; Lin, M. R.; Scott, B. L.; Eichhorn, B. W.; Runde, W. H. Coordination Trends in Alkali Metal Crown Ether Uranyl Halide Complexes: The Series $[A(Crown)]_2[UO_2X_4]$ Where A = Li, Na, K and X = Cl, Br. *Inorg. Chem.* **2001**, *40*, 3389-3394.
(46) Coughlin, E. J.; Qiao, Y.; Lapsheva, E.; Zeller, M.; Schelter, E. J.; Bart, S. C. Uranyl functionalization mediated by redox-active ligands: generation of O–C bonds via acylation. *J. Am. Chem. Soc.* **2018**, *141*, 1016-1026.
(47) Lu, G.; Haes, A. J.; Forbes, T. Z. Detection and identification of solids, surfaces, and solutions of uranium using vibrational spectroscopy. *Coord. Chem. Rev.* **2018**, *374*, 314-344.
(48) Autschbach, J.; Zheng, S. Chapter 1 Relativistic Computations of NMR Parameters from First Principles: Theory and Applications. In *Annu. Rep. NMR Spectrosc.*, Webb, G. A. Ed.; Vol. 67; Academic Press, 2009; pp 1-95.
(49) Autschbach, J. The role of the exchange-correlation response kernel and scaling corrections in relativistic density functional nuclear magnetic shielding calculations with the zeroth-order regular approximation. *Mol. Phys.* **2013**, *111*, 2544-2554.
(50) Mullane, K. C.; Hrobárik, P.; Cheisson, T.; Manor, B. C.; Carroll, P. J.; Schelter, E. J. ^{13}C NMR Shifts as an Indicator of U–C Bond Covalency in Uranium(VI) Acetylide Complexes: An Experimental and Computational Study. *Inorg. Chem.* **2019**, *58*, 4152-4163.
(51) Greif, A. H.; Hrobárik, P.; Autschbach, J.; Kaupp, M. Giant spin–orbit effects on ^1H and ^{13}C NMR shifts for uranium(vi) complexes revisited: role of the exchange–correlation

response kernel, bonding analyses, and new predictions. *Phys. Chem. Chem. Phys.* **2016**, *18*, 30462-30474.
(52) Hrobárik, P.; Hrobáriková, V.; Greif, A. H.; Kaupp, M. Giant Spin-Orbit Effects on NMR Shifts in Diamagnetic Actinide Complexes: Guiding the Search of Uranium(VI) Hydride Complexes in the Correct Spectral Range. *Angew. Chem., Int. Ed.* **2012**, *51*, 10884-10888.
(53) Smiles, D. E.; Wu, G.; Hrobárik, P.; Hayton, T. W. Synthesis, Thermochemistry, Bonding, and ^{13}C NMR Chemical Shift Analysis of a Phosphorano-Stabilized Carbene of Thorium. *Organometallics* **2017**, *36*, 4519-4524.
(54) Pedrick, E. A.; Hrobárik, P.; Seaman, L. A.; Wu, G.; Hayton, T. W. Synthesis, structure and bonding of hexaphenyl thorium(IV): observation of a non-octahedral structure. *Chem. Commun.* **2016**, *52*, 689-692.
(55) Wolford, N. J.; Sergentu, D.-C.; Brennessel, W. W.; Autschbach, J.; Neidig, M. L. Homoleptic Aryl Complexes of Uranium (IV). *Angew. Chem., Int. Ed.* **2019**, *58*, 10266-10270.
(56) Harris, R. K.; Becker, E. D.; Cabral de Menezes, S. M.; Goodfellow, R.; Granger, P. NMR nomenclature. Nuclear spin properties and conventions for chemical shifts (IUPAC Recommendations 2001). *Pure Appl. Chem.* **2001**, *73*, 1795-1818.
(57) Harris, R. K.; Becker, E. D.; Cabral De Menezes, S. M.; Granger, P.; Hoffman, R. E.; Zilm, K. W. Further conventions for NMR shielding and chemical shifts (IUPAC Recommendations 2008). *Pure Appl. Chem.* **2008**, *80*, 59-84.
(58) SMART Apex II, Version 2.1; Bruker AXS Inc.: Madison, WI; 2005.
(59) SAINT Software User's Guide, Version 7.34a; Bruker AXS Inc.: Madison, WI; 2005.
(60) Sheldrick, G. M. SADABS, University of Gottingen, Germany; 2005.
(61) SHELXTL PC, Version 6.12; Bruker AXS Inc.: Madison, WI; 2005.
(62) Diamond - Crystal and Molecular Structure Visualization. Crystal Impact - Dr. H. Putz & Dr. K. Brandenburg GbR, Kreuzherrenstr. 102, 53227 Bonn, Germany. http://www.crystalimpact.com/diamond.
(63) E. J. Baerends, T. Ziegler, A. J. Atkins, J. Autschbach, O. Baseggio, D. Bashford, A. Bérces, F. M. Bickelhaupt, C. Bo, P. M. Boerrigter, L. Cavallo, C. Daul, D. P. Chong, D. V. Chulhai, L. Deng, R. M. Dickson, J. M. Dieterich, D. E. Ellis, M. v. Faassen, L. Fan, T. H. Fischer, C. F. Guerra, M. Franchini, A. Ghysels, A. Giammona, S. J. A. v. Gisbergen, A. Goez,; A. W. Götz, J. A. Groeneveld, O. V. Gritsenko, M. Grüning, S. Gusarov, F. E. Harris, P. v. d. Hoek, Z. Hu, C. R. Jacob, H. Jacobsen, L. Jensen, L. Joubert, J. W. Kaminski, G. v. Kessel, C. König, F. Kootstra, A. Kovalenko, M. V. Krykunov, E. v. Lenthe, D. A. McCormack, A. Michalak, M. Mitoraj, S. M. Morton, J. Neugebauer, V. P. Nicu, L. Noodleman, V. P. Osinga, S. Patchkovskii, M. Pavanello, C. A. Peeples, P. H. T. Philipsen, D. Post, C. C. Pye, H. Ramanantoanina, P. Ramos, W. Ravenek, J. I. Rodríguez, P. Ros, R. Rüger, P. R. T. Schipper, D. Schlüns, H. v. Schoot, G. Schreckenbach, J. S. Seldenthuis, M. Seth, J. G. Snijders, M. Solà, M. Stener, M. Swart, D. Swerhone, V. Tognetti, G. t. Velde, P. Vernooijs, L. Versluis, L. Visscher, O. Visser, F. Wang, T. A. Wesolowski, E. M. v. Wezenbeek, G. Wiesenekker, S. K. Wolff, T. K. Woo, A. L. Yakovlev, Amsterdam Density Functional. 2017 Ed.; SCM, Theoretical Chemistry, Vrije Universiteit Amsterdam, The Netherlands, 2017. https://www.scm.com.
(64) Perdew, J. P.; Burke, K.; Ernzerhof, M. Generalized gradient approximation made simple. *Physical review letters* **1996**, *77*, 3865.

(65) Lenthe, E. v.; Baerends, E.-J.; Snijders, J. G. Relativistic regular two-component Hamiltonians. *The Journal of chemical physics* **1993**, *99*, 4597-4610.
(66) Weigend, F.; Ahlrichs, R. Balanced basis sets of split valence, triple zeta valence and quadruple zeta valence quality for H to Rn: Design and assessment of accuracy. *Physical Chemistry Chemical Physics* **2005**, *7*, 3297-3305.
(67) Grimme, S.; Ehrlich, S.; Goerigk, L. Effect of the damping function in dispersion corrected density functional theory. *J. Comput. Chem.* **2011**, *32*, 1456-1465.
(68) Pye, C. C.; Ziegler, T. An implementation of the conductor-like screening model of solvation within the Amsterdam density functional package. *Theor. Chem. Acc.* **1999**, *101*, 396-408.
(69) Adamo, C.; Barone, V. Toward chemical accuracy in the computation of NMR shieldings: the PBE0 model. *Chem. Phys. Lett.* **1998**, *298*, 113-119.
(70) Fulmer, G. R.; Miller, A. J.; Sherden, N. H.; Gottlieb, H. E.; Nudelman, A.; Stoltz, B. M.; Bercaw, J. E.; Goldberg, K. I. NMR chemical shifts of trace impurities: common laboratory solvents, organics, and gases in deuterated solvents relevant to the organometallic chemist. *Organometallics* **2010**, *29*, 2176-2179.
(71) Glendening, E. D.; Landis, C. R.; Weinhold, F. NBO 6.0: Natural bond orbital analysis program. *J. Comput. Chem.* **2013**, *34*, 1429-1437.

Chapter 3. Homoleptic Perchlorophenyl "Ate" Complexes of Thorium(IV) and Uranium(IV)

Portions of this work were published in:

Osvaldo Ordoñez, Xiaojuan Yu, Guang Wu, Jochen Autschbach, and Trevor W. Hayton, Homoleptic Perchlorophenyl "Ate" Complexes of Thorium(IV) and Uranium(IV). *Inorg. Chem.* **2021**, 60, 12436–12444

Table of Contents

3.1 Introduction

Homoleptic actinide alkyl complexes have proven to be excellent testbeds for the study of electronic structure and bonding within these enigmatic elements.[1-3] As a result, a number of homoleptic actinide alkyl complexes have been synthesized in the last 10 years.[4-18] These complexes include $[Li(DME)_n][An(CH_2SiMe_3)_5]$ (An = Th, n = 2; An = U, n = 3),[8, 10] reported by us, $[Li(THF)_4][Li(THF)_2][UMe_6]$,[4] reported by Neidig and co-workers, and $[U(CH_2Ph)_4]$,[7] reported by Bart and co-workers. In contrast, homoleptic actinide aryl complexes remain exceedingly rare, in part because of their tendency to undergo facile *ortho* C-H bond activation.[19-21] For example, the first structurally characterized homoleptic uranium aryl, $[U(C_6H_3\text{-}2,6\text{-}(C_6H_4\text{-}4\text{-}^tBu)_2)_3]$, was only isolated in 2016 by Arnold and co-workers. Its isolation required the use of 4-^{t}BuC_6H_4 *ortho* substituents on the aryl ligand to prevent *ortho* C-H bond activation.[20] Even with the 4-^{t}BuC_6H_4 substituents, however, $[U(C_6H_3\text{-}2,6\text{-}(C_6H_4\text{-}4\text{-}^tBu)_2)_3]$ still decomposes on standing at room temperature, specifically by activation of an *ortho* C-H bond located on the 4-^{t}BuC_6H_4 substituent. Additionally, we and others have used "ate" complex formation to generate homoleptic An(IV) aryl complexes, including $[Li(DME)_3]_2[Th(C_6H_5)_6]$[19] and $[Li(THF)_4][(THF)LiU(C_6H_5)_6]$.[22] These complexes are stabilized by saturation of the actinide coordination sphere, which presumably disfavors the *ortho* C-H bond activation reaction.[19] Nonetheless, $[Li(THF)_4][(THF)LiU(C_6H_5)_6]$ is still exceptionally thermally sensitive, and could only be isolated at -80 °C.[22] The use of pendant donor groups can also stabilize An-C_{aryl} bonds, as was observed for $[Th(\eta^2\text{-}N,C\text{-}C_6H_4\text{-}o\text{-}CH_2NMe_2)_4]$,[21] $[Cp^*_2U(\eta^2\text{-}N,C\text{-}(o\text{-}C_6H_4)NPh)]$,[23] and $[Cp^*_2U(\eta^2\text{-}Te,C\text{-}(o\text{-}C_6H_4)Te)]$.[24]

Many of these actinide aryl complexes are attractive targets for studying covalency via ^{13}C NMR spectroscopy. NMR spectroscopy has been previously used as a tool to evaluate

covalency in An-L and Ln-L bonding.[19, 25-33] In the case of actinide aryl complexes, the ^{13}C NMR chemical shifts for the C_{ipso} environments are strongly affected by spin-orbit (SO) coupling, a consequence of 5f (and to a lesser extent, 6d) orbital participation in the An-C σ-bond.[25] In particular, in $5f^0$ systems with low-lying, empty 5f or 6d orbitals, SO coupling tends to cause ^{13}C deshielding as long as the An-C σ-bond has sizable C 2s character.[34] For example, the ^{13}C NMR spectrum of $[Li(DME)_3]_2[Th(C_6H_5)_6]$ features a C_{ipso} chemical shift of 220.5 ppm, with a calculated 44 ppm downfield contribution from SO coupling.[19] This SO deshielding correlates to the 5f (and 6d) participation in the Th-C bond. In the case of $[Th(C_6H_5)_6]^{2-}$, specifically, the Th-C bonds were calculated to have 15% weight each from Th atomic orbitals (AOs), of which 71/15% was from 6d/5f participation, respectively.

In Chapter 2, I reported the synthesis of the first structurally characterized uranyl(VI) aryl complexes, $[Li(Et_2O)_2(THF)][UO_2(C_6Cl_5)_3]$ ([Li][**2.1**]) and $[Li(THF)_4][UO_2(C_6Cl_5)_3(THF)]$ ([Li][**2.2**]), via reaction of $[UO_2Cl_2(THF)_2]$ with 3 equiv of LiC_6Cl_5. These complexes feature surprisingly good thermal stability,[25] which I ascribed, in part, to the *ortho*-Cl substitution of the $[C_6Cl_5]^-$ ligand. Given this precedent, we rationalized that the $[C_6Cl_5]^-$ ligand could also stabilize homoleptic U(IV) and Th(IV) complexes. Additional support for this hypothesis comes from large number of homoleptic transition metal perhalophenyl complexes that have been reported over the past 25 years.[35-44] Despite these past synthetic achievements, however, no homoleptic perhalophenyl complexes are known for actinides. Additionally, the only heteroleptic perhalophenyl actinide complexes are the aforementioned uranyl(VI) species (Chapter 2),[25] making this a potentially fruitful avenue of investigation. Herein, I describe the synthesis and characterization of two homoleptic actinide-aryl "ate" complexes $[Li(DME)_2(Et_2O)]_2[Li(DME)_2][Th(C_6Cl_5)_5]_3$ ([Li][**3.1**]) and $[Li(Et_2O)_4][U(C_6Cl_5)_5]$

([Li][**3.2**]) . During the course of these investigations, we also isolated the closely related heteroleptic actinide-aryl "ate" complexes, $[Li(DME)_2(Et_2O)][Li(Et_2O)_2][ThCl_3(C_6Cl_5)_3]$ ([Li][**3.3**]) and $[Li(Et_2O)_3][UCl_2(C_6Cl_5)_3]$ ([Li][**3.4**]). The electronic structures of all four complexes were analyzed using relativistic density functional theory (DFT) calculations, with the aim of quantifying the 5f subshell participation in the An-C_{ipso} bonds.

3.2 Results and Discussion

3.2.1 Synthesis and Characterization

Addition of cold (-25 °C) solutions of 5 equiv of LiC_6Cl_5[45] to cold (-25 °C) suspensions of $AnCl_4(DME)_n$ (An = Th, n = 2; U, n = 0) in Et_2O results in immediate formation of orange solutions, concomitant with the deposition of flocculent brown-orange precipitates. Work-up of the thorium reaction mixture, followed by crystallization from dichloromethane, affords $[Li(DME)_2(Et_2O)]_2[Li(DME)_2][Th(C_6Cl_5)_5]_3$ ([Li][**3.1**]), which can be isolated as colorless plates in 20% yield (Scheme 3.1). Work-up of the uranium reaction mixture, followed by crystallization from Et_2O, affords $[Li(Et_2O)_4][U(C_6Cl_5)_5]$ ([Li][**3.2**]), which can be isolated as yellow plates in 57% yield (Scheme 3.1). Interestingly, we see no evidence for the formation of octahedral $[An(C_6Cl_5)_6]^{2-}$-type complexes, even when 6 equiv of $Li(C_6Cl_5)$ are used in the reaction.

Scheme 3.1. Synthesis of [Li][**3.1**] and [Li][**3.2**]**.**

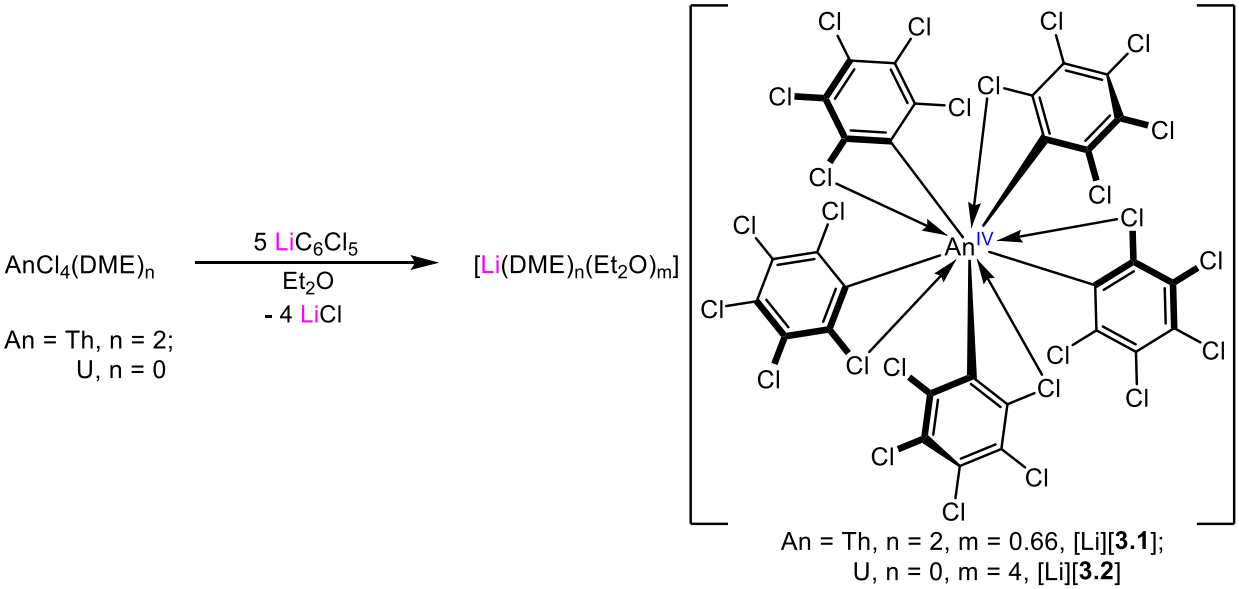

Curiously, the reaction of $ThCl_4(DME)_2$ with 4 equiv of LiC_6Cl_5, performed in an attempt to make the neutral perchlorophenyl complex, $[Th(C_6Cl_5)_4]$, resulted in isolation of heteroleptic Th aryl complex, $[Li(DME)_2(Et_2O)][Li(Et_2O)_2][ThCl_3(C_6Cl_5)_3]$ ([Li][**3.3**]), in low yield, according to an X-ray crystallographic analysis of the crystals isolated upon work-up. Complex [Li][**3.3**] can be made rationally by addition of 3 equiv of LiC_6Cl_5 to a cold (-25 °C) suspension $ThCl_4(DME)_2$ in Et_2O. When synthesized using this stoichiometry, [Li][**3.3**] can be isolated as colorless plates in 54% yield (Scheme 3.2). Similarly, addition of 3 equiv of LiC_6Cl_5 to a cold (-25 °C) suspension UCl_4 in Et_2O results in formation of $[Li(Et_2O)_3][UCl_2(C_6Cl_5)_3]$ ([Li][**3.4**]), which can be isolated as amber plates in 40% yield after work-up (Scheme 3.2). The reactions of UCl_4 with 4 equiv of LiC_6Cl_5 also results in formation of [Li][**3.4**], in similar yields to the 3 equiv reaction.

Scheme 3.2. Synthesis of [Li][**3.3**] and [Li][**3.4**].

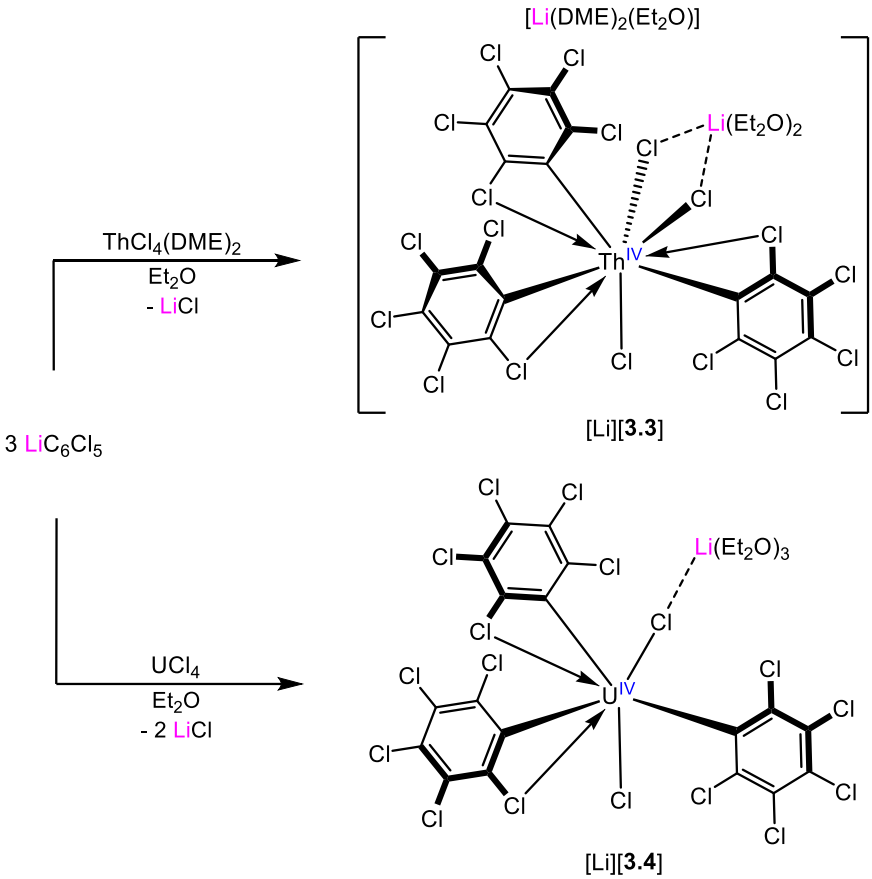

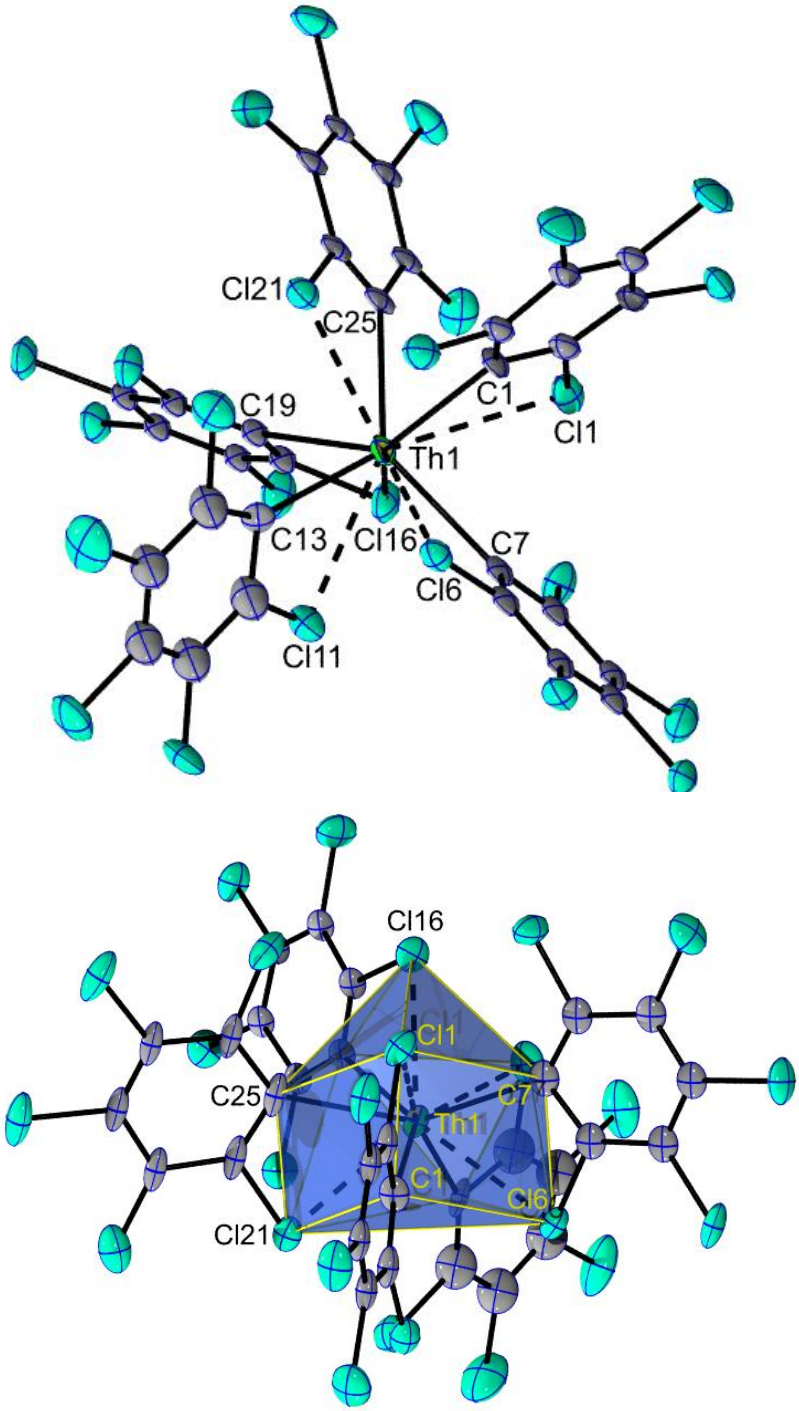

Figure 3.1 Solid-state molecular structure of [Li][**3.1**]·2.5Et_2O·2CH_2Cl_2 shown with 50% probability ellipsoids (top). Solid-state molecular structure of [Li][**3.1**]·2.5Et_2O·2CH_2Cl_2 with

the sphenocorona polygon shown in blue (bottom). All hydrogen atoms, solvate molecules, two $[Th(C_6Cl_5)_5]^-$ moieties, and Li^+ counterions have been omitted for clarity.

Both [Li][**3.1**] and [Li][**3.2**] are air- and moisture-sensitive crystalline solids that are soluble in ethereal solvents, methylene chloride, and benzene, and slightly soluble in hexanes. Additionally, [Li][**3.1**] is soluble in pyridine and acetonitrile, however [Li][**3.2**] reacts immediately upon dissolution in pyridine, resulting in formation of an intractable dark brown solution. Similarly, dissolution of [Li][**3.2**] in acetonitrile results in immediate formation of an intractable orange-brown solution concomitant with precipitation of a dark brown solid. Both [Li][**3.1**] and [Li][**3.2**] exhibit moderate thermal stability in solution. For example, solutions of [Li][**3.1**] or [Li][**3.2**] in CH_2Cl_2 exhibit minimal evidence of decomposition after standing at room temperature for 1 h. However, on standing at room temperature for 24 h, solutions of [Li][**3.1**] in methylene chloride-d_2 exhibit partial conversion to [Li][**3.3**], according to $^{13}C\{^1H\}$ NMR spectroscopy (Figure 3.13), presumably via C-Cl bond activation of the solvent. In contrast, solutions of [Li][**3.2**] completely convert into intractable mixtures in methylene chloride-d_2 over this time frame (Figure 3.15). It is not immediately apparent why [Li][**3.2**] is more reactive that [Li][**3.1**], but we note that a similar reactivity pattern is observed for $[An(C_6H_5)_6]^{2-}$ and $[Cp^*_2An(C_6H_5)_2]$ (An = Th, U),[19, 22, 46] where the uranium analogues exhibit greater thermal sensitivity than the thorium analogues.

Complex [Li][**3.1**] crystallizes in the monoclinic space group $P2_1/n$ with three independent molecules in the asymmetric unit (Figure 3.1 and Table 3.1). It crystallizes as the Et_2O and CH_2Cl_2 solvate, [Li][**3.1**]·2.5Et_2O·2CH_2Cl_2. Its asymmetric unit reveals one ten-coordinate thorium center and two nine-coordinate thorium centers. According to the continuous shape measure,[47] the 10-coordinate Th center, Th1, is best described as a C_{2v}-symmetric

sphenocorona, wherein the two square faces are defined by C1, C7, Cl1, and Cl16, and C1, C25, Cl1, and Cl21, respectively. This geometry is common for 10-coordinate complexes featuring bidentate ligands.[48] The two 9-coordinate metal centers are best described as distorted tricapped trigonal prisms.[49, 50] For Th2, the three capping atoms are C31, C43, and Cl46, whereas for Th3, the three capping atoms are C73, C85, and Cl51. The ten coordinate center in [Li][**3.1**] features five Th-C σ-bonds and five Cl→Th dative interactions involving the *ortho*-Cl atoms of the C_6Cl_5 ligands, although one of these Cl→Th dative interactions is quite long (Th1-Cl1 = 3.257(5) Å; see below for more discussion). The nine coordinate centers in [Li][**3.1**] are formed by five An-C σ-bonds and four Cl→An dative interactions. The κ^2 coordination mode generated by the Cl→An dative interaction has been previously observed for a handful of $[C_6Cl_5]^-$ complexes, including $Pt(C_6Cl_5)_4$.[38, 42, 43] The average Th-C bond length in [Li][**3.1**] is 2.65 Å (range = 2.628(18) – 2.693(18) Å), which is similar those found in other σ-bonded thorium aryl complexes.[19, 21] For example, the Th-C bond length in $[Li(DME)_3]_2[Th(C_6H_5)_6]$[19] is 2.589(3) Å, whereas the average Th-C bond length in $[Th(2\text{-}C_6H_4CH_2NMe_2)_4]$[21] is 2.549(2) Å (range = 2.497(3) – 2.544(3) Å). Additionally, both the 10-coordinate and 9-coordinate Th centers in [Li][**3.1**] exhibit identical average Th-C bond lengths. The aryl rings in [Li][**3.1**] feature disparate Th-C_{ipso}-C_{ortho} angles, a consequence of the Cl→An dative interactions. For example, the Th-C1-C2 angle is 110(1)°, whereas the Th1-C1-C6 angle is 134(1)°. The average Cl→Th bond length in [Li][**3.1**] is 3.09 Å (range = 3.018(5) – 3.257(5) Å). No other complexes with Cl→An interactions are available for comparison, but several complexes with F→An interactions are known.[51] For example, the F→U distances in $[Cp^*_2Co][U(OB(C_6F_5)_3)_2(^{Ar}acnac)(OEt_2)]$[52] are 2.762(6) and 2.789(5) Å, whereas the F→U distances in $[U(N(C_6F_5)_2)_4]$ are 2.6480(11) and 2.5989(11) Å.[53] Not

surprisingly, these values are much shorter than the Cl→An interactions observed in [Li][**3.1**]. One ten-coordinate and one nine-coordinate center in [Li][**3.1**] each exhibit an outer sphere cation $[Li(DME)_2(Et_2O)]^+$, while the other nine-coordinate thorium center in [Li][**3.1**] features a $[Li(DME)_2]^+$ cation that also interacts with the *ortho*-Cl and *meta*-Cl atoms of one C_6Cl_5 ligand. The observation of two different Th coordination geometries in the solid-state can be explained by small differences in local crystal packing, and indicates that the long Cl→Th dative interaction (e.g., Th1-Cl1) is not particularly strong.

Complex [Li][**3.2**] crystallizes in the monoclinic space group $P2_1/c$ (Figure S15). The solid-state molecular structure of [Li][**3.2**] reveals a ten-coordinate uranium center formed by five An-C σ-bonds and five Cl→An dative interactions involving the *ortho*-Cl atoms of the C_6Cl_5 ligands.[48] According to the continuous shape measure,[47] the coordination geometry about the U center is best described as a C_{2v}-symmetric sphenocorona, wherein the two square faces are defined by Cl16, C13, Cl6, and Cl1, and C13, C25, Cl11, Cl16, respectively. The average U-C bond length in [Li][**3.2**] is 2.55 Å (range = 2.52(2) – 2.59(2) Å), which is shorter than the Th-C distances in [Li][**3.1**], consistent with smaller ionic radius of the U(IV) ion.[54] The U-C bond lengths in [Li][**3.2**] are also similar to those observed in other uranium aryl complexes, such as $[Li(Et_2O)_2(THF)][UO_2(C_6Cl_5)_3]$,[25] which features U-C distances from 2.55(1) to 2.63(1) Å, and $[Li(THF)_4][Li(THF)][U(C_6H_5)_6]$,[22] which features an average U-C bond length of 2.52 Å. The latter structure also features H→U agostic interactions, which are similar to the Cl→An interactions found in [Li][**3.1**] and [Li][**3.2**]. The aryl rings in [Li][**3.2**] feature disparate U-C_{ipso}-C_{ortho} angles (e.g., U1-C1-C2 = 113(1)°, U1-C1-C6 = 135(1)°), which is a consequence of the Cl→An dative interactions. Finally, the average Cl→U distance

in [Li][**3.2**] is 3.13 Å (range = 3.006(4) – 3.250(4) Å), which is similar to that found in [Li][**3.1**].

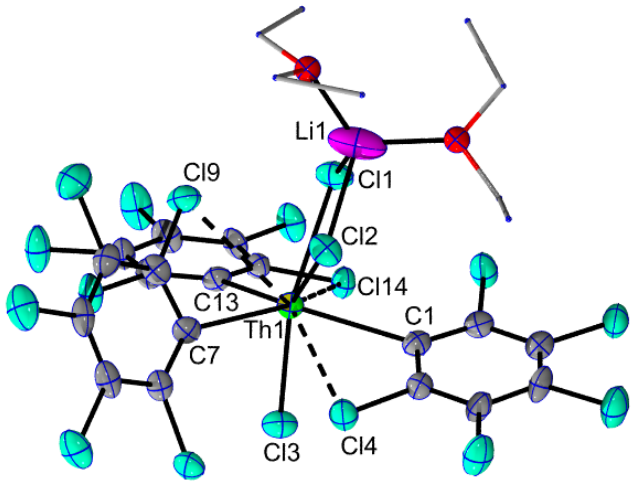

Figure 3.2. Solid-state molecular structure of [Li][**3.3**] shown with 50% probability ellipsoids. All hydrogen atoms and a $[Li(DME)_2(Et_2O)]^+$ counterion have been omitted for clarity.

Complex [Li][**3.3**] crystallizes in the triclinic space group *P*1 (Figure 3.2). Its solid-state molecular structure reveals a 9-coordinate thorium center bound by three chloride ligands, three carbon atoms of the pentachlorophenyl ligands, and three Cl→Th dative interactions involving the *ortho*-Cl atoms of the pentachlorophenyl ligands. The coordination geometry about its Th center can be described as distorted tricapped trigonal prism,[47, 55] wherein the three capping atoms are Cl4, Cl9, and Cl14. The average Th-C bond length in [Li][**3.3**] is 2.65 Å (range = 2.631(6) – 2.654(6) Å), which is similar to Th-C bond lengths in [Li][**3.1**]. The average Th-Cl distance in [Li][**3.3**] is 2.77 Å (range = 2.671(2) – 2.839(2) Å), which is

slightly longer than the average Th-Cl bond length in $ThCl_4(DME)_2$ (2.690 Å),[56] whereas the average Cl→An dative interactions in [Li][**3.3**] is 3.19 Å (range = 3.148(2) – 3.248(2) Å). Finally, the $[Li(Et_2O)_2]^+$ cation in [Li][**3.3**] features bridging interaction with two chloride ligands. The resulting Li-Cl distances are 2.37(2) Å and 2.39(2) Å.

Complex [Li][**3.4**] also crystallizes in the triclinic space group *P*1 (Figure 3.3). Its solid-state molecular structure reveals a 7-coordinate uranium center bound by two chloride ligands, three carbon atoms of the pentachlorophenyl ligand, and two long Cl→U dative interactions involving the *ortho*-Cl atoms of the pentachlorophenyl ligands (e.g., U1-Cl3 = 3.226(4), U1-Cl8 = 3.227(3) Å). Ignoring the long Cl→U dative interactions, the coordination geometry about the U center is best described as trigonal bipyramid. The average U-C bond length in [Li][**3.4**] is 2.50 Å (range = 2.50(1) – 2.51(1) Å) and is similar to that seen in [Li][**3.2**] but shorter than that seen in [Li][**3.3**], consistent with smaller ionic radius of U(IV) ion.[54] The average U-Cl bond length in [Li][**3.4**] is 2.59 Å (range = 2.591(4) – 2.594(4) Å), consistent with the average U-Cl bond length of 2.62 Å in $UCl_4(DME)_2$.[57] Finally, the $[Li(Et_2O)_3]^+$ cation in [Li][**3.4**] features a bridging interaction with a chloride ligand. The resulting Li-Cl distance is 2.69(5) Å.

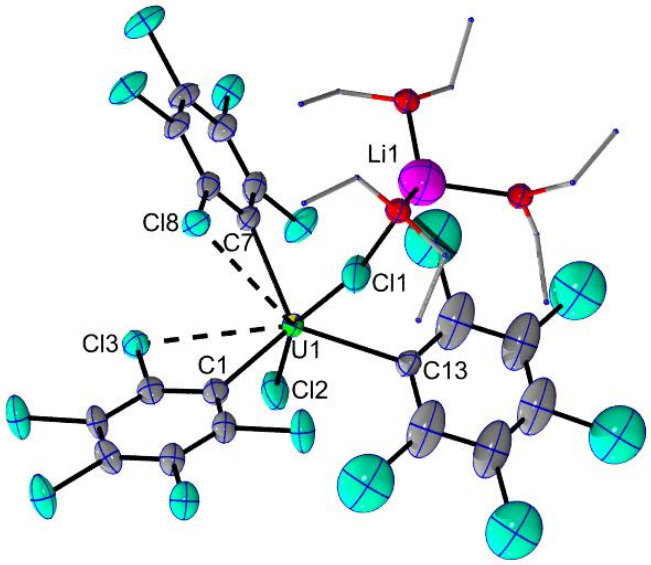

Figure 3.3. Solid-state molecular structure of [Li][**3.3**] shown with 50% probability ellipsoids. All hydrogen atoms and a $[Li(DME)_2(Et_2O)]^+$ counterion have been omitted for clarity.

Table 3.1. Selected metrical parameters for [Li][**3.1**]·2.5Et_2O·2CH_2Cl_2, [Li][**3.2**], [Li][**3.3**], and [Li][**3.4**].

Complex	[Li][**3.1**]·2.5Et_2O·2CH_2Cl_2			[Li][**3.2**]	[Li][**3.3**]	[Li][**3.4**]
An-C	Th1	Th2	Th3	2.518(17) 2.537(15) 2.541(12) 2.555(17) 2.592(16)	2.631(6) 2.653(6) 2.654(6)	2.497(13) 2.504(13) 2.505(14)
	2.633(16) 2.646(17) 2.649(18) 2.670(19) 2.673(17)	2.628(18) 2.637(17) 2.639(16) 2.656(19) 2.678(19)	2.631(18) 2.641(18) 2.645(17) 2.66(2) 2.693(18)			
Cl→An	3.018(5) 3.068(5) 3.073(5) 3.101(4) 3.257(5)	3.033(5) 3.064(5) 3.069(4) 3.107(5)	3.073(5) 3.092(6) 3.115(5) 3.122(5)	3.006(4) 3.071(5) 3.121(4) 3.197(4) 3.255(4)	3.1489(19) 3.1776(17) 3.2477(17)	3.226(4) 3.227(3)
An-Cl					2.6702(17) 2.7887(18) 2.8390(18)	2.591(4) 2.594(4)

The $^{13}C\{^1H\}$ NMR spectrum of [Li][**3.1**], recorded at room temperature in dichloromethane-d_2, features a resonance at 198.78 ppm (Figure 3.4), attributable to the *ipso* carbon of the pentachlorophenyl ligand, as well as resonances at 138.66, 131.03, and 130.13 ppm, assignable to the *ortho*, *meta*, and *para* resonances of the pentachlorophenyl ligand, respectively. The $^{13}C\{^1H\}$ NMR spectrum of [Li][**3.3**], recorded at room temperature in dichloromethane-d_2, features a resonance at 201.01 ppm (Figure 3.18), attributable to the *ipso* carbon of the pentachlorophenyl ligand, as well as resonances at 137.20, 131.96, and 129.53 ppm, assignable to the *ortho*, *meta*, and *para* resonances of the pentachlorophenyl ligand, respectively. The observation of only one aryl environment for both [Li][**3.1**] and [Li][**3.3**] in their $^{13}C\{^1H\}$ NMR spectra is evidence for exchange of the Cl→Th dative interactions at a rate faster than the NMR time scale, which renders the aryl ligands magnetically equivalent. The $^{13}C\{^1H\}$ NMR spectra of both [Li][**3.1**] and [Li][**3.3**] feature smaller downfield C_{ipso}

resonances compared to $[Li(Et_2O)_2(THF)][UO_2(C_6Cl_5)_3]$ ([Li][**2.1**]), which featured a C_{ipso} resonance at 236.7 ppm.[25]

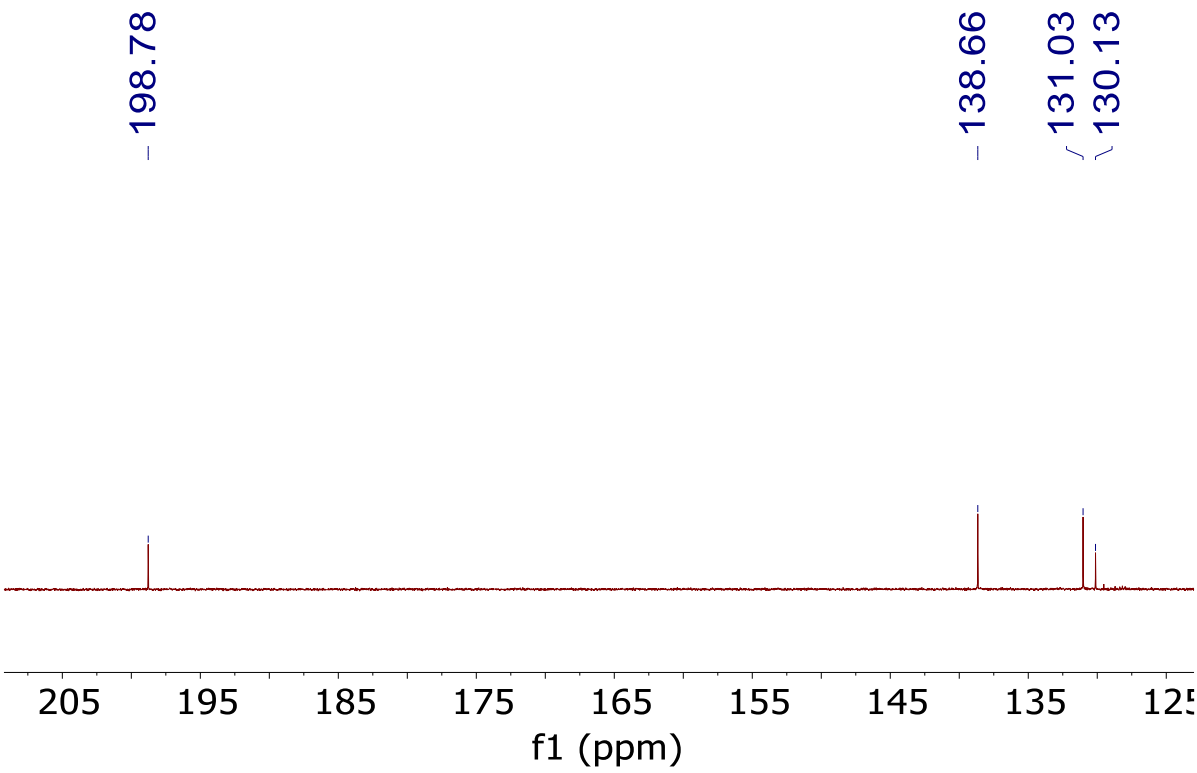

Figure 3.4. Partial $^{13}C\{^1H\}$ NMR spectrum of [Li][**3.1**] in methylene chloride-d_2.

The $^7Li\{^1H\}$ NMR spectra for [Li][**3.1**] and [Li][**3.3**] in dichloromethane-d_2 feature sharp resonances at -0.79 ppm and -0.83 ppm, respectively (Figure 3.10 and Figure 3.17). In contrast, the $^7Li\{^1H\}$ NMR spectrum of [Li][**3.2**] in dichloromethane-d_2 features a broad resonance at 0.52 ppm (Figure 3.14), consistent with the paramagnetism of this material. The $^7Li\{^1H\}$ NMR spectrum of [Li][**3.4**] in benzene-d_6 features a broad resonance at 29.59 ppm (Figure 3.20). The large downfield shift is consistent with formation of a contact ion pair in solution. Similar behavior has been observed previously for uranium aryl and uranium benzyne complexes.[58]

3.2.2 Computational Analysis

To gain a detailed understanding of the electronic structures and bonding interactions within [Li][**3.1**], [Li][**3.2**], [Li][**3.3**], and [Li][**3.3**], Dr. Xiaojuan Yu and Prof. Jochen Autschbach at the State University of New York at Buffalo carried out relativistic DFT calculations on their anionic components, namely, [**3.1**]$^-$, [**3.2**]$^-$, [**3.3**]$^-$, and [**3.4**]$^-$.[59-61] Full computational details are described in the Supporting Information. The ground states of [**3.1**]$^-$ and [**3.3**]$^-$ are closed-shell spin singlet configurations, whereas the ground states of [**3.2**]$^-$ and [**3.4**]$^-$ are spin triplets because of the two unpaired electrons of the U^{4+} ion. As shown previously by wavefunction calculations,[62, 63] the ground state for Th(IV) is not strongly multi-configurational, and can therefore be described by (single determinant) Kohn-Sham DFT calculations with approximate functionals. Further evidence for the lack of multi-configurational character in the present systems are the large HOMO and LUMO gaps calculated for [**3.1**]$^-$ and [**3.3**]$^-$, at 3.0 and 3.4 eV, respectively. In other words, there are no complications due to the presence of nearly degenerate frontier orbitals in the DFT calculations for these molecules. Natural localized molecular orbital (NLMO) analysis (Figure 3.5 and Table 3.5) confirms the Cl→An dative bonding from the close-contact chlorine atoms of the C_6Cl_5 ligands that is evident from the crystal structures. The lone pair donation from these chlorines have on average 7/8/6/5% weight at the actinide center in **[3.1/3.2/3.3/3.4]**$^-$, respectively. Not surprisingly, however, the dative bonding from the chloride ligands in [**3.3**]$^-$ and [**3.4**]$^-$ is stronger, with an average of 12 and 14% weight, respectively, at the actinide.

The NLMO analysis further shows that the Th-C_{ipso} interactions in [**3.1**]$^-$ and [**3.3**]$^-$ are quite similar (Figure 3.5). This similarity is also indicated by averaged Th-C_{ipso} Wiberg bond orders of 0.47 for [**3.1**]$^-$ and 0.49 for [**3.3**]$^-$, respectively. The interactions between the *ipso*-

carbon atoms and thorium can be viewed as two-center two-electron (2c-2e) σ-donation bonding from the negatively charged ligand, with the Th weight in the corresponding σ-bonding NLMOs ranging from 14 to 15%. Of these weights, the Th 5f contributions are 24% in [**3.1**]$^-$ and 22% in [**3.3**]$^-$. In comparison, the two uranium complexes, [**3.2**]$^-$ and [**3.4**]$^-$, feature stronger covalency in their U-C bonds, along with more pronounced participation of the 5f AOs. The U weights in the σ-bonding NLMOs range from 18% in [**3.2**]$^-$ to 21% in [**3.4**]$^-$, of which the 5f contributions are 36% and 30%, respectively. The increased covalency, compared to the Th complexes, is reflected in increased averaged U-C_{ipso} Wiberg bond orders of 0.56 in [**3.2**]$^-$ and 0.64 in [**3.4**]$^-$, respectively. Similar bonding trends are observed for both $[An(C_6H_5)_6]^{2-}$ (An = Th, U) and $[AnMe_6]^{2-}$ (An = Th, U).[4, 10, 22] For example, the An-C bonds in $[U(C_6H_5)_6]^{2-}$ feature both a greater degree of covalency (23% total metal character for U vs. 16% for Th) and 5f character (38% for U vs. 20% for Th) than its Th analogue.[22]

Various approximate density functionals (BP86, PBE, and PBE0) were used for calculating the ^{13}C NMR chemical shifts for the *ipso*-carbon in [**3.1**]$^-$ and [**3.3**]$^-$. As seen in Table 3.2, the averaged calculated chemical shifts for both complexes are only weakly dependent on the choice of the functional. The calculated chemical shifts are in acceptable agreement with the measurements. We focus on the PBE/SO-PBE results in the following discussion, unless stated otherwise. For [**3.1**]$^-$, the calculated C_{ipso} chemical shift is 203 ppm (expt. = 199 ppm), including a 27 ppm deshielding due to SO coupling. The C_{ipso} chemical shift in [**3.3**]$^-$ is calculated to be a bit larger than that in [**3.1**]$^-$, in agreement with the experiments, although the shift difference is slightly exaggerated in the calculations. The deshielding caused by SO coupling effects (ca. 29 ppm) is comparable that found in [**3.1**]$^-$, which reflects the similarity in their chemical bonding. The *ipso*-carbon SO deshielding in

both [**3.1**]$^-$ and [**3.3**]$^-$ is correlated to the Th 5f and 6d character of the σ(Th-C) NLMO, and the overall weights of actinide AOs in these bonds (i.e., the degree of covalency). Our previous calculation[25] for $[Li(Et_2O)_2(THF)][UO_2(C_6Cl_5)_3]$ found a significantly larger SO deshielding, up to 68 ppm, due to a combination of large U weight (20% overall) and 5f contribution (43% of the U weight). This difference reflects both the change in element and the higher oxidation state in the uranyl example. Similarly, we would expect stronger SO effects for the *ipso*-carbon chemical shifts in our U(IV) complexes, compared to their thorium counterparts. However, the paramagnetism of [**3.2**]$^-$ and [**3.4**]$^-$ causes too much broadening of the relevant NMR signals for them to be observed. It also renders calculations of the NMR chemical shifts much more difficult,[64] and the role of SO coupling would not be as clear-cut as it is in the diamagnetic counterparts. Thus, we decided to forego calculations of the shifts for [**3.2**]$^-$ and [**3.4**]$^-$, because the bond analyses already paint a clear picture. Interestingly, the SO-induced chemical shift in $[Th(C_6H_5)_6]^{2-}$ (40 ppm, present work) is calculated to be 13 ppm larger than that of [**3.1**]$^-$ (27 ppm), despite the former complex having a smaller 5f weight in the Th contributions to the Th-C bonds. This decrease, however, is more than compensated for by the slightly greater overall Th weight and carbon 2s character in its Th-C bonds (Table 3.2 and Table 3.5).

Table 3.2. Calculated carbon shielding (σ) and chemical shift (δ) for the C_{ipso} atom center of [**3.1**]$^-$, [**3.3**]$^-$, and $[Th(C_6H_5)_6]^{2-}$(*C*$_3$), using various functionals.[a]

Complex	Functional	σ_{calc} (ppm)	δ_{calc} (ppm)	δ_{expt} (ppm)
TMS	BP86/SO-BP86	186.9 / 187.8	-	-
	PBE/SO-PBE	187.5 / 188.4	-	
	PBE0/SO-PBE0 (25%)[b]	192.2 / 193.0	-	
	PBE0/SO-PBE0 (40%)[b]	194.7 / 195.6	-	
[3.1]$^-$	BP86/SO-BP86	10.7 / –16.8	176.2 / 204.6	198.78
	PBE/SO-PBE	11.3 / –14.8	176.2 / 203.2	
	PBE0/SO-PBE0 (25%)	13.9 / –10.8	178.3 / 203.8	
	PBE0/SO-PBE0 (40%)	15.8 / –8.3	178.9 / 203.9	
[3.3]$^-$	BP86/SO-BP86	3.9 / –25.3	183.0 / 213.1	201.01
	PBE/SO-PBE	4.5 / –23.3	183.0 / 211.7	
	PBE0/SO-PBE0 (25%)	5.5 / –20.8	186.7 / 213.8	
	PBE0/SO-PBE0 (40%)	6.8 / –19.0	187.9 / 214.6	
$[Th(C_6H_5)_6]^{2-}$[c]	PBE/SO-PBE	–21.2 /–60.1	208.7 / 248.5	220.5
	PBE0/SO-PBE0 (40%)	–15.5 / –53.4	210.2 / 249.0	

[a] NMR shifts calculated at the SO ZORA- level using the TZ2P basis set, with 'FXC' option. The calculated chemical shifts were averaged over equivalent C_{ipso} nuclei. Dichloromethane (solvent) was considered in the COSMO model for all the computations.

[b] The percentages in parentheses of functional column indicate the portion of exact exchange in the functional.

[c] For comparison, the carbon shielding and chemical shift for the C_{ipso} atom in *C*$_3$-symmetric $[Th(C_6H_5)_6]^{2-}$ was re-calculated using the same procedure as other complexes, such as using the 'FXC' option and same solvent (see computational details). The experimental chemical shift for this complex was taken from Ref.[19]

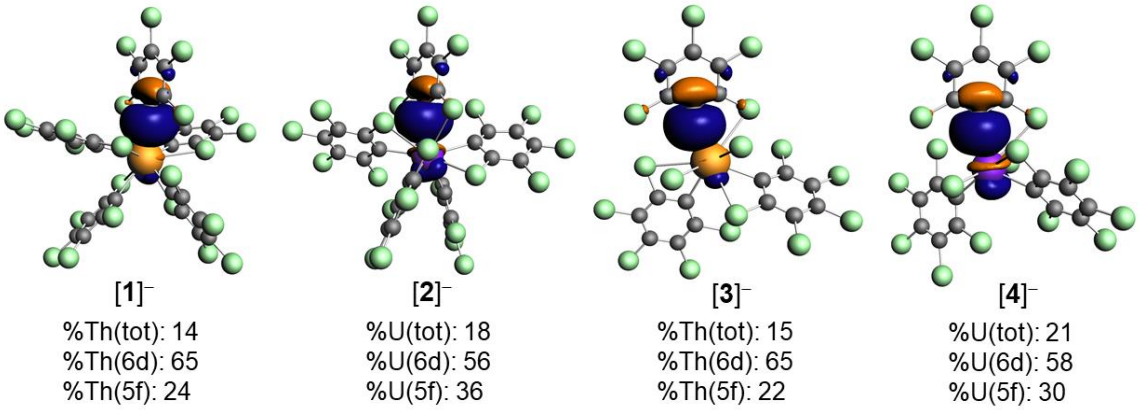

Figure 3.5. Representative An-C bonding NLMOs (An=Th or U) in [**3.1**]$^{-}$, [**3.2**]$^{-}$, [**3.3**]$^{-}$, and [**3.4**]$^{-}$. Weight-% metal character and 6d vs. 5f contributions at the metal averaged over equivalent NLMOs. (Isosurface values ±0.03 a.u. Color code for atoms: Th orange, U purple, Cl green, C gray.)

3.3 Summary

In summary, I have prepared and characterized two homoleptic actinide-aryl "ate" complexes, $[Li(DME)_2(Et_2O)]_2[Li(DME)_2][Th(C_6Cl_5)_5]_3$ and $[Li(Et_2O)_4][U(C_6Cl_5)_5]$, and have confirmed their formulation by X-ray crystallography. These two complexes represent the first isolated homoleptic perhaloaryl complexes of the actinides. They exhibit remarkable thermal stability – much greater than past homoleptic actinide aryl complexes – likely on account of the *o*-chloro substitution of the $[C_6Cl_5]^-$ ligand, combined with the many Cl→An dative interactions. Additionally, I prepared and characterized two heteroleptic actinide-aryl "ate" complexes, $[Li(DME)_2(Et_2O)][Li(Et_2O)_2][ThCl_3(C_6Cl_5)_3]$ and $[Li(Et_2O)_3][UCl_2(C_6Cl_5)_3]$. Analysis of the An-C bonding with these complexes by DFT reveals both greater covalency and greater 5f orbital participation in the U(IV) derivatives, consistent with past periodic trends. In addition, a DFT analysis of the C_{ipso} chemical shifts

in the two Th complexes reveals modest levels of spin-orbit induced shielding due to 5f participation in the Th-C bonds, providing us with an opportunity to further refine the ^{13}C NMR spectroscopic analysis of An-L bonding.

3.4 Experimental

3.4.1 General Procedures

All reactions and subsequent manipulations were performed under anaerobic and anhydrous conditions under an atmosphere of dinitrogen. Hexanes, diethyl ether (Et_2O), and toluene were dried using a Vacuum Atmospheres DRI-SOLV Solvent Purification system and stored over 3Å sieves for 24 h prior to use. Tetrahydrofuran (THF) was distilled over Na/benzophenone and stored over activated 3 Å molecular sieves for 24 h prior to use. Benzene-d_6 and thf-d_8 were dried over 3Å molecular sieves for 24 h prior to use. LiC_6Cl_5,[45] UCl_4,[65] and $ThCl_4(DME)_2$[56] were synthesized according to the previously reported procedures. All other reagents were purchased from commercial suppliers and used as received.

^1H, $^{13}C\{^1H\}$, and $^7Li\{^1H\}$ NMR spectra were recorded on an Agilent Technologies 400-MR DD2 400 MHz spectrometer or a Bruker AVANCE NEO 500 MHz spectrometer. ^1H and $^{13}C\{^1H\}$ NMR spectra were referenced to external tetramethylsilane (TMS) using the residual protio solvent peaks as internal standards. $^7Li\{^1H\}$ NMR spectra are referenced indirectly with the ^1H chemical shift of TMS at 0 ppm, according to IUPAC standard.[66, 67] IR spectra were recorded on a Nicolet 6700 FT-IR spectrometer. Elemental analyses were performed by the Microanalytical Laboratory at the University of California (Berkeley, CA).

Caution! *Depleted uranium (isotope ^{238}U) and naturally-abundant thorium are weak alpha emitters with a half-life of 4.47×10^9 years and 1.41×10^{10} years, respectively.*

Manipulations and reactions should be carried out in a fume hood or inert atmosphere glovebox in a laboratory equipped with α- and β-counting equipment.

3.4.2 Synthesis of [LiC_6Cl_6]

The synthesis of LiC_6Cl_5 was done according to the literature procedure with slight modifications.[45] A cold solution (–25 °C) of *n*-BuLi in hexanes (0.2 mL, 0.50 mmol, 2.5 M) was added dropwise to a cold, stirring suspension (–25 °C) of C_6Cl_6 (142.4 mg, 0.50 mmol) in Et_2O (2 mL). Upon addition of *n*-BuLi, the solids dissolved and solution became a golden color. The resulting LiC_6Cl_5 solution was used as is, and assumed to be 0.25 M. The $^7Li\{^1H\}$ NMR spectrum of LiC_6Cl_5 in benzene-d_6 displays a single resonance at 0.89 ppm.

3.4.3 Synthesis of [$Li(DME)_2$][$Li(DME)_2(Et_2O)$]$_2$[$Th(C_6Cl_5)_5$]$_3$ ([Li][3.1])

A cold (-25 °C) solution of LiC_6Cl_5 (2 mL in Et_2O, 0.50 mmol, 0.25 M) was added to a cold (-25 °C), stirring suspension of $ThCl_4(DME)_2$ (55.4 mg, 0.1 mmol) in Et_2O (2 mL). This resulted in an immediate color change to yellow, concomitant with the deposition of a flocculent yellow precipitate. After 10 min of stirring, the reaction mixture was filtered through a Celite column (0.5 cm × 5 cm) supported on glass wool to afford a clear, yellow filtrate. The volume of the filtrate was reduced to 2 mL *in vacuo*, hexanes (3 mL) was layered onto the solution, and the sample was stored at –25 °C for 24 h, which resulted in the deposition of amorphous solid. The yellow-orange amorphous solid was isolated by decanting the supernatant and then dissolved in CH_2Cl_2 (4 mL) to afford a pale yellow solution. The solution was filtered through a Celite column (0.5 cm × 5 cm) supported on glass wool to afford a clear, pale yellow filtrate. The volume of the filtrate was reduced to 2 mL *in vacuo*, pentane (5 mL) was layered onto the solution, and the sample was stored at –25 °C for 24 h,

which resulted in the deposition of colorless plates. The solid was isolated by decanting the supernatant and then dried briefly *in vacuo* (34 mg, 20% yield). Anal. Calcd for $C_{122}H_{80}Li_3O_{14}Cl_{75}Th_3$: C, 28.47; H, 1.57 Found: C, 28.16; H, 1.21. ^{1}H NMR (500 MHz, 25 °C, methylene chloride-d_2): δ 3.70 (s, $CH_3OC\mathit{H}_2$), 3.51 (s, $C\mathit{H}_3OCH_2$), 3.43 (m, $OC\mathit{H}_2CH_3$), 1.15 (t, $OCH_2C\mathit{H}_3$). ^{13}C{^{1}H} NMR (500 MHz, 25 °C, methylene chloride-d_2): δ 198.78 (*i*-C), 138.66 (*o*-C), 131.03 (*m*-C), 130.31 (*p*-C), 70.99 ($\mathit{C}H_3OCH_2$), 60.11 ($CH_3O\mathit{C}H_2$). ^{7}Li{^{1}H} NMR (400 MHz, 25 °C, methylene chloride-d_2): δ -0.79 (s). IR (KBr pellet, cm^{-1}): 3461 (w), 3112 (vw), 3066 (w), 3004 (w), 2933 (w), 2931 (w), 2885 (w), 2850 (w), 2833 (m), 2337 (vw), 2088 (vw), 1945 (vw), 1729 (w), 1556 (w), 1541 (w), 1523 (m), 1506 (s), 1473 (s), 1452 (s), 1419 (m), 1396 (s), 1369 (m), 1334 (s), 1319 (s), 1307 (s), 1276 (s), 1245 (s), 1226 (s), 1191 (s), 1170 (s), 1120 (s), 1108 (s), 1079 (s), 1054 (s), 1029 (s), 987 (m), 944 (m) 906 (w), 866 (s), 840 (w), 815 (s), 738 (m), 701 (w), 684 (s), 661 (s), 578 (w), 563 (m), 555 (m), 526 (w), 457 (w), 433 (w), 408 (w).

3.4.4 Synthesis of $[Li(Et_2O)_4][U(C_6Cl_5)_5]$ ([Li][3.2])

A cold (-25 °C) solution of LiC_6Cl_5 (2 mL in Et_2O, 0.5 mmol, 0.25 M) was added to a cold (-25 °C), suspension of UCl_4 (37.9 mg, 0.1 mmol) in Et_2O (2 mL). This resulted in an immediate color change to orange concomitant with the deposition of a flocculent orange-brown precipitate. After 10 min, the reaction mixture was filtered through a Celite column (0.5 cm × 5 cm) supported on glass wool to afford a clear, orange filtrate. The volume of the filtrate was reduced to 2 mL *in vacuo*, hexanes (5 mL) was layered onto the solution, and the sample was stored at –25 °C for 24 h, which resulted in the deposition of yellow plates. The solid was isolated by decanting the supernatant and then dried *in vacuo* (102.4 mg, 57% yield). Anal. Calcd for $C_{46}H_{40}LiO_5Cl_{25}U$: C, 30.90; H, 2.26. Found: C, 29.41; H, 1.91. ^{1}H NMR (500

MHz, 25 °C, methylene chloride-d_2): δ 3.62 (br s, 16H, OCH_2CH$_3$), 1.30 (br s, 24H, OCH$_2$CH_3). ^{7}Li{^{1}H} NMR (400 MHz, 25 °C, methylene chloride-d_2): δ 0.52 (br s). IR (KBr pellet, cm^{-1}): 3419 (w), 3110 (w), 3066 (w), 2975 (w), 2933 (w), 2883 (w), 1637 (w), 1558 (w), 1535 (w), 1525 (m), 1506 (m), 1490 (m), 1473 (w), 1452 (m), 1446 (m), 1421 (w), 1411 (w), 1396 (s), 1334 (s), 1307 (s), 1319 (s), 1278 (s), 1226 (m), 1180 (w), 1170 (s), 1151 (m), 1128 (m), 1087 (s), 1056 (s), 943 (vw), 900 (w), 890 (w), 865 (m), 838 (w), 831 (w), 819 (s), 755 (w), 701 (w), 682 (s), 665 (s), 582 (m), 563 (m), 557 (m), 526 (w), 408 (w).

3.4.5 Synthesis of [Li(DME)$_2$(Et$_2$O)][Li(Et$_2$O)$_2$][ThCl$_3$(C$_6$Cl$_5$)$_3$] ([Li][3.3])

Method A. A cold (-25 °C) solution of LiC$_6$Cl$_5$ (2 mL in Et$_2$O, 0.5 mmol, 0.25 M) was added to a cold (-25 °C), stirring suspension of ThCl$_4$(DME)$_2$ (92.3 mg, 0.167 mmol) in Et$_2$O (2 mL). This resulted in an immediate color change to yellow-orange, concomitant with the deposition of a flocculent yellow-orange precipitate. After 10 min of stirring, the reaction mixture was filtered through a Celite column (0.5 cm × 5 cm) supported on glass wool to afford a clear, yellow-orange filtrate. The volume of the filtrate was reduced to 2 mL *in vacuo*, hexanes (5 mL) was layered onto the solution, and the sample was stored at –25 °C for 24 h, which resulted in the deposition of pale orange plates. The solid was isolated by decanting the supernatant and then dried *in vacuo* (136 mg, 54 % yield). Anal. Calcd for C$_{38}$H$_{50}$Cl$_{18}$Li$_2$O$_7$Th: C, 30.37; H, 3.35. Found (1st attempt): C, 27.06; H, 3.19. Found (2nd attempt):C, 27.49; H, 2.86. Elemental analysis consistently showed low carbon content, possibly due to incomplete combustion. ^{1}H NMR (500 MHz, 25 °C, methylene chloride-d_2): δ 3.62 (s, 8H, CH$_3$OCH_2), 3.45 (s, 12H, CH_3OCH$_2$), 3.43 (m, 12H, OCH_2CH$_3$), 1.15 (t, 18H, OCH$_2$CH_3). ^{13}C{^{1}H} NMR (500 MHz, 25 °C, methylene chloride-d_2): δ 201.01 (*i*-C), 137.20 (*o*-C), 131.96 (*m*-C), 129.53 (*p*-C), 71.20 (*C*H$_3$OCH$_2$), 66.07 (O*C*H$_2$CH$_3$), 59.91 (CH$_3$O*C*H$_2$),

15.49 (CH_2CH_3). $^{7}Li\{^{1}H\}$ NMR (400 MHz, 25 °C, methylene chloride-d_2): δ -0.83 (s). IR (KBr pellet, cm^{-1}): 3415 (w), 3110 (w), 3066 (w), 2931 (m), 2883 (m), 2831 (m), 2753 (w), 2724 (w), 2339 (w), 2183 (w), 2092 (w), 1945 (w), 1729 (w), 1637 (w), 1629 (w), 1556 (m), 1538 (w), 1523 (s), 1506 (s), 1473 (s), 1452 (s), 1396 (s), 1367 (s), 1334 (s), 1317 (s), 1313 (s), 1276 (s), 1243 (m), 1226 (m), 1211 (m), 1191 (m), 1170 (s), 1122 (s), 1108 (s), 1083 (s), 1052 (s), 1027 (s), 981 (m), 946 (w), 912 (w), 865 (s), 838 (m), 821 (s), 813 (s), 721 (w), 701 (w), 684 (s), 659 (s), 570 (w), 563 (m), 526 (w).

Method B. A cold (-25 °C) solution of LiC_6Cl_5 (2 mL in Et_2O, 0.5 mmol, 0.25 M) was added to a cold (-25 °C), stirring suspension of $ThCl_4(DME)_2$ (69.3 mg, 0.125 mmol) in Et_2O (2 mL). This resulted in an immediate color change to yellow, concomitant with the deposition of a flocculent yellow-orange precipitate. After 10 min of stirring, the reaction mixture was filtered through a Celite column (0.5 cm × 5 cm) supported on glass wool to afford a clear, yellow-orange filtrate. The volume of the filtrate was reduced to 2 mL *in vacuo*, hexanes (5 mL) was layered onto the solution, and the sample was stored at –25 °C for 24 h, which resulted in the deposition of pale orange plates. The solid was isolated by decanting the supernatant and then dried *in vacuo* (71 mg, 38 % yield).

3.4.6 Synthesis of $[Li(Et_2O)_3][UCl_2(C_6Cl_5)_3]$ ([Li][3.4])

Method A. A cold (-25 °C) solution of LiC_6Cl_5 (2 mL in Et_2O, 0.5 mmol, 0.25 M) was added to a cold (-25 °C), suspension of UCl_4 (63.3 mg, 0.167 mmol) in Et_2O (2 mL). This resulted in an immediate color change to orange, concomitant with the deposition of a flocculent brown precipitate. After 5 min, the reaction mixture was filtered through a Celite column (0.5 cm × 5 cm) supported on glass wool to afford a clear, orange filtrate. The volume of the filtrate was reduced to 2 mL *in vacuo*, hexanes (5 mL) was layered onto the solution,

and the sample was stored at –25 °C for 24 h, which resulted in the deposition of yellow plates. The solid was isolated by decanting the supernatant and then dried *in vacuo* (87 mg, 40 % yield). Anal. Calcd for $C_{46}H_{40}LiO_5Cl_{25}U$: C, 28.01; H, 2.35. Found: C, 27.80; H, 2.03. ^{1}H NMR (500 MHz, 25 °C, benzene-d_6): δ 3.56 (br s, 12H, OCH_2CH$_3$), 1.34 (br s, 18H, OCH$_2$CH_3). ^{7}Li{^{1}H} NMR (500 MHz, 25 °C, benzene-d_6): δ 29.59 (br s). IR (KBr pellet, cm^{-1}): 3415 (w), 3110 (w), 3066 (w), 2975 (w), 2933 (w), 2873 (w), 2562 (w), 2339 (w), 1729 (w), 1629 (w), 1556 (w), 1542 (w), 1523 (m), 1508 (w), 1483 (w), 1440 (w), 1421 (w), 1396 (s), 1332 (s), 1297 (m), 1284 (m), 1226 (m), 1170 (s), 1151 (w), 1139 (w), 1122 (w), 1087 (s), 1062 (s), 943 (w), 914 (w), 896 (w), 865 (s), 823 (s), 784 (w), 742 (w), 700 (w), 684 (s), 665 (m), 563 (m), 526 (m), 406 (m).

Method B. A cold (-25 °C) solution of LiC_6Cl_5 (2 mL in Et_2O, 0.5 mmol, 0.25 M) was added to a cold (-25 °C), suspension of UCl_4 (47.5 mg, 0.125 mmol) in Et_2O (2 mL). This resulted in an immediate color change to orange, concomitant with the deposition of a flocculent orange-brown precipitate. After 10 min, the reaction mixture was filtered through a Celite column (0.5 cm × 5 cm) supported on glass wool to afford a clear, orange filtrate. The volume of the filtrate was reduced to 2 mL *in vacuo*, hexanes (5 mL) was layered onto the solution, and the sample was stored at –25 °C for 24 h, which resulted in the deposition of yellow plates. The solid was isolated by decanting the supernatant and then dried *in vacuo* (107.4 mg, 67 % yield).

3.4.7 X-Ray Crystallography

Data for all complexes were collected on a Bruker KAPPA APEX II diffractometer equipped with an APEX II CCD detector using a TRIUMPH monochromator with a Mo Kα X-ray source (α = 0.71073 Å). The crystals were mounted on a cryoloop under Paratone-N

oil, and all data were collected at 100(2) K using an Oxford nitrogen gas cryostream. Data were collected using ω scans with 0.5° frame widths. Frame exposures of 10 seconds were used for [Li][**3.1**]·2.5Et_2O·2CH_2Cl_2, [Li][**3.3**], and [Li][**3.4**]. Frame exposures of 20 seconds were used for [Li][**3.2**]. Data collection and cell parameter determination were conducted using the SMART program.[68] Integration of the data frames and final cell parameter refinement were performed using SAINT software.[69] Absorption correction of the data was carried out using the multi-scan method SADABS.[70] Subsequent calculations were carried out using SHELXTL.[71] Structure determination was done using direct or Patterson methods and difference Fourier techniques. All hydrogen atom positions were idealized and rode on the atom of attachment. Structure solution and refinement were performed using SHELXTL.[71] Graphics, and creation of publication materials were performed using Diamond.[72]

For complex [Li][**3.1**]·2.5Et_2O·2CH_2Cl_2, two Et_2O solvate molecules exhibited positional disorder, which was addressed by constraining the affected atoms with the SADI and EADP commands. In addition, the Li counterions and solvent ligands exhibited positional disorder, which was addressed by constraining the affected atoms with the SADI and EADP commands. The atoms of the disordered solvate molecules were refined isotropically. The C_6Cl_5 carbon atoms exhibited minor positional disorder that was addressed by use of the EADP command. For complex [Li][**3.2**], the four Et_2O molecules exhibited positional disorder, which was addressed by modelling each Et_2O molecule over two positions in a 54:46 ratio. In addition, the affected O and C atoms were constrained with the SADI and EADP commands. Hydrogen atoms were not added to disordered Et_2O solvate molecules. For complex [Li][**3.3**], two Et_2O ligands coordinated to Li counterion exhibited positional disorder, which was addressed by constraining the affected atoms with SADI and EADP. For

complex [Li][**3.4**], three Et_2O ligands coordinated to the Li counterion exhibited positional disorder, which was addressed by constraining the affected atoms SADI and EADP. Additionally, the Li atom was refined isotropically.

Further crystallographic details of complexes [Li][**3.1**]·2.5Et_2O·2CH_2Cl_2 , [Li][**3.2**], [Li][**3.3**], and [Li][**3.4**] can be found in Table 3.3 and Table 3.4. Complexes [Li][**3.1**]·2.5Et_2O·2CH_2Cl_2, [Li][**3.2**], [Li][**3.3**], and [Li][**3.4**] have been deposited in the Cambridge Structural Database ([Li][**3.1**]·2.5Et_2O·2CH_2Cl_2: CCDC 2087696; [Li][**3.2**]: CCDC 2087697; [Li][**3.3**]: CCDC 2087698; [Li][**3.4**]: CCDC 2087699).

Table 3.3 X-ray crystallographic data for complexes [Li][**3.1**]·2.5Et_2O·2CH_2Cl_2 and [Li][**3.2**].

	[Li][**3.1**]·2.5Et_2O·2CH_2Cl_2	[Li][**3.2**]
Formula	$C_{122}H_{80}Li_3O_{14}Cl_{75}Th_3$	$C_{46}H_{40}LiO_5Cl_{25}U$
Crystal Habit, Color	Colorless	Yellow
Crystal Size (mm)	0.2 × 0.1 × 0.05	0.2 × 0.1 × 0.05
MW (g/mol)	5145.8	1788.1
crystal system	Monoclinic	Monoclinic
space group	$P2_1/n$	$P2_1/c$
a (Å)	26.231(7)	16.935(3)
b (Å)	18.950(5)	16.462(3)
c (Å)	38.591(10)	23.352(4)
α (°)	90	90
β (°)	97.035(5)	94.907(4)
γ (°)	90	90
V ($Å^3$)	19038(9)	6486.4(18)
Z	4	4
T (K)	100(2)	100(2)
λ (Å)	0.71073	0.71073
GOF	1.180	1.015
Density (calcd) (Mg/m^3)	1.919	1.831
Absorption coefficient (mm^{-1})	3.503	3.573
F_{000}	10668	3472
Total no Reflections	140040	24527
Unique Reflections	30313	10322
Final R indices*	R_1 = 0.0889 wR_2 = 0.1678	R_1 = 0.0781 wR_2 = 0.2246
Largest Diff. peak and hole ($e^- A^{-3}$)	5.368, -2.264	2.197, -1.121

*For [I>2σ(I)

Table 3.4. X-ray crystallographic data for complexes [Li][**3.3**] and [Li][**3.4**].

	[Li][**3.3**]	[Li][**3.4**]
Formula	$C_{38}H_{50}Li_2O_7Cl_{18}Th$	$C_{30}H_{30}LiO_3Cl_{17}U$
Crystal Habit, Color	Pale Orange	Yellow
Crystal Size (mm)	0.2 × 0.1 × 0.05	0.2 × 0.1 × 0.05
MW (g/mol)	1502.80	1286.16
crystal system	Triclinic	Triclinic
space group	P -1	P -1
a (Å)	13.366(4)	11.158(3)
b (Å)	14.221(4)	13.511(5)
c (Å)	17.545(5)	16.518(5)
α (°)	76.549(3)	85.635(8)
β (°)	85.498(4)	79.000(5)
γ (°)	64.312(3)	65.731(5)
V ($Å^3$)	2921.9(14)	2227.3(12)
Z	2	2
T (K)	100(2)	100(2)
λ (Å)	0.71073	0.71073
GOF	1.095	1.047
Density (calcd) (Mg/m^3)	1.708	1.917
Absorption coefficient (mm^{-1})	3.416	4.693
F_{000}	1472	1236
Total no Reflections	64878	40326
Unique Reflections	13023	9974
Final R indices*	$R_1 = 0.0551$ $wR_2 = 0.1760$	$R_1 = 0.1061$ $wR_2 = 0.2696$
Largest Diff. peak and hole ($e^- A^{-3}$)	4.137, -2.001	7.457, -5.514

*For [I>2σ(I)

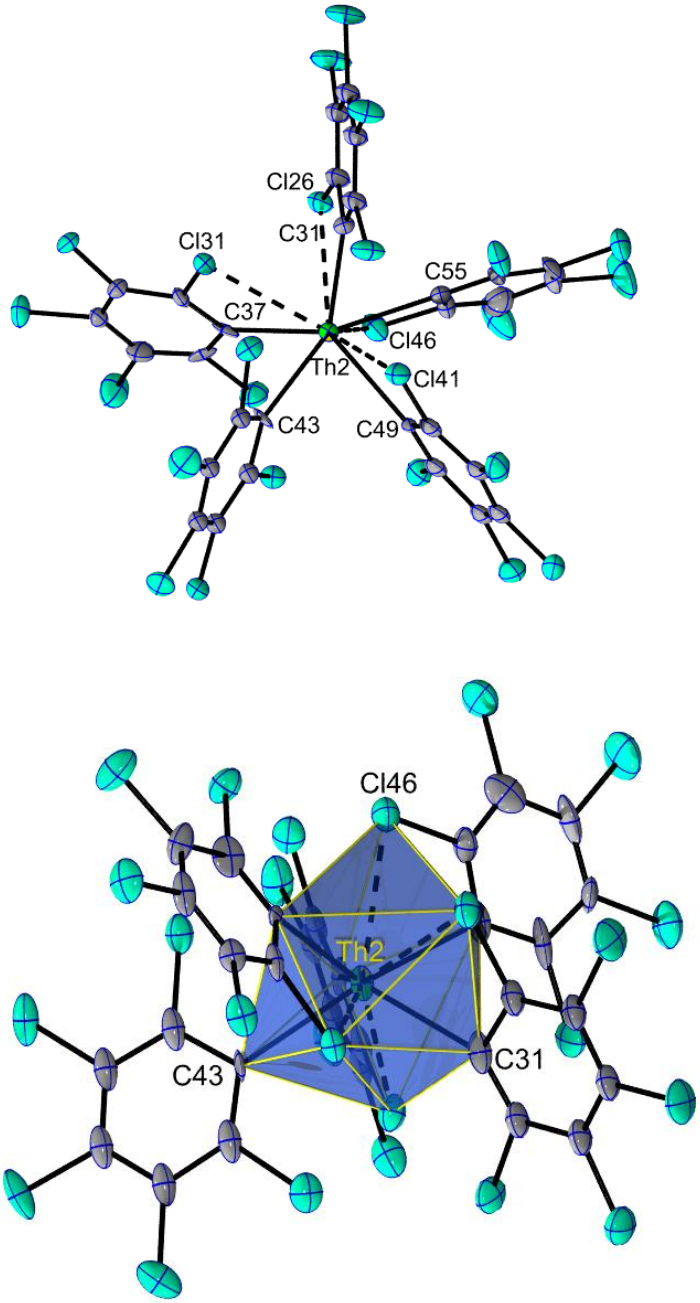

Figure 3.6. Solid-state molecular structure of Th2 in [Li][**3.1**]·2.5Et_2O·2CH_2Cl_2 shown with 50% probability ellipsoids. All hydrogen atoms, solvate molecules, and a $[Li(DME)_2(Et_2O)]^+$ counterion have been omitted for clarity.

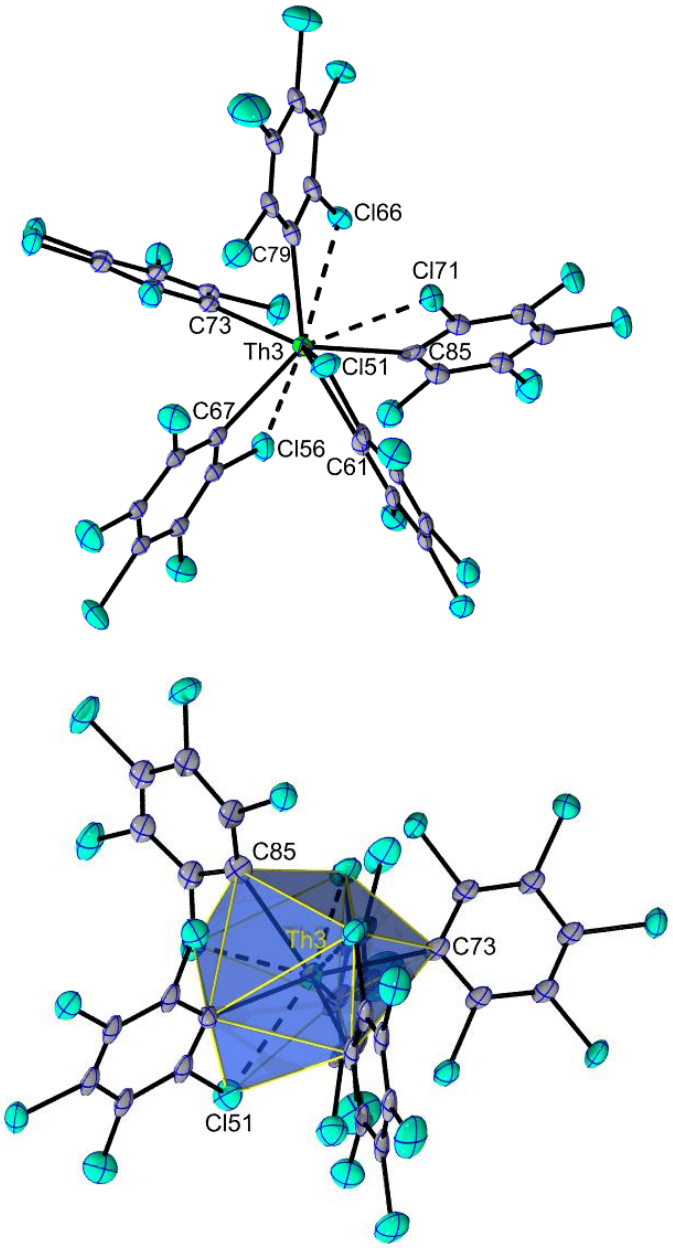

Figure 3.7. Solid-state molecular structure of Th3 in [Li][**3.1**]·2.5Et_2O·2CH_2Cl_2 shown with 50% probability ellipsoids. All hydrogen atoms, solvate molecules, and a $[Li(DME)_2]^+$ counterion have been omitted for clarity.

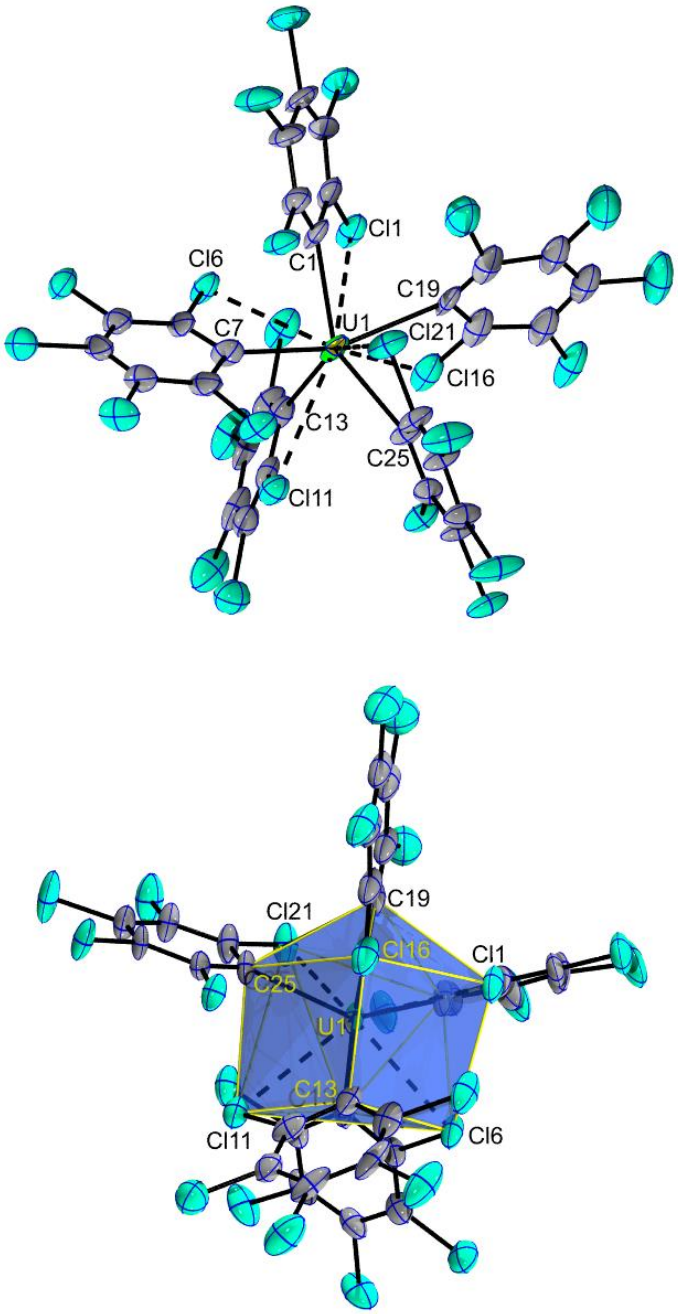

Figure 3.8. Solid-state molecular structure of [Li][**3.2**] shown with 30% probability ellipsoids. All hydrogen atoms and a $[Li(Et_2O)_4]^+$ counterion have been omitted for clarity.

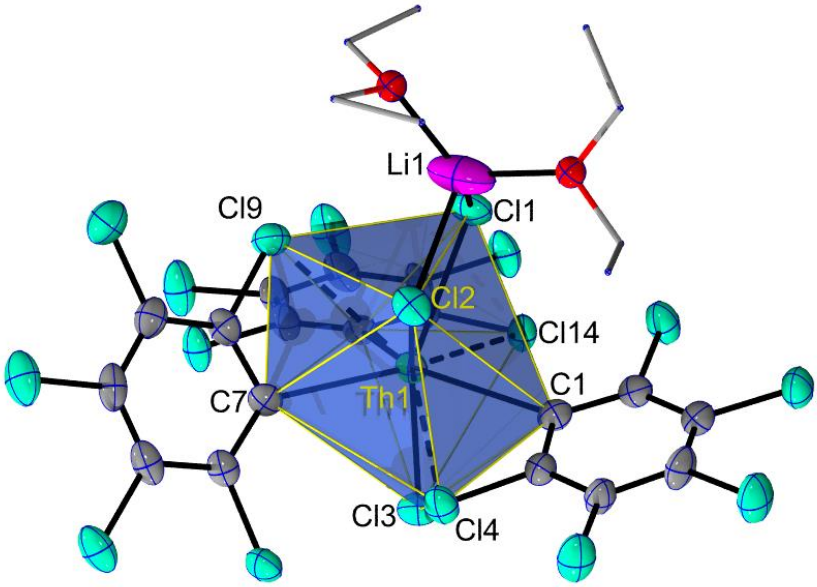

Figure 3.9. Solid-state molecular structure of [Li][**3.3**] shown with 50% probability ellipsoids. All hydrogen atoms and a $[Li(DME)_2(Et_2O)]^+$ counterion have been omitted for clarity.

3.4.8 Computational Data Details

Kohn-Sham density functional theory (DFT) calculations were performed based on crystal structure coordinates, unless stated otherwise, using the 2017 release of the Amsterdam Density Functional (ADF) suite.[61] The Perdew–Burke–Ernzerhof[73] (PBE) exchange-correlation functional, all-electron scalar-relativistic Zeroth-Order Regular Approximation[74] (ZORA) Hamiltonian, and the Slater-type atomic orbital (STO) basis sets of triple-ζ doubly polarized (TZ2P)[75] quality were employed for the single-point calculations. The conductor-like screening model (COSMO) was used to describe solvent effect (dichloromethane).[76] The bond analysis for the complexes was based on natural localized molecular orbitals (NLMOs) generated with NBO6.[59]

The computations of the NMR shielding tensors[60] (σ, ppm) for [**3.1**]$^-$ and [**3.3**]$^-$ were performed with the NMR module of ADF, using both the scalar relativistic and spin-orbit all electron ZORA Hamiltonian. Functionals used for the NMR calculations were BP86, PBE, PBE0 (25% exact exchange), and PBE0 (40% exact exchange).[77, 78] The ^{13}C chemical shifts (δ, ppm) were obtained by subtracting the *ipso*-carbon nuclear magnetic shielding of interest from the reference compound (tetramethylsilane, TMS), with the latter calculated at the same level of theory.

Table 3.5. % compositions (averaged) of the An-C_{ipso} and An-Cl bonding NLMOs in [**3.1**]$^-$, [**3.2**]$^-$, [**3.3**]$^-$, [**3.4**]$^-$,and $[Th(C_6H_5)_6]^{2-}$.[a]

Complexes	**Orbital**	**Total C**	**2s**	**2p**	**Total An**	**7s**	**7p**	**6d**	**5f**
[**3.1**]$^-$	σ(Th-C)	78	28	72	14	11	0	65	24
[**3.2**]$^-$	σ(U-C)	74	27	73	18	8	0	56	36
[**3.3**]$^-$	σ(Th-C)	78	28	72	15	13	0	65	22
[**3.4**]$^-$	σ(U-C)	74	29	71	21	12	0	58	30
$[Th(C_6H_5)_6]^{2-}$ [b]	σ(Th-C)	81	30	70	15	12	0	68	20
Complexes	**Orbital**	**Total Cl**	**3s**	**3p**	**Total An**	**7s**	**7p**	**6d**	**5f**
[**3.1**]$^-$	σ(Th-Cl)	91	32	68	7	13	0	56	31
[**3.2**]$^-$	σ(U-Cl)	90	27	73	8	12	0	54	34
[**3.3**]$^-$	σ(Th-Cl)[c]	87	50	50	12	14	0	61	25
	σ(Th-Cl)	92	25	75	6	14	0	54	32
[**3.4**]$^-$	σ(U-Cl)[c]	85	40	60	14	12	0	50	38
	σ(U-Cl)	93	17	83	5	11	0	52	37

[a] NLMO bonding analysis performed at the scalar ZORA level using the PBE functional and TZ2P basis set.

[b] The geometry for the $[Th(C_6H_5)_6]^{2-}$ complex was taken from Ref 19 with C_3 symmetry.[19]

[c] The Cl atom directly bound to An.

3.5 Appendix

3.5.1 NMR Spectra

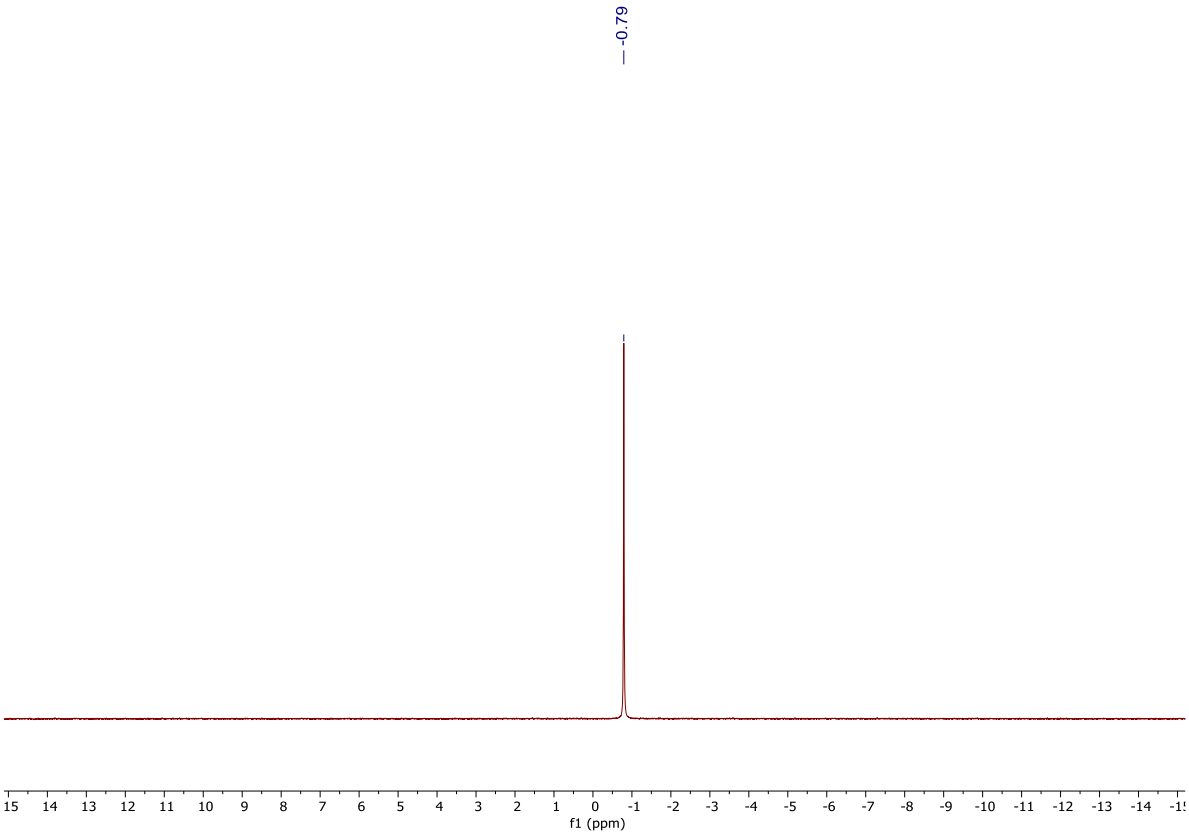

Figure 3.10. $^{7}Li\{^{1}H\}$ NMR spectrum of [Li][**3.1**] in methylene chloride-d_2.

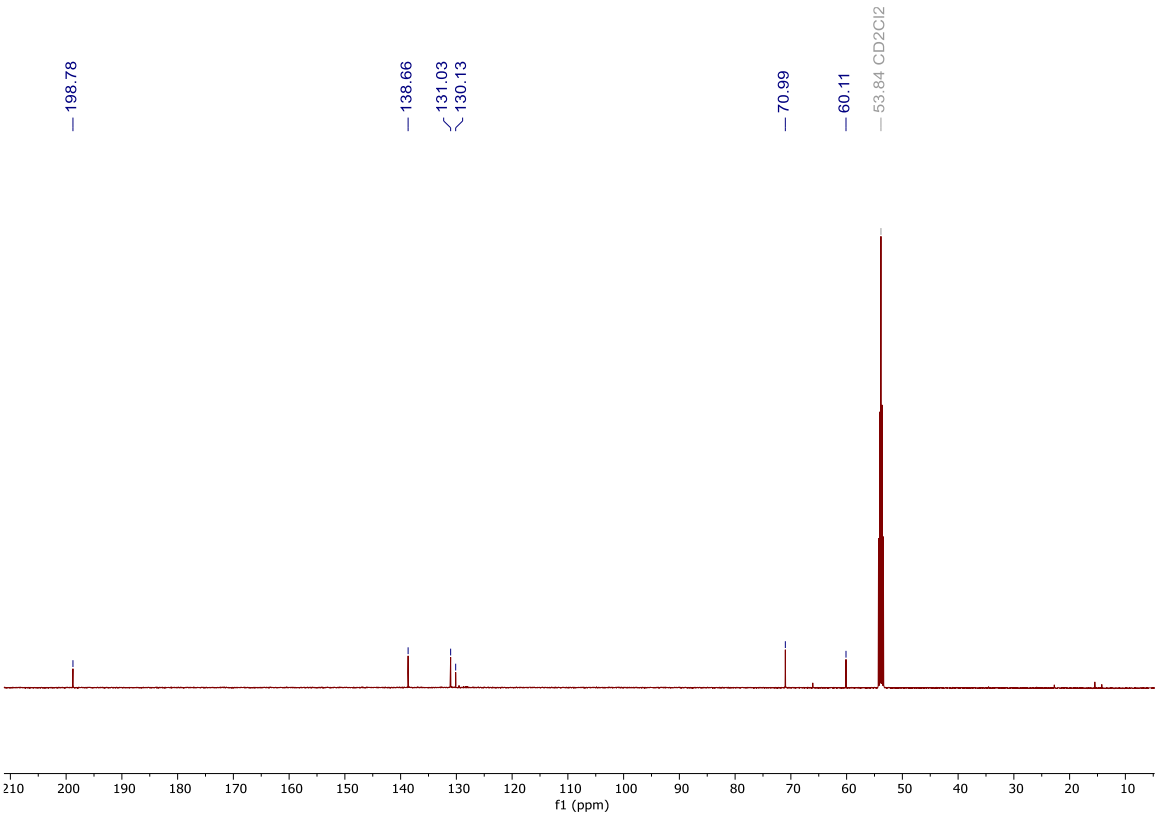

Figure 3.11. $^{13}C\{^{1}H\}$ NMR spectrum of [Li][**3.1**] in methylene chloride-d_2.

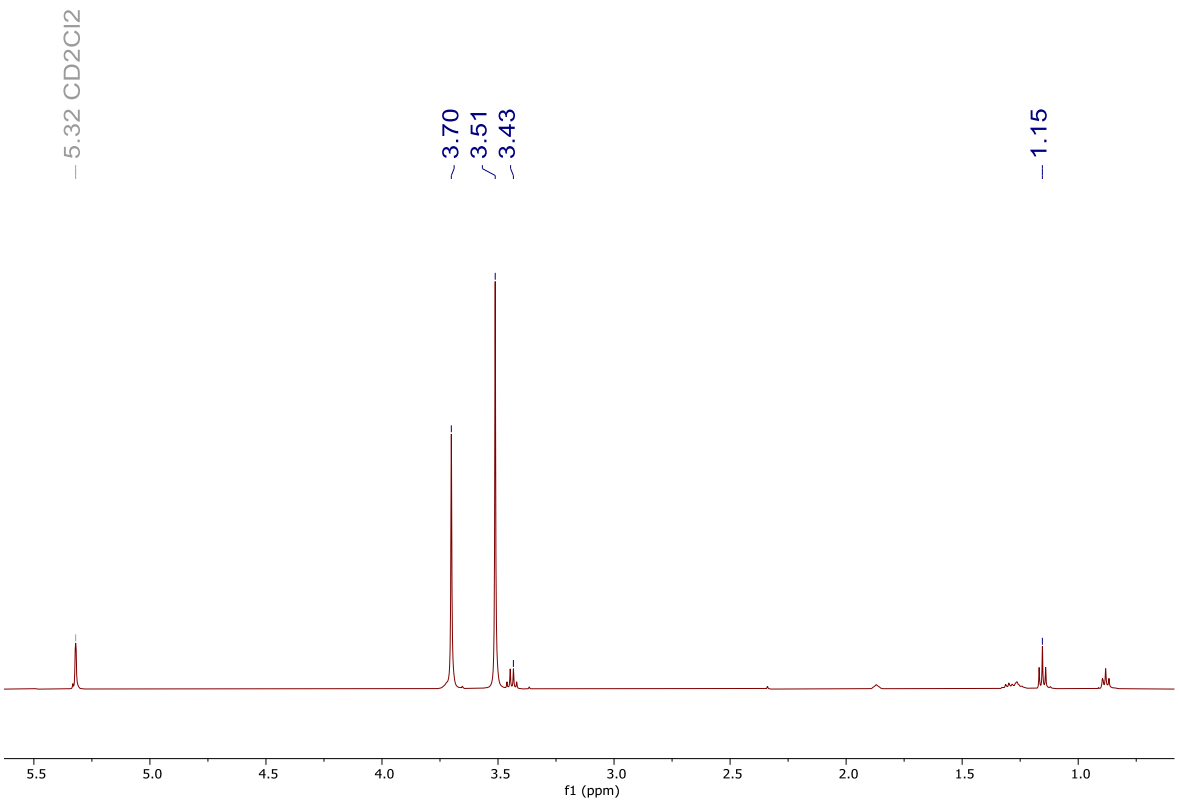

Figure 3.12. ^{1}H NMR spectrum of [Li][**3.1**] in methylene chloride-d_2.

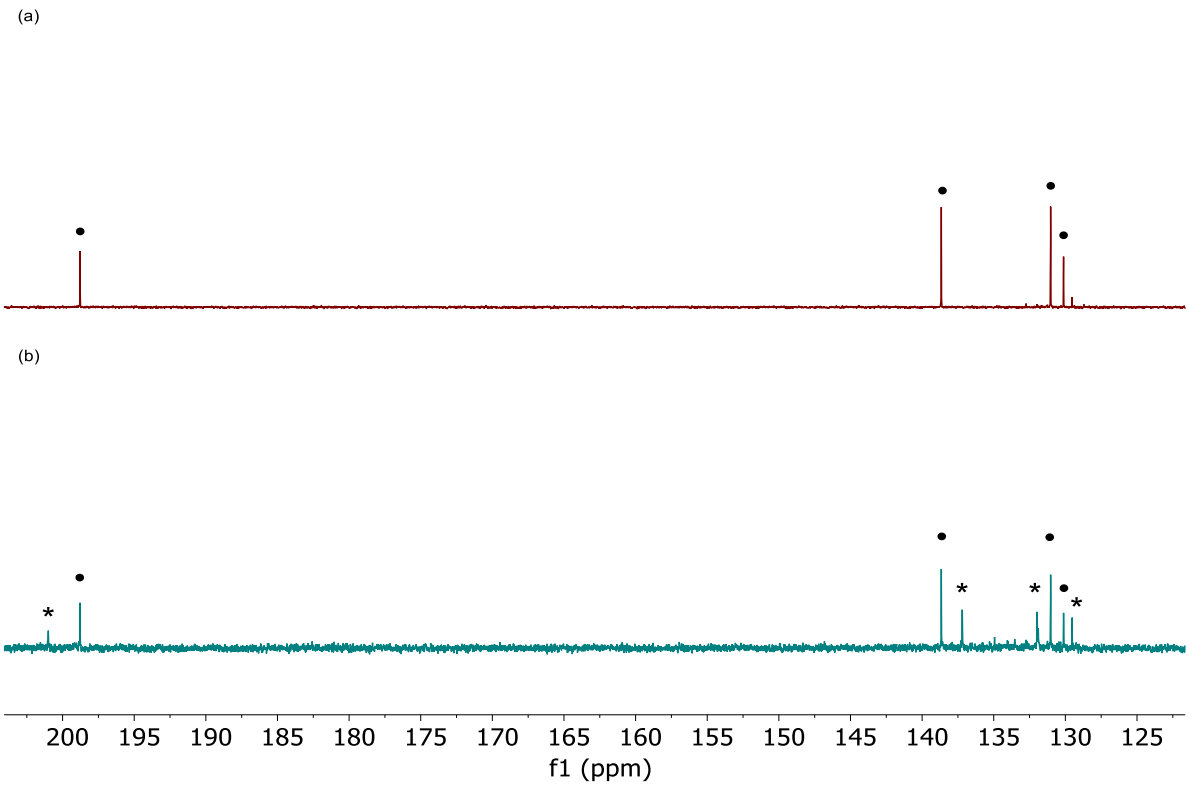

Figure 3.13. (a) Partial $^{13}C\{^{1}H\}$ NMR spectrum of [Li][**3.1**] in methylene chloride-d_2. (b) Partial $^{13}C\{^{1}H\}$ NMR spectrum of [Li][**3.1**] in methylene chloride-d_2 after standing for 24 h in solution at room temperature. (•) indicates the presence of [Li][**3.1**] and (*) indicates the presence of [Li][**3.3**].

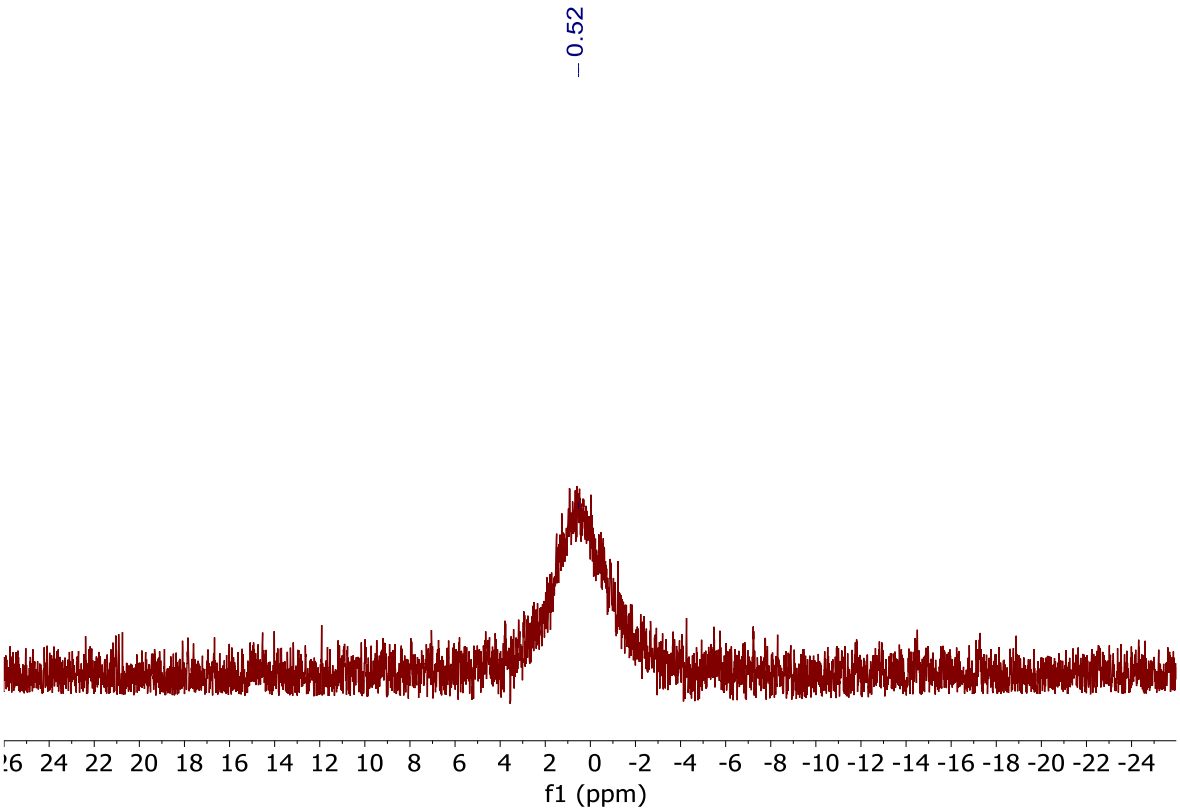

Figure 3.14. ^{7}Li{^{1}H} NMR spectrum of [Li][**3.2**] in methylene chloride-d_2.

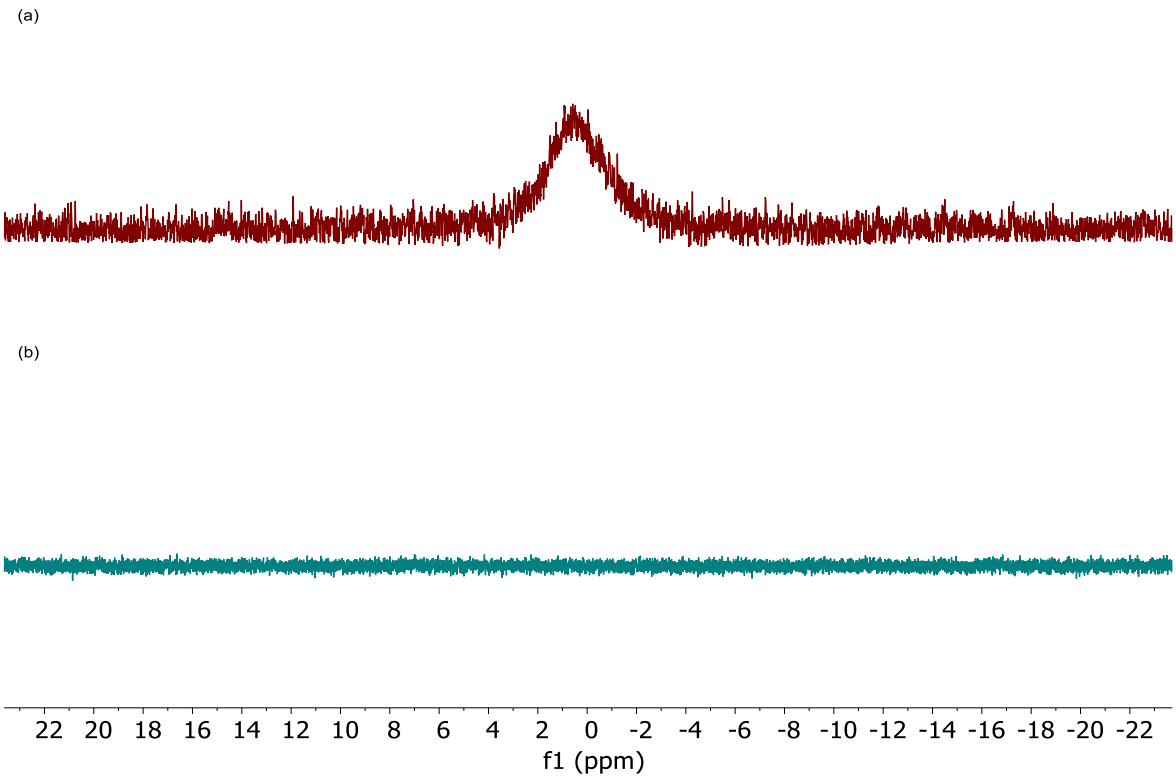

Figure 3.15. (a) ^{7}Li{^{1}H} NMR spectrum of [Li][**3.2**] in methylene chloride-d_2. (b) ^{7}Li{^{1}H} NMR spectrum of [Li][**3.2**] in methylene chloride-d_2 after standing for 24 h in solution at room temperatre.

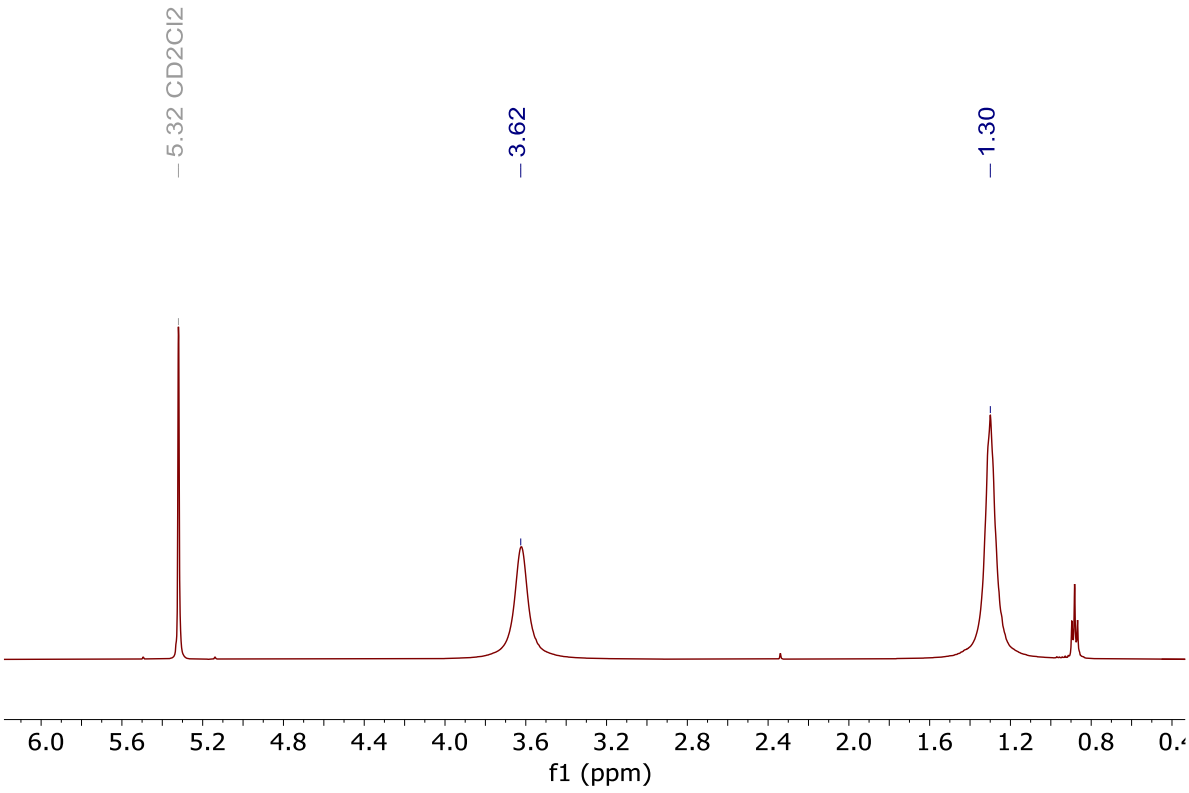

Figure 3.16. ^{1}H NMR spectrum of [Li][**3.2**] in methylene chloride-d_2.

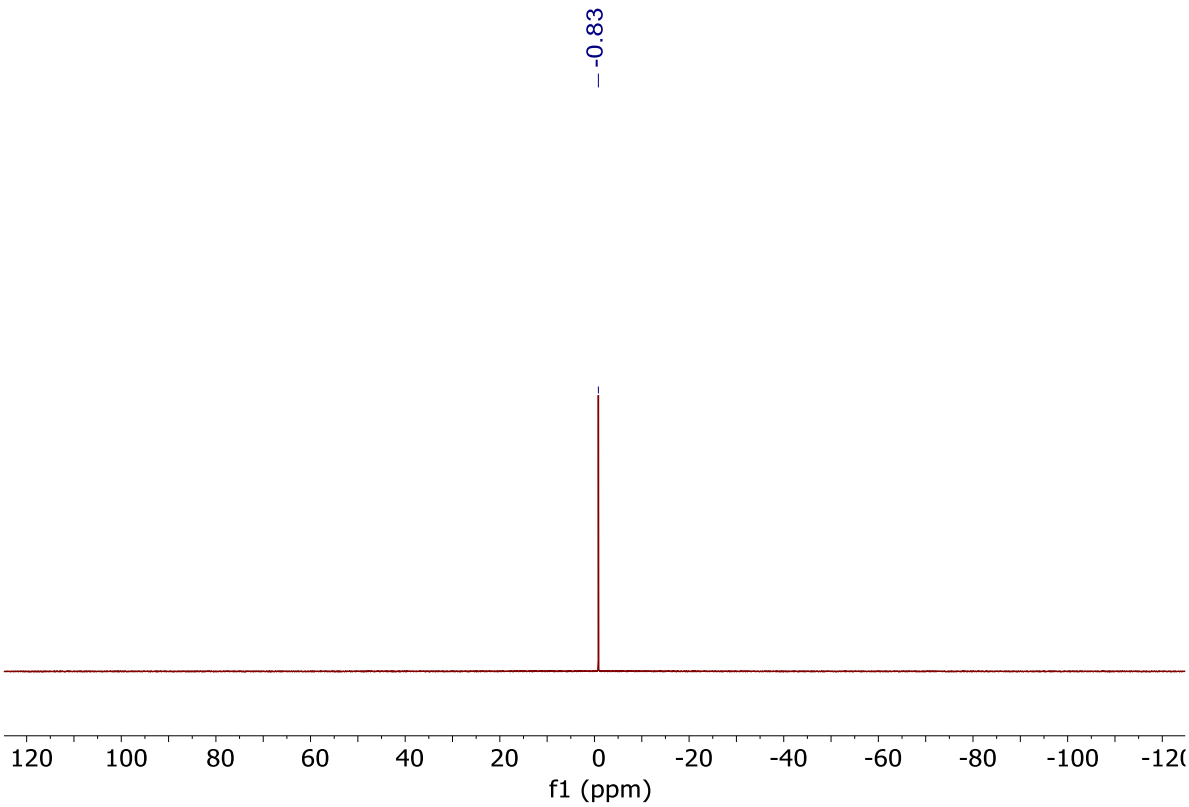

Figure 3.17. ^{7}Li{^{1}H} NMR spectrum of [Li][**3.3**] in methylene chloride-d_2.

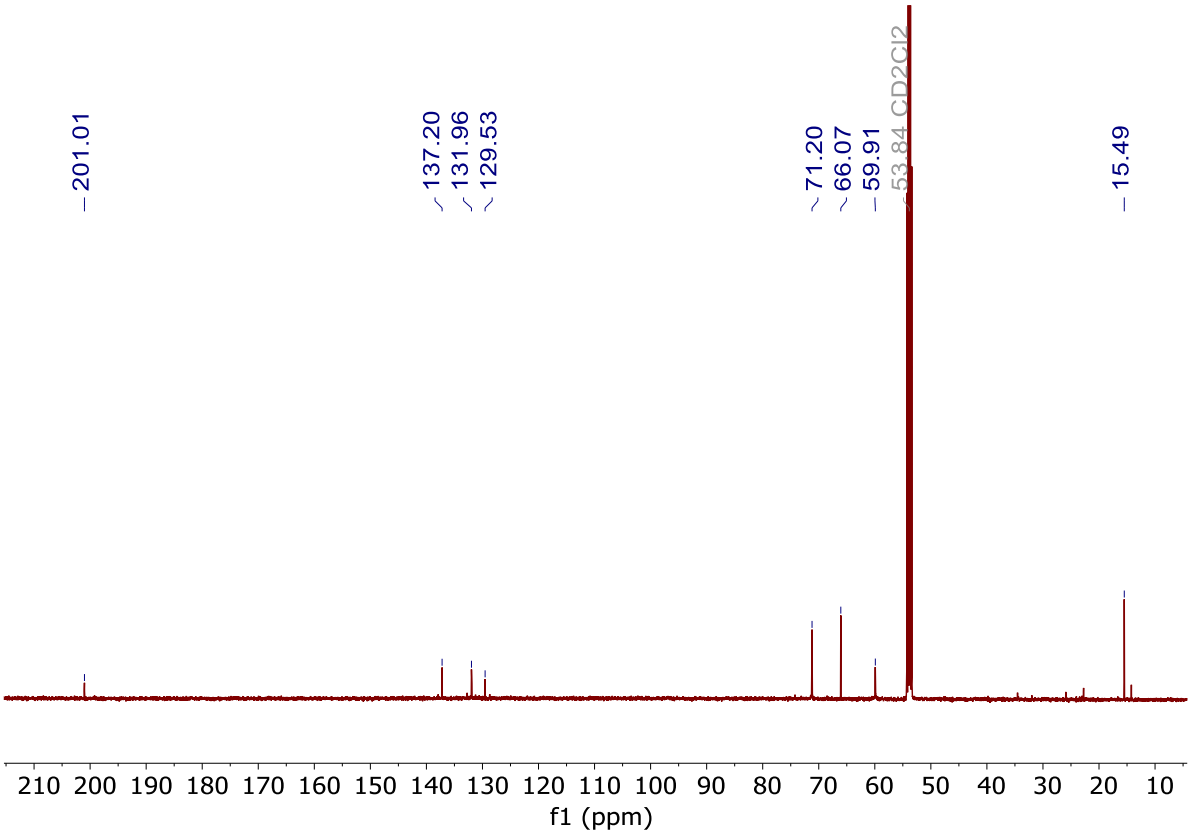

Figure 3.18. $^{13}C\{^{1}H\}$ NMR spectrum of [Li][**3.3**] in methylene chloride-d_2.

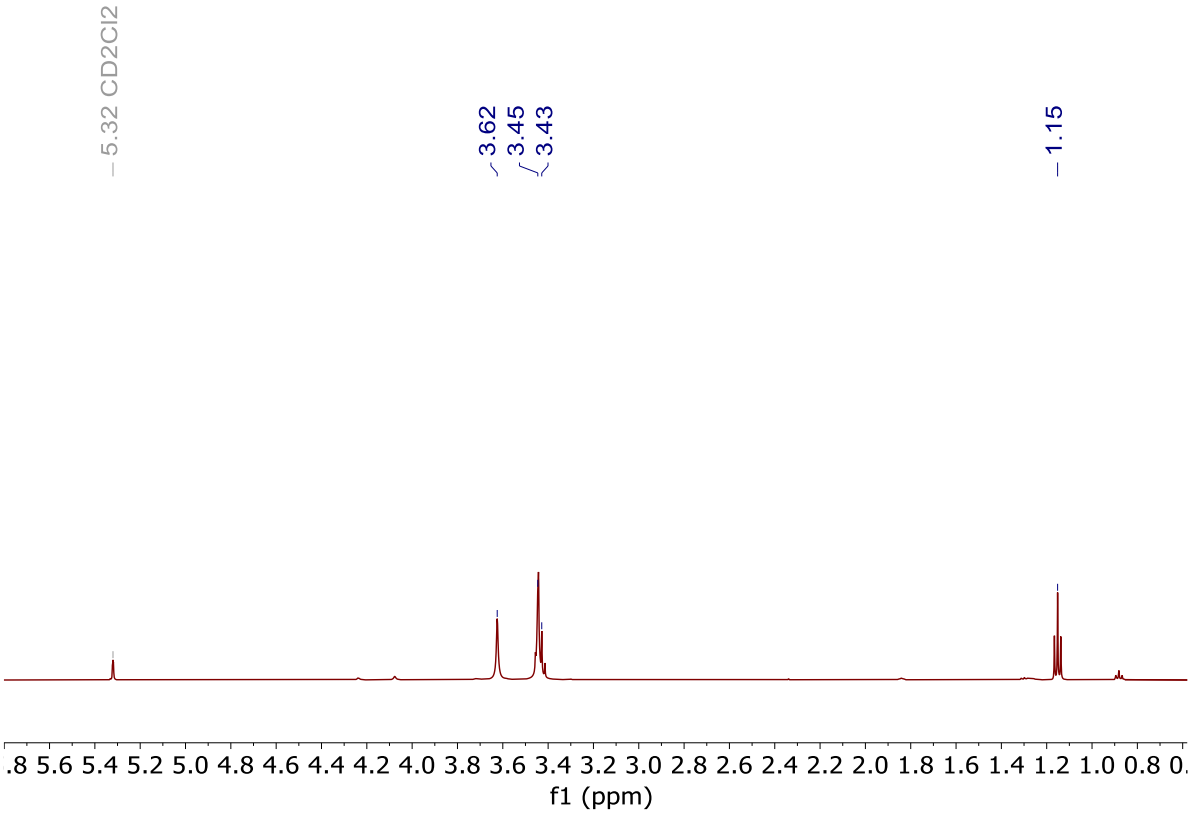

Figure 3.19. ^{1}H NMR spectrum of [Li][**3.3**] in methylene chloride-d_2.

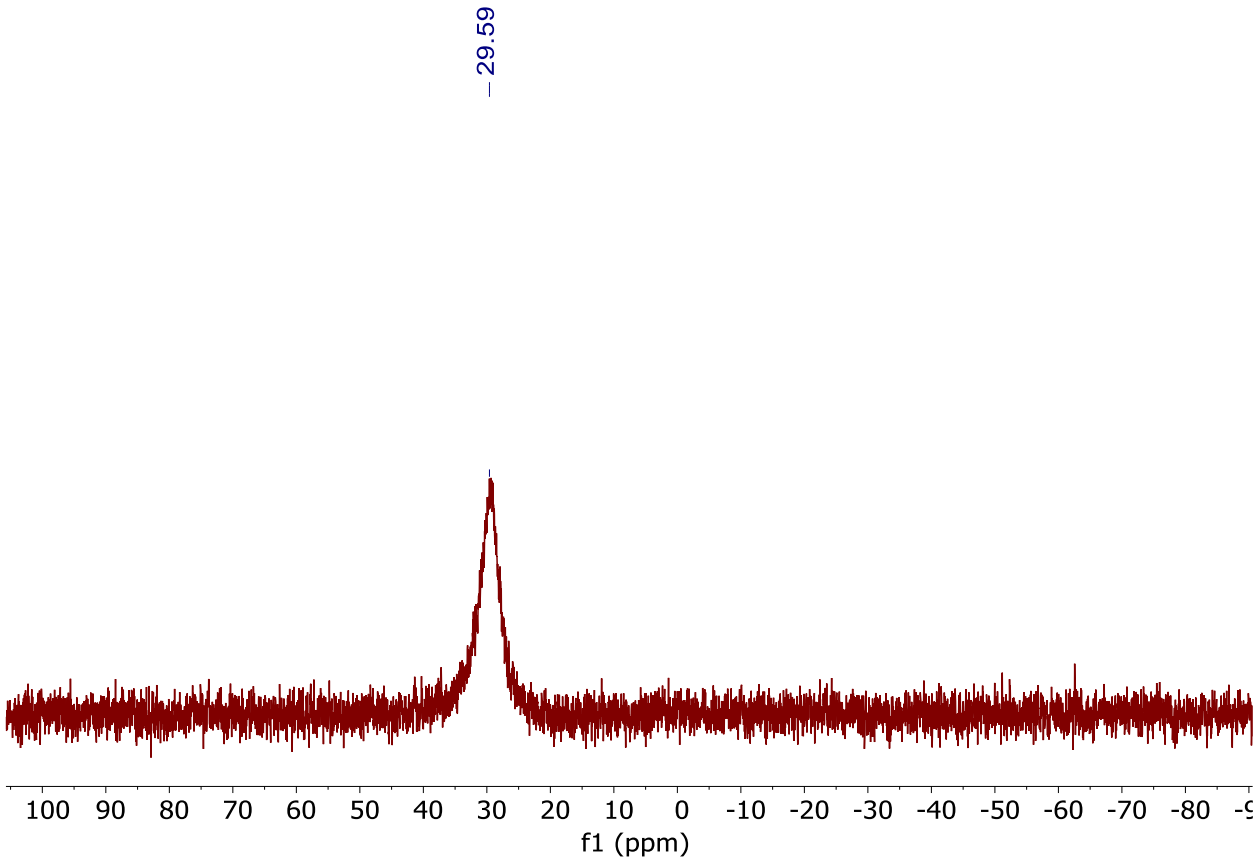

Figure 3.20. $^{7}Li\{^{1}H\}$ NMR spectrum of [Li][**3.4**] in benzene-d_6.

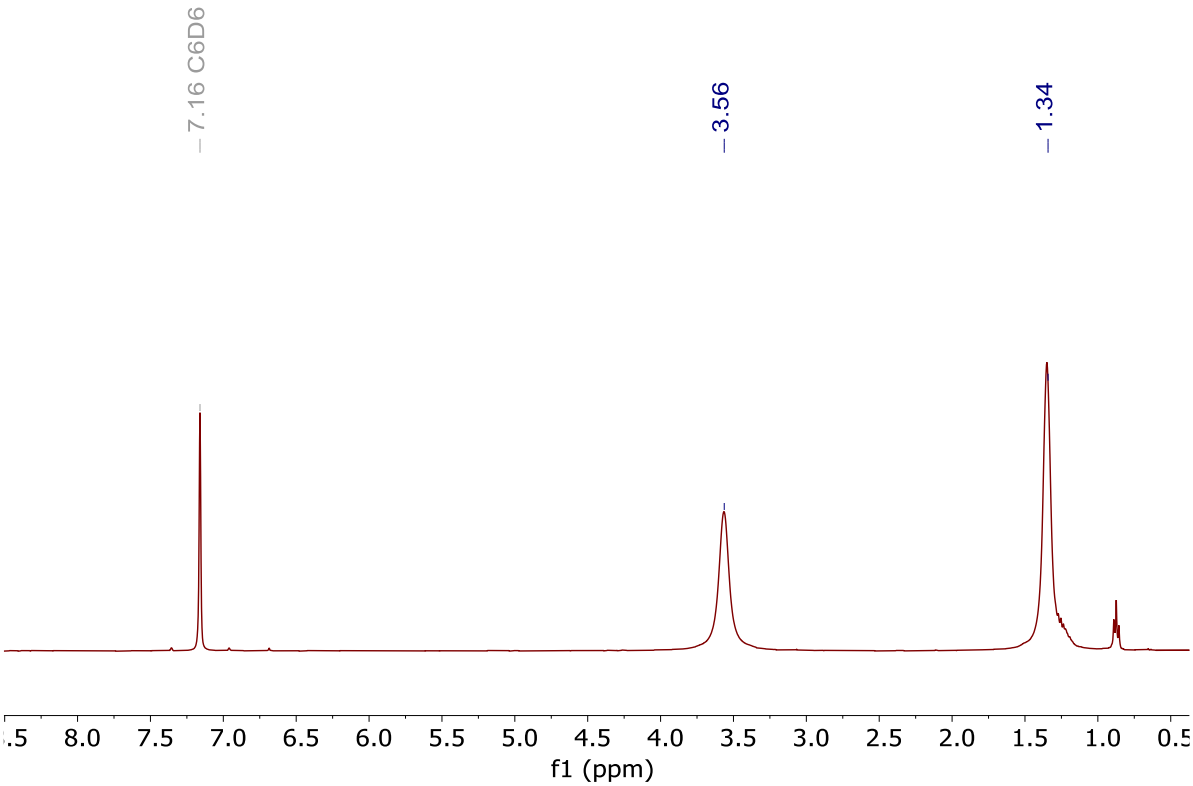

Figure 3.21. ^{1}H NMR spectrum of [Li][**3.4**] in benzene-d_6.

3.5.2 IR Spectra

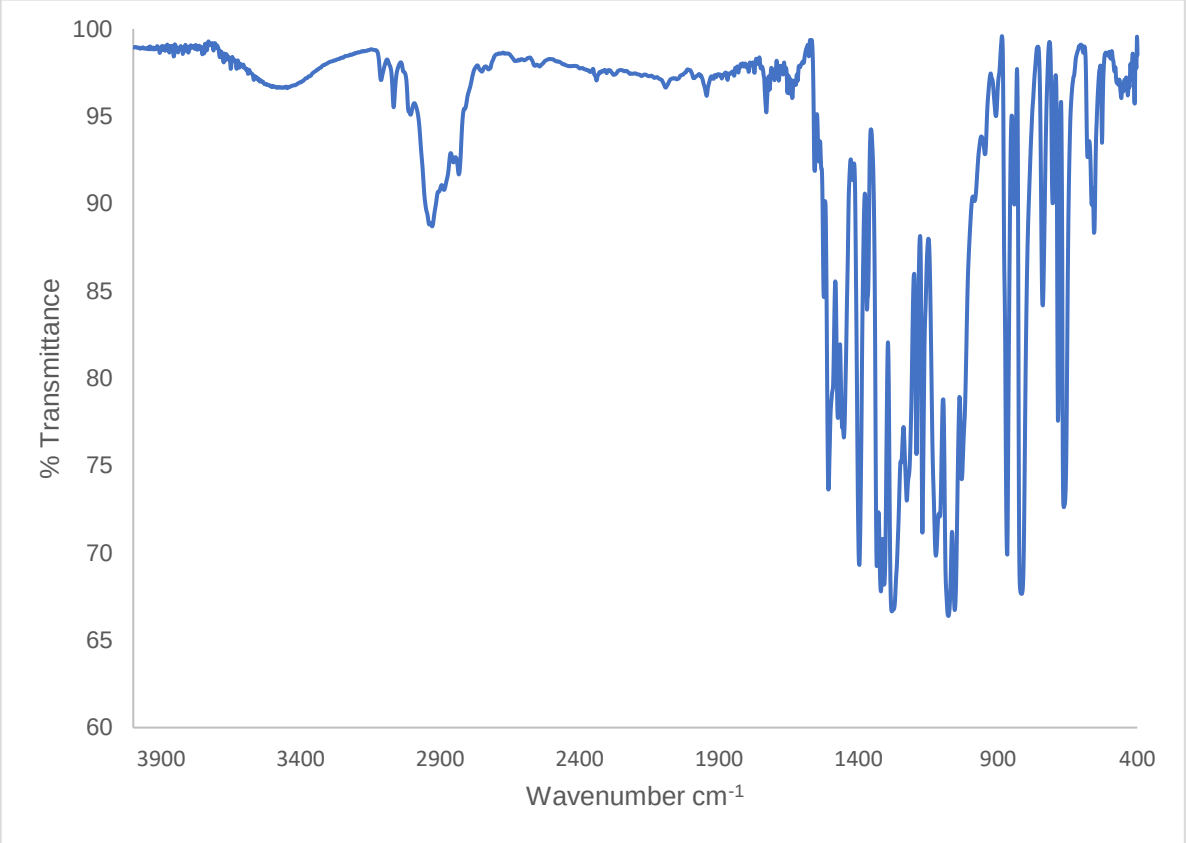

Figure 3.22. IR spectrum of [Li][**3.1**] (KBr pellet).

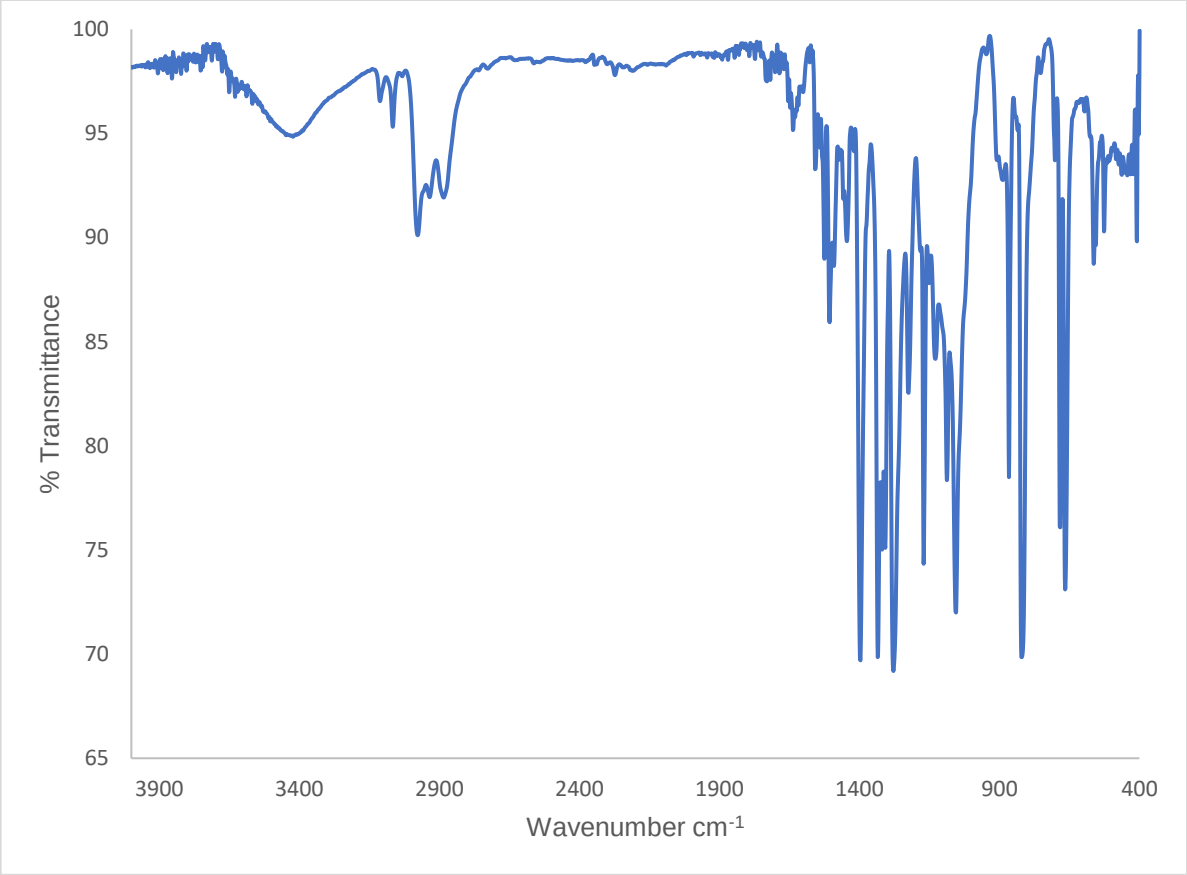

Figure 3.23. IR spectrum of [Li][**3.2**] (KBr pellet).

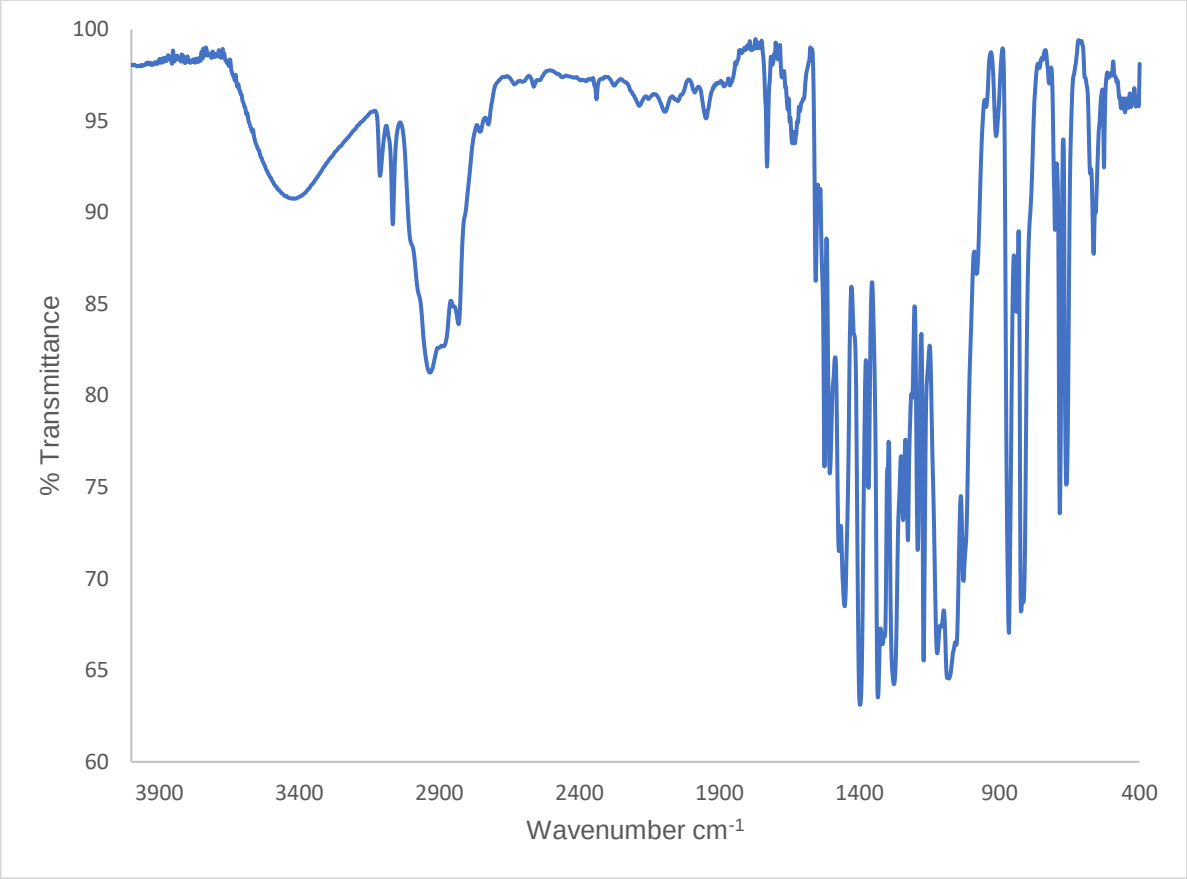

Figure 3.24. IR spectrum of [Li][**3.3**] (KBr pellet).

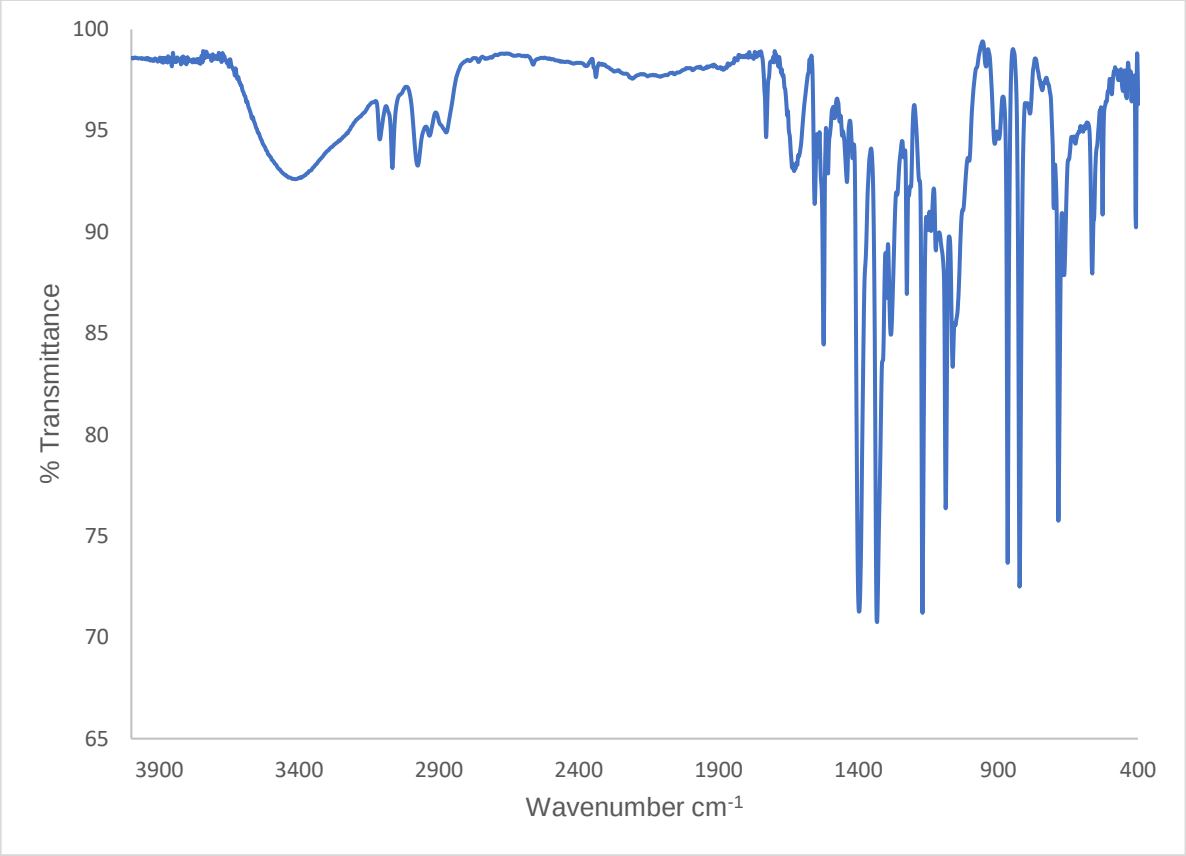

Figure 3.25. IR spectrum of [Li][**3.4**] (KBr pellet).

3.6 References

(1) Jones, M. B.; Gaunt, A. J. Recent Developments in Synthesis and Structural Chemistry of Nonaqueous Actinide Complexes. *Chem. Rev.* **2013**, *113*, 1137-1198.
(2) Liddle, S. T. The Renaissance of Non-Aqueous Uranium Chemistry. *Angew. Chem. Int. Ed.* **2015**, *54*, 8604-8641.
(3) Johnson, S. A.; Bart, S. C. Achievements in uranium alkyl chemistry: celebrating sixty years of synthetic pursuits. *Dalton Trans.* **2015**, *44*, 7710-7726.
(4) Sears, J. D.; Sergentu, D.-C.; Baker, T. M.; Brennessel, W. W.; Autschbach, J.; Neidig, M. L. The Exceptional Diversity of Homoleptic Uranium–Methyl Complexes. *Angew. Chem. Int. Ed.* **2020**, *132*, 13688-13692.
(5) Van der Sluys, W. G.; Burns, C. J.; Sattelberger, A. P. First example of a neutral homoleptic uranium alkyl. Synthesis, properties, and structure of $U[CH(SiMe_3)_2]_3$. *Organometallics* **1989**, *8*, 855-857.
(6) Kraft, S. J.; Fanwick, P. E.; Bart, S. C. Carbon–Carbon Reductive Elimination from Homoleptic Uranium(IV) Alkyls Induced by Redox-Active Ligands. *J. Am. Chem. Soc.* **2012**, *134*, 6160-6168.
(7) Johnson, S. A.; Kiernicki, J. J.; Fanwick, P. E.; Bart, S. C. New Benzylpotassium Reagents and Their Utility for the Synthesis of Homoleptic Uranium(IV) Benzyl Derivatives. *Organometallics* **2015**, *34*, 2889-2895.
(8) Fortier, S.; Melot, B. C.; Wu, G.; Hayton, T. W. Homoleptic Uranium(IV) Alkyl Complexes: Synthesis and Characterization. *J. Am. Chem. Soc.* **2009**, *131*, 15512-15521.
(9) Fortier, S.; Walensky, J. R.; Wu, G.; Hayton, T. W. High-Valent Uranium Alkyls: Evidence for the Formation of $U^{VI}(CH_2SiMe_3)_6$. *J. Am. Chem. Soc.* **2011**, *133*, 11732-11743.
(10) Seaman, L. A.; Walensky, J. R.; Wu, G.; Hayton, T. W. In Pursuit of Homoleptic Actinide Alkyl Complexes. *Inorg. Chem.* **2013**, *52*, 3556-3564.
(11) Lauke, H.; Swepston, P. J.; Marks, T. J. Synthesis and characterization of a homoleptic actinide alkyl. The heptamethylthorate(IV) ion: a complex with seven metal-carbon .sigma. bonds. *J. Am. Chem. Soc.* **1984**, *106*, 6841-6843.
(12) Cruz, C. A.; Emslie, D. J. H.; Harrington, L. E.; Britten, J. F.; Robertson, C. M. Extremely Stable Thorium(IV) Dialkyl Complexes Supported by Rigid Tridentate 4,5-Bis(anilido)xanthene and 2,6-Bis(anilidomethyl)pyridine Ligands. *Organometallics* **2007**, *26*, 692-701.
(13) Behrle, A. C.; Myers, A. J.; Rungthanaphatsophon, P.; Lukens, W. W.; Barnes, C. L.; Walensky, J. R. Uranium(III) and thorium(IV) alkyl complexes as potential starting materials. *Chem. Commun.* **2016**, *52*, 14373-14375.
(14) Myers, A. J.; Tarlton, M. L.; Kelley, S. P.; Lukens, W. W.; Walensky, J. R. Synthesis and Utility of Neptunium(III) Hydrocarbyl Complex. *Angew. Chem. Int. Ed.* **2019**, *58*, 14891-14895.
(15) Kraft, S. J.; Fanwick, P. E.; Bart, S. C. Exploring the Insertion Chemistry of Tetrabenzyluranium Using Carbonyls and Organoazides. *Organometallics* **2013**, *32*, 3279-3285.
(16) Matson, E. M.; Franke, S. M.; Anderson, N. H.; Cook, T. D.; Fanwick, P. E.; Bart, S. C. Radical Reductive Elimination from Tetrabenzyluranium Mediated by an Iminoquinone Ligand. *Organometallics* **2014**, *33*, 1964-1971.

(17) Duhović, S.; Khan, S.; Diaconescu, P. L. In situ generation of uranium alkyl complexes. *Chem. Commun.* **2010**, *46*, 3390-3392.
(18) Johnson, S. A.; Higgins, R. F.; Abu-Omar, M. M.; Shores, M. P.; Bart, S. C. Mechanistic Insights into Concerted C–C Reductive Elimination from Homoleptic Uranium Alkyls. *Organometallics* **2017**, *36*, 3491-3497.
(19) Pedrick, E. A.; Hrobárik, P.; Seaman, L. A.; Wu, G.; Hayton, T. W. Synthesis, structure and bonding of hexaphenyl thorium(IV): observation of a non-octahedral structure. *Chem. Commun.* **2016**, *52*, 689-692.
(20) Boreen, M. A.; Parker, B. F.; Lohrey, T. D.; Arnold, J. A Homoleptic Uranium(III) Tris(aryl) Complex. *J. Am. Chem. Soc.* **2016**, *138*, 15865-15868.
(21) Seaman, L. A.; Pedrick, E. A.; Tsuchiya, T.; Wu, G.; Jakubikova, E.; Hayton, T. W. Comparison of the Reactivity of 2-Li-$C_6H_4CH_2NMe_2$ with MCl_4 (M=Th, U): Isolation of a Thorium Aryl Complex or a Uranium Benzyne Complex. *Angew. Chem. Int. Ed.* **2013**, *52*, 10589-10592.
(22) Wolford, N. J.; Sergentu, D.-C.; Brennessel, W. W.; Autschbach, J.; Neidig, M. L. Homoleptic Aryl Complexes of Uranium (IV). *Angew. Chem. Int. Ed.* **2019**, *58*, 10266-10270.
(23) Graves, C. R.; Schelter, E. J.; Cantat, T.; Scott, B. L.; Kiplinger, J. L. A Mild Protocol To Generate Uranium(IV) Mixed-Ligand Metallocene Complexes using Copper(I) Iodide. *Organometallics* **2008**, *27*, 5371-5378.
(24) Evans, W. J.; Miller, K. A.; Ziller, J. W.; DiPasquale, A. G.; Heroux, K. J.; Rheingold, A. L. Formation of $(C_5Me_5)_2U(EPh)Me$, $(C_5Me_5)_2U(EPh)_2$, and $(C_5Me_5)_2U(\eta^2\text{-}TeC_6H_4)$ from $(C_5Me_5)_2UMe_2$ and PhEEPh (E = S, Se, Te). *Organometallics* **2007**, *26*, 4287-4293.
(25) Ordoñez, O.; Yu, X.; Wu, G.; Autschbach, J.; Hayton, T. W. Synthesis and Characterization of Two Uranyl-Aryl "Ate" Complexes. *Chem. Eur. J.* **2021**, *27*, 5885-5889.
(26) Mullane, K. C.; Hrobárik, P.; Cheisson, T.; Manor, B. C.; Carroll, P. J.; Schelter, E. J. ^{13}C NMR Shifts as an Indicator of U–C Bond Covalency in Uranium(VI) Acetylide Complexes: An Experimental and Computational Study. *Inorg. Chem.* **2019**, *58*, 4152-4163.
(27) Smiles, D. E.; Wu, G.; Hrobárik, P.; Hayton, T. W. Synthesis, Thermochemistry, Bonding, and ^{13}C NMR Chemical Shift Analysis of a Phosphorano-Stabilized Carbene of Thorium. *Organometallics* **2017**, *36*, 4519-4524.
(28) Seaman, L. A.; Hrobárik, P.; Schettini, M. F.; Fortier, S.; Kaupp, M.; Hayton, T. W. A Rare Uranyl(VI)–Alkyl Ate Complex $[Li(DME)_{1.5}]_2[UO_2(CH_2SiMe_3)_4]$ and Its Comparison with a Homoleptic Uranium(VI)–Hexaalkyl. *Angew. Chem. Int. Ed.* **2013**, *52*, 3259-3263.
(29) Staun, S. L.; Sergentu, D.-C.; Wu, G.; Autschbach, J.; Hayton, T. W. Use of ^{15}N NMR spectroscopy to probe covalency in a thorium nitride. *Chem. Sci.* **2019**, *10*, 6431-6436.
(30) Smiles, D. E.; Wu, G.; Hrobárik, P.; Hayton, T. W. Use of ^{77}Se and ^{125}Te NMR Spectroscopy to Probe Covalency of the Actinide-Chalcogen Bonding in $[Th(E_n)\{N(SiMe_3)_2\}_3]^-$ (E = Se, Te; n = 1, 2) and Their Oxo-Uranium(VI) Congeners. *J. Am. Chem. Soc.* **2016**, *138*, 814-825.
(31) Wu, W.; Rehe, D.; Hrobárik, P.; Kornienko, A. Y.; Emge, T. J.; Brennan, J. G. Molecular Thorium Compounds with Dichalcogenide Ligands: Synthesis, Structure, ^{77}Se NMR Study, and Thermolysis. *Inorg. Chem.* **2018**, *57*, 14821-14833.
(32) Hrobárik, P.; Hrobáriková, V.; Greif, A. H.; Kaupp, M. Giant Spin-Orbit Effects on NMR Shifts in Diamagnetic Actinide Complexes: Guiding the Search of Uranium(VI) Hydride Complexes in the Correct Spectral Range. *Angew. Chem. Int. Ed.* **2012**, *51*, 10884-10888.

(33) Panetti, G. B.; Sergentu, D.-C.; Gau, M. R.; Carroll, P. J.; Autschbach, J.; Walsh, P. J.; Schelter, E. J. Isolation and characterization of a covalent Ce^{IV}-Aryl complex with an anomalous ^{13}C chemical shift. *Nat. Commun.* **2021**, *12*, 1713.
(34) Vícha, J.; Novotný, J.; Komorovsky, S.; Straka, M.; Kaupp, M.; Marek, R. Relativistic Heavy-Neighbor-Atom Effects on NMR Shifts: Concepts and Trends Across the Periodic Table. *Chem. Rev.* **2020**, *120*, 7065-7103.
(35) García-Monforte, M. A.; Alonso, P. J.; Forniés, J.; Menjón, B. New advances in homoleptic organotransition-metal compounds: The case of perhalophenyl ligands. *Dalton Trans.* **2007**, 3347-3359.
(36) Alonso, P. J.; Forniés, J.; García-Monforte, M. A.; Martín, A.; Menjón, B. New Homoleptic Organometallic Derivatives of Vanadium(III) and Vanadium(IV): Synthesis, Characterization, and Study of Their Electrochemical Behaviour. *Chem. Eur. J.* **2005**, *11*, 4713-4724.
(37) Alonso, P. J.; Arauzo, A. B.; Forniés, J.; García-Monforte, M. A.; Martín, A.; Martínez, J. I.; Menjón, B.; Rillo, C.; Sáiz-Garitaonandia, J. J. A Square-Planar Organoiron(III) Compound with a Spin-Admixed State. *Angew. Chem. Int. Ed.* **2006**, *45*, 6707-6711.
(38) Alonso, P. J.; Forniés, J.; García-Monforte, M. A.; Martín, A.; Menjón, B.; Rillo, C. A New Series of Homoleptic, Paramagnetic Organochromium Derivatives: Synthesis, Characterization, and Study of Their Magnetic Properties. *Chem. Eur. J.* **2002**, *8*, 4056-4065.
(39) J. Alonso, P.; R. Falvello, L.; Forniés, J. Synthesis and first structural characterisation of a homoleptic tetraorganochromate(III) salt. *Chem. Commun.* **1998**, 1721-1722.
(40) Alonso, P. J.; Forniés, J.; García-Monforte, M. A.; Martín, A.; Menjón, B. The first structurally characterised homoleptic organovanadium(III) compound. *Chem. Commun.* **2001**, 2138-2139.
(41) Garcia, M. P.; Jimenez, M. V.; Oro, L. A.; Lahoz, F. J.; Tiripicchio, M. C.; Tiripicchio, A. A homoleptic mononuclear iridium(II) organometallic complex: synthesis and x-ray structure of $[Ir(C_6Cl_5)_4]_2$. *Organometallics* **1993**, *12*, 4660-4663.
(42) P. García, M.; Victoria Jiménez, M.; J. Lahoz, F.; A. López, J.; A. Oro, L. Synthesis of the homoleptic rhodium(III) complex $[Rh(C_6Cl_5)_3]$. Molecular structures of $[Rh(C_6Cl_5)_3]$ and $[Rh(C_6Cl_4–C_6Cl_4)(C_6Cl_5)(SC_4H_8)_2]$. *J. Chem. Soc., Dalton Trans.* **1998**, 4211-4214.
(43) Fornies, J.; Menjon, B.; Sanz-Carrillo, R. M.; Tomas, M.; Connelly, N. G.; Crossley, J. G.; Orpen, A. G. Synthesis and Structural Characterization of the First Isolated Homoleptic Organoplatinum(IV) Compound: $[Pt(C_6Cl_5)_4]$. *J. Am. Chem. Soc.* **1995**, *117*, 4295-4304.
(44) Ara, I.; Forniés, J.; García-Monforte, M. A.; Martín, A.; Menjón, B. Synthesis and Characterization of Pentachlorophenyl–Metal Derivatives with d^0 and d^{10} Electron Configurations. *Chem. Eur. J.* **2004**, *10*, 4186-4197.
(45) Rausch, M. D.; Tibbetts, F. E.; Gordon, H. B. Perhaloaryl-metal chemistry: II. Pentachlorophenyllithium. *J. Organomet. Chem.* **1966**, *5*, 493-500.
(46) Fagan, P. J.; Manriquez, J. M.; Maatta, E. A.; Seyam, A. M.; Marks, T. J. Synthesis and properties of bis(pentamethylcyclopentadienyl) actinide hydrocarbyls and hydrides. A new class of highly reactive f-element organometallic compounds. *J. Am. Chem. Soc.* **1981**, *103*, 6650-6667.
(47) Cirera, J.; Ruiz, E.; Alvarez, S. Continuous Shape Measures as a Stereochemical Tool in Organometallic Chemistry. *Organometallics* **2005**, *24*, 1556-1562.
(48) Ruiz-Martínez, A.; Alvarez, S. Stereochemistry of Compounds with Coordination Number Ten. *Chem. Eur. J.* **2009**, *15*, 7470-7480.

(49) Ruiz-Martínez, A.; Casanova, D.; Alvarez, S. Polyhedral structures with an odd number of vertices: nine-atom clusters and supramolecular architectures. *Dalton Trans.* **2008**, 2583-2591.
(50) Ruiz-Martínez, A.; Casanova, D.; Alvarez, S. Polyhedral Structures with an Odd Number of Vertices: Nine-Coordinate Metal Compounds. *Chem. Eur. J.* **2008**, *14*, 1291-1303.
(51) Pedrick, E. A.; Wu, G.; Kaltsoyannis, N.; Hayton, T. W. Reductive silylation of a uranyl dibenzoylmethanate complex: an example of controlled uranyl oxo ligand cleavage. *Chem. Sci.* **2014**, *5*, 3204-3213.
(52) Schnaars, D. D.; Wu, G.; Hayton, T. W. Reduction of Pentavalent Uranyl to U(IV) Facilitated by Oxo Functionalization. *J. Am. Chem. Soc.* **2009**, *131*, 17532-17533.
(53) Yin, H.; Lewis, A. J.; Williams, U. J.; Carroll, P. J.; Schelter, E. J. Fluorinated diarylamide complexes of uranium(III, IV) incorporating ancillary fluorine-to-uranium dative interactions. *Chem. Sci.* **2013**, *4*, 798-805.
(54) Shannon, R. Revised effective ionic radii and systematic studies of interatomic distances in halides and chalcogenides. *Acta Cryst. A* **1976**, *32*, 751-767.
(55) Zabrodsky, H.; Peleg, S.; Avnir, D. Continuous symmetry measures. *J. Am. Chem. Soc.* **1992**, *114*, 7843-7851.
(56) Cantat, T.; Scott, B. L.; Kiplinger, J. L. Convenient access to the anhydrous thorium tetrachloride complexes $ThCl_4(DME)_2$, $ThCl_4(1,4\text{-dioxane})_2$ and $ThCl_4(THF)_{3.5}$ using commercially available and inexpensive starting materials. *Chem. Commun.* **2010**, *46*, 919-921.
(57) Schnaars, D. D.; Wu, G.; Hayton, T. W. Reactivity of UH_3 with mild oxidants. *Dalton Trans.* **2008**, 6121-6126.
(58) Pedrick, E. A.; Seaman, L. A.; Scott, J. C.; Griego, L.; Wu, G.; Hayton, T. W. Synthesis and Reactivity of a U(IV) Dibenzyne Complex. *Organometallics* **2016**, *35*, 494-502.
(59) Glendening, E. D.; Landis, C. R.; Weinhold, F. NBO 6.0: Natural bond orbital analysis program. *J. Comput. Chem.* **2013**, *34*, 1429-1437.
(60) Autschbach, J. The role of the exchange-correlation response kernel and scaling corrections in relativistic density functional nuclear magnetic shielding calculations with the zeroth-order regular approximation. *Mol. Phys.* **2013**, *111*, 2544-2554.
(61) Baerends, E.; Autschbach, J.; Bérces, A.; Bo, C.; Boerrigter, P.; Cavallo, L.; Chong, D.; Deng, L.; Dickson, R.; Ellis, D. Amsterdam density functional. *Theoretical Chemistry, Vrije Universiteit, Amsterdam, URL http://www. scm. com* **2006**, *42*.
(62) Assefa, M. K.; Sergentu, D.-C.; Seaman, L. A.; Wu, G.; Autschbach, J.; Hayton, T. W. Synthesis, Characterization, and Electrochemistry of the Homoleptic f Element Ketimide Complexes $[Li]_2[M(N{=}CtBuPh)_6]$ (M = Ce, Th). *Inorg. Chem.* **2019**, *58*, 12654-12661.
(63) Ganguly, G.; Sergentu, D.-C.; Autschbach, J. Ab Initio Analysis of Metal–Ligand Bonding in $An(COT)_2$ with An=Th, U in Their Ground- and Core-Excited States. *Chem. Eur. J.* **2020**, *26*, 1776-1788.
(64) Autschbach, J. Chapter One - NMR Calculations for Paramagnetic Molecules and Metal Complexes. In *Annual Reports in Computational Chemistry*, Dixon, D. A. Ed.; Vol. 11; Elsevier, 2015; pp 3-36.
(65) Kiplinger, J. L.; Morris, D. E.; Scott, B. L.; Burns, C. J. Convenient Synthesis, Structure, and Reactivity of $(C_5Me_5)U(CH_2C_6H_5)_3$: A Simple Strategy for the Preparation of Monopentamethylcyclopentadienyl Uranium(IV) Complexes. *Organometallics* **2002**, *21*, 5978-5982.

(66) Harris, R. K.; Becker, E. D.; Cabral de Menezes, S. M.; Goodfellow, R.; Granger, P. NMR nomenclature. Nuclear spin properties and conventions for chemical shifts(IUPAC Recommendations 2001). **2001**, *73*, 1795-1818.
(67) Harris, R. K.; Becker, E. D.; Cabral de Menezes, S. M.; Granger, P.; Hoffman, R. E.; Zilm, K. W. Further conventions for NMR shielding and chemical shifts (IUPAC Recommendations 2008). **2008**, *80*, 59-84.
(68) SMART Apex II, Version 2.1; Bruker AXS Inc.: Madison, WI; 2005.
(69) SAINT Software User's Guide, Version 7.34a; Bruker AXS Inc.: Madison, WI; 2005.
(70) Sheldrick, G. M. SADABS, University of Gottingen, Germany; 2005.
(71) SHELXTL PC, Version 6.12; Bruker AXS Inc.: Madison, WI; 2005.
(72) Diamond - Crystal and Molecular Structure Visualization. Crystal Impact - Dr. H. Putz & Dr. K. Brandenburg GbR, Kreuzherrenstr. 102, 53227 Bonn, Germany. http://www.crystalimpact.com/diamond.
(73) Paier, J.; Hirschl, R.; Marsman, M.; Kresse, G. The Perdew–Burke–Ernzerhof exchange-correlation functional applied to the G2-1 test set using a plane-wave basis set. *J. Chem. Phys.* **2005**, *122*.
(74) Lenthe, E. v.; Baerends, E.-J.; Snijders, J. G. Relativistic regular two-component Hamiltonians. *J. Chem. Phys.* **1993**, *99*, 4597-4610.
(75) Weigend, F.; Ahlrichs, R. Balanced basis sets of split valence, triple zeta valence and quadruple zeta valence quality for H to Rn: Design and assessment of accuracy. *Phys. Chem. Chem. Phys.* **2005**, *7*, 3297-3305.
(76) Pye, C. C.; Ziegler, T. An implementation of the conductor-like screening model of solvation within the Amsterdam density functional package. *Theor. Chem. Acc.* **1999**, *101*, 396-408.
(77) Adamo, C.; Barone, V. Toward chemical accuracy in the computation of NMR shieldings: the PBE0 model. *Chem. Phys. Lett.* **1998**, *298*, 113-119.
(78) Perdew, J. P.; Burke, K.; Ernzerhof, M. Generalized gradient approximation made simple. *Phys. Rev. Lett.* **1996**, *77*, 3865.

Chapter 4. Assessing the 4f orbital participation in the Ln-C bonds of $[Li(THF)_4][Ln(C_6Cl_5)_4]$ (Ln = La, Ce)

Portions of this work were published in:

Osvaldo Ordoñez, Xiaojuan Yu, Guang Wu, Jochen Autschbach, and Trevor W. Hayton, Assessing the 4f orbital participation in the Ln-C bonds of $[Li(THF)_4][Ln(C_6Cl_5)_4]$ (Ln = La, Ce). *Inorg.* **2022**, 61, 15138–15143

Table of Contents

4.1 Introduction

Homoleptic lanthanide aryl complexes have a long and rich history.[1-5] The first structurally characterized example, $[Li(THF)_4][Lu(2,6\text{-}Me_2C_6H_3)_4]$, was isolated in 1972 by Hursthouse and co-workers.[2] Since that time, a large number homoleptic Ln aryl complexes have been reported in the literature. Many of these complexes utilize pendant donor groups to stabilize the Ln-C_{aryl} bonds,[1, 3, 4] such as $[Ln(\eta^2\text{-}N,C\text{-}C_6H_4\text{-}o\text{-}CH_2NMe_2)_3]$ (Ln = Er, Yb, Lu, Y),[4] $[Ln(\eta^2\text{-}N,C\text{-}C_6H_4\text{-}o\text{-}CH(Me)NMe_2)_3]$ (Ln = Y, Dy, Nd, Sm),[1] $[Sm(\eta^2\text{-}N,C\text{-}C_6H_4\text{-}o\text{-}C(Me)_2NMe_2)_3]$,[1] and $[La\{(S,S,)\text{-Phebox-}^iPr\}_3]$,[3] among others.[1, 4, 6-8] However, many solvent-stabilized Ln aryl complexes are also known, which do not feature stabilizing pendant donor groups. Among these examples are several $[Ln(Ar)_3(solvent)_x]$- and $[Ln(Ar)_2(solvent)_x]$-type complexes,[9-12] including $[Yb(C_6F_5)_2(THF)_4]$ and $[Eu(Dpp)_2(THF)_2]$ (Dpp = 2,6-$Ph_2C_6H_3$).[11, 12] These complexes are functionally homoleptic due to the lability of their solvent donor ligands. Yet, despite this rich history, there are no reported lanthanide complexes containing the perchlorophenyl ligand (C_6Cl_5), which is remarkable given the large number of homoleptic C_6Cl_5 complexes reported for the transition metals,[13-22] and more recently, the actinides as discussed in chapters 2 and 3.[23, 24]

Previously, I and others have shown that ^{13}C NMR spectroscopy is a valuable tool to evaluate covalency in actinide-ligand bonding.[23-31] In particular, the ^{13}C chemical shifts of organometallic ligands have proven to be highly sensitive to the degree of 5f orbital participation in the An-C bonds. Actinide perchlorophenyl complexes have also proven useful in this regard.[23, 24] For example, in chapter 2 the C_{ipso} chemical shift in the uranyl C_6Cl_5

complex $[Li(Et_2O)_2(THF)][UO_2(C_6Cl_5)_3]$ ([Li][**2.1**]) was found at 236.7 ppm. Calculations reveal a 62 ppm downfield spin-orbit (SO) induced shift due to the involvement of the 5f orbitals in the U-C bonding.[23] Additionally, in chapter 3 the C_{ipso} chemical shift in the homoleptic thorium C_6Cl_5 complex $[Li(Et_2O)_2(THF)][Th(C_6Cl_5)_5]$ ([Li][**3.1**]) was found at 203 ppm, including a 27 ppm deshielding due to SO coupling.[24] In contrast, this method of analysis has not been widely applied to the lanthanides. In one case, reported by Schelter and co-workers, an analysis of the ^{13}C NMR spectrum of $[Li(THF)_4][Ce^{IV}(\kappa^2\text{-}ortho\text{-oxa})(MBP)_2]$ (*ortho*-oxa = dihydro-dimethyl-2-[4-(trifluoromethyl)phenyl]-oxazolide, MBP^{2-} = 2,2′-methylenebis(6-*tert*-butyl-4-methylphenolate)) reveals a calculated 40 ppm SO–induced shift for the C_{ipso} resonance, which is compelling evidence of 4f involvement in lanthanide(IV)-ligand bonding.[32] Additionally, Liddle and co-workers reported an analysis of the ^{13}C chemical shifts in a cerium(IV)-diphosphonioalkylidene complex, $[Ce(BIPM^{TMS})_2]$ ($BIPM^{TMS}$ = $\{C(PPh_2NSiMe_3)_2\}^{2-}$), which reveals a calculated 82.9 ppm, SO-induced shift for the Ce=C double bonds.[33] That said, to our knowledge this method has not been applied to Ln(III) organometallics.

In an effort to expand this method of analysis to lanthanide organometallics, I targeted the synthesis of two homoleptic lanthanide-aryl "ate" complexes $[Li(THF)_4][La(C_6Cl_5)_4]$ ([Li][**4.1**]) and $[Li(THF)_4][Ce(C_6Cl_5)_4]$ ([Li][**4.2**]). These complexes proved to be highly thermally sensitive; nonetheless, both complexes were characterized by X-ray crystallography and $^{13}C\{^1H\}$ NMR spectroscopy, and their electronic structures were examined by density functional theory (DFT) with a relativistic Hamiltonian.

4.2 Results and Discussion

4.2.1 Synthesis and Characterization

Reaction of $[La(NO_3)_3(THF)_4]$ with 4 equiv of LiC_6Cl_5[34] in cold Et_2O (-25 °C) resulted in immediate formation of an orange-yellow solution, concomitant with the deposition of copious amounts of tan precipitate. Work-up of reaction mixture afforded $[Li(THF)_4][La(C_6Cl_5)_4]$ ([Li][**4.1**]), which as isolated as colorless plates in 20% yield (Scheme 4.1). I also sought to synthesize the analogous cerium(III) aryl complex $[Li(THF)_4][Ce(C_6Cl_5)_4]$ ([Li][**4.2**]), which was prepared by reaction of $[Ce(NO_3)_3(THF)_4]$ with 4 equiv of LiC_6Cl_5 in cold Et_2O (-25 °C) (Scheme 4.1). Work-up of the reaction mixture followed by recrystallization from concentrated toluene afforded [Li][**4.2**] as yellow plates in 16% yield. Importantly, [Li][**4.1**] and [Li][**4.2**] represent the first homoleptic perchlorophenyl complexes of the lanthanides.

The low yields observed for [Li][**4.1**] and [Li][**4.2**] reflect their high thermal sensitivity (see below). Indeed, the highest yields were achieved when the reaction time and temperature were minimized. In particular, reaction times were kept to 2 min, and the work-up was performed using cold pentane and toluene. Longer reaction times (e.g., 1 h at room temperature) resulted in substantially reduced yields. Attempts to improve the yields of [Li][**4.1**] and [Li][**4.2**]were met with limited success. For example, reaction of LiC_6Cl_5 with $CeCl_3$ or $[CeCl_3(THF)_4]$ did not generate [Li][**4.2**], likely because the low solubility of either starting material in Et_2O resulted in minimal conversion. In this regard, the successful use of $[Ln(NO_3)_3(THF)_4]$ in this chemistry likely reflects its higher solubility in Et_2O. Additionally, our choice of solvents was somewhat limited because LiC_6Cl_5 reacts rapidly with THF.

Moreover, attempts to understand the mass balance of each transformation was complicated by the absence of a convenient NMR handle.

Scheme 4.1 Synthesis of Complexes [Li][**4.1**] and [Li][**4.2**].

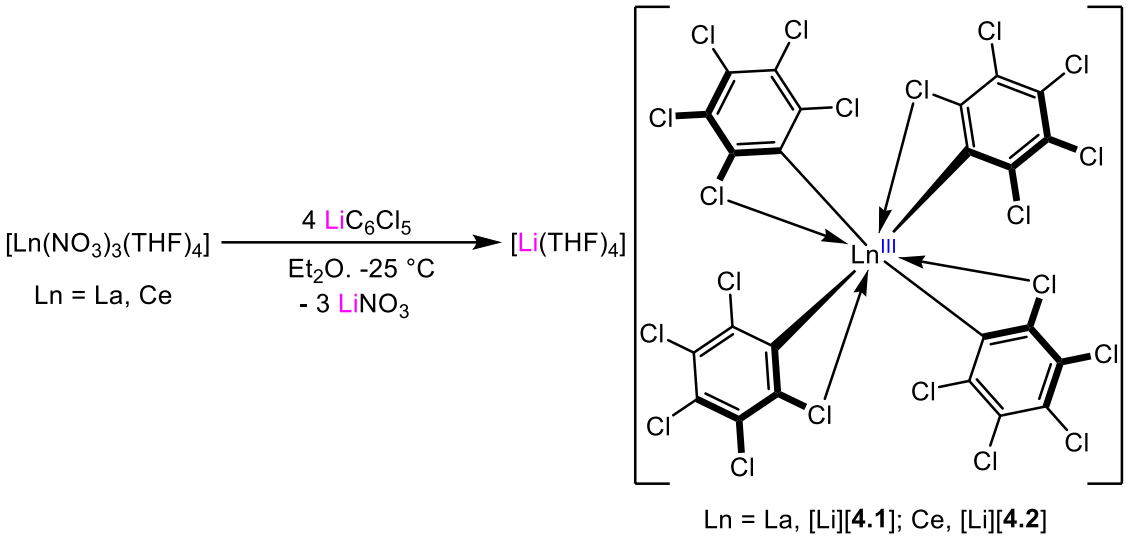

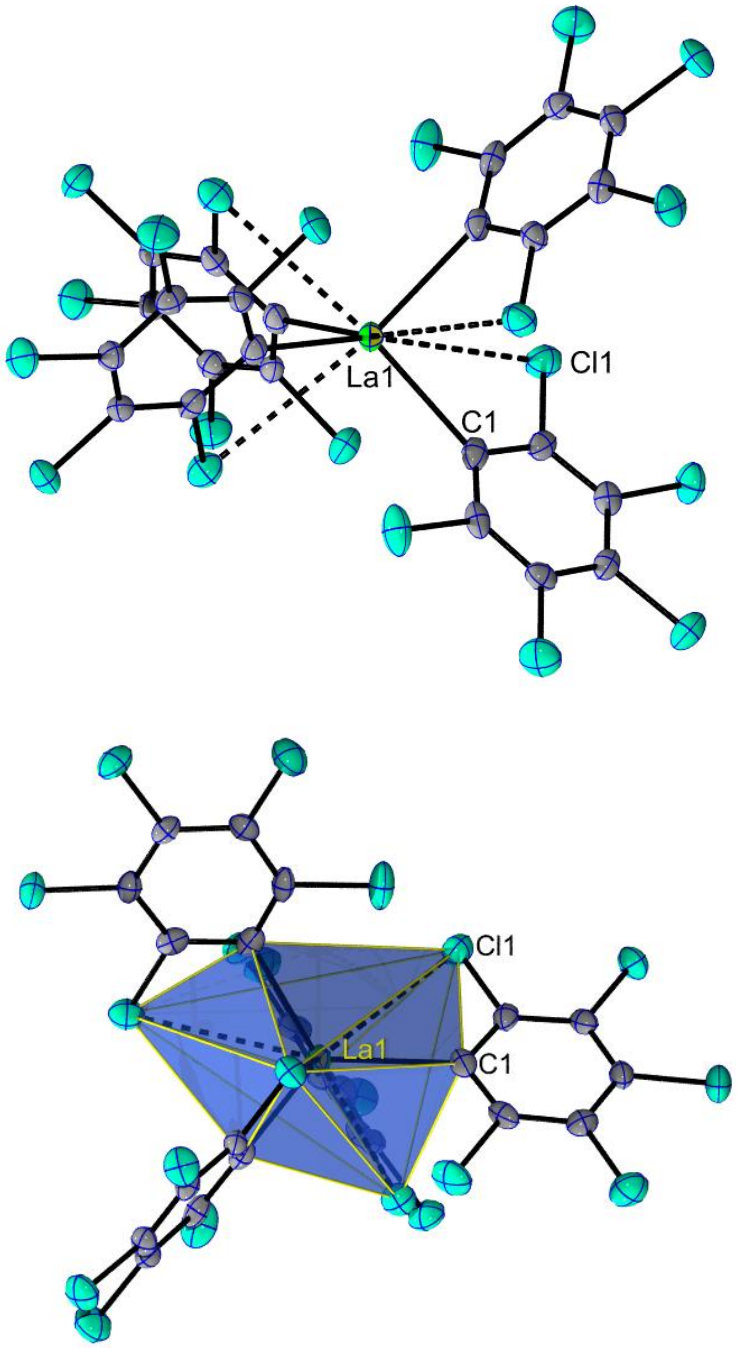

Figure 4.1 Solid-state molecular structure of [Li][**4.1**] shown with 50% probability ellipsoids (top). Solid-state molecular structure of [Li][**4.1**] with the triakis tetrahedron polygon shown in blue (bottom). The $[Li(THF)_4]^+$ counterion was omitted for clarity.

Complex [Li][**4.1**] crystallizes in the tetragonal space group $I4_1/a$ and features only one crystallographically independent aryl ligand (Figure 4.1). The eight-coordinate lanthanum center is coordinated by four *ipso* carbons and four "short" Ln—Cl contacts involving the *ortho*-Cl atoms of the C_6Cl_5 ligands. However, calculations suggest that the La center forms dative interactions of varying strengths with all eight *ortho*-Cl atoms (see below). According to the continuous shape measure,[35] the coordination geometry is best described as a T_d-symmetric triakis tetrahedron. Cl→M dative interactions were previously observed in $[Li(DME)_2(Et_2O)]_2[Li(DME)_2][Th(C_6Cl_5)_5]_3$ and $[Li(Et_2O)_4][U(C_6Cl_5)_5]$, as well as several transition metal examples.[14, 15, 19, 24] Despite these nominally stabilizing interactions, [Li][**4.1**] still exhibits appreciable thermal sensitivity (see below). The La-C distance in [Li][**4.1**] is 2.594(3) Å (Table 4.1), which is similar to those seen in other σ-bonded lanthanum aryl complexes,[3, 8, 36] such as $[Cp_2La(2,6\text{-}(Me_2NCH_2)C_6H_3]$ (2.548(3) Å).[36] The Cl→Ln distance in [Li][**4.1**] (3.5193(9) Å) is significantly longer than the Cl→An interactions observed for $[Li(DME)_2(Et_2O)]_2[Li(DME)_2][Th(C_6Cl_5)_5]_3$ (av. 3.09 Å) and $[Li(Et_2O)_4][U(C_6Cl_5)_5]$ (av. 3.13 Å), despite their relatively similar ionic radii (i.e., La^{3+} = 1.032 Å; Th^{4+} = 0.94 Å; U^{4+} = 0.89 Å).[24, 37]

Complex [Li][**4.2**] crystallizes in the monoclinic space group $P2_1/c$ as the toluene solvate, [Li][**4.2**]·C_7H_8 (Figure 4.5). The solid-state molecular structure of [Li][**4.2**] reveals an eight-coordinate cerium center formed by four Ln-C σ-bonds and four "short" Cl→Ln dative interactions. According to the continuous shape measure,[35] its coordination geometry is best described as a highly distorted triakis tetrahedron. The average Ce-C distance in [Li][**4.2**] is 2.559(7) Å (range = 2.542(7) – 2.579(7) Å; Table 4.1), which is shorter than the La-C distance in [Li][**4.1**], consistent with smaller ionic radius of the Ce(III) ion.[37] These values are also

shorter than the Ce-C_{ipso} distances in [Cp'$_2$Ce(C_6F_5)] (Cp' = 1,2,4-^{t}Bu$_3$$C_5H_2$; 2.621(4) Å),[38] [Cp'$_2$Ce(2,3,4,6-$C_6HF_4$)] (2.623(3) Å),[38] and [Cp'$_2$Ce(2,3,4,5-C_6HF_4)] (2.64(2) Å).[39] Interestingly, these examples also feature F→Ce dative interactions similar to the Cl→Ce interactions found in [Li][**4.2**].[40] In this regard, the "short" Cl→Ce distances in [Li][**4.2**] range from 3.455(2) to 3.558(2) Å. These values bracket that found in [Li][**4.1**].

Table 4.1 Selected metrical parameters for [Li][**4.1**] and [Li][**4.2**]·C_7H_8

Complex	[Li][**4.1**]	[Li][**4.2**]·C_7H_8
Ln-C	2.594(3)	2.557(6), 2.542(7), 2.579(7), 2.552(7)
Cl→Ln	3.5193(9)	3.455(2), 3.470(2), 3.545(2), 3.558(2)
Ln-C_{ipso}-C_{ortho}	118.5(3)°, 126.1(2)°	118.8(5)°, 127.6(5)° 119.1(4)°, 126.1(5)° 120.3(5)°, 124.2(4)° 121.9(5)°, 123.0(5)°

Both [Li][**4.1**] and [Li][**4.2**] exhibit appreciable thermal sensitivity, as evidenced by a $^{13}C\{^1H\}$ NMR spectrum of an *in situ* prepared sample of [Li][**4.1**] that was allowed to stand at room temperature for 1 h (Figure 4.18). This spectrum reveals the formation of a number of decomposition products, including C_6Cl_5H, and while the other decomposition products could not be definitively identified, the number of peaks, and their positions, suggest that they could be chlorinated biphenyls.[41] Similar products are generated upon decomposition of Ln-C_6F_5 complexes.[11, 40, 42, 43] Additionally, both [Li][**4.1**] and [Li][**4.2**] quickly decompose upon dissolution in tetrahydrofuran, CH_2Cl_2, pyridine, dimethoxyethane, and dimethylacetamide, as evidenced by the rapid formation of intractable deep orange-brown solutions. Isolated

samples of [Li][**4.1**] and [Li][**4.2**] are insoluble hexanes and Et_2O, and only somewhat soluble in arene solvents. Curiously, however, the solubility of material prepared *in situ* in Et_2O is much improved. Accordingly, I recorded their $^{13}C\{^1H\}$ NMR spectra with material generated *in situ* in this solvent. These spectra were also recorded at -35 °C to minimize thermal decomposition. The *in situ* $^{13}C\{^1H\}$ NMR spectrum of complex [Li][**4.1**], recorded in a mixture of Et_2O/benzene-d_6, features a resonance at 185.41 ppm (Figure 4.2), which I assign to the *ipso* carbon environment of its pentachlorophenyl ligands. This resonance is much more upfield than the C_{ipso} resonances of $[Li(Et_2O)_2(THF)][UO_2(C_6Cl_5)_3]$ ([Li][**2.1**])[23] from chapter 2, which appear at 236.7 ppm and $[Li(DME)_2(Et_2O)]_2[Li(DME)_2][Th(C_6Cl_5)_5]_3$ ([Li][**3.1**])[24] from chapter 3, which appear at 198.78 ppm. This difference suggests a much less covalent M-C interaction (see below for more discussion). This spectrum also features resonances at 139.80, 128.73, and 128.47 ppm, which I ascribe to the *ortho*, *meta*, and *para* resonances of the pentachlorophenyl ligand, respectively. Additionally, I observe resonances at 184.35, 141.06, 127.74, and 127.38 ppm, which I ascribe to the *ipso*, *ortho*, *meta*, and *para* resonances of unreacted LiC_6Cl_5, respectively. Confirmation of these assignments comes from a ^{13}C NMR spectrum of [Li][**4.1**] prepared with 10 equiv of LiC_6Cl_5 (Figure 4.12), as well as ^{13}C NMR spectrum of a sample of LiC_6Cl_5 prepared *in situ* (Figure 4.17). The *in situ* $^{13}C\{^1H\}$ NMR spectrum of [Li][**4.2**], recorded Et_2O/benzene-d_6, features a distinctive downfield resonance at 557.87 ppm (Figure 4.3), tentatively attributable to the *ipso* carbon of the pentachlorophenyl ligand. In addition, I observe resonances at 150.92, 149.83, and 129.66 ppm, which are assigned to the *ortho/meta*, *para*, and *ortho/meta* resonances of the pentachlorophenyl ligand, respectively. The large downfield shift of the C_{ipso} peak is consistent with the paramagnetism

expected for [Li][**4.2**]. This spectrum also exhibits resonances assignable to unreacted LiC_6Cl_5.

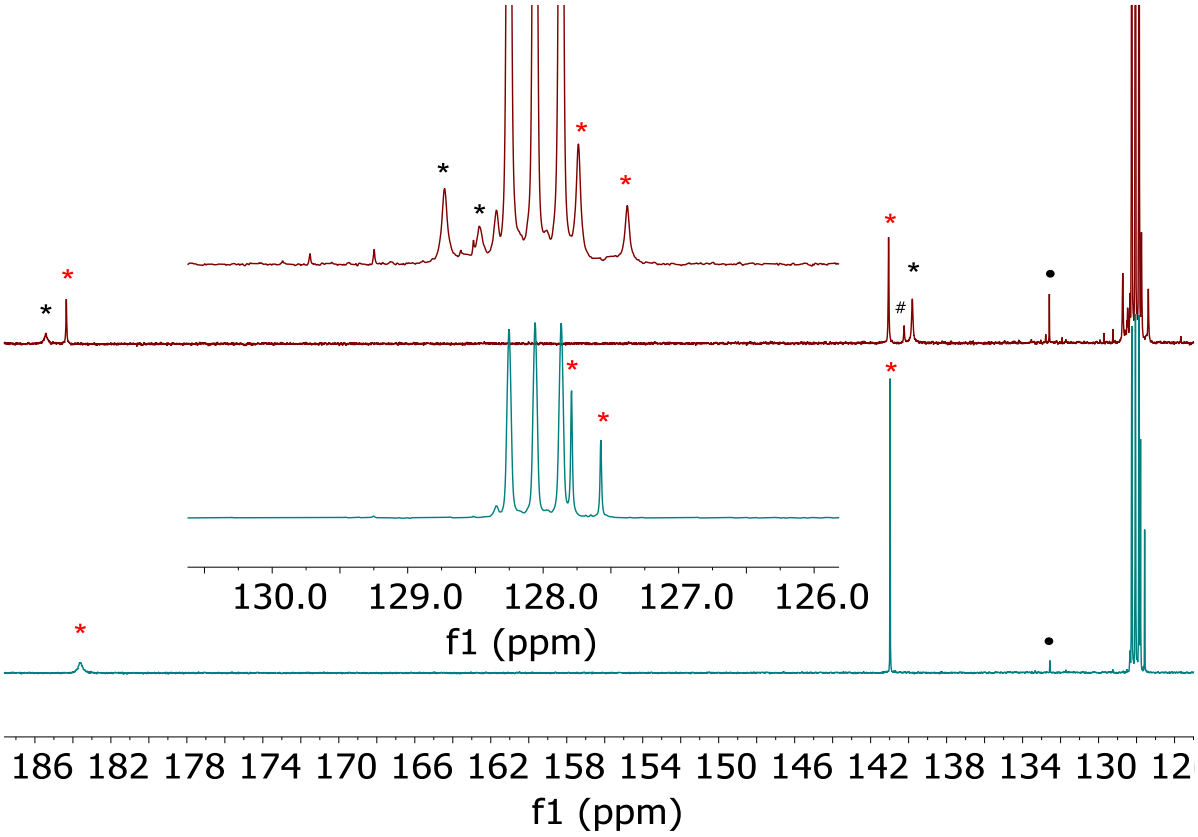

Figure 4.2. Partial $^{13}C\{^1H\}$ NMR spectrum of *in situ* generated [Li][**4.1**] in Et_2O/benzene-d_6 at –35 °C (top). Partial $^{13}C\{^1H\}$ NMR spectrum of *in situ* generated LiC_6Cl_5 in Et_2O/benzene-d_6 at –35 °C (bottom). Inserts display enlarged section of $^{13}C\{^1H\}$ NMR spectra for clarity. (*) indicates the presence of [Li][**4.1**], (*) indicates the presence of LiC_6Cl_5, (•) indicates the presence of C_6Cl_6, and (#) indicates an unidentified impurity.

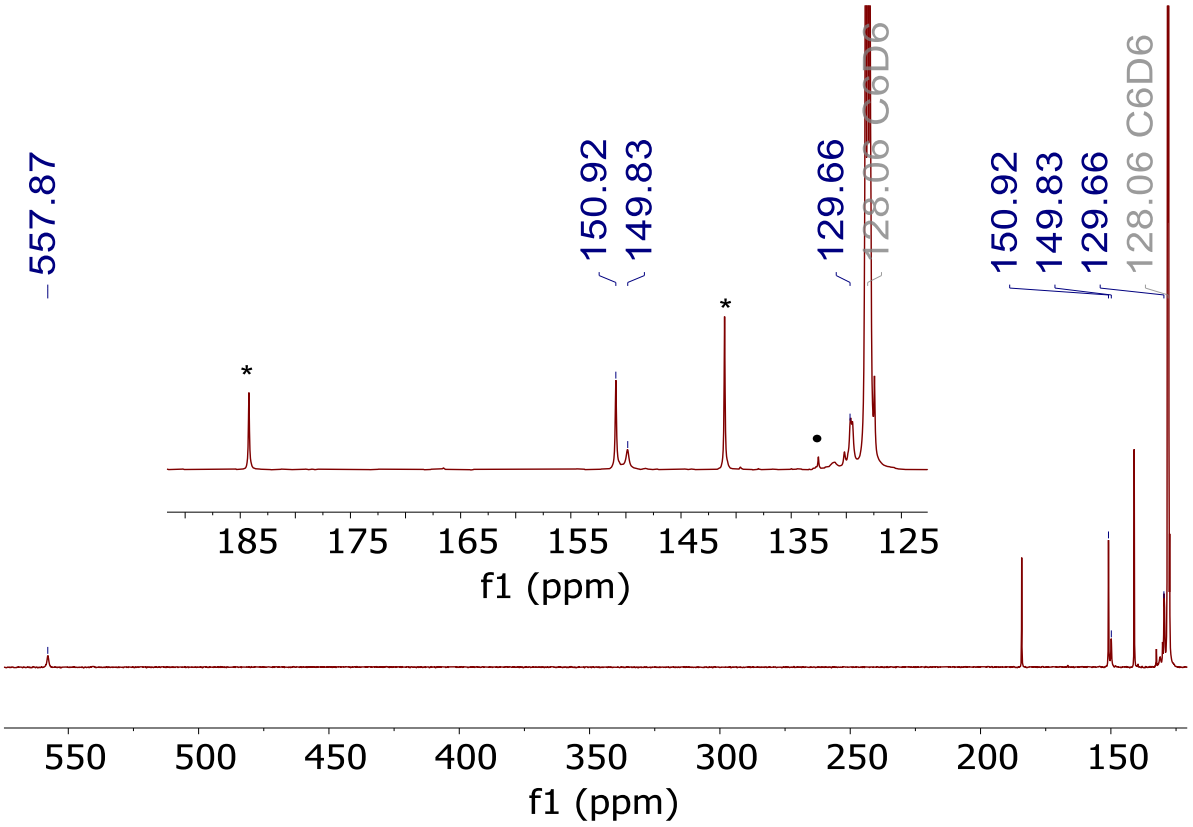

Figure 4.3. $^{13}C\{^{1}H\}$ NMR spectrum of *in situ* generated [Li][**4.2**] in Et_2O/benzene-d_6 at –35 °C. (•) indicates the presence of C_6Cl_6 and (*) indicates the presence of LiC_6Cl_5. Insert displays enlarged section of $^{13}C\{^{1}H\}$ NMR spectrum for clarity.

4.2.2 Computational Analysis

To understand the electronic structures and bonding interactions within [Li][**4.1**] and [Li][**4.2**], Dr. Xiaojuan Yu and Prof. Jochen Autschbach at the State University of New York at Buffalo carried out DFT calculations with various hybrid and non-hybrid functionals, and a relativistic Hamiltonian, on the anionic components, [**4.1**]$^-$ and [**4.2**]$^-$.[44-46] Complete computational details are given in the Supporting Information. The calculated NMR shifts of [**4.1**]$^-$ were insensitive to the choice of functional, and therefore only the NMR data and corresponding bonding analysis obtained with the PBE functional are discussed in the

following paragraphs. Complex [**4.1**]$^-$ is a closed-shell spin singlet, whereas complex [**4.2**]$^-$ exhibits a spin doublet configuration, as expected for a Ce(III) complex. The spin density is effectively localized at cerium, as evidenced by the Ce spin population of 0.986 (idealized 1.0) (Figure 4.6). The singly occupied molecular orbital (MO) is mostly of non-bonding 4f character. Natural localized MO (NLMO) analysis of the Ln-C_{ipso} interactions reveals nearly identical orbital compositions for La and Ce (Figure 4.4), which is also indicated by the similar Ln-C_{ipso} Wiberg bond orders (WBOs) of 0.30 and 0.33 for [**4.1**]$^-$ and [**4.2**]$^-$, respectively. The Ln weights in the σ-bonding NLMOs range from 8% (for [**4.1**]$^-$) to 9% (for [**4.2**]$^-$). Within these weights, the 4f and 5d contributions are 11% and 73% for [**4.1**]$^-$, respectively, and 17% and 69% for [**4.2**]$^-$, respectively, with the balance being 6s character in both cases (Table 4.2). The C_{ipso} weights in the σ-bonding NLMOs are 84% for both [**4.1**]$^-$ and [**4.2**]$^-$. Within these weights, the 2s and 2p contributions are 25% and 75% for [**4.1**]$^-$, respectively, and 26% and 74% for [**4.2**]$^-$, respectively. In other words, there is an appreciable degree of donation bonding, but weaker than what is known from similar actinide complexes,[24, 27, 47] and the involvement of the 4f orbitals in the donation bonds is overall very minor. For comparison, the An-C_{ipso} WBOs for $[An(C_6Cl_5)_5]^-$ discussed in chapter 3 are much larger, ranging from 0.47 for the Th analogue and 0.56 in the U analogue.[24] This difference reflects both the greater expected M-L covalency for the early actinides vs. the lanthanides, as well as the greater expected M-L covalency for M^{4+} vs M^{3+}.[32, 48] The NLMO analysis of [**4.1**]$^-$ and [**4.2**]$^-$ also reveals the presence of eight weak Cl→An dative interactions in each complex. The average Ln weight in the NLMOs of these dative interactions is 2% for both [**4.1**]$^-$ and [**4.2**]$^-$ (Figure 4.7 and Table 4.2), which are commensurate with the experimentally measured (relatively long) Cl→Ln distances.

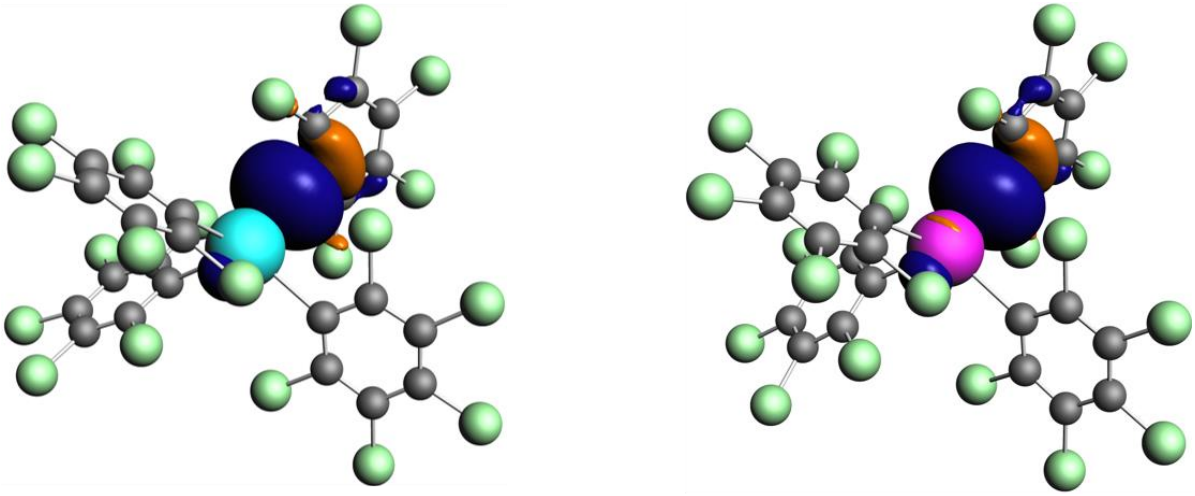

Figure 4.4 Representative Ln–C bonding NLMOs in [**4.1**]$^-$ and [**4.2**]$^-$. (Isosurface values ±0.03 au.)

Table 4.2 % weight compositions of the Ln-C (Ln = La, Ce) bonding and Lone pair (LP) NLMOs in [**4.1**]$^-$ and [**4.2**]$^-$. % orbital character averaged over equivalent NLMOs.

Complex	Orbital	Total L	*n*s	*n*p	Total Ln	6s	5d	4f
[**4.1**]$^-$	σ(La-C)	84	25	75	8	15	73	11
	LP(Cl)	96	26	74	2	19	76	5
[**4.2**]$^-$	σ(Ce-C)	84	26	74	9	14	69	17
	LP(Cl)	96	27	73	2	20	75	5

The ^{13}C NMR chemical shifts of the C_{ipso} nuclei for $[(Et_2O)_3Li(C_6Cl_5)]$ and [**4.1**]$^-$ were calculated with and without SO coupling effects. Repeated attempts to model the paramagnetic NMR (pNMR) ligand shifts for [**4.2**]$^-$ with DFT or wavefunction calculations were unsuccessful, likely because of a strong sensitivity of the spin delocalization and spin population to the dynamics of the system;[49-51] therefore, the chemical shifts for [**4.2**]$^-$ **are not included in this analysis.** The calculated C_{ipso}, C_{ortho}, C_{meta}, and C_{para} chemical shifts for $[(Et_2O)_3Li(C_6Cl_5)]$ are 180.9 ppm (exp = 183.63 ppm), 145.1 ppm (exp = 140.97 ppm), 132.6 ppm (exp = 127.79 ppm), and 131.7 ppm (exp = 127.57 ppm). These predictions match the experimental values reasonably well, and further confirm our assignments for the unreacted LiC_6Cl_5 in the *in situ* ^{13}C NMR spectra. The calculated C_{ipso}, C_{ortho}, C_{meta}, and C_{para} chemical shifts for [**4.1**]$^-$ are 184.0 ppm (exp = 185.41 ppm), 140.6 ppm (exp = 139.80 ppm), 131.6 ppm (exp = 128.73 ppm), and 132.3 ppm (exp = 128.47 ppm). These values, especially the C_{ipso} and C_{ortho} chemical shifts, are in excellent agreement with experiment.

The diamagnetic, paramagnetic, and spin-orbit shielding (σ) contributions to the C_{ipso} chemical shifts for both [**4.1**]$^-$ and $[Th(C_6Cl_5)_5]^-$ ([**3.1**]$^-$) are provided in Table 4.3. Note, for

both [**4.1**]$^-$ and [Th(C_6Cl_5)$_5$]$^-$ ([**3.1**]$^-$), the 2s contributions to the M-C_{ipso} bonding are similar (25 and 28%, respectively).[24] Likewise, σ_d contributions are essentially identical and the σ_p contributions are very similar. The only substantive difference is the σ_{SO} contribution (-7.9 and -26.1 ppm, respectively), which can be explained by the greater covalency (and greater valence f-shell contributions) in the M-C_{ipso} donation bonds of [Th(C_6Cl_5)$_5$]$^-$ vs. [**4.1**]$^-$. [Ce^{IV}(κ^2-*ortho*-oxa)(MBP)$_2$]$^-$ features a large (40 ppm) deshielding due to SO coupling for the same reason.[32] Nonetheless, while the SO contribution to the C_{ipso} chemical shift in [**4.1**]$^-$ is relatively small, as expected given the weak 4f (and to a lesser extent 5d) participation in the La-C_{ipso} bonds, its inclusion is unequivocally necessary to achieve good agreement between theory and experiment.

Table 4.3 Calculated C_{ipso} NMR chemical shift (δ, in ppm) and individual isotropic shielding contributions (σ, in ppm) in [**4.1**]$^-$ and [Th(C_6Cl_5)$_5$]$^-$ at the SO-PBE level of theory.[a]

Compound	Method	σ_d	σ_p	σ_{so}	σ_{calc}	δ_{calc}	δ_{expt}	Ref
[**4.1**]$^-$	SO-PBE	248.7	-244.6	-7.9	-3.8	184.0	185.4	This work
[Th(C_6Cl_5)$_5$]$^-$ ([**3.1**]$^-$)	SO-PBE	248.4	-237.1	-26.1	-14.8	203.2	198.8	Ch. 3

[a] σ_d, σ_p and σ_{so} indicate the diamagnetic, paramagnetic, and SO shielding, respectively, as partitioned in the NMR calculations.

4.3 Summary

In summary, I have prepared and characterized the first structurally authenticated homoleptic perchlorophenyl complexes of the lanthanides, [Li(THF)$_4$][La(C_6Cl_5)$_4$] ([Li][**4.1**]) and [Li(THF)$_4$][Ce(C_6Cl_5)$_4$] ([Li][**4.2**]), and I have confirmed their formulations by X-ray crystallography. A combined ^{13}C NMR spectroscopic and DFT study found that the Ln-C_{ipso}

bonds are mostly ionic, with the donation bonding mainly involving the Ln 5d orbitals and only minimal 4f orbital participation. Indeed, the spin-orbit-induced deshielding of the C_{ipso} chemical shift was only ca. 8 ppm – much less than that calculated for comparable An^{4+} perchlorophenyl complexes. Yet, while the SO contribution to the C_{ipso} chemical shift is small, it must be included in the DFT calculations to accurately match theory to experiment, highlighting the sensitivity of this approach to unravel electronic structure.

4.4 Experimental

4.4.1 General Procedures

All reactions and subsequent manipulations were performed under anaerobic and anhydrous conditions under an atmosphere of dinitrogen. Hexanes, diethyl ether (Et_2O), and toluene were dried using a Vacuum Atmospheres DRI-SOLV Solvent Purification system and stored over 3Å sieves for 24 h prior to use. Tetrahydrofuran (THF) was distilled over Na/benzophenone and stored over activated 3 Å molecular sieves for 24 h prior to use. Benzene-d_6 was dried over 3Å molecular sieves for 24 h prior to use. LiC_6Cl_5,[34] $[La(NO_3)_3(THF)_4]$,[52] and $[Ce(NO_3)_3(THF)_4]$[52] were synthesized according to the previously reported procedures. All other reagents were purchased from commercial suppliers and used as received.

^1H, $^{13}C\{^1H\}$, and $^7Li\{^1H\}$ NMR spectra were recorded on an Agilent Technologies 400-MR DD2 400 MHz spectrometer or a Bruker AVANCE NEO 500 MHz spectrometer. ^1H and $^{13}C\{^1H\}$ NMR spectra were referenced to external tetramethylsilane (TMS) using the residual protio solvent peaks as internal standards. $^7Li\{^1H\}$ NMR spectra were referenced indirectly with the ^1H chemical shift of TMS at 0 ppm, according to IUPAC standard.[53, 54] IR spectra

were recorded on a Nicolet 6700 FT-IR spectrometer. Elemental analyses were performed by the Microanalytical Laboratory at the University of California (Berkeley, CA).

4.4.2 Synthesis of [LiC_6Cl_6]

The synthesis of LiC_6Cl_5 was performed according to the literature procedure with slight modifications.[34] *Caution! LiC_6Cl_5 reportedly detonates upon attempted isolation from ethereal solvents.*[55] *Accordingly, it should only be handled in situ.* A cold solution (–25 °C) of *n*-BuLi in hexanes (0.2 mL, 0.50 mmol, 2.5 M) was added dropwise to a cold, stirring suspension (–25 °C) of C_6Cl_6 (142.4 mg, 0.50 mmol) in Et_2O (2 mL). Upon addition of *n*-BuLi, the solids dissolved and the solution became a golden color. The resulting LiC_6Cl_5 solution was used immediately, as prepared, and assumed to be 0.25 M.

4.4.3 Synthesis of [$Li(THF)_4$][$La(C_6Cl_5)_4$] ([Li][4.1])

A cold (–25 °C) solution of LiC_6Cl_5 (2 mL in Et_2O, 0.50 mmol, 0.25 M) was added to a cold (–25 °C), stirring suspension of [$La(NO_3)_3(THF)_4$] (76.6 mg, 0.125 mmol) in Et_2O (2 mL), which resulted in an immediate color change to orange-yellow, concomitant with the deposition of a flocculent brown precipitate. After 2 min of stirring, the reaction mixture was filtered through a Celite column (0.5 cm × 5 cm) supported on glass wool to afford a clear, orange-yellow filtrate. The volatiles were removed *in vacuo* and the resulting tacky solid was triturated with cold pentane (–25 °C; 2 × 1 mL) to yield a light-orange solid. The solid was then extracted into cold toluene (–25 °C; 3 mL) and the resulting orange solution was filtered through a Celite column (0.5 cm × 5 cm) supported on glass wool to afford a clear, orange filtrate. The volume of the filtrate was reduced to 1 mL *in vacuo* and the sample was stored at –25 °C for 24 h, which resulted in the deposition of colorless plates. The solid was isolated

by decanting the supernatant and then dried briefly *in vacuo* (35.9 mg, 20% yield). Anal. Calcd for $C_{40}H_{32}LiO_4Cl_{20}La$: C, 33.56; H, 2.25 Found: C, 32.11; H, 1.99. IR (KBr pellet, cm^{-1}): 3108 (vw), 3066 (vw), 2977 (w), 2960 (w), 2883 (w), 1729 (vw), 1556 (w), 1523 (m). 1502 (m), 1457 (m), 1446 (m), 1419 (w), 1396 (s), 1332 (s), 1309 (s), 1278 (s), 1241 (m), 1238 (m), 1226 (m), 1170 (s), 1128 (m), 1087 (s), 1051 (s), 954 (vw), 946 (vw), 916 (w), 889 (m), 865 (s), 813 (s), 809 (s), 730 (m), 696 (m), 684 (s), 653 (s), 563 (m), 545 (w), 526 (w), 428 (w).

4.4.4 Synthesis of $[Li(THF)_4][Ce(C_6Cl_5)_4]$ ([Li][4.2])

A cold (–25 °C) solution of LiC_6Cl_5 (2 mL in Et_2O, 0.50 mmol, 0.25 M) was added to a cold (–25 °C), stirring suspension of $[Ce(NO_3)_3(THF)_4]$ (76.8 mg, 0.125 mmol) in Et_2O (2 mL), which resulted in an immediate color change to yellow, concomitant with the deposition of a flocculent brown precipitate. After 2 min of stirring, the reaction mixture was filtered through a Celite column (0.5 cm × 5 cm) supported on glass wool to afford a clear, yellow filtrate. The volatiles were removed *in vacuo* and the resulting tacky solid was triturated with cold pentane (25 °C; 2 × 1 mL) to yield a pale-yellow solid. The solid was then extracted into cold toluene (25 °C; 3 mL) and the resulting orange solution was filtered through a Celite column (0.5 cm × 5 cm) supported on glass wool to afford a clear, orange filtrate. The volume of the filtrate was reduced to 1 mL *in vacuo* and the sample was stored at –25 °C for 24 h, which resulted in the deposition of yellow plates. The solid was isolated by decanting the supernatant and then dried briefly *in vacuo* (28 mg, 15.6% yield). Anal. Calcd for $C_{40}H_{32}Li_1O_4Cl_{20}Ce$: C, 33.53; H, 2.25 Found: C, 33.91; H, 2.37. IR (KBr pellet, cm^{-1}): 3106 (vw), 3064 (w), 3031 (vw), 2975 (w), 2950 (w), 2881 (w), 1729 (w), 1602 (vw), 1556 (w), 1523 (m), 1502 (m), 1496 (m), 1457 (m), 1434 (m), 1427 (m). 1396 (s), 1332 (s), 1309 (s), 1276 (s), 1241 (m), 1236 (m), 1226 (m), 1170 (s), 1130 (m), 1087 (m), 1051 (s), 1000 (w),

946 (vw), 916 (m), 889 (m), 865 (s), 829 (w), 808 (s), 811 (s), 775 (w), 730 (m), 688 (m), 684 (s), 655 (s), 580 (vw), 563 (m), 545 (w), 526 (w), 464 (w), 431 (w).

4.4.5 *In Situ* Preparation of [Li][4.1]

A cold (–25 °C) solution of LiC_6Cl_5 (2 mL in Et_2O, 0.50 mmol, 0.25 M) was added to a cold (–25 °C), stirring suspension of $[La(NO_3)_3(THF)_4]$ (76.6 mg, 0.125 mmol) in Et_2O (2 mL). After 2 min, the reaction mixture was filtered through a Celite column (0.5 cm × 5 cm) supported on glass wool to afford an orange-yellow filtrate. The volume of the filtrate was reduced to 1 mL *in vacuo*. An aliquot (0.6 mL) of the concentrated reaction filtrate and 4 drops (ca. 0.03 mL) of benzene-d_6 was then transferred to an NMR tube. $^{13}C\{^1H\}$ NMR (500 MHz, –35 °C, Et_2O/benzene-d_6): δ 185.41 (*i*-C, [Li][**4.1**]), 184.35 (*i*-C, LiC_6Cl_5), 141.06 (*o*-C, LiC_6Cl_5), 139.80 (*o*-C, [Li][**4.1**]), 128.73 (*m*-C, [Li][**4.1**]), 128.47 (*p*-C, [Li][**4.1**]), 127.74 (*m*-C, LiC_6Cl_5), 127.38 (*p*-C, LiC_6Cl_5). $^7Li\{^1H\}$ NMR (500 MHz, –35 °C, Et_2O/benzene-d_6): δ 0.10 (s).

4.4.6 *In Situ* Preparation of [Li][4.1] using 10 equiv of LiC_6Cl_5

A cold (–25 °C) solution of LiC_6Cl_5 (2 mL in Et_2O, 0.50 mmol, 0.25 M) was added to a cold (–25 °C), stirring suspension of $[La(NO_3)_3(THF)_4]$ (30.6 mg, 0.05 mmol) in Et_2O (2 mL). After 2 min, the reaction mixture was filtered through a Celite column (0.5 cm × 5 cm) supported on glass wool to afford a clear amber reaction filtrate. The volume of the filtrate was reduced to 1 mL *in vacuo*. An aliquot (0.6 mL) of the concentrated reaction filtrate and 4 drops (ca. 0.03 mL) of benzene-d_6 was then transferred to an NMR tube. $^{13}C\{^1H\}$ NMR (500 MHz, –35 °C, Et_2O/benzene-d_6): δ 185.32 (*i*-C, [Li][**4.1**]), 183.88 (*i*-C, LiC_6Cl_5), 141.02 (*o*-

C, LiC_6Cl_5), 139.84 (*o*-C, [Li][**4.1**]). $^7Li\{^1H\}$ NMR (500 MHz, –35 °C, Et_2O/benzene-d_6): δ 0.57 (s).

4.4.7 *In Situ* Preparation of [Li][4.2]

A cold (–25 °C) solution of LiC_6Cl_5 (2 mL in Et_2O, 0.50 mmol, 0.25 M) was added to a cold (–25 °C), stirring suspension of $[Ce(NO_3)_3(THF)_4]$ (76.8 mg, 0.125 mmol) in Et_2O (2 mL). After 2 min, the reaction mixture was filtered through a Celite column (0.5 cm × 5 cm) supported on glass wool to afford a yellow filtrate. The volume of the filtrate was reduced to 1 mL *in vacuo*. An aliquot (0.6 mL) of the concentrated reaction filtrate and 4 drops (ca. 0.03 mL) of benzene-d_6 was then transferred to an NMR sample tube. $^{13}C\{^1H\}$ NMR (500 MHz, –35 °C, Et_2O/benzene-d_6): δ 557.87 (*i*-C, [Li][**4.2**]), 184.21 (*i*-C, LiC_6Cl_5), 150.92 (*o*-C or *m*-C, [Li][**4.2**]), 149.83 (*p*-C, [Li][**4.2**]), 141.05 (*o*-C, LiC_6Cl_5), 129.66 (*o*-C or *m*-C, [Li][**4.2**]). $^7Li\{^1H\}$ NMR (500 MHz, –35 °C, Et_2O/benzene-d_6): δ –0.79 (s).

4.4.8 *In Situ* Preparation of [Li][4.2] using 10 equiv of LiC_6Cl_5

A cold (–25 °C) solution of LiC_6Cl_5 (2 mL in Et_2O, 0.50 mmol, 0.25 M) was added to a cold (–25 °C), stirring suspension of $[Ce(NO_3)_3(THF)_4]$ (30.7 mg, 0.05 mmol) in Et_2O (2 mL). After 2 min, the reaction mixture was filtered through a Celite column (0.5 cm × 5 cm) supported in glass wool to afford orange-yellow filtrate. The volume of the filtrate was reduced to 1 mL *in vacuo*. An aliquot (0.6 mL) of the concentrated reaction filtrate and 4 drops (ca. 0.03 mL) of benzene-d_6 was then transferred to an NMR sample tube. $^{13}C\{^1H\}$ NMR (500 MHz, –35 °C, Et_2O/benzene-d_6): δ 558.36 (*i*-C, [Li][**4.2**]), 183.91 (*i*-C, LiC_6Cl_5), 151.03 (*o*-C or *m*-C, [Li][**4.2**]), 150.11 (*p*-C, [Li][**4.2**]), 141.02 (*o*-C, LiC_6Cl_5), 129.84 (*o*-C or *m*-C, [Li][**4.2**]). (500 MHz, –35 °C, Et_2O/benzene-d_6): δ 0.14 (s).

4.4.9 Spectroscopic Characterization of *In Situ* Generated LiC_6Cl_5

A cold solution (–25 °C) of *n*-BuLi in hexanes (0.2 mL, 0.50 mmol, 2.5 M) was added dropwise to a cold, stirring suspension (–25 °C) of C_6Cl_6 (142.4 mg, 0.50 mmol) in Et_2O (2 mL). Upon addition of *n*-BuLi, the solids dissolved and solution became a golden color. The volume of the filtrate was reduced to 1 mL *in vacuo*. An aliquot (0.6 mL) of the reaction mixture and 4 drops (ca. 0.03 mL) of benzene-d_6 was then transferred to an NMR sample tube. $^{13}C\{^1H\}$ NMR (500 MHz, –35 °C, Et_2O/benzene-d_6): δ 183.63 (*i*-C, LiC_6Cl_5), 140.97 (*o*-C, LiC_6Cl_5), 127.79 (*m*-C, LiC_6Cl_5), 127.57 (*p*-C, LiC_6Cl_5). $^7Li\{^1H\}$ NMR (500 MHz, –35 °C, Et_2O/benzene-d_6): δ 0.76 (s).

4.4.10 X-Ray Crystallography

Data for all complexes were collected on a Bruker KAPPA APEX II diffractometer equipped with an APEX II CCD detector using a TRIUMPH monochromator with a Mo Kα X-ray source (α = 0.71073 Å). The crystals were mounted on a cryoloop under Paratone-N oil, and all data were collected at 100(2) K using an Oxford nitrogen gas cryostream. Data were collected using ω scans with 0.5° frame widths. Frame exposures of 15 s were used for [Li][**4.1**] and [Li][**4.2**]·C_7H_8. Data collection and cell parameter determinations were conducted using the SMART program.[56] Integration of the data frames and final cell parameter refinement were performed using SAINT software.[57] Absorption correction of the data was carried out using the multi-scan method SADABS.[58] Subsequent calculations were carried out using SHELXTL.[59] Structure determination was done using direct or Patterson methods and difference Fourier techniques. All hydrogen atom positions were idealized and rode on the atom of attachment. Structure solution and refinement were performed using SHELXTL.[59] Graphics, and creation of publication materials were performed using Diamond.[60]

For complex [Li][**4.2**]·C_7H_8, the toluene solvate molecule exhibited positional disorder, which was addressed by constraining the affected atoms with the SADI command. These carbon atoms were refined isotropically.

Further crystallographic details of complexes [Li][**4.1**] and [Li][**4.2**]·C_7H_8 can be found in Table 4.4. Complexes [Li][**4.1**] and [Li][**4.2**]·C_7H_8 have been deposited in the Cambridge Structural Database ([Li][**4.1**]: CCDC 2164822; [Li][**4.2**]·C_7H_8: CCDC 2164823).

Table 4.4 X-ray crystallographic data for complexes **[Li][4.1]** and **[Li][4.2]**·C_7H_8**.**

	[Li][**4.1**]	[Li][**4.2**]·C_7H_8
Formula	$C_{40}H_{32}LiO_4Cl_{20}La$	$C_{47}H_{40}LiO_4Cl_{20}Ce$
Crystal Habit, Color	Colorless	Yellow
Crystal Size (mm)	0.2 × 0.2 × 0.1	0.2 × 0.2 × 0.1
MW (g/mol)	1431.5	1524.85
crystal system	Tetragonal	Monoclinic
space group	$I4_1/a$	$P2_1/c$
a (Å)	18.0573(15)	15.741(4)
b (Å)	18.0573(15)	19.055(5)
c (Å)	16.7394(16)	20.461(5)
α (°)	90	90
β (°)	90	106.246(6)
γ (°)	90	90
V ($Å^3$)	5458.2(10)	5892(2)
Z	4	4
T (K)	110(2)	110(2)
λ (Å)	0.71073	0.71073
GOF	1.469	1.006
Density (calcd) (Mg/m^3)	1.742	1.719
Absorption coefficient (mm^{-1})	1.801	1.721
F_{000}	2816	3020
Total no Reflections	9295	35930
Unique Reflections	2763	12046
Final R indices*	$R_1 = 0.0389$ $wR_2 = 0.0552$	$R_1 = 0.0589$ $wR_2 = 0.1196$
Largest Diff. peak and hole ($e^- A^{-3}$)	0.459, -0.531	1.579, -1.020

*For [I>2σ(I)

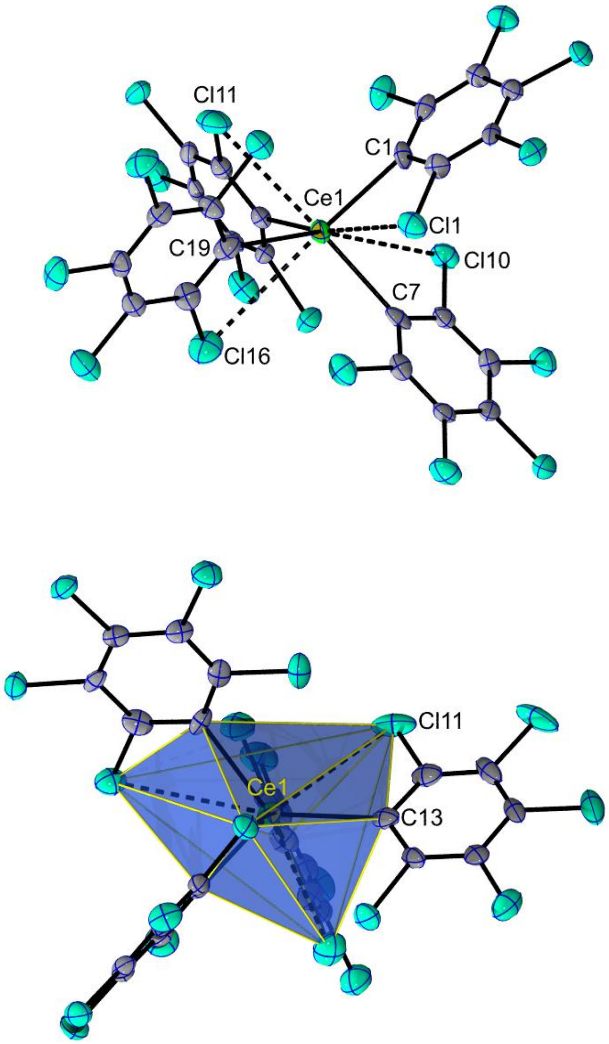

Figure 4.5 Solid-state molecular structure of [Li][**4.2**]·C_7H_8 shown with 50% probability ellipsoids. Solvate molecule and $[Li(THF)_4]^+$ counterion have been omitted for clarity.

4.4.11 Computational Data Details

Calculations were performed with the Amsterdam Density Functional (ADF) suite (version 2017)[46] using the PBE[61] functional, the scalar relativistic (SR) all-electron Zeroth-Order Regular Approximation[62] (ZORA) Hamiltonian, and Slater-type orbital (STO) basis sets of triple-ζ doubly polarized (TZ2P)[63] quality for all atoms. Based on this setup, the structure of $[(Et_2O)_3Li(C_6Cl_5)]$ was fully optimized. An atom-pairwise correction for dispersion forces was considered via Grimme's D3 model augmented with the Becke-Johnson (BJ) damping.[64] Calculations for [**4.1**]$^-$ and [**4.2**]$^-$ employed the experimental structures instead. The conductor-like screening model (COSMO) was used to describe solvent effects.[65] To quantify the compositions of the chemical bonds, natural localized molecular orbital (NLMO) analyses were carried out with the NBO program, version 6.0, as interfaced with ADF.[44]

Nuclear magnetic shielding constants for $[(Et_2O)_3Li(C_6Cl_5)]$ and [**4.1**]$^-$, were calculated at the DFT/ZORA-SR and DFT/spin-orbit (SO) ZORA levels of theory and TZ2P basis sets. The computations of the NMR shielding tensors[66] employed the GGA functional BP86 and PBE, as well as the hybrid PBE0[45] exchange-correlation functional with 25% (standard) and 40% exact exchange. The ^{13}C shifts δ_i were calculated via $\delta_i = \sigma_{benz} - \sigma_i + \delta_{benz}$. Here, σ_i is the calculated shielding of the carbon of interest, σ_{benz} and δ_{benz} are the calculated carbon shielding and the experimental chemical shift of benzene (128.8 ppm), respectively.[67] However, it is noted that using the secondary benzene reference in the calculations, instead of TMS directly, did not make a substantial difference in the calculated chemical shifts.

Table 4.5 Calculated carbon shielding (σ) and chemical shift (δ) for the reference and [**4.1**]$^-$.

Compounds	**Method**	**Label**	**σ_{calc} (ppm)**	**δ_{calc} (ppm)**	**Δ_{SO} $\delta(C_{ipso})$**	**δ_{expt} (ppm)**
Benzene	BP86/SO-BP86	C	50.2 / 50.9	-		
	PBE/SO-PBE	C	50.7 / 51.4	-		
	PBE0/SO-PBE0 (HF=25%)	C	51.7 / 52.4	-		128.8[67]
	PBE0/SO-PBE0 (HF=40%)	C	52.9 / 53.6	-		128.8[67]
[**4.1**]$^-$	BP86/SO-BP86	C_{ipso}, C_{ortho}, C_{meta}, C_{para}	3.4, 35.8, 46.1, 44.2 / -4.6, 39.0, 47.8, 47.1	175.6, 143.2, 132.9, 134.8 / 184.3, 140.7, 131.9, 132.6	8.7	185.4, 139.9, 128.7, 128.5 (This work)
	PBE/SO-PBE	C_{ipso}, C_{ortho}, C_{meta}, C_{para}	4.1, 36.5, 46.9, 44.9 / -3.8, 39.6, 48.6, 47.9	175.4, 143.0, 132.6, 134.6 / 184.0, 140.6, 131.6, 132.3	8.6	
	PBE0/SO-PBE0 (HF=25%)	C_{ipso}, C_{ortho}, C_{meta}, C_{para}	5.5, 38.3, 48.8, 47.0 / -3.2, 41.6, 50.9, 50.0	175.0, 142.2, 131.7, 133.5 / 184.4, 139.6, 130.3, 131.2	9.4	
	PBE0/SO-PBE0 (HF=40%)	C_{ipso}, C_{ortho}, C_{meta}, C_{para}	6.7, 39.9, 50.0, 48.6 / -2.6, 43.3, 52.3, 51.8	175.0, 141.8, 131.7, 133.1 / 185.0, 139.1, 130.1, 130.6	10.0	

Solvent effects were considered in the calculations via COSMO, using benzene parameters. The calculated NMR shielding and chemical shifts are averaged for ^{13}C environments in [**4.1**]$^-$.

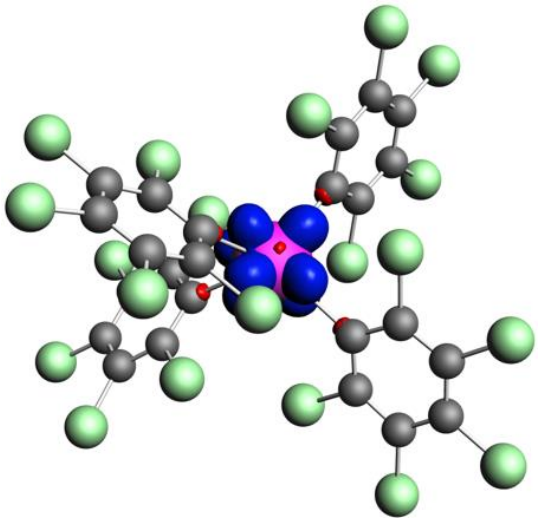

Figure 4.6 Isosurfaces (±0.001 au) of the spin density for [**4.2**]$^{-}$.

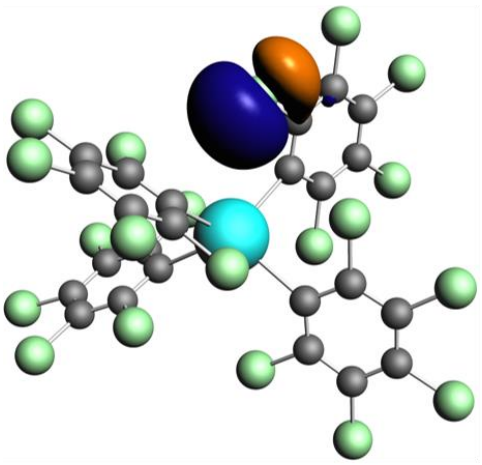

[**1**]$^{-}$

%La(tot): 2
%La(5d): 76
%La(4f): 5

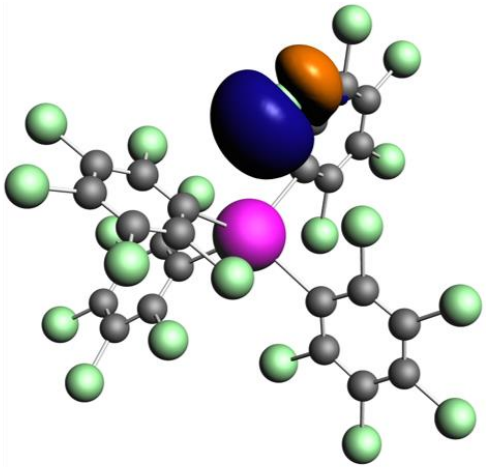

[**2**]$^{-}$

%Ce(tot): 2
%Ce(5d): 75
%Ce(4f): 5

Figure 4.7 Representative Ln–Cl bonding (LP) NLMOs in [**4.1**]$^{-}$ and [**4.2**]$^{-}$. Weight % metal character and 5d vs 4f contributions at the metal averaged over equivalent NLMOs. (Isosurface values ±0.03 au.).

4.5 Appendix

4.5.1 NMR Spectra

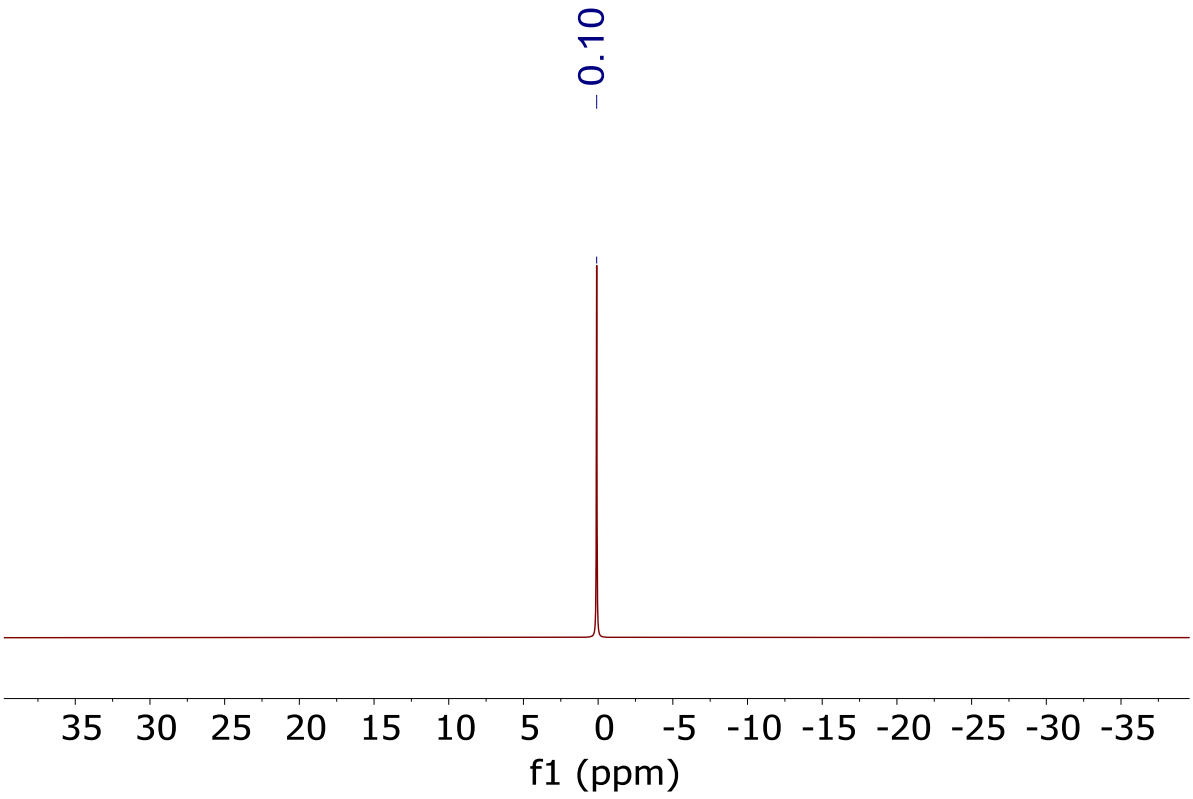

Figure 4.8 $^{7}Li\{^{1}H\}$ NMR spectrum of *in situ* generated [Li][**4.1**] in Et_2O/benzene-d_6 at –35 °C.

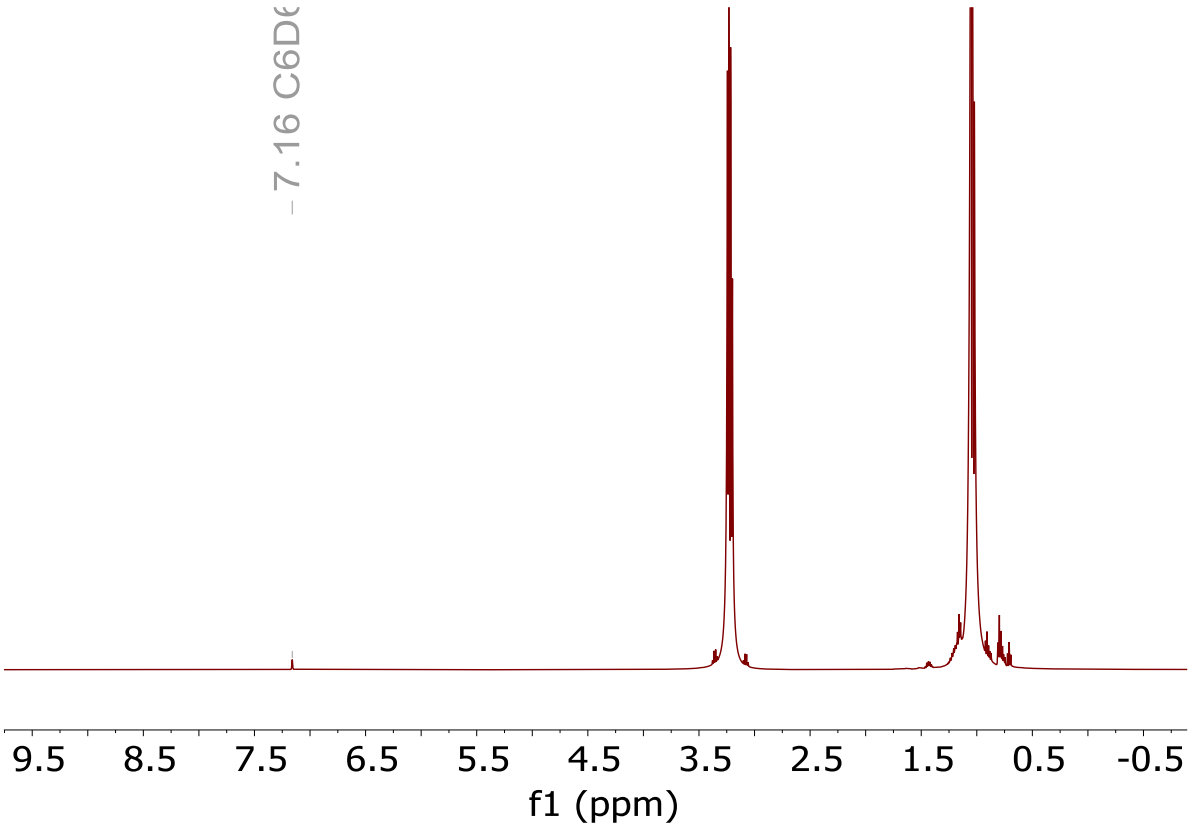

Figure 4.9 ^{1}H NMR spectrum of *in situ* generated [Li][**4.1**] in Et_2O/benzene-d_6 at –35 °C.

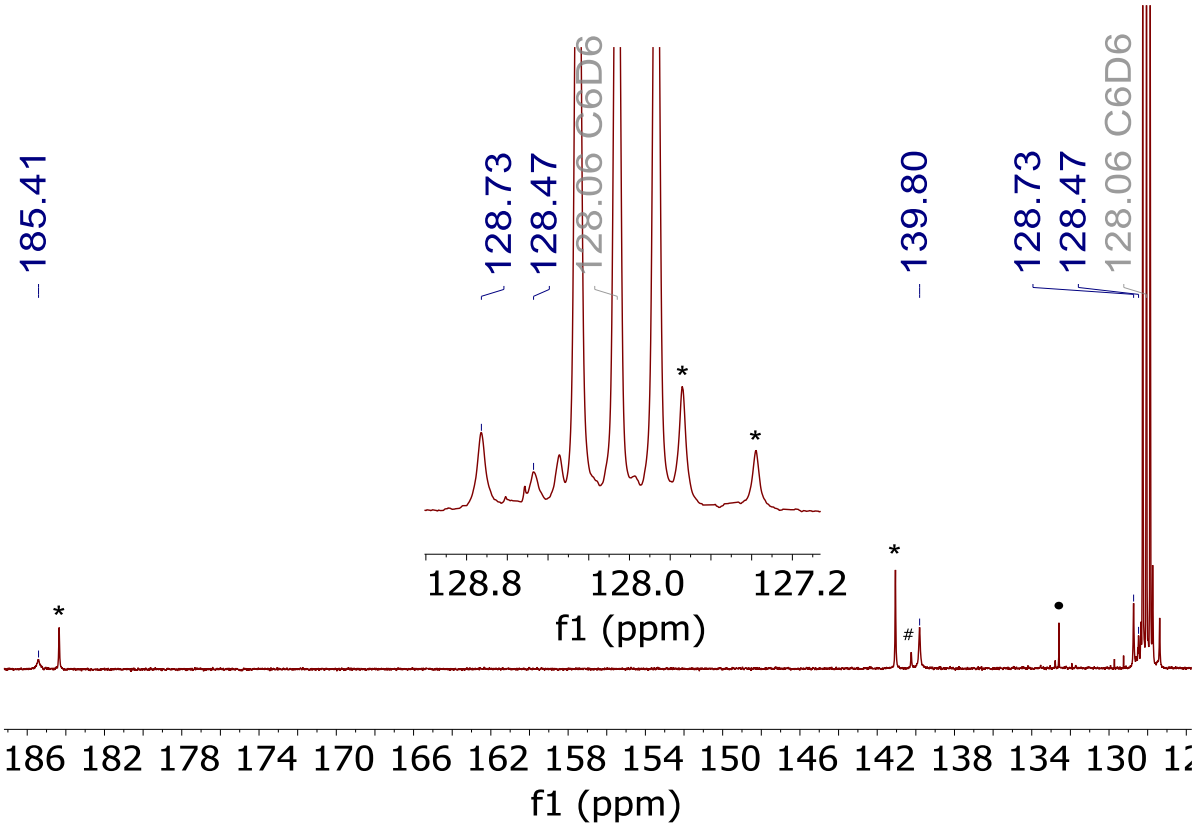

Figure 4.10 $^{13}C\{^{1}H\}$ NMR spectrum of *in situ* generated [Li][**4.1**] in Et_2O/benzene-d_6 at –35 °C. (•) indicates the presence of C_6Cl_6, (*) indicates the presence of LiC_6Cl_5, and (#) indicates an unidentified impurity.

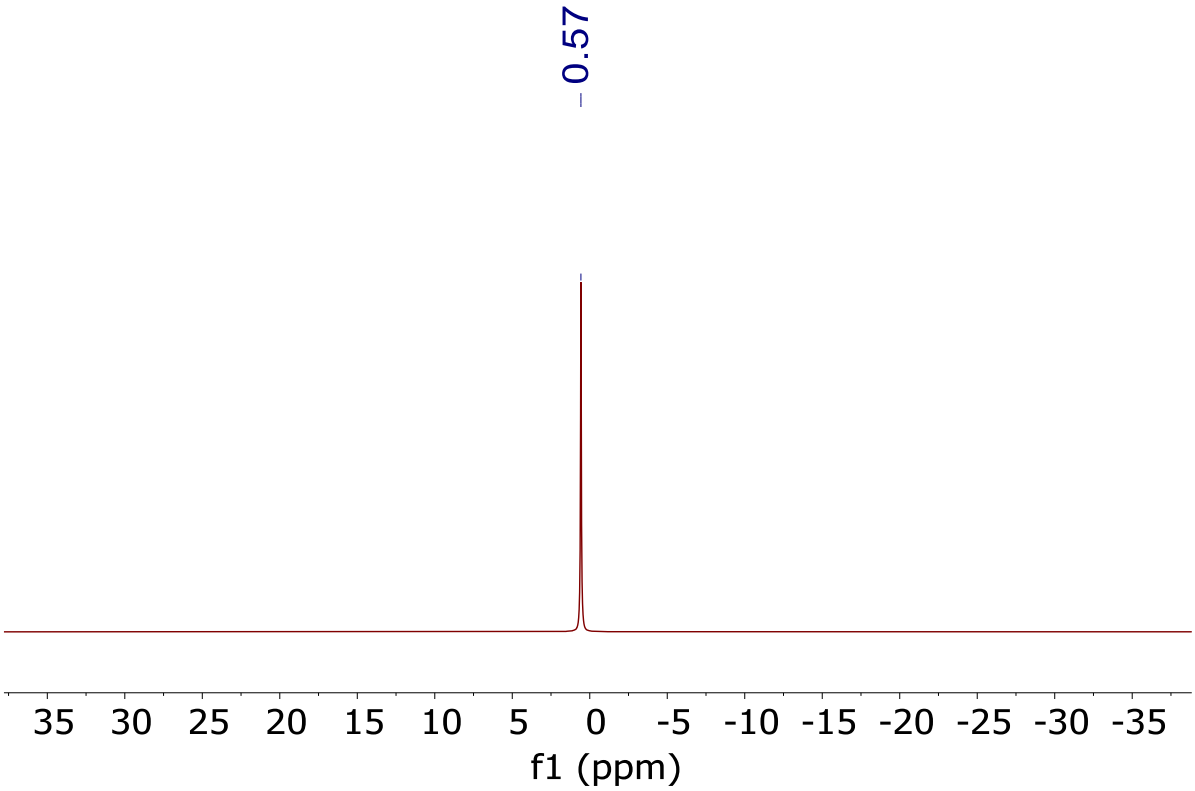

Figure 4.11 $^{7}Li\{^{1}H\}$ NMR spectrum of *in situ* generated [Li][**4.1**] using 10 equiv of LiC_6Cl_5 in Et_2O/benzene-d_6 at –35 °C.

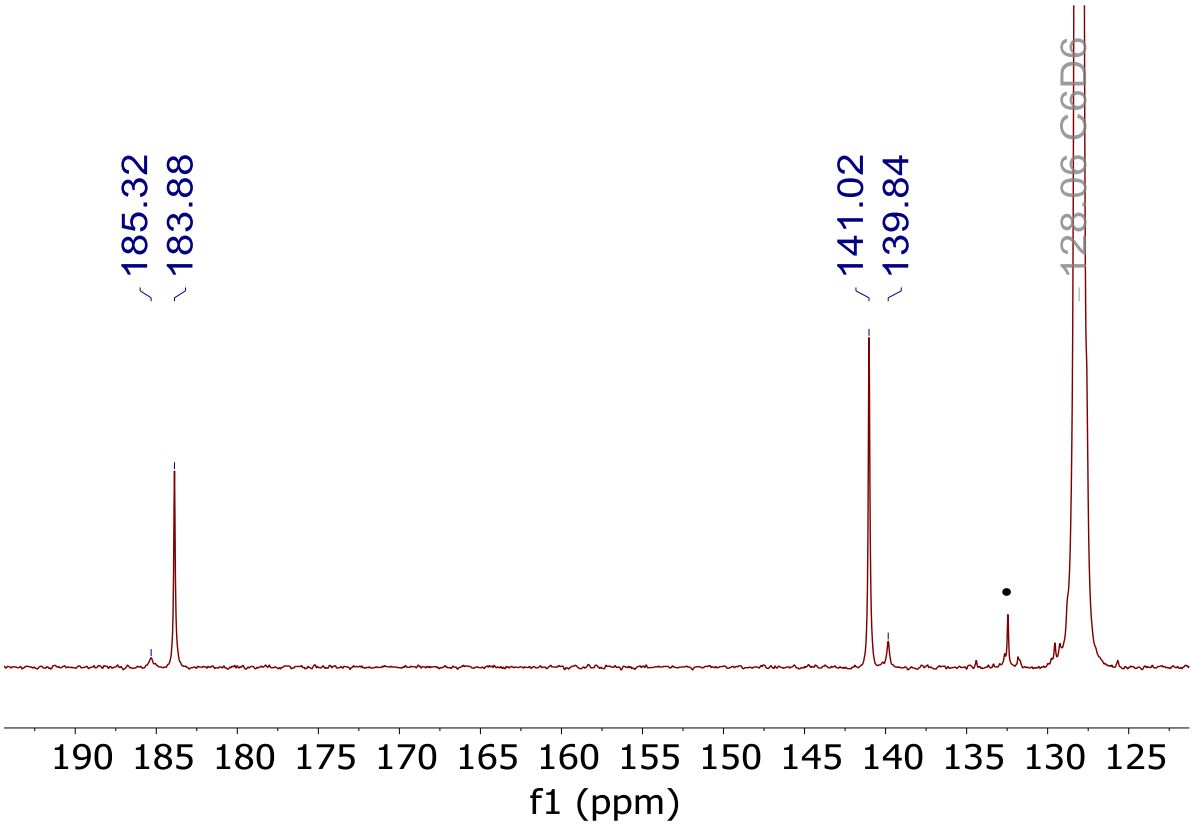

Figure 4.12 Partial $^{13}C\{^{1}H\}$ NMR spectrum of *in situ* generated [Li][**4.1**] using 10 equiv LiC_6Cl_5 in Et_2O/benzene-d_6 at –35 °C. (•) indicates the presence of C_6Cl_6.

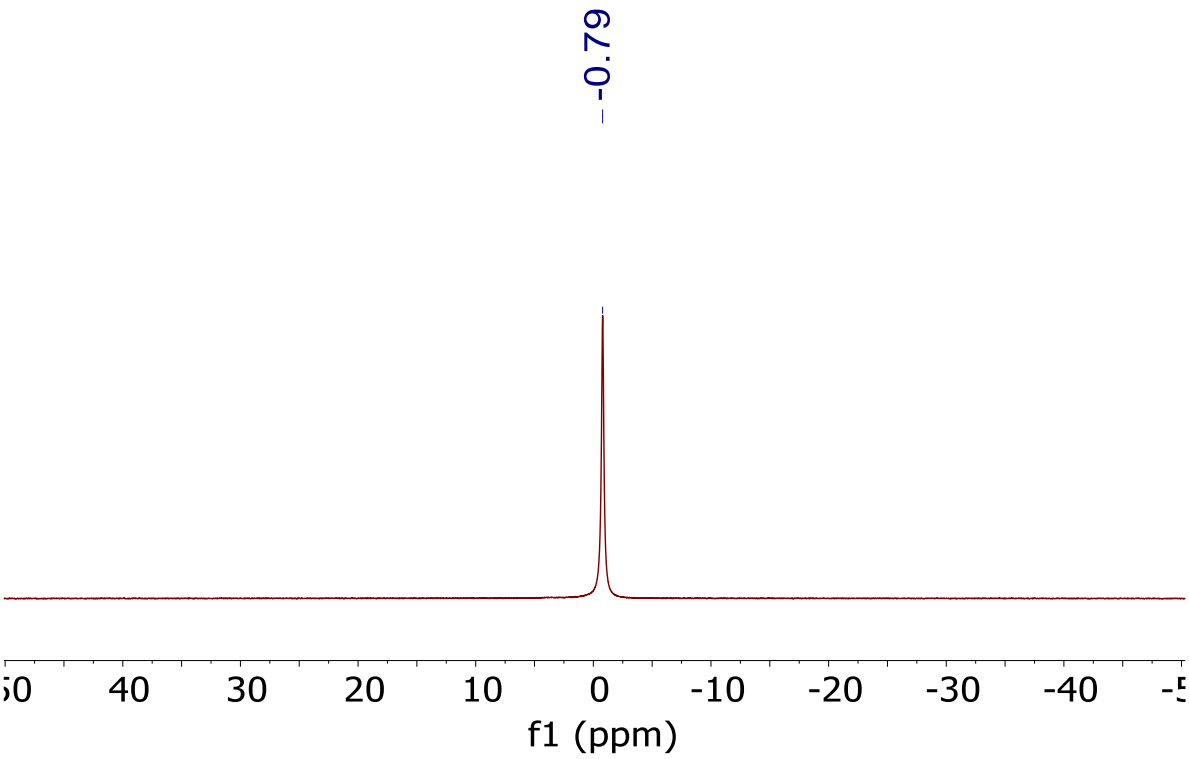

Figure 4.13 $^{7}Li\{^{1}H\}$ NMR spectrum of *in situ* generated [Li][**4.2**] in Et_2O/benzene-d_6 at –35 °C.

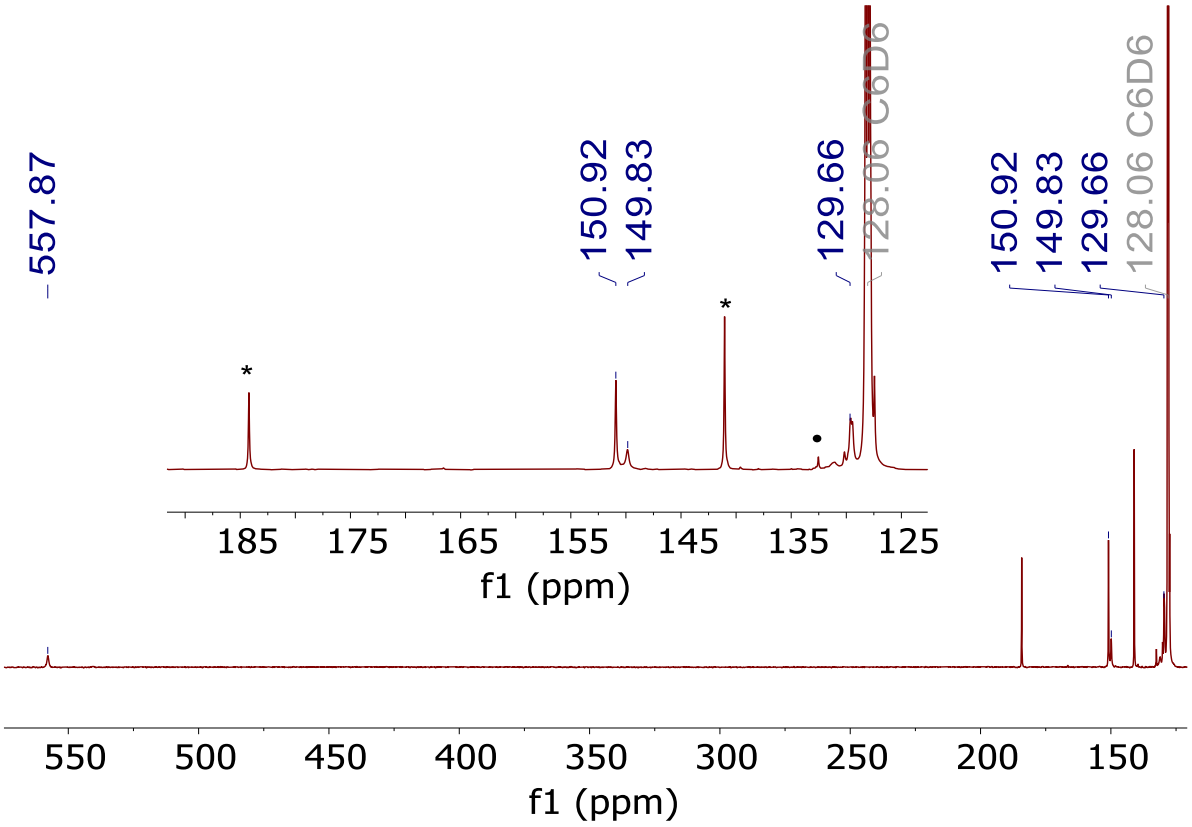

Figure 4.14. $^{13}C\{^{1}H\}$ NMR spectrum of *in situ* generated [Li][**4.2**] in Et_2O/benzene-d_6 at –35 °C. (•) indicates the presence of C_6Cl_6 and (*) indicates the presence of LiC_6Cl_5. Insert displays enlarged section of $^{13}C\{^{1}H\}$ NMR spectrum for clarity.

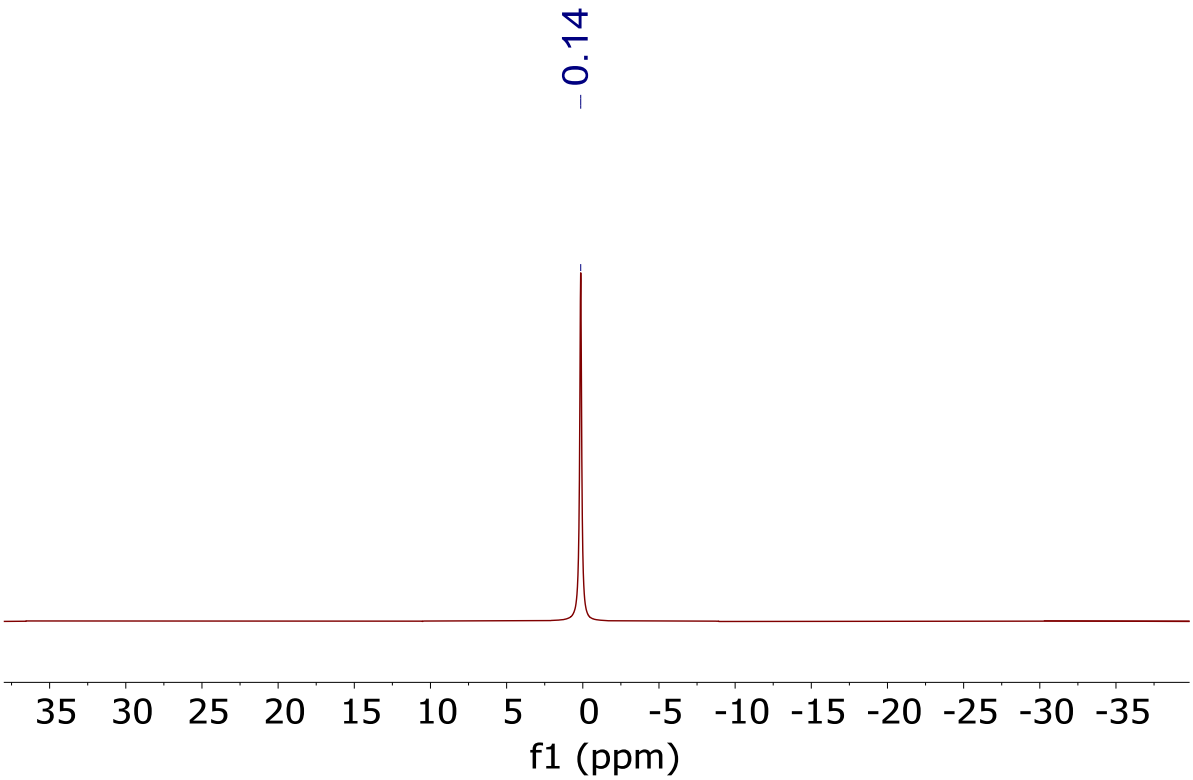

Figure 4.15. $^{7}Li\{^{1}H\}$ NMR spectrum of *in situ* generated [Li][**4.2**] using 10 equiv of LiC_6Cl_5 in Et_2O/benzene-d_6 at –35 °C.

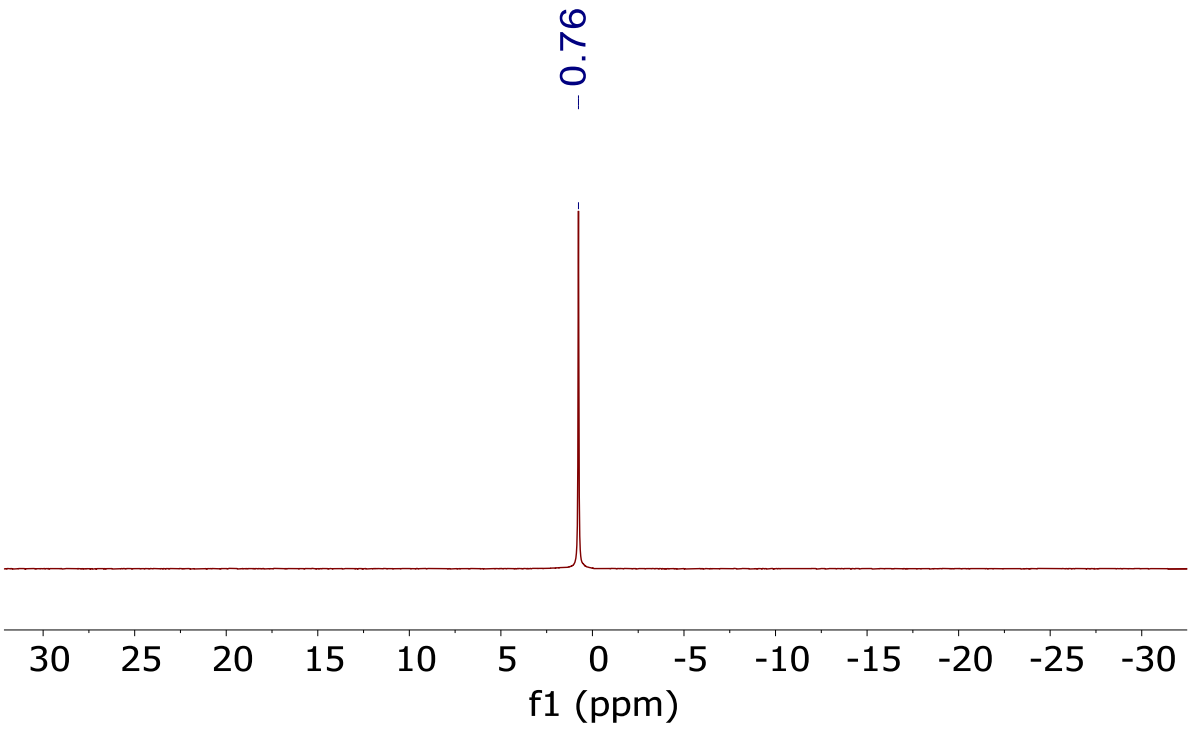

Figure 4.16. $^{7}Li\{^{1}H\}$ NMR spectrum of *in situ* generated LiC_6Cl_5 in Et_2O/benzene-d_6 at –35 °C.

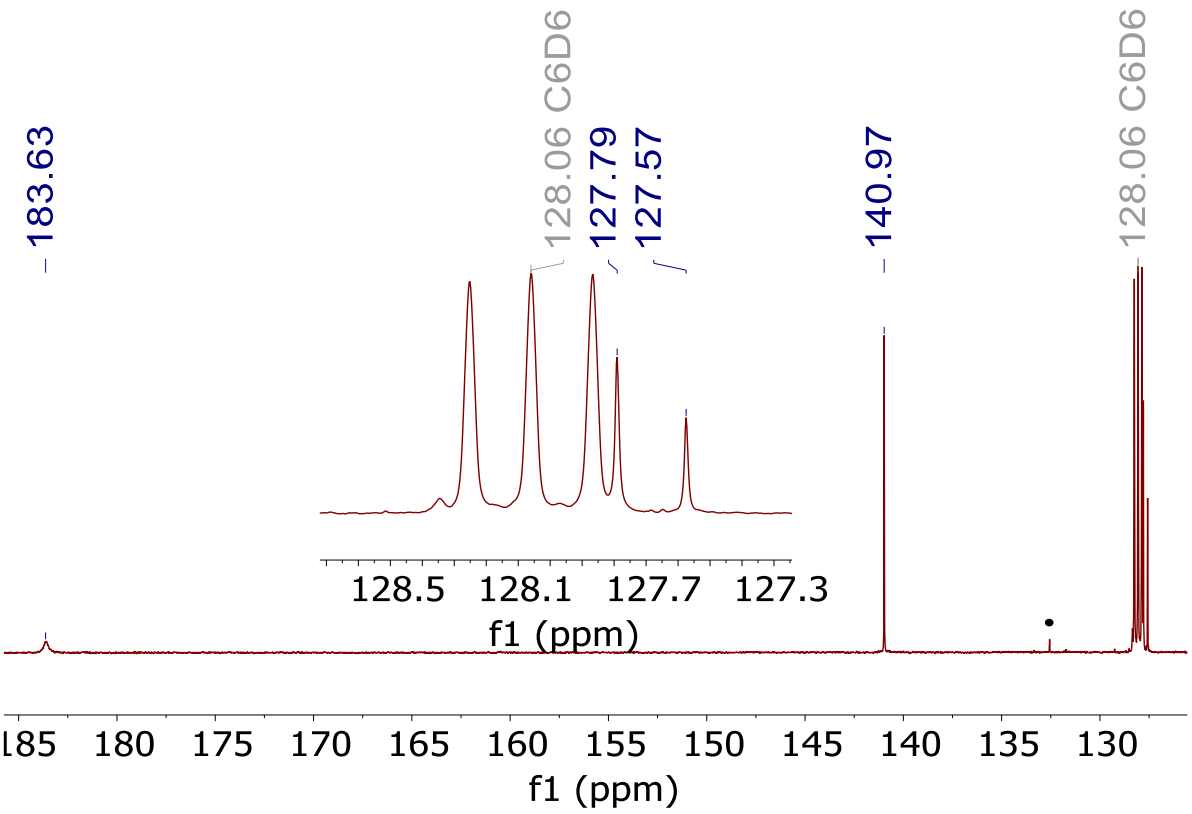

Figure 4.17. Partial $^{13}C\{^{1}H\}$ NMR spectrum of *in situ* generated LiC_6Cl_5 in Et_2O/benzene-d_6 at –35 °C. (•) indicates the presence of C_6Cl_6.

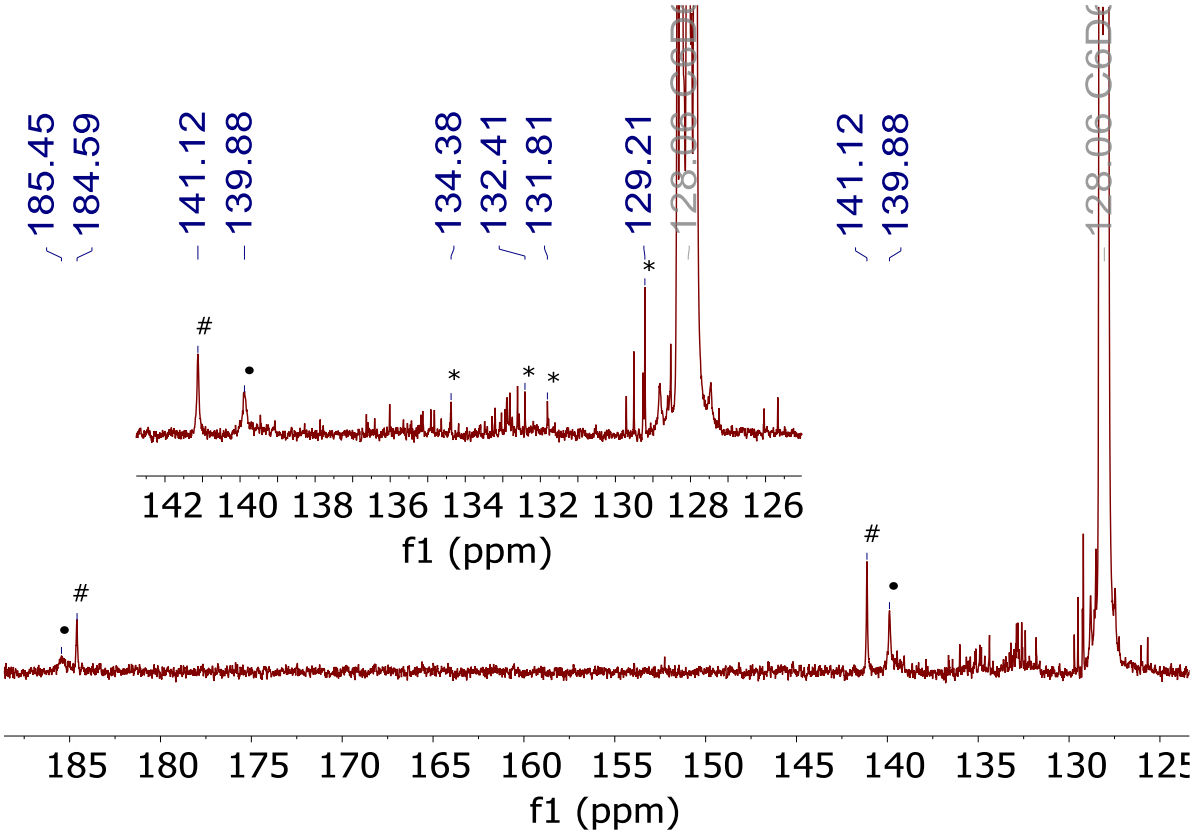

Figure 4.18. $^{13}C\{^{1}H\}$ NMR spectrum of *in situ* generated [Li][**4.1**] in Et_2O/benzene-d_6 at –35 °C. (•) indicates the presence of [Li][**4.1**], (#) indicates the presence of LiC_6Cl_5, and (*) indicates the presence of pentachlorobenzene (C_6Cl_5H).[68]

Experimental details: A cold (–25 °C) solution of LiC_6Cl_5 (2 mL in Et_2O, 0.50 mmol, 0.25 M) was added to a cold (–25 °C), stirring suspension of $[La(NO_3)_3(THF)_4]$ (76.6 mg, 0.125 mmol) in Et_2O (2 mL). After stirring for 1 h at room temperature, the reaction mixture was filtered through a Celite column (0.5 cm × 5 cm) supported on glass wool to afford an orange-yellow filtrate. The volume of the filtrate was reduced to 1 mL *in vacuo*. An aliquot (0.6 mL) of the concentrated reaction filtrate and 4 drops (ca. 0.03 mL) of benzene-d_6 was then transferred to an NMR tube and a $^{13}C\{^{1}H\}$ NMR spectrum was recorded.

4.5.2 IR Spectra

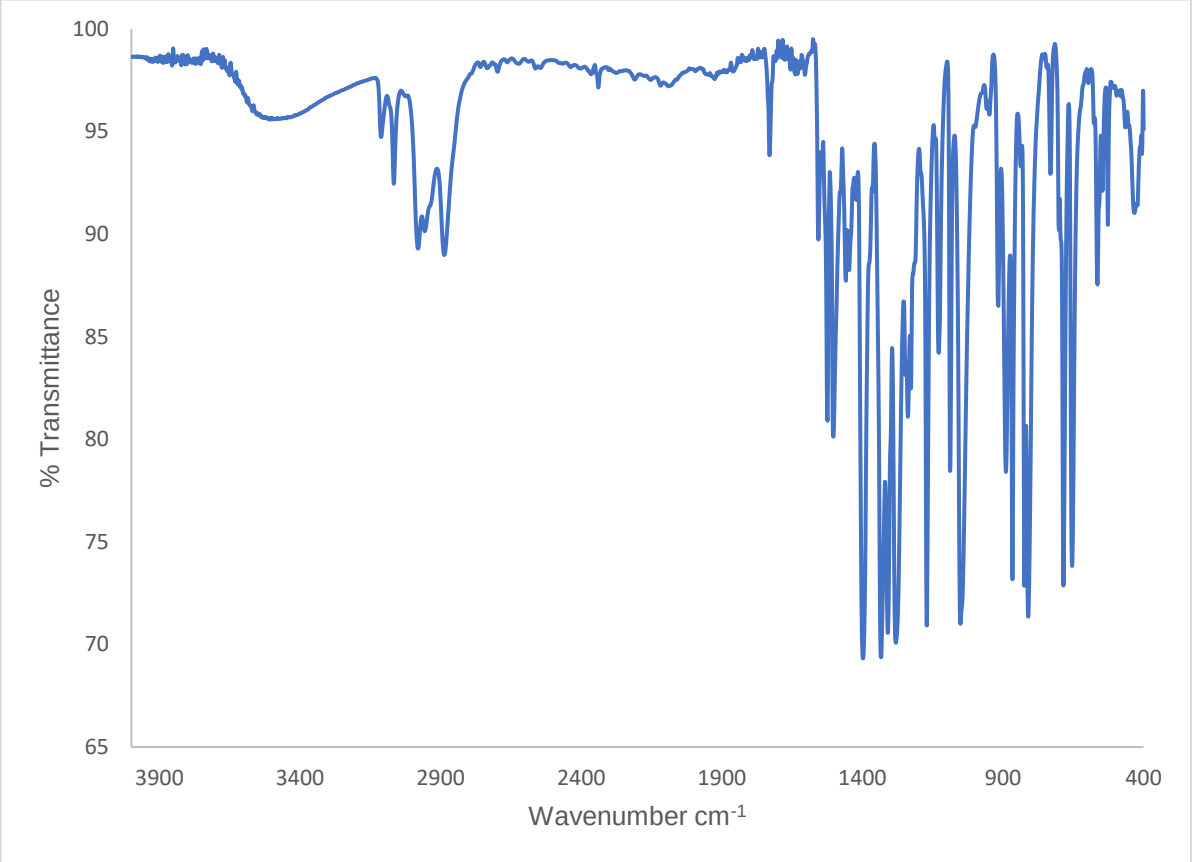

Figure 4.19. IR spectrum of [Li][**4.1**] (KBr pellet).

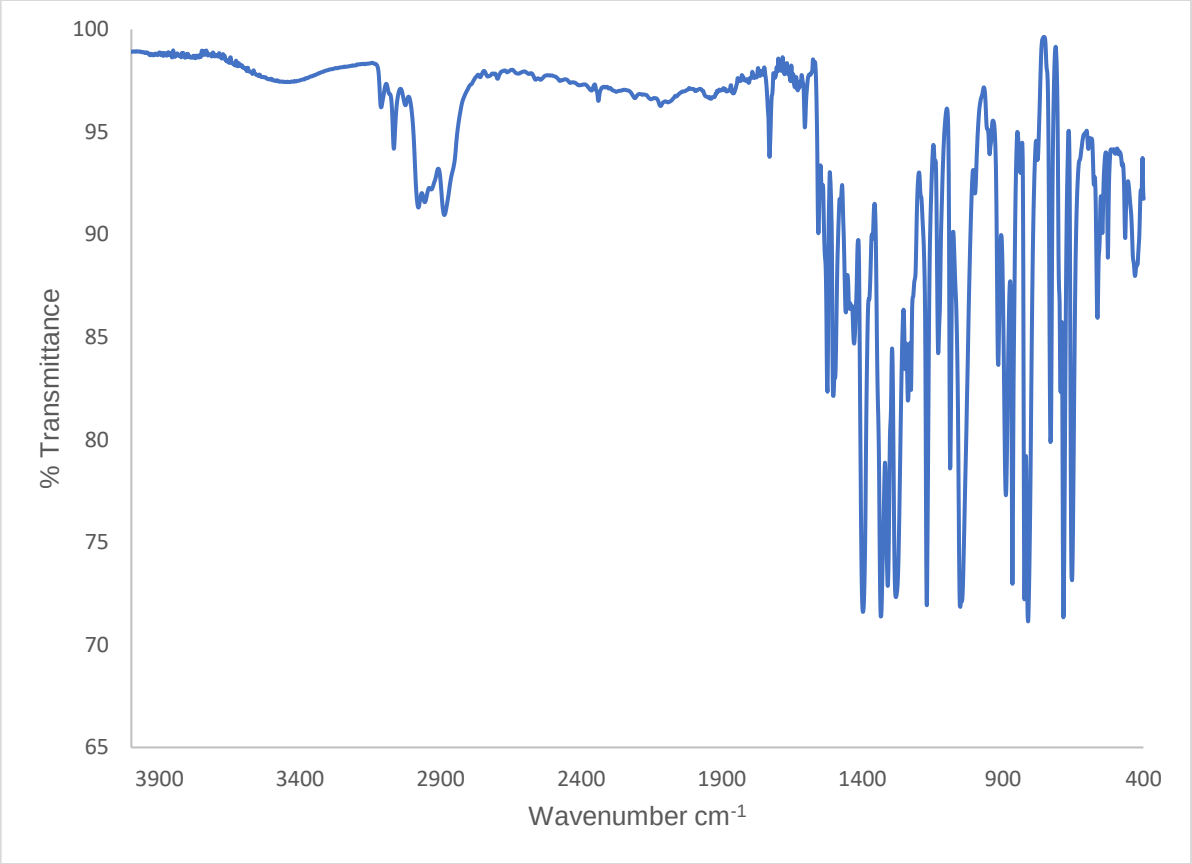

Figure 4.20. IR spectrum of [Li][**4.2**] (KBr pellet).

4.6 References

(1) Petrov, A. R.; Thomas, O.; Harms, K.; Rufanov, K. A.; Sundermeyer, J. Dramatic enhancement of the stability of rare-earth metal complexes with α-methyl substituted N,N-dimethylbenzylamine ligands. *J. Organomet. Chem.* **2010**, *695*, 2738-2746.

(2) Cotton, S. A.; Hart, F. A.; Hursthouse, M. B.; Welch, A. J. Preparation and molecular structure of a σ-bonded lanthanide phenyl. *J. Chem. Soc., Chem. Commun.* **1972**, 1225-1226.

(3) Pan, Y.; Xu, T.; Yang, G.-W.; Jin, K.; Lu, X.-B. Bis(oxazolinyl)phenyl-Ligated Rare-Earth-Metal Complexes: Highly Regioselective Catalysts for cis-1,4-Polymerization of Isoprene. *Inorg. Chem.* **2013**, *52*, 2802-2808.

(4) Petrov, A. R.; Rufanov, K. A.; Harms, K.; Sundermeyer, J. Re-investigation of ortho-metalated N,N-dialkylbenzylamine complexes of rare-earth metals. First structurally characterized arylates of neodymium and gadolinium Li[$LnAr_4$]. *J. Organomet. Chem.* **2009**, *694*, 1212-1218.

(5) Zimmermann, M.; Anwander, R. Homoleptic Rare-Earth Metal Complexes Containing Ln−C σ-Bonds. *Chem. Rev.* **2010**, *110*, 6194-6259.

(6) Ihara, E.; Adachi, Y.; Yasuda, H.; Hashimoto, H.; Kanehisa, N.; Kai, Y. Synthesis of 2,6-dialkoxylphenyllanthanoid complexes and their polymerization catalysis1Dedicated to Professor Akira Nakamura on the occasion of his retirement.1. *J. Organomet. Chem.* **1998**, *569*, 147-157.

(7) Wayda, A. L.; Atwood, J. L.; Hunter, W. E. Homoleptic organolanthanoid hydrocarbyls. The synthesis and x-ray crystal structure of tris[o-((dimethylamino)methyl)phenyl]lutetium. *Organometallics* **1984**, *3*, 939-941.

(8) Martinez-Arripe, E.; Jean-Baptiste-dit-Dominique, F.; Auffrant, A.; Le Goff, X.-F.; Thuilliez, J.; Nief, F. Synthesis and Characterization of Bidentate Rare-Earth Iminophosphorane o-Aryl Complexes and Their Behavior As Catalysts for the Polymerization of 1,3-Butadiene. *Organometallics* **2012**, *31*, 4854-4861.

(9) Bochkarev, L. N.; Stepantseva, T. A.; Zakharov, L. N.; Fukin, G. K.; Yanovsky, A. I.; Struchkov, Y. T. Synthesis and Crystal Structure of $Ph_3Ln(THF)_3$ (Ln = Er, Tm). *Organometallics* **1995**, *14*, 2127-2129.

(10) Forsyth, C. M.; Deacon, G. B. The First Crystallographically Characterized (Perfluoroaryl)lanthanoid(II) Complex, $Eu(C_6F_5)_2(OC_4H_8)_5$. *Organometallics* **2000**, *19*, 1205-1207.

(11) Deacon, G. B.; Forsyth, C. M. A Half-Sandwich Perfluoroorganoytterbium(II) Complex from a Simple Redox Transmetalation/Ligand Exchange Synthesis. *Organometallics* **2003**, *22*, 1349-1352.

(12) Heckmann, G.; Niemeyer, M. Synthesis and First Structural Characterization of Lanthanide(II) Aryls: Observation of a Schlenk Equilibrium in Europium(II) and Ytterbium(II) Chemistry. *J. Am. Chem. Soc.* **2000**, *122*, 4227-4228.

(13) Ara, I.; Forniés, J.; García-Monforte, M. A.; Martín, A.; Menjón, B. Synthesis and Characterization of Pentachlorophenyl–Metal Derivatives with d^0 and d^{10} Electron Configurations. *Chem. Eur. J.* **2004**, *10*, 4186-4197.

(14) Fornies, J.; Menjon, B.; Sanz-Carrillo, R. M.; Tomas, M.; Connelly, N. G.; Crossley, J. G.; Orpen, A. G. Synthesis and Structural Characterization of the First Isolated Homoleptic Organoplatinum(IV) Compound: $[Pt(C_6Cl_5)_4]$. *J. Am. Chem. Soc.* **1995**, *117*, 4295-4304.

(15) P. García, M.; Victoria Jiménez, M.; J. Lahoz, F.; A. López, J.; A. Oro, L. Synthesis of the homoleptic rhodium(III) complex [Rh(C_6Cl_5)$_3$]. Molecular structures of [Rh(C_6Cl_5)$_3$] and [Rh(C_6Cl_4–C_6Cl_4)(C_6Cl_5)(SC_4H_8)$_2$]. *J. Chem. Soc., Dalton Trans.* **1998**, 4211-4214.
(16) Garcia, M. P.; Jimenez, M. V.; Oro, L. A.; Lahoz, F. J.; Tiripicchio, M. C.; Tiripicchio, A. A homoleptic mononuclear iridium(II) organometallic complex: synthesis and x-ray structure of [Ir(C_6Cl_5)$_4$]$_2$. *Organometallics* **1993**, *12*, 4660-4663.
(17) Alonso, P. J.; Forniés, J.; García-Monforte, M. A.; Martín, A.; Menjón, B. The first structurally characterised homoleptic organovanadium(III) compound. *Chem. Commun.* **2001**, 2138-2139.
(18) J. Alonso, P.; R. Falvello, L.; Forniés, J. Synthesis and first structural characterisation of a homoleptic tetraorganochromate(III) salt. *Chem. Commun.* **1998**, 1721-1722.
(19) Alonso, P. J.; Forniés, J.; García-Monforte, M. A.; Martín, A.; Menjón, B.; Rillo, C. A New Series of Homoleptic, Paramagnetic Organochromium Derivatives: Synthesis, Characterization, and Study of Their Magnetic Properties. *Chem. Eur. J.* **2002**, *8*, 4056-4065.
(20) Alonso, P. J.; Arauzo, A. B.; Forniés, J.; García-Monforte, M. A.; Martín, A.; Martínez, J. I.; Menjón, B.; Rillo, C.; Sáiz-Garitaonandia, J. J. A Square-Planar Organoiron(III) Compound with a Spin-Admixed State. *Angew. Chem. Int. Ed.* **2006**, *45*, 6707-6711.
(21) Alonso, P. J.; Forniés, J.; García-Monforte, M. A.; Martín, A.; Menjón, B. New Homoleptic Organometallic Derivatives of Vanadium(III) and Vanadium(IV): Synthesis, Characterization, and Study of Their Electrochemical Behaviour. *Chem. Eur. J.* **2005**, *11*, 4713-4724.
(22) García-Monforte, M. A.; Alonso, P. J.; Forniés, J.; Menjón, B. New advances in homoleptic organotransition-metal compounds: The case of perhalophenyl ligands. *Dalton Trans.* **2007**, 3347-3359.
(23) Ordoñez, O.; Yu, X.; Wu, G.; Autschbach, J.; Hayton, T. W. Synthesis and Characterization of Two Uranyl-Aryl "Ate" Complexes. *Chem. Eur. J.* **2021**, *27*, 5885-5889.
(24) Ordoñez, O.; Yu, X.; Wu, G.; Autschbach, J.; Hayton, T. W. Homoleptic Perchlorophenyl "Ate" Complexes of Thorium(IV) and Uranium(IV). *Inorg. Chem.* **2021**, *60*, 12436-12444.
(25) Kent, G. T.; Yu, X.; Pauly, C.; Wu, G.; Autschbach, J.; Hayton, T. W. Synthesis of Parent Acetylide and Dicarbide Complexes of Thorium and Uranium and an Examination of Their Electronic Structures. *Inorg. Chem.* **2021**, *60*, 15413-15420.
(26) Kent, G. T.; Yu, X.; Wu, G.; Autschbach, J.; Hayton, T. W. Synthesis and electronic structure analysis of the actinide allenylidenes, [{(NR_2)$_3$}An($CCCPh_2$)]$^-$ (An = U, Th; R = $SiMe_3$). *Chem. Sci.* **2021**, *12*, 14383-14388.
(27) Pedrick, E. A.; Hrobárik, P.; Seaman, L. A.; Wu, G.; Hayton, T. W. Synthesis, structure and bonding of hexaphenyl thorium(IV): observation of a non-octahedral structure. *Chem. Commun.* **2016**, *52*, 689-692.
(28) Mullane, K. C.; Hrobárik, P.; Cheisson, T.; Manor, B. C.; Carroll, P. J.; Schelter, E. J. ^{13}C NMR Shifts as an Indicator of U–C Bond Covalency in Uranium(VI) Acetylide Complexes: An Experimental and Computational Study. *Inorg. Chem.* **2019**, *58*, 4152-4163.
(29) Smiles, D. E.; Wu, G.; Hrobárik, P.; Hayton, T. W. Synthesis, Thermochemistry, Bonding, and ^{13}C NMR Chemical Shift Analysis of a Phosphorano-Stabilized Carbene of Thorium. *Organometallics* **2017**, *36*, 4519-4524.
(30) Seaman, L. A.; Hrobárik, P.; Schettini, M. F.; Fortier, S.; Kaupp, M.; Hayton, T. W. A Rare Uranyl(VI)–Alkyl Ate Complex [Li(DME)$_{1.5}$]$_2$[UO_2(CH_2SiMe_3)$_4$] and Its Comparison with a Homoleptic Uranium(VI)–Hexaalkyl. *Angew. Chem. Int. Ed.* **2013**, *52*, 3259-3263.

(31) Kent, G. T.; Yu, X.; Wu, G.; Autschbach, J.; Hayton, T. W. Ring-opening of a thorium cyclopropenyl complex generates a transient thorium-bound carbene. *Chem. Commun.* **2022**, *58*, 6805-6808.
(32) Panetti, G. B.; Sergentu, D.-C.; Gau, M. R.; Carroll, P. J.; Autschbach, J.; Walsh, P. J.; Schelter, E. J. Isolation and characterization of a covalent Ce^{IV}-Aryl complex with an anomalous ^{13}C chemical shift. *Nat. Commun.* **2021**, *12*, 1713.
(33) Baker, C. F.; Seed, J. A.; Adams, R. W.; Lee, D.; Liddle, S. T. $^{13}C_{carbene}$ nuclear magnetic resonance chemical shift analysis confirms Ce^{IV}=C double bonding in cerium(IV)–diphosphonioalkylidene complexes. *Chem. Sci.* **2024**, *15*, 238-249.
(34) Rausch, M. D.; Tibbetts, F. E.; Gordon, H. B. Perhaloaryl-metal chemistry: II. Pentachlorophenyllithium. *J. Organomet. Chem.* **1966**, *5*, 493-500.
(35) Cirera, J.; Ruiz, E.; Alvarez, S. Continuous Shape Measures as a Stereochemical Tool in Organometallic Chemistry. *Organometallics* **2005**, *24*, 1556-1562.
(36) Hogerheide, M. P.; Boersma, J.; Spek, A. L.; van Koten, G. Synthesis of a Bis(cyclopentadienyl)lanthanum Aryl Complex with a Pseudofacially Bound Bis(ortho)-Chelating Aryldiamine Ligand. X-ray Structure of $(\eta^5\text{-}C_5H_5)_2La(C_6H_3\{CH_2NMe_2\}2\text{-}2,6)$. *Organometallics* **1996**, *15*, 1505-1507.
(37) Shannon, R. Revised effective ionic radii and systematic studies of interatomic distances in halides and chalcogenides. *Acta Cryst. A* **1976**, *32*, 751-767.
(38) Maron, L.; Werkema, E. L.; Perrin, L.; Eisenstein, O.; Andersen, R. A. Hydrogen for Fluorine Exchange in C_6F_6 and C_6F_5H by Monomeric $[1,3,4\text{-}(Me_3C)_3C_5H_2]_2CeH$: Experimental and Computational Studies. *J. Am. Chem. Soc.* **2005**, *127*, 279-292.
(39) Werkema, E. L.; Andersen, R. A. Fluorine for Hydrogen Exchange in the Hydrofluorobenzene Derivatives $C_6H_xF_{(6-x)}$, where x = 2, 3, 4 and 5 by Monomeric $[1,2,4\text{-}(Me_3C)_3C_5H_2]_2CeH$: The Solid State Isomerization of $[1,2,4\text{-}(Me_3C)_3C_5H_2]_2Ce(2,3,4,5\text{-}C_6HF_4)$ to $[1,2,4\text{-}(Me_3C)_3C_5H_2]_2Ce(2,3,4,6\text{-}C_6HF_4)$. *J. Am. Chem. Soc.* **2008**, *130*, 7153-7165.
(40) Yin, H.; Zabula, A. V.; Schelter, E. J. C–F→Ln/An interactions in synthetic f-element chemistry. *Dalton Trans.* **2016**, *45*, 6313-6323.
(41) Yanagisawa, M.; Hayamizu, K.; Yamamoto, O. ^{13}C chemical shifts of chlorinated biphenyls. *Magn. Reson. Chem.* **1986**, *24*, 1013-1014.
(42) Deacon, G. B.; Jaroschik, F.; Junk, P. C.; Kelly, R. P. A divalent heteroleptic lanthanoid fluoride complex stabilised by the tetraphenylcyclopentadienyl ligand, arising from C–F activation of pentafluorobenzene. *Chem. Commun.* **2014**, *50*, 10655-10657.
(43) Deacon, G. B.; Koplick, A. J.; Raverty, W. D.; Vince, D. G. Organolanthanoids: II. Preparation and identification of some organolanthanoid species in solution. *J. Organomet. Chem.* **1979**, *182*, 121-141.
(44) Glendening, E. D.; Landis, C. R.; Weinhold, F. NBO 6.0: Natural bond orbital analysis program. *J. Comput. Chem.* **2013**, *34*, 1429-1437.
(45) Autschbach, J. The role of the exchange-correlation response kernel and scaling corrections in relativistic density functional nuclear magnetic shielding calculations with the zeroth-order regular approximation. *Mol. Phys* **2013**, *111*, 2544-2554.
(46) Baerends, E. J.; Ziegler, T.; Atkins, A. J.; Autschbach, J.; Baseggio, O.; Bashford, D.; Bérces, A.; Bickelhaupt, F. M.; Bo, C.; Boerrigter, P. M.; Cavallo, L.; Daul, C.; Chong, D. P.; Chulhai, D. V.; Deng, L.; Dickson, R. M.; Dieterich, J. M.; Ellis, D. E.; van Faassen, M.; Fan, L.; Fischer, T. H.; Guerra, C. F.; Franchini, M.; Ghysels, A.; Giammona, A.; van Gisbergen, S. J. A.; Goez, A.; Götz, A. W.; Groeneveld, J. A.; Gritsenko, O. V.; Grüning, M.; Gusarov,

S.; Harris, F. E.; van den Hoek, P.; Hu, Z.; Jacob, C. R.; Jacobsen, H.; Jensen, L.; Joubert, L.; Kaminski, J. W.; van Kessel, G.; König, C.; Kootstra, F.; Kovalenko, A.; Krykunov, M. V.; van Lenthe, E.; McCormack, D. A.; Michalak, A.; Mitoraj, M.; Morton, S. M.; Neugebauer, J.; Nicu, V. P.; Noodleman, L.; Osinga, V. P.; Patchkovskii, S.; Pavanello, M.; Peeples, C. A.; Philipsen, P. H. T.; Post, D.; Pye, C. C.; Ramanantoanina, H.; Ramos, P.; Ravenek, W.; Rodríguez, J. I.; Ros, P.; Rüger, R.; Schipper, P. R. T.; Schlüns, D.; van Schoot, H.; Schreckenbach, G.; Seldenthuis, J. S.; Seth, M.; Snijders, J. G.; Solà, M.; Stener, M.; Swart, M.; Swerhone, D.; Tognetti, V.; te Velde, G.; Vernooijs, P.; Versluis, L.; Visscher, L.; Visser, O.; Wang, F.; Wesolowski, T. A.; van Wezenbeek, E. M.; Wiesenekker, G.; Wolff, S. K.; Woo, T. K.; Yakovlev, A. L. ADF, ver. 2017; SCM, Theoretical Chemistry, Vrije Universiteit: Amsterdam, The Netherlands, 2017. https://www.scm.com.

(47) Wolford, N. J.; Sergentu, D.-C.; Brennessel, W. W.; Autschbach, J.; Neidig, M. L. Homoleptic Aryl Complexes of Uranium (IV). *Angew. Chem. Int. Ed.* **2019**, *58*, 10266-10270.

(48) Löble, M. W.; Keith, J. M.; Altman, A. B.; Stieber, S. C. E.; Batista, E. R.; Boland, K. S.; Conradson, S. D.; Clark, D. L.; Lezama Pacheco, J.; Kozimor, S. A.; et al. Covalency in Lanthanides. An X-ray Absorption Spectroscopy and Density Functional Theory Study of $LnCl_6^{x-}$ (x = 3, 2). *J. Am. Chem. Soc.* **2015**, *137*, 2506-2523.

(49) Martin, B.; Autschbach, J. Temperature dependence of contact and dipolar NMR chemical shifts in paramagnetic molecules. *J. Chem. Phys.* **2015**, *142*, 054108.

(50) Gendron, F.; Sharkas, K.; Autschbach, J. Calculating NMR Chemical Shifts for Paramagnetic Metal Complexes from First-Principles. *J. Phys. Chem. Lett.* **2015**, *6*, 2183-2188.

(51) Autschbach, J. Chapter One - NMR Calculations for Paramagnetic Molecules and Metal Complexes. In *Annual Reports in Computational Chemistry*, Dixon, D. A. Ed.; Vol. 11; Elsevier, 2015; pp 3-36.

(52) Niemeyer, M. 1,2-Dimethoxyethan- und Tetrahydrofuran-Komplexe der Seltenerdmetallnitrate. *Z. Anorg. Allg. Chem.* **2006**, *632*, 1449-1456.

(53) Harris, R. K.; Becker, E. D.; Cabral de Menezes, S. M.; Goodfellow, R.; Granger, P. NMR nomenclature. Nuclear spin properties and conventions for chemical shifts(IUPAC Recommendations 2001). **2001**, *73*, 1795-1818.

(54) Harris, R. K.; Becker, E. D.; Cabral de Menezes, S. M.; Granger, P.; Hoffman, R. E.; Zilm, K. W. Further conventions for NMR shielding and chemical shifts (IUPAC Recommendations 2008). **2008**, *80*, 59-84.

(55) Rausch, M. D.; Moser, G. A.; Meade, C. F. The isolation, characterization and synthetic utility of several solid organolithium compounds. *J. Organomet. Chem.* **1973**, *51*, 1-11.

(56) SMART Apex II, Version 2.1; Bruker AXS Inc.: Madison, WI; 2005.

(57) SAINT Software User's Guide, Version 7.34a; Bruker AXS Inc.: Madison, WI; 2005.

(58) Sheldrick, G. M. SADABS, University of Gottingen, Germany; 2005.

(59) SHELXTL PC, Version 6.12; Bruker AXS Inc.: Madison, WI; 2005.

(60) Diamond - Crystal and Molecular Structure Visualization. Crystal Impact - Dr. H. Putz & Dr. K. Brandenburg GbR, Kreuzherrenstr. 102, 53227 Bonn, Germany. http://www.crystalimpact.com/diamond.

(61) Perdew, J. P.; Burke, K.; Ernzerhof, M. Generalized Gradient Approximation Made Simple. *Phys. Rev. Lett.* **1996**, *77*, 3865-3868.

(62) Lenthe, E. v.; Baerends, E. J.; Snijders, J. G. Relativistic regular two-component Hamiltonians. *J. Chem. Phys.* **1993**, *99*, 4597-4610.

(63) Weigend, F.; Ahlrichs, R. Balanced basis sets of split valence, triple zeta valence and quadruple zeta valence quality for H to Rn: Design and assessment of accuracy. *PCCP* **2005**, *7*, 3297-3305.
(64) Grimme, S.; Ehrlich, S.; Goerigk, L. Effect of the damping function in dispersion corrected density functional theory. *J. Comput. Chem.* **2011**, *32*, 1456-1465.
(65) Pye, C. C.; Ziegler, T. An implementation of the conductor-like screening model of solvation within the Amsterdam density functional package. *Theor. Chem. Acc.* **1999**, *101*, 396-408.
(66) Adamo, C.; Barone, V. Toward chemical accuracy in the computation of NMR shieldings: the PBE0 model. *Chem. Phys. Lett.* **1998**, *298*, 113-119.
(67) Fulmer, G. R.; Miller, A. J. M.; Sherden, N. H.; Gottlieb, H. E.; Nudelman, A.; Stoltz, B. M.; Bercaw, J. E.; Goldberg, K. I. NMR Chemical Shifts of Trace Impurities: Common Laboratory Solvents, Organics, and Gases in Deuterated Solvents Relevant to the Organometallic Chemist. *Organometallics* **2010**, *29*, 2176-2179.
(68) Takeuchi, Y.; Furuyama, H.; Fukushi, S.; Fujiwara, S. Carbon-13 nuclear magnetic resonance spectra of polychloro- and polybromo-benzenes. *J. Chem. Soc., Perkin Trans. 2* **1985**, 175-177.

Chapter 5. Quantifying Actinide-Carbon Bond Covalency in Uranyl-Aryl Complex Utilizing Solution ^{13}C NMR Spectroscopy

Portions of this work were published in:

Osvaldo Ordoñez, Xiaojuan Yu, Guang Wu, Jochen Autschbach, and Trevor W. Hayton, Quantifying Actinide-Carbon Bond Covalency in Uranyl-Aryl Complex Utilizing Solution ^{13}C NMR Spectroscopy. *Inorg. Chem.* **2024**, *63*, 9427-9433.

Table of Contents

5.1 Introduction

The field of uranium organometallic chemistry has seen significant advancements over the past two decades.[1-6] However, reports of uranyl (UO_2^{2+}) organometallic chemistry remain remarkably rare.[7-23] The first uranyl hydrocarbyl complex was characterized as recently as 2002,[11] and since then only a handful of uranyl hydrocarbyl complexes have been reported.[7-13, 16-19, 21, 22] This scarcity is due to the reducing ability of many alkylating reagents, which results in unwanted uranyl reduction to insoluble U(IV) oxides.[24-26] However, several synthetic strategies have been adopted that can impart significant kinetic stability to uranyl-carbon bonds. For example, several research groups have used chelating ligands, such as bis(iminophosphorano)methanide,[11, 12] bis(iminophosphorano)methandiide,[16, 17] bis(thiophosphorano)methanide,[18] and calix[4]pyrrole[8] to generate stable uranyl hydrocarbyl complexes. Saturation of the uranium coordination sphere can also stabilize U-C bonds, as illustrated by $[Li(MeIm)][(UO_2(Ar_2nacnac)(C_4H_5N_2)_2]$[10] and $[Li(DME)_{1.5}]_2[UO_2(CH_2SiMe_3)_4]$.[9] In Chapter 2, I described the first structurally authenticated uranyl-aryl complexes, $[Li(Et_2O)_2(THF)][UO_2(C_6Cl_5)_3]$ ([Li][**2.1**]) and $[Li(THF)_4][UO_2(C_6Cl_5)_3(THF)]$ ([Li][**2.2**]).[7] Their surprisingly good thermal stability is likely the result of the poor reducing ability of the $[C_6Cl_5]^-$ ligand, in combination with the lack of easily activated *ortho*-H atoms on the aryl ring. Several uranyl *N*-heterocyclic carbene (NHC) complexes have been reported, as well.[14, 15, 21, 23, 27] Presumably, their stability is due to the lower reducing ability of neutral NHC donors vs. anionic hydrocarbyl ligands.[24, 25]

In chapter 2, diamagnetic $[Li(Et_2O)_2(THF)][UO_2(C_6Cl_5)_3]$ ([Li][**2.1**]) and $[Li(THF)_4][UO_2(C_6Cl_5)_3(THF)]$ ([Li][**2.1**]) also proved to be good substrates for evaluating U-C bond covalency using ^{13}C NMR spectroscopy combined with density functional theory

(DFT) calculations. This approach is emerging as a valuable means to examine An–C and Ln-C bonding.[7, 9, 28-36] In particular, the ^{13}C NMR resonances for An- or Ln-bound carbon nuclei may exhibit large downfield shifts due to the relativistic spin-orbit (SO) interaction, a result of the 5f and 6d orbital participation in the An-C and Ln-C σ-bonds.[37, 38] In the case of $[Li(Et_2O)_2(THF)][UO_2(C_6Cl_5)_3]$ (**2.1**), discussed in chapter 2, the C_{ipso} chemical shift was calculated to feature a 62 ppm downfield contribution from SO coupling, which was due to the uranium valence orbitals mixing into the U-C bonds.[7]

Building on my past efforts in uranyl hydrocarbyl chemistry, I searched for other aryl ligands that could produce a stable uranyl aryl complex. In this regard, the 2,4,6-tris(trifluoromethyl)phenyl fragment ($[Fmes]^-$) is an intriguing candidate because of its similar electron withdrawing character to $[C_6Cl_5]^-$ and lack of *ortho*-H atoms. Additionally, I hypothesized that the relatively bulky *ortho*-CF_3 substituents would impart further kinetic stability to the U-C bonds. In fact, Fmes is known for its ability to stabilize unusual fragments, especially those of with low coordination numbers and unstable oxidation states.[39-62] For example, the Fmes ligand was used to stabilize the first bis(aryl) plumbylene, $[Pb(Fmes)_2]$, and the first monomeric bis(aryl) stannylene, $[Sn(Fmes)_2]$.[47, 49] Fmes was also used to stabilize $[(Fmes)_2MM(Fmes)_2]$ (M = Ga, In), which represent early examples of complexes with stable In-In and Ga-Ga bonds.[57]

Herein, I describe the synthesis and characterization of the two new structurally-characterized uranyl aryl complexes, namely, $[Li(THF)_3][UO_2(Fmes)_3]$ ($[Li(THF)_3][$**5.1**$]$) and $[Li(Et_2O)_3(THF)][UO_2(Fmes)_3]$ ($[Li(Et_2O)_3(THF)][$**5.1**$]$). To our knowledge, this ligand had not been previously employed in f element chemistry. In addition, I applied a combination of

^{13}C NMR spectroscopy and relativistic DFT calculations to study the nature of their uranium-carbon bonds.

5.2 Results and Discussion

5.2.1 Synthesis and Characterization

The preparation of the *in situ* generated LiFmes (FmesH = 1,3,5-$(CF_3)_3C_6H_3$) was done according to the literature procedure with slight modifications.[51] A slow addition of a cold (-25 °C) solution of 2.5 M *n*-BuLi in hexanes was added dropwise to a cold (-25 °C) colorless stirring solution of FmesH in Et_2O. After 30 min of stirring, the reaction mixture became a clear pale-yellow color. It is important to note that the inefficiency of *n*-BuLi in deprotonation of FmesH leads to incomplete conversion and prolonging reaction times does not enhance conversion.[51] Notably, as discussed in chapter 2, LiFmes exhibits less thermal sensitivity compared to LiC_6Cl_5. Subsequent, addition of a cold (–25 °C) solution of LiFmes,[51] generated *in situ*, to a cold (–25 °C) suspension of $[UO_2Cl_2(THF)_2]_2$ in Et_2O results in the formation of an orange solution. Extraction of the reaction mixture with hexanes affords an orange solution, from which $[Li(THF)_3][UO_2(Fmes)_3]$ ($[Li(THF)_3][$**5.1**$]$) was isolated as pale orange plates in 84% yield, calculated assuming that THF was the limiting reagent (Scheme 5.1). In contrast, extraction of a comparably prepared reaction mixture with Et_2O affords a yellow solution, from which $[Li(Et_2O)_3(THF)][UO_2(Fmes)_3]$ ($[Li(Et_2O)_3(THF)][$**5.1**$]$) was isolated as bright yellow plates in 60% yield. The highest yields were achieved when 6 equiv of FmesH (per U) were used in the reactions to form $[Li(THF)_3][$**5.1**$]$ and $[Li(Et_2O)_3(THF)][$**5.1**$]$. Presumably, the large excess was required because of the inefficiency of FmesH deprotonation by *n*-BuLi.[51] Interestingly, upon standing at room temperature, crystals of

[Li(Et$_2$O)$_3$(THF)][**5.1**] slowly change color from yellow to bright orange over the course of several hours. I hypothesize that, in the solid state, the Li^+ cation loses solvent and subsequently coordinates to a uranyl oxo ligand, forming orange [Li(solvent)$_3$][UO$_2$(Fmes)$_3$].

Scheme 5.1. Synthesis of Complexes [Li(THF)$_3$][**5.1**] and [Li(Et$_2$O)$_3$(THF)][**5.1**].

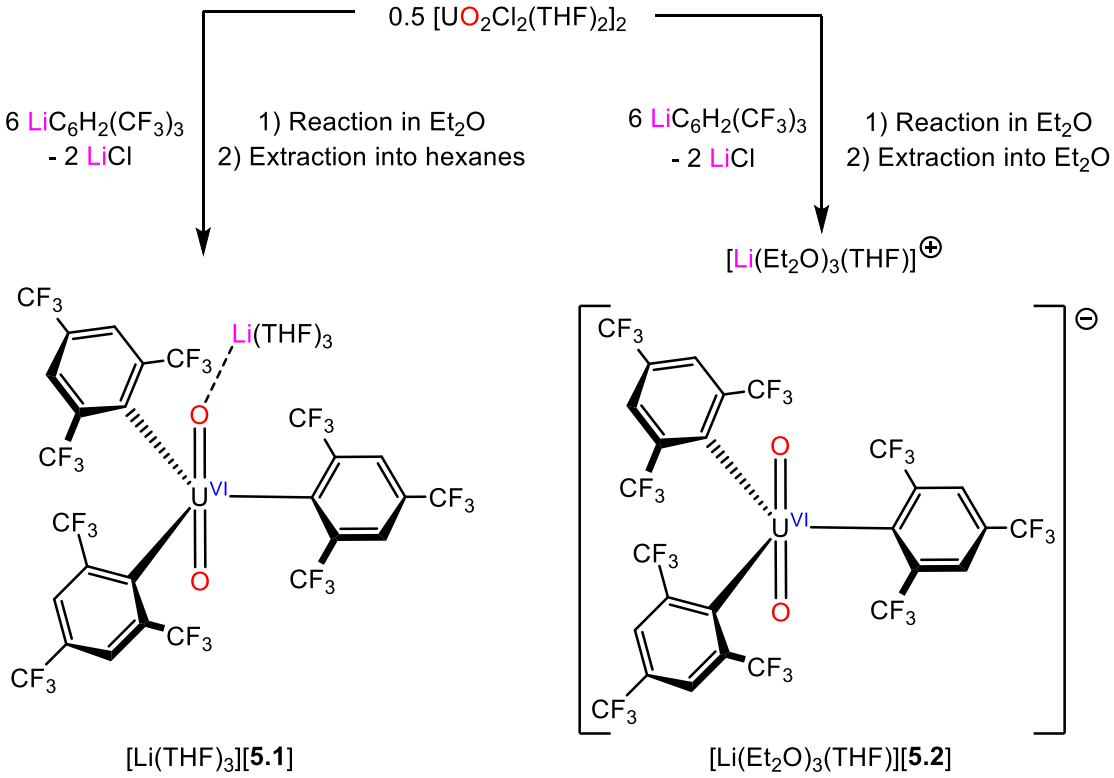

Complex [Li(THF)$_3$][**5.1**] crystallizes in the triclinic space group $P\bar{1}$ as the THF solvate [Li(THF)$_3$][**5.1**]·0.5THF (Figure 5.1), whereas [Li(Et$_2$O)$_3$(THF)][**5.1**] crystallizes in the monoclinic space group $P2_1$ with two independent molecules in the asymmetric unit (Figure 5.4). The metrical parameters of the two molecules are similar, and only one will be discussed in detail. Both [Li(THF)$_3$][**5.1**] and [Li(Et$_2$O)$_3$(THF)][**5.1**] feature trigonal bipyramidal geometries about their uranium centers. Complex [Li(THF)$_3$][**5.1**] also features a close contact between the $[Li(THF)_3]^+$ cation and a uranyl oxo ligand (Li1-O1 = 2.001(16) Å), whereas [Li(Et$_2$O)$_3$(THF)][**5.1**] is a discrete cation/anion pair. Coordination of Li^+ to the oxo ligand

in [Li(THF)$_3$][**5.1**] appears to result in a small, but statistically significant, perturbation of the U-O$_{yl}$ bond length (e.g., U1-O1 = 1.772(6), U1-O2 = 1.720(7) Å; Table 5.1). However, these values are still within the normal range of U-O$_{yl}$ distances.[63-65] The average U-C distances in [Li(THF)$_3$][**5.1**] (2.57(4) Å) and 5.2 (2.58(3) Å) are similar to those found in other σ-bonded uranyl aryl complexes.[7] For example, in chapter 2 the average U-C bond distance in [Li(THF)$_4$][UO$_2$(C$_6$Cl$_5$)$_3$(THF)] ([Li][**2.1**]) is 2.58(4) Å. The closest F→U contact in 5.1 is U1-F9 = 2.877(6) Å, and the closest F→U contact in [Li(Et$_2$O)$_3$(THF)][**5.1**] is U2-F54 = 2.88(2) Å. These distances are longer than the F→U contacts observed for [Cp*$_2$Co][U(OB(C$_6$F$_5$)$_3$)$_2$(^{Ar}acnac)(OEt$_2$)] (^{Ar}acnac = Ar*NC*(Ph)CHC(Ph)*O*; Ar = 3,5-tBu$_2$C$_6$H$_3$)[66] (2.762(6) and 2.789(5) Å) and [U(N(C$_6$F$_5$)$_2$)$_4$][67] (2.6480(11) and 2.5989(11) Å). Although F→M interactions are common for the Fmes ligand,[49, 52] the comparatively large

distances in the present study suggest that F→U dative interactions in $[UO_2(Fmes)_3]^-$, if present, are weak. This conclusion is supported by the DFT calculations (vide infra).

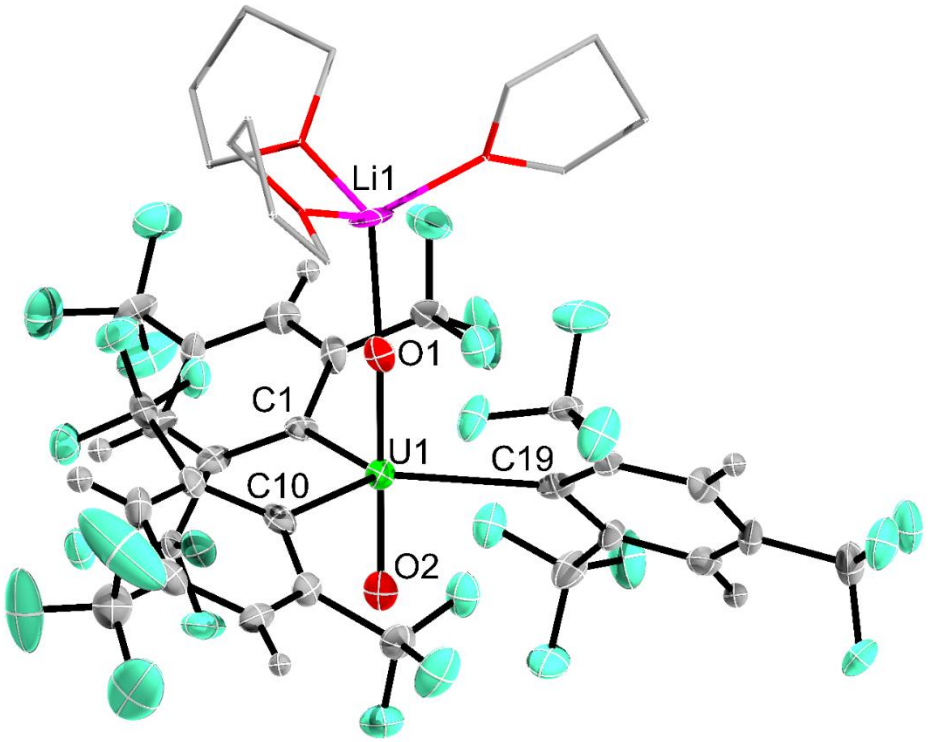

Figure 5.1. Solid-state molecular structure of $[Li(THF)_3]$[**5.1**]·0.5THF shown with 50% probability ellipsoids. The THF ligands are shown in wireframe style and their H atoms are omitted for clarity.

Table 5.1. Selected metrical parameters for [Li(THF)$_3$][**5.1**]·0.5THF and [Li(Et$_2$O)$_3$(THF)][**5.1**].

Complex	[Li(THF)$_3$][**5.1**]·0.5THF	[Li(Et$_2$O)$_3$(THF)][**5.1**]	
U-C	2.554(9), 2.609(9), 2.537(10)	U1	U2
		2.55(4), 2.57(3), 2.57(4)	2.58(4), 2.61(4), 2.63(4)
U=O	1.772(6), 1.720(7)	1.71(2), 1.70(2)	1.73(2), 1.72(2)
Li-O$_{yl}$	2.001(16)	-	-
O-U-O	179.9(4)	179.0(10)	179.3(11)

The ^{1}H NMR spectrum of [Li(THF)$_3$][**5.1**] in benzene-d_6 exhibits a singlet at 8.40 ppm, assigned to the *meta*-CH environment of the Fmes ligand (Figure 5.6). Additionally, the ^{19}F{^{1}H} spectrum for [Li(THF)$_3$][**5.1**] in benzene-d_6 features two resonances, in a 2:1 ratio, at –56.70 and –62.60 ppm, which are assigned to the *ortho* and *para* trifluoromethyl resonances, respectively (Figure 5.8). The ^{7}Li{^{1}H} NMR spectrum of [Li(THF)$_3$][**5.1**] in benzene-d_6 features a broad resonance at –3.27 ppm (Figure 5.7). A uranyl amide complex with oxo-coordinated Li$^+$ cations exhibits a similar upfield ^{7}Li chemical shift.[68] The orange color of this solution, in combination with the relatively upfield ^{7}Li resonance suggest that a Li-O$_{yl}$ dative interaction is present in the system and is maintained in benzene-d_6. In contrast, the dissolution of [Li(THF)$_3$][**5.1**] in THF-d_8 resulted in an immediate color change to yellow. The ^{7}Li{^{1}H} NMR spectrum of this solution features a broad resonance at 0.06 ppm, suggesting the formation of discrete cation/anion pair. Finally, the low solubility of [Li(THF)$_3$][**5.1**] in benzene-d_6 precluded the collection of a ^{13}C{^{1}H} NMR spectrum in this solvent. While

[Li(THF)$_3$][**5.1**] is very soluble in THF-d_8, I did not record its ^{13}C NMR spectrum in THF-d_8 because I assumed that it would convert into fully-solvated Li^+ and $[UO_2(Fmes)_3]^-$ (see below).

The ^{1}H NMR spectrum of [Li(Et$_2$O)$_3$(THF)][**5.1**] in THF-d_8, recorded at room temperature, exhibits a sharp resonance at 8.30 ppm attributed to the *meta*-CH environment (Figure 5.13). Additionally, the ^{19}F{^{1}H} spectrum for [Li(Et$_2$O)$_3$(THF)][**5.1**] in THF-d_8 feature two resonances at –58.15 and –63.38, in a 2:1 ratio, corresponding to the *ortho* and *para* trifluoromethyl environments, respectively (Figure 5.15). The ^{7}Li{^{1}H} NMR spectrum [Li(Et$_2$O)$_3$(THF)][**5.1**] in THF-d_8 features a sharp resonance at –0.28 ppm (Figure 5.14), consistent with the presence of a fully solvated Li^+ cation.[7, 29] The ^{13}C{^{19}F} NMR spectrum of [Li(Et$_2$O)$_3$(THF)][**5.1**] in THF-d_8, recorded at –35 °C to minimize decomposition, features a distinctive downfield resonance at 240.03 ppm, which is attributable to the C_{ipso} environment of the Fmes ligands (Figure 5.2). In addition, the spectrum features resonances at 142.94, 128.92, and 126.26 ppm, which are assigned to the C_{ortho}, C_{para}, C_{meta} environments of the Fmes ligand, respectively. The ^{13}C{^{1}H} NMR spectrum of [Li(Et$_2$O)$_3$(THF)][**5.1**] in THF-d_8, recorded at –35 °C, features an identical C_{ipso} resonance at 240.03 ppm. For comparison, in chapter 2 the C_{ipso} resonance of [Li(Et$_2$O)$_2$(THF)][$UO_2(C_6Cl_5)_3$] ([Li][**2.1**]) in benzene-d_6 was

also shifted significantly downfield (236.7 ppm).[7] Raman spectra for [Li(THF)$_3$][**5.1**] and [Li(Et$_2$O)$_3$(THF)][**5.1**] were not recorded.

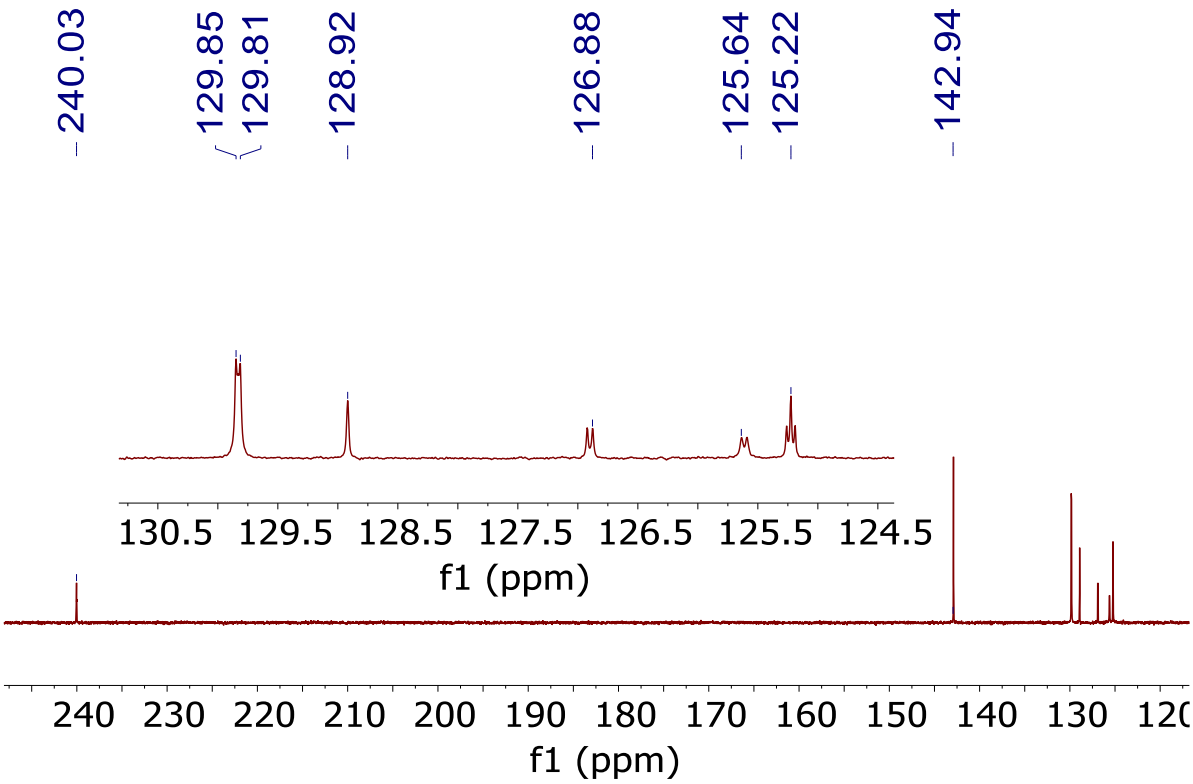

Figure 5.2. Partial $^{13}C\{^{19}F\}$ NMR spectrum of [Li(Et$_2$O)$_3$(THF)][**5.1**] in THF-d_8 at –35 °C. Insert displays enlarged section of $^{13}C\{^{19}F\}$ NMR spectrum for clarity.

5.2.2 Computational Analysis

Dr. Xiaojuan Yu and Prof. Jochen Autschbach at the State University of New York at Buffalo performed DFT calculations with the zeroth-order relativistic approximation (ZORA) Hamiltonian on the anionic component of [**5.1**]$^-$, using a selection of functionals (BP86, PBE, PBE0, and B3LYP). The calculations employed the Amsterdam Density Functional program along with the NBO code included with ADF, for analyses of the bonding in terms of natural localized molecular orbitals (NLMOs).[69-71] Complete computational details are provided in

the Supporting Information (SI). PBE0 gave the best agreement with the experiments for structural parameters, and this functional is also commonly used for NMR calculations.[72] Therefore, the following discussion is based on results obtained with this functional. The average optimized U-C and U-O_{yl} distances of [**5.1**]$^-$ are within 0.02 and 0.04 Å, respectively, of the experimentally-determined values. An NMLO analysis of [**5.1**]$^-$ reveals (Figure 5.3) that the σ(U-C) bond features 21% total uranium weight (62/25% 6d/5f at U), with a Wiberg bond order (WBO) of 0.63. For comparison, a previous NMLO analysis of the U-C σ-bonds in $[UO_2(C_6Cl_5)_3]^-$ revealed 22% uranium weight (59/28% 6d/5f at U) with a WBO of 0.67.[7] Similar uranium participation has been calculated for the U-C σ bonds in $[UO_2(CH_2SiMe_3)_4]^{2-}$,[9] which features 18% uranium weight albeit with larger 5f character (40/45% 6d/5f at U). The bonding analyses also show F→U dative interactions (Table 5.4), but only involving 2% weight of uranium in the relevant NLMOs (Figure 5.5). The halide donation is therefore much weaker than the Cl→U dative interactions (with 5 to 8% metal weights in the relevant NLMOs) observed for the U(IV) aryl complexes, $[Li(Et_2O)_3][UCl_2(C_6Cl_5)_3]$ ([Li][**3.4**]) and $[Li(Et_2O)_4][U(C_6Cl_5)_5]$ ([Li][**3.2**]) as discussed in chapter 3.[29]

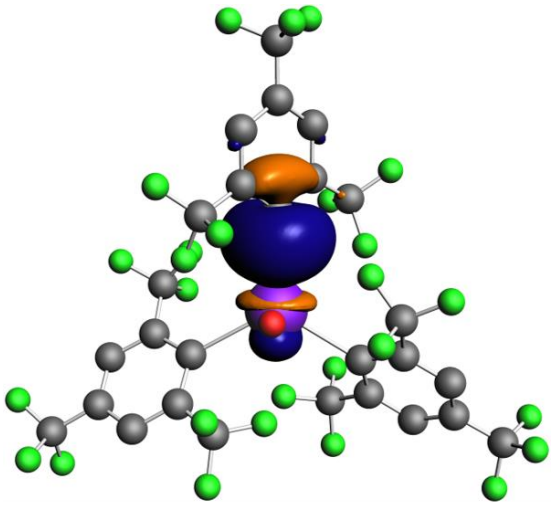

Figure 5.3. A representative U-C bonding NLMO in [**5.1**]$^{-}$. Weight-% metal character and 6d vs. 5f contribution at the metal averaged over equivalent NLMOs. Isosurfaces at ±0.03 a.u. Color code for atoms: U purple, O red, F seafoam green, C dark gray.

The ^{13}C NMR chemical shifts for [**5.1**]$^{-}$ were also calculated, with and without SO effects included, using a PBE0 variant with 40% exact exchange. This methodology has been used successfully by us, and others, to accurately calculate ^{13}C chemical shifts for actinide organometallics complexes, including $[UO_2(C_6Cl_5)_3]^{-}$ ([**2.1**]$^{-}$) and $[UO_2(CH_2SiMe_3)_4]^{2-}$.[7, 9, 35, 73, 74] The averaged calculated C_{ipso} chemical shift for [**5.1**]$^{-}$ is 238 ppm, which is in excellent agreement with the experimentally-determined value (240 ppm). SO effects contribute 51 ppm to this shift, which must be attributed to the 5f and 6d orbital involvement in the U-C bonds. Interestingly, this downfield shift is somewhat smaller than the one calculated for $[UO_2(C_6Cl_5)_3]^{-}$ ([**2.1**]$^{-}$) (62 ppm),[7] and much smaller than that calculated for $[UO_2(CH_2SiMe_3)_4]^{2-}$ (177 ppm),[9] which reflects the sensitivity of ^{13}C chemical shifts to the

varying degrees of 5f/6d orbital participation in the U-C interactions, as well as minor variations in the overall U weights and the 2s contribution from the carbon center.[75] $[UO_2(CH_2SiMe_3)_4]^{2-}$, in particular, is calculated to much have greater 5f character in its U-C bonds vs. [**5.1**]$^-$ and $[UO_2(C_6Cl_5)_3]^-$ ([**2.1**]$^-$), although the overall U weights are similar. The other Fmes ^{13}C chemical shifts in [**5.1**]$^-$ are also predicted well by the calculations (Table 5.5), including C_{ortho} (Calc. = 139.2 ppm; Expt. = 142.9 ppm), C_{meta} (Calc. = 125.1 ppm; exp. = 126.3 ppm), and C_{para} (Calc.= 125.4 ppm; Expt. = 128.9 ppm); however, these resonances do not display any appreciable SO-induced changes, as expected.

5.3 Summary

I have prepared and characterized a rare example of a uranyl aryl "ate" complex supported by two different cations, namely, $[Li(THF)_3][UO_2(Fmes)_3]$ and $[Li(Et_2O)_3(THF)][UO_2(Fmes)_3]$. They represent rare examples of well-characterized uranyl organometallic complexes, as well as the first examples of f element Fmes complexes. Their unusual stability is likely a consequence of their CF_3 substituents, which imparts significant kinetic stability to the U-C bonds due to their steric bulk in combination with their electron withdrawing ability. Unlike many other Fmes systems, however, I do not observe significant F→M dative interactions, likely due to the rigidity of the uranyl fragment, which would restrict any F→M interactions to the nearly saturated equatorial plane. The C_{ipso} resonance of $[UO_2(Fmes)_3]^-$ was observed at 240 ppm in its $^{13}C\{^{19}F\}$ NMR spectrum. DFT calculations were able to reproduce this chemical shift almost perfectly when the relativistic SO interaction was included. In particular, SO effects are responsible for a 51 ppm downfield shift of this resonance, due to covalent mixing of the uranium valence orbitals with those of the *ipso* carbon atoms. Consistent with this finding, an NMLO analysis of $[UO_2(Fmes)_3]^-$ shows an

appreciable covalency in the U-C bonding interaction. Overall, this work highlights the continuing utility of NMR spectroscopy in the evaluation of An-L bonding within diamagnetic actinide complexes. In addition, it adds to a growing body of uranyl organometallic chemistry. For many years, uranyl hydrocarbyl complexes were thought to be inherently unstable,[24, 25] but recent work shows that uranyl-carbon bonds can be kinetically stabilized through careful ligand choice.

5.4 Experimental

5.4.1 General Procedures

All reactions and subsequent manipulations were performed under anaerobic and anhydrous conditions under an atmosphere of dinitrogen. Hexanes, pentane, and diethyl ether (Et_2O) were dried using a Vacuum Atmospheres DRI-SOLV Solvent Purification system and stored over 3Å sieves for 24 h prior to use. Tetrahydrofuran (THF) was distilled over Na/benzophenone and stored over activated 3 Å molecular sieves for 24 h prior to use. Benzene-d_6 and THF-d_8 was dried over 3Å molecular sieves for 24 h prior to use. $[UO_2Cl_2(THF)_2]_2$ was synthesized according to the previously reported procedures.[76] All other reagents were purchased from commercial suppliers and used as received.

^{1}H, $^{13}C\{^{1}H\}$, $^{13}C\{^{19}F\}$, $^{19}F\{^{1}H\}$, and $^{7}Li\{^{1}H\}$ NMR spectra were recorded on a Bruker AVANCE NEO 500 MHz spectrometer or a Bruker AVANCE III HD 400 MHz spectrometer. ^{1}H, $^{13}C\{^{1}H\}$, and $^{13}C\{^{19}F\}$ NMR spectra were referenced to external tetramethylsilane (TMS) using the residual protio solvent peaks as internal standards. $^{7}Li\{^{1}H\}$ and $^{19}F\{^{1}H\}$ NMR spectra were referenced indirectly with the ^{1}H chemical shift of TMS at 0 ppm, according to IUPAC standard.[77, 78] IR spectra were recorded on a Nicolet 6700 FT-IR spectrometer.

Elemental analyses were performed by the Microanalytical Laboratory at the University of California (Berkeley, CA).

5.4.2 Synthesis of [LiFmes]

The synthesis of LiFmes was performed according to the literature procedure with slight modifications.[51] A cold solution (–25 °C) of *n*-BuLi in hexanes (0.2 mL, 0.50 mmol, 2.5 M) was added dropwise to a cold, stirring solution (–25 °C) of 1,3,5-$(CF_3)_3C_6H_3$ (0.093 mL, 0.50 mmol) in Et_2O (2 mL). After 30 min of stirring, the reaction mixture became a clear pale-yellow color. The resulting LiFmes solution was used as is.

5.4.3 Synthesis of [Li(THF)$_3$][UO$_2$(Fmes)$_3$] ([Li(THF)$_3$][5.1])

A solution of LiFmes (2 mL in Et_2O, 0.50 mmol, 0.25 M) was added to a cold (–25 °C), stirring suspension of $[UO_2Cl_2(THF)_2]_2$ (40.4 mg, 0.042 mmol) in Et_2O (2 mL), which resulted in a gradual color change to orange, concomitant with the deposition of a pale-yellow precipitate. After 30 min of stirring, the reaction mixture was filtered through a Celite column (0.5 cm × 5 cm) supported on glass wool to afford a clear, orange filtrate. The volatiles were removed *in vacuo* and the resulting orange solid was triturated with pentane (2 × 1 mL). The solid was then extracted into hexanes (4 × 2 mL) and the resulting orange solution was filtered through a Celite column (0.5 cm × 5 cm) supported on glass wool to afford a clear, orange filtrate. The volume of the filtrate was reduced to 2 mL *in vacuo* and the sample was stored at –25 °C for 24 h, which resulted in the deposition of orange plates. The solid was isolated by decanting the supernatant and then dried briefly *in vacuo* (62.3 mg, 84% yield). The yield was calculated by assuming that THF was the limiting reagent. Anal. Calcd for $C_{39}H_{30}LiO_5F_{27}U$: C, 35.05; H, 2.26 Found: C, 34.29; H, 2.28. ^{1}H NMR (25 °C, 500 MHz,

benzene-d_6): δ 8.40 (s, *m*-H). ^{7}Li{^{1}H} NMR (25 °C, 194.4 MHz, benzene-d_6): δ –3.27 (br s). ^{19}F{^{1}H} NMR (25 °C, 470.6 MHz, benzene-d_6): δ –56.70 (s, 18F, *o*-CF_3), –62.60 (s, 9F, *p*-CF_3). ^{1}H NMR (25 °C, 400 MHz, THF-d_8): δ 8.30 (s, *m*-H). ^{7}Li{^{1}H} NMR (25 °C, 155.51 MHz, THF-d_8): δ 0.06 (br s). ^{19}F{^{1}H} NMR (25 °C, 376.5 MHz, THF-d_8): δ –58.08 (s, 18F, *o*-CF_3), –63.40 (s, 9F, *p*-CF_3). IR (KBr pellet, cm^{-1}): 3432 (w), 2975 (w), 2958 (w), 2929 (w), 2875 (w), 2233 (w), 1830 (w), 1619 (m), 1560 (w), 1452 (w), 1384 (m), 1251 (m), 1060 (s), 1035 (s), 1008 (m), 933 (s), 908 (s), 887 (s), 846 (s), 835 (s), 794 (m), 792 (m), 734 (s), 686 (s), 667 (s), 578 (w), 557 (w), 511 (w), 430 (m).

5.4.4 Synthesis of [Li(Et$_2$O)$_3$(THF)][UO$_2$(Fmes)$_3$] ([Li(Et$_2$O)$_3$(THF)][5.1])

A solution of LiFmes (2 mL in Et$_2$O, 0.50 mmol, 0.25 M) was added to a cold (–25 °C), stirring suspension of [UO$_2$Cl$_2$(THF)$_2$]$_2$ (40.4 mg, 0.042 mmol) in Et$_2$O (2 mL), which resulted in a gradual color change to orange, concomitant with the deposition of a pale-yellow precipitate. After 30 min of stirring, the reaction mixture was filtered through a Celite column (0.5 cm × 5 cm) supported on glass wool to afford a clear, orange filtrate. The volatiles were removed *in vacuo* and the resulting orange solid was triturated with pentane (2 × 1 mL). The solid was then extracted into Et$_2$O (2 × 1.5 mL) and the resulting yellow solution was filtered through a Celite column (0.5 cm × 5 cm) supported on glass wool to afford a clear, yellow filtrate. The volume of the filtrate was reduced to 2 mL *in vacuo*, pentane (3 mL) was layered onto the solution, and the sample was stored at –25 °C for 24 h, which resulted in the deposition of yellow plates. The solid was isolated by decanting the supernatant and dried briefly *in vacuo* (70.5 mg, 60% yield). Anal. Calcd for $C_{43}H_{44}LiO_6F_{27}U$: C, 36.51; H, 3.13. Found (1st attempt): C, 33.14; H, 2.66. Found (2nd attempt): C, 33.52; H, 2.44. I attribute the low C% for both attempts to loss of Li$^+$-bound THF on standing. ^{1}H NMR (25 °C, 400 MHz,

THF-d_8): δ 8.30 (s, *m*-H). ^{7}Li{^{1}H} NMR (25 °C, 155.5 MHz, THF-d_8): δ –0.28 (br s). ^{19}F{^{1}H} NMR (25 °C, 376.6 MHz, THF-d_8): δ –58.15 (s, 18F, *o*-CF_3), –63.38 (s, 9F, *p*-CF_3). ^{13}C{^{19}F} NMR (–35 °C, 125.8 MHz, THF-d_8): δ 240.03 (s, *i*-C),142.94 (s, *o*-C), 129.83 (d, J_{CH} = 4.52 Hz, *o*-CF_3), 128.92 (s, *p*-C), 126.26 (dd, J_{CH} = 5.65, 161.63 Hz, *m*-C), 125.22 (t, J_{CH} = 4.52 Hz, *p*-CF_3). ^{13}C{^{1}H} NMR (–35 °C, 125.8 MHz, THF-d_8): δ 240.03 (s, *i*-C), 142.9 (q, J_{CF} = 32.78 Hz, *o*-C), 129.83 (q, J_{CF} = 274.94 Hz, *o*-CF_3), 128.92 (q, J_{CF} = 128.92 Hz, *p*-C), 126.26 (s, *m*-C), 125.23 (q, J_{CF} = 271.27 Hz, *p*-CF_3). IR (KBr pellet, cm^{-1}): 3415 (w), 2993 (w), 2894 (w), 2227 (w), 1826 (w), 1616 (m), 1560 (m), 1450 (m), 1388 (m), 1027 (m), 935 (s), 902 (s), 883 (s), 846 (s), 833 (s), 792 (s), 734 (s), 684 (s), 694 (s), 572 (w), 559 (m), 534 (m), 516 (m), 511 (m), 478 (m), 460 (m), 457 (m), 426 (m).

5.4.5 X-Ray Crystallography

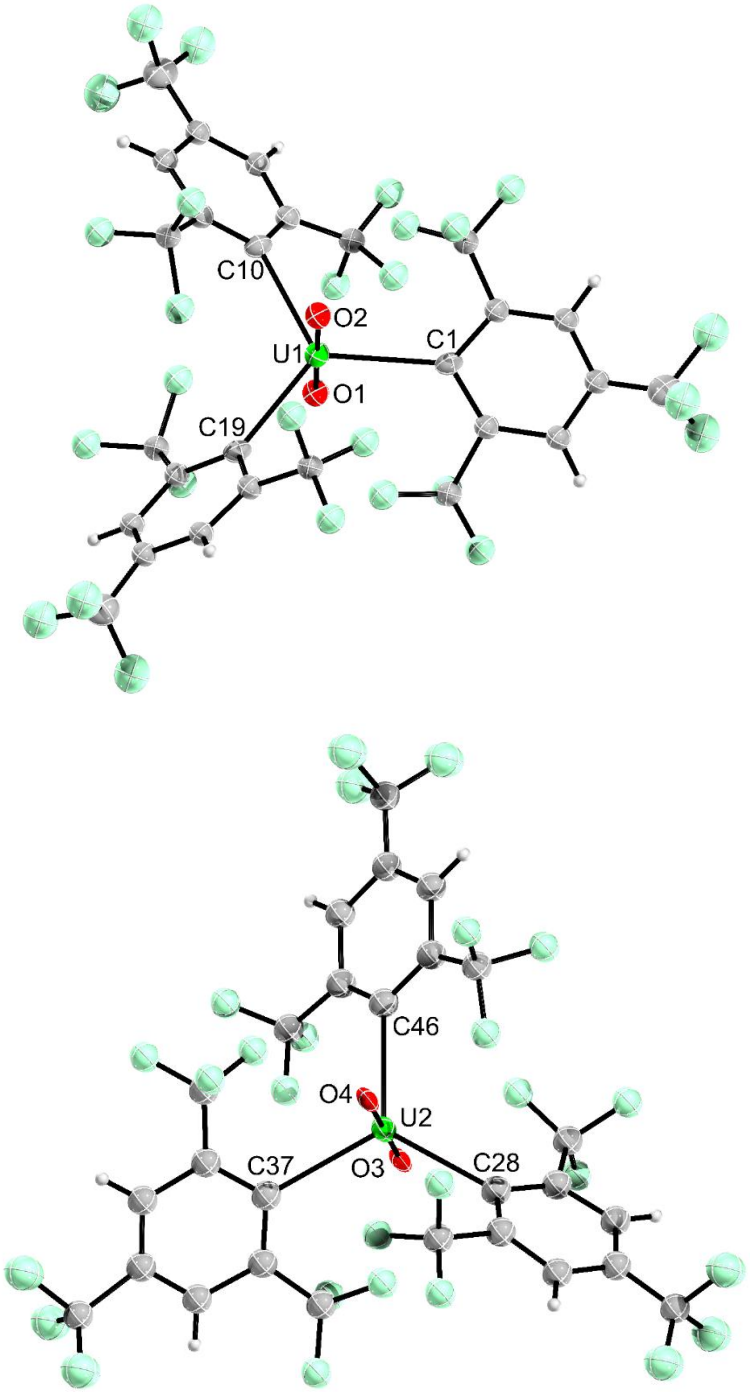

Figure 5.4. Solid-state molecular structure of $[Li(Et_2O)_3(THF)]$[**5.1**] shown with 30% probability ellipsoids. $[Li(Et_2O)_3(THF)]$ counterions are omitted for clarity.

Data for all complexes were collected on a Bruker KAPPA APEX II diffractometer equipped with an APEX II CCD detector using a TRIUMPH monochromator with a Mo Kα X-ray source (α = 0.71073 Å). The crystals were mounted on a cryoloop under Paratone-N oil, and all data were collected at 100(2) K using an Oxford nitrogen gas cryostream. Data were collected using ω scans with 0.5° frame widths. Frame exposures of 15 s were used for both $[Li(THF)_3][\mathbf{5.1}]\cdot 0.5THF$ and $[Li(Et_2O)_3(THF)][\mathbf{5.1}]$. Data collection and cell parameter determinations were conducted using the SMART program.[79] Integration of the data frames and final cell parameter refinement were performed using SAINT software.[80] Absorption correction of the data was carried out using the multi-scan method SADABS.[81] Subsequent calculations were carried out using SHELXTL.[82] Structure determination was done using direct or Patterson methods and difference Fourier techniques. All hydrogen atom positions were idealized and rode on the atom of attachment. Structure solution and refinement were performed using SHELXTL.[82] Graphics, and creation of publication materials were performed using Diamond.[83]

Complex $[Li(THF)_3][\mathbf{5.1}]\cdot 0.5THF$ exhibited positional disorder within the THF solvate molecule, which was address by constraining the affected atoms with EAPD and DFIX commands and setting their occupancies to 50%. Because of this disorder, hydrogen atoms were not added to the THF solvate molecule. Complex $[Li(Et_2O)_3(THF)][\mathbf{5.1}]$ exhibited positional disorder on the Fmes ligands, which was addressed by constraining the affected atoms with EADP and SADI commands. In addition, Li counterions and solvent ligands exhibited positional disorder, which was addressed by constraining the affected atoms with EADP and SADI commands. Because of this disorder, the $[Li(Et_2O)_3(THF)]^+$ counterions were not refined anisotropically.

Further crystallographic details of complexes [Li(THF)$_3$][**5.1**]·0.5THF and [Li(Et$_2$O)$_3$(THF)][**5.1**] can be found in Table 5.2. Complexes [Li(THF)$_3$][**5.1**]·0.5THF and [Li(Et$_2$O)$_3$(THF)][**5.1**] have been deposited in the Cambridge Structural Database ([Li(THF)$_3$][**5.1**]·0.5THF: CCDC 2278342; [Li(Et$_2$O)$_3$(THF)][**5.1**]: CCDC 2278343).

Table 5.2. X-ray crystallographic data for complexes $[Li(THF)_3][\mathbf{5.1}]\cdot 0.5THF$ and $[Li(Et_2O)_3(THF)][\mathbf{5.1}]$.

	$[Li(THF)_3][\mathbf{5.1}]\cdot 0.5THF$	$[Li(Et_2O)_3(THF)][\mathbf{5.1}]$
Formula	$C_{41}H_{34}F_{27}LiO_{5.5}U$	$C_{86}H_{88}F_{54}Li_2O_{12}U_2$
Crystal Habit, Color	Plates, Orange	Plates, Yellow
Crystal Size (mm)	0.2 × 0.1 × 0.05	0.1 × 0.1 × 0.05
MW (g/mol)	1372.65	2829.50
crystal system	Triclinic	Monoclinic
space group	P -1	$P2_1$
a (Å)	11.422(10)	13.582(3)
b (Å)	13.504(14)	27.739(4)
c (Å)	18.136(16)	13.805(3)
α (°)	99.04(3)	90
β (°)	101.49(3)	103.046(14)
γ (°)	114.602(18)	90
V ($Å^3$)	2400(4)	5066.6(16)
Z	2	2
T (K)	100(2)	100(2)
λ (Å)	0.71073	0.71073
GOF	0.994	1.034
Density (calcd) (Mg/m^3)	1.899	1.855
Absorption coefficient (mm^{-1})	3.530	3.348
F_{000}	1324	2752
Total no Reflections	14396	31581
Unique Reflections	8230	17281
Final R indices*	$R_1 = 0.0571$ $wR_2 = 0.1157$	$R_1 = 0.0999$ $wR_2 = 0.2089$
Largest Diff. peak and hole ($e^- A^{-3}$)	1.787, -1.749	1.476, -0.946

* $I > 2\sigma(I)$

5.4.6 Computational Data Details

Kohn-Sham density functional calculations for [**5.1**]$^-$ were performed with the Amsterdam Density Functional (ADF) suite (version 2017)[69] using the PBE0[84-88] functional, the scalar relativistic (SR) all-electron Zeroth-Order Regular Approximation[71] (ZORA) Hamiltonian, and Slater-type orbital (STO) basis sets of triple-ζ doubly polarized (TZ2P)[89] quality for all atoms. An atom-pairwise correction for dispersion forces was considered via Grimme's D3 model augmented with the Becke-Johnson (BJ) damping.[90] The conductor-like screening model (COSMO) was used to describe solvent effects (tetrahydrofuran).[91] To quantify the compositions of the chemical bonds, natural localized molecular orbital (NLMO) analyses were carried out with the NBO program, version 6.0, as interfaced with ADF.[92]

Nuclear magnetic shielding constants for [**5.1**]$^-$, were calculated at the DFT/ZORA-SR and DFT/spin-orbit (SO) ZORA levels of theory and TZ2P basis sets. The computations of the NMR shielding tensors employed the hybrid PBE0 exchange-correlation functional with 40% exact exchange, which previously applied to the reliable chemical shifts of actinide complexes.[9, 74, 87] The ^{13}C shifts δ_i were calculated via $\delta_i = \sigma_{benz} - \sigma_i + \delta_{benz}$. Here, σ_i is the calculated shielding of the carbon of interest, σ_{benz} and δ_{benz} are the calculated carbon shielding and the experimental chemical shift of benzene (128.8 ppm), respectively.[93] However, it is noted that using the secondary benzene reference in the calculations, instead of TMS directly, did not make a substantial difference in the calculated chemical shifts.

Table 5.3. The optimized structural parameters vs experimental data for [**5.1**]$^{-}$.

Bond length	BP86	PBE	PBE0	B3LYP	Expt.
U-C_{avg}	2.573	2.584	2.575	2.596	2.56
U-C_{range}	2.572-2.574	2.583-2.585	2.575-2.576	2.596-2.597	2.54-2.56
U-O	1.792	1.789	1.753	1.772	1.719
O-U-O(°)	179.9	179.9	179.9	179.9	179.3

Table 5.4. % weight compositions of the U-L (L = C, O) bonding NLMOs in [**5.1**]$^{-}$.

Complex	**Orbital**	**Total L**	**2s**	**2p**	**Total U**	**7s**	**7p**	**6d**	**5f**
5.1	σ(U-C)	76	31	79	21	13	0	62	25
	σ(U-O)	72	26	74	27	0	0	17	83
	π(U-O)	79	0	100	21	0	0	40	60
	LP(F)	96	13	87	2	12	1	46	42

Table 5.5. Calculated carbon shielding (σ) and chemical shift (δ) for the reference and [**5.1**]$^-$ using PBE0 (40%)[a] functionals.

Complex	**Nuclei**	**σ_{calc}(ppm) scalar/SO**	**δ_{calc}(ppm)**	**Δ_{SO} (ppm)**	**δ_{expt}(ppm)**
Benzene	C	52.9/53.4	/	/	128.8[93]
[**5.1**]$^-$	C_{ipso}	-4.8/-55.5	186.3/237.7	51.4	240.03
	C_{ortho}	44.4/43.0	137.3/139.2	1.9	142.94
	C_{meta}	57.9/57.1	123.8/125.1	1.3	126.26
	C_{para}	55.9/56.8	125.8/125.4	-0.4	128.92

[a] Fraction of exact exchange in the functional in parentheses. Standard PBE0 has 25% exact exchange. Scalar relativistic calculations ('scalar') versus calculations that include scalar and spin-orbit (SO) relativistic effects.

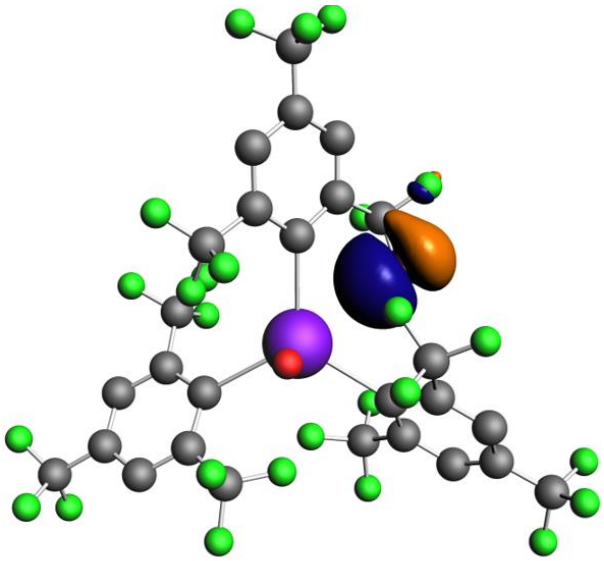

Figure 5.5. Representative fluorine lone-pair NLMO in [**5.1**]$^{-}$ showing minor donation to the uranium center. Weight-% metal character and relative 6d vs. 5f contribution at the metal averaged over equivalent NLMOs. Isosurfaces at ±0.03 a.u. Color code for atoms: U purple, O red, F seafoam green, C dark gray.

5.5 Appendix

5.5.1 NMR Spectra

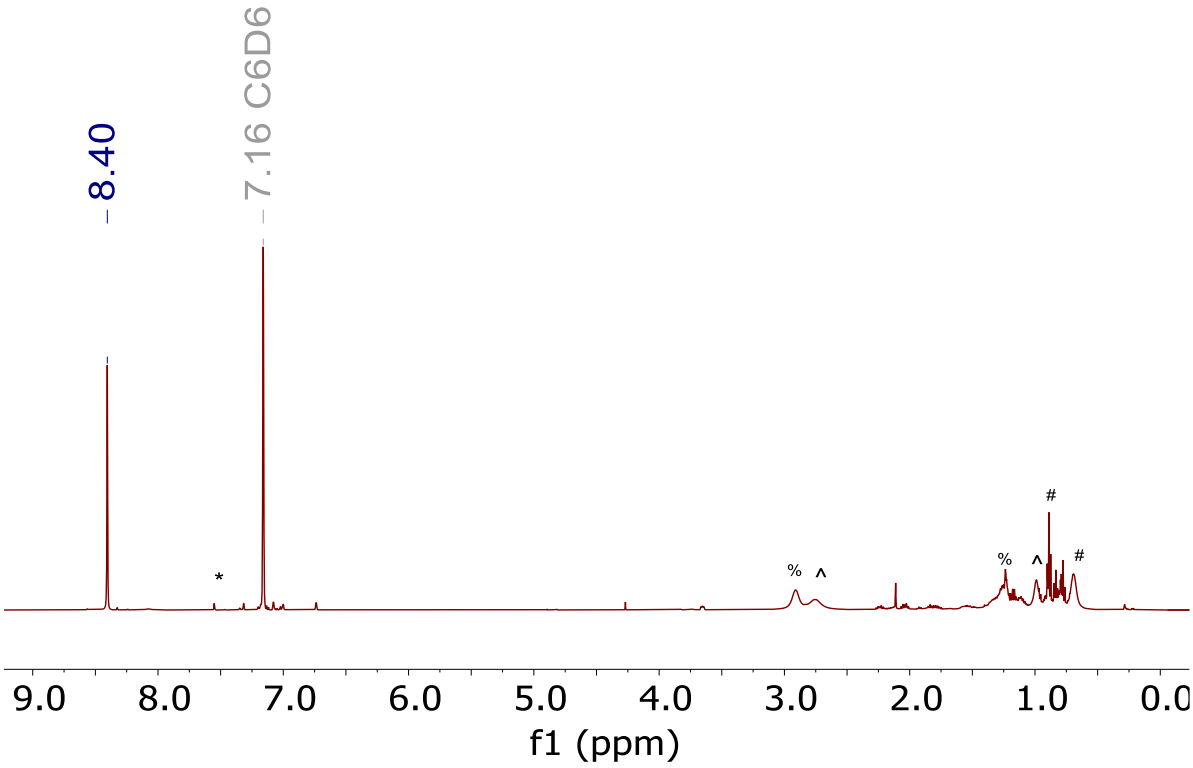

Figure 5.6. ^{1}H NMR spectrum of [Li(THF)$_3$][**5.1**] in benzene-d_6 at room temperature. (*) indicates the presence of FmesH. (#) indicates the presence of hexanes. (^) indicates the presence of Et_2O. (%) indicates the presence of THF.

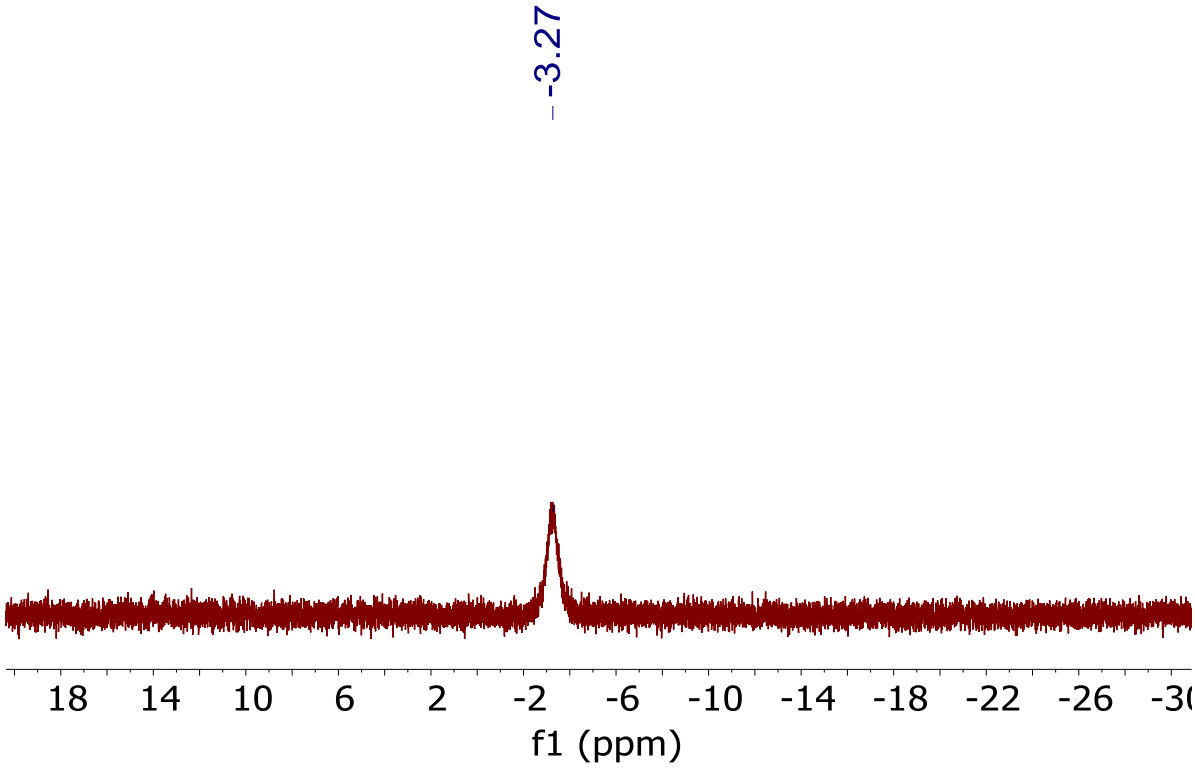

Figure 5.7. $^{7}Li\{^{1}H\}$ NMR spectrum of $[Li(THF)_3]$[**5.1**] in benzene-d_6 at room temperature.

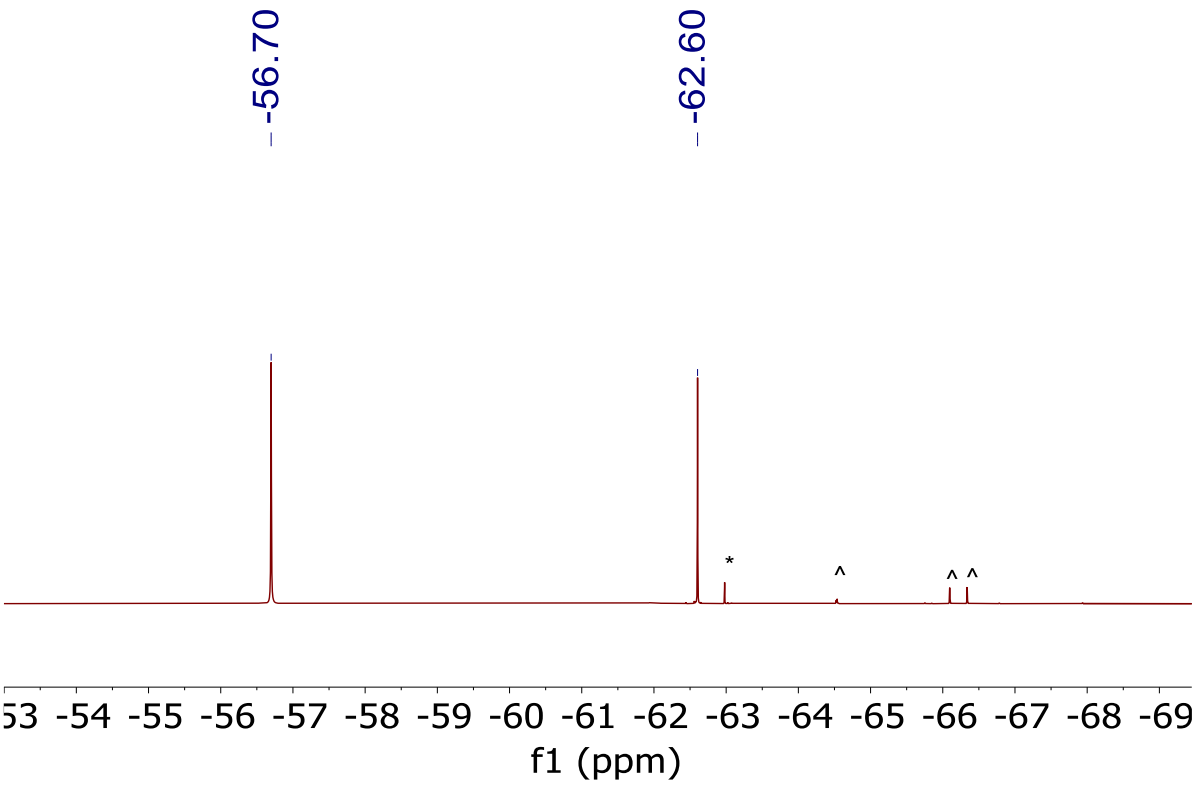

Figure 5.8. $^{19}F\{^{1}H\}$ NMR spectrum of [Li(THF)$_3$][**5.1**] in benzene-d_6 at room temperature. (*) indicates the presence of FmesH. (^) indicates the presence of unidentified impurities.

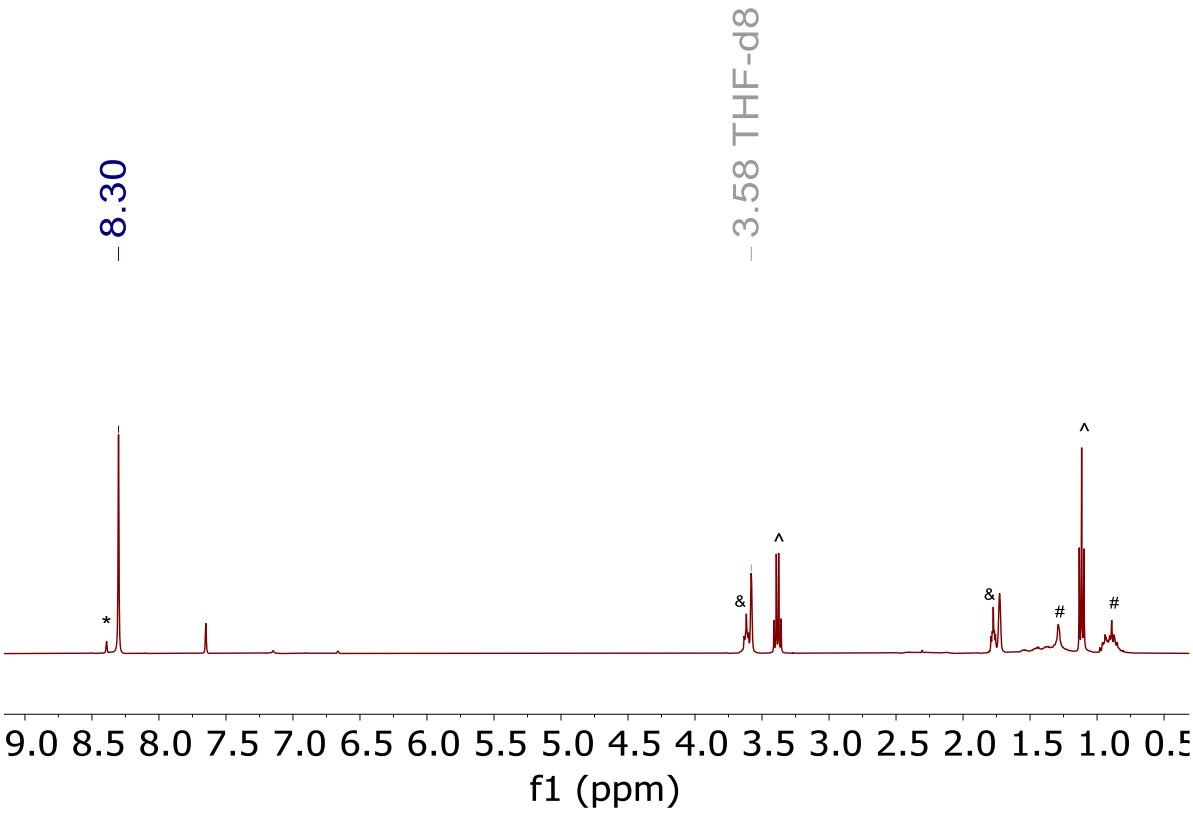

Figure 5.9. ^{1}H NMR spectrum of [Li(THF)$_3$][**5.1**] in THF-d_8 at room temperature. (*) indicates the presence of FmesH. (#) indicates the presence of hexanes. (^) indicates the presence of Et_2O. (&) indicates the presence of THF.

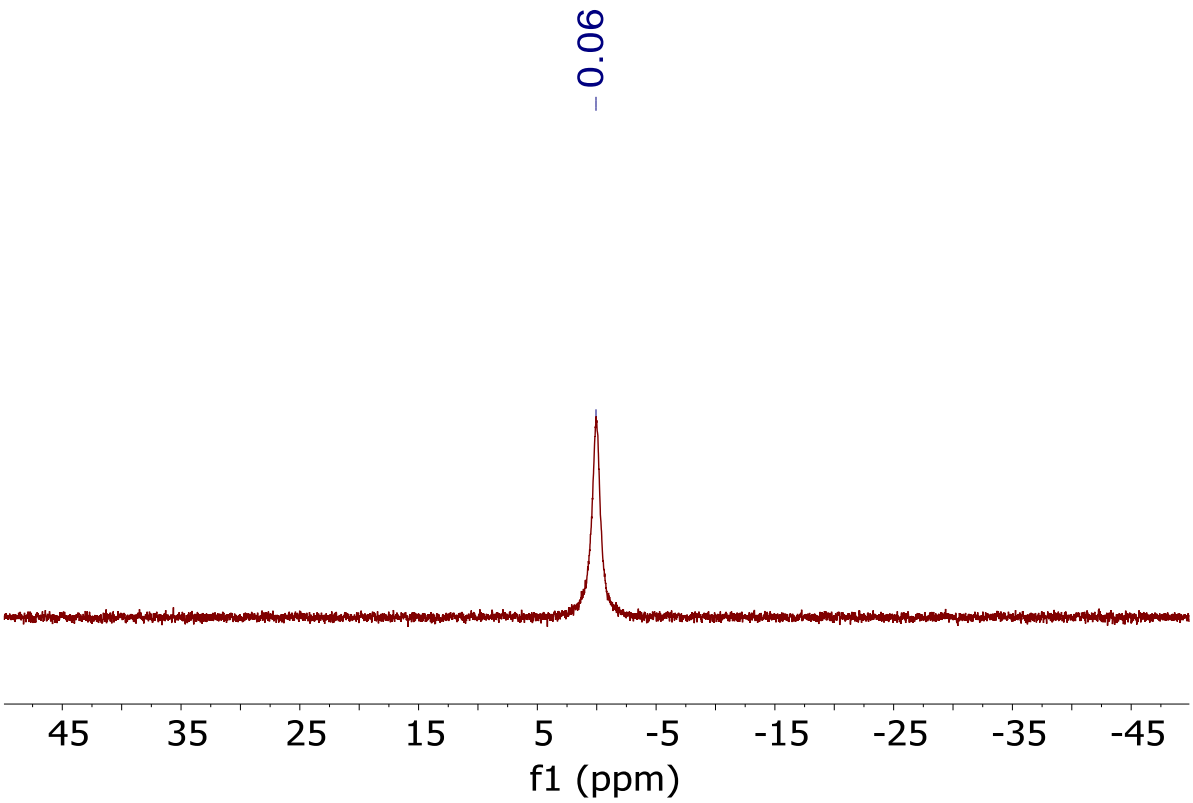

Figure 5.10. $^{7}Li\{^{1}H\}$ NMR spectrum of $[Li(THF)_3]$[**5.1**] in THF-d_8 at room temperature.

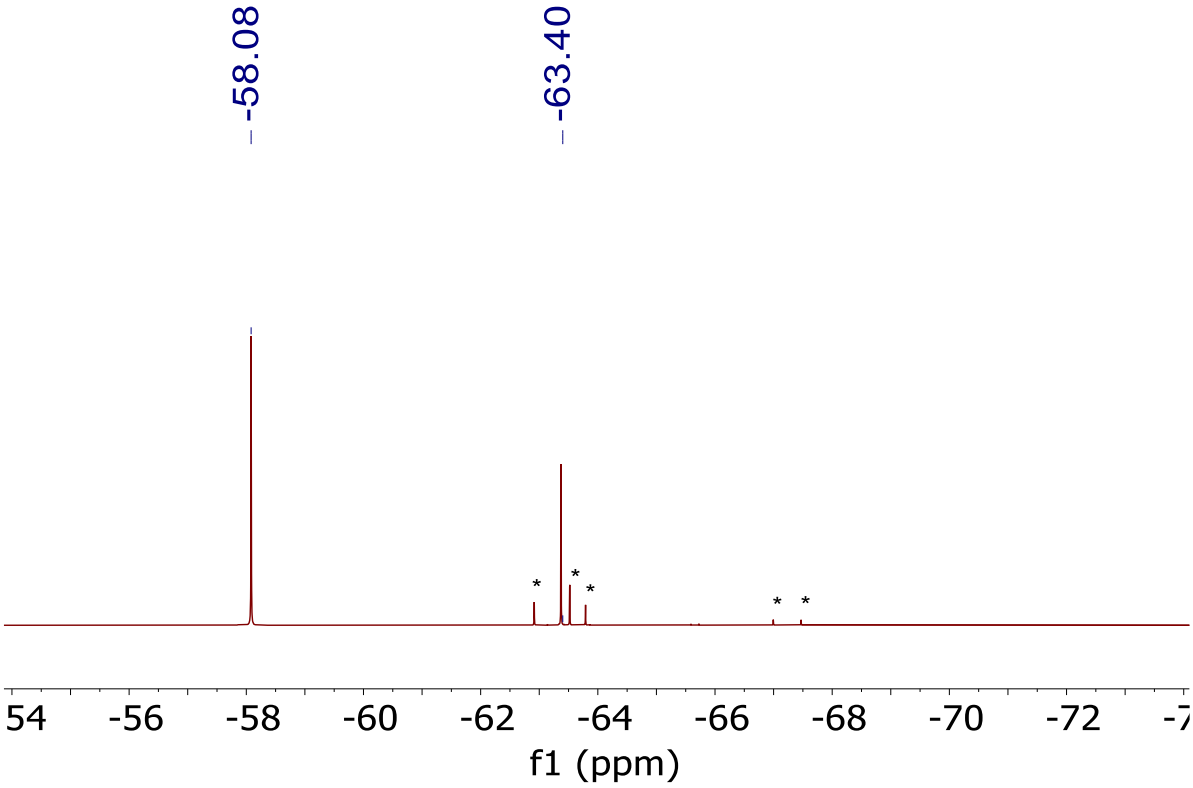

Figure 5.11. $^{19}F\{^{1}H\}$ NMR spectrum of [Li(THF)$_3$][**5.1**] in THF-d_8 at room temperature. (*) indicates the presence of unidentified impurities.

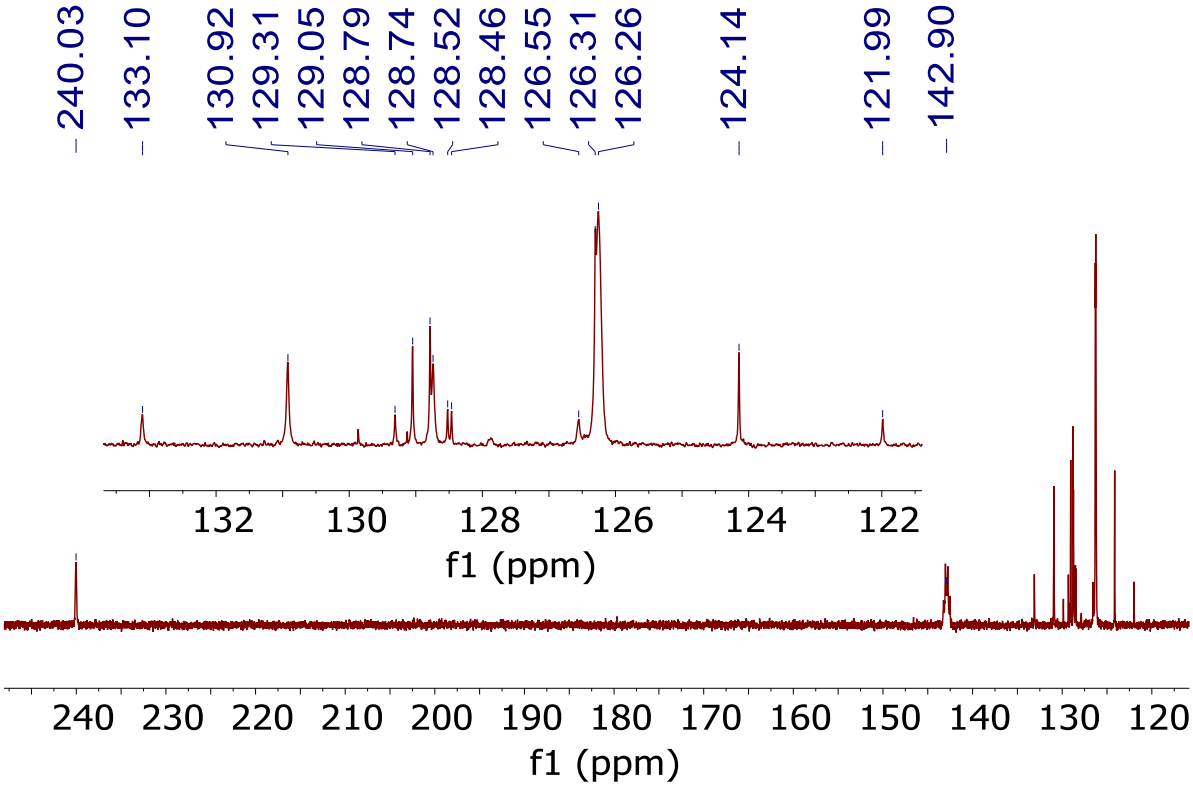

Figure 5.12. Partial $^{13}C\{^{1}H\}$ NMR spectrum of $[Li(Et_2O)_3(THF)]$[**5.1**] in THF-d_8 at –35 °C.

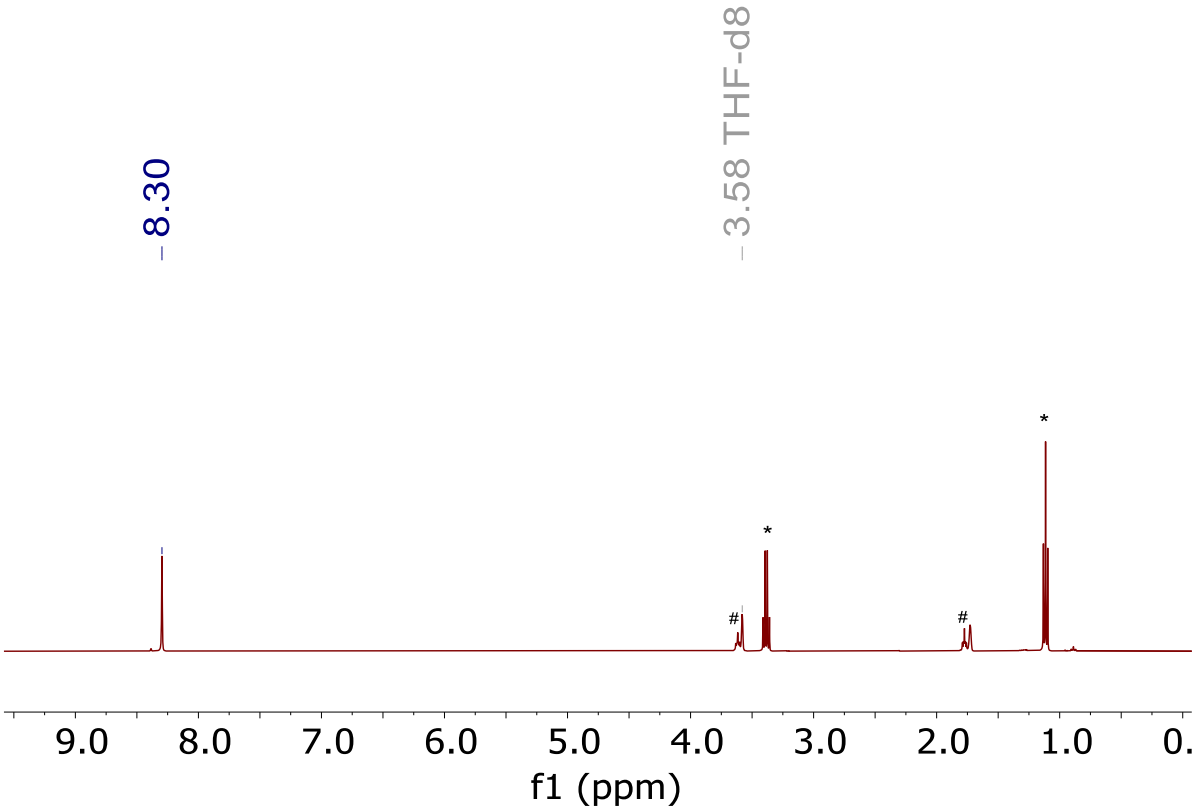

Figure 5.13. ^{1}H NMR spectrum of [Li(Et_2O)$_3$(THF)][**5.1**] in THF-d_8 at 25 °C. (*) indicates the presence of Et_2O, and (#) indicates the presence of THF.

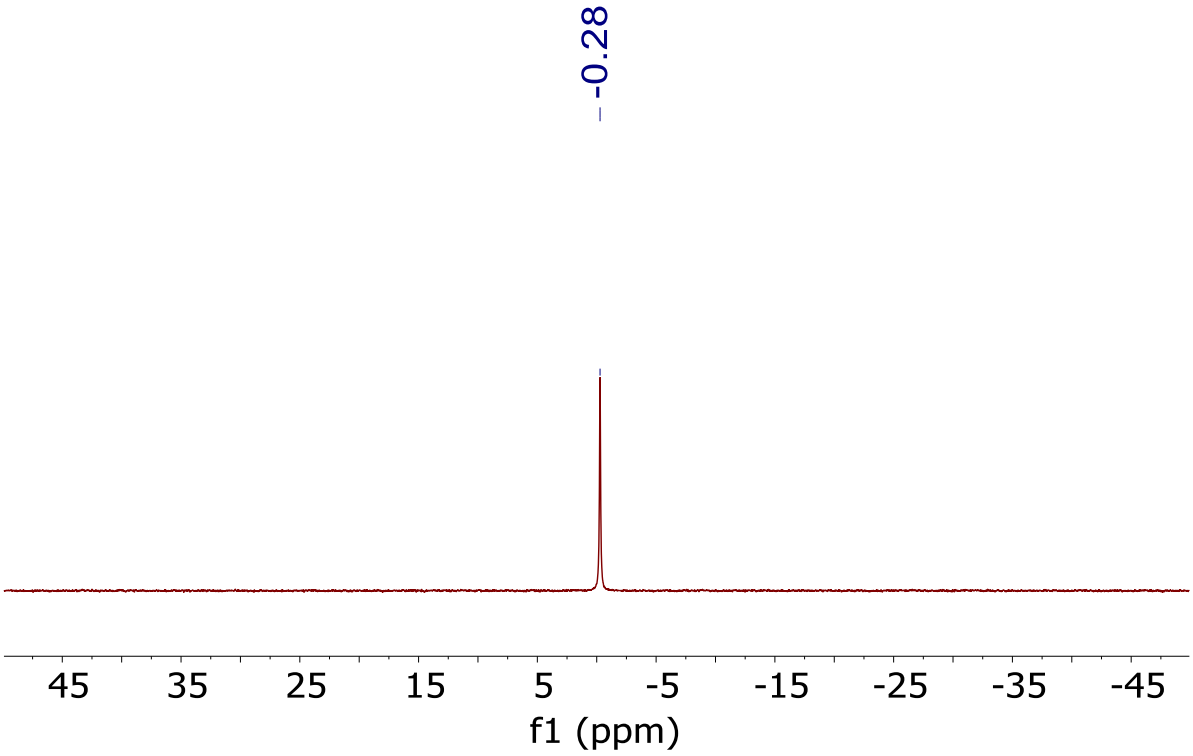

Figure 5.14. $^{7}Li\{^{1}H\}$ NMR spectrum of $[Li(Et_2O)_3(THF)]$[**5.1**] in THF-d_8 at 25 °C.

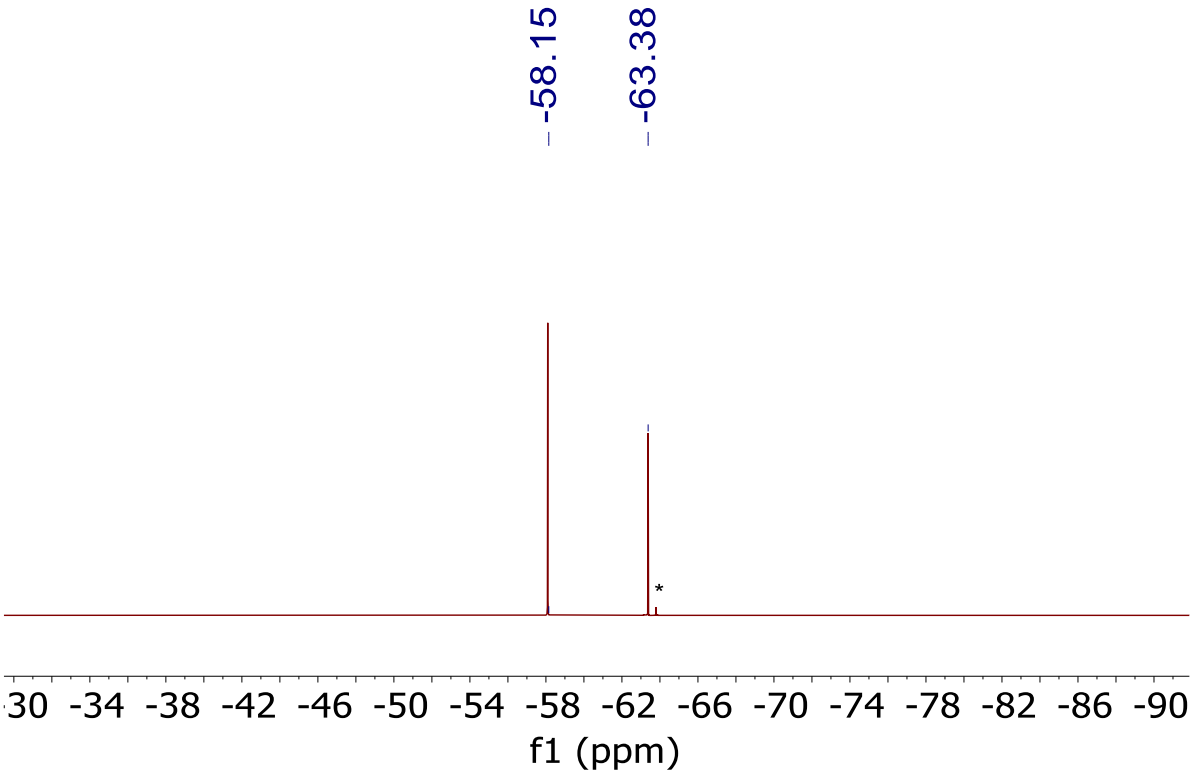

Figure 5.15. $^{19}F\{^{1}H\}$ NMR spectrum of $[Li(Et_2O)_3(THF)]$[**5.1**] in THF-d_8 at 25 °C. (*) indicates the presence of an unidentified impurity.

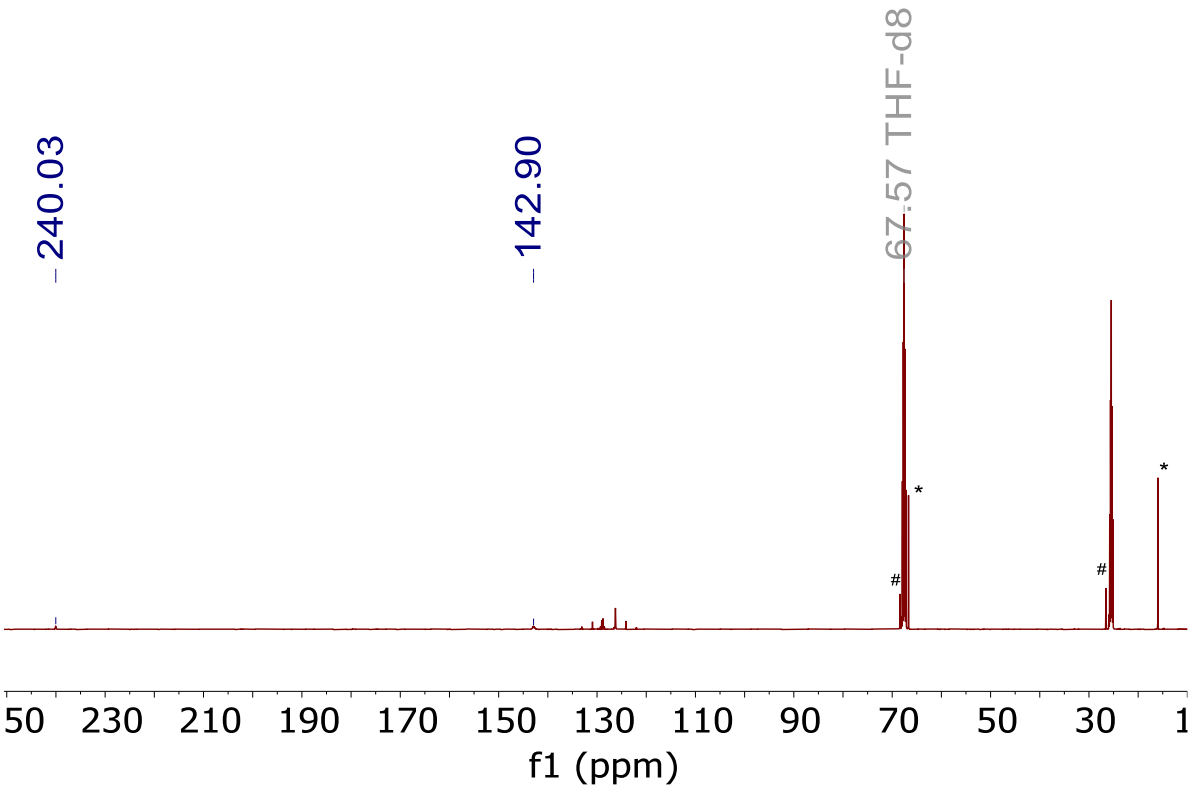

Figure 5.16. $^{13}C\{^{1}H\}$ NMR spectrum of [Li(Et_2O)$_3$(THF)][**5.1**] in THF-d_8 at –35 °C. (*) indicates the presence of Et_2O. (#) indicates the presence of THF.

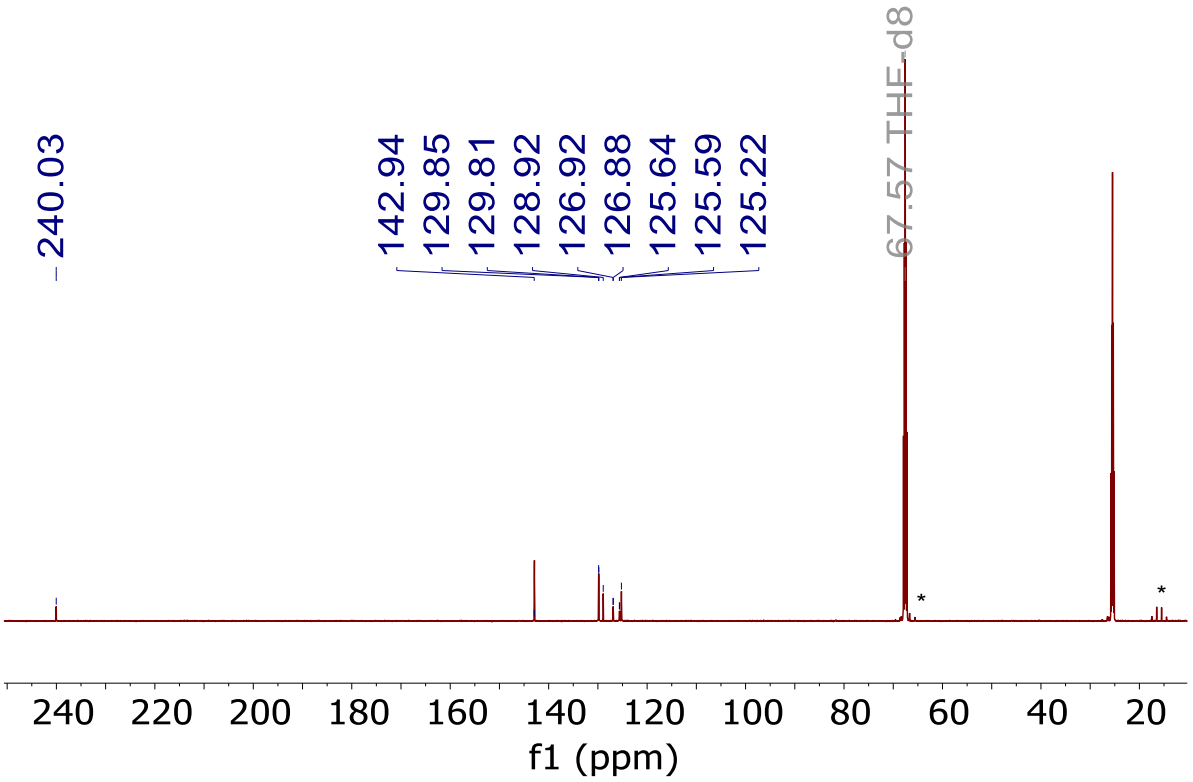

Figure 5.17. $^{13}C\{^{19}F\}$ NMR spectrum of [Li(Et_2O)$_3$(THF)][**5.1**] in THF-d_8 at –35 °C. (*) indicates the presence of Et_2O.

5.5.2 IR Spectra

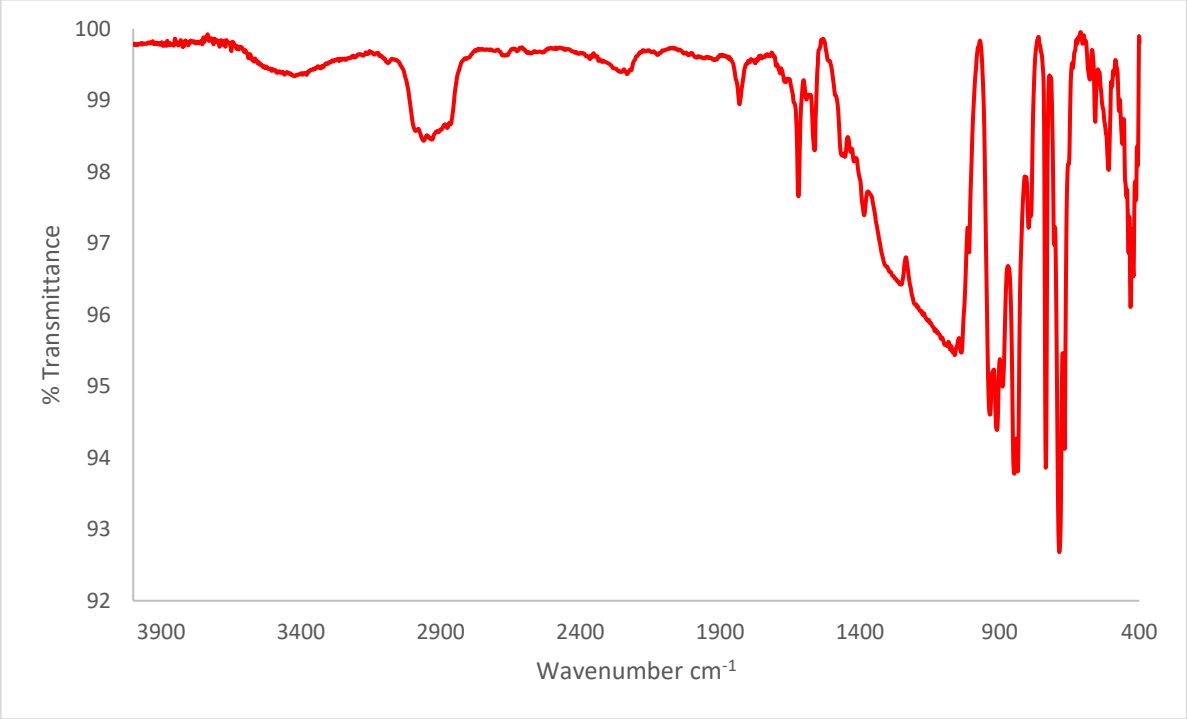

Figure 5.18. IR spectrum of [Li(THF)$_3$][**5.1**] (KBr pellet).

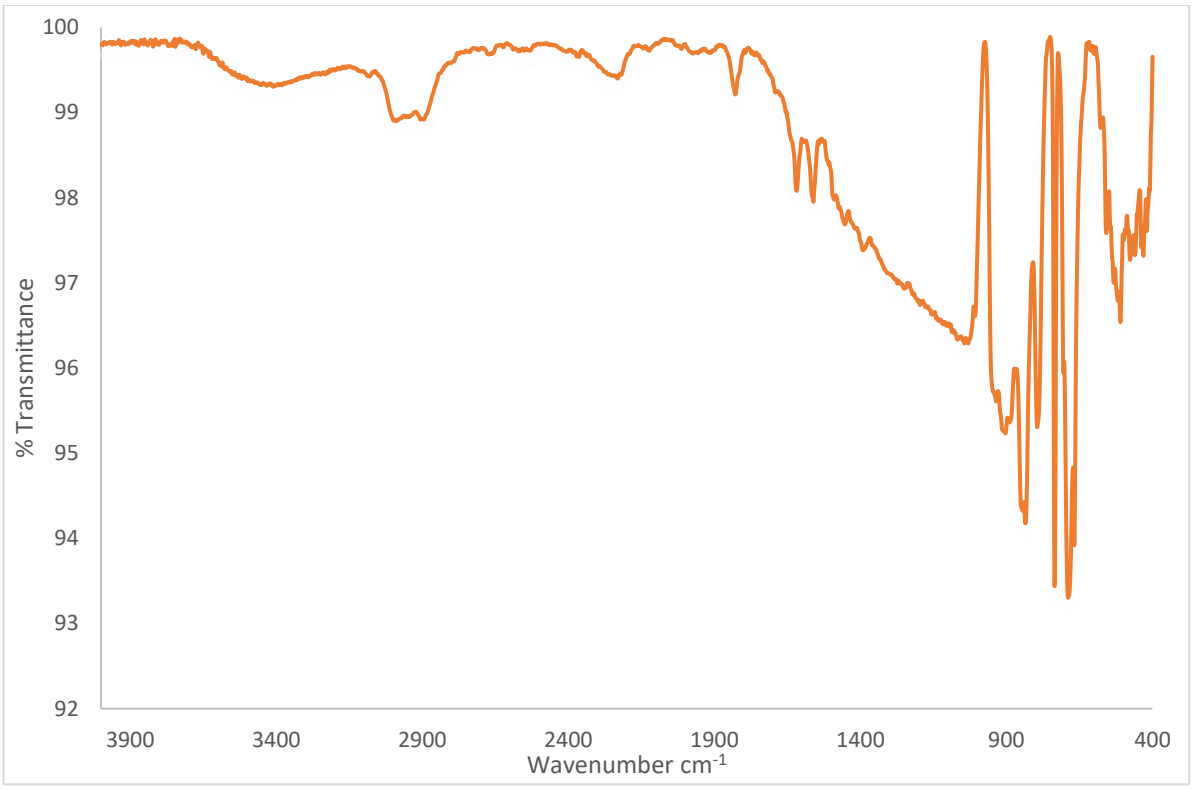

Figure 5.19. IR spectrum of $[Li(Et_2O)_3(THF)]$[**5.1**] (KBr pellet).

5.6 References

(1) Jones, M. B.; Gaunt, A. J. Recent Developments in Synthesis and Structural Chemistry of Nonaqueous Actinide Complexes. *Chemical Reviews* **2013**, *113*, 1137-1198.
(2) Seaman, L. A.; Walensky, J. R.; Wu, G.; Hayton, T. W. In Pursuit of Homoleptic Actinide Alkyl Complexes. *Inorg. Chem.* **2013**, *52*, 3556-3564.
(3) Johnson, S. A.; Bart, S. C. Achievements in uranium alkyl chemistry: celebrating sixty years of synthetic pursuits. *Dalton Trans.* **2015**, *44*, 7710-7726.
(4) Liddle, S. T. The Renaissance of Non-Aqueous Uranium Chemistry. *Angew. Chem. Int. Ed.* **2015**, *54*, 8604-8641.
(5) Gregson, M.; Wooles, A. J.; Cooper, O. J.; Liddle, S. T. Covalent Uranium Carbene Chemistry. *Comments Inorg. Chem.* **2015**, *35*, 262-294.
(6) Hayton, T. W. 3.03 - Hydride, Alkyl, Aryl, Acetylide, Carbonyl, and Cyanide Complexes of the Actinides. In *Comprehensive Organometallic Chemistry IV*, Parkin, G., Meyer, K., O'hare, D. Eds.; Elsevier, 2022; pp 58-84.
(7) Ordoñez, O.; Yu, X.; Wu, G.; Autschbach, J.; Hayton, T. W. Synthesis and Characterization of two Uranyl-Aryl "Ate" Complexes. *Chem. Eur. J.* **2021**, *27*, 5885-5889.
(8) Kent, G. T.; Murillo, J.; Wu, G.; Fortier, S.; Hayton, T. W. Coordination of Uranyl to the Redox-Active Calix[4]pyrrole Ligand. *Inorg. Chem.* **2020**, *59*, 8629-8634.
(9) Seaman, L. A.; Hrobárik, P.; Schettini, M. F.; Fortier, S.; Kaupp, M.; Hayton, T. W. A Rare Uranyl(VI)–Alkyl Ate Complex $[Li(DME)_{1.5}]_2[UO_2(CH_2SiMe_3)_4]$ and Its Comparison with a Homoleptic Uranium(VI)–Hexaalkyl. *Angew. Chem. Int. Ed.* **2013**, *52*, 3259-3263.
(10) Schettini, M. F.; Wu, G.; Hayton, T. W. Synthesis and reactivity of a uranyl-imidazolyl complex. *Chem. Commun.* **2012**, *48*, 1484-1486.
(11) Sarsfield, M. J.; Helliwell, M.; Collison, D. The first uranyl–methine carbon bond; a complex with out-of-plane uranyl equatorial coordination. *Chem. Commun.* **2002**, 2264-2265.
(12) Sarsfield, M. J.; Steele, H.; Helliwell, M.; Teat, S. J. Uranyl *bis*-iminophosphorane complexes with in- and out-of-plane equatorial coordination. *Dalton Trans.* **2003**, 3443-3449.
(13) Sarsfield, M. J.; Helliwell, M.; Raftery, J. Distorted Equatorial Coordination Environments and Weakening of UO Bonds in Uranyl Complexes Containing NCN and NPN Ligands. *Inorg. Chem.* **2004**, *43*, 3170-3179.
(14) Mungur, S. A.; Liddle, S. T.; Wilson, C.; Sarsfield, M. J.; Arnold, P. L. Bent metal carbene geometries in amido *N*-heterocyclic carbene complexes. *Chem. Commun.* **2004**, 2738-2739.
(15) Oldham Jr., W. J.; Oldham, S. M.; Scott, B. L.; Abney, K. D.; Smith, W. H.; Costa, D. A. Synthesis and Structure of *N*-Heterocyclic Carbene Complexes of Uranyl Dichloride. *Chem. Commun.* **2001**, 1348-1349.
(16) Lu, E.; Cooper, O. J.; McMaster, J.; Tuna, F.; McInnes, E. J. L.; Lewis, W.; Blake, A. J.; Liddle, S. T. Synthesis, Characterization, and Reactivity of a Uranium(VI) Carbene Imido Oxo Complex. *Angew. Chem. Int. Ed.* **2014**, *53*, 6696-6700.
(17) Mills, D. P.; Cooper, O. J.; Tuna, F.; McInnes, E. J. L.; Davies, E. S.; McMaster, J.; Moro, F.; Lewis, W.; Blake, A. J.; Liddle, S. T. Synthesis of a Uranium(VI)-Carbene: Reductive Formation of Uranyl(V)-Methanides, Oxidative Preparation of a $[R_2C{=}U{=}O]^{2+}$ Analogue of the $[O{=}U{=}O]^{2+}$ Uranyl Ion ($R = Ph_2PNSiMe_3$), and Comparison of the Nature of U^{IV}=C, U^{V}=C, and U^{VI}=C Double Bonds. *J. Am. Chem. Soc.* **2012**, *134*, 10047-10054.

(18) Tourneux, J.-C.; Berthet, J.-C.; Cantat, T.; Thuéry, P.; Mézailles, N.; Ephritikhine, M. Exploring the Uranyl Organometallic Chemistry: From Single to Double Uranium−Carbon Bonds. *J. Am. Chem. Soc.* **2011**, *133*, 6162-6165.
(19) Maynadié, J.; Berthet, J.-C.; Thuéry, P.; Ephritikhine, M. The first cyclopentadienyl complex of uranyl. *Chem. Commun.* **2007**, 486-488.
(20) Berthet, J.-C.; Thuery, P.; Ephritikhine, M. The first actinyl cyanide. *Chem. Commun.* **2007**, 604-606.
(21) Maity, A. K.; Ward, R. J.; Rupasinghe, D. M. R. Y. P.; Zeller, M.; Walensky, J. R.; Bart, S. C. Organometallic Uranyl Complexes Featuring a Carbodicarbene Ligand. *Organometallics* **2020**, *39*, 783-787.
(22) Kiernicki, J. J.; Cladis, D. P.; Fanwick, P. E.; Zeller, M.; Bart, S. C. Synthesis, Characterization, and Stoichiometric U–O Bond Scission in Uranyl Species Supported by Pyridine(diimine) Ligand Radicals. *J. Am. Chem. Soc.* **2015**, *137*, 11115-11125.
(23) Arnold, P. L.; Casely, I. J.; Turner, Z. R.; Carmichael, C. D. Functionalised Saturated-Backbone Carbene Ligands: Yttrium and Uranyl Alkoxy–Carbene Complexes and Bicyclic Carbene–Alcohol Adducts. *Chem. Eur. J.* **2008**, *14*, 10415-10422.
(24) Seyam, A. M. Observations on the reaction of uranium tetrachloride and dichlorodioxouranium(VI) with lithium alkyls. *Inorg. Chim. Acta* **1985**, *110*, 123-126.
(25) Seyam, A. M. Thermal studies of "dialkyldioxouranium(VI)". *Inorg. Chim. Acta* **1982**, *58*, 71-74.
(26) Berthet, J.-C.; Siffredi, G.; Thuéry, P.; Ephritikhine, M. Easy access to stable pentavalent uranyl complexes. *Chem. Commun.* **2006**, 3184-3186.
(27) Oldham, S. M.; Scott, B. L.; Oldham, W. J. Reaction of the N-heterocyclic carbene, 1,3-dimesityl-imidazol-2-ylidene, with a uranyl triflate complex, $UO_2(OTf)_2(thf)_3$. *Appl. Organometal. Chem.* **2006**, *20*, 39-43.
(28) Ordoñez, O.; Yu, X.; Wu, G.; Autschbach, J.; Hayton, T. W. Assessing the 4f Orbital Participation in the Ln–C Bonds of $[Li(THF)_4][Ln(C_6Cl_5)_4]$ (Ln = La, Ce). *Inorg. Chem.* **2022**, *61*, 15138-15143.
(29) Ordoñez, O.; Yu, X.; Wu, G.; Autschbach, J.; Hayton, T. W. Homoleptic Perchlorophenyl "Ate" Complexes of Thorium(IV) and Uranium(IV). *Inorg. Chem.* **2021**, *60*, 12436-12444.
(30) Kent, G. T.; Yu, X.; Wu, G.; Autschbach, J.; Hayton, T. W. Ring-opening of a thorium cyclopropenyl complex generates a transient thorium-bound carbene. *Chem. Commun.* **2022**, *58*, 6805-6808.
(31) Kent, G. T.; Yu, X.; Wu, G.; Autschbach, J.; Hayton, T. W. Synthesis and electronic structure analysis of the actinide allenylidenes, $[\{(NR_2)_3\}An(CCCPh_2)]^-$ (An = U, Th; R = $SiMe_3$). *Chem. Sci.* **2021**, *12*, 14383-14388.
(32) Kent, G. T.; Yu, X.; Pauly, C.; Wu, G.; Autschbach, J.; Hayton, T. W. Synthesis of Parent Acetylide and Dicarbide Complexes of Thorium and Uranium and an Examination of Their Electronic Structures. *Inorg. Chem.* **2021**, *60*, 15413-15420.
(33) Pedrick, E. A.; Hrobarik, P.; Seaman, L. A.; Wu, G.; Hayton, T. W. Synthesis, structure and bonding of hexaphenyl thorium(IV): observation of a non-octahedral structure. *Chem. Commun.* **2016**, *52*, 689-692.
(34) Smiles, D. E.; Wu, G.; Hrobárik, P.; Hayton, T. W. Synthesis, Thermochemistry, Bonding, and ^{13}C NMR Chemical Shift Analysis of a Phosphorano-Stabilized Carbene of Thorium. *Organometallics* **2017**, *36*, 4519-4524.

(35) Mullane, K. C.; Hrobárik, P.; Cheisson, T.; Manor, B. C.; Carroll, P. J.; Schelter, E. J. ^{13}C NMR Shifts as an Indicator of U–C Bond Covalency in Uranium(VI) Acetylide Complexes: An Experimental and Computational Study. *Inorg. Chem.* **2019**, *58*, 4152-4163.
(36) Panetti, G. B.; Sergentu, D.-C.; Gau, M. R.; Carroll, P. J.; Autschbach, J.; Walsh, P. J.; Schelter, E. J. Isolation and characterization of a covalent Ce^{IV}-Aryl complex with an anomalous ^{13}C chemical shift. *Nature Commun.* **2021**, *12*, 1713.
(37) Vícha, J.; Komorovsky, S.; Repisky, M.; Marek, R.; Straka, M. Relativistic Spin–Orbit Heavy Atom on the Light Atom NMR Chemical Shifts: General Trends Across the Periodic Table Explained. *J. Chem. Theory Comput.* **2018**, *14*, 3025-3039.
(38) Vícha, J.; Novotný, J.; Komorovsky, S.; Straka, M.; Kaupp, M.; Marek, R. Relativistic Heavy-Neighbor-Atom Effects on NMR Shifts: Concepts and Trends Across the Periodic Table. *Chem. Rev.* **2020**, *120*, 7065-7103.
(39) Burford, N.; Macdonald, C. L. B.; LeBlanc, D. J.; Cameron, T. S. Synthesis and Characterization of Bis(2,4,6-tris(trifluoromethyl)phenyl) Derivatives of Arsenic and Antimony: X-ray Crystal Structures of $As(R_F)_2Cl$, $Sb(R_F)_2Cl$, and $Sb(R_F)_2OSO_2CF_3$. *Organometallics* **2000**, *19*, 152-155.
(40) Bartolomé, C.; Villafañe, F.; Martín-Alvarez, J. M.; Martínez-Ilarduya, J. M.; Espinet, P. $[Pd(Fmes)_2(tmeda)]$: A Case of Intermittent C-H···F-C Hydrogen-Bond Interaction in Solution. *Chem. Eur. J.* **2013**, *19*, 3702-3709.
(41) Bartolomé, C.; Espinet, P.; Martín-Álvarez, J. M.; Villafañe, F. Bis(fluoromesityl) Palladium Complexes, Archetypes of Steric Crowding and Axial Protection by *ortho* Effect − Evidence for Dissociative Substitution Processes − Observation of ^{19}F–^{19}F Through-Space Couplings. *Eur. J. Inorg. Chem.* **2004**, *2004*, 2326-2337.
(42) Bartolomé, C.; Espinet, P.; Martín-Álvarez, J. M.; Villafañe, F. $[Pd(Fmes)I\{NMe_2(CH_2\text{-}o\text{-}C_6H_4\text{-}I)\text{-}N,I\}]$, a palladium(II) complex with I^- and organic iodide as *trans* ligands. *Inorg. Chim. Acta* **2003**, *347*, 49-52.
(43) Bartolomé, C.; Espinet, P.; Martín-Alvarez, J. M.; Villafañe, F. Monoarylated Fluoromesitylpalladium Complexes. *Eur. J. Inorg. Chem.* **2003**, *2003*, 3127-3138.
(44) Bartolomé, C.; Espinet, P.; Vicente, L.; Villafañe, F.; Charmant, J. P. H.; Orpen, A. G. Neutral Organometallic Palladium(II) Aquo Complexes. *Organometallics* **2002**, *21*, 3536-3543.
(45) Bartolomé, C.; Espinet, P.; Villafañe, F.; Giesa, S.; Martín, A.; Orpen, A. G. (2,4,6-Tris(trifluoromethyl)phenyl)palladium(II) Complexes. *Organometallics* **1996**, *15*, 2019-2028.
(46) Bender; Banaszak Holl, M. M.; Mitchell, A.; Wells, N. J.; Kampf, J. W. *o*-(Trifluoromethyl)aryl Interactions and Stabilization in Hypervalent Germanium Compounds. *Organometallics* **1998**, *17*, 5166-5171.
(47) Gruetzmacher, H.; Pritzkow, H.; Edelmann, F. T. Synthesis and structure of a monomeric diarylstannylene. *Organometallics* **1991**, *10*, 23-25.
(48) Brooker, S.; Bertel, N.; Stalke, D.; Noltemeyer, M.; Roesky, H. W.; Sheldrick, G. M.; Edelmann, F. T. Main-group chemistry of the 2,4,6-tris(trifluoromethyl)phenyl substituent: X-ray crystal structures of $[2,4,6\text{-}(CF_3)_3C_6H_2]_2Zn$, $[2,4,6\text{-}(CF_3)_3C_6H_2]_2Cd(MeCN)$ and $[2,4,6\text{-}(CF_3)_3C_6H_3]_2Hg$. *Organometallics* **1992**, *11*, 192-195.
(49) Brooker, S.; Buijink, J. K.; Edelmann, F. T. Synthesis, structure, and reactivity of the first stable diaryllead(II) compound. *Organometallics* **1991**, *10*, 25-26.

(50) Whitmire, K. H.; Labahn, D.; Roesky, H. W.; Noltemeyer, M.; Sheldrick, G. M. Sterically crowded aryl bismuth compounds: synthesis and characterization of bis{2,4,6-tris(trifluoromethyl)phenyl} bismuth chloride and tris{2,4,6-tris(trifluoromethyl)phenyl} bismuth. *J. Organomet. Chem.* **1991**, *402*, 55-66.
(51) Stalke, D.; Whitmire, K. H. Spectroscopic and structural characterization of 2,4,6-tris(trifluoromethyl)phenyllithium·Et_2O: a dimer stabilized by lithium ⋯ fluorine contacts. *J. Chem. Soc., Chem. Commun.* **1990**, 833-834.
(52) Batsanov, A. S.; Dillon, K. B.; Gibson, V. C.; Howard, J. A. K.; Sequeira, L. J.; Yao, J. W. Synthesis and crystal structures of chromium and molybdenum complexes containing the 2,4,6-tris(trifluoromethyl)phenyl ligand. *J. Organomet. Chem.* **2001**, *631*, 181-187.
(53) Dillon, K. B.; Gibson, V. C.; Howard, J. A. K.; Redshaw, C.; Sequeira, L.; Yao, J. W. Group 6 transition metal complexes containing the σ-bonded 2,4,6-tris(trifluoromethyl) phenyl ("fluoromes") ligand. *J. Organomet. Chem.* **1997**, *528*, 179-183.
(54) Gibson, V. C.; Redshaw, C.; Sequeira, L. J.; Dillon, K. B.; Clegg, W.; Elsegood, M. R. J. Vanadium complexes containing the 2,4,6-tris(trifluoromethyl)phenyl ('fluoromes') ligand. *Chem. Commun.* **1996**, 2151-2152.
(55) Espinet, P.; Martín-Barrios, S.; Villafañe, F.; Jones, P. G.; Fischer, A. K. [2,4,6-Tris(trifluoromethyl)phenyl]gold(I) and -gold(III) Complexes. *Organometallics* **2000**, *19*, 290-295.
(56) Schluter, R. D.; Isom, H. S.; Cowley, A. H.; Atwood, D. A.; Jones, R. A.; Olbrich, F.; Corbelin, S.; Lagow, R. J. Use of the 2,4,6-Tris(trifluoromethyl)phenyl Ligand in Organogallium Chemistry. *Organometallics* **1994**, *13*, 4058-4063.
(57) Schluter, R. D.; Cowley, A. H.; Atwood, D. A.; Jones, R. A.; Bond, M. R.; Carrano, C. J. Use of the 2,4,6-tris(trifluoromethyl)phenyl ligand to stabilize indium-indium and gallium-gallium bonds. *J. Am. Chem. Soc.* **1993**, *115*, 2070-2071.
(58) Benedikt, G. M.; Goodall, B. L.; Iyer, S.; McIntosh, L. H.; Mimna, R.; Rhodes, L. F.; Day, C. S.; Day, V. W. Synthesis, Solution Dynamics, and X-ray Crystal Structure of Bis(2,4,6-tris(trifluoromethyl)phenyl)(1,2-dimethoxyethane)nickel. *Organometallics* **2001**, *20*, 2565-2569.
(59) Bardají, M.; Jones, P. G.; Laguna, A.; Moracho, A.; Fischer, A. K. Synthesis of 2,4,6-tris(trifluoromethyl)phenyl complexes of gold and thallium. *J. Organomet. Chem.* **2002**, *648*, 1-7.
(60) Cornet, S. M.; Dillon, K. B.; Entwistle, C. D.; Fox, M. A.; Goeta, A. E.; Goodwin, H. P.; Marder, T. B.; Thompson, A. L. Synthesis and characterisation of some new boron compounds containing the 2,4,6-$(CF_3)_3C_6H_2$ (fluoromes = Ar), 2,6-$(CF_3)_2C_6H_3$ (fluoroxyl = Ar′), or 2,4-$(CF_3)_2C_6H_3$ (Ar″) ligands. *Dalton Trans.* **2003**, 4395-4405.
(61) Batsanov, A. S.; Cornet, S. M.; Dillon, K. B.; Goeta, A. E.; Hazendonk, P.; Thompson, A. L. New group 15 compounds containing the 2,4,6-$(CF_3)_3C_6H_2$ (fluoromes = Ar), 2,6-$(CF_3)_2C_6H_3$ (fluoroxyl = Ar′) or 2,4-$(CF_3)_2C_6H_3$ (Ar″) ligands. *J. Chem. Soc., Dalton Trans.* **2002**, 4622-4628.
(62) Belay, M.; Edelmann, F. T. 2,4,6-Tris(trifluormethyl)phenyl und 2,4,6-Tris(trifluormethyl)-dithiobenzoat als Liganden in Cobalt(II)-und Nickel(II)-Verbindungen. *J. Organomet. Chem.* **1994**, *479*, c21-c24.
(63) Denning, R. G. Electronic Structure and Bonding in Actinyl Ions and their Analogs. *J. Phys. Chem. A* **2007**, *111*, 4125-4143.

(64) Denning, R. Electronic Structure and Bonding in Actinyl Ions. *Struct. Bonding* **1992**, *79*, 215-276.
(65) Fortier, S.; Hayton, T. W. Oxo ligand functionalization in the uranyl ion (UO_2^{2+}). *Coord. Chem. Rev.* **2010**, *254*, 197-214.
(66) Schnaars, D. D.; Wu, G.; Hayton, T. W. Reduction of Pentavalent Uranyl to U(IV) Facilitated by Oxo Functionalization. *J. Am. Chem. Soc.* **2009**, *131*, 17532-17533.
(67) Yin, H.; Lewis, A. J.; Williams, U. J.; Carroll, P. J.; Schelter, E. J. Fluorinated diarylamide complexes of uranium(III, IV) incorporating ancillary fluorine-to-uranium dative interactions. *Chem. Sci.* **2013**, *4*, 798-805.
(68) Seaman, L. A.; Schnaars, D. D.; Wu, G.; Hayton, T. W. Isolation of a uranyl amide by "ate" complex formation. *Dalton Trans.* **2010**, *39*, 6635-6637.
(69) Baerends, E. J.; Ziegler, T.; Atkins, A. J.; Autschbach, J.; Baseggio, O.; Bashford, D.; Bérces, A.; Bickelhaupt, F. M.; Bo, C.; Boerrigter, P. M.; Cavallo, L.; Daul, C.; Chong, D. P.; Chulhai, D. V.; Deng, L.; Dickson, R. M.; Dieterich, J. M.; Ellis, D. E.; van Faassen, M.; Fan, L.; Fischer, T. H.; Guerra, C. F.; Franchini, M.; Ghysels, A.; Giammona, A.; van Gisbergen, S. J. A.; Goez, A.; Götz, A. W.; Groeneveld, J. A.; Gritsenko, O. V.; Grüning, M.; Gusarov, S.; Harris, F. E.; van den Hoek, P.; Hu, Z.; Jacob, C. R.; Jacobsen, H.; Jensen, L.; Joubert, L.; Kaminski, J. W.; van Kessel, G.; König, C.; Kootstra, F.; Kovalenko, A.; Krykunov, M. V.; van Lenthe, E.; McCormack, D. A.; Michalak, A.; Mitoraj, M.; Morton, S. M.; Neugebauer, J.; Nicu, V. P.; Noodleman, L.; Osinga, V. P.; Patchkovskii, S.; Pavanello, M.; Peeples, C. A.; Philipsen, P. H. T.; Post, D.; Pye, C. C.; Ramanantoanina, H.; Ramos, P.; Ravenek, W.; Rodríguez, J. I.; Ros, P.; Rüger, R.; Schipper, P. R. T.; Schlüns, D.; van Schoot, H.; Schreckenbach, G.; Seldenthuis, J. S.; Seth, M.; Snijders, J. G.; Solà, M.; Stener, M.; Swart, M.; Swerhone, D.; Tognetti, V.; te Velde, G.; Vernooijs, P.; Versluis, L.; Visscher, L.; Visser, O.; Wang, F.; Wesolowski, T. A.; van Wezenbeek, E. M.; Wiesenekker, G.; Wolff, S. K.; Woo, T. K.; Yakovlev, A. L. ADF, ver. 2017; SCM, Theoretical Chemistry, Vrije Universiteit: Amsterdam, The Netherlands, 2017. https://www.scm.com.
(70) Glendening, E. D.; Landis, C. R.; Weinhold, F. Natural bond orbital methods. *WIREs. Comput. Mol. Sci.* **2012**, *2*, 1-42.
(71) Lenthe, E. v.; Baerends, E. J.; Snijders, J. G. Relativistic regular two-component Hamiltonians. *J. Chem. Phys.* **1993**, *99*, 4597-4610.
(72) Adamo, C.; Barone, V. Toward chemical accuracy in the computation of NMR shieldings: the PBE0 model. *Chem. Phys. Lett.* **1998**, *298*, 113-119.
(73) Greif, A. H.; Hrobárik, P.; Autschbach, J.; Kaupp, M. Giant spin–orbit effects on ^{1}H and ^{13}C NMR shifts for uranium(vi) complexes revisited: role of the exchange–correlation response kernel, bonding analyses, and new predictions. *Phys. Chem. Chem. Phys.* **2016**, *18*, 30462-30474.
(74) Hrobarik, P.; Hrobarikova, V.; Greif, A. H.; Kaupp, M. Giant Spin-Orbit Effects on NMR Shifts in Diamagnetic Actinide Complexes: Guiding the Search for Uranium(VI) Hydrides Complexes in the Correct Spectral Range. *Angew. Chem. Int. Ed.* **2012**, *51*, 10884–10888.
(75) There is also a SO effect on the carbon shielding from other ligand atoms, such as Cl and Si, which may or may not be additive.
(76) Wilkerson, M. P.; Burns, C. J.; Paine, R. T.; Scott, B. L. Synthesis and Crystal Structure of $UO_2Cl_2(THF)_3$: A Simple Preparation of an Anhydrous Uranyl Reagent. *Inorg. Chem.* **1999**, *38*, 4156-4158.

(77) Harris, R. K.; Becker, E. D.; Cabral De Menezes, S. M.; Granger, P.; Hoffman, R. E.; Zilm, K. W. Further Conventions for NMR Shielding and Chemical Shifts. *Pure Appl. Chem.* **2008**, *80*, 59-84.
(78) Harris, R. K.; Becker, E. D.; Cabral De Menezes, S. M.; Goodfellow, R.; Granger, P. NMR Nomenclature. Nuclear Spin Properties and Conventions for Chemical Shifts. *Pure Appl. Chem.* **2001**, *73*, 1795-1818.
(79) SMART Apex II, Version 2.1; Bruker AXS Inc.: Madison, WI; 2005.
(80) SAINT Software User's Guide, Version 7.34a; Bruker AXS Inc.: Madison, WI; 2005.
(81) Sheldrick, G. M. SADABS, University of Gottingen, Germany; 2005.
(82) SHELXTL PC, Version 6.12; Bruker AXS Inc.: Madison, WI; 2005.
(83) Diamond - Crystal and Molecular Structure Visualization. Crystal Impact - Dr. H. Putz & Dr. K. Brandenburg GbR, Kreuzherrenstr. 102, 53227 Bonn, Germany. http://www.crystalimpact.com/diamond.
(84) Perdew, J. P. Density-functional approximation for the correlation energy of the inhomogeneous electron gas. *Phys. Rev. B* **1986**, *33*, 8822-8824.
(85) Perdew, J. P. Erratum: Density-functional approximation for the correlation energy of the inhomogeneous electron gas. *Phys. Rev. B* **1986**, *34*, 7406-7406.
(86) Perdew, J. P.; Chevary, J. A.; Vosko, S. H.; Jackson, K. A.; Pederson, M. R.; Singh, D. J.; Fiolhais, C. Atoms, molecules, solids, and surfaces: Applications of the generalized gradient approximation for exchange and correlation. *Phys. Rev. B* **1992**, *46*, 6671-6687.
(87) Autschbach, J. The role of the exchange-correlation response kernel and scaling corrections in relativistic density functional nuclear magnetic shielding calculations with the zeroth-order regular approximation. *Molecular Physics* **2013**, *111*, 2544-2554.
(88) Autschbach, J.; Zheng, S. Relativistic Computations of NMR Parameters from First Principles: Theory and Applications. *Ann. Rep. NMR Spectrosc.* **2009**, *67*, 1-95.
(89) Van Lenthe, E.; Baerends, E. J. Optimized Slater-type basis sets for the elements 1–118. *J. Comput. Chem.* **2003**, *24*, 1142-1156.
(90) Grimme, S.; Ehrlich, S.; Goerigk, L. Effect of the damping function in dispersion corrected density functional theory. *J. Comput. Chem.* **2011**, *32*, 1456-1465.
(91) Pye, C. C.; Ziegler, T. An implementation of the conductor-like screening model of solvation within the Amsterdam density functional package. *Theor. Chem. Acc.* **1999**, *101*, 396-408.
(92) Glendening, E. D.; Landis, C. R.; Weinhold, F. NBO 6.0: Natural bond orbital analysis program. *J. Comput. Chem.* **2013**, *34*, 1429-1437.
(93) Fulmer, G. R.; Miller, A. J. M.; Sherden, N. H.; Gottlieb, H. E.; Nudelman, A.; Stoltz, B. M.; Bercaw, J. E.; Goldberg, K. I. NMR Chemical Shifts of Trace Impurities: Common Laboratory Solvents, Organics, and Gases in Deuterated Solvents Relevant to the Organometallic Chemist. *Organometallics* **2010**, *29*, 2176-2179.

Chapter 6. Ring-opening in the actinide cyclopropyl complexes $[Cp_3U(2,2\text{-diphenylcyclopropyl})]^{n-}$ (n = 0, 1)

Portions of this work were published in:

Osvaldo Ordoñez, Greggory T. Kent, Megan A. Schuerlein, Guang Wu, Trevor W. Hayton, Ring-opening in the actinide cyclopropyl complexes $[Cp_3U(2,2\text{-diphenylcyclopropyl})]^{n-}$ (n = 0, 1). *Organometallics.* **2023**, 42, 2347–2352

Table of Contents

6.1 Introduction

The synthetic methods used by transition metal chemists to make carbene complexes do not often translate to the actinides.[1-4] For example, addition of diphenyldiazomethane to [$Cp^*_2U^{IV}$(NAr)] (Ar = 2,4,6-$^tBu_3C_6H_2$) results in formation of the U(VI) hydrazido complex, [$Cp^*_2U^{VI}$(NAr)(N_2CPh_2)], and not in N_2 elimination and carbene formation, as intended.[5] Similarly, reaction of [(($^{t\text{-}Bu}$ArO)$_3$tacn)U^{III}] with

diphenyldiazomethane results in formation of [(($^{t\text{-Bu}}$ArO)$_3$tacn)U^{IV}(η^2-NNCPh$_2$)], which features an unusual open-shell mono-anionic hydrazido ligand.[6] Several other examples of similar diazoalkane reactivity with the actinides are also known.[6-13] α-H elimination, another common way to make transition metal carbenes,[14] has also never been seen in the actinides. Instead, other modes of reactivity are observed. For example, thermolysis of [Cp*$_2$Th(CH$_2$^{t}Bu)$_2$] result in formation of [Cp*$_2$Th(*cyclo*-*C*H$_2$CMe$_2$*C*H$_2$)] and neopentane via γ-H activation of a neopentyl ligand.[15] At this point, the only reliable synthetic route to an An=C bond is ligation of a deprotonated Wittig reagent or bis(iminophosphorane) to an actinide ion, which results in formation of heteroatom-stabilized actinide carbene complexes,[4, 16-21] such as [Cp*$_2$U(X)(CHPPh$_3$)] (X= Cl, Br, I),[17] [U{C(SiMe$_3$)(PPh$_2$)}(BIPM^{TMS})(Cl)]$^-$ (BIPM^{TMS} = C(PPh$_2$NSiMe$_3$)$_2$),[22] and [An(CHPPh$_3$)(NR$_2$)$_3$] (An = Th, U; R = SiMe$_3$).[23, 24]

In an effort to find new routes to An=C and An≡C bonds, we have turned our attention to less common carbene and carbyne sources. For example, we recently reported the isolation of the first An allenylidenes, [{(NR$_2$)$_3$}An(CCCPh$_2$)]$^-$ (An = U, Th; R = SiMe$_3$), which were accessed by deprotonation of the An-allenyl complexes [{(NR$_2$)$_3$}An(CH=C=CPh$_2$)],[25] which themselves were made via reaction of [AnCl(NR$_2$)$_3$] with 1-lithium-3,3-diphenylcyclopropene. Notably, [{(NR$_2$)$_3$}An(CCCPh$_2$)]$^-$ were the first reported An carbenes that contain no heteroatom stabilization. In addition, we reported the thermal ring-opening of [Cp$_3$Th(3,3-diphenylcyclopropenyl) to give [Cp$_3$Th(3-phenyl-1*H*-inden-1-yl)].[26] Calculations suggest that this reaction proceeds via a triplet metallocarbene. However,

this proposed intermediate could not be observed. Similarly, the U(III) bis(diisopropylamino)cyclopropenylidene adduct, [$(NR_2)_3U$(BAC)] (R = $SiMe_3$) rearranges upon heating to give the ring-opened U(IV) product, [$(NR_2)_2U\{N(R)(SiMe_2CH{=}C(N^iPr_2)C(N^iPr_2){=}CH)\}$], which we hypothesized was also formed via an unobserved carbene intermediate.[27] Finally, reduction of the U(III) isocyanide, [$U(NR_2)_3$(CN-2,6-$Me_2C_6H_3)_2$], resulted in isocyanide coupling, and not aminocarbyne formation, as originally hoped.[28, 29]

Building on this work, we have continued to search for non-traditional routes to actinide carbenes. One possible route to a metal carbene is the ring-opening of a cyclopropyl ligand via a proximal C-C bond (Scheme 6.1).[30, 31] In particular, Jones and co-workers reported that photolysis of [$CpFe(CO)_2$(1-ethoxycyclopropyl)] generates a transient metallocyclocarbene **A**, which was identified by an Fe=C resonance at 335.0 ppm in its ^{13}C NMR spectrum.[30] This species subsequently isomerized to an η^3-allyl complex on standing. Also of note, [$Cp^*_2Y(\mu$-*cyclo*-$C_3H_5)_2Li$(THF)], [$Tp^{Me2}NbCl$(*cyclo*-$C_3H_5)(\eta^2$-MeC≡CMe)], and [^{Me}LSc(*cyclo*-$C_3H_5)_2$] (^{Me}L = ArNC(Me)CHC(Me)NAr, Ar = 2,6-$^iPr_2C_6H_3$) exhibit α-C–C agostic interactions in the solid-state, which can be viewed as a prelude to proximal C-C activation.[32-34] However, ring-opening via a distal C-C bond has also be observed. This mechanism of cyclopropyl ring-opening directly provides an η^3-allyl complex and is likely operative in [Cp*W(NO)(*cyclo*-C_3H_5)R] (R = CH_2SiMe_3, CH_2Ph, $CH_2{}^tBu$)[35, 36] and [$Tp^{Me2}Nb$(*cyclo*-$C_3H_5)(C_6F_5)(\eta^2$-MeC≡CMe)].[37] The mechanism of cyclopropyl ring opening in [Cp^*_2Sm(*cyclo*-1-Me-2-Ph-C_3H_3)] has also been calculated using DFT. In this particular case, distal C-C activation was calculated to occur with an activation

barrier of 27-35 kcal/mol, depending on the conformer.[38] Intriguingly, coordination of the phenyl substituent to the Sm center was found to lower the barrier of activation.

Scheme 6.1. Generation of an iron carbene via cyclopropyl ring-opening.[30]

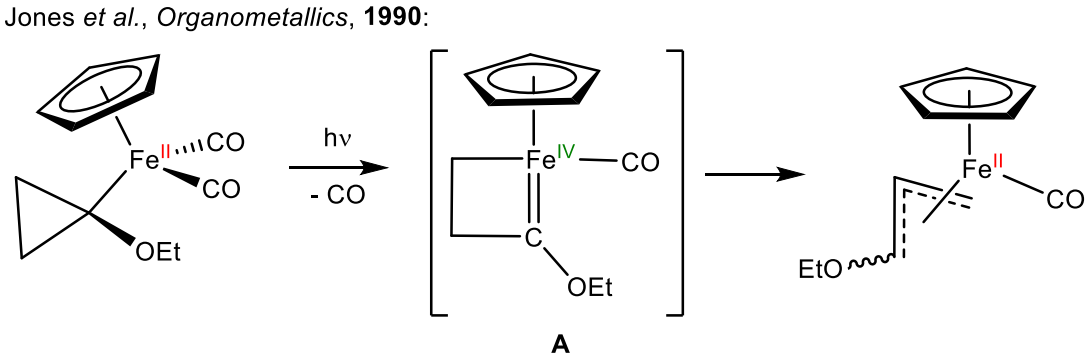

Herein, I report the synthesis, isolation, and ring-opening reactivity of [Cp_3U(2,2-diphenylcyclopropyl)] and its isostructural U(III) analogue, which represent the first structurally-characterized f element cyclopropyl complexes. Additionally, I investigate the mechanism of ring-opening by selectively labelling the cyclopropyl ligand with deuterium. This cyclopropyl ligand was chosen, in part, because I thought the phenyl groups at the 2-position would bias the ring in favor of proximal activation, either via steric or electronic effects.

6.2 Results and Discussion

6.2.1 Synthesis and Characterization

The synthesis and characterization of complexes **6.1** and **6.2** were first reported by Greggory T. Kent in their dissertation titled "Development of New Methods Towards Actinide-Carbene Fragments".[39] Reaction of [Cp_3UCl] with *in situ* generated 1-lithium-2,2-diphenylcyclopropane[40] in Et_2O results in formation of [Cp_3U(2,2-diphenylcyclopropyl)] (**6.1**), which can be isolated as brown plates in 63% yield after removal of the volatiles,

extraction into toluene, filtration, and crystallization (Scheme 6.2)**.** The ^{1}H NMR spectrum of **6.1** in benzene-d_6 features a diagnostic H_α resonance at –170.26 ppm and diastereotopic H_β resonances at –17.07 and –23.12 ppm. These three resonances are present in a 1:1:1 ratio, consistent with the proposed formulation. In addition, complex **6.1** exhibits a single Cp environment at –3.41 ppm (Figure 6.1). The UV-vis spectrum of **6.1** features a broad transition centered at 475 nm (ε = 835 $cm^{-1}\cdot M^{-1}$), which we have tentatively assigned to a LMCT transition (Figure 6.32)**.** This spectrum also features many sharp, weak absorptions between 500 to 750 nm, which are assignable to Laporte forbidden 5f $\rightarrow$ 5f transitions.[12, 41, 42] Additionally, reaction of [Cp_3ThCl] with *in situ* generated 1-lithium-2,2-diphenylcyclopropane[40] in Et_2O results in formation of the Th analog, [Cp_3Th(2,2-diphenylcyclopropyl)] (**6.2**), which can be isolated as colorless plates in 82% yield. The ^{1}H NMR spectrum of **6.2** in benzene-d_6 features a diagnostic H_α resonance at 0.88 ppm and diastereotopic H_β resonances at 1.93 ppm and 1.83 ppm. Dr. Greggory T. Kent in their dissertation reports the $^{13}C\{^{1}H\}$ NMR spectrum of **6.2** in benzene-d_6. Complexes **6.1** and **6.2** represent a rare example of an actinide cyclopropyl complexes. To our knowledge, only one other example is known, namely, [Cp^*_2Th(*cyclo*-$C_3H_5)_2$], but it was not structurally characterized.[43]

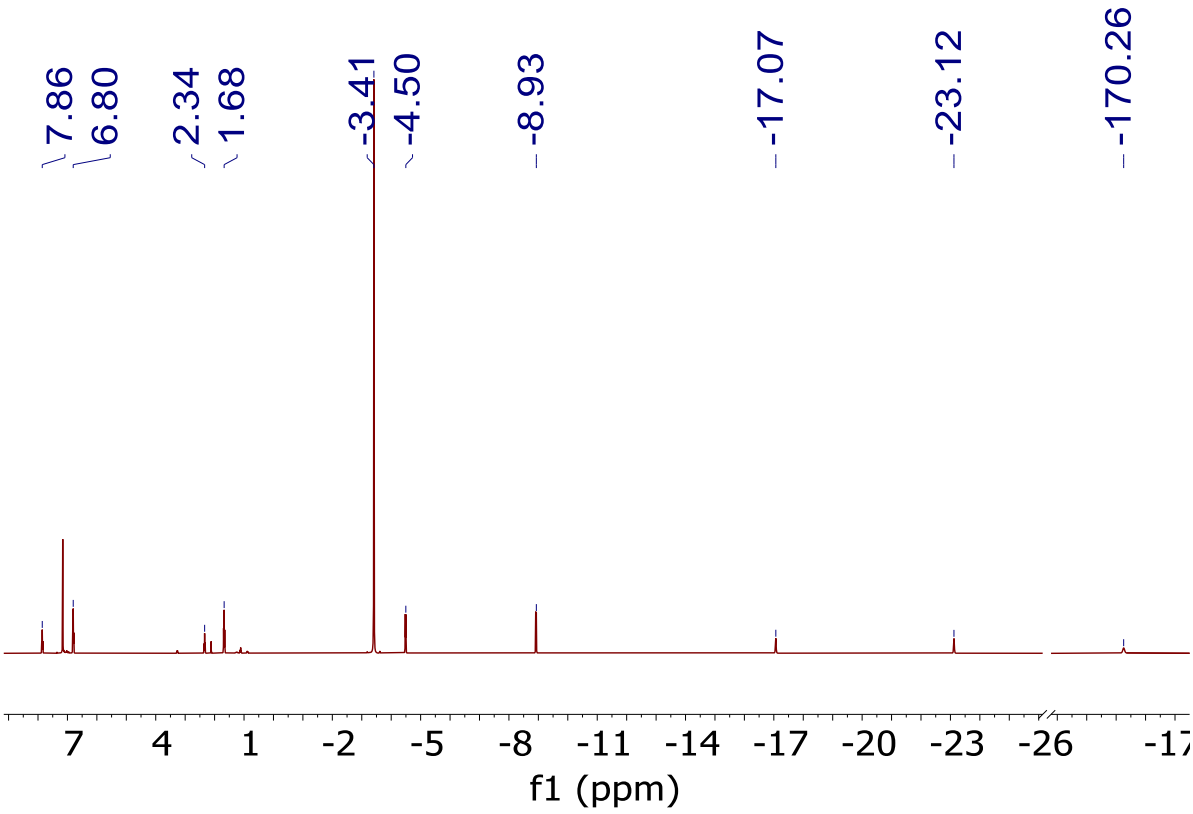

Figure 6.1. ^{1}H NMR spectrum of **6.1** in benzene-d_6 at room temperature.

Scheme 6.2. Synthesis of complexes **6.1** and **6.2**.

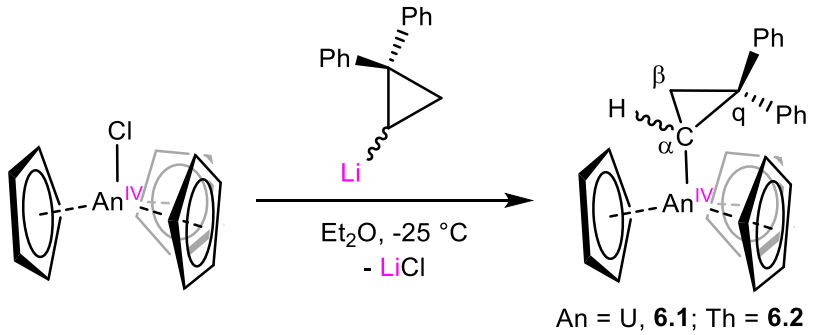

The solid-state structures of both complexes **6.1** and **6.2** were first collected by Greggory T. Kent.[39] Both complexes **6.1** and **6.2** crystallizes in the orthorhombic space group *C*mca. Both exhibits substantial positional disorder of both the Cp and 2,2-diphenylcyclopropyl

ligands. Due to the extreme positional disorder, H atoms were not assigned to either the Cp and 2,2-diphenylcyclopropyl ligands. Nonetheless, the connectivity of **6.1** and **6.2** were confirmed (Figure 6.2). In an attempt to grow crystals of both complexes **6.1** and **6.2** in a different crystal system, they were crystalized from Et_2O, THF, dichloromethane, chlorobenzene, and dimethoxyethane. In all instances, however, these crystallizations result in nicely-diffracting needles that still featured the same *C*mca unit cell.

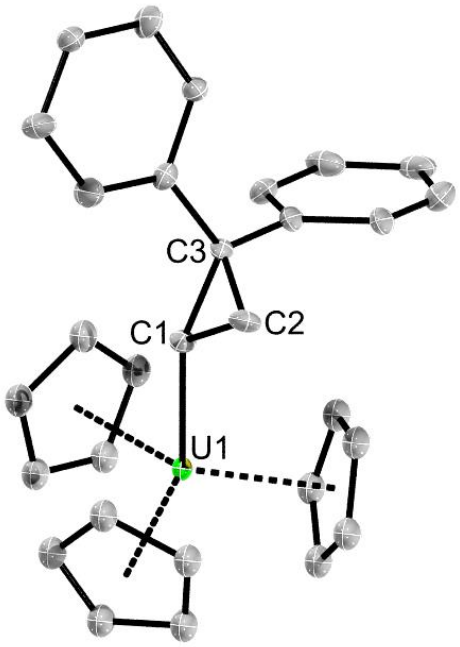

Figure 6.2. Solid State molecular structure of **6.1**, shown with thermal ellipsoids set at 50% probability. A second molecule in the asymmetric unit is omitted for clarity.

Scheme 6.3. Synthesis of complexes **6.3**, **6.4**, and **6.5**.

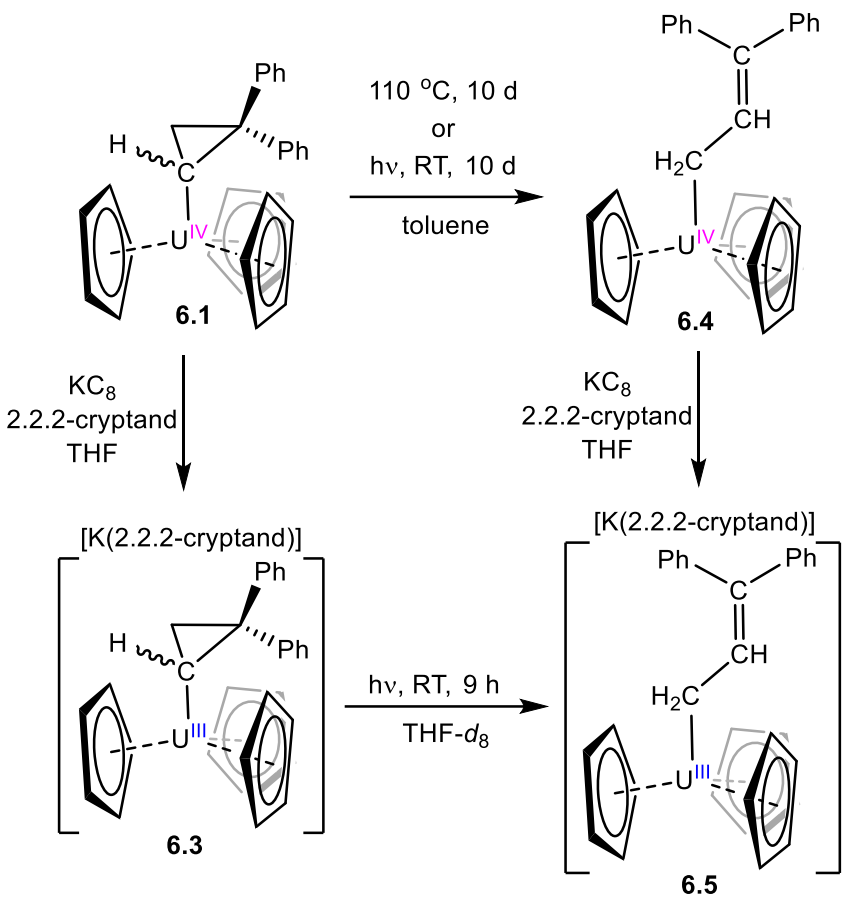

In a collaborative effort with Megan A. Schuerlein, an undergraduate researcher in the Hayton group, we examined the reactivity of **6.1** towards reducing agents. In this regards, reaction of **6.1** with 1 equiv of KC_8 in THF, in the presence of 2.2.2-cryptand, results in formation of a dark red solution, from which [K(2.2.2-cryptand**)]**[Cp_3U(2,2-diphenylcyclopropyl)] (**6.3**) can be isolated in 88% yield after work-up (Scheme 6.3). The ^{1}H NMR spectrum of **6.3** in THF-d_8 features a diagnostic H_α resonance at –88.03 ppm and diastereotopic H_β resonances at –1.32 and –5.46 ppm. These resonances are present in a 1:1:1 ratio. In addition, complex **6.3** exhibits a single Cp environment at –15.05 ppm (Figure 6.3). Its UV-vis spectrum of **6.3** features broad transitions centered at 385 nm (ε = 880 $cm^{-1}\cdot M^{-1}$)

and 478 (ε = 765 $cm^{-1} \cdot M^{-1}$), which we have tentatively assigned to 6d → 5f transitions. In addition, we observe several weak, broad absorptions between 530 to 800 nm, which are consistent with Laporte forbidden 5f → 5f transitions (Figure 6.34).

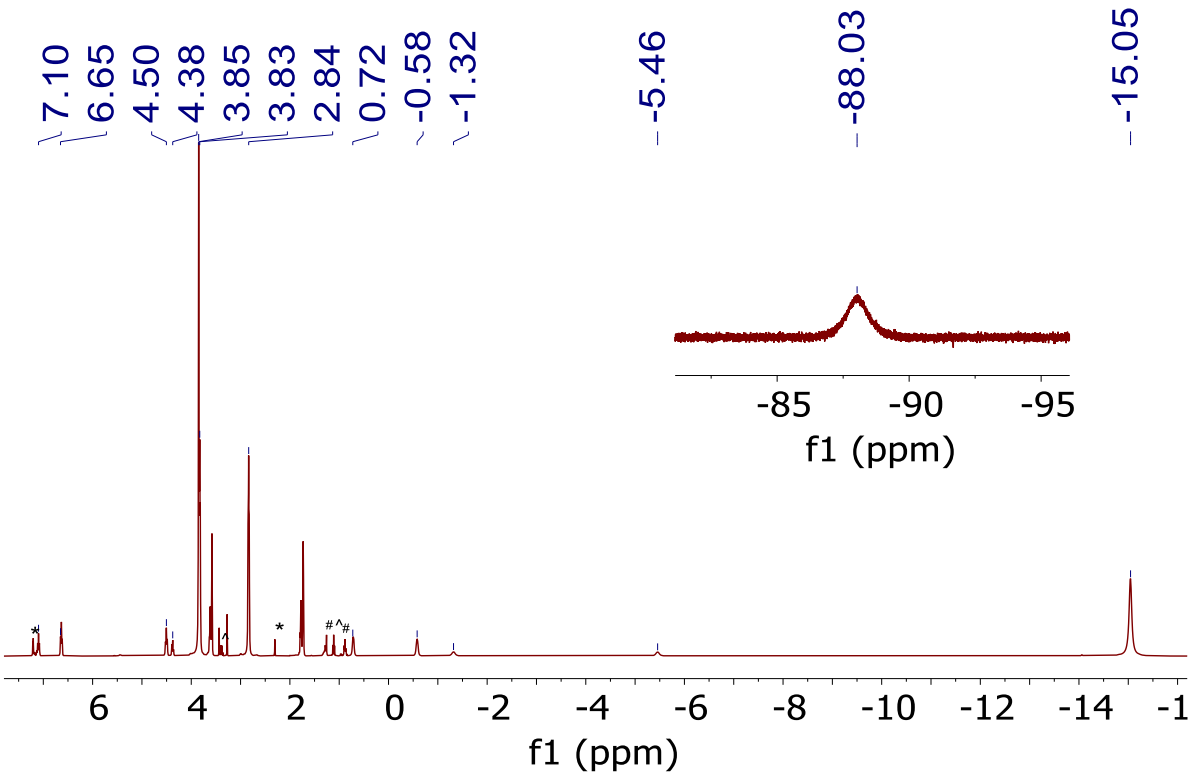

Figure 6.3. ^{1}H NMR spectrum of **6.3** in THF-d_8 at room temperature. (*) indicates the presence of toluene, (#) indicates the presence of hexanes, and (^) indicates the presence of Et_2O.

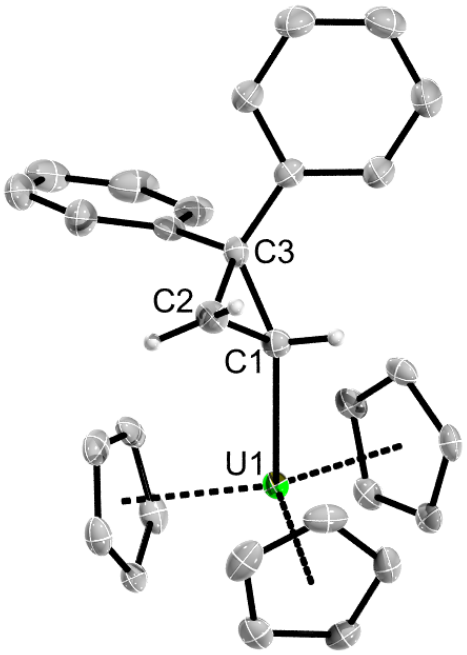

Figure 6.4. Solid state molecular structure of **6.3**·0.5THF, shown with thermal ellipsoids set at 50% probability. The $[K(2.2.2\text{-cryptand})]^+$ cation, THF solvate, and hydrogen atoms (except those of C_α and C_β) are omitted for clarity. Selected bond lengths [Å] and angles [deg]: U–C1 = 2.526(4), C1–C2 = 1.533(5), C1–C3 = 1.525(5), C2–C3 = 1.506(5), U–C1–C2 = 126.7(3), U–C1–C3 = 142.8(3).

Complex **6.3** crystallizes in the triclinic space group $P\bar{1}$ as the THF solvate, **6.3**·0.5THF (Figure 6.4). Unlike **6.1**, complex **6.3** crystallizes without disorder, permitting an accurate assessment of its metrical parameters. The U-C distance in **6.3** is 2.526(4) Å, which is similar to those of other σ-bonded uranium(III) hydrocarbyl complexes.[44-47] For example, the U–C bond distances in $[Li(2.1.1\text{-cryptand})][Cp_3U(n\text{-}C_4H_9)]$, $[Tp^*U(CH_2Ph)_2(THF)]$, $[Tp^*_2UMe]$, and $[Cp^*TpU(CH_2SiMe_3)(THF)]$ are 2.557(9), 2.604(9) and 2.615(7), 2.54(3), and 2.557(12) Å, respectively.[44, 45, 48, 49] Moreover, the C_α–C_β (1.533(5) Å), C_α–C_q (1.525(5)

Å), and C_β–C_q (1.506(5) Å) distances in **6.3** are consistent with the presence of C-C single bonds. Additionally, the sum of interatomic angles around C_α (329°) is consistent with sp^3 hybridization at this atom. To our knowledge, complexes **6.1** and **6.3** represent the first structurally characterized cyclopropyl complexes of the actinides, although many actinide metallacycles are known.[50]

Given the reactivity reported for [$CpFe(CO)_2$(1-ethoxycyclopropyl)],[30] I hypothesized that thermolysis of **6.1** could induce isomerization to afford a ring-opened uranium carbene complex. To this end, a red-brown toluene solution of **6.1**, in an NMR tube equipped with a J-Young valve, was thermolyzed for 10 d at 110 °C. The reaction mixture gradually changed from red-brown to dark yellow. Work-up of the resulting dark yellow solution resulted isolation of the U(IV) allyl complex, [$Cp_3U(\eta^1$-3,3-diphenylallyl)] (**6.4**), as dark yellow blocks in 35% yield (Scheme 6.3). The ^{1}H NMR spectrum of **6.4** in toluene-d_8 features a diagnostic H_α resonance at –212.5 ppm and an H_β resonance at –31.76 ppm. These resonances are present in a 2:1 ratio, consistent with the proposed formulation. In addition, complex **6.4** exhibits a single Cp environment at –2.87 ppm (Figure 6.5). Complex **6.4** can also be accessed by photolysis of **6.1**. In particular, photolysis of a red-brown toluene solution of **6.1**, using a water-jacketed, medium-pressure Hg lamp, for 10 d at room temperature also results in formation of a dark yellow solution. Work-up of this solution results in the isolation of **6.4** in 38% yield (Scheme 6.3). Note that the ^{1}H NMR spectra of the crude reaction mixtures, for either the photolysis or thermolysis reactions, are quite clean, suggesting that the modest yields are due to challenges with crystallization. To our knowledge, these reactions represent the first examples of cyclopropyl ring-opening in complexes of the actinides.

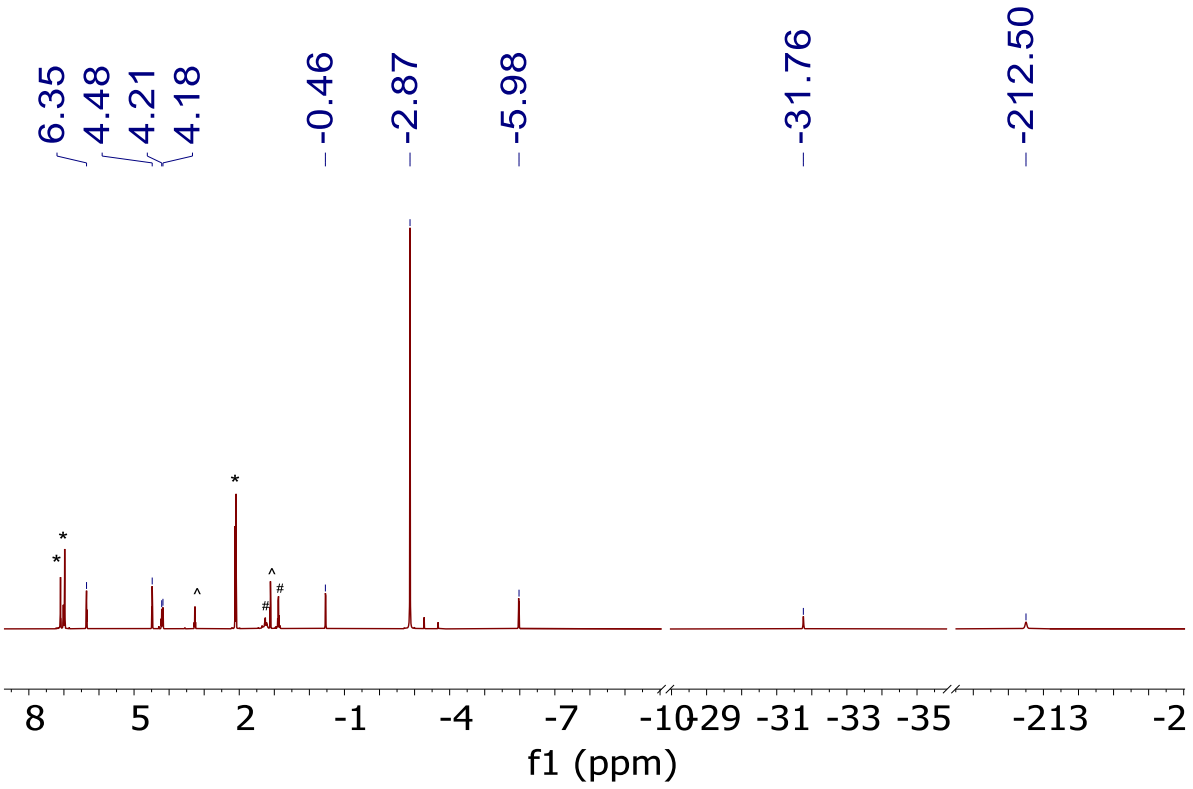

Figure 6.5. ^{1}H NMR spectrum of **6.4** via thermolysis of **6.1** in toluene-d_8 at room temperature. (*) indicates the presence of toluene, (#) indicates the presence of hexanes, and (^) indicates the presence of Et2O.

Complex **6.3** can also undergo cyclopropyl ring opening. In particular, photolysis of a dark red THF solution of **6.3** using a water-jacketed, medium-pressure Hg lamp, in an NMR tube equipped with a J-Young valve, for 9 h at room temperature resulted in a color change to dark yellow-orange. Work-up of the reaction mixture resulted the isolation of the ring-opened product, [K(2.2.2-cryptand)][$Cp_3U(\eta^1$-3,3-diphenylallyl)] (**6.5**), as dark yellow plates in 53% yield (Scheme 6.3). The ^{1}H NMR spectrum of 4 in THF-d_8 features a diagnostic H_α resonance at –118.19 ppm and a H_β resonance at –20.13 ppm, which are present in a 2:1 ratio, respectively**.** In addition, complex **6.5** exhibits a single Cp environment at –14.98 ppm (Figure

6.6). Complex **6.5** can also be access by reduction of **6.5**. In particular, reaction of **6.4** with 1 equiv of KC_8 in THF, in the presence of 2.2.2-cryptand, affords **6.5** in 40% yield after work-up (Scheme 6.3). Interestingly, attempts to effect the thermal ring-opening of complex **6.3** were unsuccessful. Complex **6.3** is insoluble in toluene, which precluded thermolysis in that solvent, while thermolysis of a THF solution of **6.3** at 65 °C resulted in no reaction over the course of 48 h. The synthesis and characterization of ring-opened products **6.4** and **6.5** was performed in collaboration with Megan A. Schuerlein.

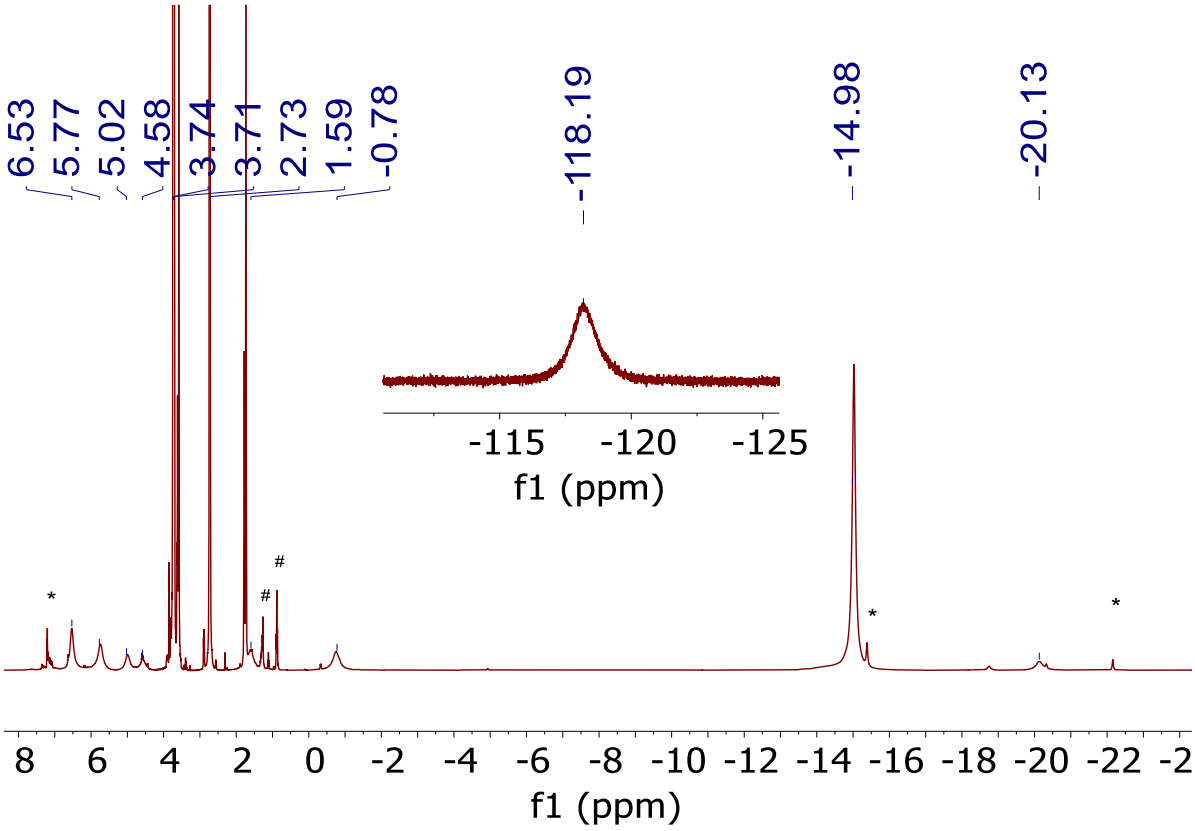

Figure 6.6. ^{1}H NMR spectrum of **6.5** formed via photolysis of **6.3** in THF-d_8 at room temperature. (*) indicates the presence of an unidentified decomposition product, (#) indicates the presence of hexanes, and (^) indicates the presence of Et2O.

Complexes **6.4** and **6.5** both crystallize in the triclinic space group $P\bar{1}$ (Figure 6.7, Figure 6.11, and Table 6.1). Complex **6.4** crystallizes as the toluene solvate, **6.4**·C_7H_8, whereas **6.5** crystallizes as the THF solvate, **6.5**·THF. The U-C distance in **6.4** is 2.532(4) Å, which is consistent with those found in other U(IV) η^1-allyl complexes. For example, the relevant U-C distances in [Cp*$_2$U(η^3-$CH_2C(R)CH_2$)(η^1-$CH_2C(R)$═CH_2)] (R = H, Me) are 2.526(3) Å and 2.538(1) Å, respectively.[51] Not surprisingly, the U-C distance in **6.5** (2.59(1) Å) is longer than that observed for **6.4**, consistent with the larger ionic radius of U(III).[52] The C_α–C_β distances in **6.4** and **6.5** are 1.463(6) Å and 1.42(1) Å, respectively, which are consistent with C-C single bonds, whereas the C_β–C_γ distances in **6.4** (1.364(6) Å) and **6.5** (1.39(1) Å) are consistent with double bond character. The sum of angles around C_γ are also consistent with sp^2 hybridization (**6.4**: Σ(C-C_γ-C) = 360°; **6.5**: Σ(C-C_γ-C) = 360°). Overall, these data confirm the presence of a η^1-allyl ligand in **6.4** and **6.5.**

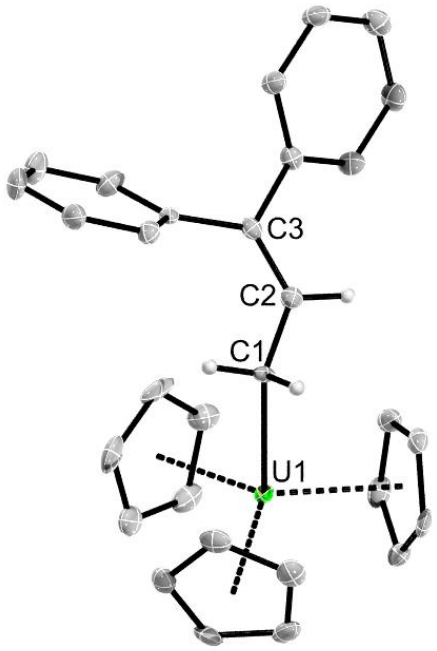

Figure 6.7. Solid state molecular structure of **6.4**, shown with thermal ellipsoids set at 50% probability. The toluene solvate and hydrogen atoms (except those of C_α and C_β) are omitted for clarity. Selected bond lengths [Å] and angles [deg]: 6.4: U–C1 = 2.532(4), C1–C2 = 1.463(6), C2–C3 = 1.364(6), U–C1–C2 = 119.5(3), C1–C2–C3 = 129.7(4). 6.5: U–C1 = 2.59(1), C1–C2 = 1.42(1), C2–C3 = 1.39(1), U–C1–C2 = 121.1(8), C1–C2–C3 = 133(1).

To probe if the cyclopropyl ring-opening is occuring via proximal or distal C-C activation, we selectively labelled the C_α position of **6.1** with deuterium. Access to **6.1**-d_1 was achieved by reaction of [Cp_3UCl] with *in situ* generated 1-lithium-1-deuterio-2,2-diphenylcyclopropane in Et_2O.[53] Complex **6.1**-d_1 can be isolated as brown plates in 65% yield after work up. Its ^{1}H NMR spectrum is nearly identical to that of **6.1**, except that the H_α resonance is absent (Figure 6.8). As expected, the ^{2}H NMR spectrum of **6.1**-d_1 features a single resonance at –171.54 ppm, assignable to the D_α environment (Figure 6.13). Subsequent

reaction of **6.1**-d_1 with 1 equiv of KC_8 in THF, in the presence of 2.2.2-cryptand, results in formation of a dark red solution, from which **6.3**-d_1 can be isolated in 67% yield. Its ^{2}H NMR spectrum features a single resonance at –87.43 ppm assignable to the D_α environment (Figure 6.16). Importantly, no other resonances are present in the ^{2}H NMR spectra of **6.1**-d_1 and **6.3**-d_1, indicative of selective labelling at the C_α position without any deuterium scrambling.

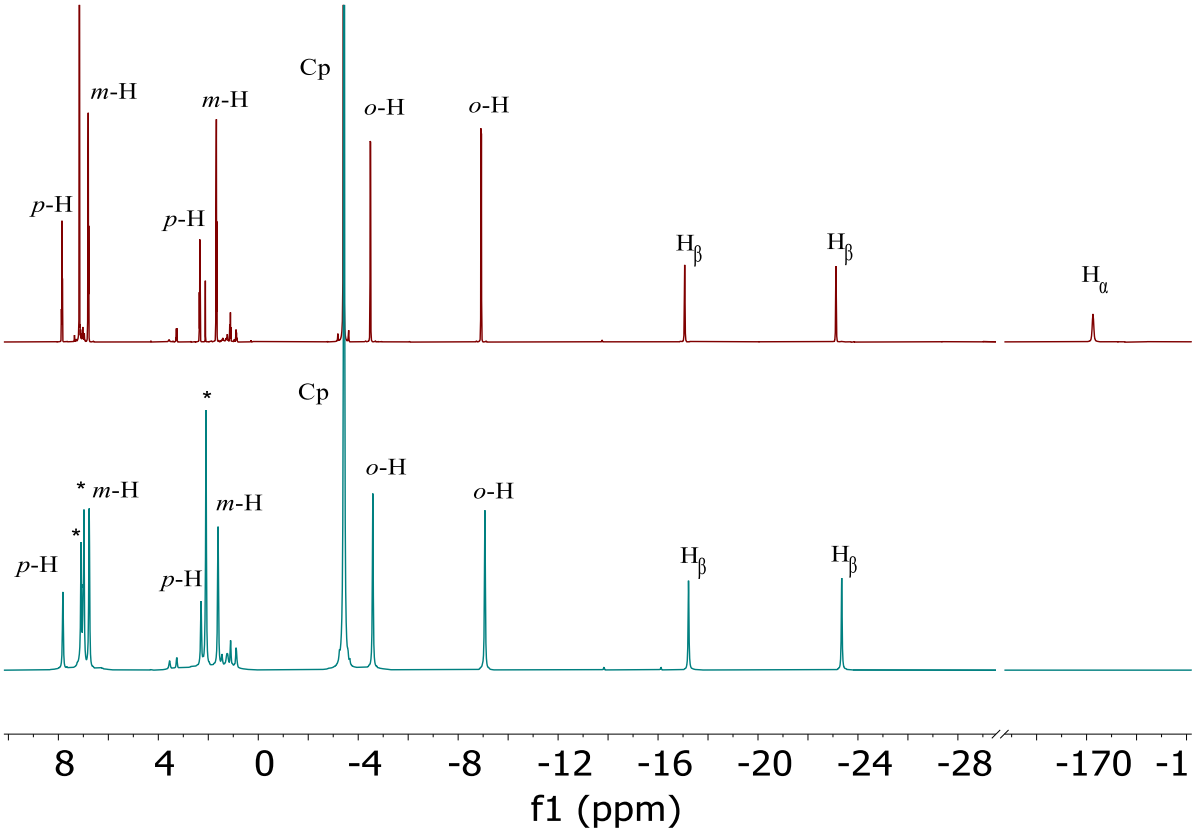

Figure 6.8. ^{1}H NMR spectrum of **6.1** in benzene-d_6 at room temperature (top). ^{1}H NMR spectrum of **6.1**-d_1 toluene-d_8 at room temperature (bottom). (*) indicates the presence of toluene-d_8.

Thermolysis of a red-brown toluene solution of **6.1**-d_1, in an NMR tube equipped with a J-Young valve, at 110 °C for 11 d resulted in formation of a deep yellow solution. Work-up

of this solution provided the U(IV) allyl complex, [$Cp_3U(\eta^1$-2-deutero-3,3-diphenylallyl)] (**6.4**-d_1), as dark yellow blocks in 42% yield (Scheme 6.4). Its ^{2}H NMR spectrum in toluene-h_8 features one resonance at –31.82 ppm assignable to the D_β environment (Figure 6.19). No other resonances are present in this spectrum. In addition, the ^{1}H NMR spectrum of **6.4**-d_1 in toluene-d_8 features a diagnostic H_α resonance at –212.5 ppm (Figure 6.18)**.** No resonance is observed for the H_β environment in this spectrum. Overall, the ^{2}H and ^{1}H NMR spectra are consistent with a distal ring-opening pathway to afford an η^3-allyl intermediate (**B**), which then isomerizes to give the η^1-allyl product, **6.4**-d_1. Photolysis of a red-brown toluene solution of **6.1**-d_1 using a water-jacketed, medium-pressure Hg lamp for 8 d at room temperature, also results in formation of **6.4**-d_1. The ^{1}H and ^{2}H NMR spectra of this material are also consistent with isomerization via selective distal C-C bond cleavage (Figure 6.20 and Figure 6.21).

Scheme 6.4. Synthesis of complex **6.4**-d_1.

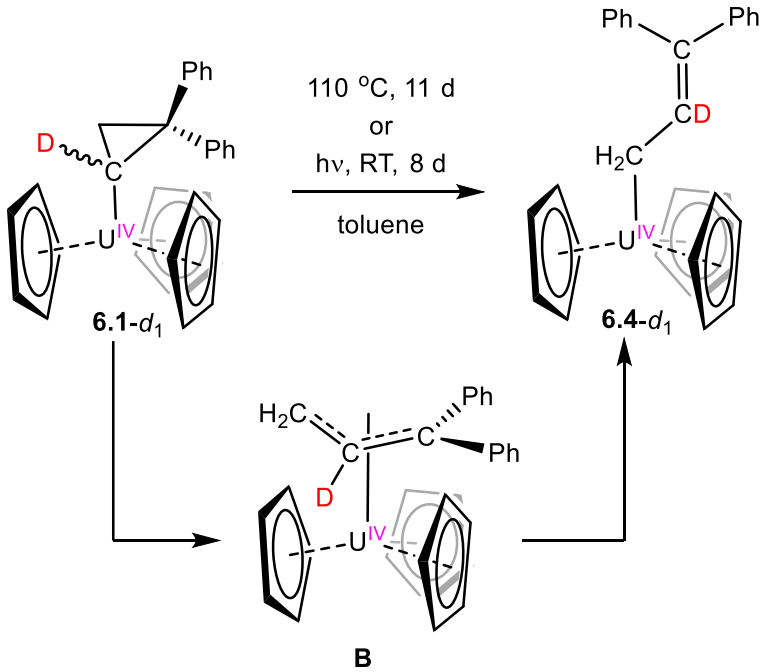

We also examined the cyclopropyl ring-opening of complex **6.3**. In particular, photolysis of a dark red THF solution of **6.3**-d_1 using a water-jacketed, medium-pressure Hg lamp, in an NMR tube equipped with a J-Young valve, for 24 h at room temperature resulted in a color change to dark yellow-orange (Scheme 6.5). The ^{2}H NMR spectrum of this mixture in THF-h_8 featured a single resonance at –19.36 ppm, which assignable to the D_β environment of **6.5**-d_1 (Figure 6.24). The ^{1}H NMR spectrum of a comparably generated reaction mixture in THF-d_8 features a diagnostic H_α resonance at –118.30 ppm, but no resonance assignable to the H_β environment (Figure 6.23). As was observed for **6.4**-d_1, the spectral data for **6.5**-d_1 are consistent with selective distal C-C bond cleavage. Interestingly, Chen and co-workers also utilized selective deuterium labelling to investigate cyclopropyl reactivity. In their case, they discovered that cyclopropane elimination from [L^{Me}Sc(*cyclo*-$C_3H_5)_2$] occurs via direct hydrogen abstraction from an isopropyl methine carbon.[33]

Scheme 6.5. Synthesis of complex **6.5**-d_1.

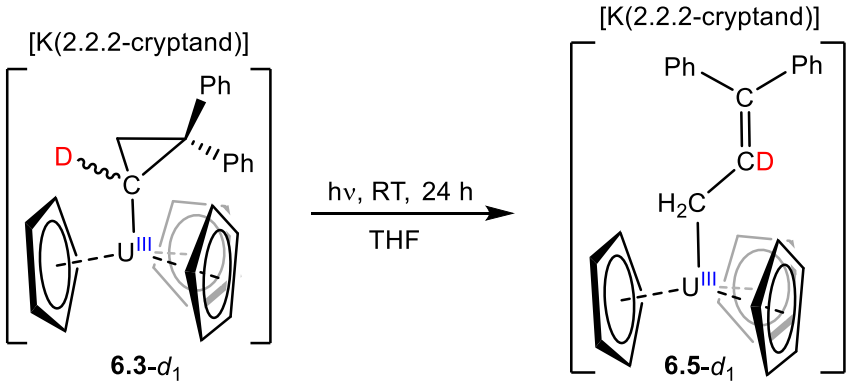

Given the ring-opening in the uranium cyclopropyl complexes, I hypothesized that thermolysis or photolysis could induce isomerization to afford a ring-opened product of the thorium cyclopropyl complex, **6.2**. However, thermolysis of a colorless toluene-d_8 of **6.2** at

110 °C resulted in no reaction over the course of 4d. Considering that ring-open in the uranium cyclopropyl was induces via photolysis, I examined the UV-vis spectrum of **6.2** in THF, which reveals a transition centered at 220 nm (ε = 67000 $cm^{-1}\cdot M^{-1}$) and broad transition at 290 nm (ε = 17800 $cm^{-1}\cdot M^{-1}$), which we have tentatively assigned to LMCT transitions (Figure 6.33). Interestingly, photolysis of a colorless THF-d_8 of **6.2**, using a water-jacketed, medium-pressure Hg lamp, for 1 h at room temperature results in color change to yellow. The ^{1}H NMR spectrum of this reaction mixture in THF-d_8 reveals three new Cp environments at 6.34 ppm, 6.22 ppm, and 6.16 ppm, as well as the presence of **6.2**, suggesting the formation of several Cp-containing products (Figure 6.25). Work-up of this solution resulted in the deposition of a few pale yellow plates and colorless solids affording the isolation of the Th(IV) allyl complex, [$Cp_3U(\eta^1$-3,3-diphenylallyl)] (**6.6**), however the yield was not record because the material was not analytically pure. The ^{1}H NMR spectrum of **6.6** in benzene-d_6 reveals a resonance at 5.85 ppm, assignable to the Cp environment, however, it also reveals the presence of **6.2** and Cp_3ThCl (Figure 6.26). These resonances are present in a 2:1:2 ratio, suggesting a mixture of products in sample. The ^{13}C NMR spectrum of **6.6** was not recorded due to a mixture of products and the presence of **6.2** and Cp_3ThCl. Multiple attempts to isolate pure material of complex **6.6** proved unsuccessful and resulted in intractable mixtures. Specifically, attempts to isolate **6.6** from photolysis of **6.2** in various solvents such as THF-d_8, toluene-d_8, benzene-d_6, dichloromethane-d_2, and pyridine-d_5, along with various reaction times resulting in appearance of multiple Cp environment, complicating the isolation of analytical pure material. Interesting, in a few instances photolysis of colorless solution of **6.2** resulted in color change to dark green solution and deposition of dark green crystals. Specifically, photolysis of solution of **6.2** (9.3 mg, 0.015 mmol) in THF-d_8 (0.7 mL) for 3 h at room temperature using a

water-jacketed, medium-pressure Hg lamp, resulted in a dark green solution and deposition of dark green solids. Interestingly, the crude ^{1}H NMR spectrum of reaction mixture reveals three distinct minor resonance at 14.48, 14.29, and 13.03 ppm, which are significantly downfield for typical diamagnetic Th(IV) complexes (Figure 6.27). Additionally, the sample contains several Cp-containing products, as indicated by resonances at 6.34, 6.21, and 6.16 ppm, in a 1:1.5:1 ratio, respectively. However, these remain unassigned. I attempted to characterize the solid-state structure of the dark green solids, however due to suboptimal data quality and substantial disorder, I was unable to determine the structure. Nonetheless, I tentatively attributed the emergence of the green color to the presence of a thorium(III) complex, [Cp_3Th^{III}]. Despite subsequent efforts, attempts to isolate XRD-quality samples proved unsuccessful. The examination of the ring-opening of **6.2** was performed in collaboration with Megan A. Schuerlein.

Complex **6.6** crystallizes in the monoclinic space group $P2_1/c$ as the THF solvate, **6.6**·THF (Figure 6.9 and Table 6.1). The solid-state structure of **6.6** is isostructural to that observed in **6.4**. Additionally, the Th-C_α-bond distance is 2.556(4) Å, which is slight longer that observed for **6.4**, consistent with the larger ionic radius of the Th(IV) ion.[52] The C_α–C_β and C_β–C_γ distances in **6.6** are 1.457(6) Å and 1.355(6) Å, respectively, which are similar to those found in **6.4** and **6.5**. The C_α–C_β distance is consistent with C-C single bonds, whereas the C_β–C_γ distance is consistent with double bond character. Finally, the sum of angles around C_γ are also consistent with sp^2 hybridization (**6.6**: Σ(C-C_γ-C) = 359.9°).

Table 6.1. Selected metrical parameters for complexes **6.4**·C_7H_8, **6.5**·THF, and **6.6**·THF**.**

Bond (Å, °)	**6.4**·C_7H_8	**6.5**·THF	**6.6**·THF
An–C_α	2.532(4)	2.59(1)	2.556(4)
C_α–C_β	1.463(6)	1.42(1)	1.457(6)
C_β–C_γ	1.364(6)	1.39(1)	1.355(6)
C_γ–C_{ipso}	1.486(6), 1.503(6)	1.469(13), 1.485(13)	1.481(6), 1.489(6)
An–C_α–C_β	119.5(3)	121.1(8)	117.6(3)
C_α–C_β–C_γ	129.7(4)	133(1)	131.1(4)
$\Sigma(\angle C_{ipso/\beta}$–$C_\gamma$–$C_{ipso})$	360.0	360.0	359.9

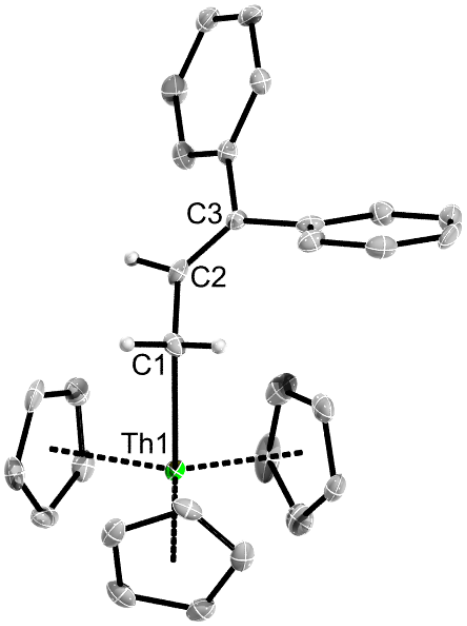

Figure 6.9. Solid state molecular structure of **6.6**·THF, shown with thermal ellipsoids set at 50% probability. The THF solvate and hydrogen atoms (except those of C_α and C_β) are omitted for clarity.

6.3 Summary

In summary, I isolated [Cp_3U(2,2-diphenylcyclopropyl)] via salt metathesis of [Cp_3UCl] with *in situ* generated 1-lithium-2,2-diphenylcyclopropane. Thermolysis or photolysis of this complex results in ring-opening of the cyclopropyl ring, which results in formation of an η^1-allyl complex, [$Cp_3U(\eta^1$-3,3-diphenylallyl)]**.** Similar results are observed upon photolysis of its U(III) analogue, [K(2.2.2-cryptand)][Cp_3U(2,2-diphenylcyclopropyl)]. Deuterium labelling studies demonstrate that ring-opening occurs exclusively via distal C-C bond cleavage, via an unobserved η^3-allyl intermediate, despite the apparent steric unfavorability of the diphenyl-substituted η^3-3,3-diphenylallyl ligand. Notably, I observed no evidence for proximal activation, regardless of uranium oxidation state or mechanism of activation (i.e., thermolysis or photolysis), demonstrating that the phenyl substituents cannot override the preference for distal activation. This reactivity contrasts with that observed for [$CpFe(CO)_2$(1-ethoxycyclopropyl)],[30] which can exhibit proximal C-C cleavage, and highlights the potential importance of the α-carbon substituent in directing the mode of activation (Scheme 6.1). Moving forward, we plan to further examine the reactivity of actinide cyclopropyl complexes, especially cyclopropyl complexes with heteroatom substituents on the α-carbon, in pursuit of non-traditional routes to access actinide carbon multiple bonds.

6.4 Experimental

6.4.1 General Procedures

All reactions and subsequent manipulations were performed under anaerobic and anhydrous conditions under an atmosphere of dinitrogen. Diethyl ether (Et_2O), pentane, toluene, and hexanes were dried using a Vacuum Atmospheres DRI-SOLV Solvent

Purification system and stored over 3Å sieves for 24 h prior to use. Tetrahydrofuran (THF) was distilled over calcium hydride then distilled over sodium benzophenone, collected, and stored over 3Å sieves for 24 h prior to use. THF-d_8, toluene-d_8, and C_6D_6 were stored over 3Å sieves for 24 h prior to use. [Cp_3UCl], 1-bromo-2,2-diphenylcyclopropane, and 1-deutero-1-bromo-2,2-diphenylcyclopropane were synthesized according to previously reported literature procedures.[53-55] All other reagents were purchased from commercial vendors and used as received.

^1H, $^{13}C\{^1H\}$, and ^2H NMR spectra were recorded on a **Bruker Avance III HD 400 MHz**, a Varian UNITY INOVA 500 MHz, a **Bruker Avance NEO 500 MHz,** or a Varian Unity Inova AS600 600 MHz spectrometer. ^1H, ^2H, and $^{13}C\{^1H\}$ NMR spectra were referenced to external $SiMe_4$ using the residual protio (or deutero) solvent peaks as internal standards.[56, 57] IR spectra were recorded on a Nicolet 6700 FT-IR spectrometer. Electronic absorption spectra were recorded on a Shimadzu UV3600 UV-NIR Spectrometer. Elemental analyses were performed by the Microanalytical Laboratory at University of California (Berkeley, CA).

6.4.2 Synthesis of [Cp_3U(2,2-diphenylcyclopropyl)] (6.1).

To a cold (–25 °C), stirring, colorless Et_2O solution (0.5 mL) of 1-bromo-2,2-diphenylcyclopropane (139.2 mg, 0.510 mmol) was added dropwise a cold (–25 °C), colorless pentane solution of 1.5 M ^{t}BuLi (0.3 mL, 0.510 mmol). The solution immediately turned pale yellow. This solution was then added dropwise to a cold (–25 °C), stirring brown slurry of [Cp_3UCl] (159.3 mg, 0.340 mmol) suspended in Et_2O (3 mL). The solution immediately turned red-brown, concomitant with the deposition of a red-brown precipitate. After stirring for 45 min, the volatiles were removed from the filtrate *in vacuo*. The red-brown powder was then extracted into toluene (3 mL) and filtered through a Celite column supported on glass

wool (0.5 cm × 2 cm), leaving a tan precipitate on the Celite pad. This red-brown solution was then layered with hexanes (5 mL). Storage of this vial at –25 ºC for 24 h resulted in the deposition of brown plates, which were isolated by decanting the supernatant, rinsing the crystals with cold (-25 °C) pentane (2 mL), and drying *in vacuo* (142.7 mg, 63 % yield). Anal. Calcd for $UC_{30}H_{28}$: C, 57.51; H, 4.50. Found: C, 57.35; H, 4.50. ^{1}H NMR (25 °C, 400 MHz, benzene-d_6): δ 7.86 (t, *J* = 7.0 Hz, 1H, *p*-H), 6.80 (t, *J* = 6.9 Hz, 2H, *m*-H), 2.34 (t, *J* = 7.2 Hz, 1H, *p*-H), 1.68 (t, *J* = 7.8 Hz, 2H, *m*-H), –3.41 (s, 15H, Cp), –4.50 (d, *J* = 7.3 Hz, 2H, *o*-H), –8.93 (d, *J* = 8.4 Hz, 2H, *o*-H), –17.07 (s, 1H, H_β), –23.12 (s, 1H, H_β), –170.26 (s, 1H, H_α). IR (KBr pellet, cm^{-1}): 3026 (w), 2960 (w), 2873 (w), 1595 (w), 1491 (w), 1441 (w), 1124 (w), 1065 (w), 1011 (m), 924 (w), 891 (w), 781 (s), 758 (s), 696 (m), 592 (w), 540 (w).

6.4.3 Synthesis of [Cp$_3$U(1-deutero-2,2-diphenylcyclopropyl)] (6.1-d_1).

To a cold (–25 °C), stirring, colorless Et_2O solution (0.5 mL) of 1-bromo-1-deuterio-2,2-diphenylcyclopropane (87.4 mg, 0.318 mmol) was added dropwise a cold (–25 °C), colorless pentane solution of 1.5 M ^{t}BuLi (0.199 mL, 0.318 mmol). The solution immediately turned pale yellow. This solution was then added dropwise to a cold (–25 °C), stirring brown slurry of [Cp$_3$UCl] (74.7 mg, 0.159 mmol) suspended in Et_2O (3 mL). The solution immediately turned red-brown, concomitant with the deposition of a red-brown precipitate. After stirring for 1h, the volatiles were removed *in vacuo*. The red-brown powder was then extracted into toluene (6 mL) and filtered through a Celite column supported on glass wool (0.5 cm × 2 cm), leaving behind a tan precipitate on the Celite pad. The volume of the red-brown filtrate was reduced to 2 mL *in vacuo*, pentane (5 mL) was then layered onto the solution, and the vial was stored at –25 °C for 24 h, which resulted in the deposition of red-brown plates. The solid was isolated by decanting the supernatant and drying briefly *in vacuo* (65 mg, 65% yield). ^{1}H NMR

(25 °C, 500 MHz, toluene-d_8): δ 7.82 (s, 1H, *p*-H), 6.78 (s, 2H, *m*-H), 2.29 (s, 1H, *p*-H), 1.63 (s, 2H, *m*-H), –3.43 (s, 15H, Cp), –4.59 (s, 2H, *o*-H), –9.06 (s, 2H, *o*-H), –17.22 (s, 1H, H_β), –23.35 (s, 1H, H_β). ^{2}H NMR (25 °C, 76.75 MHz, toluene-h_8): δ –171.54 (s, H_α).

6.4.4 Synthesis of [Cp_3Th(2,2-diphenylcyclopropyl)] (6.2).

To a cold (–25 °C), stirring, colorless Et_2O solution (0.5 mL) of 1-bromo-2,2-diphenylcyclopropane (97.9 mg, 0.36 mmol) was added dropwise a cold (–25 °C), colorless pentane solution of 1.5 M ^{t}BuLi (0.23 mL, 0.36 mmol). The solution immediately turned pale yellow. This solution was then added dropwise to a cold (–25 °C), stirring brown slurry of [Cp_3ThCl] (110.5 mg, 0.23 mmol) suspended in Et_2O (3 mL). The stirring solution immediately turned grey concomitant with the deposition of a grey precipitate. After stirring for 45 min the volatiles were removed from the filtrate *in vacuo*. The colorless powder was then extracted into toluene (3 mL) and filtered through a Celite column supported on glass wool (0.5 cm × 2 cm) leaving behind a grey precipitate on the Celite column. Layering this solution with hexanes (5 mL) and storage of this vial at -25 ºC for 24 h resulted in the deposition of colorless plates. The solid was isolated by decanting the supernatant and drying briefly *in vacuo* (99.0 mg, 67% yield). Anal. Calcd for $ThC_{30}H_{28}$: C, 58.06; H, 4.55. Found: C, 57.79; H, 4.61. ^{1}H NMR (500 MHz, Benzene-d_6) δ 7.65 (d, 2H, H_o), 7.45 (d, 2H, H_o), 7.22 (t, 2H, H_m), 7.21 (t, 2H, H_m) 7.10 (t, 1H, H_p), 7.03 (t, 1H, H_p), 5.83 (s, 13H), 1.90 (dd, J = 9.6, 2.8 Hz, 1H, H_β), 1.80 (dd, J = 10.8, 2.8 Hz, 1H, H_β), 0.85 (dd, J = 10.2 Hz, 1H, H_α).

6.4.5 Synthesis of [K(2.2.2-cryptand)][Cp_3U(1-deutero-2,2-diphenylcyclopropyl)] (6.3).

To a cold (–25 °C), stirring, red-brown THF solution (1 mL) of **6.1** (59.7 mg, 0.095 mmol) and 2.2.2-cryptand (35.9 mg, 0.095 mmol) was added KC_8 (14.2 mg, 0.105 mmol) as a bronze

solid. Upon addition, the solution turned dark red. After 2 min, the solution was filtered through a Celite column supported on glass wool (0.5 cm × 2 cm), affording a clear, dark red filtrate. Pentane (5 mL) was then layered onto the solution, and the vial was stored at –25 °C for 24 h, which resulted in the deposition of red plates. The solid was isolated by decanting the supernatant and drying briefly *in vacuo* (87 mg, 88% yield). Anal. Calcd for $UC_{48}H_{64}KO_6N_2$: C, 55.32; H, 6.19, N, 2.69. Found: C, 54.99; H, 6.17, N, 2.78. ^{1}H NMR (25 °C, 400 MHz, THF-d_8): δ 7.10 (t, J = 7.2 Hz, 1H, *p*-H), 6.65 (t, J = 7.0 Hz, 2H, *m*-H), 4.50 (t, J = 7.5 Hz, 2H, *m*-H), 4.38 (t, J = 7.1 Hz, 1H, *p* -H), 3.85 (s, 12H, OCH_2CH_2O), 3.83 (t, J = 4.6 Hz, 12H, OCH_2CH$_2$N), 2.84 (t, J = 4.7 Hz, 12H, OCH$_2$CH_2N), 0.72 (s, 2H, *o*-H), –0.58 (s, 2H, *o*-H), –1.32 (s, 1H, H$_\beta$), –5.46 (s, 1H, H$_\beta$), –15.05 (s, 15H, Cp), –88.03 (s, 1H, H$_\alpha$). IR (KBr pellet, cm^{-1}): 3052 (m), 2956 (m), 2815 (m), 1957 (w), 1596 (m), 1492 (s), 1475 (s), 1 (w), 1448 (s), 1440 (s), 1361 (s), 1292 (s), 1257 (s), 1238 (m), 1174 (w), 1078 (s), 1012 (s), 948 (s), 933 (s), 831 (s), 763 (s), 744 (s), 831 (m), 763 (s), 746 (s), 700 (s), 678 (s), 676 (m), 590 (m), 547 (m) 522 (m).

6.4.6 Synthesis of [K(2.2.2-cryptand)][Cp$_3$U(1-deutero-2,2-diphenylcyclopropyl)] (6.3-d_1).

To a cold (–25 °C), stirring, red-brown THF solution (1 mL) of **1**-d_1 (53.5 mg, 0.085 mmol) and 2.2.2-cryptand (32.1 mg, 0.085 mmol) was added KC_8 (12.7 mg, 0.093 mmol) as a bronze solid. Upon addition, the solution turned dark red. After 2 min, the solution was filtered through a Celite column supported on glass wool (0.5 cm × 2 cm), affording a clear dark red filtrate. Pentane (5 mL) was then layered onto the solution, and the vial was stored at –25 °C for 24 h, which resulted in the deposition of red plates. The solid was isolated by decanting the supernatant and drying briefly *in vacuo* (59.1 mg, 67 % yield). ^{1}H NMR (25 °C,

500 MHz, THF-d_8): δ 7.07 (t, J = 7.2 Hz, 1H, p-H), 6.62 (t, J = 6.9 Hz, 2H, m-H), 4.56 (t, J = 7.6 Hz, 2H, m-H), 4.41 (t, J = 7.2 Hz, 2H, p -H), 3.85 (s, 12H, OCH_2CH_2O), 3.83 (t, J = 4.8 Hz, 12H, OCH_2CH$_2$N), 2.84 (t, J = 4.7 Hz, 12H, OCH$_2$CH_2N), 0.82 (s, 2H, o-H), –0.44 (s, 2H, o-H), –0.92 (s, 1H, H$_\beta$), –5.07 (s, 1H, H$_\beta$), –15.31 (s, 15H, Cp). ^{2}H NMR (25 °C, 76.75 MHz, THF-h_8): δ –87.43 (s, H$_\alpha$).

6.4.7 Synthesis of [Cp$_3$U(η^1-3,3-diphenylallyl)] (6.4) via thermolysis of [Cp$_3$U(2,2-diphenylcyclopropyl)] (6.1).

Red-brown crystals of **6.1** (117.4 mg, 0.187 mmol) were dissolved in toluene (6 mL) resulting in formation of a clear red brown solution. This solution was transferred to a Schlenk tube equipped with a Teflon valve, brought out of the glovebox and thermolyzed for 10 d at 110 °C. The color of the solution gradually changed from red brown to dark yellow over the course of the thermolysis. After 10 d, the Schlenk tube was brought back into glovebox and the solution was filtered through a Celite column (0.5 cm × 2 cm) supported on glass wool to afford a clear dark yellow filtrate. The volume of the filtrate was reduced to 2 mL *in vacuo*. Pentane (5 mL) was layered onto the solution, and the vial was stored at –25 °C for 24 h, which resulted in the deposition of yellow plates. The solid was isolated by decanting the supernatant and drying briefly *in vacuo* (41 mg, 35% yield). Anal. Calcd for $UC_{30}H_{28}$: C, 57.51; H, 4.50. Found: C, 57.87; H, 4.64. ^{1}H NMR (25 °C, 600 MHz, toluene-d_8): δ 6.35 (t, J = 7.6 Hz, 2H, m-H), 4.48 (t, J = 6.4 Hz, 2H, m-H), 4.21 (t, J = 8.2 Hz, 1H, p-H), 4.18 (t, J = 6.4 Hz, 1H, p-H), –0.46 (d, J = 7.3 Hz, 2H, o-H), –2.87 (s, 15H, Cp), –5.98 (d, J = 6.4 Hz, 2H, o-H), –31.76 (s, 1H, H$_\beta$), –212.50 (s, 2H, H$_\alpha$) (**Error! Reference source not found.**). IR (KBr pellet, cm^{-1}): 3399 (w), 3079 (w), 3048 (w), 3021 (w), 2989 (w), 2923 (w), 2852 (w), 2086 (w), 1959 (w), 1793 (w), 1693 (w), 1594 (m), 1579 (s), 1560 (s), 1490 (s), 1440 (s), 1390

(w), 1361 (w), 1263 (w), 1170 (m), 1072 (m), 1041 (s), 1012 (s), 931 (s), 792 (s), 760 (s), 734 (s), 696 (s), 646 (s), 605 (s), 568 (m), 539 (m), 493 (w), 466 (m), 418 (m).

6.4.8 Synthesis of [$Cp_3U(\eta^1$-2-deutero-3,3-diphenylallyl)] (6.4-d_1) via thermolysis of [Cp_3U(1-deutero-2,2-diphenylcyclopropyl)] (6.1-d_1).

Red-brown crystals of **6.1**-d_1 (20.0 mg, 0.0319 mmol) were dissolved in toluene-d_8 (0.7 mL) resulting in formation of a clear red brown solution. This solution was transferred to an NMR tube equipped with a J-Young valve, brought out of the glovebox and thermolyzed for 11 d at 110 °C. The color of the solution gradually changed from red brown to dark yellow over the course of the thermolysis. After 11 d, the NMR tube was brought back into glovebox and the solution was filtered through Celite column (0.5 cm × 2 cm) supported on glass wool to afford a clear dark yellow filtrate. Pentane (2 mL) was then layered onto the solution, and the vial was stored at –25 °C for 24 h, which resulted in the deposition of yellow plates. The solid was isolated by decanting the supernatant and drying briefly *in vacuo* (8.4 mg, 42% yield). ^{1}H NMR (25 °C, 500 MHz, toluene-d_8): δ 6.36 (t, J = 7.4 Hz, 2H, *m*-H), 4.48 (t, J = 6.7 Hz, 2H, *m*-H), 4.21 (t, J = 7.9 Hz, 1H, *p*-H), 4.17 (t, J = 6.7 Hz, 1H, *p*-H), –0.46 (d, J = 7.6 Hz, 2H, *o*-H), –2.87 (s, 15H, Cp), -5.96 (d, J = 7.6 Hz, 2H, *o*-H), –212.50 (s, 2H, H_α). ^{2}H NMR (25 °C, 76.75 MHz, toluene-h_8): δ –31.82 (s, H_β).

6.4.9 Synthesis of [$Cp_3U(\eta^1$-3,3-diphenylallyl)] (6.4) via photolysis of [Cp_3U(2,2-diphenylcyclopropyl)] (6.1)

Red-brown crystals of **6.1** (22 mg, 0.035 mmol) were dissolved in toluene-d_8 (0.7 mL) resulting in formation of a clear red brown solution. This solution was transferred to an NMR tube equipped with a J-Young valve, brought out of the glovebox and was exposed to light

from a water-jacketed, medium-pressure mercury lamp for 10 d at room temperature. The color of the solution gradually changed from red brown to dark yellow over the course of the photolysis. After 10 d, the solution was filtered through Celite column (0.5 cm × 2 cm) supported on glass wool to afford a clear dark yellow filtrate. Pentane (2 mL) was layered onto the solution, and the vial was stored at –25 °C for 24 h, which resulted in the deposition of yellow plates. The solid was isolated by decanting the supernatant and drying briefly *in vacuo* (8.4 mg, 38% yield). ^{1}H NMR (25 °C, 500 MHz, toluene-d_8): δ 6.35 (t, J = 7.7 Hz, 2H, *m*-H), 4.48 (t, J = 6.8 Hz, 2H, *m*-H), 4.21 (t, J = 7.9 Hz, 1H, *p*-H), 4.18 (t, J = 6.7 Hz, 1H, *p*-H), –0.47 (d, J = 7.3 Hz, 2H, *o*-H), –2.87 (s, 15H, Cp), –5.98 (d, J = 7.6 Hz, 2H, *o*-H), –31.76 (s, 1H, H_β), –212.45 (s, 2H, H_α).

6.4.10 Synthesis of [Cp$_3$U(η^1-2-deutero-3,3-diphenylallyl)] (6.4-d_1) via photolysis of [Cp$_3$U(1-deutero-2,2-diphenylcyclopropyl)] (6.1-d_1).

Red-brown crystals of **6.1**-d_1 (15 mg, 0.024 mmol) were dissolved in toluene-d_8 (0.7 mL), resulting in formation of a clear red brown solution. This solution was transferred to an NMR tube equipped with a J-Young valve, brought out of the glovebox and was exposed to light from a water-jacketed, medium-pressure mercury lamp for 8 d at room temperature. The color of the solution gradually changed from red brown to dark yellow over the course of the photolysis. After 8 d, the NMR tube was brought back into glovebox and the solution was filtered through Celite column (0.5 cm × 2 cm) supported on glass wool to afford a clear dark yellow filtrate. Pentane (2 mL) was layered onto the solution, and the vial was stored at –25 °C for 24 h, which resulted in the deposition of yellow plates. The solid was isolated by decanting the supernatant and drying briefly *in vacuo* (2.2 mg, 15% yield). ^{1}H NMR (25 °C, 500 MHz, toluene-d_8): δ 6.37 (t, J = 7.7 Hz, 2H, *m*-H), 4.48 (t, J = 6.8 Hz, 2H, *m*-H), 4.21 (t,

J = 7.9 Hz, 1H, *p*-H), 4.17 (t, *J* = 6.7 Hz, 1H, *p*-H), –0.46 (d, *J* = 7.9 Hz, 2H, *o*-H), –2.87 (s, 15H, Cp), –5.98 (d, *J* = 6.2 Hz, 2H, *o*-H), –212.48 (s, 2H, H_α). ^{2}H NMR (25 °C, 76.75 MHz, toluene-h_8): δ –31.79 (s, H_β).

6.4.11 Synthesis of [K(2.2.2-cryptand)][Cp$_3$U(η^1-3,3-diphenylallyl)] (6.5) via Photolysis of [K(2,2,2-cryptand)][Cp$_3$U(2,2-diphenylcyclopropyl)] (6.3).

Dark red crystals of **6.3** (31.4 mg, 0.0301 mmol) were dissolved in THF-d_8 (2 mL), resulting in formation of a dark red solution. This solution was transferred to an NMR tube equipped with a J-Young valve, brought out of the glovebox and exposed to light from a water-jacketed, medium-pressure mercury lamp at room temperature. After 9h, the NMR tube was brought back into glovebox and the solution was filtered through a Celite column (0.5 cm × 2 cm) supported on glass wool to afford a dark yellow-orange filtrate. The volume of the filtrate was reduced to 1 mL *in vacuo*. Pentane (3 mL) was then layered onto the solution, and the vial was stored at –25 °C for 24 h, which resulted in the deposition of dark yellow plates. The solid was isolated by decanting the supernatant and drying briefly *in vacuo* (16.5 mg, 53% yield). ^{1}H NMR (25 °C, 400 MHz, THF-d_8): δ 6.53 (br s, 2H, *m*-H), 5.77 (br s, 2H, *m*-H), 5.02 (br s, 1H, *p*-H), 4.58 (br s, 1H, *p*-H), 3.74 (s, 12H, OCH_2CH_2O), 3.71 (t, *J* = 4.5 Hz, 12H, OCH_2CH$_2$N), 2.73 (t, *J* = 4.5 Hz, 12H, OCH$_2$CH_2N), 1.59 (br s, 2H, *o*-H), –0.78 (br s, 2H, *o*-H), –14.98 (s, 15H, Cp), –20.13 (s, 1H, H_β), –118.19 (s, 2H, H_α).

6.4.12 *In Situ* Preparation of [K(2.2.2-cryptand)][Cp$_3$U(η^1-2-deutero-3,3-diphenylallyl)] (6.5-d_1) in THF-d_8.

Dark red crystals of **6.3**-d_1 (8.1 mg, 0.008 mmol) were dissolved in THF-d_8 (1 mL), resulting in formation of a dark red solution. This solution was transferred to an NMR tube

equipped with a J-Young valve, brought out of the glovebox and exposed to light from a water-jacketed, medium-pressure mercury lamp, for 24 h at room temperature. A ^{1}H NMR spectrum of the dark yellow-orange solution was then recorded, which revealed clean formation of **6.5-*d*$_1$** (**Error! Reference source not found.**). ^{1}H NMR (25 °C, 500 MHz, THF-*d*$_8$): δ 6.54 (br s, 2H, *m*-H), 5.72 (br s, 2H, *m*-H), 4.98 (br s, 1H, *p*-H), 4.53 (br s, 1H, *p*-H), 3.66 (s, 12H, OC*H*$_2$C*H*$_2$O), 3.63 (t, *J* = 4.6 Hz, 12H, OC*H*$_2$CH$_2$N), 2.64 (t, *J* = 4.6 Hz, 12H, OCH$_2$C*H*$_2$N), 1.59 (br s, 2H, *o*-H), –0.76 (br s, 2H, *o*-H), –15.06 (s, 15H, Cp), –118.30 (s, 2H, H$_\alpha$).

6.4.13 Synthesis of [K(2.2.2-cryptand)][Cp$_3$U(η^1-3,3-diphenylallyl)] (6.5) via reduction of [Cp$_3$U(η^1-3,3-diphenylallyl)] (6.4).

To a cold (-25 °C), stirring, yellow THF solution (2 mL) of **6.4** (21.8 mg, 0.035 mmol) and 2.2.2-cryptand (13.1 mg, 0.035 mmol) was added KC_8 (5.2 mg, 0.038 mmol) as a brown solid. Upon addition, the solution turned dark yellow-orange. After 10 min, the solution was filtered through a Celite column supported on glass wool (0.5 cm × 2 cm), affording a clear, dark yellow filtrate. Pentane (5 mL) was layered onto the solution, and the vial was stored at –25 °C for 24 h, which resulted in the deposition of dark yellow plates. The solid was isolated by decanting the supernatant and drying briefly *in vacuo* (14.6 mg, 40% yield). Anal. Calcd for $UC_{48}H_{64}KO_6N_2$: C, 55.32; H, 6.19, N, 2.69. Found: C, 55.09; H, 6.35, N, 2.65. ^{1}H NMR (500 MHz, THF-*d*$_8$): δ 6.53 (br s, 2H, *m*-H), 5.73 (br s, 2H, *m*-H), 4.99 (br s, 1H, *p*-H), 4.55 (br s, 1H, *p*-H), 3.66 (s, 12H, OC*H*$_2$C*H*$_2$O), 3.63 (t, *J* = 4.8 Hz, 12H, OC*H*$_2$CH$_2$N), 2.64 (t, *J* = 5.1 Hz, 12H, OCH$_2$C*H*$_2$N), 1.60 (br s, 2H, *o*-H), –0.76 (br s, 2H, *o*-H), –15.05 (s, 15H, Cp), –20.16 (s, 1H, H$_\beta$), –118.23 (s, 2H, H$_\alpha$). IR (KBr pellet, cm^{-1}): 3081 (w), 3052 (w), 2962 (w), 2879 (w), 2819 (w), 2751 (w), 1951 (w), 1592 (w), 1569 (w), 1531 (w), 1479 (m), 1442 (m),

1357 (s), 1294 (m), 1257 (m), 1174 (w), 1130 (s), 1106 (s), 1010 (m), 950 (s), 931 (s), 892 (w), 831 (m), 771 (s), 746 (s), 701 (s), 665 (m) 642 (m), 611 (w), 563 (m), 524 (m).

6.4.14 Synthesis of [Cp$_3$Th(3,3-diphenylallyl)] (6.6) via photolysis of [Cp$_3$Th(2,2-diphenylcyclopropyl)] (6.2).

Colorless crystals of **6.2** (18.5 mg, 0.029 mmol) were dissolved in THF-d_8 (0.7 mL), resulting in formation of a clear colorless solution. This solution was transferred to an NMR tube equipped with a J-Young valve, brought out of the glovebox and was exposed to light from a water-jacketed, medium-pressure mercury lamp for 1 h at room temperature. The color of the solution gradually changed from colorless to yellow over the course of the photolysis. After 1 h, the NMR tube was brought back into glovebox and the solution was filtered through Celite column (0.5 cm × 2 cm) supported on glass wool to afford a clear yellow filtrate. Pentane (2 mL) was layered onto the solution, and the vial was stored at –25 °C for 24 h, which resulted in the deposition of pale yellow plates, however yield was not recorded.

6.4.15 X-Ray Crystallography

Data for all complexes were collected on a Bruker KAPPA APEX II diffractometer equipped with an APEX II CCD detector using a TRIUMPH monochromator with a Mo Kα X-ray source (α = 0.71073 Å). The crystals were mounted on a cryoloop under Paratone-N oil, and all data were collected at 100(2) K using an Oxford nitrogen gas cryostream. Data were collected using ω scans with 0.5° frame widths. X-ray data for **6.1**, **6.3**·0.5THF, **6.4**·toluene, **6.5**·THF, and **6.6**·THF were collected utilizing frame exposures of 15 s, 15 s, 10 s, 30 s, and 15 s respectively. Data collection and cell parameter determination were conducted using the SMART program.[58] Integration of the data frames and final cell parameter refinement were performed using SAINT software.[59] Absorption correction of the data was carried out using the multi-scan method SADABS.[60] Subsequent calculations were carried out using SHELXTL.[61] Structure determination was done using direct or Patterson methods and difference Fourier techniques. All hydrogen atom positions were idealized and rode on the atom of attachment. Structure solution and refinement were performed using SHELXTL.[61] Graphics and creation of publication materials were performed using Diamond.[62]

Complex **6.1** exhibited significant positional disorder, which was addressed by constraining the affected carbon atoms with EADP commands and setting their occupancies to 50%. Because of the severe disorder, hydrogen atoms were not added to the 2,2-diphenylcyclopropyl ligand and three Cp ligands. For complex **6.3**, a THF solvate molecule that sits on a special position exhibited positional disorder, which was addressed by constraining the bond lengths within this fragment with the DFIX command. Hydrogen atoms were not added to disordered THF solvate molecule. For complex **6.4**, a toluene solvate molecule was disordered over two positions in a 50:50 ratio. Hydrogen atoms were not added

to the toluene solvate. For complex **6.5**, one Cp ligand and a THF solvate molecule exhibited unresolved positional disorder, which was addressed by constraining the affected atoms with SADI and EADP commands. For complex **6.6**, one Cp ligand exhibited unresolved positional disorder, which was addressed by constraining the affected atoms with EADP commands.

Complexes **6.1**, **6.3**·0.5THF, **6.4**·toluene, and **6.5**·THF have been deposited in the Cambridge Structural Database (**6.1**: CCDC 2260884; **6.3**·0.5THF: CCDC 2260885; **6.4**·toluene: CCDC 2260886; **6.5**·THF: CCDC 2260887). Further crystallographic details can be found in Table 6.2.

Table 6.2. X-ray Crystallographic Data for Complexes **6.1** and **6.3**·0.5THF, **6.4**·toluene, and **6.5**·THF.

	6.1	**6.3**·0.5THF	**6.4**·toluene	**6.5**·THF
Formula	$C_{30}H_{28}U$	$C_{50}H_{68}KN_2O_{6.5}U$	$C_{37}H_{36}U$	$C_{52}H_{72}KN_2O_7U$
Crystal Habit, Color	Plate, Brown	Plate, Red	Plate, Yellow	Plate, Dark Yellow
Crystal Size (mm)	0.2 × 0.10 × 0.05	0.2 × 0.2 × 0.1	0.25 × 0.25 × 0.1	0.2 × 0.15 × 0.05
MW (g/mol)	626.55	1078.19	718.69	1114.24
crystal system	Orthorhombic	Triclinic	Triclinic	Triclinic
space group	Cmca	P -1	P -1	P -1
a (Å)	8.0925(19)	12.5459(10)	8.9068(8)	9.9866(6)
b (Å)	28.423(6)	14.8402(12)	11.0786(10)	15.5809(10)
c (Å)	20.107(5)	15.4620(11)	14.7983(14)	16.7843(10)
α (°)	90.00	63.405(4)	98.266(5)	88.520(3)
β (°)	90.00	83.565(4)	93.680(5)	87.419(3)
γ (°)	90.00	67.160(4)	91.987(5)	76.486(3)
V ($Å^3$)	4625.0(19)	2365.7(3)	1440.6(2)	2536.4(3)
Z	8	2	2	2
T (K)	100(2)	100(2)	100(2)	100(2)
λ (Å)	0.71073	0.71073	0.71073	0.71073
GOF	1.193	1.344	1.034	1.002
Density (calcd) (Mg/m^3)	1.800	1.514	1.657	1.459
Absorption coefficient (mm^{-1})	7.034	3.569	5.657	3.332
F_{000}	2400	1090	700	1130
Total no Reflections	32510	30512	13000	11284
Unique Reflections	3038	10001	6397	7872
Final R indices*	R_1 = 0.0425, wR_2 = 0.1051	R_1 = 0.0325 wR_2 = 0.0557	R_1 = 0.0322 wR_2 = 0.0658	R_1 = 0.0618 wR_2 = 0.1097
Largest Diff. peak and hole ($e^- A^{-3}$)	2.770, -3.738	1.559, -1.493	1.578, -1.627	1.376, -1.888

*For [I>2σ(I)]

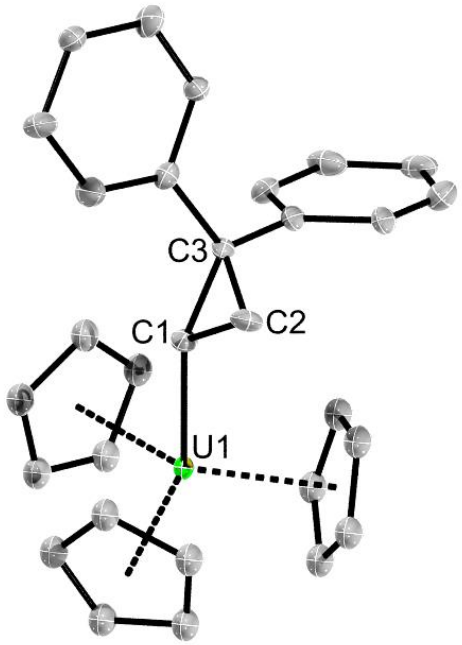

Figure 6.10. Solid state molecular structure of **6.1**, shown with thermal ellipsoids set at 50% probability. A second molecule in the asymmetric unit is omitted for clarity.

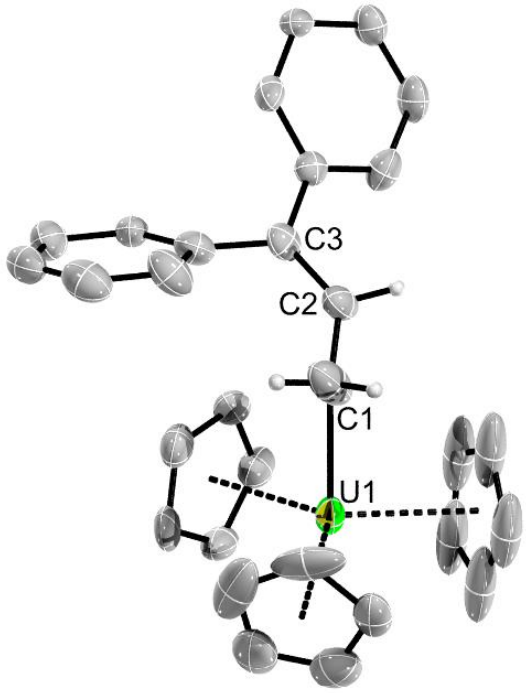

Figure 6.11. Solid state molecular structure of **6.5**, shown with thermal ellipsoids set at 50% probability. A $[K(2.2.2\text{-cryptand})]^+$ counterion, THF solvate, and hydrogen atoms (except those of C_α and C_β) are omitted for clarity.

6.5 Appendix

6.5.1 NMR Spectra

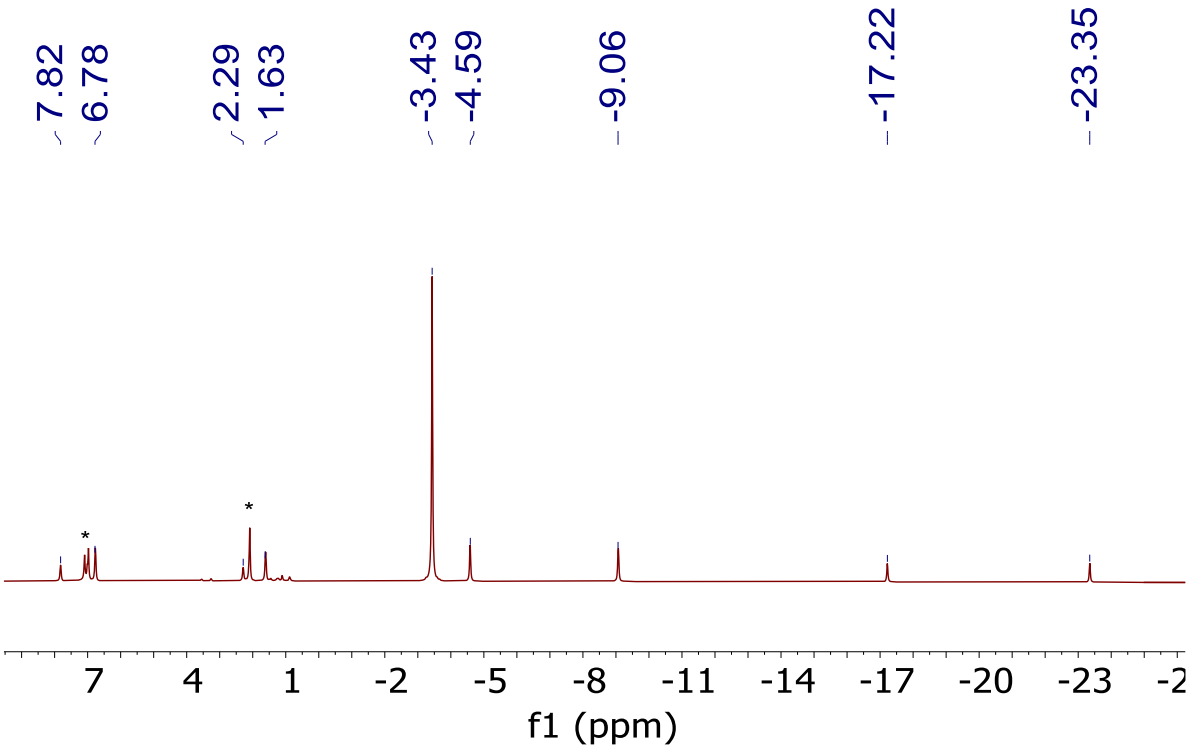

Figure 6.12. ^{1}H NMR spectrum of [Cp_3U(1-deutero-2,2-diphenylcyclopropyl)] (**6.1**-d_1) in toluene-d_8 at room temperature. (*) indicates the presence of toluene-d_8.

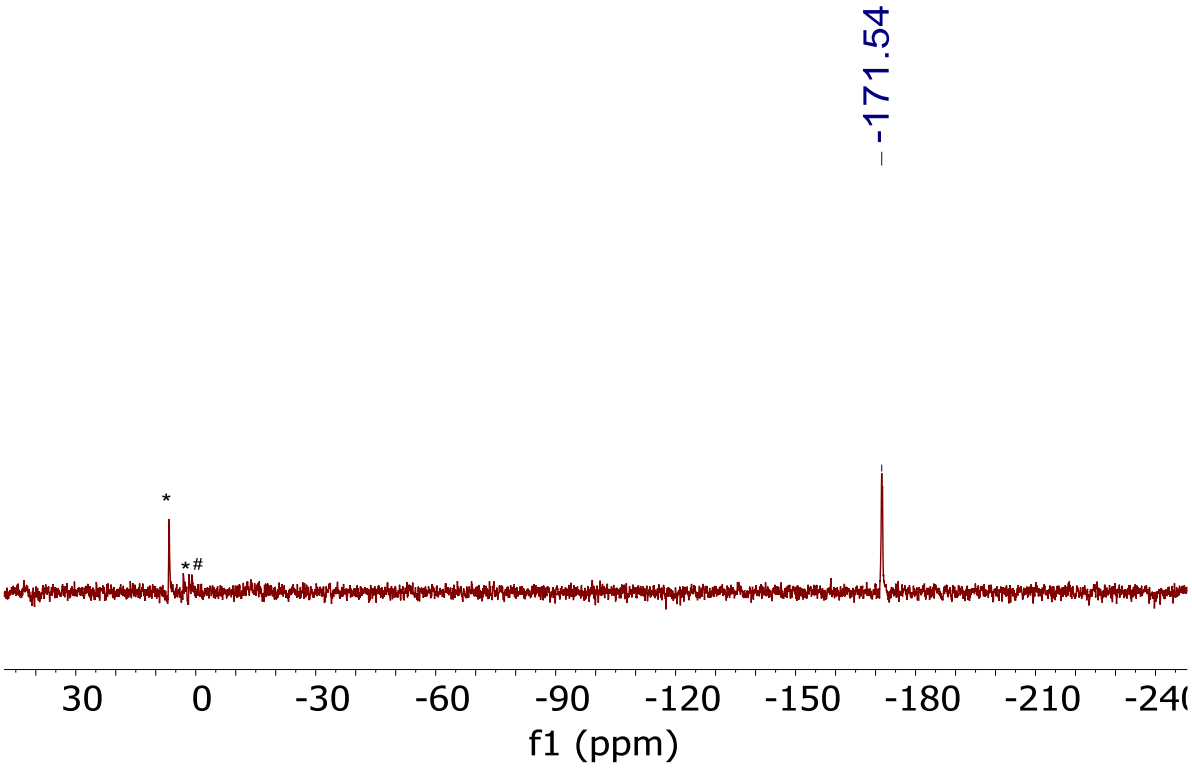

Figure 6.13. ^{2}H NMR spectrum of [Cp_3U(1-deutero-2,2-diphenylcyclopropyl)] (**6.1**-d_1) in toluene at room temperature. (*) indicates the presence of toluene. (#) indicates the presence of hexanes.

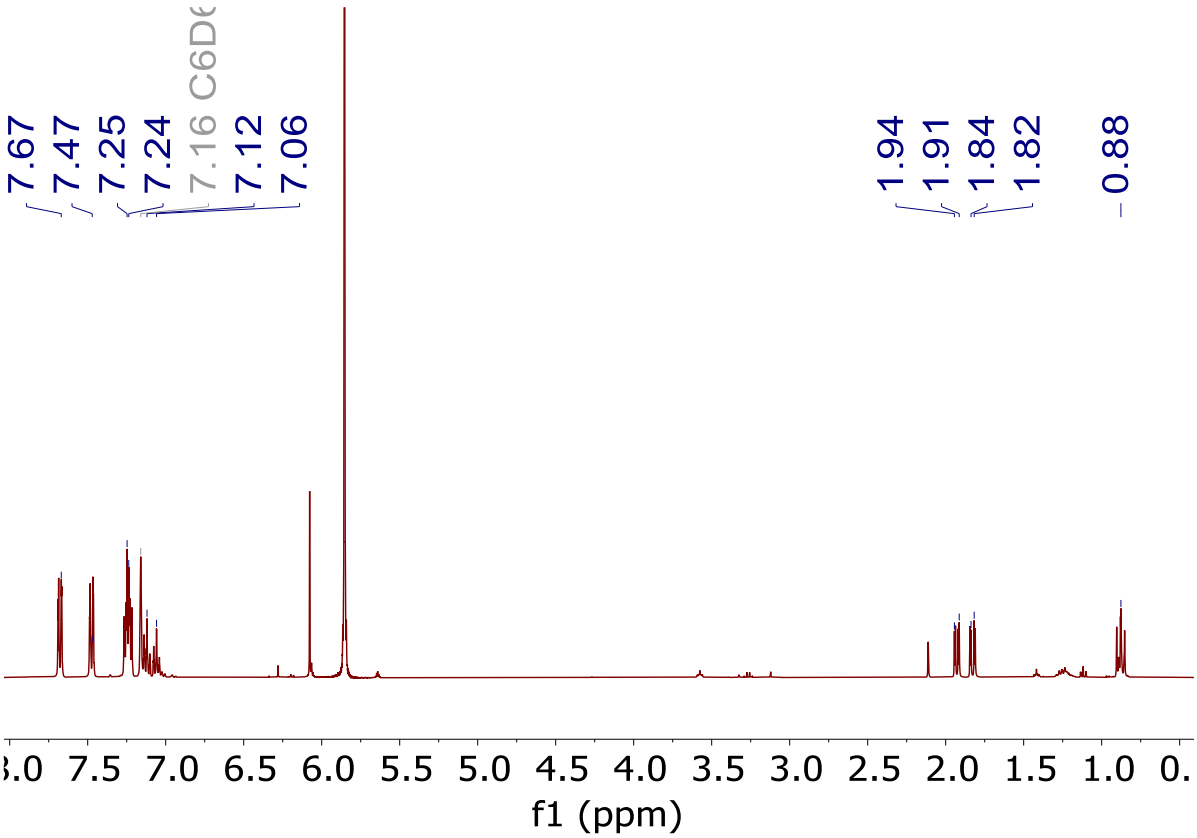

Figure 6.14. ^{1}H NMR spectrum of [Cp3Th(2,2-diphenylcyclopropyl)] (**6.2**) in benzene-d6 at room temperature

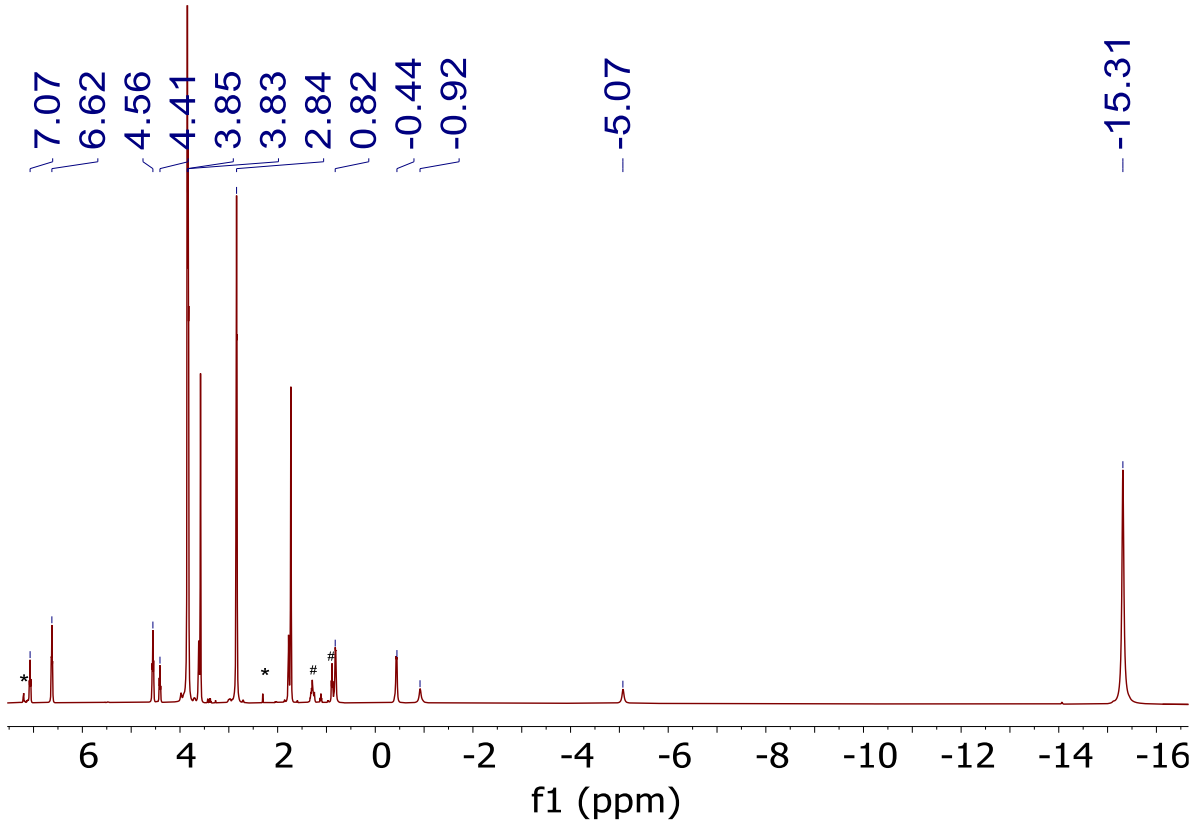

Figure 6.15. ^{1}H NMR spectrum of [K(2.2.2-cryptand)][Cp_3U(1-deutero-2,2-diphenylcyclopropyl)] (**6.3**-d_1) in THF-d_8 at room temperature. (*) indicates the presence of toluene and (#) indicates the presence of hexanes.

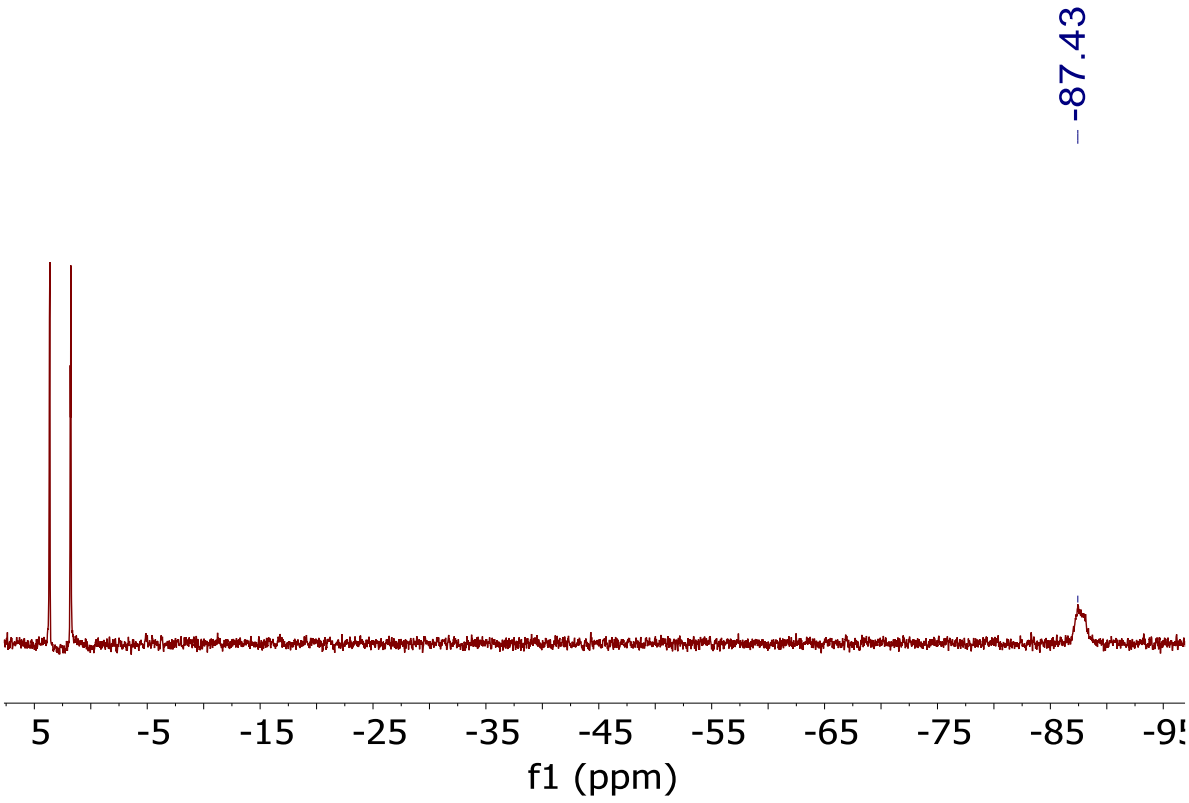

Figure 6.16. ^{2}H NMR spectrum of [K(2.2.2-cryptand)][Cp_3U(1-deutero-2,2-diphenylcyclopropyl)] (**6.3**-d_1) in THF-d_8 at room temperature.

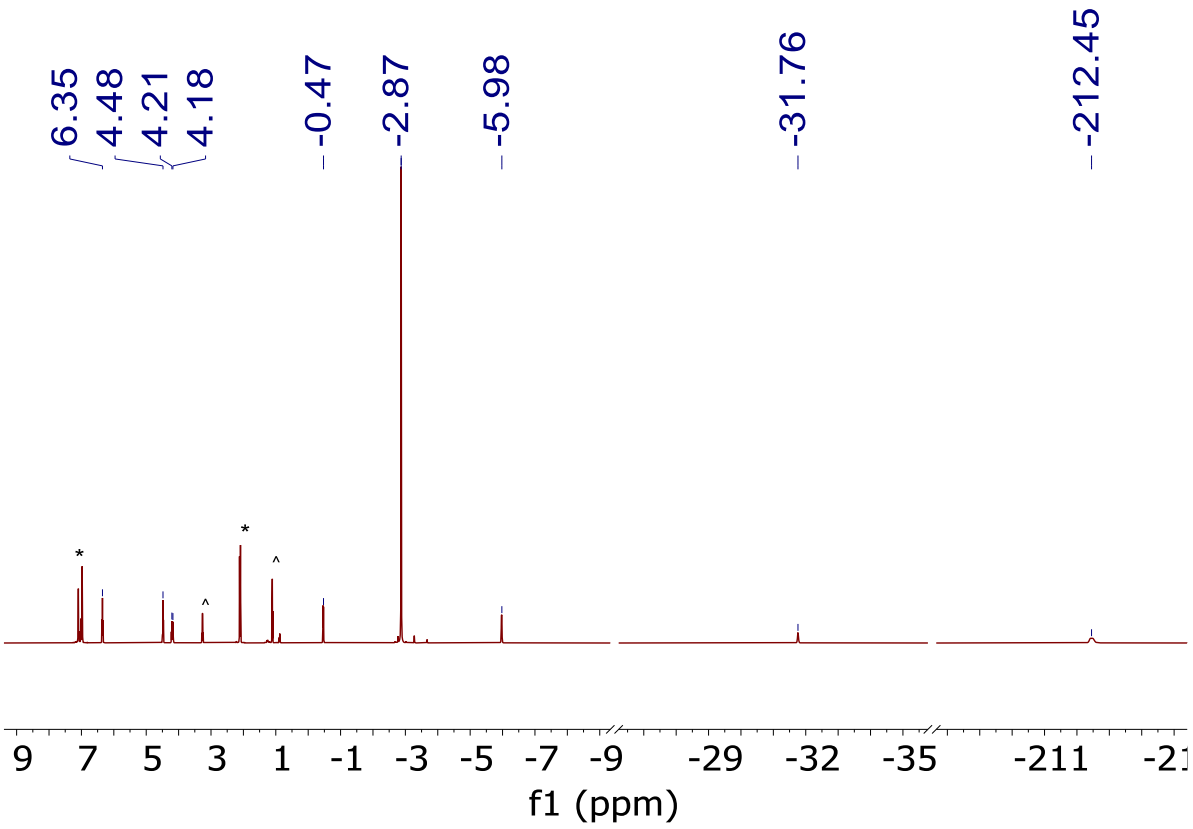

Figure 6.17. ^{1}H NMR spectrum of [$Cp_3U(\eta^1$-3,3-diphenylallyl)] (**6.4**) via photolysis of **6.1** in toluene-d_8 at room temperature. (*) indicates the presence of toluene. (^) indicates the presence of Et_2O.

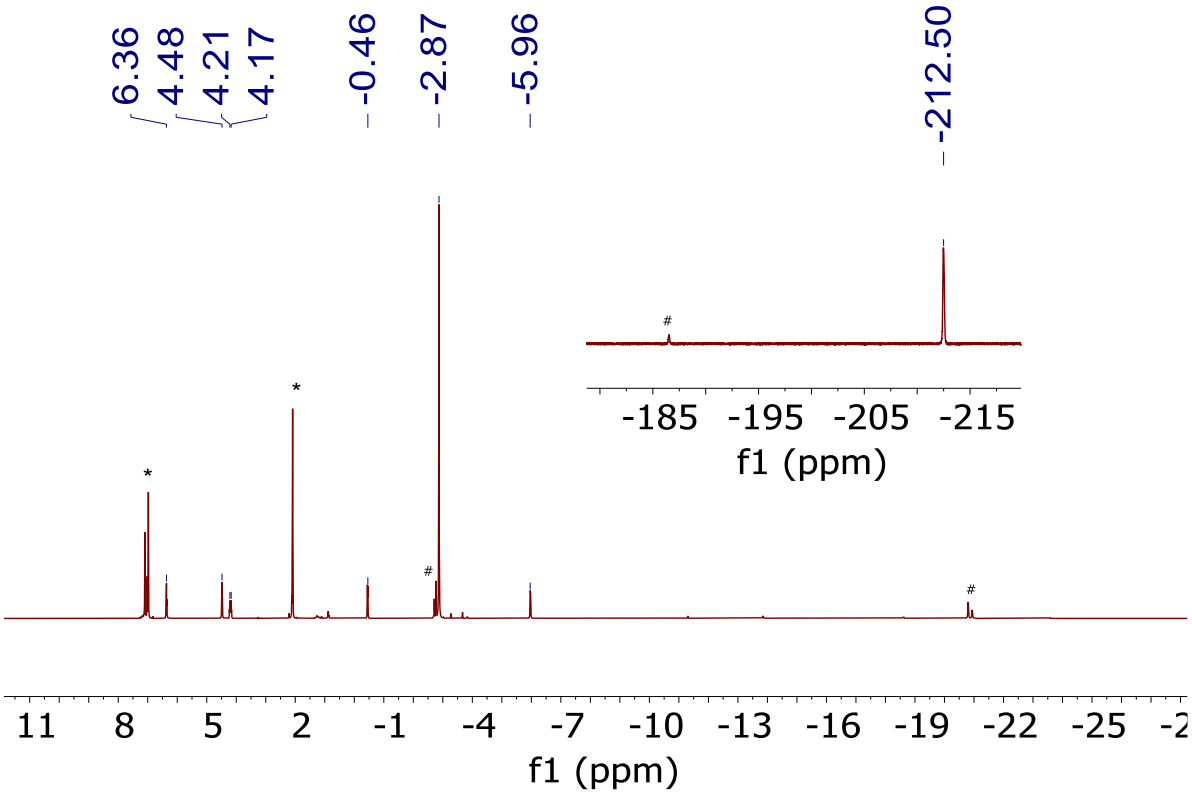

Figure 6.18. ^{1}H NMR spectrum of [Cp3U(η1-2-deutero-3,3-diphenylallyl)] (**6.4**-d_1) formed via thermolysis of **6.1**-d_1 in toluene-d_8 at room temperature. (*) indicates the presence of toluene. (#) indicates the presence of an unidentified decomposition product.

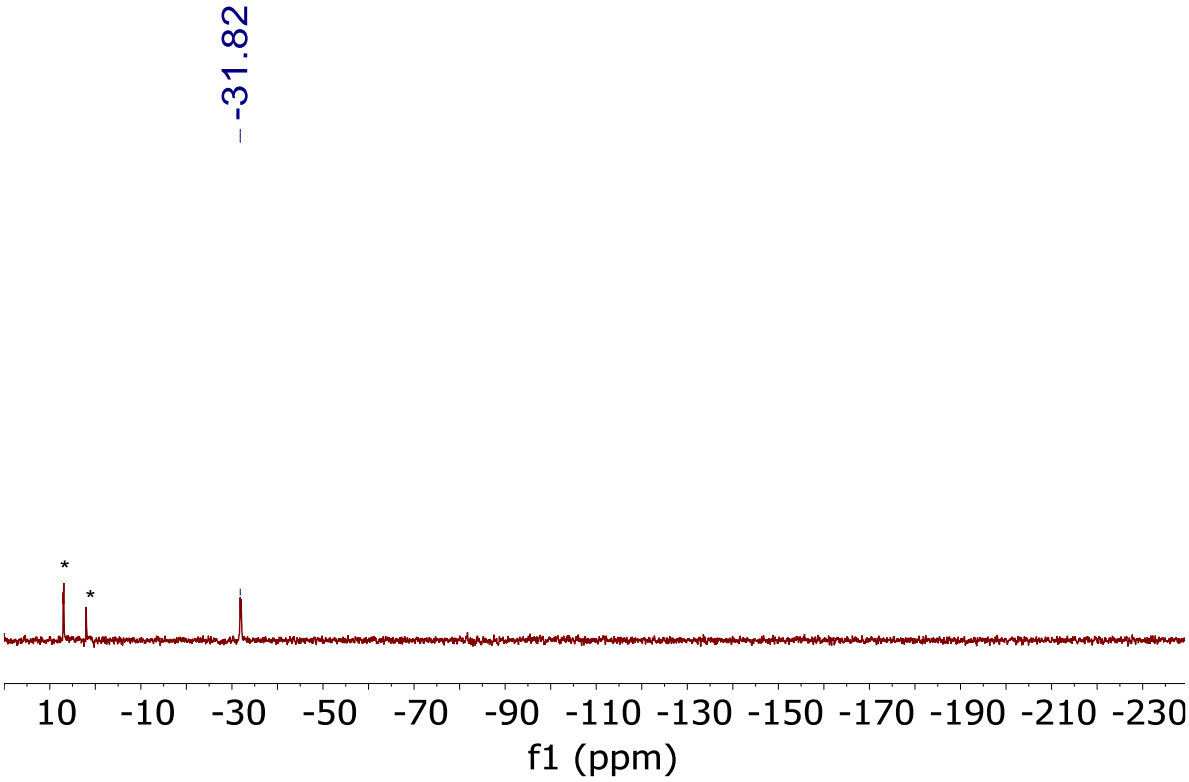

Figure 6.19. ^{2}H NMR spectrum of [$Cp_3U(\eta^1$-2-deutero-3,3-diphenylallyl)] (**6.4**-d_1) formed via thermolysis of **6.1**-d_1 in toluene-h_8 at room temperature. (*) indicates the presence of toluene.

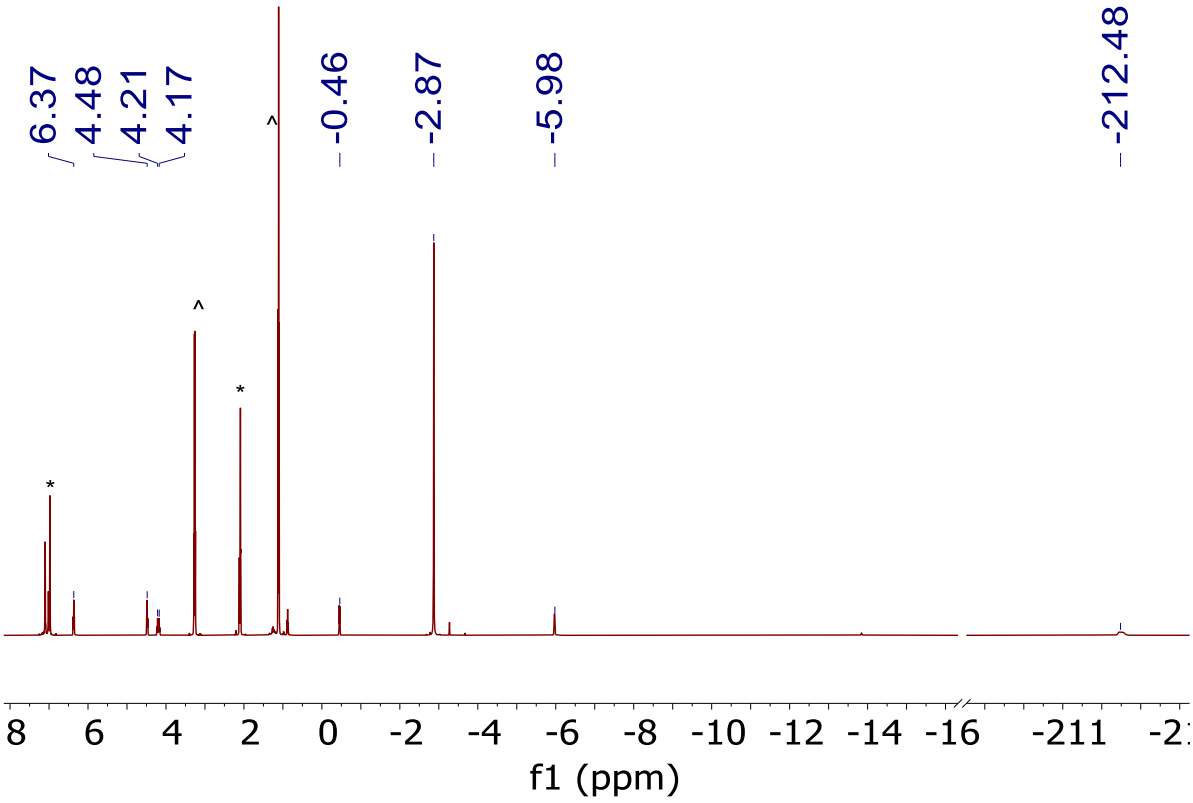

Figure 6.20. ^{1}H NMR spectrum of [$Cp_3U(\eta^1$-2-deutero-3,3-diphenylallyl)] (**6.4**-d_1) formed via photolysis of **6.1**-d_1 in toluene-d_8 at room temperature. (*) indicates the presence of toluene and (^) indicates the presence of Et_2O.

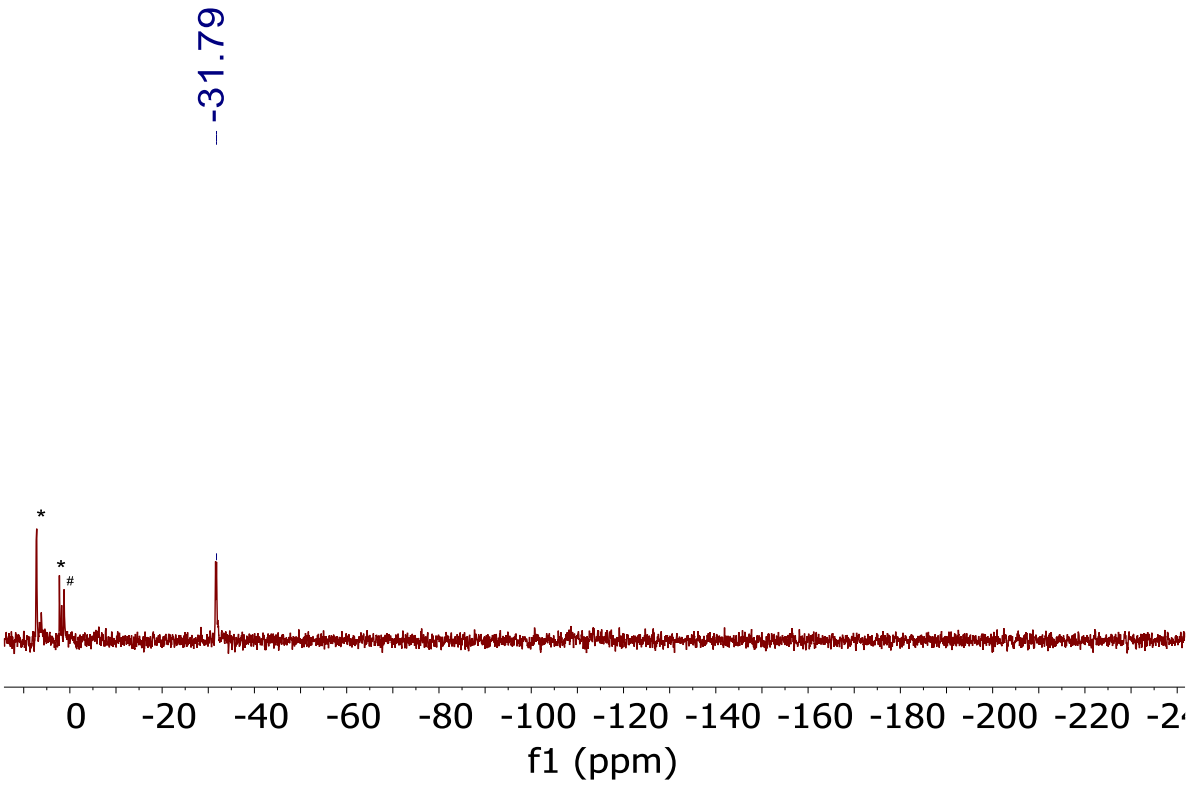

Figure 6.21. ^{2}H NMR spectrum of [$Cp_3U(\eta^1$-2-deutero-3,3-diphenylallyl)] (**6.4**-d_1) formed via photolysis of **6.1**-d_1 in toluene-h_8 at room temperature. (*) indicates the presence of toluene. (#) indicates the presence of hexanes.

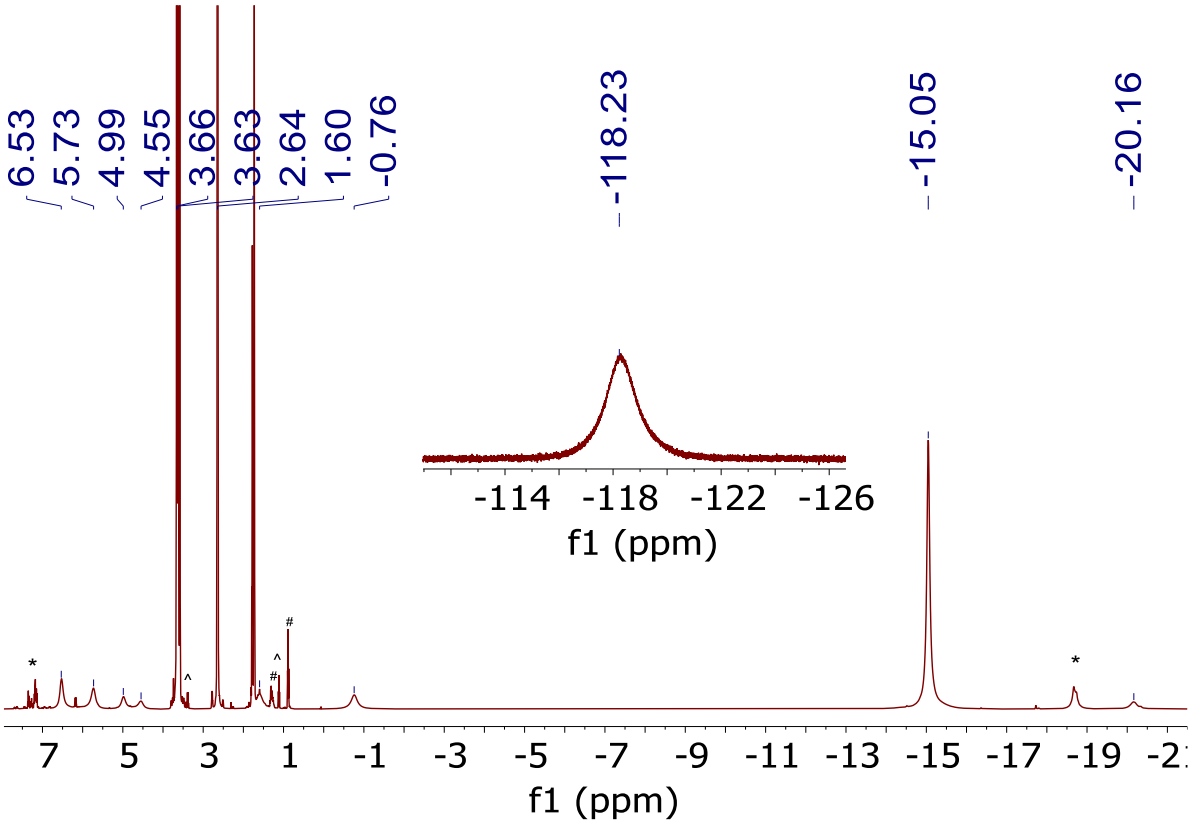

Figure 6.22. ^{1}H NMR spectrum of [K(2.2.2-cryptand)][$Cp_3U(\eta^1$-3,3-diphenylallyl)] (**6.5**) formed via reduction of **6.4** in THF-d_8 at room temperature. (*) indicates the presence of an unidentified decomposition product, (#) indicates the presence of hexanes, and (^) indicates the presence of Et_2O.

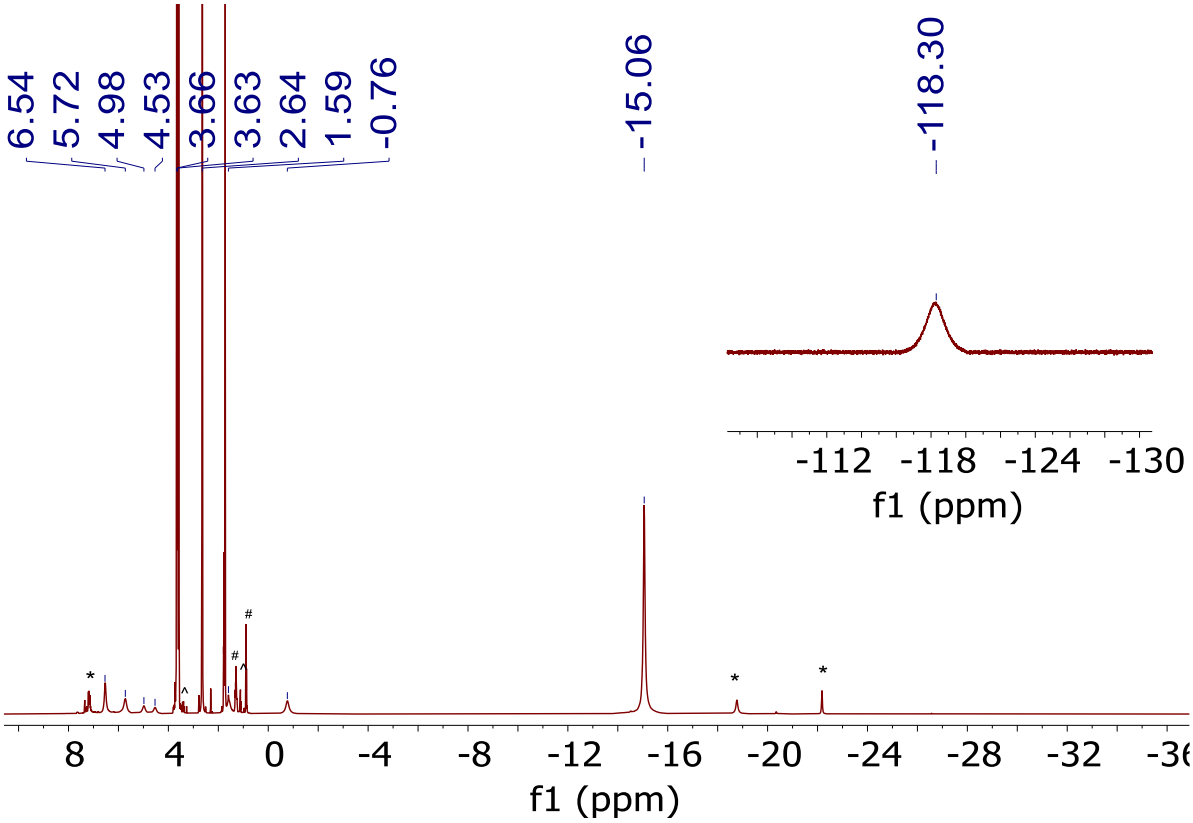

Figure 6.23. ^{1}H NMR spectrum of in situ generated **6.5**-d_1 in THF-d_8 at room temperature. (*) indicates the presence of an unidentified decomposition product, (#) indicates the presence of hexanes, and (^) indicates the presence of Et2O.

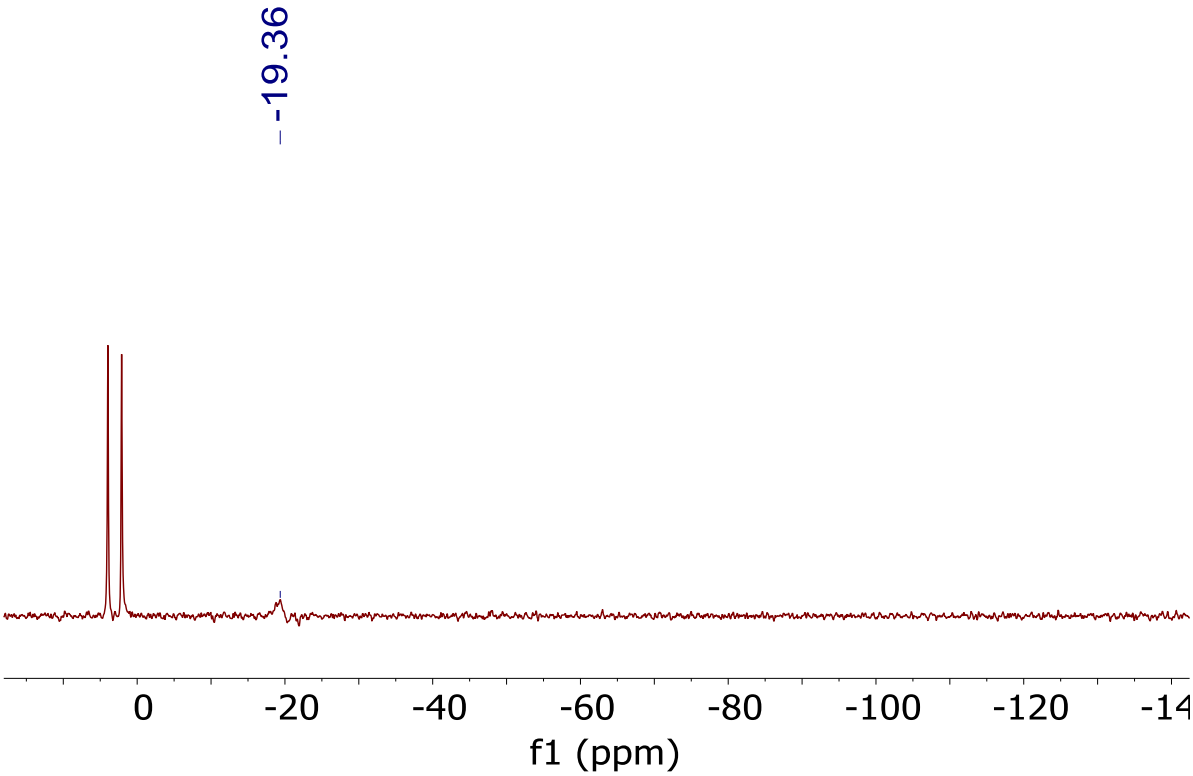

Figure 6.24. ^{2}H NMR spectrum of *in situ* generated **6.5**-d_1 in THF-h_8 at room temperature.

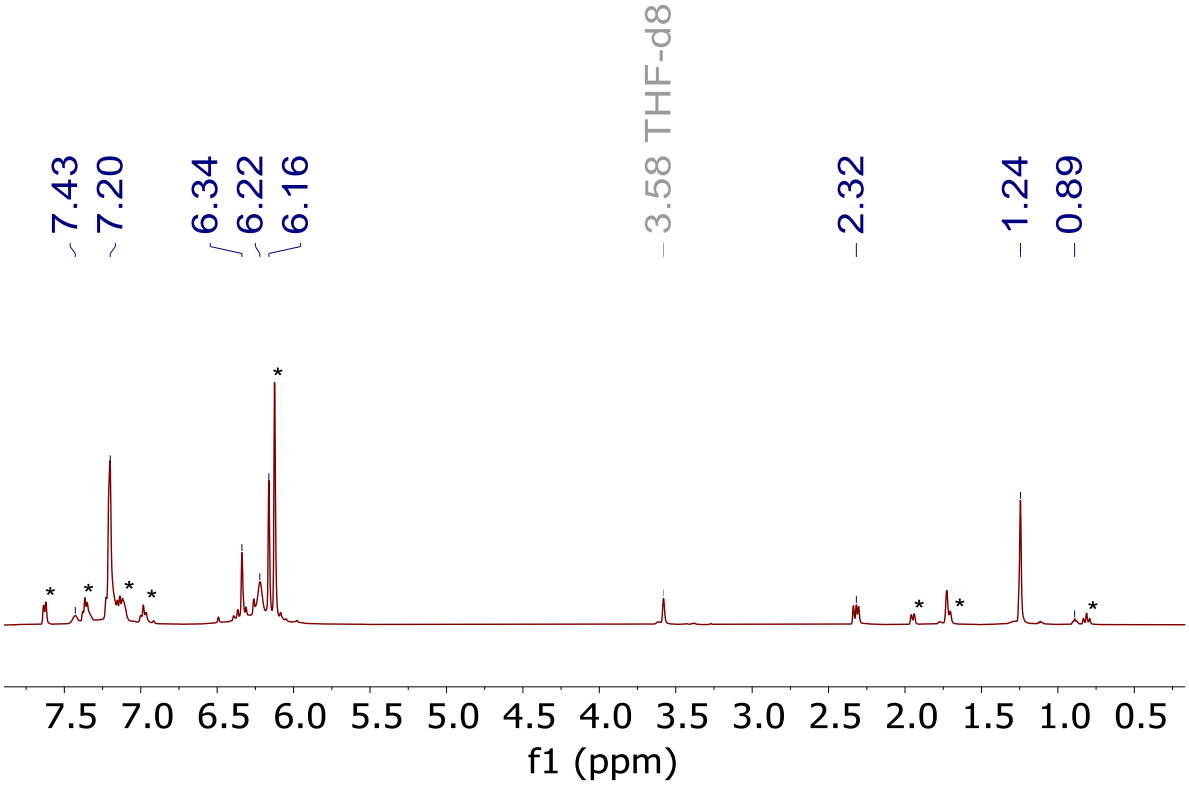

Figure 6.25. ^{1}H NMR spectrum of **6.2** after photolysis using a water-jacketed, medium-pressure Hg lamp, for 1 h at room temperature inTHF-d_8.

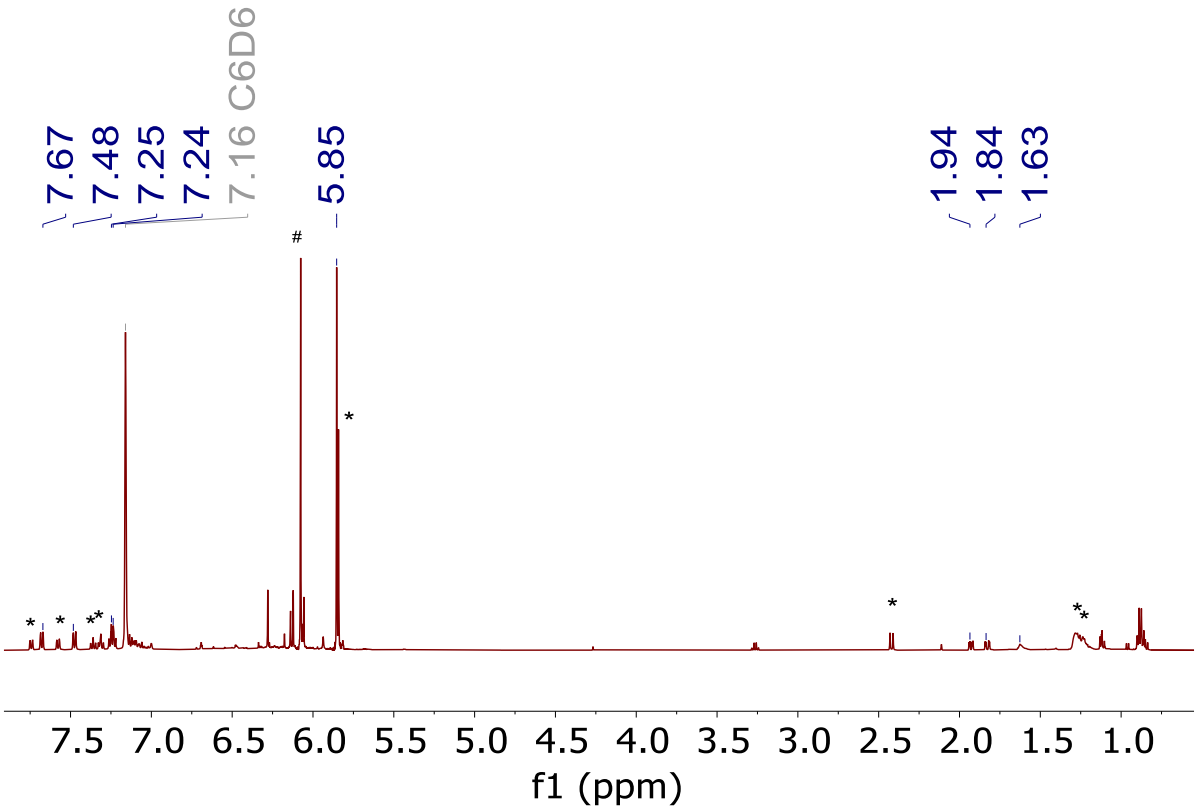

Figure 6.26. ^{1}H NMR spectrum of **6.6** in benzene-d_6 at room temperature. (*) indicates the presence of **6.2** and (#) indicates the presence of Cp_3ThCl.

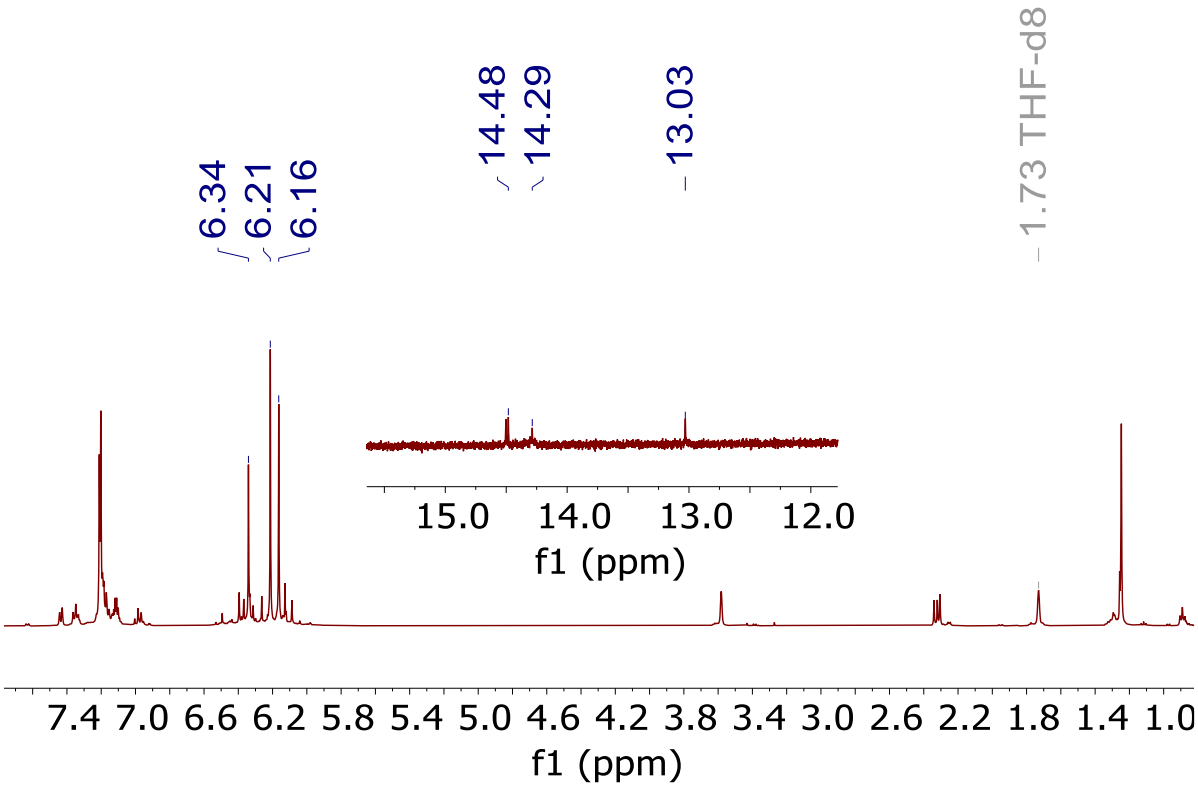

Figure 6.27. ^{1}H NMR spectrum of **6.2** in THF-d_8 after photolysis for 3 h at room temperature.

Experimental details: Colorless crystals of **6.2** (9.3 mg, 0.015 mmol) were dissolved in THF-d_8 (0.7 mL), resulting in formation of a clear colorless solution. This solution was transferred to an NMR tube equipped with a J-Young valve, brought out of the glovebox, and was exposed to light from a water-jacketed, medium-pressure mercury lamp for 3 h at room temperature. The color of the solution changed from colorless to dark green over the course of the photolysis. The ^{1}H NMR spectrum was recorded.

6.5.2 IR Spectra

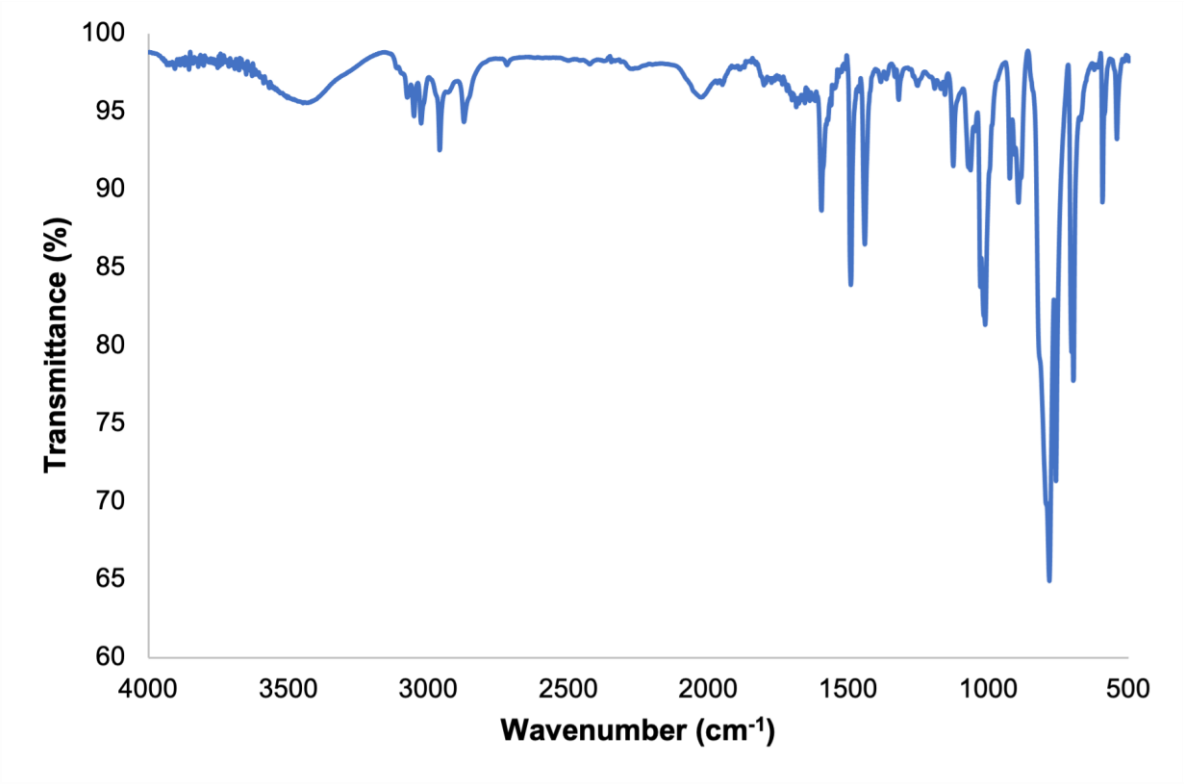

Figure 6.28. IR spectrum of **6.1** (KBr Pellet).

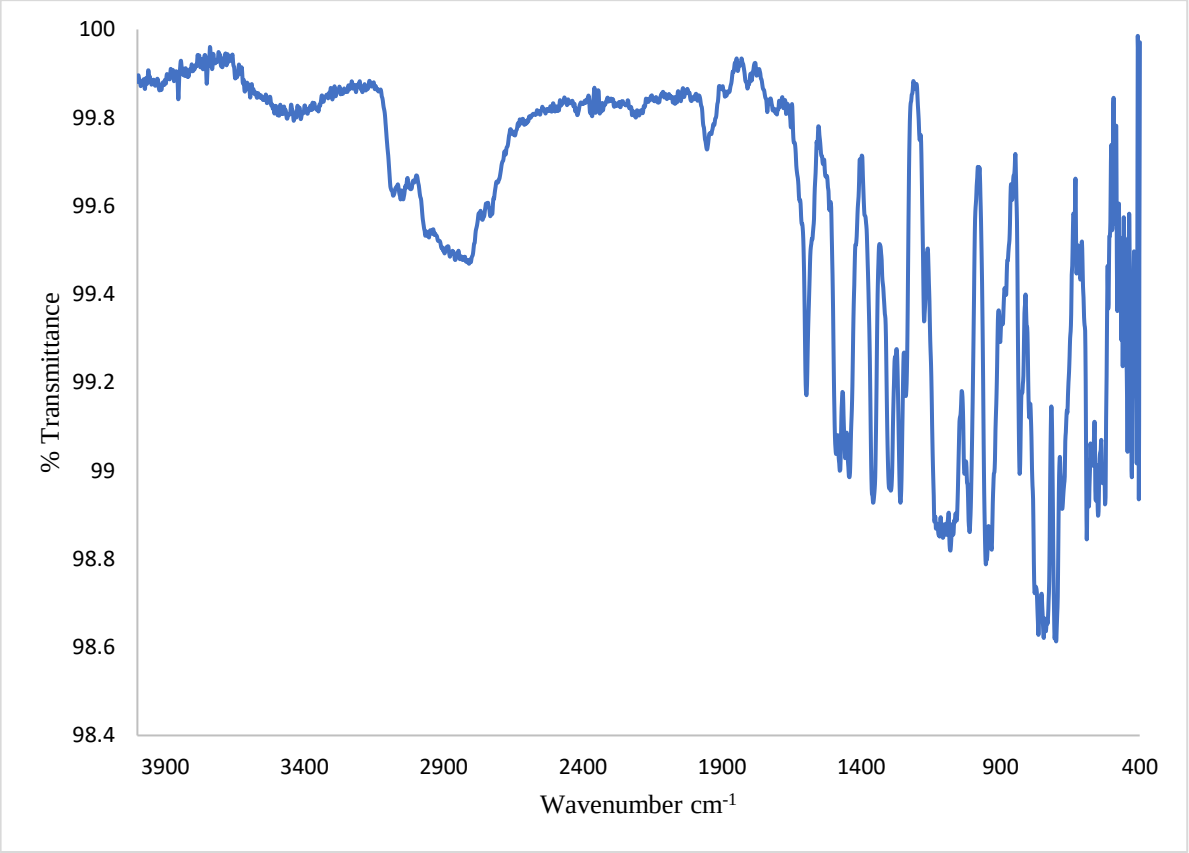

Figure 6.29. IR spectrum of **6.3** (KBr Pellet).

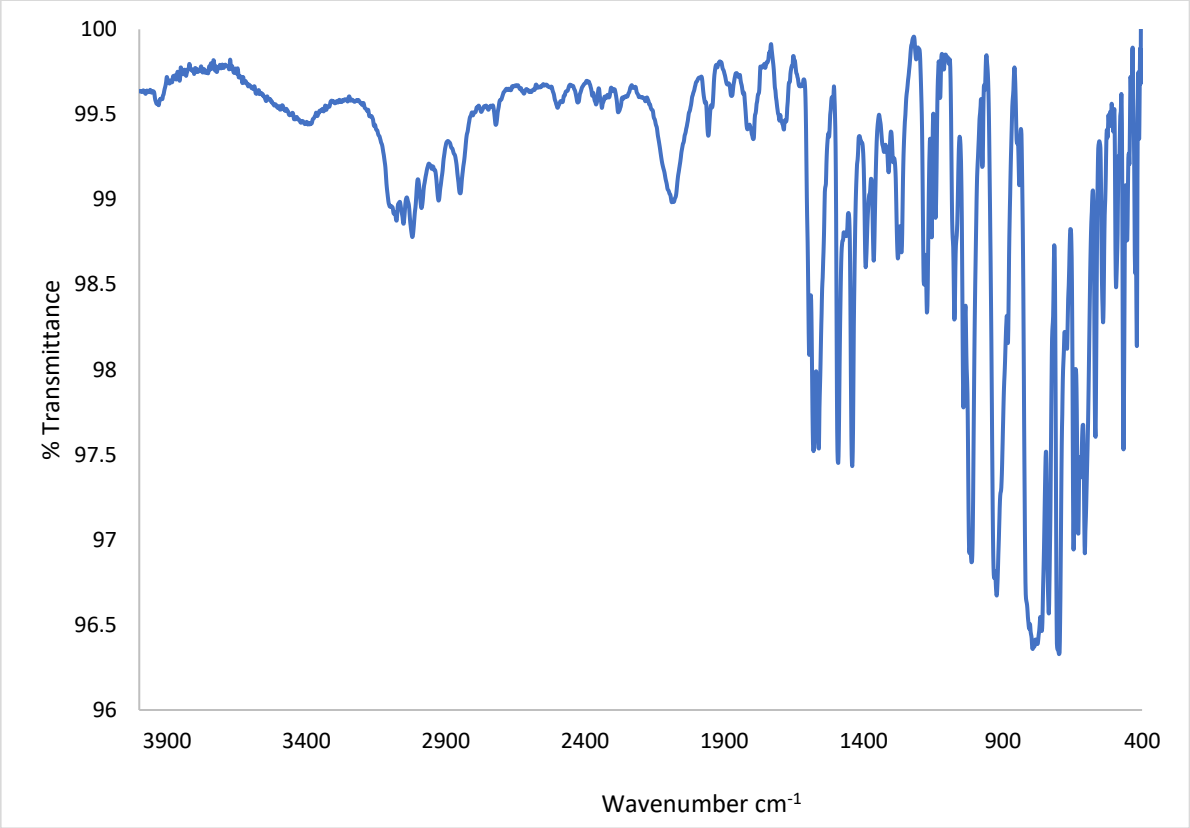

Figure 6.30. IR spectrum of **6.4** (KBr Pellet).

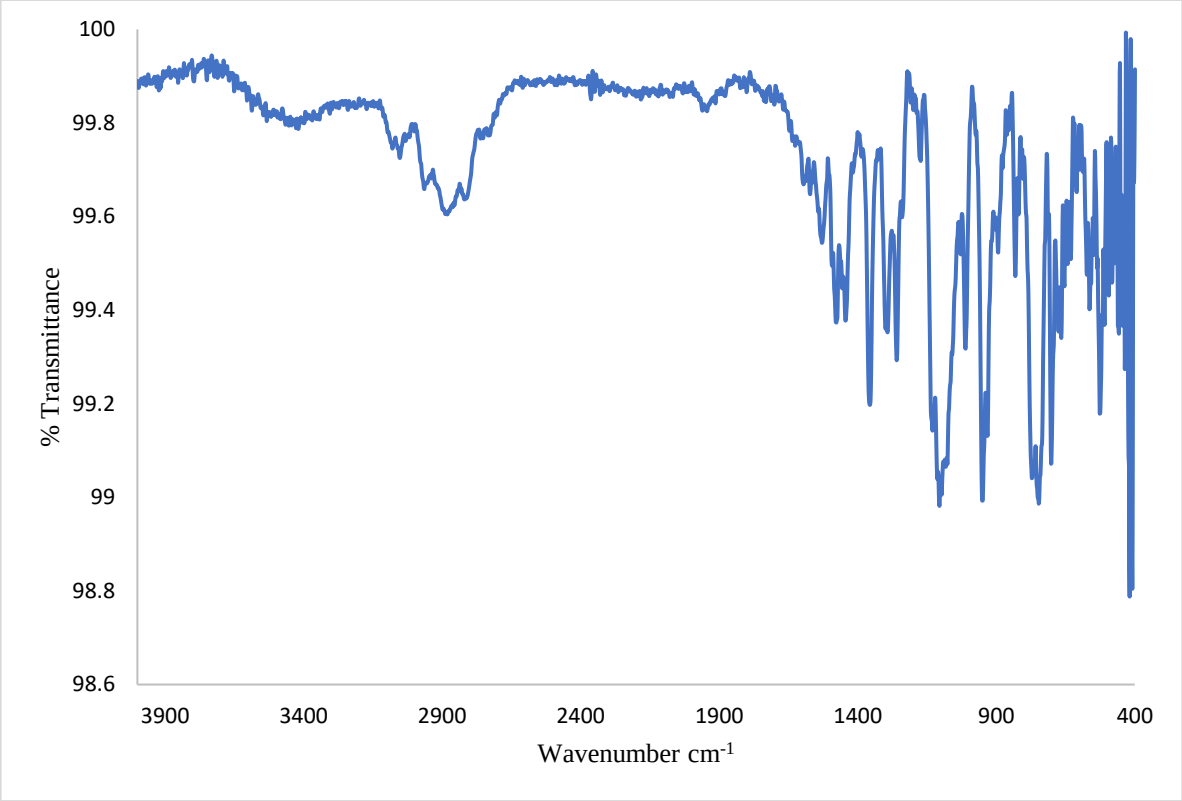

Figure 6.31. IR spectrum of **6.5** (KBr Pellet).

6.5.3 UV-vis Spectra

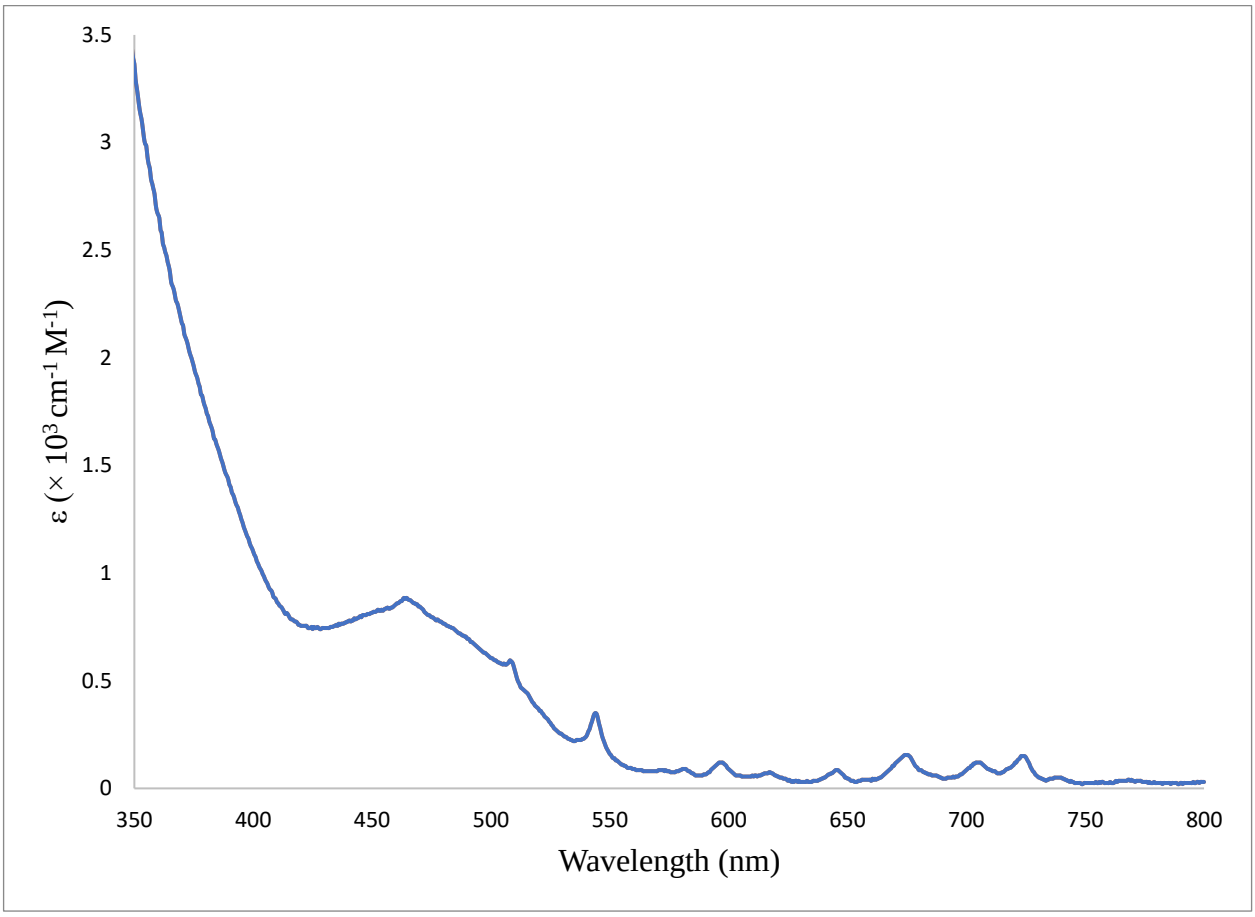

Figure 6.32. Electronic absorption spectrum of **6.1** (0.2 mM, THF).

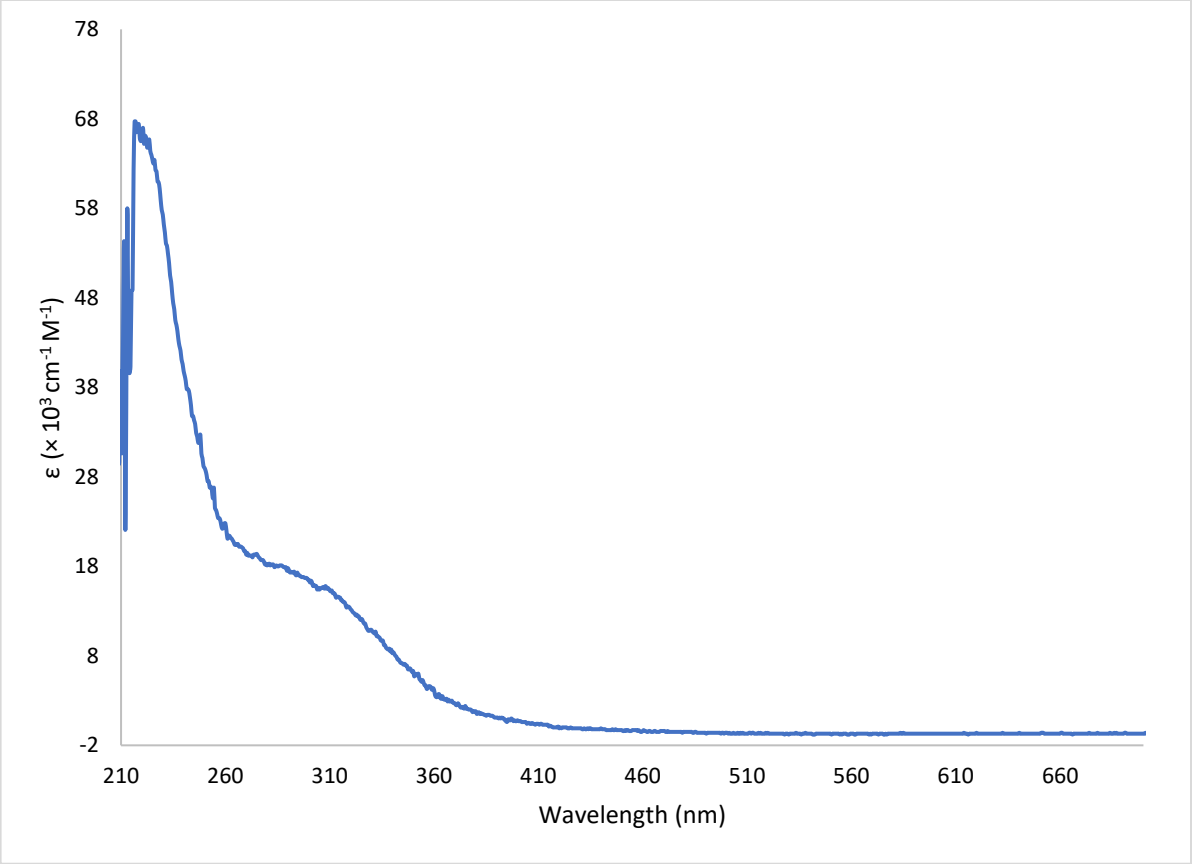

Figure 6.33. Electronic absorption spectrum of **6.2** (10 μM, THF).

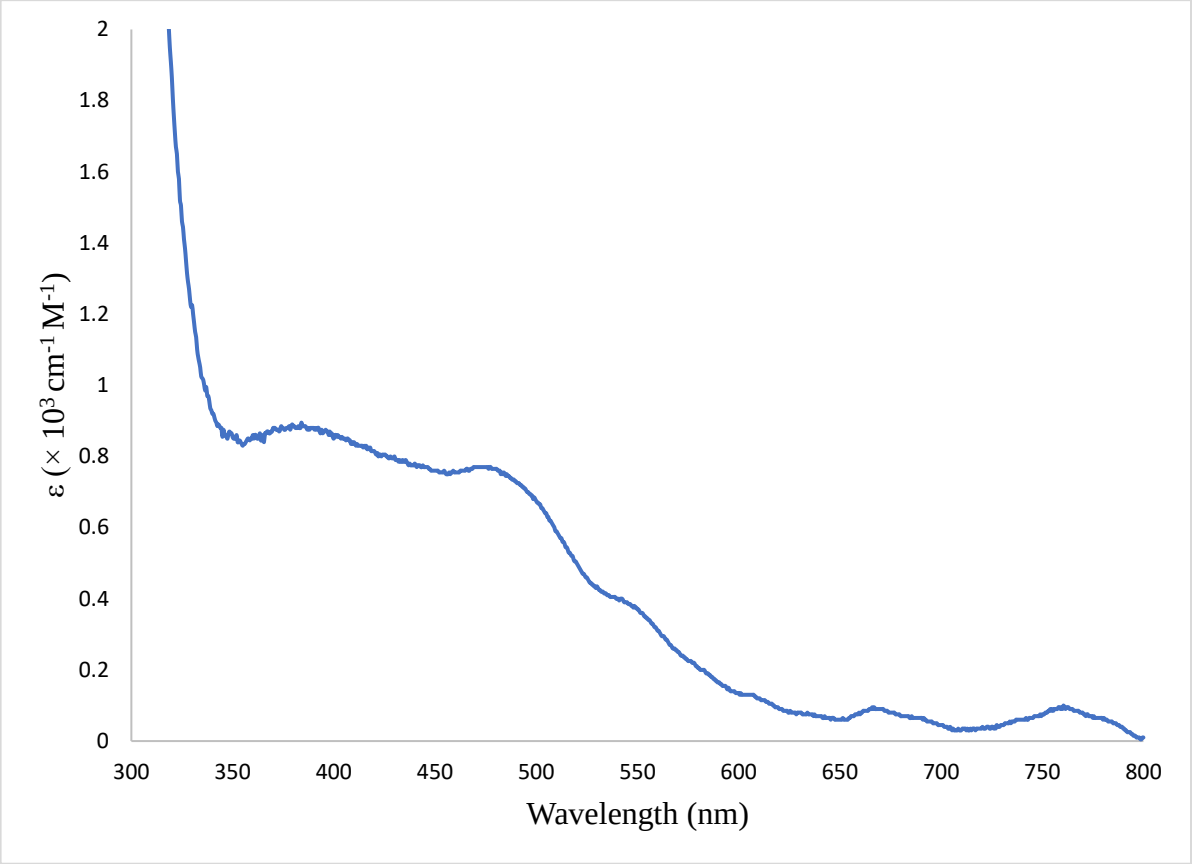

Figure 6.34. Electronic absorption spectrum of **6.3** (0.2 mM, THF).

6.6 References

(1) Hayton, T. W. Recent developments in actinide-ligand multiple bonding. *Chem. Commun.* **2013**, *49*, 2956-2973.
(2) Hayton, T. W. Metal-ligand multiple bonding in uranium: structure and reactivity. *Dalton Trans.* **2010**, *39*, 1145-1158.
(3) Liddle, S. T. The Renaissance of Non-Aqueous Uranium Chemistry. *Angew. Chem. Int. Ed.* **2015**, *54*, 8604-8641.
(4) Gregson, M.; Wooles, A. J.; Cooper, O. J.; Liddle, S. T. Covalent Uranium Carbene Chemistry. *Comments Inorg. Chem.* **2015**, *35*, 262-294.
(5) Kiplinger, J. L.; Morris, D. E.; Scott, B. L.; Burns, C. J. Enhancing the reactivity of uranium(vi) organoimido complexes with diazoalkanes. *Chem. Commun.* **2002**, 30-31.
(6) Lam, O. P.; Feng, P. L.; Heinemann, F. W.; O'Connor, J. M.; Meyer, K. Charge-Separation in Uranium Diazomethane Complexes Leading to C-H Activation and Chemical Transformation. *J. Am. Chem. Soc.* **2008**, *130*, 2806-2816.
(7) Roussel, P.; Boaretto, R.; Kingsley, A. J.; Alcock, N. W.; Scott, P. Reactivity of a triamidoamine complex of trivalent uranium. *J. Chem. Soc., Dalton Trans.* **2002**, 1423-1428.
(8) Ren, W.; Zhou, E.; Fang, B.; Hou, G.; Zi, G.; Fang, D.-C.; Walter, M. D. Experimental and Computational Studies on the Reactivity of a Terminal Thorium Imidometallocene towards Organic Azides and Diazoalkanes. *Angew. Chem. Int. Ed.* **2014**, *53*, 11310-11314.
(9) Matson, E. M.; Fanwick, P. E.; Bart, S. C. Diazoalkane Reduction for the Synthesis of Uranium Hydrazonido Complexes. *Eur. J. Inorg. Chem.* **2012**, *2012*, 5471-5478.
(10) Settineri, N. S.; Shiau, A. A.; Arnold, J. Two-electron oxidation of a homoleptic U(III) guanidinate complex by diphenyldiazomethane. *Chem. Commun.* **2018**, *54*, 10913-10916.
(11) Cantat, T.; Graves, C. R.; Scott, B. L.; Kiplinger, J. L. Challenging the Metallocene Dominance in Actinide Chemistry with a Soft PNP Pincer Ligand: New Uranium Structures and Reactivity Patterns. *Angew. Chem. Int. Ed.* **2009**, *48*, 3681-3684.
(12) Gardner, B. M.; Patel, D.; Lewis, W.; Blake, A. J.; Liddle, S. T. Photochemically Promoted Bond-Cleavage and -Capture in a Diazomethane Derivative of a Triamidoamine Uranium(IV) Complex. *Angew. Chem. Int. Ed.* **2011**, *50*, 10440-10443.
(13) Kiplinger, J. L.; John, K. D.; Morris, D. E.; Scott, B. L.; Burns, C. J. [(C5Me5)2U(Me)(OTf)]2: A New Reagent for Uranium Metallocene Chemistry. Preparation of the First Actinide Hydrazonato Complexes. *Organometallics* **2002**, *21*, 4306-4308.
(14) Crabtree, R. H. The Organometallic Chemistry of the Transition Metals. 3rd ed.; John Wiley & Sons, 2001; pp 292-337.
(15) Bruno, J. W.; Smith, G. M.; Marks, T. J.; Fair, C. K.; Schultz, A. J.; Williams, J. M. C-H Activation Mechanisms and Regioselectivity in the Cyclometallation Reactions of Bis(pentamethylcyclopentadienyl)thorium Dialkyl Complexes. *J. Am. Chem. Soc.* **1986**, *108*, 40-56.
(16) Rungthanaphatsophon, P.; Bathelier, A.; Castro, L.; Behrle, A. C.; Barnes, C. L.; Maron, L.; Walensky, J. R. Formation of Methane versus Benzene in the Reactions of $(C_5Me_5)_2Th(CH_3)_2$ with $[CH_3PPh_3]X$ (X=Cl, Br, I) Yielding Thorium-Carbene or Thorium-Ylide Complexes. *Angew. Chem. Int. Ed.* **2017**, *56*, 12925-12929.
(17) Rungthanaphatsophon, P.; Huang, P.; Walensky, J. R. Phosphorano-Stabilized Carbene Complexes with Short Thorium(IV)– and Uranium(IV)–Carbon Bonds. *Organometallics* **2018**, *37*, 1884-1891.

(18) Cantat, T.; Arliguie, T.; Noël, A.; Thuéry, P.; Ephritikhine, M.; Floch, P. L.; Mézailles, N. The U=C Double Bond: Synthesis and Study of Uranium Nucleophilic Carbene Complexes. *J. Am. Chem. Soc.* **2009**, *131*, 963-972.
(19) Ma, G.; Ferguson, M. J.; McDonald, R.; Cavell, R. G. Actinide Metals with Multiple Bonds to Carbon: Synthesis, Characterization, and Reactivity of U(IV) and Th(IV) Bis(iminophosphorano)methandiide Pincer Carbene Complexes. *Inorg. Chem.* **2011**, *50*, 6500-6508.
(20) Gregson, M.; Lu, E.; Mills, D. P.; Tuna, F.; McInnes, E. J. L.; Hennig, C.; Scheinost, A. C.; McMaster, J.; Lewis, W.; Blake, A. J.; et al. The inverse-trans-influence in tetravalent lanthanide and actinide bis(carbene) complexes. *Nat. Commun.* **2017**, *8*, 14137.
(21) Ren, W.; Deng, X.; Zi, G.; Fang, D.-C. The Th=C double bond: an experimental and computational study of thorium poly-carbene complexes. *Dalton Trans.* **2011**, *40*, 9662-9664.
(22) Lu, E.; Boronski, J. T.; Gregson, M.; Wooles, A. J.; Liddle, S. T. Silyl-Phosphino-Carbene Complexes of Uranium(IV). *Angew. Chem. Int. Ed.* **2018**, *57*, 5506-5511.
(23) Fortier, S.; Walensky, J. R.; Wu, G.; Hayton, T. W. Synthesis of a Phosphorano-Stabilized U(IV)-Carbene via One-Electron Oxidation of a U(III)-Ylide Adduct. *J. Am. Chem. Soc.* **2011**, *133*, 6894-6897.
(24) Smiles, D. E.; Wu, G.; Hrobárik, P.; Hayton, T. W. Synthesis, Thermochemistry, Bonding, and ^{13}C NMR Chemical Shift Analysis of a Phosphorano-Stabilized Carbene of Thorium. *Organometallics* **2017**, *36*, 4519-4524.
(25) Kent, G. T.; Yu, X.; Wu, G.; Autschbach, J.; Hayton, T. W. Synthesis and electronic structure analysis of the actinide allenylidenes, $[\{(NR_2)_3\}An(CCCPh_2)]^-$ (An = U, Th; R = SiMe3). *Chem. Sci.* **2021**, *12*, 14383-14388.
(26) Kent, G. T.; Yu, X.; Wu, G.; Autschbach, J.; Hayton, T. W. Ring-opening of a thorium cyclopropenyl complex generates a transient thorium-bound carbene. *Chem. Commun.* **2022**, *58*, 6805-6808.
(27) Nguyen, T. H.; Yu, X.; Kent, G. T.; Autschbach, J.; Hayton, T. W. U-C Bond Insertion, Ring-opening, and C-H activation in a Uranium Bis(diisopropylamino)cyclopropenylidene (BAC) Adduct. *Organometallics* **2023**, *42*, 1005–1012.
(28) Staun, S. L.; Kent, G. T.; Gomez-Torres, A.; Wu, G.; Fortier, S.; Hayton, T. W. Reductive Coupling of Xylyl Isocyanide Mediated by Low-Valent Uranium. *Organometallics* **2021**, *40*, 2934-2938.
(29) Mokhtarzadeh, C. C.; Moore, C. E.; Rheingold, A. L.; Figueroa, J. S. A Highly-Reduced Cobalt Terminal Carbyne: Divergent Metal- and α-Carbon-Centered Reactivity. *J. Am. Chem. Soc.* **2018**, *140*, 8100-8104.
(30) Conti, N. J.; Crowther, D. J.; Tivakornpannarai, S.; Jones, W. M. Rearrangements of cyclopropanes .sigma. bonded to iron: .alpha.-eliminations to carbene complexes and ring opening to .pi.-allyl complexes. *Organometallics* **1990**, *9*, 175-184.
(31) Omrcen, T.; Conti, N. J.; Jones, W. M. Synthesis and ring-opening reactions of .alpha.-fluoro-substituted cyclopropanes .sigma.-bonded to iron. *Organometallics* **1991**, *10*, 913-917.
(32) Jaffart, J.; Etienne, M.; Reinhold, M.; McGrady, J. E.; Maseras, F. An unprecedented α-C–C agostic interaction in a cyclopropyl tris(pyrazolyl)boratoniobium complex. *Chem. Commun.* **2003**, 876-877.
(33) Xu, C.; Li, G.; Etienne, M.; Leng, X.; Chen, Y. α-C–C agostic interactions and C–H bond activation in scandium cyclopropyl complexes. *Inorganic Chemistry Frontiers* **2020**, *7*, 4822-4831.

(34) Escudié, Y.; Dinoi, C.; Allen, O.; Vendier, L.; Etienne, M. An Unsymmetrical bis C-C Agostic Heterobimetallic Lithium Yttrium Complex. *Angew. Chem. Int. Ed.* **2012**, *51*, 2461-2464.
(35) Parker, K. D. J.; Labat, S.; Sotiropoulos, J.-M.; Miqueu, K.; Pimienta, V.; Vendier, L.; Etienne, M. Allyl Complexes of Tungsten from the Rearrangement of Transient Cyclopropyl Precursors. *Eur. J. Inorg. Chem.* **2019**, *2019*, 4555-4563.
(36) Parker, K. D. J.; Vendier, L.; Etienne, M. Synthesis, Characterization, and Ligand Rearrangement of Tungsten Cyclopropyl Complexes. *Organometallics* **2018**, *37*, 1221-1224.
(37) Oulié, P.; Dinoi, C.; Li, C.; Sournia-Saquet, A.; Jacob, K.; Vendier, L.; Etienne, M. CH Bond Activation of Unsaturated Hydrocarbons by a Niobium Methyl Cyclopropyl Precursor. Cyclopropyl Ring Opening and Alkyne Coupling Reaction. *Organometallics* **2017**, *36*, 53-63.
(38) Tobisch, S. Organolanthanide-Mediated Ring-Opening Ziegler Polymerization (ROZP) of Methylenecycloalkanes: A Theoretical Mechanistic Investigation of Alternative Mechanisms for Chain Initiation of the Samarocene-Promoted ROZP of 2-Phenyl-1-methylenecyclopropane. *Chemistry – A European Journal* **2005**, *11*, 3113-3126.
(39) Kent, G. T. Development of New Methods Towards Actinide-Carbene Fragments. UC Santa Barbara, 2022.
(40) Maercker, A.; Oeffner, K. S.; Girreser, U. Polylithiumorganic compounds. Part 29: C,C Bond cleavage of phenyl substituted and strained carbocycles using lithium metal. *Tetrahedron* **2004**, *60*, 8245-8256.
(41) Morris, D. E.; Da Re, R. E.; Jantunen, K. C.; Castro-Rodriguez, I.; Kiplinger, J. L. Trends in Electronic Structure and Redox Energetics for Early-Actinide Pentamethylcyclopentadienyl Complexes. *Organometallics* **2004**, *23*, 5142-5153.
(42) Mills, D. P.; Moro, F.; McMaster, J.; van Slageren, J.; Lewis, W.; Blake, A. J.; Liddle, S. T. A delocalized arene-bridged diuranium single-molecule magnet. *Nat. Chem.* **2011**, *3*, 454-460.
(43) Fendrick, C. M.; Marks, T. J. Actinacyclobutanes. Thermochemistry based strategies for the ring-opening stoichiometric activation of saturated and olefinic hydrocarbons. *Journal of the American Chemical Society* **1986**, *108*, 425-437.
(44) Matson, E. M.; Kiernicki, J. J.; Fanwick, P. E.; Bart, S. C. Expanding the Family of Uranium(III) Alkyls: Synthesis and Characterization of Mixed-Ligand Derivatives. *European Journal of Inorganic Chemistry* **2016**, *2016*, 2527-2533.
(45) Matson, E. M.; Forrest, W. P.; Fanwick, P. E.; Bart, S. C. Synthesis and Reactivity of Trivalent Tp*U(CH2Ph)2(THF): Insertion vs Oxidation at Low-Valent Uranium–Carbon Bonds. *Organometallics* **2013**, *32*, 1484-1492.
(46) Johnson, S. A.; Bart, S. C. Achievements in uranium alkyl chemistry: celebrating sixty years of synthetic pursuits. *Dalton Transactions* **2015**, *44*, 7710-7726.
(47) Matson, E. M.; Forrest, W. P.; Fanwick, P. E.; Bart, S. C. Functionalization of Carbon Dioxide and Carbon Disulfide Using a Stable Uranium(III) Alkyl Complex. *J. Am. Chem. Soc.* **2011**, *133*, 4948-4954.
(48) Arnaudet, L.; Charpin, P.; Folcher, G.; Lance, M.; Nierlich, M.; Vigner, D. Characterization of the anion $[(\eta^5\text{-}C_5H_5)_3U^{III}\text{-}n\text{-}C_4H_9]^-$. Synthesis and crystal structure of tricyclopentadienyl n-butyluranium(III) lithium cryptate: $[(C_5H_5)_3UC_4H_9]^-[LiC_{14}H_{28}N_2O_4]^+$. *Organometallics* **1986**, *5*, 270-274.

(49) Matson, E. M.; Forrest, W. P.; Fanwick, P. E.; Bart, S. C. Use of Alkylsodium Reagents for the Synthesis of Trivalent Uranium Alkyl Complexes. *Organometallics* **2012**, *31*, 4467-4473.
(50) Zi, G. Recent developments in actinide metallacycles. *Chem. Commun.* **2018**, *54*, 7412-7430.
(51) Webster, C. L.; Ziller, J. W.; Evans, W. J. Synthesis and CO2 Insertion Reactivity of Allyluranium Metallocene Complexes. *Organometallics* **2012**, *31*, 7191-7197.
(52) Shannon, R. D. Revised Effective Ionic Radii and Systematic Studies of Interatomic Distances in Halide and Chalcogenides. *Acta Crystallogr. Sect. A* **1976**, *A32*, 751-767.
(53) Baird, M. S.; Nizovtsev, A. V.; Bolesov, I. G. Bromine–magnesium exchange in gem-dibromocyclopropanes using Grignard reagents. *Tetrahedron* **2002**, *58*, 1581-1593.
(54) Marks, T. J.; Seyam, A. M.; Wachter, W. A.; Halstead, G. W.; Raymond, K. N. Chlorotris(η-Cyclopentadienyl)Complexes of Uranium(IV) and Thorium(IV). In *Inorganic Syntheses*, 1976; pp 147-151.
(55) Huang, J.-H.; Lee, T.-Y.; Swenson, D. C.; Messerle, L. An alkylidene-tethered tantallanorbornadiene from reduction of a tantalum(phenylalkenyl)alkylidene derived from 3,3-diphenylcyclopropene ring opening by $(\eta\text{-}C_5Me_4R)_2Ta_2(\mu\text{-}X)_4$ (Ta=Ta). *Inorganica Chimica Acta* **2003**, *345*, 209-215.
(56) Harris, R. K.; Becker, E. D.; De Menezes, S. M. C.; Granger, P.; Hoffman, R. E.; Zilm, K. W. Further Conventions for NMR Shielding and Chemical Shifts (IUPAC Recommendations 2008). *Magn. Reson. Chem.* **2008**, *46*, 582-598.
(57) Harris, R. K.; Becker, E. D.; Cabral de Menezes, S. M.; Goodfellow, R.; Granger, P. NMR nomenclature: nuclear spin properties and conventions for chemical shifts. IUPAC Recommendations 2001. International Union of Pure and Applied Chemistry. Physical Chemistry Division. Commission on Molecular Structure and Spectroscopy. *Magn. Reson. Chem.* **2002**, *40*, 489-505.
(58) *SMART Apex II*, Version 2.1 ed.; Bruker AXS Inc.: Madison WI, 2005.
(59) *SAINT Software User's Guide*, Version 7.34a ed.; Bruker AXS Inc.: Madison, WI, 2005.
(60) *Sheldrick, G. M. SADABS, University of Gottingen, Germany; 2005*.
(61) *SHELXTL PC*, Version 6.12 ed.; Bruker AXS Inc.:Madison, WI, 2005.
(62) Diamond - Crystal and Molecular Structure Visualization. Crystal Impact - Dr. H. Putz & Dr. K. Brandenburg GbR, Kreuzherrenstr. 102, 53227 Bonn, Germany. http://www.crystalimpact.com/diamond.

Chapter 7. An Actinide Complex with a Nucleophilic Allenylidene Ligand

Portions of this work were published in:

Osvaldo Ordoñez, Xiaojuan Yu, Megan A. Schuerlein, Guang Wu, Jochen Autschbach, and Trevor W. Hayton, An Actinide Complex with a Nucleophilic Allenylidene Ligand. Submitted

Table of Contents

7.1 Introduction

Since their first isolation in 1976,[1, 2] transition metal allenylidenes have elicited considerable interest due to their diverse stoichiometric and catalytic reactivity.[3-16] The observed regiochemistry can generally be understood by examining the underlying electronic structure (and corresponding resonance form) of the allenylidene intermediate involved in these transformations (Scheme 7.1).[17] In particular, calculations on a Ru allenylidene show that the LUMO is located predominately on C_α and C_γ, while the HOMO is on C_β.[18] Calculations on other metal allenylidenes provide a similar bonding picture.[17, 19-21] These findings are consistent with predominance of resonance form **III**, at least for mid- and late-

transition metals, and explains why nucleophiles attack C_α and C_γ, whereas electrophiles attack C_β.[22, 23] Numerous reactivity studies support this bonding picture. For example, ruthenium-catalyzed substitutions of propargylic alcohols occurs via regioselective nucleophilic attack at C_γ of the allenylidene intermediate.[24-35] Similarly, reaction of [(η^5-1,2,3-$Me_3C_9H_4$)Ru($CCCPh_2$)(CO)(PPh_3)][BF_4] with ROH (R= Me, Et) or NaR (R = OMe, CCH) results in nucleophilic addition to C_α and C_γ, respectively.[36] Finally, reaction of [{CpFe}$_2$(μ-dppe)(μ-CO)(μ:η^1:η^1-$CCC(CN)_2$)] with HBF_4 results in formation of [{CpFe}$_2$(μ-dppe)(μ-CO)(μ:η^1:η^1-$CC(H)C(CN)_2$)][BF_4] via protonation at C_β.[37] Similar regiochemistry is observed upon protonation of [(η^6-*p*-cymene)RuCl($CCCPh_2$)(PCy_3)][OTf] and [CpOsCl(P^iPr_3)($CCCPh_2$)].[38, 39]

Scheme 7.1. Allenylidene resonance forms.

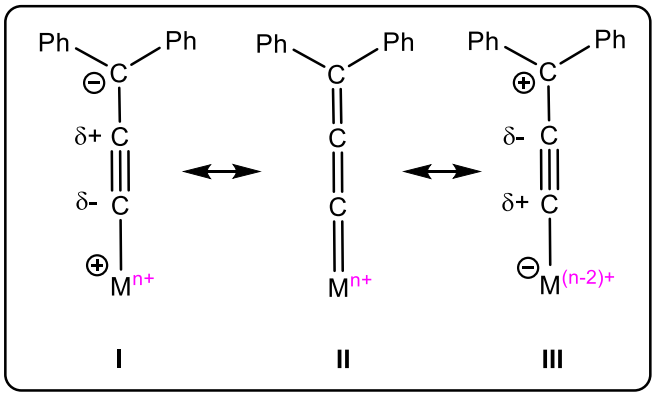

In contrast to the mid- and late-transition metals, early metal or f element allenylidenes should favor resonance form **I**. However, very few allenylidenes are known for the early metals or f elements, making it difficult to verify this hypothesis. The vast majority of allenylidene complexes are in groups 6, 8, and 9. The scarcity of early metal allenylidenes is partially due to the lack of viable synthetic routes. For example, the first allenylidenes, [M{$CCCPh(NMe_2)$}$(CO)_5$] (M = Cr, W), were made by reaction of

[M{C(OEt)C(H)CPh(NMe$_2$)}(CO)$_5$] with a Lewis acid (i.e., BF_3 or $AlEt_3$), which results in elimination of EtOH.[1] Similarly, Selegue and co-workers reported the synthesis of [CpRu(CCCPh$_2$)(PMe$_3$)$_2$][PF_6] by reaction of [CpRuCl(PMe$_3$)$_2$] with propargyl alcohol and NH_4PF_6 via elimination of H_2O.[40] The formation of the EtOH and H_2O by-products in these synthetic protocols would seemingly limit their applicability to the oxophilic early metals. Perhaps as a result, only two early transition metal allenylidenes are known, namely, [Cp$_2$Ti(CCCPh$_2$)(PMe$_3$)] and [{Cp$_2$ZrEt}$_2$(μ:η^1:η^2-CCCMe$_2$)].[41, 42] However, the former complex was only characterized in solution and its solid-state molecular structure was not determined.[41] With respect to the f elements, we recently reported the first structurally characterized actinide allenylidene complexes, [Li(2.2.2-cryptand)][{(NR$_2$)$_3$}An(CCCPh$_2$)] (An = U, Th). These complexes were formed by deprotonation of the An(IV) allenyls, [{(NR$_2$)$_3$}An(CH=C=CPh$_2$)], which themselves were formed by reaction of lithium-3,3-diphenylcyclopropene with [AnCl(NR$_2$)$_3$].[43] This paucity of examples has hindered our ability to study the reactivity of the allenylidene ligand at electropositive metal center.

Recently, Hayton and co-workers report the reaction of [Cp$_3$ThCl] with *in situ* generated 1-lithium-3,3-diphenylcyclopropene that affords a thorium cyclopropenyl complex, [Cp$_3$Th(3,3-diphenylcyclopropenyl)].[44] Interestingly, subsequent thermolysis induces ring opening to generate the *ortho* C-H activated product, [Cp$_3$Th(3-phenyl-1H-inden-1-yl)] (Scheme 7.2), illustrating a new mode of reactivity of 3,3-diphenylcyclopropene with the actinides. Computation analysis indicated that this reaction proceeds through a triplet metallocarbene. However, the proposed intermediate was not experimentally observed.

Scheme 7.2. Synthesis and Thermolysis of [Cp_3Th(3,3-diphenylcyclopropenyl)].

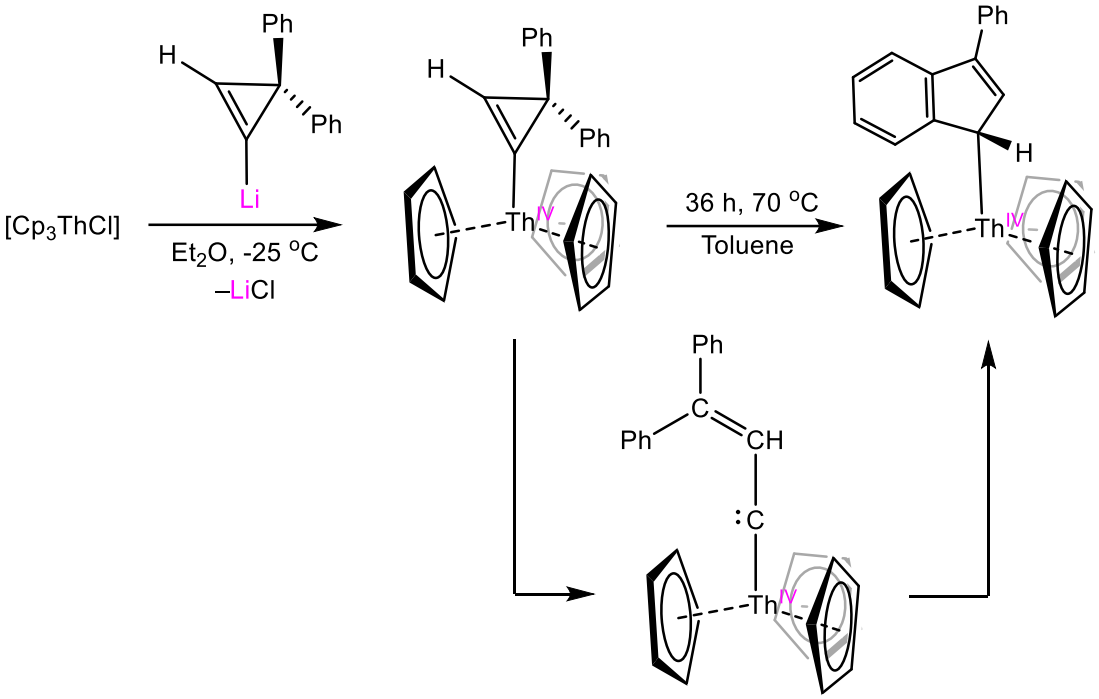

Herein, I report the synthesis and characterization thorium allenylidene complexes, [Li(Et_2O)$_2$][Cp_3Th($CCCPh_2$)] ([Li(Et_2O)$_2$][**7.1**]), [Li(12-c-4)(THF)][Cp_3Th($CCCPh_2$)] ([Li(12-crown-4)(THF)][**7.1**]) and [Li(2.2.2-cryptand)][Cp_3Th($CCCPh_2$)] ([Li(2.2.2-cryptand)][**7.1**]). Importantly, I perform the first reactivity study for early metal allenylidene, establishing that resonance form **I** is a valid description of its electronic structure. The synthesis, characterization, and reactivity studies of [Li(Et_2O)$_2$][**7.1**], [Li(12-crown-4)(THF)][**7.1**], and [Li(2.2.2-cryptand)][**7.1**] were performed in collaboration with Megan A. Schuerlein. In collaboration with Dr. Xiaojuan Yu and Prof. Jochen Autschbach at the State University of New York at Buffalo performed DFT calculations to examine the electronic structure and chemical bonding [**7.1**]$^-$, **7.2**, and **7.3**. Interestingly, NLMO analysis of [**7.1**]$^-$ and **7.2** reveal highly delocalized electronic structures and provides further evidence for involvement of resonance forms **I** and **II**. Significantly, evaluation of the Th-C bond

covalency in [**7.1**]$^-$ and **7.2** using ^{13}C NMR spectroscopy combined with DFT calculations revealing spin-orbit induced downfield shift, due to participation of the 5f orbitals.

7.2 Results and Discussion

7.2.1 Synthesis and Characterization

Slow dropwise addition of a cold (–25 °C) Et_2O solution of 1 equiv of LDA to a cold (–25 °C) Et_2O solution of [Cp_3Th(3,3-diphenylcyclopropenyl)][44] results in an immediate color change to bright orange. Removal of the volatiles, extraction into Et_2O, filtration, and crystallization results in the isolation of the allenylidene complex, [Li(Et_2O)$_2$][Cp_3Th($CCCPh_2$)] ([Li(Et_2O)$_2$][**7.1**]), as orange plates in 54% yield (Scheme 7.3). The ^{1}H NMR spectrum of [Li(Et_2O)$_2$][**7.1**] in benzene-d_6 features three resonances present in a 2:2:1 ratio at 7.88, 7.19, and 6.57 ppm, which are assignable to the *ortho*, *meta*, and *para* positions of the phenyl substituents of the allenylidene ligand (Figure 7.22). In addition, complex [Li(Et_2O)$_2$][**7.1**] exhibits a single Cp environment at 6.18 ppm, integrating to 15H. The ^{13}C{^{1}H NMR spectrum of [Li(Et_2O)$_2$][**7.1**] in THF-d_8 features resonances at 161.12, 146.65, and 70.72 ppm assigned to the C_α, C_β, and C_γ environments of the allenylidene ligand, respectively (Figure 7.1). For comparison, the only other reported Th allenylidene complex, [Li(2.2.2-cryptand)][{(NR_2)$_3$}Th($CCCPh_2$)] (R = $SiMe_3$), features C_α, C_β, and C_γ resonances at 205.4, 128.5, and 70.6 ppm, respectively.[43]

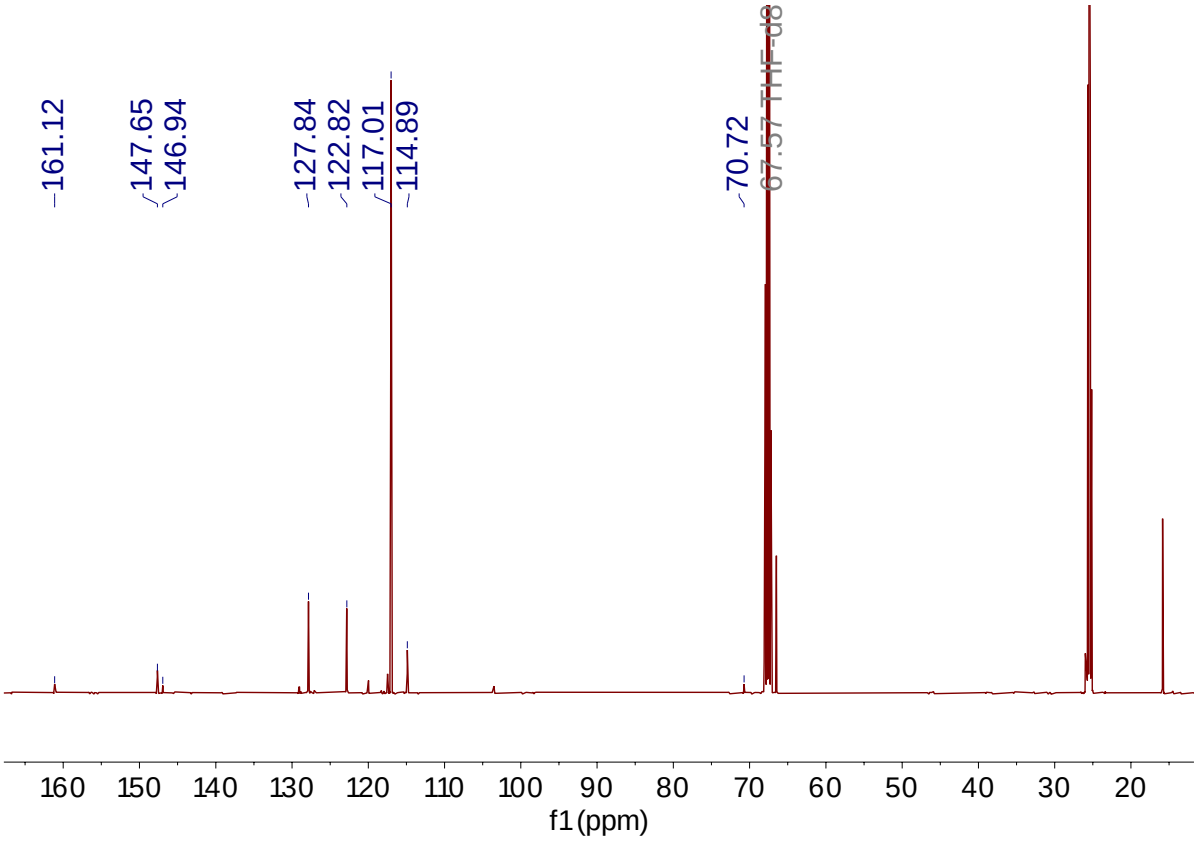

Figure 7.1. $^{13}C\{^{1}H\}$ NMR spectrum of $[Li(Et_2O)_2]$[**7.1**] in THF-d_8 at room temperature.

To our knowledge, the conversion of cyclopropenyl to allenylidene by deprotonation via an exogenous base is unprecedented and promises the potential of a general route to allenylidene complexes. The closest precedent is the reaction of 3,3-dimethylcyclopropene with $[Cp_2Zr(\eta^2\text{-}C_2H_4)(PMe_3)]$, which provides the bridged allenlyidene complex, $[\{Cp_2Zr_(Et)\}_2(\mu{:}\eta^1{:}\eta^2\text{-}CCCMe_2)]$, presumably also via ring-opening of a cyclopropenyl intermediate.[42] In contrast, previous examples of cyclopropenyl ring-openings were mediated by addition of electrophiles.[45-49] For example, protonation of the Ru cyclopropenyl complex, $[CpRu(2\text{-phenyl-3-cyano-1-cyclopropenyl})(PPh_3)_2]$ gives the vinylidene complex, $[CpRu(CC(Ph)(CH_2CN)(PPh_3)_2]^+$, whereas reaction with $[CPh_3]^+$ gives the vinylidene complex, $[CpRu(CC(Ph)\{CH(CPh_3)(CN)\})(PPh_3)_2]^+$.[47, 50-53] Similarly, reaction of [TpRu(2-

phenyl-3-cyano-1-cyclopropenyl)(PPh_3)$_2$] (Tp = HB(pz)$_3$, pz = pyrazolyl) with I_2 results in formation of the vinylidene, [TpRu(CC(Ph){CH(I)(CN)})(PPh_3)$_2$]$^+$.[54] Cyclopropenyl ligands can also undergo thermolytic ring opening. For instance, we reported that thermolysis of [Cp_3Th(3,3-diphenylcyclopropenyl)] affords the ring-open product [Cp_3Th(3-phenyl-1*H*-inden-1-yl] via a hypothesized carbene intermediate (Scheme 7.2).[44] Likewise, Hashmi and co-workers observed similar transformation upon thermolysis of [(IPr)Au(3,3-diphenylcyclopropenyl)].[55] However, in neither transformation is an allenylidene generated. The thermolysis of [(NR_2)$_3$U(BAC)] (R = $SiMe_3$) generates a cyclopropenyl intermediate that rearranges to afford the ring-opened product [(NR_2)$_2$U{*N*(R)($SiMe_2$CH═C(N^iPr$_2$)C(N^iPr$_2$)═*C*H)}].[56]

Scheme 7.3. Synthesis of [Li(Et$_2$O)$_2$][**7.1**], [Li(2.2.2-cryptand)][**7.1**], [Li(12-crown-4)(THF)][**7.1**] and **7.2**.

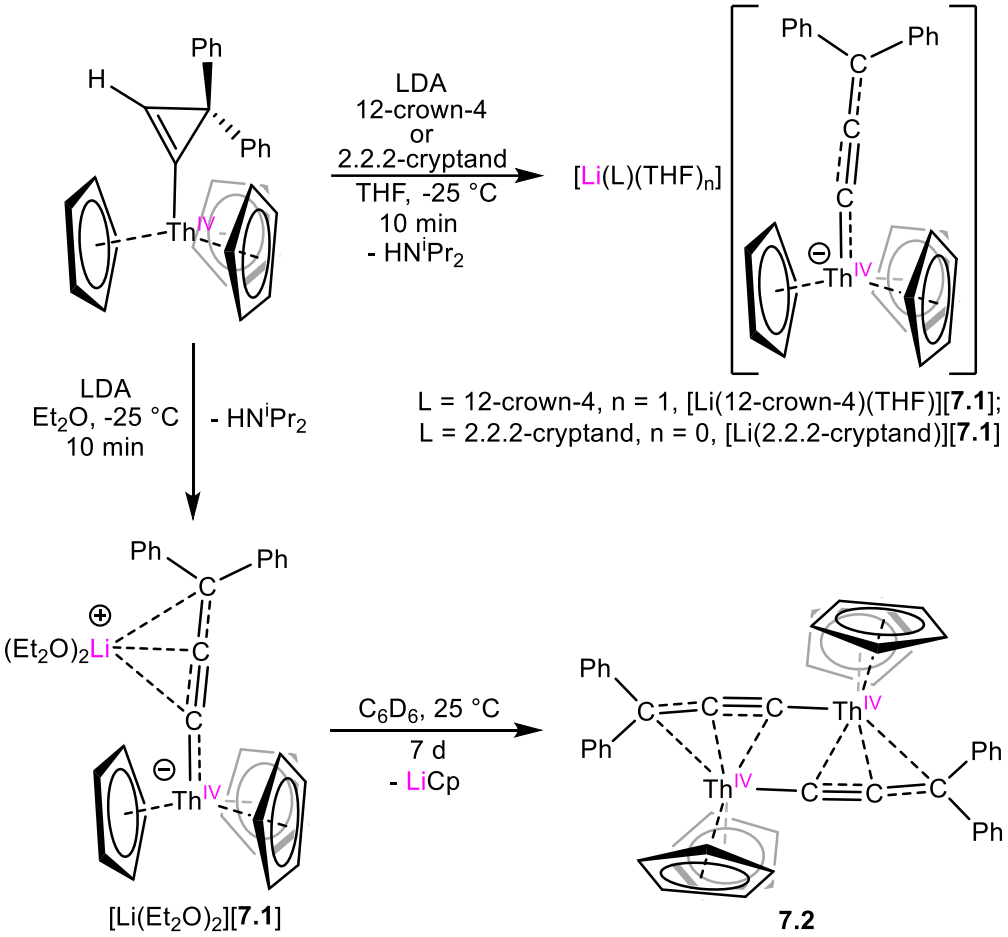

Complex [Li(Et$_2$O)$_2$][**7.1**] is insoluble in hexanes and pentane, but is soluble in Et$_2$O and benzene, where it generates bright orange solutions. In contrast, dissolution of [Li(Et$_2$O)$_2$][**7.1**] in THF results in formation of a dark red solution, presumably due to the formation of a separated cation/anion pair. In support of this hypothesis, the ^{7}Li{^{1}H} spectrum of [Li(Et$_2$O)$_2$][**7.1**] in benzene-d_6 features a singlet at –2.34 ppm, whereas the ^{7}Li{^{1}H} spectrum of [Li(Et$_2$O)$_2$][**7.1**] in THF-d_8 features a singlet at –0.69 ppm, indicating the change in Li coordination environment. Complex [Li(Et$_2$O)$_2$][**7.1**] is thermally sensitive in solution. For example, the ^{1}H NMR spectrum of [Li(Et$_2$O)$_2$][**7.1**] in benzene-d_6 reveals ca. 60%

conversion to allenylidene-bridged dimer, $[Cp_2Th(CCCPh_2)]_2$ (**7.2**), after standing for 1 d in solution at room temperature (Figure 7.25).[57] In contrast, a THF-d_8 solution of $[Li(Et_2O)_2]$[**7.1**] only exhibits ca. 20% conversion to **7.2** after standing for 1 d at room temperature. A ^{1}H NMR spectrum of this reaction mixture also features a resonance at 5.71 ppm, which is assignable to LiCp (Figure 7.26).[58] We ascribe the greater thermal stability of $[Li(Et_2O)_2]$[**7.1**] in THF to that solvent's higher dielectric constant, which can better support an anionic complex.

Complex **7.2** can also be made on preparative scale. Thus, storage of a bright red solution of $[Li(Et_2O)_2]$[**7.1**] in benzene-d_6 for 7 d at room temperature results in a color change to pale yellow, concomitant with the deposition of bright orange red plates and a colorless powder. Work-up of the reaction mixture affords **7.2** as bright orange red plates in a 54% yield (Scheme 7.3). The conversion of $[Li(Et_2O)_2]$[**7.1**] to **7.2** in C_6D_6 is likely driven by the precipitation of insoluble LiCp. The ^{1}H NMR spectrum of **7.2** in dichloromethane-d_2 features resonances at 7.56, 7.46, and 7.11 ppm, which are assignable to the *ortho*, *meta*, and *para* positions of the phenyl substituents of the allenylidene ligand, respectively (Figure 7.33). These resonances are present in 2:2:1 ratio. The ^{1}H NMR spectrum of **7.2** also displays a single Cp environment at 6.11 ppm, integrating to 10H (Figure 7.33). The $^{13}C\{^1H\}$ NMR spectrum of **7.2** in dichloromethane-d_2 features resonances at 178.42, 160.77, and 89.14 ppm, which are assignable to the C_α, C_β, and C_γ environments of the allenylidene ligand, respectively (Figure 7.2). These resonances are shifted downfield relative to those observed in $[Li(Et_2O)_2]$[**7.1**] (Table 7.1), likely due to the μ:η^1:η^3 binding mode of the allenylidene ligand, which increases the metal involvement in bonding.

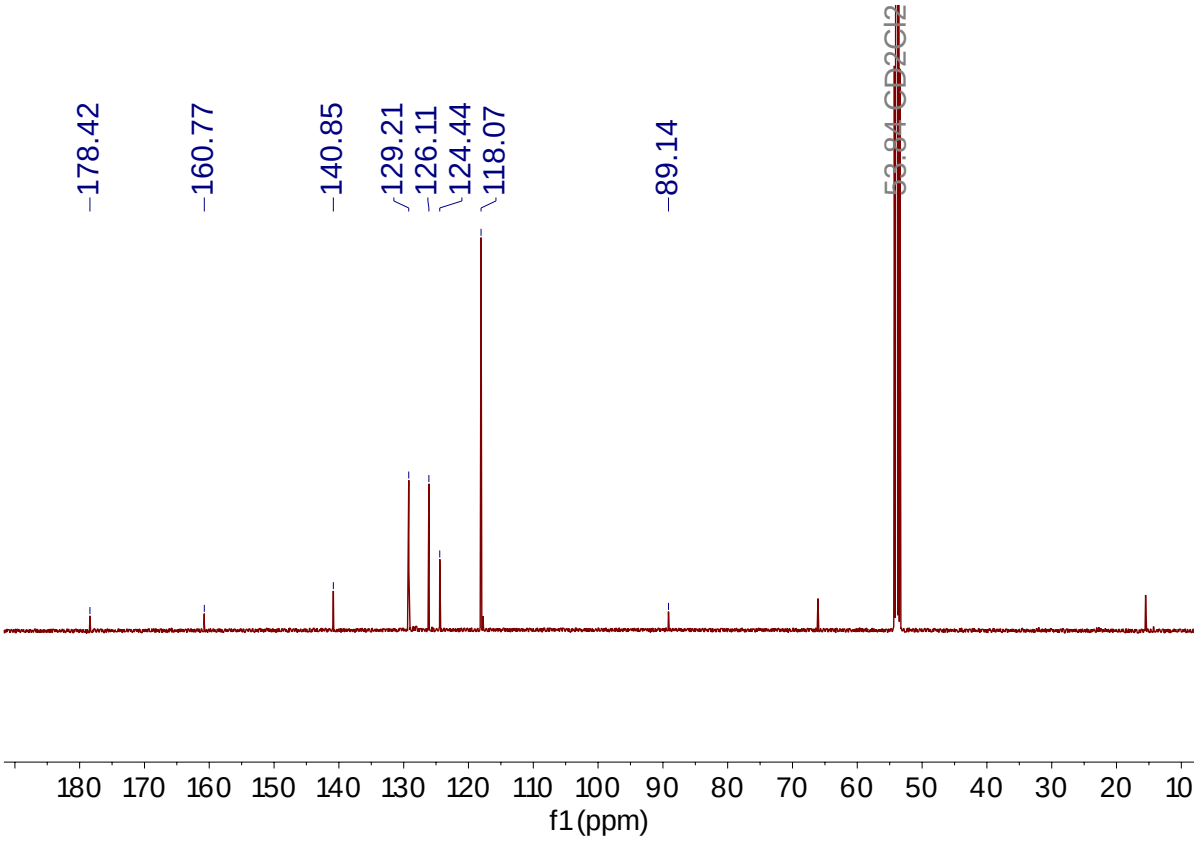

Figure 7.2. $^{13}C\{^{1}H\}$ NMR spectrum of **7.2** in dichloromethane-d_2 at room temperature.

We hypothesized that addition of a crown ether to $[Li(Et_2O)_2]$[**7.1**] would enhance its thermal stability by disfavoring formation of LiCp. Thus, slow dropwise addition of a cold (–25 °C) THF solution of 1 equiv of LDA to a cold (–25 °C), colorless THF solution of [Cp_3Th(3,3-diphenylcyclopropenyl)], in the presence of 1 equiv of 12-crown-4, result in immediate formation of dark red solution. Work-up of the reaction mixture affords [Li(12-crown-4)(THF)][**7.1**] as red plates in 72% yield (Scheme 7.3). The ^{1}H NMR spectrum of [Li(12-crown-4)(THF)][**7.1**] in THF-d_8 features three resonances 7.58, 6.87, and 6.16 ppm, which are assignable to the *ortho*, *meta*, and *para* positions of the allenylidene fragment, respectively (Figure 7.27). Additionally, the ^{1}H NMR spectrum exhibits a single Cp environment at 6.31 ppm. The $^{13}C\{^{1}H\}$ NMR spectrum of [Li(12-crown-4)(THF)][**7.1**]

features resonances at 164.80, 141.77, and 72.48 ppm, which are assignable to the C_α, C_β, and C_γ environments of the allenylidene ligand, respectively (Figure 7.3). Finally, the $^{7}Li\{^{1}H\}$ spectrum of [Li(12-crown-4)(THF)][**7.1**] in THF-d_8 features a singlet at –0.95 ppm.

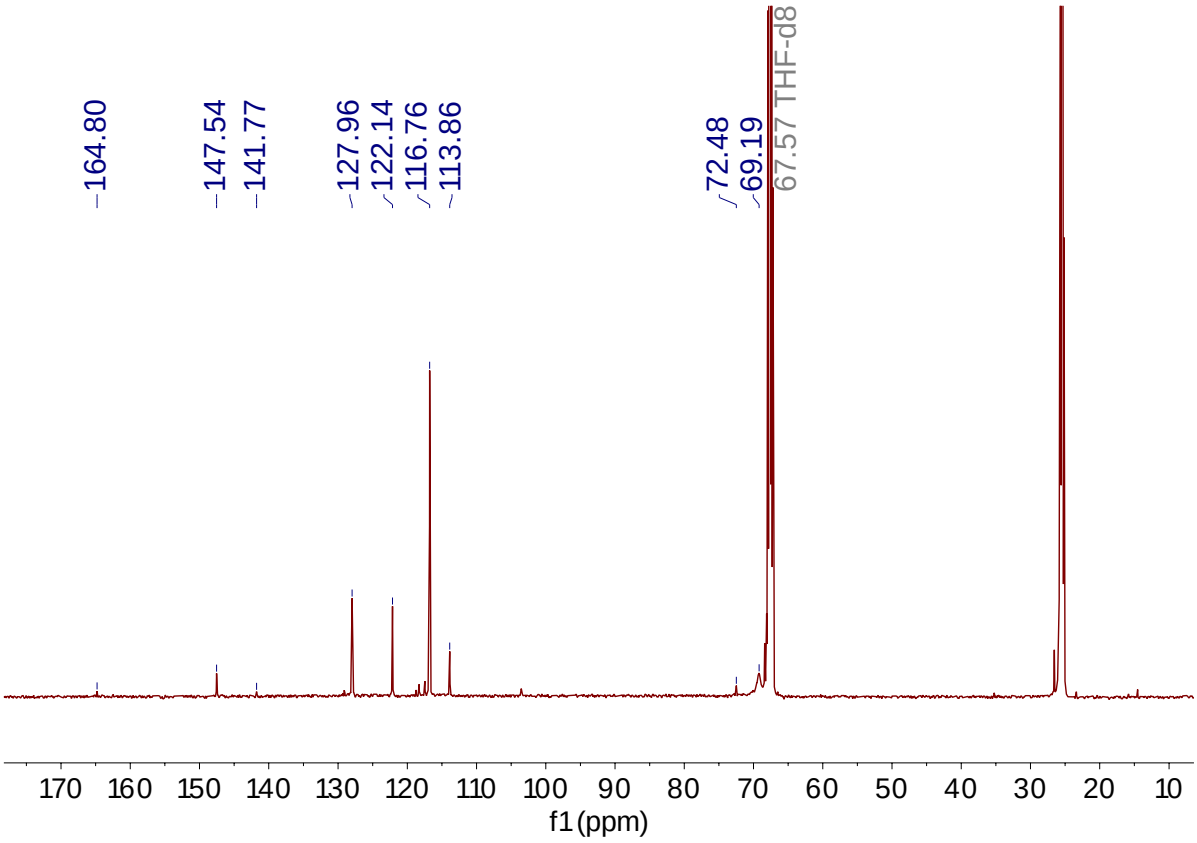

Figure 7.3. $^{13}C\{^{1}H\}$ NMR spectrum of [Li(12-crown-4)(THF)][**7.1**] in THF-d_8 at room temperature.

Similarly, dropwise addition of a cold (–25 °C) THF solution of 1 equiv of LDA to a cold (–25 °C) THF solution of [Cp_3Th(3,3-diphenylcyclopropenyl)], in the presence of 1 equiv of 2.2.2-cryptand, results in an immediate color change to a dark red solution. Work-up of the reaction mixture after 10 min affords [Li(2.2.2-cryptand)][**7.1**], which can be isolated as dark red plates in 79% yield. Its ^{1}H NMR spectrum in THF-d_8 displays a single Cp environment at 6.31 ppm and three resonances at 7.53, 6.79, and 6.06 ppm, which are assignable to the *ortho*,

meta, and *para* positions of phenyl substituent the allenylidene ligand, respectively (Figure 7.30). The $^{13}C\{^{1}H\}$ NMR spectrum of [Li(2.2.2-cryptand)][**7.1**] features resonances at 166.86, 138.78, and 73.64 ppm, attributable to the C_α, C_β, and C_γ environments of the allenylidene ligand (Figure 7.5). Its $^{7}Li\{^{1}H\}$ spectrum in THF-d_8 features a singlet at –1.24 ppm. Finally, the UV-vis spectra of [Li(2.2.2-cryptand)][**7.1**] in THF displays λ_{max} centered at 440 nm (ε = 3792 $cm^{-1}\cdot M^{-1}$) and two shoulders at 396 nm (ε = 3260 $cm^{-1}\cdot M^{-1}$) and 510 nm (ε = 1924 $cm^{-1}\cdot M^{-1}$) (Figure 7.4). The UV-vis spectrum of **7.2** in THF is similar and features λ_{max} centered at 336 nm **(**ε = 2589 $cm^{-1}\cdot M^{-1}$**)** and at 436 nm **(**ε = 3803 $cm^{-1}\cdot M^{-1}$**)** and a shoulder at 395 nm (ε = 2839 $cm^{-1}\cdot M^{-1}$) (Figure 7.4). We attribute these bands to a ligand-based absorption, as Th(IV) complexes are typically colorless. In this regard, the UV-vis spectrum reported for both [Li(2.2.2-cryptand)][$\{(NR_2)_3\}$Th($CCCPh_2$)] and $[CPh_3]^-$ are qualitatively similar to those of [Li(2.2.2-cryptand)][**7.1**] and **7.2**,[43] suggesting that the color has a similar origin.[59-61]

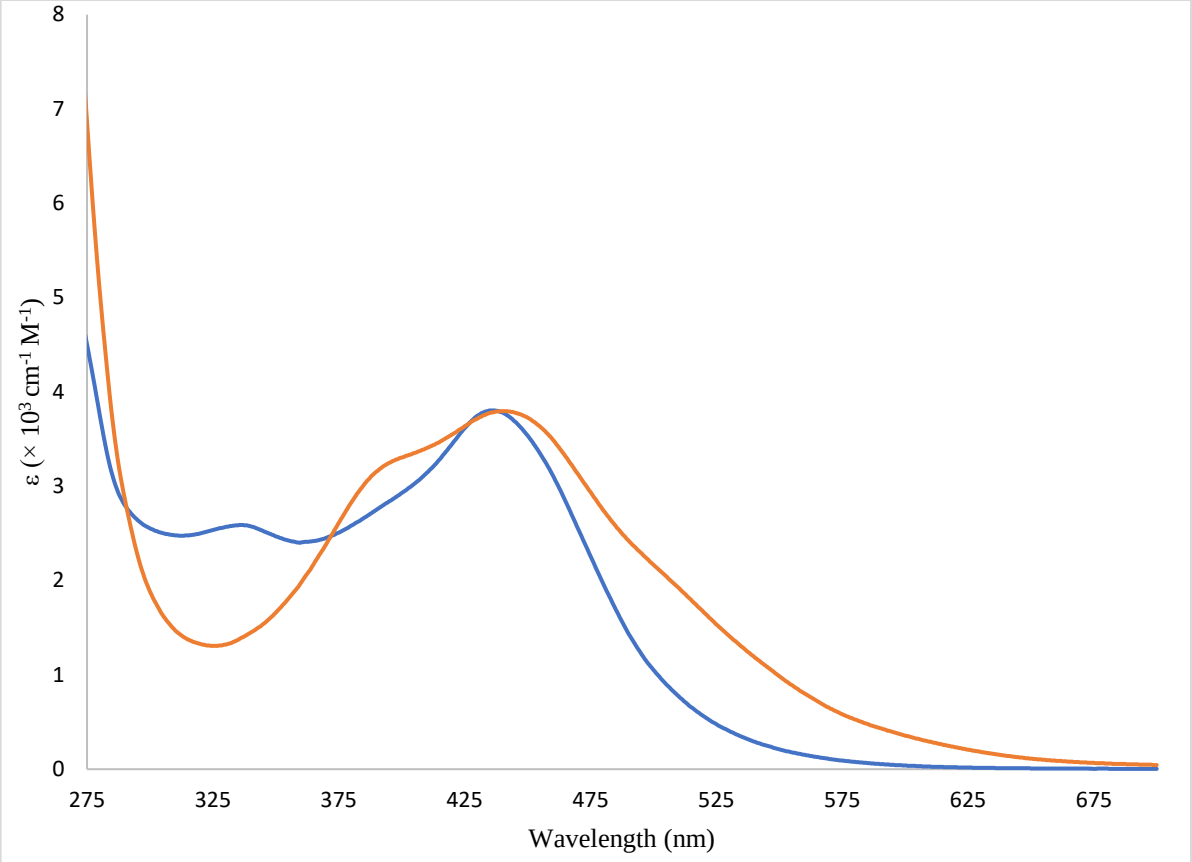

Figure 7.4. Electronic absorption spectra of [Li(2.2.2-cryptand)][**7.1**] (0.25 mM, THF) (orange) and **7.2** (0.28 mM, THF) (blue).

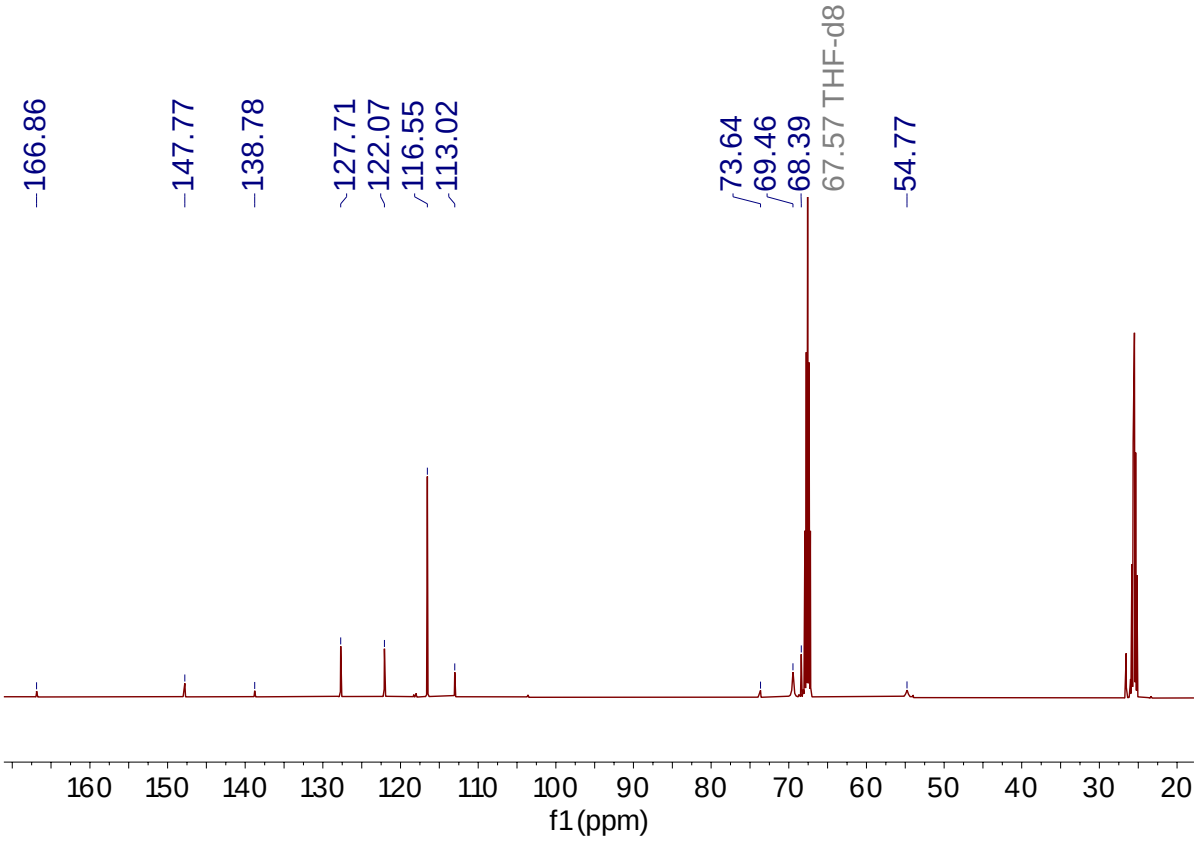

Figure 7.5. $^{13}C\{^{1}H\}$ NMR spectrum of [Li(2.2.2-cryptand)][**7.1**] in THF-d_8 at room temperature.

Both [Li(12-crown-4)(THF)][**7.1**] and [Li(2.2.2-cryptand)] [**7.1**] are soluble in THF and DME, but insoluble in Et_2O, benzene, hexanes, and pentane. Surprisingly, the ^{1}H NMR spectrum of both Li(12-crown-4)(THF)][**7.1**] and [Li(2.2.2-cryptand)] [**7.1**] in THF-d_8 after standing for 2 d in solution at room temperature exhibit a negligible amount of decomposition. (Figure S11 and S15). We hypothesize the improved thermal stability of both [Li(12-crown-4)(THF)][**7.1**] and [Li(2.2.2-cryptand)][**7.1**], relative to [Li$(Et_2O)_2$][**7.1**], is due to strong complexation of Li^+ which disfavors the formation LiCp.

We also examined the IR spectra of [**7.1**]$^-$ and **7.2**. Complex [Li$(Et_2O)_2$][**7.1**] exhibits a C_α–C_β stretch at 1914 cm^{-1}, whereas [Li(2.2.2-cryptand)][**7.1**] exhibits a C_α–C_β stretch at 1945

cm^{-1}. The lower value observed for [Li(Et_2O)$_2$][**7.1**] is evidence for coordination of Li^+ to the allenylidene ligand in the solid-state, which weakens the C_α–C_β bond relative to [Li(2.2.2-cryptand)][**7.1**]. Complex **7.2** also exhibits a reduced C_α–C_β stretch (1906 cm^{-1}) in comparison to [Li(2.2.2-cryptand)][**7.1**], likely for the same reason. For comparison, the Re allenylidene complex, [Re($CCCPh_2$)(N^tBu)$_2$(S-1-Ad)], features a C_α–C_β stretch at 1810 cm^{-1} in its IR spectrum,[62] suggesting an electronic structure closer to resonance form **II** for its allenylidene ligand vs. that found for [Li(2.2.2-cryptand)][**7.1**]. Nonetheless, the C_α–C_β stretch observed for [Li(2.2.2-cryptand)][**7.1**] is well below that observed for a true actinide acetylide complex, such as [U(NR_2)$_3$(CCPh)] (R = $SiMe_3$), which exhibits a C≡C stretch at 2072 cm^{-1}. This large difference is strong evidence for contribution of resonance form **II** to its electronic structure.[63]

Table 7.1. $^{13}C\{^1H\}$ NMR Chemical Shift Data for Complexes [Li(Et_2O)$_2$][**7.1**], [Li(2.2.2-cryptand)][**7.1**], [Li(12-crown-4)(THF)][**7.1**], **7.2**, **7.3** [Li(2.2.2cryptand)][{(NR_2)$_3$}Th($CCCPh_2$)]

	Solvent	C_α	C_β	C_γ	Cp
[Li(Et_2O)$_2$][**7.1**]	THF-d_8	161.12	146.94	70.72	117.01
[Li(12-crown-4)(THF)][**7.1**]	THF-d_8	164.80	141.77	72.48	116.76
[Li(2.2.2-cryptand)][**7.1**]	THF-d_8	166.86	138.78	73.64	116.55
7.2·C_6D_6	CD_2Cl_2	178.42	160.77	89.14	118.07
[Li(2.2.2cryptand)][{(NR_2)$_3$}Th($CCCPh_2$)][43]	C_6D_6/ THF-d_8	205.4	128.5	70.6	-
7.3	THF-d_8	146.38	126.71	46.82	117.45

7.2.2 X-ray Crystallographic Characterization

Complex [Li(Et$_2$O)$_2$][**7.1**] crystallizes in the triclinic space group $P\bar{1}$ (Figure 7.6). It features a close contact between the [Li(Et$_2$O)$_2$]$^+$ cation and the C_α, C_β, and C_γ carbon atoms of the allenylidene fragment. The corresponding Li-C_α, Li-C_β, and Li-C_γ distances are 2.390(11) Å, 2.151(12) Å, and 2.507(13), respectively, which are consistent with those previously reported for organolithium compounds with similar contact ion pair bonding (range = 2.128(6) – 2.511(3) Å).[64-68] The Th-C_α distance in [Li(Et$_2$O)$_2$][**7.1**] (2.446(5) Å) is longer than that reported for our Th allenylidene complex, [Li(2.2.2-cryptand)][{(NR$_2$)$_3$}Th(CCCPh$_2$)] (2.368(16) Å), as well as those found in the thorium phosphorano-stabilized carbene complexes, [Th(CHPPh$_3$)(NR$_2$)$_3$] (2.362(2) Å) and [Cp*$_2$Th(CHPPh$_3$)I] (2.299(6) Å),[43, 69, 70] likely on account of the Li$^+$ interaction with the allenylidene fragment, as well as the higher coordination number at the thorium center (see below for more discussion). The C_α–C_β distance in [Li(Et$_2$O)$_2$][**7.1**] (1.244(7) Å) is slight longer than a C-C triple bond, whereas the C_β–C_γ (1.402(7) Å) distance is significantly shorter than a C-C single bond.[71] The C_α–C_β and C_β–C_γ distances reflect the contribution from both resonance forms **I** and **II**, in accord with the previously reported thorium allenylidene complex.[43] In addition, the Th-C_α-C_β and C_α-C_β-C_γ angles are 154.9(5)° and 172.1(6)°, respectively. These values differ from those observed for [Li(2.2.2-cryptand)][{(NR$_2$)$_3$}Th(CCCPh$_2$)] (i.e., 172.0(14)° and 174.6(16)°), likely on account of Li$^+$ coordination to the allenylidene unit.[43] Finally, the sum of angles around the C_γ (360°) is indicative of sp^2 hybridization.

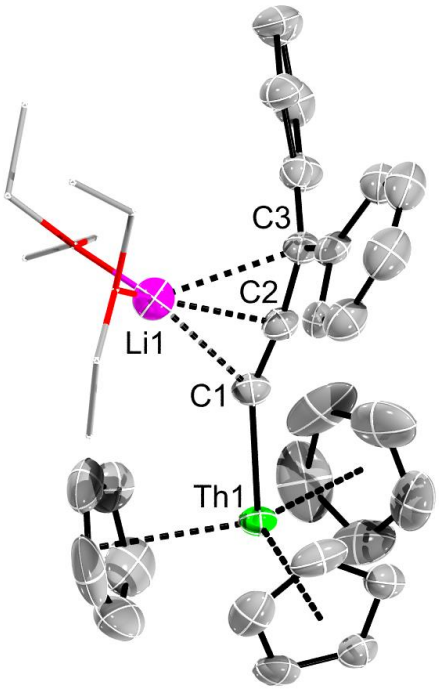

Figure 7.6. Solid-state molecular structure of [Li(Et_2O)$_2$][**7.1**]. Thermal ellipsoids set at 50% probability. The Et_2O ligand are shown in wireframe style and hydrogen atoms are omitted for clarity.

Table 7.2. Selected metrical parameters for complexes $[Li(Et_2O)_2]$[**7.1**], [Li(2.2.2-cryptand)][**7.1**], [Li(12-crown-4)(THF)][**7.1**], **7.2, 7.3**

Bond (Å, °)	$[Li(Et_2O)_2]$[**7.1**]	[Li(12-crown-4)(THF)][**7.1**]	[Li(2.2.2-cryptand)][**7.1**]	**7.2**·C_6D_6	**7.3**
An–C_α	2.447(5)	2.406(6)	2.411(10)	2.487(7)	2.499(8)
C_α–C_β	1.244(7)	1.230(7)	1.228(12)	1.251(10)	1.176(11)
C_β–C_γ	1.402(7)	1.431(7)	1.388(12)	1.407(10)	1.509(11)
C_γ–C_{ipso}	1.458(8), 1.476(8)	1.434(7), 1.479(6)	1.447(13), 1.474(13)	1.489(10), 1.501(11)	1.538(11), 1.541(10)
An–C_α–C_β	154.9(5)	162.1(5)	174.6(8)	176.8(6)	175.9(7)
C_α–C_β–C_γ	172.2(6)	177.1(6)	178.3(10)	164.8(7)	178.0(8)
$\Sigma(\angle C_{ipso/\beta}$–$C_\gamma$–$C_{ipso})$	360.0	359.7	359.9	354.8	656.9

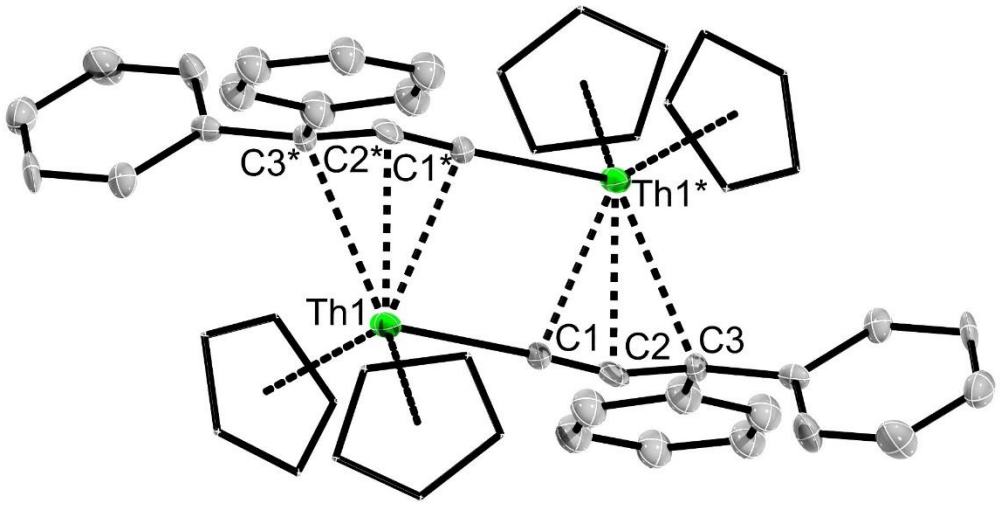

Figure 7.7. Solid-state molecular structure of **7.2**. Thermal ellipsoids set at 50 % probability. The Cp ligands are shown in wireframe style, hydrogen atoms are omitted for clarity.

Complex **2** crystallizes in the triclinic space group $P\bar{1}$ as a C_6D_6 solvate, **7.2**·C_6D_6 (Figure 7.7). The structure features two Th atoms related by an inversion center. Its allenylidene ligand adopts an unprecedented μ:η^1:η^3 binding mode, although μ:η^1:η^2 and μ:η^1:η^1 binding modes are also known.[19, 72-76] The Th1-C_α distance (2.48(1) Å) is similar to those found in σ-bonded thorium acetylide complexes,[77-80] such as [Th(C≡CH)(NR_2)$_3$] (R = $SiMe_3$; 2.481(8) Å), [{Th(NR_2)$_3$}$_2$(μ:η^1:η^1-C_2)] (R = $SiMe_3$; 2.484(6) Å, 2.501(5) Å), and [(L)Th(C≡CR')$_2$] (L = *trans*-calix[2]benzene[2]pyrrolide; R' = $SiMe_3$, Si^iPr_3; 2.479(4) Å, 2.482(3) Å), suggesting a single Th-C bond.[77, 81] Additionally, the Th1*-C_α (2.667(9) Å), Th1*-C_β (2.629(10) Å), and Th1*-C_γ (2.923(10) Å) distances are similar to the Th-C distances in the homoleptic thorium η^3-allyl complexes, [Th{η^3-1,3-$R_2C_3H_3$}$_4$] and [Th{η^3-1-RC_3H_4}$_4$] (R = $SiMe_3$) (range = 2.617(5) – 2.892(5) Å).[82] Furthermore, the C_α-C_β-C_γ angle (165.0(10)°) is notably perturbed due to the η^3 binding to Th1*. The C_α–C_β (1.248(14) Å) and C_β–C_γ (1.413(14) Å) distances are similar to those of [Li(Et_2O)$_2$][**7.1**] and [Li(2.2.2-cryptand)][{(NR_2)$_3$}Th($CCCPh_2$)].[43] Finally, the sum of angles around C_γ (354.8°) deviates slightly from 360° due to the Th1*–C_γ interaction.

Complex [Li(12-crown-4)(THF)][**7.1**] crystallizes in the monoclinic space group $P2_1/n$ (Figure 7.8), whereas [Li(2.2.2-cryptand)][**7.1**] crystallizes in the orthorhombic space group $P2_12_12_1$ (Figure 7.9). Both [Li(12-crown-4)(THF)][**7.1**] and [Li(2.2.2-cryptand)][**7.1**] crystallize as discrete cation-anion pairs. The Th-C_α distances in [Li(12-crown-4)(THF)][**7.1**] (2.411(10) Å) and [Li(2.2.2-cryptand)][**7.1**] (2.41(2) Å) are shorter than that of **7.2**, due to the terminal allenylidene binding mode. However, they are slightly longer than the Th-C_α distance in [Li(2.2.2-cryptand)][{(NR_2)$_3$}Th($CCCPh_2$)] (2.368(16) Å), likely due to their higher coordination number at the thorium metal center. They are also slightly longer than the Th-C_α

distances observed in thorium phosphorano-stabilized carbene complexes, [Th(CHPPh$_3$)(NR$_2$)$_3$] (R = SiMe$_3$) (2.362(2) Å) and [Cp*$_2$ThCl(CHPPh$_3$)] (2.3235(1) Å).[69, 70] Nonetheless, the Th-C$_\alpha$ distances are comparable to those reported for the thorium methanediides, such as [Th(BIPM^{TMS})$_2$] (BIPM^{TMS} = C(PPh$_2$NSiMe$_3$)$_2$) (2.514(3) Å, 2.516(3) Å), [Th(BIPM^{TMS}){N(SiMe$_3$)$_2$}(N=CPh$_2$)] (2.474(8) Å), [Th(BIPM^{TMS}){N(SiMe$_3$)$_2$}(μ-Cl)]$_2$ (2.410(8) Å), and [{(Ph$_2$P=S)$_2$C}$_2$Th(DME)] (2.485(7) Å, 2.498(7) Å).[83-86] Intriguingly, the Th-C$_\alpha$-C$_\beta$ angle in [Li(12-crown-4)(THF)][**7.1**] (162.1(5)°) is more acute than that of [Li(2.2.2-cryptand)][**7.1**] (172(4)°) and [Li(2.2.2-cryptand)][{(NR$_2$)$_3$}Th(CCCPh$_2$)] (172.0(14)°).[43] We attribute this difference to crystal packing and not to an electronic effect.

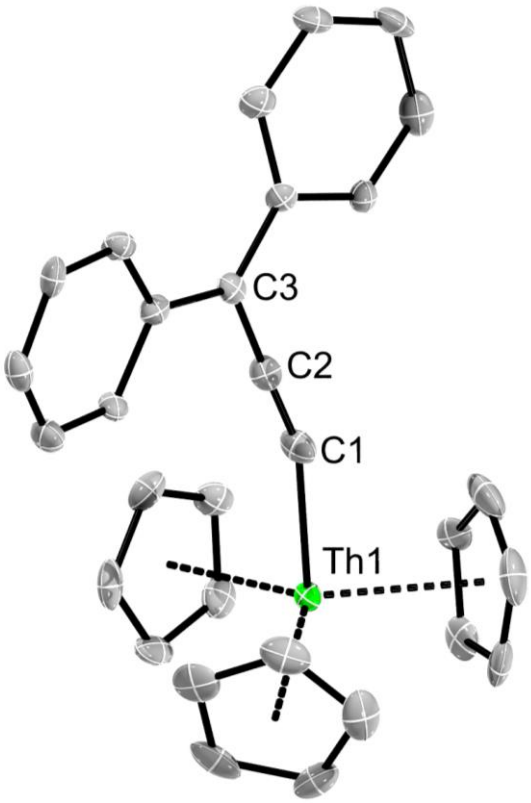

Figure 7.8. Solid-state molecular structure of [Li(12-crown-4)(THF)][**7.1**]. Thermal ellipsoids set at 50% probability. The $[Li(12\text{-crown-4})(THF)]^+$ cation and hydrogen atoms are omitted for clarity.

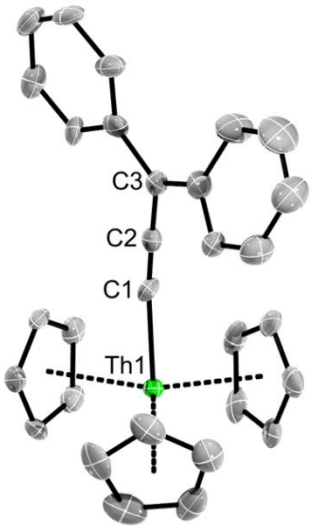

Figure 7.9. Solid-state molecular structure of [Li(2.2.2-cryptand)][**7.1**]. Thermal ellipsoids set at 50% probability. The $[Li(2.2.2\text{-cryptand})]^+$ cation and hydrogen atoms are omitted for clarity.

7.2.3 Reactivity Studies

In efforts to further understand its electronic structure, I investigated the reactivity of $[Li(Et_2O)_2]$[**7.1**] with an electrophile. Thus, addition of 1 equiv of MeI to a cold (–25 °C) THF solution of $[Li(Et_2O)_2]$[**7.1**] results in immediate formation of a pale yellow solution. Work-up of this solution, followed by crystallization from hexanes, affords $[Cp_3Th(CCC(Me)Ph_2)]$ (**7.3**), which can be isolated as colorless plates in 83% yield (Scheme 7.4). The ^{1}H NMR spectrum of **7.3** in THF-d_8 displays a single Cp environment at 6.32 ppm and a methyl resonance at 2.01 ppm (Figure 7.34). These resonances are present in a 15:3 ratio. The $^{13}C\{^1H\}$ NMR spectrum of **7.3** in THF-d_8 features resonances at 146.38, 126.71, and 46.82 ppm, which are assignable to the C_α, C_β, and C_γ environments of the acetylide ligand, respectively (Figure 7.10). For comparison, the C_α and C_β chemical shifts in **7.3** are upfield

shifted to those observed in [**7.1**]$^{-}$ (Table 7.1). This upfield shift is attributed to reduced spin orbit induced deshielding between **7.3** and [**7.1**]$^{-}$, indicating a decrease in 5f participation in the Th-C bonds (see below). Finally, the IR spectra of **7.3** exhibits a characteristic C≡C stretch at 2071 cm^{-1} consistent with those of other thorium acetylide complexes,[63, 79, 81] and ca. 150 cm^{-1} higher than the C_α–C_β stretch of [**7.1**]$^{-}$.

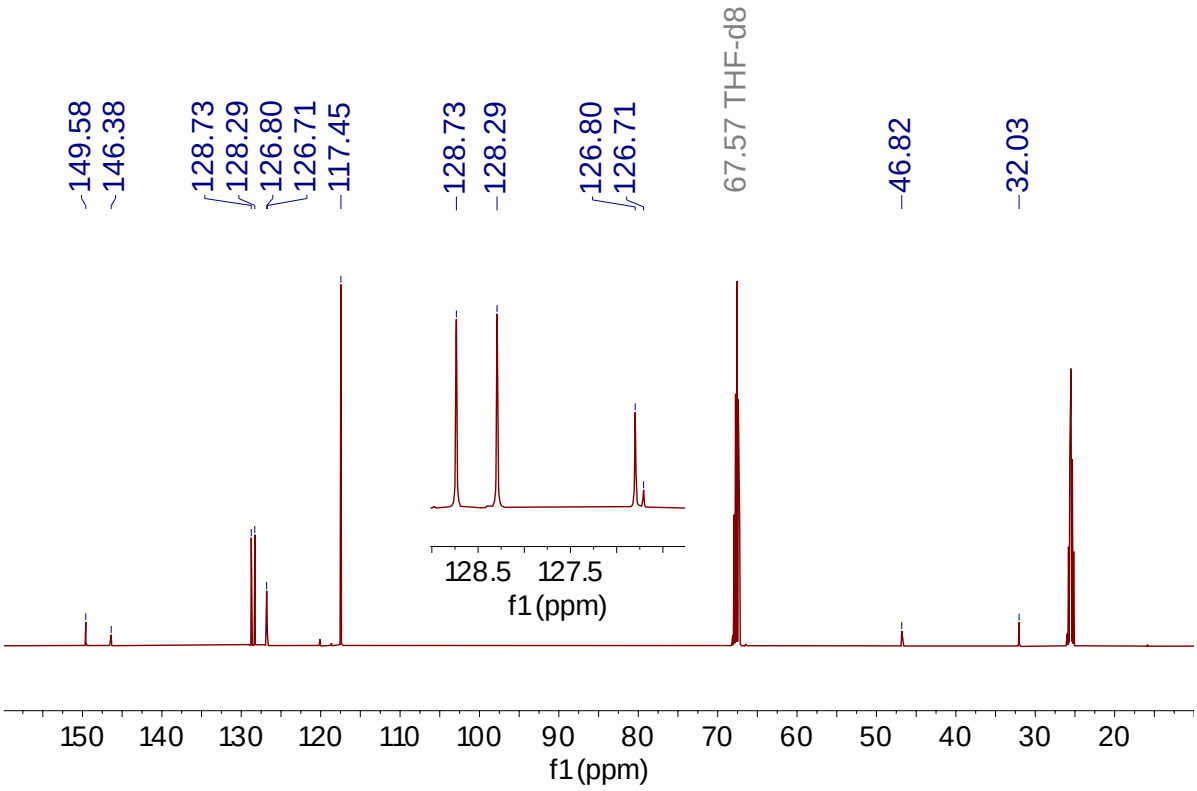

Figure 7.10. $^{13}C\{^{1}H\}$ NMR spectrum of **7.3** in THF-d_8 at room temperature.

Scheme 7.4. Synthesis of complexes **7.3** and **7.4**.

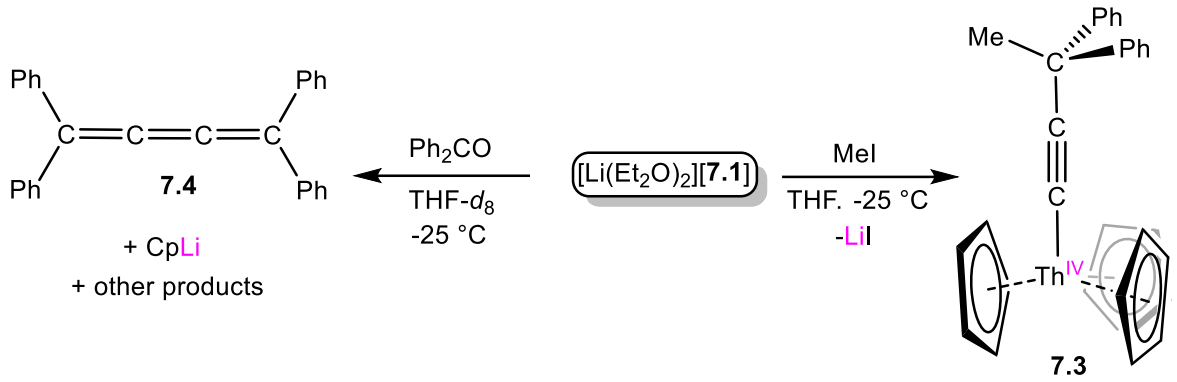

Complex **7.3** crystallizes in the monoclinic space group $P2_1/c$ as a THF solvate, **7.3**·THF (Figure 7.11). Its Th-C_α distance (2.499(8) Å) is longer than those observed for [**7.1**]$^-$ and **7.2**, but is consistent with those previously reported for thorium acetylides,[79-81] such as [Th(C≡CH)(NR_2)$_3$] (2.481(8) Å)[81], [(η^5-1,3-(^{t}Bu)$_2$$C_5H_3$)$_2$Th(C≡CPh)$_2$] (2.461(4) Å, 2.462(4) Å)[80], [(L)Th(C≡CR)$_2$] (R = $SiMe_3$, Si^iPr_3)$_2$; L = *trans*-calix[2]benzene[2]pyrrolide) (2.479(4) Å, 2.482(3) Å),[77] and [Th(Bc^{Mes})$_2$(C≡C-*p*-tolyl)$_2$] (Bc^{Mes} = bis(NHC)borate) (2.497(5) Å, 2.508(5) Å).[78] The C_α–C_β distance of 1.18(1) Å is consistent with a C≡C triple bond, and is shorter than the C_α–C_β distances found in [**7.1**]$^-$. The C_β–C_γ distance (1.51(1) Å) is consistent with a C-C single bond and is significantly longer than the C_β–C_γ distance observed in [**7.1**]$^-$ (Table 7.2). The difference in metrical parameters observe in **7.3** vs [**7.1**]$^-$, further supports the contribution of resonance form **I** and **II** in the electronic structure of [**7.1**]$^-$.

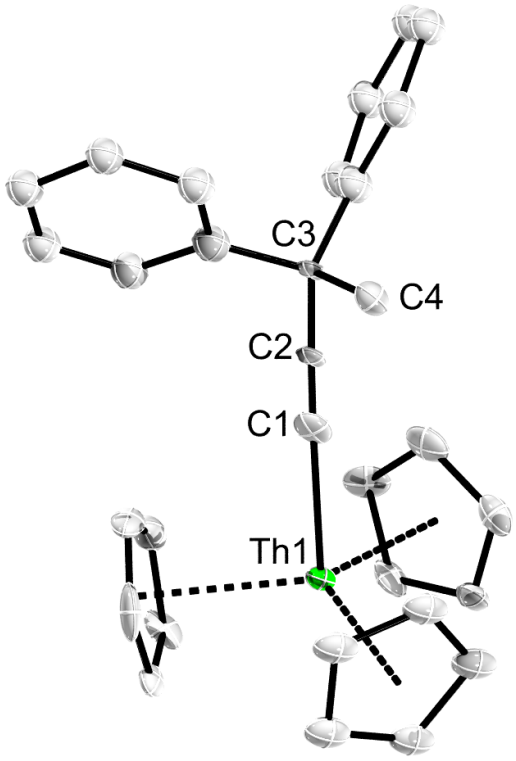

Figure 7.11. Solid-state molecular structure of **7.3**·THF. Thermal ellipsoids set at 50% probability and hydrogen atoms are omitted for clarity.

To our knowledge, the formation of **7.3** represents the first example of regioselective electrophilic attack at the C_γ atom in a metal allenylidene complex. This regioselectivity supports the contribution of resonance form **I** to the electronic structure of [Li(Et_2O)$_2$][**7.1**]. In contrast, transition metal allenylidenes typically react with electrophiles at C_β, consistent with resonance form **III**.[4, 87, 88] For example, reaction of [Re($CCCPh_2$)(CO)$_2$(triphos)][OTf] (triphos = $MeC(CH_2PPh_2)_3$) with excess ROTf (R = H, Me) results in formation of the carbyne complexes, [Re(≡CC(R)═CPh_2)(CO)$_2$(triphos)][OTf]$_2$ (R = H, Me).[87]

I also examined the reaction of [Li(Et_2O)$_2$][**7.1**] with benzophenone. Thus, a slow dropwise addition of a cold (–25 °C) THF-d_8 solution of 1 equiv of Ph_2CO to a cold (–25 °C) THF-d_8 solution of [Li(Et_2O)$_2$][**7.1**] results in immediate formation of a bright yellow solution. The ^{1}H NMR spectrum of the reaction mixture reveals complete consumption of benzophenone, along with the appearance of three new aryl CH resonances at 7.55 ppm, 7.38 ppm, and 7.32 ppm, which are assignable to the *ortho*, *meta*, and *para* positions of the phenyl substituents of 1,1,4,4-tetraphenylbutatriene (**7.4**), respectively (Figure 7.12). This species is formed in 99% yield, according to integration against an internal standard (C_6Me_6).[89] The ^{13}C{^{1}H} NMR spectrum of this mixture features diagnostic resonances at 152.72 and 123.80 ppm, which are assignable to the $C_{2,3}$ and $C_{1,4}$ cumulene carbons of **7.4**, respectively (Figure 7.35).[89] I also observe a singlet at 5.71 ppm in the ^{1}H NMR spectrum along with a corresponding resonance at 103.53 ppm in the ^{13}C{^{1}H} NMR spectrum, which are both assignable to LiCp. The yield of LiCp was determined to be 78% by integration of the ^{1}H resonance against the internal standard and calculated by assuming that Li^+ was the limiting reagent.[58] Several other Cp-containing products are also present in the sample, as evidenced by resonances at 6.61, 6.50, and 6.39 ppm in the ^{1}H NMR spectrum; however, these remain unassigned. I hypothesize that the allenylidene metathesis proceeds via initial formation of 1,1,4,4-tetraphenylbutatriene and [Li(solvent)$_x$][Cp_3Th(O)], which is evidently unstable and prone to loss of $[Cp]^-$. However, all attempts to isolate and identify the Th-containing product in this transformation have proven unsuccessful.

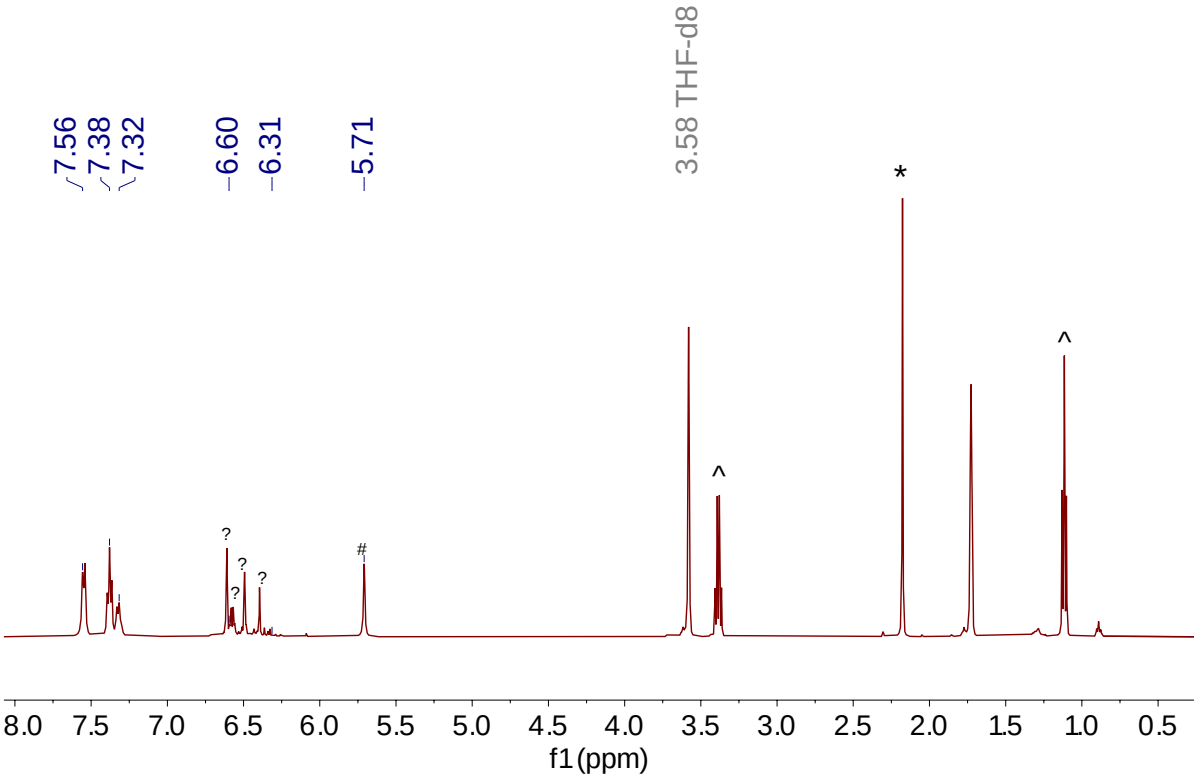

Figure 7.12. ^{1}H NMR spectrum of *in situ* reaction of [Li(Et_2O)$_2$][**7.1**] with 1 equiv of Ph_2CO in THF-d_8 at room temperature. (*) indicates the presence of hexamethylbenzene, (#) indicates the presence of LiCp, (^) indicates the presence of Et_2O, and (?) indicates the presence of unidentified Cp-containing products.

To our knowledge, this reactivity represents the first example of carbonyl-olefin metathesis reported for an allenylidene ligand,[90] and provides further support for the presence of resonances forms **I** and **II** in [**7.1**]$^{-}$. Similar reactivity is observed for transition metal alkylidenes. For example, reaction of [Ta($CH_2{}^tBu$)$_3$(=CH^tBu)] with Ph_2CO gives $Ph_2CC(H)^tBu$ and "[Ta(O)($CH_2{}^tBu$)$_3$]".[91] Similarly, reaction of [(PNP)Ti=CH^tBu(OTf)] (PNP = N[2-P^iPr_2-4-methylphenyl]$_2$) with 2 equiv of Ph_2CO results in formation of $Ph_2CC(H)^tBu$ and [(PNP)Ti(O)(OTf)($OCPh_2$)].[92]

Scheme 7.5. Synthesis of complex **7.5**.

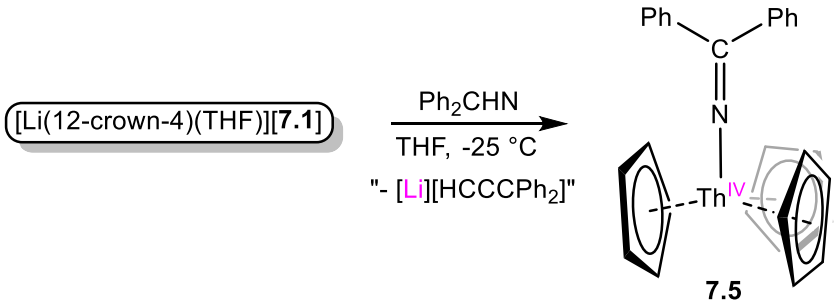

Additionally, I examined the reaction of $[Li(Et_2O)_2][$**7.1**$]$ with benzophenone imine in an efforts to isolate a thorium parent imido complex. This complex would be analogous to the proposed formation of thorium oxo from reaction of reaction of $[Li(Et_2O)_2][$**7.1**$]$ with benzophenone. Thus, a slow dropwise addition of a cold (–25 °C) THF solution of 1 equiv of Ph_2CNH to a cold (–25 °C) THF solution of $[Li(Et_2O)_2][$**7.1**$]$ results in immediate formation of a bright orange solution. After stirring for 20 min at room temperature, the ^{1}H NMR spectrum of the reaction mixture reveals complete consumption of benzophenone imine, along with the appearance of three new aryl CH resonances at 7.66 ppm, 7.25 ppm, and 7.21 ppm. Additionally, the ^{1}H NMR spectrum displays a major Cp environment at 6.16 ppm (Figure 7.40). However, reaction of $[Li(Et_2O)_2][$**7.1**$]$ with benzophenone imine does not reveal the formation of 1,1,4,4-tetraphenylbutatriene (**7.4**), indicating that this reaction proceeds differently compared to the reaction towards benzophenone. Interestingly, extraction of the reaction mixture with pentane affords a pale orange solution, from which $[Cp_3Th(N{=}CPh_2)]$ (**7.5**) was isolated a pale orange plates. I hypothesized that reaction of $[Li(Et_2O)_2][$**7.1**$]$ with benzophenone imine proceeds via protonation of the allenylidene fragment, leading to the generation of **7.5** and $[Li][HCCCPh_2]$. Complex **7.5** was characterized via X-ray crystallography, however NMR and UV-vis spectra, and a yield, were not recorded. Complex

7.5 crystallizes in the orthorhombic space group $P2_12_12_1$ (Figure 7.13). The Th-N bond distance in **7.5** is 2.250(14) Å, which is consistent with previous reports of thorium ketimide complexes.[93] Additionally, the N═C bond distance is 1.29(2) Å, consistent with N═C double bond.[93] Furthermore, the Th-N-C angle in **7.5** is 162.7(13)°, which is similar to that observed in previous reported thorium ketamide complex. For example, the Th-N-C angle $[Li]_2[Th(N{=}C(^tBu)Ph)_6]$ of 166.24(14)°.[94]

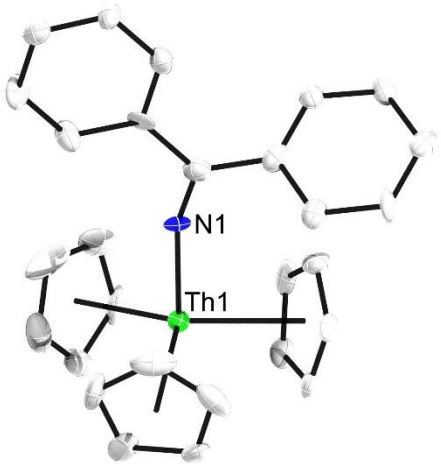

Figure 7.13. Solid-state molecular structure of **7.5**. Thermal ellipsoids set at 50% probability. The hydrogen atoms are omitted for clarity.

I also examined the reactivity of [Li(2.2.2-cryptand)][**7.1**] towards norbornene and diphenylacetylene in THF-d_8, however no reaction was observed in either case. In contrast, Dixneuf and co-workers have shown that ruthenium allenylidenes are competent pre-catalysts for ring-closing metathesis, enyne metathesis, and ring-opening metathesis polymerization (ROMP).[8, 38, 95-98 99] It is not immediately clear why [Li(2.2.2-cryptand)][**7.1**] is unreactive towards olefins and alkynes, but it may be due to the steric inaccessibility of the Th center caused by the presence of three cyclopentadienyl co-ligands.

Scheme 7.6. Synthesis of complex **7.6**.

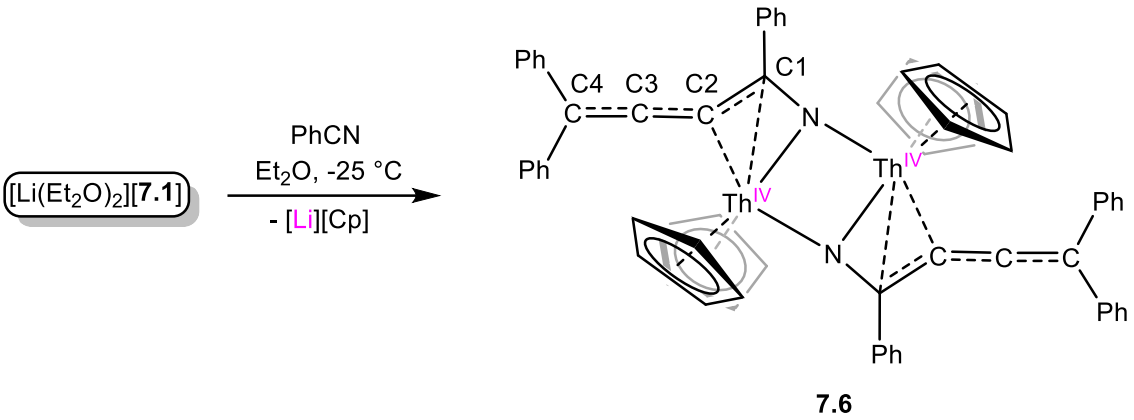

Additionally, I investigated the reactivity of $[Li(Et_2O)_2][$**7.1**$]$ with PhCN. Thus, addition of 1 equiv of PhCN to cold (–25 °C) Et_2O solution of $[Li(Et_2O)_2][$**7.1**$]$ results in immediate formation of a dark red solution (Scheme 7.6). Work-up of this solution, followed by crystallization from Et_2O, affords $[Cp_2Th(\mu\text{-}NC(Ph)CCCPh_2)]_2$ (**7.6**), as dark red plates. However, the yield was not recorded. The ^{1}H NMR spectrum of **7.6** in benzene-d_6 displays a single Cp environment at 6.21 ppm. Additionally, the ^{1}H NMR features an aryl resonance at 7.81, 7.33, and 7.22 ppm attributed to the phenyl substituents on C4 atom. The ^{1}H NMR exhibits additional aryl resonances at 8.16, 7.14, and 7.11 ppm that are assignable to the phenyl substituents on C1 atom (Figure 7.39). The ^{13}C{^{1}H} NMR and IR spectra were not recorded. Complex **7.6** crystallizes in the triclinic space group $P\bar{1}$ as a Et_2O solvate, **7.6**·3Et_2O (Figure 7.14). However, because of significant disorder and poor data quality, it was not possible to refine the nitrogen atoms anisotropically, and therefore, the metrical parameters will not be addressed. Importantly, the structural analysis confirms the insertion of PhCN into the Th- C_α bond. Similar PhCN insertion is observed in actinide alkyl and aryl complexes. For example, reaction of $Cp^*_2AnR_2$ (An = Th, U; R = Ph, CH_2Ph, CH_3) with excess PhCN results in nitrile insertion to generate actinide bis(ketimide) complexes, $Cp^*_2AnR_2$.[93]

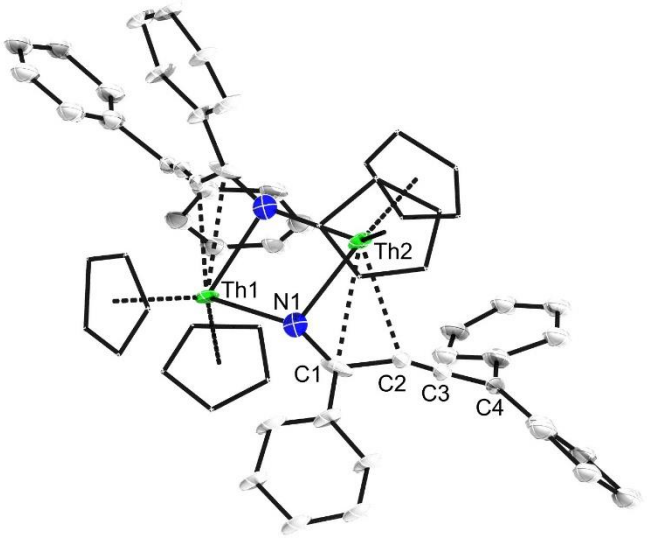

Figure 7.14. Solid-state molecular structure of **7.6**. Thermal ellipsoids set at 50% probability. The hydrogen atoms are omitted for clarity.

7.2.4 Computational Analysis

Actinide carbenes have proven to be valuable substrates for interrogating actinide-ligand bonding.[69, 70, 84, 100-114] Accordingly, the electronic structure and bonding interactions in [**7.1**]$^{-}$, **7.2**, and **7.3** was analyzed by Dr. Xiaojuan Yu and Prof. Jochen Autschbach at the State University of New York at Buffalo using density functional theory (DFT) using the B3LYP hybrid functional. Complete computational details are provided in section 7.4.15 Computational Data Details. The natural localized molecular orbital (NLMO) analysis reveals strong electron delocalization across the allenylidene fragment for three complexes (Figure 7.15, Figure 7.16, and Figure 7.20). For [**7.1**]$^{-}$, NLMO analysis showed three orbitals within the Th(CCCPh$_2$) fragment with appreciable Th character, including a σ(Th–C$_\alpha$) bond with 23% total Th weight (9% 7s; 75% 6d; 16% 5f) and two orthogonal π(C$_\alpha$–C$_\beta$) bonds with sizable Th weights [3% (47% 6d; 52% 5f) and 4% (46% 6d; 54% 5f), respectively]. The latter

two orbitals, along with the presence of a delocalized π lone-pair NLMO on C_γ, provide clear evidence for a dominance of resonance form **I**, which predicts triple bond character in the C_α-C_β bond along with a C_γ, lone pair in [**7.1**]$^-$. This assignment is also supported by the Wiberg bond orders (WBO): Th-C_α = 0.82, C_α-C_β = 2.58, C_β-C_γ = 1.19. However, the partial delocalization of the π(C_α–C_β) orbital onto Th indicates that resonance form **II** provides a secondary contribution to the electronic structure. The previously reported Th allenylidene, [{$(NR_2)_3$}Th($CCCPh_2$)]$^-$, exhibits similar delocalization, with comparable levels of Th participation in the σ(Th–C_α) and π(Th–C_α–C_β) orbitals.[115]

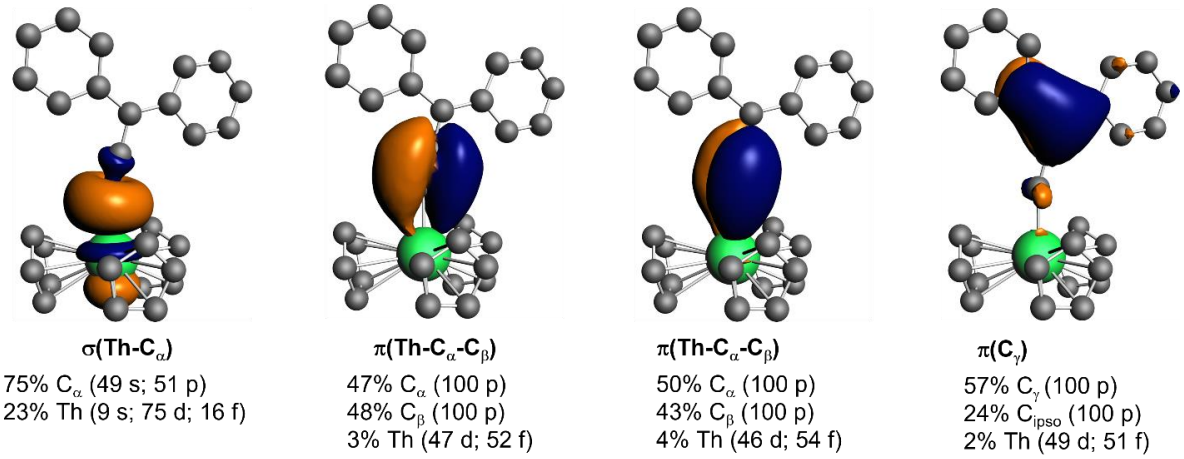

Figure 7.15. Isosurfaces (±0.03 a.u.) and atomic orbital weight compositions of selected NLMOs for [**7.**1]$^-$. Hydrogen atoms are omitted for clarity. (Color code: thorium = green; carbon = gray.)

The bonding picture with **7.2** is necessarily more complex, but also indicative of a highly delocalized electronic structure containing elements of resonance forms **I** and **II**. The NLMO analysis identified four orbitals within the [Th($CCCPh_2$)]$_2$ fragment with appreciable Th character (Figure 7.16). The σ(Th–C_α) bond exhibits 18% total weight (9% 7s; 72% 6d; 19% 5f) from Th and 4% total weight (20% 7s; 53% 6d; 26% 5f) from the bridging Th atom (Th*).

The two orthogonal π(Th–C_α–C_β) bonds each only exhibit 2% total weight from Th, but ca. 4% and 7% total weight, respectively, from Th*. Finally, the π-type NLMO on C_γ exhibits 2% total weight from Th, but 12% total weight from Th*. The electronic structure assignment is therefore similar to [**7.1**]$^-$ in terms of the dominance of resonance structure **I**, but the allenylidene orbitals are also clearly donating to the bridging Th* atom, which therefore reduces the bond orders within the ligand and between C_α and Th. This donation is also reflected in the averaged WBOs of the allenylidene unit: Th-C_α = 0.63, C_α-C_β = 2.33, C_β-C_γ = 1.26. The relatively large Th* contribution in the C_γ lone-pair NLMO is reflected in the ^{13}C spectral data for this complex (see below).

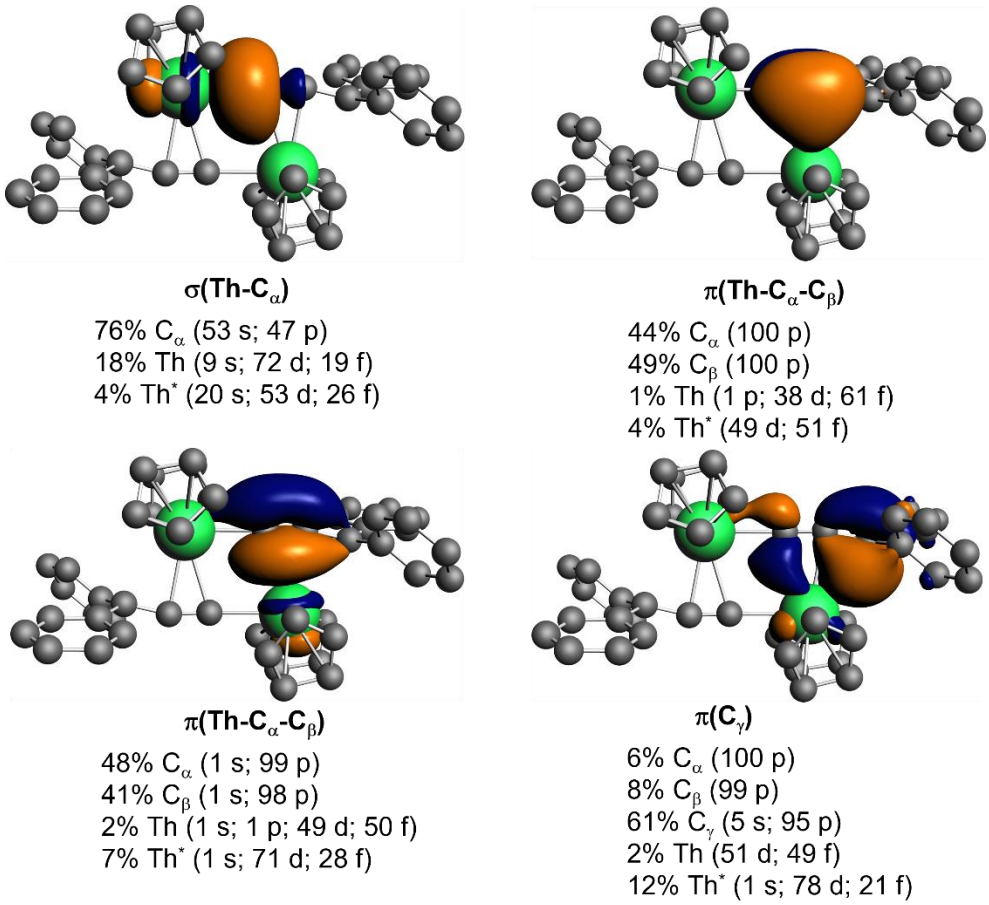

Figure 7.16. Isosurfaces (±0.03 a.u.) and atomic orbital weight compositions of selected NLMOs for **7.2**. Hydrogen atoms are omitted for clarity. (Color code: thorium = green; carbon = gray.)

For complex **7.3**, a natural localized molecular orbital (NLMO) analysis identified three orbitals within the Th(CCC(Me)Ph_2) fragment with Th character (Figure S29), including a σ(Th–C_α) bond with 22% total Th weight (9% 7s; 74% 6d; 16% 5f), and two orthogonal π(C_α–C_β) bonds with minor Th weights [2% (43% 6d; 57% 5f) and 2% (44% 6d; 55% 5f), respectively]. The σ(Th–C_α) bond in **7.3** is similar to that seen for [**7.1**]$^-$**, but the** π(C_α–C_β) interactions with Th are reduced, consistent with the pure acetylide resonance form expected for **7.3**. This resonance form is also reflected by the C_α–C_β WBO of 2.82. Furthermore, when

going from [**7.1**]$^-$ to **7.3**, the replacement of the delocalized π-lone pair on C_γ by –Me causes the C_β-C_γ WBO to decrease from 1.19 to 1.00.

The ^{13}C NMR chemical shifts for complexes [**7.1**]$^-$**, 7.2, and 7.3** were calculated using a hybrid version of the PBE functional with 40% exact exchange, with and without SO effects. See Table S5 for a summary of all calculated shifts. We have previously shown that the chosen functional can accurately predict ^{13}C NMR chemical shifts in thorium organometallics.[44] Indeed, the calculated NMR carbon chemical shifts are in excellent agreement the experimental values. For example, the calculated C_α shift for [**7.1**]$^-$ is 166.4 ppm (expt. = 164.8 ppm), which includes a 25.6 ppm deshielding contribution due to SO coupling (SOC) that is primarily attributed to the strong SO coupling within, and the involvement in chemical bonding of, the actinide ion's 5f shell. The calculated C_β and C_γ shifts for [**7.1**]$^-$ are 136.5 ppm (expt. = 141.8 ppm) and 74.2 ppm (expt. = 72.5 ppm), respectively. The former value includes 5.5 ppm deshielding is due to SOC. The SO-induced deshielding at C_β is therefore not negligible and a reflection of the Th-C covalency in combination with the delocalization in the allenylidene ligand. Generally speaking, the SO effects on the NMR shifts of neighboring light atoms indicate covalent bonding to a nearby heavy metal center.[44] For comparison, the C_α and C_β shifts in [{$(NR_2)_3$}Th($CCCPh_2$)]$^-$ include 36 and 9 ppm of SO-induced deshielding, respectively.[115] These values are comparable to those calculated for [**7.1**]$^-$ and reflect the similar bonding arrangements in their allenylidene ligands. The calculated C_α shift for **7.2** is 182.2 ppm (expt. = 178.4 ppm), which includes a 21.2 ppm deshielding contribution due to SOC. The calculated C_β and C_γ shifts for **7.2** are 163.8 ppm (expt. = 160.8 ppm) and 90.4 ppm (expt. = 89.1 ppm), respectively, including 2.9 and 3.5 ppm deshielding due to SOC. The latter value reflects the presence of the orbital

interaction between C_γ and Th^* (Figure 7.16). For comparison, the calculated C_α shift for **7.3** is 141.7 ppm (expt. = 146.4 ppm), which includes a 20.3 ppm deshielding contribution due to SOC. The reduced SOC deshielding for **7.3** relative to [**7.1**]$^-$ is consistent with its reduced Th-C_α covalency.

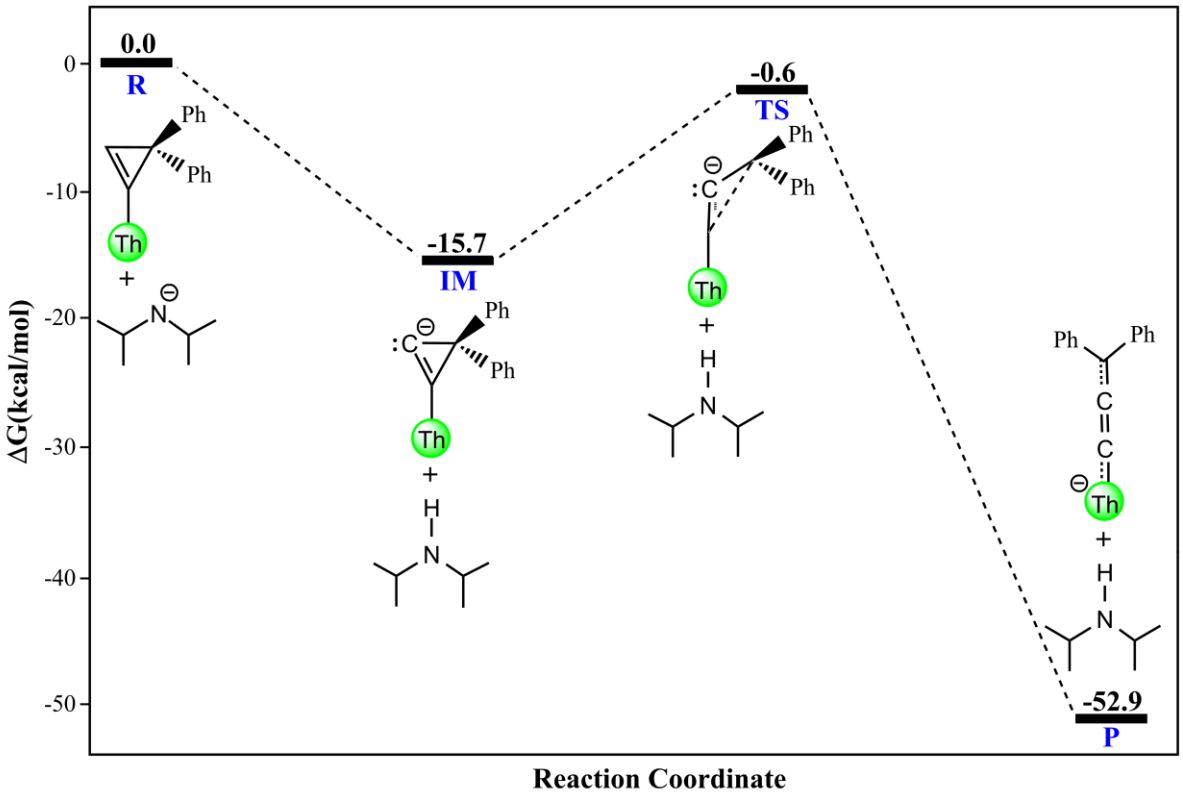

Figure 7.17. Computed DFT (B3LYP) Gibbs energy profile for the formation of [**7.**1]$^-$.

The reaction pathway from [Cp_3Th(3,3-diphenylcyclopropenyl)] to [Li(12-crown-4)(THF)][**7.1**] was also studied by DFT calculations (B3LYP functional), with the aim of elucidating the mechanism of cyclopropenyl ring-opening. Computational details are provided in section 7.4.15 Computational Data Details. The Gibbs energy reaction profile for the formation of [**7.1**]$^-$ is displayed in Figure 7.17. Structural details of the corresponding

stationary points are highlighted in Figure 7.21. The presence of the Li^+ ion was not explicitly modeled.

Starting from reactants diisopropylamide and [Cp_3Th(3,3-diphenylcyclopropenyl)] (designated as **R)**, the reaction proceeds via two primary steps: (1) deprotontation of **R** resulting in the formation of [$Cp_3Th(\eta^1$-3,3-Ph_2-*cyclo*-$C_3)]^-$ (denoted as **IM**) and diisopropylamine; and, (2) subsequent ring opening of **IM**, yielding products [**7.1**]$^-$ (denoted as **P**) and diisopropylamine. Following the formation of **IM**, in the subsequent ring-opening process (Figure S30), the C_α–C_β–C_γ angle changes from 63° in **IM** to 97° in the transition state (**TS**) and further to 176° (Expt. = 172°) for **P**. Notably, the energy of **TS** lies below that of the reactants, and the product formation is highly exothermic (52.9 kcal/mol). Therefore, the formation of [**1**]$^-$ is both kinetically and thermodynamically favorable, which is consistent with the rapid reaction rate observed experimentally.

We also considered an alternative structure for the intermediate, **IM***, with both C_α and C_β coordinated to Th, as depicted in Figure 7.21. The Gibbs energy of **IM*** was found to be 11.3 kcal/mol lower than that of **IM**. The structure of **IM*** exhibits an isosceles triangular configuration, not unlike a recently reported endohedral fullerene triangular thorium carbide cluster, $ThC_2@C_{82}$.[116] However, despite numerous attempts, our calculations did not reveal a viable pathway connecting **IM*** to [**7.1**]$^-$. Likewise, no reaction pathway connecting **IM** and **IM*** could be found. Therefore, we prefer a reaction pathway that proceeds via a C_β carbanion along the effectively barrierless pathway depicted in Figure 7.17.

7.2.5 Reactivity of Uranyl Towards 1-lithium-3,3-diphenylcyclopropene

Expanding upon my past efforts in uranyl hydrocarbyl chemistry, as discussed in chapter 2 and chapter 5, I aimed to explore alternative ligands to stabilize the uranyl fragment. Thus, I investigated the reactivity of 1-lithium-3,3-diphenylcyclopropene with uranyl in efforts to further isolate f-elements allenylidene complexes. The, addition of 2 equiv *in situ* generated 1-lithium-3,3-diphenylcyclopropene to an Et_2O solution of $[UO_2Cl_2(THF)_2]$ results in the formation of a red bright solution. Removal of the volatiles, extraction into hexanes, filtration, and crystallization results in the isolation of 1,1,6,6-tetraphenylhex-1,5-diene-3-yne (**7.7**), as red plates. The yield was not recorded. The ^{1}H NMR spectrum of **7.7** in benzene-d_6 features a diagnostic C*H* resonance at 6.11 ppm (Figure 7.37).[117] The $^{13}C\{^1H\}$ NMR spectrum of **7.7** in benzene-d_6 features resonances at 142.03, 139.87, 130.47, and 128.50 ppm attributable to *ipso*, *para*, *ortho*, and *meta* positions of the phenyl substituents. Additionally, the $^{13}C\{^1H\}$ NMR spectrum displays resonances present at 152.31, 108.38, and 94.09 ppm, which are assignable to the C1, C2, and C3 atoms, respectively (Figure 7.38). I hypothesize that the formation of compound **7.7** occurs initially through salt metathesis, generating "$[UO_2$(3,3-diphenylcyclopropenyl)$_2]$". This complex undergoes reduction of the uranium center and 3,3-diphenylcyclopropenyl oxidation, leading to the formation of a bicyclopropene compound. Subsequent isomerization affords the ring-opened product, **7.7**. The conversion of bicyclopropene to ring-open alkyne has been previous demonstrated. For instance, 3,3,3',3'-tetramethyl-2,2'-bis(trimethylsilyl)-1,1'-bicyclopropenyl converts thermally to the ring-opened isomerized product, 2,7-dimethyl-3,6-bis(trimethylsilyl)-octa-2,6-dien-4-yne.[118] Additionally, previous attempts to isolate uranyl organometallics has resulted in reductive elimination due to the reducing properties of numerous alkylating agents. For example, the

reaction between $[U^{VI}O_2Cl_2]$ with 2 equiv of phenyllithium resulted in uranium center reduction to afford $[U^{IV}O_2]$ alongside biphenyl.[119, 120]

Scheme 7.7. Synthesis of **7.7**.

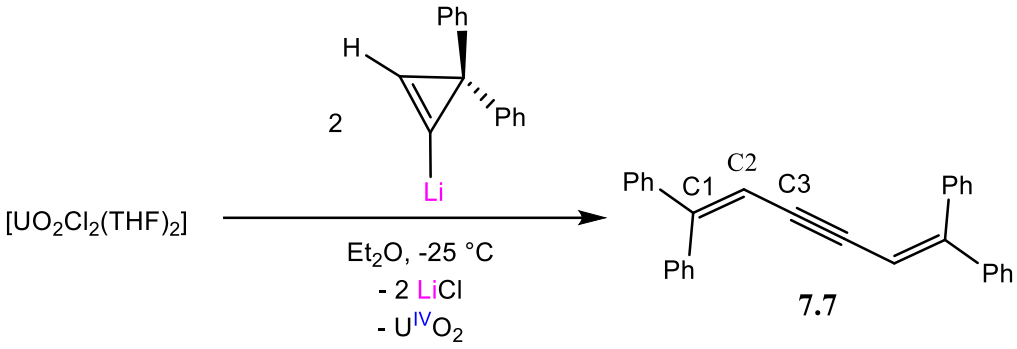

7.2.6 Reactivity of a Neptunium Complex Towards 3,3-diphenylcyclopropene

As previously reported by Dr. Greggory T. Kent from our group, reaction of $[AnCl(NR_2)_3]$ (An = U, Th, R = $SiMe_3$) with *in situ* generated lithium-3,3-diphenylcyclopropene results in the formation of the actinide allenyl complexes $[\{(NR_2)_3\}An(CH{=}C{=}CPh_2)]$ (An = U, Th). Subsequent deprotonation of $[\{(NR_2)_3\}An(CH{=}C{=}CPh_2)]$ with LDA in the presence of 2,2,2-cryptand results in formation of the anionic allenylidenes, [Li(2.2.2-cryptand)]$[\{(NR_2)_3\}An(CCCPh_2)]$ (An = U, Th), which are the first An-C multiple bonds that do not feature heteroatom stabilization.[43]

Scheme 7.8. Proposed Synthesis of Neptunium Allenylidene Complex.

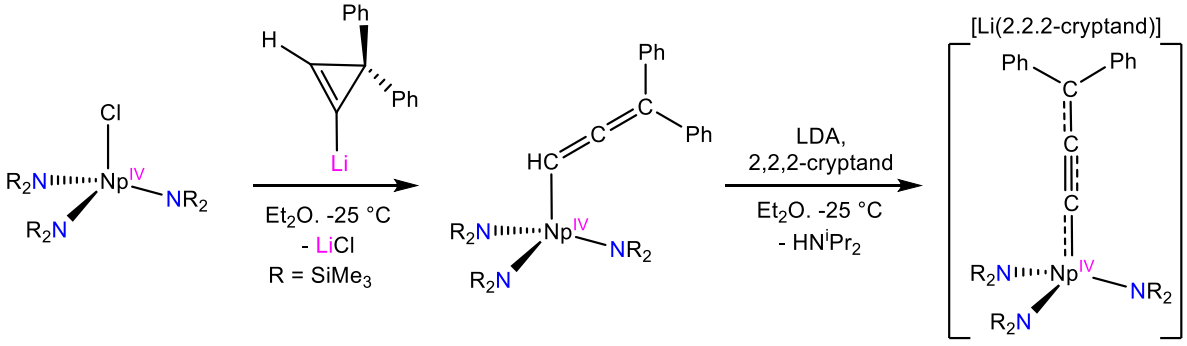

Inspired by this chemistry, I proposed to investigate the reactivity of previously reported neptunium (Np) silylamide complex, [$NpCl(NR_2)_3$] (R = $SiMe_3$)[121] with *in situ* generated lithium-3,3-diphenylcyclopropene, aiming to afford a neptunium allenyl complex. The subsequent treatment of the neptunium allenyl complex with 1 equiv of LDA could potentially yield a first neptunium allenylidene complex. Due to the limited Np stocks and relatively high-specific radioactivity of ^{237}Np, this chemistry requires small-cale preoptimized reaction conditions using analog complexes, namely, uranium or thorium. In efforts to develop preoptimized small-scale strategy, approximately 20 mg small scale reaction of a uranium silylamide complex, [$UCl(NR_2)_3$], was used to establish the synthetic methods at the University of California, Santa Barbara. Notably, small-scale reaction of [$AnCl(NR_2)_3$] (An = U, Th) with *in situ* generated lithium-3,3-diphenylcyclopropene led to the formation of uranium allenyl complex, [{$(NR_2)_3$}$An(CH{=}C{=}CPh_2)$] (An = U, Th). However, various attempts to crystallize were unsuccessful, likely due to its high solubility in hexanes. Consequently, treating the *in situ generated uranium or thorium allenyl complex with LDA in the presence of 2,2,2-cryptand result in the formation of crystals suitable for solid-state analysis.* In efforts to expand the chemistry to transuranic elements, I investigated the reactivity of [$NpCl(NR_2)_3$] (R= $SiMe_3$)[121] towards 3,3-diphenylcyclopropene (Scheme 7.8). The neptunium work was conducted at Los Alamos National Laboratory (LANL) under the guidance of Dr. Andrew J. Gaunt and Dr. Jesse Murillo. In this regard, slow dropwise addition of a cold (–35 °C) Et_2O solution of 1 equiv of *in situ* generated lithium-3,3-diphenylcyclopropene to an Et_2O solution of [$NpCl(NR_2)_3$] results in an immediate color change to amber brown color, presumably due to formation of a neptunium allenyl complex, [{$(NR_2)_3$}$Np(CH{=}C{=}CPh_2)$]. Subsequent slow dropwise addition of a cold (–35 °C) Et_2O

solution of 1 equiv of LDA to a cold (–35 °C) Et_2O solution of "[{$(NR_2)_3$}Np(CH=C=CPh_2)]" in the presence of 2,2,2-cryptand resulted in formation of dark yellow solution with precipitation of yellow solids. After stirring for 2 min, filtration of the reaction mixture with glass fiber filter and crystallization from Et_2O layered with pentane results in the isolation of the [Li(2,2,2-cryptand)][$NpCl(NR_2)_3$] (R = $SiMe_3$) (**7.8**), isolated as light yellow plates in a 10.5 % yield (Scheme 7.9). Complex **7.8** was characterized via X-ray crystallography, however the NMR and UV-vis spectrum were not recorded. In addition, a dark yellow oil was concurrently formed. Subsequent extraction into THF, filtration, and crystallization results in the isolation of the [Li(2,2,2-cryptand)] [$NpCl_2(NR_2)_3$] (R = $SiMe_3$) (**7.9**), which was isolated as yellow orange plates (Scheme 7.10). Complex **7.9** was characterized via X-ray crystallography, however NMR and UV-vis spectra, and a yield, were not recorded. I hypothesize that the lithium-3,3-diphenylcyclopropene reduces the [$NpCl(NR_2)_3$], resulting in the formation of complex **7.8** and the 3,3-diphenylcyclopropyl radical, while the formation of complex **7.9** is likely due to the subsequent reaction of LiCl and 2,2,2-cryptand with [$NpCl(NR_2)_3$] in solution.

Scheme 7.9. Isolation of complexes **7.8** and **7.9**.

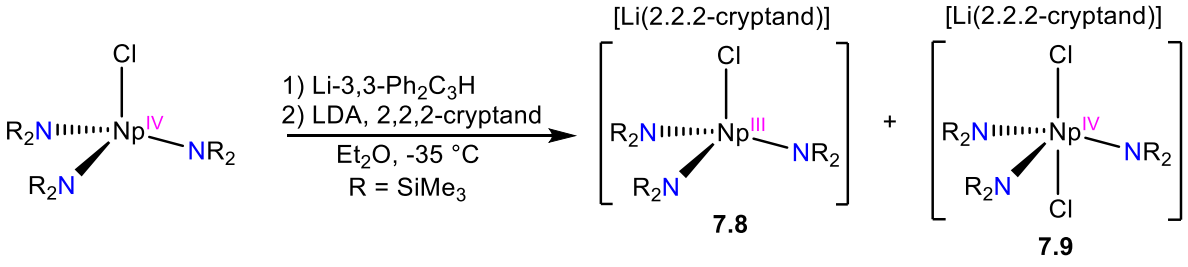

In an efforts to isolate a neptunium cyclopropenyl complex, I explored the reactivity of 7.6 with lithium-3,3-diphenylcyclopropene. Thus, a slow dropwise addition of a cold (–25 °C) Et_2O solution of 1 equiv of *in situ* generated lithium-3,3-diphenylcyclopropene to a yellow

Et_2O solution of **7.8** results in an immediate color change to dark yellow solution (Scheme 7.10).Work-up and extraction of the reaction mixture into pentane affords a clear yellow filtrate and leaves dark solids behind. Further extraction of the dark solids into Et_2O affords a dark orange filtrate. Storage of the yellow pentane filtrate at –35 °C afford light yellow plates, similar in appearance to those isolate for **7.8**. However, a yield was not recorded, and further characterization was not performed. Storage of the orange Et_2O filtrate at –35 °C afforded dark red plates, but attempts to characterize using X-ray crystallography were unsuccessful. The yield was not recorded, and characterization methods, such as NMR and UV-vis spectroscopy were not performed on the reaction mixture.

Scheme 7.10. Reaction of **7.8** with lithium-3,3-diphenylcyclopropene.

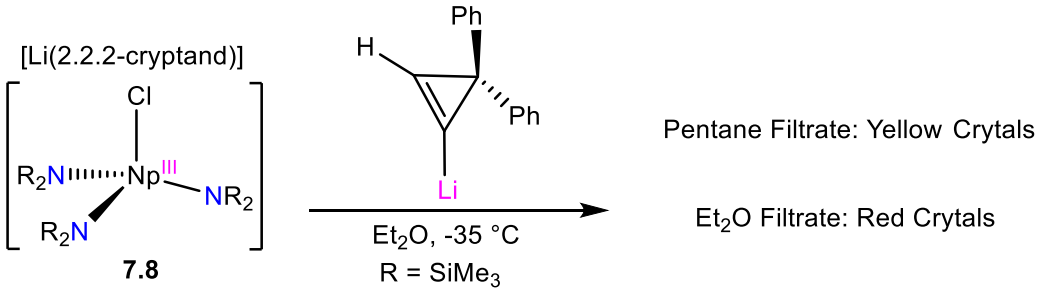

Complex **7.8** crystallizes in the monoclinic space group $P2_1/c$ (Figure 7.18), whereas **7.9** crystallizes in the triclinic space group $P\bar{1}$ (Figure 7.19). The solid-state molecular structure of **7.8** reveals a pseudotetrahedral geometry around the neptunium coordinated by three amide ligands and Cl ligand. The solid-state molecular structure of **7.9** reveals a trigonal bipyramidal neptunium center coordinated by three amide ligands and two Cl ligand. Additionally, both **7.8** and **7.9** feature a $[Li(2,2,2\text{-cryptand})]^+$ counterion as discrete anion-cation pairs. The average Np-N distance in **7.8** is 2.364 Å (range = 2.360(2) – 2.369(2) Å), which are longer than **7.9** of 2.193 Å (range = 2.14(6)- 2.25(6) Å). The longer Np-N in **7.8** is consistent with the larger ionic radius of Np^{3+}.[122] The Np-N distances in **7.8** and **7.9** are similar to those

reported in neptunium amide complexes. For example, the average Np-N distance in $[Np(NR_2)_3Cl]$ and $[\{K(DB\text{-}18\text{-}C\text{-}6)(THF)\}_3(\mu_3\text{-}Cl)][Np(NR_2)_3Cl]_2$ ($R = SiMe_3$) is 2.221(4) Å and 2.297 Å, respectively.[121]

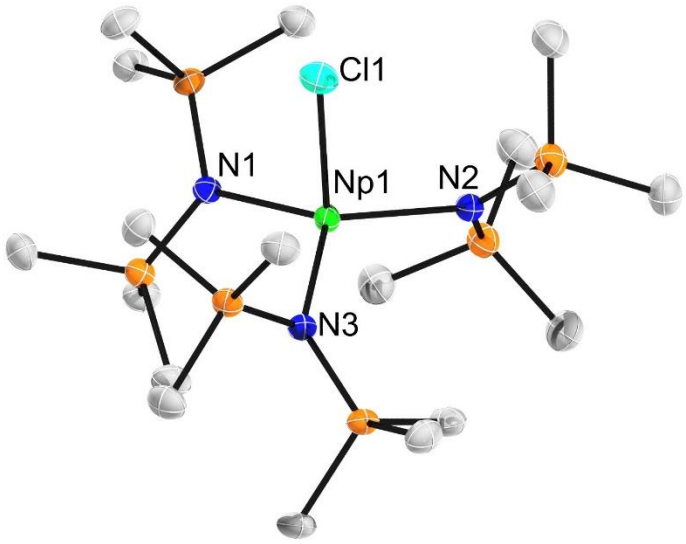

Figure 7.18. Solid-state molecular structure of **7.8**. Thermal ellipsoids set at 50% probability. The hydrogen atoms and $[Li(2,2,2\text{-cryptand})]^+$ are omitted for clarity.

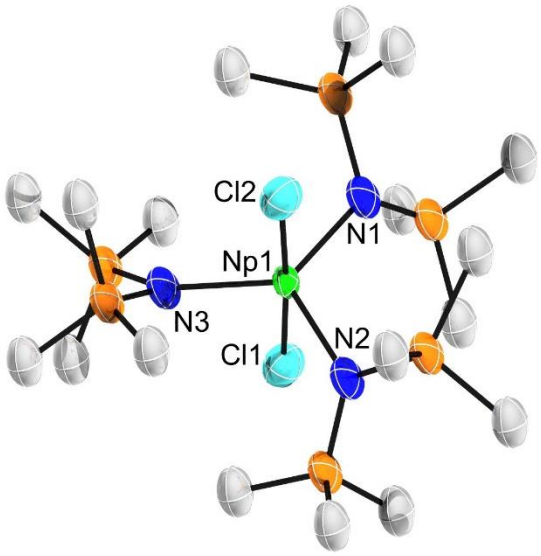

Figure 7.19. Solid-state molecular structure of **7.9**. Thermal ellipsoids set at 50% probability. The hydrogen atoms and $[Li(2,2,2\text{-cryptand})]^+$ are omitted for clarity.

Overall, the isolation of **7.8** suggests that the readily accessible trivalent oxidation state of Np hinders the ability to isolate the desired organometallic complex. This highlights the difference in reactivity towards lithium-3,3-diphenylcyclopropene between Np vs that observed in U and Th. Going forward, additional examination of reaction mixtures using NMR spectroscopy could offer valuable insights into the synthesis of the desired complex. Also the utilizing *in situ* generated Np allenyl, "$[\{(NR_2)_3\}Np(CH{=}C{=}CPh_2)]$" is not an ideal approach due to the potential presence LiCl, which could impede subsequent reactions and lead to the formation of complexes similar to **7.9**.

7.3 Summary

In summary, I have synthesized and characterized a rare example of f element allenylidene complexes, namely, $[Li(Et_2O)_2][Cp_3Th(CCCPh_2)]$, [Li(12-crown-

4)(THF)][$Cp_3Th(CCCPh_2)$], and [Li(2.2.2-cryptand)][$Cp_3Th(CCCPh_2)$]. To our knowledge, the ring-opening of the 3,3-diphenylcyclopropenyl ligand upon deprotonation via an exogenous base is unprecedented and provides a potentially important new route to the allenylidene ligand. Additionally, [$Li(Et_2O)_2$][**7.1**] demonstrated regioselective electrophilic attack at the C_γ carbon atom upon reaction with MeI leading to the formation of a thorium acetylide complex, [$Cp_3Th(C{\equiv}CC(Me)Ph_2)$] (**7.3**). Furthermore, the reactivity of [$Li(Et_2O)_2$][**7.1**] towards benzophenone represents the first example of carbonyl-olefin metathesis reported for an allenylidene ligand. Importantly, this works showcases several novel modes of allenylidene reactivity, providing a new avenue of reactivity in comparison to the more common late transition metal allenylidenes. The NLMO analysis of the bonding in [**7.1**]$^-$ and **7.2** by DFT reveal a delocalized electronic structure with contributions from both resonance forms **I** and **II**. In addition, a DFT analysis of the ^{13}C NMR chemical shifts in [**7.1**]$^-$ and **7.2** show modest levels of nuclear magnetic shielding induced by the spin-orbit coupling due to 5f participation on the Th-C_α bonds. Furthermore, I examined the reactivity between [$NpCl(NR_2)_3$] with lithium-3,3-diphenylcyclopropene, which resulted in reduction of the neptunium center and isolation of a neptunium(III) silylamide complexes, [Li(2,2,2-cryptand)][$NpCl(NR_2)_3$] (R = $SiMe_3$) (**7.8**). Additionally, from the same reaction, a neptunium(IV) silylamide complex, [Li(2,2,2-cryptand)][$NpCl_2(NR_2)_3$] (R = $SiMe_3$) (**7.9**), was obtained, which was attributed due to the presence of LiCl in solution. Moving forward, it is crucial to examine the neptunium reduction in efforts to prevent unwanted reduction. Importantly, additional pre-optimization is required to minimize the presence of LiCl in subsequent reaction, thereby facilitating the isolation of the desire neptunium organometallic complexes.

7.4 Experimental

7.4.1 General Procedures

General. All reactions and subsequent manipulations were performed under anaerobic and anhydrous conditions under an atmosphere of dinitrogen. Hexanes, diethyl ether (Et_2O), and toluene were dried using a Vacuum Atmospheres DRI-SOLV Solvent Purification system and stored over 3Å sieves for 24 h prior to use. Tetrahydrofuran (THF) was distilled over Na/benzophenone and stored over activated 3 Å molecular sieves for 24 h prior to use. Benzene-d_6 and thf-d_8 were dried over 3Å molecular sieves for 24 h prior to use. [Cp_3Th(3,3-diphenylcyclopropenyl)] and LDA were synthesized according to the previously reported procedures.[44, 123, 124] All other reagents were purchased from commercial suppliers and used as received.

^{1}H, ^{13}C{^{1}H}, and ^{7}Li{^{1}H} NMR spectra were recorded on an Agilent Technologies 400-MR DD2 400 MHz spectrometer or a Bruker AVANCE NEO 500 MHz spectrometer. ^{1}H and ^{13}C{^{1}H} NMR spectra were referenced to external tetramethylsilane (TMS) using the residual protio solvent peaks as internal standards. ^{7}Li{^{1}H} NMR spectra are referenced indirectly with the ^{1}H chemical shift of TMS at 0 ppm, according to IUPAC standard.[125, 126] IR spectra were recorded on a Nicolet 6700 FT-IR spectrometer. Electronic absorption spectra were recorded on a Shimadzu UV3600 UV-NIR Spectrometer. Elemental analyses were performed by the Microanalytical Laboratory at the University of California (Berkeley, CA).

7.4.2 Synthesis of $Et_2O)_2$][Cp_3Th(CCCPh$_2$)] ([Li($Et_2O)_2$][7.1])

To a cold (–25 °C), stirring, colorless Et_2O solution (2 mL) of [Cp_3Th(3,3-diphenylcyclopropenyl)] (97.7 mg, 0.157 mmol) was added over the course of 5 min a cold

(–25 °C), colorless Et_2O (1 mL) solution of LDA (16.8 mg, 0.157 mmol). Upon addition, the solution turned bright red-orange. (Note: faster addition resulted in immediate formation of a dark red brown solution concomitant with the precipitation of a dark brown solid. Despite the formation of dark brown solids, complex $[Li(Et_2O)_2]$[7.1] can be isolated is low yields) After stirring for 10 min, the volatiles were removed *in vacuo*. The red-orange solid was then extracted into Et_2O (6 mL) and filtered through a Celite column (0.5 cm × 2 cm) supported on glass wool to afford a clear, red filtrate. The volume of the filtrate was reduced to 3 mL *in vacuo*. Storage of this vial at –25 ºC for 24 h resulted in the deposition of orange plates, which were isolated by decanting the supernatant, rinsing with cold (-25 °C) pentane (2 mL), and drying *in vacuo* (66.2 mg, 54% yield). Anal. Calcd for $ThC_{38}H_{45}LiO_2$: C, 59.06; H, 5.87. Found: C, 58.92; H, 5.87. ^{1}H NMR (25 °C, 500 MHz, benzene-d_6): δ 7.88 (d, J = 7.3 Hz, 4H, *o*-H), 7.19 (t, J = 8.39 Hz, 4H, *m*-H), 6.57 (t, J = 7.1 Hz, 2H, *p*-H), 6.18 (s, 15H, Cp), 3.23 (q, J = 7.02 Hz, 8H, O*C*H$_2$CH$_3$), 1.06 (q, J = 7.02 Hz, 12H, OCH$_2$*C*H$_3$). ^{13}C{^{1}H} NMR (25 °C, 126 MHz, THF-d_8): δ 161.12 (C_α), 147.65 (*i*-C), 146.94 (C_β), 127.84 (*o*-C), 122.82 (*m*-C), 117.01 (Cp), 114.89 (*p*-C), 70.72 (C_γ). ^{7}Li{^{1}H} NMR (25 °C, 194 MHz, THF-d_8) δ –0.69. IR (KBr pellet, cm^{-1}): 3026 (w), 3022 (w), 2971 (m), 2930 (w), 2864 (m), 2717 (w), 2592 (w), 2565 (w), 2495 (w), 2417 (w), 2356 (w), 2343 (w), 2280 (w), 2081 (w), 1914 (s, ν_{CC}), 1866 (s, ν_{CC}), 1685 (w), 1572 (s), 1554 (s), 1511 (m), 1477 (s), 1447 (s), 1384 (m), 1360 (m), 1327 (m), 1300 (s), 1286 (s), 1267 (m), 1243 (m), 1171 (s), 1152 (m), 1098 (s), 1061 (s), 1010 (s), 987 (s), 951 (w), 908 (m), 885 (w), 838 (w), 781 (s), 700 (s), 650 (m), 631 (m), 600 (w), 542 (w), 514 (w), 475 (w), 419 (w).

7.4.3 Synthesis of [Li(12-crown-4)(THF)][Cp$_3$Th(CCCPh$_2$)] ([Li(12-crown-4)(THF)][7.1])

To a cold (–25 °C), stirring, colorless THF solution (2 mL) of [Cp_3Th(3,3-diphenylcyclopropenyl)] (30.0 mg, 0.048 mmol) and 12-crown-4 (8.5 mg, 0.048 mmol) was added dropwise a cold (–25 °C), colorless THF (1 mL) solution of LDA (5.1 mg, 0.048 mmol). Upon addition, the solution turned dark red. After stirring for 10 min, the volatiles were removed *in vacuo*. The red solid was then extracted into THF (3 mL) and filtered through a Celite column (0.5 cm × 2 cm) supported on glass wool to afford a clear, dark red filtrate. The volume of the filtrate was reduced to 2 mL *in vacuo* and layered with hexanes (3 mL). Storage of this vial at –25 ºC for 24 h resulted in the deposition of red plates, which were isolated by decanting the supernatant, rinsing with cold (-25 °C) pentane (2 mL), and drying *in vacuo* (30.2 mg, 72% yield). Anal. Calcd for $ThC_{42}H_{49}LiO_5$: C, 57.80; H, 5.66. Found: C, 57.58; H, 5.74. ^{1}H NMR (25 °C, 500 MHz, THF-d_8): δ 7.58 (d, J = 7.93 Hz, 4H, *o*-H), 6.87 (t, J = 7.71 Hz, 4H, *m*-H), 6.31 (s, 15H, Cp), 6.16 (t, J = 7.02 Hz, 2H, *p*-H), 3.64 (s, 16H, 12-crown-4). $^{13}C\{^1H\}$ NMR (25 °C, 126 MHz, THF-d_8): δ 164.80 (C_α), 147.54 (*i*-C), 141.77 (C_β), 127.96 (*o*-C), 122.14 (*m*-C), 116.76 (Cp), 113.86 (*p*-C), 72.48 (C_γ), 69.19 (12-crown-4). $^7Li\{^1H\}$ NMR (25 °C, 194 MHz, THF-d_8) δ –0.95. IR (KBr pellet, cm^{-1}): 3081 (w), 3042 (w), 2935 (m), 2878 (m), 2742 (w), 2703 (w), 2607 (w), 2577 (w), 2528 (w), 2480 (w), 2412 (w), 2359 (w), 2354 (w), 2278 (w), 2076 (w), 1949 (s, ν_{CC}), 1896 (s, ν_{CC}), 1767 (w), 1715 (w), 1675 (w), 1652 (w), 1585 (s), 1545 (s), 1483 (s), 1446 (s), 1430 (s), 1401 (w), 1359 (m), 1333 (s), 1297 (s), 1241 (m), 1221 (m), 1197 (m), 1166 (s), 1132 (s), 1087 (s), 1046 (s), 1021 (s), 980 (s), 926 (s), 900 (s), 860 (s), 770 (s), 745 (s), 687 (s), 634 (m), 613 (w), 582 (m), 545 (m), 509 (w), 481 (m), 467 (m).

7.4.4 Synthesis of [Li(2.2.2-cryptand)][$Cp_3Th(CCCPh_2)$] ([Li(2.2.2-cryptand)][7.1])

To a cold (–25 °C), stirring, colorless THF solution (2 mL) of [Cp_3Th(3,3-diphenylcyclopropenyl)] (55.7 mg, 0.089 mmol) and 2.2.2-cryptand (33.8 mg, 0.089 mmol) was added dropwise a cold (–25 °C), colorless THF (1 mL) solution of LDA (9.6 mg, 0.089 mmol). Upon addition, the solution turned dark red. After stirring for 10 min, the volatiles were removed *in vacuo*. The dark red solid was then extracted into THF (3 mL) and filtered through a Celite column (0.5 cm × 2 cm) supported on glass wool to afford a clear, dark red filtrate. The volume of the filtrate was reduced to 2 mL *in vacuo* and layered with hexanes (3 mL). Storage of this vial at –25 ºC for 24 h resulted in the deposition of red plates, which were isolated by decanting the supernatant, rinsing with cold (-25 °C) pentane (2 mL), and drying *in vacuo* (71.2 mg, 79% yield). Anal. Calcd for $ThC_{48}H_{61}N_2LiO_6$: C, 57.59; H, 6.14; N, 2.80. Found: C, 57.21; H, 6.37; N, 2.54. ^{1}H NMR (25 °C, 500 MHz, THF-d_8): δ 7.53 (d, J = 8.39 Hz, 4H, *o*-H), 6.79 (t, J = 7.63 Hz, 4H, *m*-H), 6.31 (s, 15H, Cp), 6.06 (t, J = 7.63 Hz, 2H, *p*-H), 3.56 (s, 12H, CH_2), 3.52 (t, J = 5.04 Hz, 12H, CH_2), 2.59 (t, J = 5.11 Hz, 12H, CH_2). ^{13}C{^{1}H} NMR (25 °C, 126 MHz, THF-d_8): δ 166.86 (C_α), 147.77 (*i*-C), 138.78 (C_β), 127.71 (*o*-C), 122.07 (*m*-C), 116.55 (Cp), 113.02 (*p*-C), 73.64 (C_γ), 69.46 ($C_{cryptand}$), 68.39 ($C_{cryptand}$), 54.77 ($C_{cryptand}$). ^{7}Li{^{1}H} NMR (25 °C, 194 MHz, THF-d_8) δ –1.24. IR (KBr pellet, cm^{-1}): 3054 (w), 2862 (m), 2578 (w), 2494 (w), 2421 (w), 2364 (w), 2331 (w), 2282 (w), 2075 (w), 1945 (s, ν_{CC}), 1587 (s), 1571 (s), 1477 (s), 1445 (s), 1356 (s), 1333 (s), 1298 (s), 1259 (m), 1236 (m), 1144 (m), 1086 (s), 1013 (s), 979 (s), 947 (s), 930 (s), 902 (s), 764 (s), 699 (s), 688 (s), 631 (m), 609 (w), 575 (m), 550 (m), 525 (m), 480 (m), 419 (w).

7.4.5 Synthesis of [$Cp_2Th(CCCPh_2)]_2$ (7.2)

Dissolution of [$Li(Et_2O)_2$][$Cp_3Th(CCCPh_2)$] (23.9 mg, 0.031 mmol) in benzene-d_6 (1 mL) resulted in bright red solution. The solution was permitted to stand for 7 d, which resulted in

color change to pale yellow concomitant with the deposition of orange red plates and a colorless powder. The red solid was isolated from the colorless powder by decanting the supernatant, rinsing with Et_2O (2 × 2 mL), and drying *in vacuo* (9.2 mg, 54% yield). Anal. Calcd for $Th_2C_{50}H_{40}$: C, 54.35; H, 3.65. Found: C, 55.01; H, 3.86. ^{1}H NMR (25 °C, 500 MHz, dichloromethane-d_2): δ 7.56 (d, J = 7.2 Hz, 8H, *o*-H), 7.46 (t, J = 7.8 Hz, 8H, *m*-H), 7.11 (t, J = 7.2 Hz, 4H, *p*-H), 6.11 (s, 20H, Cp). ^{13}C{^{1}H} NMR (25 °C, 126 MHz, dichloromethane-d_2): δ 178.42 (C_α), 160.77 (C_β), 140.85 (*i*-C), 129.21 (*o*-C), 126.11 (*m*-C), 124.44 (*p*-C), 118.07 (Cp), 89.14 (C_γ). IR (KBr pellet, cm^{-1}): 3086 (w), 3052 (w), 3020 (w), 2273 (w), 1906 (m, ν_{CC}), 1715 (w), 1661 (w), 1638 (w), 1587 (m), 1513 (m), 1484 (m), 1445 (m), 1401 (w), 1355 (w), 1331 (w), 1292 (w), 1255 (w), 1234 (m), 1184 (w), 1157 (w), 1089 (w), 1048 (m), 1013 (s), 915 (m), 897 (m), 848 (w), 791 (s), 698 (s), 681 (m), 647 (m), 644 (m), 596 (w), 504 (w), 498 (w), 469 (m).

7.4.6 Synthesis of [Cp$_3$Th(CCC(Me)Ph$_2$)] (7.3).

To a cold (–25 °C), stirring, red THF solution (2 mL) of [Li(Et$_2$O)$_2$][Cp$_3$Th(CCCPh$_2$)] (51.6 mg, 0.067 mmol) was added cold (–25 °C) MeI (4.2 µL, 0.067 mmol). Upon addition, the solution immediately turned pale yellow. After stirring for 2 min, the volatiles were removed *in vacuo* and the resulting pale yellow tacky solid was triturated with pentane (2 × 2 mL). The solid was then extracted into pentane (10 mL) and filtered through a Celite column (0.5 cm × 2 cm) supported on glass wool to afford a clear, colorless filtrate. The volatiles were then removed *in vacuo* to provide a colorless solid. The colorless solid was then extracted into hexanes (10 mL) and filtered through a Celite column (0.5 cm × 2 cm) supported on glass wool to afford a clear, colorless filtrate. The volume of the filtrate was reduced to 5 mL *in vacuo*. Storage of this vial at –25 ºC for 24 h resulted in the deposition of colorless plates,

which were isolated by decanting the supernatant and drying *in vacuo* (34.9 mg, 83% yield). Anal. Calcd for $ThC_{31}H_{28}$: C, 58.86; H, 4.46. Found: C, 58.63; H, 4.38. ^{1}H NMR (25 °C, 500 MHz, THF-d_8): δ 7.65 (d, J = 7.8 Hz, 4H, *o*-H), 7.28 (t, J = 7.8 Hz, 4H, *m*-H), 7.15 (t, J = 7.3 Hz, 2H, *p*-H), 6.32 (s, 20H, Cp), 2.01 (s, 3H, CH_3). ^{13}C{^{1}H} NMR (25 °C, 500 MHz, THF-d_8): δ 149.58 (*i*-C), 146.38 (C_α), 128.73 (*o*-C), 128.29 (*m*-C), 126.80 (*p*-C), 126.71 (C_β), 117.45 (Cp), 46.82 (C_γ), 32.03 (CH_3). IR (KBr pellet, cm^{-1}): 3914 (w), 3454 (w), 3298 (w), 3086 (w), 3054 (w), 3029 (w), 2978 (m), 2934 (w), 2880 (m), 2715 (w), 2425 (w), 2278 (w), 2071 (m, ν_{CC}), 1948 (w), 1880 (w), 1808 (w), 1773 (w), 1683 (m), 1596 (m), 1489 (s), 1443 (s), 1368 (m), 1315 (w), 1286 (w), 1260 (w), 1199 (m), 1183 (m), 1159 (w), 1130 (m), 1127 (m), 1104 (w), 1064 (m), 1046 (s), 1027 (s), 1011 (s), 912 (m), 890 (m), 842 (w), 803 (s), 771(s), 700 (s), 653 (s), 639 (s), 613 (m), 587 (m), 535 (w), 505 (w), 453 (w), 422 (w).

7.4.7 *In Situ* Reaction of [Li(Et$_2$O)$_2$][1] with Ph$_2$CO.

To a cold (–25 °C), stirring, red THF-d_8 solution (0.5 mL) of [Li(Et$_2$O)$_2$][Cp$_3$Th(CCCPh$_2$)] (9.4 mg, 0.012 mmol) and C_6Me_6 (1.1 mg, 0.007 mmol) was added dropwise a cold (–25 °C), colorless THF-d_8 solution (0.25 mL) of Ph_2CO (2.2 mg, 0.012 mmol). Upon addition, the solution immediately turned bright yellow. After 5 min, the solution was transferred to an NMR tube equipped with a J-Young valve. ^{1}H, ^{7}Li{^{1}H}, and ^{13}C{^{1}H} NMR spectra were then recorded, which revealed formation of 1,1,4,4-tetraphenylbutatriene[89] in 99 % yield, according to integration against the internal standard. The generation of cyclolpentadienyllithium (LiCp)[58] was also observed. ^{1}H NMR (25 °C, 500 MHz, THF-d_8): δ 7.55 (d, J = 7.8 Hz, 8H, *o*-H), 7.38 (t, J = 7.6Hz, 8H, *m*-H), 7.32 (d, J = 7.8 Hz, 4H, *p*-H), 6.61 (s, unidentified), 6.58 (s, unidentified), 6.57 (s, unidentified), 6.49 (s, unidentified), 6.39 (s, unidentified), 5.71 (s, 5H, LiCp), 1.73 (s, 18H, C_6Me_6). ^{13}C{^{1}H} NMR (25 °C, 500 MHz,

THF-d_8): δ 152.72 ($C_{2,3}$), 139.82 (*i*-C), 132.23 (C_6Me_6), 130.33 (*o*-C), 122.82 (*m*-C), 129.03 (*p*-C), 123.80 ($C_{1,4}$), 118.29 (unidentified), 117.63 (unidentified), 117.49 (unidentified), 116.97 (unidentified), 114.29 (unidentified), 113.75 (unidentified), 103.53 (LiCp), 17.07 (C_6Me_6). ^{7}Li{^{1}H} NMR (25 °C, 194 MHz, THF-d_8) δ –6.02 (LiCp).

7.4.8 Synthesis of [Cp$_3$Th(N=CPh$_2$)] (7.5).

To a cold (–25 °C), stirring, red THF solution (2 mL) of [Li(12-crown-4)(THF)][**7.1**] (26.0 mg, 0.0315 mmol) was added Ph_2C=NH (5.3 µL, 0.0315 mmol). Upon addition, the solution immediately turned orange. After stirring for 20 min, the volatiles were removed *in vacuo* and the resulting orange tacky solid was triturated with pentane (2 × 2 mL). The solid was then extracted into Pent (3 mL) and filtered through a Celite column (0.5 cm × 2 cm) supported on glass wool to afford a clear pale orange filtrate. The volume of the filtrate was reduced to 1 mL *in vacuo*. Storage of this vial at –25 ºC for 24 h resulted in the deposition of pale orange plates, which were isolated by decanting the supernatant and drying *in vacuo*. The yield was not recorded. ^{1}H NMR (25 °C, 500 MHz, benzene-d_6): δ 7.65 (d, *J* = 6.8 Hz, 4H, *o*-H), 7.25 (t, *J* = 7.2 Hz, 4H, *m*-H), 7.21 (t, *J* = 1.5 Hz, 2H, *p*-H), 6.16 (s, 15H, Cp).

7.4.9 Synthesis of [Cp$_2$Th(µ-NC(Ph)CCCPh$_2$)]$_2$ (7.6).

To a cold (–25 °C), stirring, orange Et_2O solution (2 mL) of [Li(Et_2O)$_2$][**7.1**] (33.6 mg, 0.043 mmol) was added PhCN (4.5 µL, 0.044 mmol). Upon addition, the solution immediately turned dark red. After stirring for 10 min, the volatiles were removed *in vacuo* and the resulting dark red tacky solid was triturated with pentane (2 × 2 mL). The solid was then extracted into Et_2O (3 mL) and filtered through a Celite column (0.5 cm × 2 cm) supported on glass wool to afford a clear dark red filtrate. The volume of the filtrate was reduced to 1 mL

in vacuo. Storage of this vial at –25 ºC for 24 h resulted in the deposition of dark red plates, which were isolated by decanting the supernatant and drying *in vacuo*. The yield was not recorded. ^{1}H NMR (25 °C, 500 MHz, benzene-d_6):δ 8.16 (dd, J = 8.4, 1.3 Hz, 2H, *m*-H), 7.81 (dd, J = 8.4, 1.2 Hz, 4H, *m*-H), 7.34 (t, J = 9.3 Hz, 4H, *o*-H), 7.22 (t, J = 7.6 Hz, 2H, *o*-H), 7.13 (d, J = 5.6 Hz, 2H, *p*-H), 7.11 (d, J = 5.5 Hz, 1H, *p*-H), 6.21 (s, 10H, Cp)**.**

7.4.10 Synthesis of 1,1,6,6-tetraphenylhex-1,5-diene-3-yne (7.7).

To a cold (-25 °C), colorless Et_2O solution (0.5 mL) of 3,3-diphenylcyclopropene (11.5 mg, 0.107 mmol) was added quickly a cold (-25 °C), colorless Et_2O solution (0.5 mL) of LDA (20.7 mg, 0.107 mmol). The solution immediately turned pale yellow. This solution was then added dropwise to a cold (-25 °C), stirring suspension of $[UO_2Cl_2(THF)_2]$ (26.1 mg, 0.054 mmol) in Et_2O (2 mL). This resulted in an immediate color change to bright red, concomitant with the deposition of a brown precipitate. After stirring for 30 min the volatiles were removed *in vacuo* and the resulting red solid was triturated with pentane (1 mL). The red solid was then extracted into hexanes (2 mL), and the resulting bright red solution was filtered through a Celite column supported on glass wool (0.5 cm × 2 cm). Storage of this solution at -25 °C for 24 h resulted in the deposition of red plates. Decanting the supernatant and drying *in vacuo* afforded **7.7** as red plates. The yield was not recorded. ^{1}H NMR (25 °C, 500 MHz, benzene-d_6): δ 7.48 (d, J = 1.8 Hz, *o*-C), 7.46 (d, J = 1.5 Hz), 7.14-7.08 (8H), 6.99 (d, J = 1.7 Hz, 1H), 6.11 (s, C*H*, 1H). ^{13}C{^{1}H} NMR (25 °C, 126 MHz, THF-d_8): δ

7.4.11 Synthesis of [NpCl(NR$_2$)$_3$]

To a cold (–35 °C), stirring, salmon pink THF (2 mL) solution of $NpCl_4(DME)_2$ (67.6 mg, 0.121 mmol) was added dropwise over 5 min a cold (-35 °C) colorless THF (2 mL) solution

of $NaNR_2$ (66.5 mg, 363 mmol). Upon addition, the solution changed color to a slightly cloudy orange yellow solution. After stirring for 24 h, the reaction mixture is filtered through glass fiber filter to afford a clear orange filtrate. The volatiles were removed *in vacuo* and the orange solid was then extracted into hexanes (3 × 2 mL) and filter through glass fiber filter to afford a clear orange filtrate. The volume of the filtrate was reduced to 1.5 mL *in vacuo*. Storage of this vial at –35 ºC for 13 d resulted in the deposition of orange solids, which were isolated by decanting the supernatant and drying *in vacuo* (46.8 mg, 51 % yield).

To a cold (–35 °C), stirring, salmon pink THF (2 mL) solution of $NpCl_4(DME)_2$ (25.9 mg, 0.046 mmol) was added dropwise over 5 min a cold (-35 °C) colorless THF (2 mL) solution of $NaNR_2$ (25.6 mg, 0.138 mmol). Upon addition, the solution changed color to an orange yellow solution. After stirring for 24 h, the reaction mixture is filtered through glass fiber filter to afford a clear orange yellow filtrate. The volatiles were removed *in vacuo* and the orange solid was triturated with pentane (0.5 mL), then extracted into hexanes (3 × 1 mL) and filtered through glass fiber filter to afford a clear orange filtrate. The volume of the filtrate was reduced to 0.5 mL *in vacuo*. Storage of this vial at –35 ºC for 24 h resulted in the deposition of orange solids, which were isolated by decanting the supernatant and drying *in vacuo* (18.8 mg, 34.9 % yield).

7.4.12 Reaction of $[NpCl(NR_2)_3]$ with lithium-3,3-diphenylcyclopropenyl

To a cold (-35 °C), colorless Et_2O solution (0.5 mL) of 3,3-diphenylcyclopropene (15.7 mg, 0.081 mmol) was added quickly a cold (-25 °C), colorless Et_2O solution (0.5 mL) of LDA (8.3 mg, 0.078 mmol). Immediately, the solution turned light yellow. This solution was then added drop wise to a cold (-35 °C) stirring orange solution of $[NpCl(NR_2)_3]$ (43.5 mg, 0.078

mmol) in Et_2O (1.5 mL). Immediately, the solution turned amber brown color upon addition of *in situ* generated lithium-3,3-diphenylcyclopropene. The reaction mixture was stirred for 5 min, then stored at -35 °C for 2 min before stirring for another 5min. This cycle was repeated five times. The reaction mixture was filtered through a glass fiber filter to afford a clear orange filtrate. To the orange filtrate 2,2,2-cryptand (29.3 mg, 0.078 mmol) was added as a colorless solid and the vial was stored at -35 °C for 20 min. To the cold (-35 °C), orange Et_2O solution was added slow dropwise a cold (-35 °C), colorless Et_2O solution (0.5 mL) of LDA (8.3 mg, 0.078 mmol). Immediately, the solution turned dark yellow concomitant with yellow silds. After stirring for 2 min, the reaction mixture was filtered through a glass fiber filter and the volume of the filtrate was reduced to 1 mL *in vacuo*. The resulting dark yellow filtrate was layer with pentane (3 mL). Storage of this vial at –35 ºC for 2 d resulted in the deposition of light yellow plates, which were isolated by decanting the supernatant and drying *in vacuo* to afford [Li(2,2,2-cryptand)][NpCl(NR_2)$_3$] (R = $SiMe_3$) (**7.8**) (6.9 mg, 10.5 % yield). In addition, a dark yellow oil was concurrently formed, subsequent extraction into THF (1.5 mL) and filtered through a glass fiber filter to afford a dark yellow filtrate, the volume of the filtrate was reduced to 1 mL *in vacuo*, and layered with pentane (2 mL). Storage of this vial at –35 ºC for 2 d resulted in the deposition of dark yellow oil, which was isolated by decanting the supernatant and drying *in vacuo.* The dark yellow oil was washed with toluene (1mL) and extracted into THF (2 mL), the volume of the filtrate was reduced to 1 mL *in vacuo*, and layered with pentane (2 mL). Storage of this vial at –35 ºC for 2 d resulted in the deposition of dark yellow plates, which were isolated by decanting the supernatant and drying *in vacuo* to afford [Li(2,2,2-cryptand)]$_2$[NpCl$_2$(NR_2)$_3$] (R = $SiMe_3$) (**7.9**). The yield of **7.9** was not recorded.

7.4.13 Reaction of [Li(2,2,2-cryptand)][NpCl(NR_2)$_3$] with lithium-3,3-diphenylcyclopropenyl

To a cold (-35 °C), colorless Et_2O solution (0.5 mL) of 3,3-diphenylcyclopropene (1.2 mg, 0.006 mmol) was added quickly a cold (-25 °C), colorless Et_2O solution (0.5 mL) of LDA (0.6 mg, 0.006 mmol). Immediately, the solution turned light yellow. This solution was then added drop wise to a cold (-35 °C) stirring orange solution of [Li(2,2,2-cryptand)][NpCl(NR_2)$_3$] (6.9 mg, 0.006 mmol) in Et_2O (1 mL). Immediately, the solution turned into dark yellow solution with formation of dark precipitate. After stirring for 40 min, the volatiles were removed *in vacuo* and the dark yellow solid and extracted into pentane (3 × 1 mL) and filtered through glass fiber filter to afford a clear yellow filtrate. The remaining solids were extracted into Et_2O (3 × 1 mL) and filtered through glass fiber filter to afford a clear dark orange filtrate. The volume of the pentane and Et_2O filtrates were reduced to 0.5 mL *in vacuo*. Storage of the pentane filtrate at –35 ºC for 24 h resulted in the deposition of light-yellow needles, however the yield and further characterization were not performed. Storage of the Et_2O filtrate at –35 ºC for 24 h resulted in the deposition of dark red plates, however the yield and further characterization were not performed.

7.4.14 X-Ray Crystallography

Data for all complexes were collected on a Bruker KAPPA APEX II diffractometer equipped with an APEX II CCD detector using a TRIUMPH monochromator with a Mo Kα X-ray source (α = 0.71073 Å). The crystals were mounted on a cryoloop under Paratone-N oil, and all data were collected at 100(2) K using an Oxford nitrogen gas cryostream. Data were collected using ω scans with 0.5° frame widths. Frame exposures of 20 s, 30 s, 30 s, 20 s, and 60 s were used for [Li(Et_2O)$_2$][**7.1**], [Li(12-crown-4)(THF)][**7.1**], [Li(2.2.2-cryptand)][**7.1**]·2THF, **7.2**·C_6D_6 and **7.3**·THF, respectively. Data collection and cell parameter determinations were conducted using the SMART program.[127] Integration of the data frames and final cell parameter refinement were performed using SAINT software.[128] Absorption correction of the data was carried out using the multi-scan method SADABS.[129] Subsequent calculations were carried out using SHELXTL.[130] Structure determination was done using direct or Patterson methods and difference Fourier techniques. All hydrogen atom positions were idealized and rode on the atom of attachment. Structure solution and refinement were performed using SHELXTL. Graphics, and creation of publication materials were performed using Diamond.[131]

Complex [Li(Et_2O)$_2$][**7.1**] exhibited positional disorder within one of the Et_2O solvate molecule, which was address by constraining the affected atoms with SADI commands. Complex [Li(12-crown-4)(THF)][**7.1**] exhibited positional disorder within one of the THF solvate molecule, which was address by constraining the affected atoms with EADP and DFIX commands. Complex [Li(2.2.2-cryptand)][**7.1**]·2THF exhibited positional disorder within the [Li(2.2.2-cryptand)]$^+$ counterions, which was address by constraining the affected atoms with EADP commands. In addition, the THF solvate molecules in [Li(2.2.2-cryptand)][**7.1**]·2THF

were not refined anisotropically due to positional disorder. Complex **7.2**·C_6D_6 exhibited positional disorder within the Cp ligands, which was address by constraining the affected atoms with EADP and SADI commands.

Table 7.3. X-ray crystallographic data for Complexes $[Li(Et_2O)_2]$[**7.1**], [Li(12-crown-4)(THF)][**7.1**], and [Li(2.2.2-cryptand)][**7.1**]·2THF.

	$[Li(Et_2O)_2]$[**7.1**]	[Li(12-crown-4)(THF)][**7.1**]	[Li(2.2.2-cryptand)][**7.1**] ·2THF
Formula	$C_{38}H_{45}LiO_2Th$	$C_{42}H_{49}LiO_5Th$	$C_{56}H_{77}LiN_2O_8Th$
Crystal Habit, Color	Needles, Orange	Plates, Red	Needles, Red
Crystal Size (mm)	0.2 × 0.1 × 0.05	0.2 × 0.2 × 0.05	0.2 × 0.1 × 0.05
MW (g/mol)	772.72	872.79	1145.17
crystal system	triclinic	monoclinic	monoclinic
space group	P -1	P 21/n	P 21/n
a (Å)	8.886(2)	12.333(7)	18.566(2)
b (Å)	12.379(3)	15.269(8)	13.638(2)
c (Å)	15.531(4)	19.665(11)	21.957(3)
α (°)	91.617(13)	90	90
β (°)	90.367(14)	97.649(13)	113.112(8)
γ (°)	97.639(14)	90	90
V ($Å^3$)	1692.5(7)	3670(3)	5113.5(13)
Z	2	4	4
T (K)	200(2)	100(2)	100(2)
λ (Å)	0.71073	0.71073	0.71073
GOF	0.982	1.035	0.929
Density (calcd) (Mg/m^3)	1.516	1.580	1.488
Absorption coefficient (mm^{-1})	4.435	4.107	2.972
F_{000}	764	1736	2336
Total no Reflections	15304	18887	29119
Unique Reflections	7437	7757	10431
Final R indices*	R_1 = 0.0436, wR_2 = 0.0692	R_1 = 0.0392, wR_2 = 0.0501	R_1 = 0.0579, wR_2 = 0.1397
Largest Diff. peak and hole ($e^- A^{-3}$)	0.812, -0.899	1.008, -1.304	1.609, -1.171

*For [I>2σ(I)]

Table 7.4. X-ray crystallographic data for Complex **7.2**·C_6D_6 and **7.3**·THF.

	7.2·C_6D_6	**7.3**·THF
Formula	$C_{56}H_{40}D_6Th_2$	$C_{35}H_{36}OTh$
Crystal Habit, Color	Plates, Red	Plates, Colorless
Crystal Size (mm)	0.2 × 0.1 × 0.05	0.15 × 0.15 × 0.05
MW (g/mol)	1189.04	704.68
crystal system	triclinic	monoclinic
space group	P -1	P 21/c
a (Å)	8.3920(19)	16.799(3)
b (Å)	9.589(3)	10.6406(17)
c (Å)	14.262(3)	16.826(3)
α (°)	101.567(8)	90
β (°)	100.650(13)	112.361(3)
γ (°)	98.330(13)	90
V ($Å^3$)	1085.0(4)	2781.4(8)
Z	1	4
T (K)	100(2)	100(2)
λ (Å)	0.71073	0.71073
GOF	1.056	0.988
Density (calcd) (Mg/m^3)	1.810	1.683
Absorption coefficient (mm^{-1})	6.882	5.387
F_{000}	562	1376
Total no Reflections	9474	12749
Unique Reflections	4746	5871
Final R indices*	R_1 = 0.0470, wR_2 = 0.0823	R_1 = 0.0455, wR_2 = 0.0932
Largest Diff. peak and hole ($e^- A^{-3}$)	2.272, -3.742	6.003, -1.376

*For [I>2σ(I)]

Table 7.5. X-ray crystallographic data for Complex **7.5** and **7.6**·3Et_2O.

	7.5	**7.6**·3Et_2O
Formula	$C_{28}H_{25}NTh$	$C_{64}H_{50}N_2Th_2$
Crystal Habit, Color	Plates, orange	Plates, Red
Crystal Size (mm)	0.2 × 0.1 × 0.05	0.15 × 0.15 × 0.05
MW (g/mol)	607.54	1311.17
crystal system	orthorhombic	triclinic
space group	P 212121	P -1
a (Å)	8.685(2)	12.014(5)
b (Å)	8.6905(16)	14.545(8)
c (Å)	28.716(5)	17.147(9)
α (°)	90	75.54(3)
β (°)	90	85.70(3)
γ (°)	90	79.31(3)
V ($Å^3$)	2167.3(8)	2850(2)
Z	4	4
T (K)	100(2)	100(2)
λ (Å)	0.71073	0.71073
GOF	1.117	1.156
Density (calcd) (Mg/m^3)	2.304	2.604
Absorption coefficient (mm^{-1})	6.920	7.451
F_{000}	1448	2048
Total no Reflections	14881	9719
Unique Reflections	4417	9719
Final R indices*	R_1 = 0.0548, wR_2 = 0.0919	R_1 = 0.2037, wR_2 = 0.4237
Largest Diff. peak and hole ($e^- A^{-3}$)	2.530, -2.542	19.470, -5.381

*For [I>2σ(I)]

Table 7.6. X-ray crystallographic data for Complexes **7.8** and **7.9**.

	7.8	**7.9**
Formula	$C_{36}H_{90}N_5O_6Si_6LiClNp$	$C_{36}H_{90}N_5O_6Si_6LiCl_2Np$
Crystal Habit, Color	Plates, orange	Plates, Red
Crystal Size (mm)	0.2 × 0.1 × 0.05	0.15 × 0.15 × 0.05
MW (g/mol)	1138.06	1172.49
crystal system	Monoclinic	triclinic
space group	$P2_1/c$	P -1
a (Å)	16.5361(5)	15.541(5)
b (Å)	15.8045(5)	15.939(5)
c (Å)	21.9557(7)	22.607(7)
α (°)	90	110.321(8)
β (°)	109.3760(10)	90.114(10)
γ (°)	90	90.031(10)
V ($Å^3$)	5413.0(3)	5251(3)
Z	4	4
T (K)	100(2)	100(2)
λ (Å)	0.71073	0.71073
GOF	1.117	1.039
Density (calcd) (Mg/m^3)	1.396	4.988
Absorption coefficient (mm^{-1})	2.143	7.451
F_{000}	2348	6705
Total no Reflections	137117	8076
Unique Reflections	20632	5303
Final R indices*	R_1 = 0.0395, wR_2 = 0.0783	R_1 = 0.2037, wR_2 = 0.3415
Largest Diff. peak and hole ($e^- A^{-3}$)	1.832, -1.835	1.573, -1.482

*For [I>2σ(I)]

7.4.15 Computational Data Details

Kohn-Sham density functional theory (DFT) calculations were carried out for complexes [**7.1**]⁻, **7.2**, and **7.3**, with the 2023 release of the Amsterdam Modeling Suite (AMS).[132] Calculations for these three complexes were carried out based on crystal structure coordinates; only the positions of the hydrogen atoms were optimized, using the B3LYP hybrid exchange-correlation functional,[133-135] all-electron scalar-relativistic (SR) Zeroth-Order Regular Approximation[136] (ZORA) Hamiltonian, and the Slater-type atomic orbital (STO) basis sets of triple-ζ doubly polarized (TZ2P)[137] quality for all atoms. An atom-pairwise correction for dispersion forces was considered via Grimme's D3 model augmented with the Becke-Johnson (BJ) damping.[138] To analyze the chemical bonds, natural localized molecular orbital (NLMO) analyses were carried out with NBO 6.0 program as interfaced with ADF.[139]

Nuclear magnetic shielding constants for [**7.1**]⁻, **7.2**, and **7.3**, were calculated with SR and spin-orbit (SO) ZORA and TZ2P basis sets. The NMR computations employed the PBE0 exchange-correlation hybrid functional with 40% exact exchange, which previously produced reliable chemical shifts of actinide complexes.[140-142] The conductor-like screening model (COSMO) was used to describe electrostatic effects from the solvent.[143] To be consistent with the experimental conditions, COSMO models were used with parameters for tetrahydrofuran (THF) for [**7.1**]⁻ and **7.3**, whereas dichloromethane (DCM) parameters were used for **7.2**. The ^{13}C shifts δ_i were calculated via $\delta_i = \sigma_{secondary} - \sigma_i + \delta_{secondary}$. Here, σ_i is the calculated shielding of the carbon of interest, $\sigma_{secondary}$ and $\delta_{secondary}$ are the calculated ipso-carbon shielding at the same level of theory and the experimental measured chemical shift of 3,3-diphenylcyclopropene (Expt.=32.1 ppm), respectively. It is noted, however, that using the secondary reference in the NMR shift calculations, instead of using tetramethylsilane (TMS) directly as the reference in the computations, did not make a substantial difference in the calculated chemical shifts.

Kohn-Sham density functional calculations were also conducted to investigate the formation of [**7.1**]⁻, using Gaussian 16 (G16) package.[144] The geometries of complex [**7.1**]⁻ and relevant the stationary points were fully optimized with the B3LYP hybrid exchange-correlation functional. Small-core Stuttgart energy-consistent relativistic pseudopotential, ECP60MWB for Th, was utilized with matching valence basis sets.[145] The 6-31G(d) basis set

was used for the C, N, and H atoms.[146] Atom-pairwise corrections for dispersion forces were considered via Grimme's D3 model augmented with the Becke-Johnson (BJ) damping.[138] To obtain the Gibbs free energy and to characterize the stationary point (minima vs. transition states), vibrational frequency calculations were carried out at the same level of theory. The imaginary normal mode of the transitions state and the intrinsic reaction coordinate (IRC) calculations confirmed that the transition state connects properly to the intermediate and product.[147]

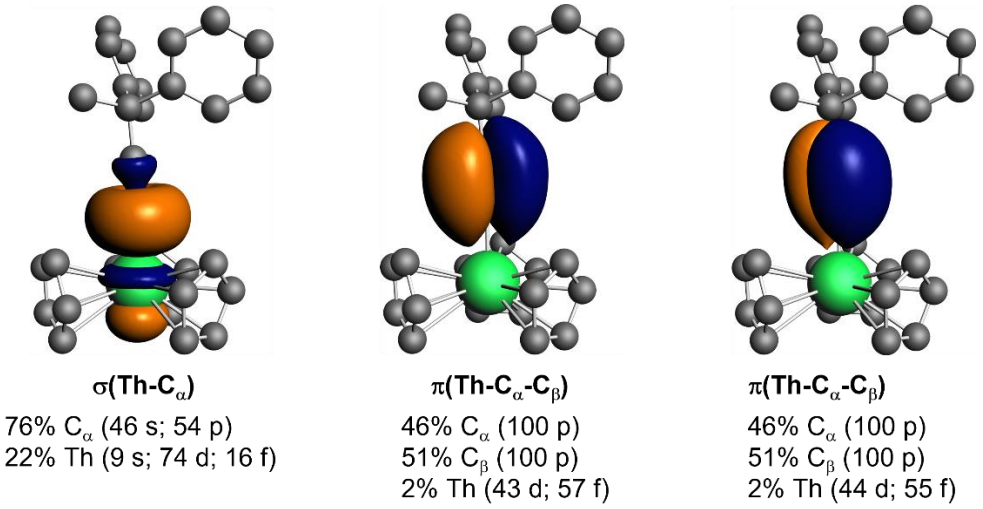

Figure 7.20. Isosurfaces (±0.03 a.u.) and atomic orbital weight compositions of selected NLMOs for **7.3**. Hydrogen atoms are omitted for clarity. (Color code: thorium = green; carbon = gray.)

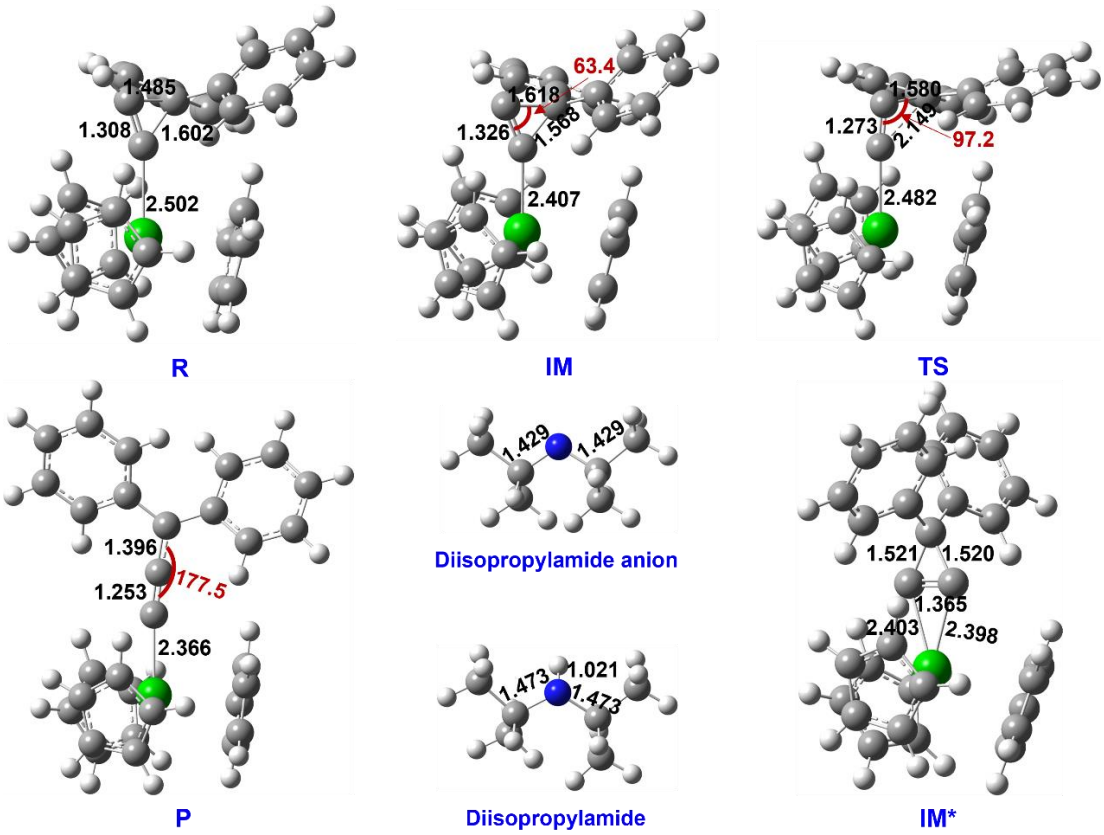

Figure 7.21. Optimized geometries of the stationary points in the formation of [**7.1**]$^{-}$. IM* is an alternative intermediate that was considered in the study (see text). Distances are in Å, angles are in degrees. Color code for atoms: Th = green, N = blue, C = dark gray, H = white.

Table 7.7. % Compositions of the Th-C bonding NLMOs of [**7.1**]$^{-}$ and **7.3**.

Complex	Orbital	Total M	7s	7p	6d	5f	Total C_α	2s	2p	Total C_β	2s	2p
[**7.1**]$^{-}$	σ(Th-C)	23	9	0	75	16	75	49	51	1	23	77
	π(Th-C)	3	0	0	47	52	47	0	100	48	0	100
	π(Th-C)	4	0	0	46	54	50	0	100	43	0	100
7.3	σ(Th-C)	22	9	0	74	16	76	46	54	1	26	74
	π(Th-C)	2	0	0	43	57	46	0	100	51	0	100
	π(Th-C)	2	0	0	44	55	46	0	100	51	0	100

Table 7.8. Selected Wiberg bond orders (WBOs) for [**7.1**]$^{-}$, **7.2**, and **7.3**.

WBO	[**7.1**]$^{-}$	**7.2**	**7.3**
Th–C_α	0.8239	0.6319	0.7002
C_α–C_β	2.5838	2.3313	2.8177
C_β–C_γ	1.1949	1.2553	1.0024

Table 7.9. Calculated carbon shielding (σ) and chemical shift (δ) for 3,3-diphenylcyclopropene and the C_α, C_β, and C_γ nuclei of [**7.1**]$^{-}$, **7.2**, and **7.3**. PBE0 (40%) [a] functional.

Complex	**Method**	**σ_{calc}(ppm)**	**δ_{calc}(ppm)**	**δ_{expt}(ppm)**	**Δ_{SO} (ppm)**
3,3-diphenyl cyclopropene	PBE0/SO-PBE0 (40%)	156.4 / 157.1	/	32.1	/
[**7.1**]$^{-}$	PBE0/SO-PBE0 (40%)	47.7, 57.5, 114.3 / 22.8, 52.7, 115.0	140.8, 131.0, 74.2 / 166.4, 136.5, 74.2	164.8, 141.8, 72.5	25.6, 5.5, 0.0
7.2	PBE0/SO-PBE0 (40%)	27.5, 27.6, 101.6 / 7.0, 25.4, 98.8	161.0, 160.9, 86.9 / 182.2, 163.8, 90.4	178.4, 160.8, 89.1	21.2, 2.9, 3.5
7.3	PBE0/SO-PBE0 (40%)	67.1, 68.3, 140.7 / 47.5, 65.1, 141.6	121.4, 120.2, 47.8 / 141.7, 124.1, 47.6	146.4, 126.7, 46.8	20.3, 3.9, -0.2

[a] Fraction of exact exchange in the functional in parentheses.

7.5 Appendix

7.5.1 NMR Spectra

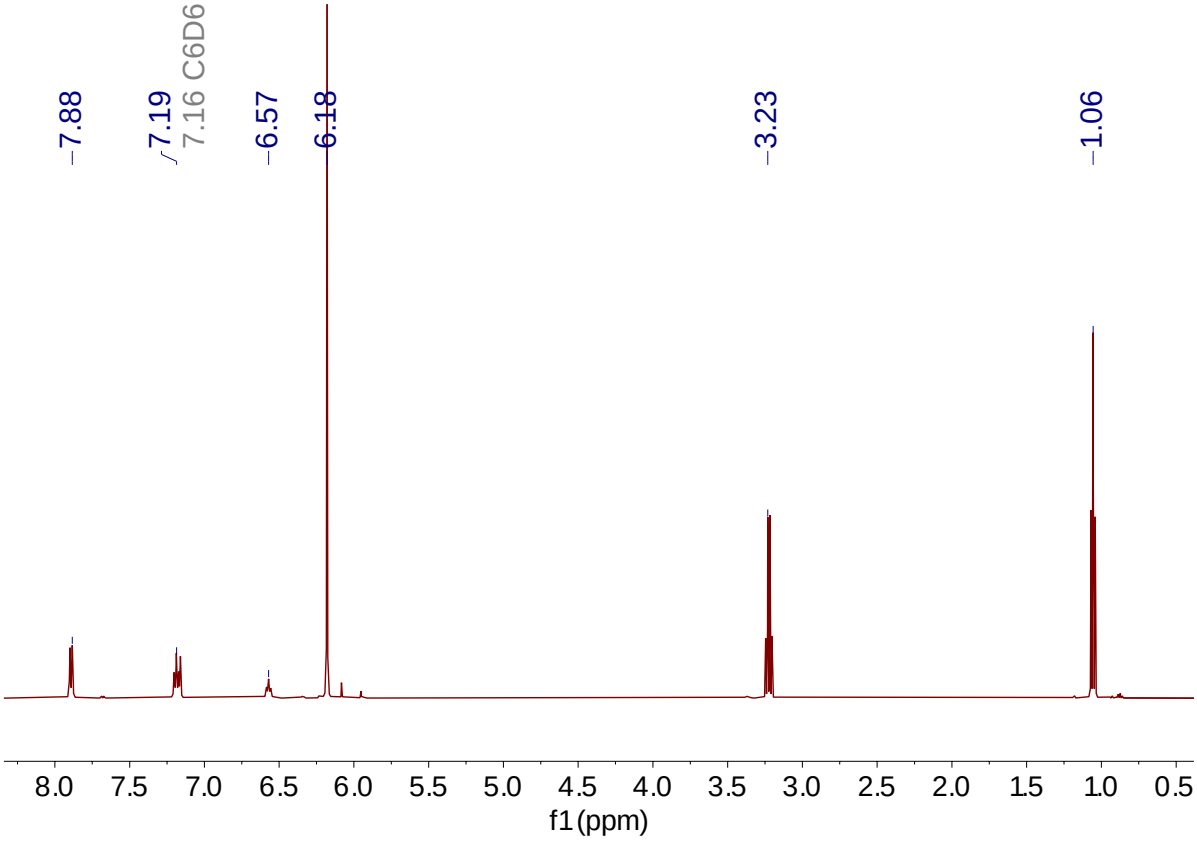

Figure 7.22. ^{1}H NMR spectrum of [Li(Et_2O)$_2$][**7.1**] in benzene-d_6 at room temperature.

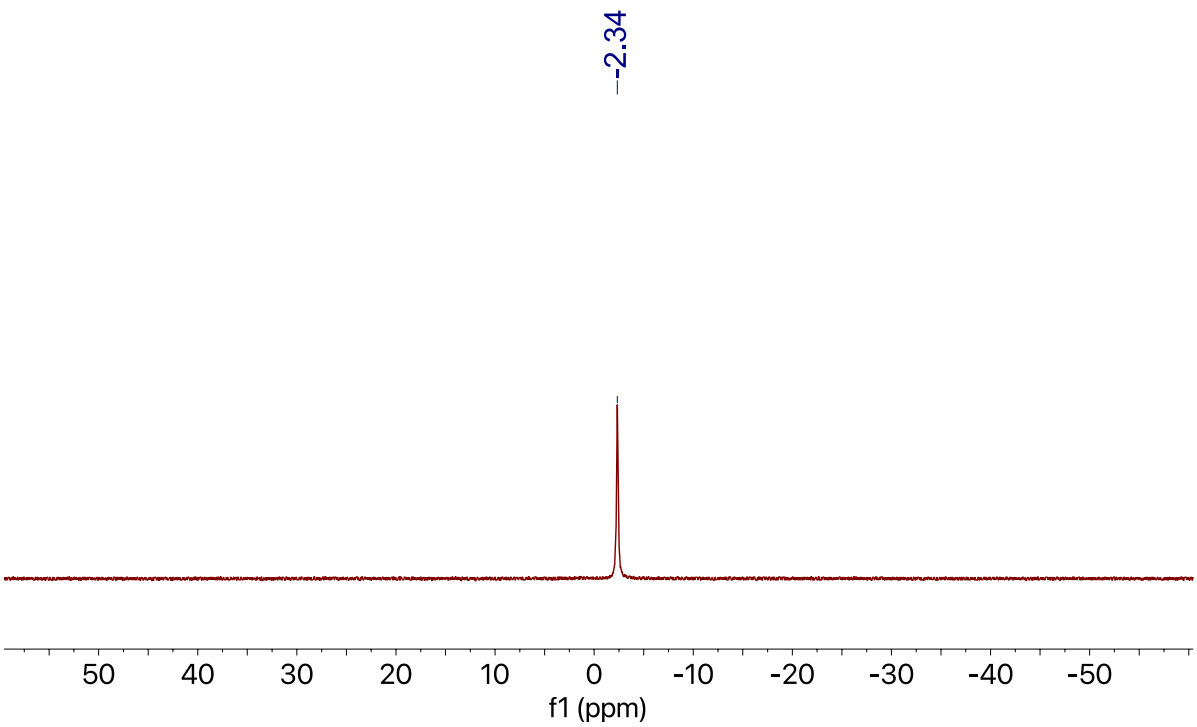

Figure 7.23. $^{7}Li\{^{1}H\}$ NMR spectrum of [[$Li(Et_2O)_2$][**7.1**] in benzene-d_8 at room temperature.

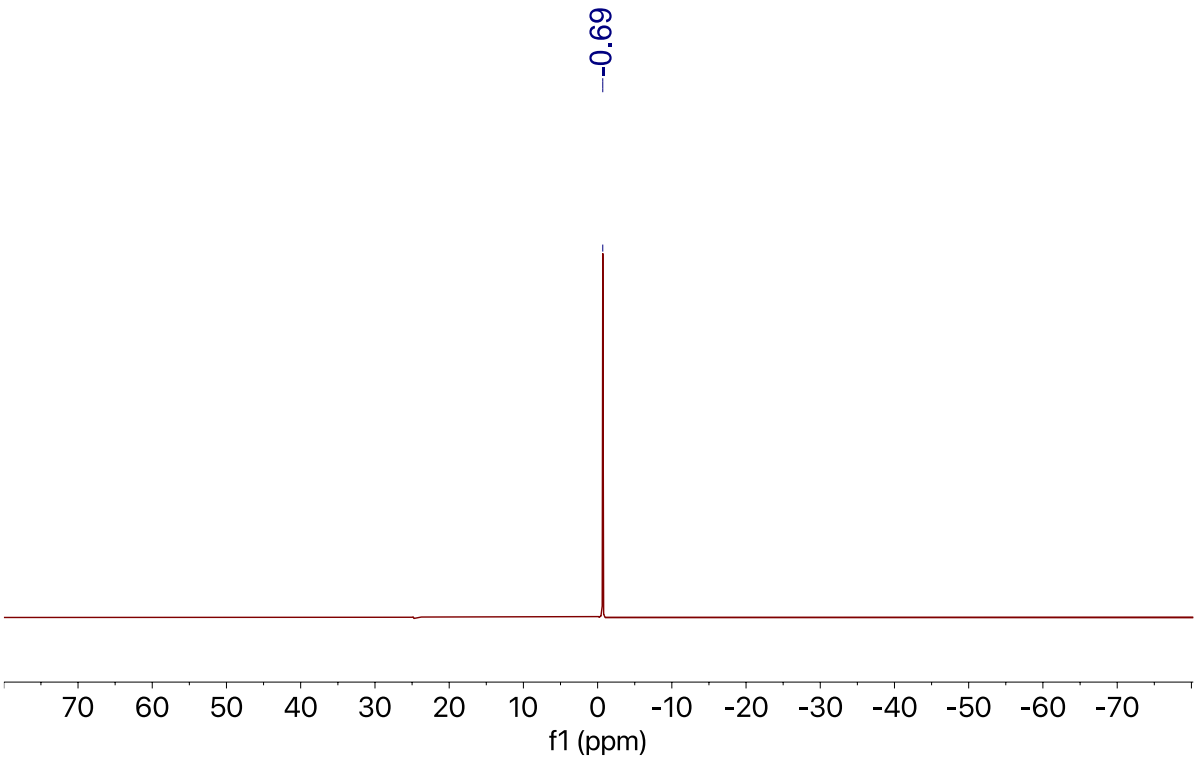

Figure 7.24. $^{7}Li\{^{1}H\}$ NMR spectrum of $[Li(Et_2O)_2]$[**7.1**] in THF-d_8 at room temperature.

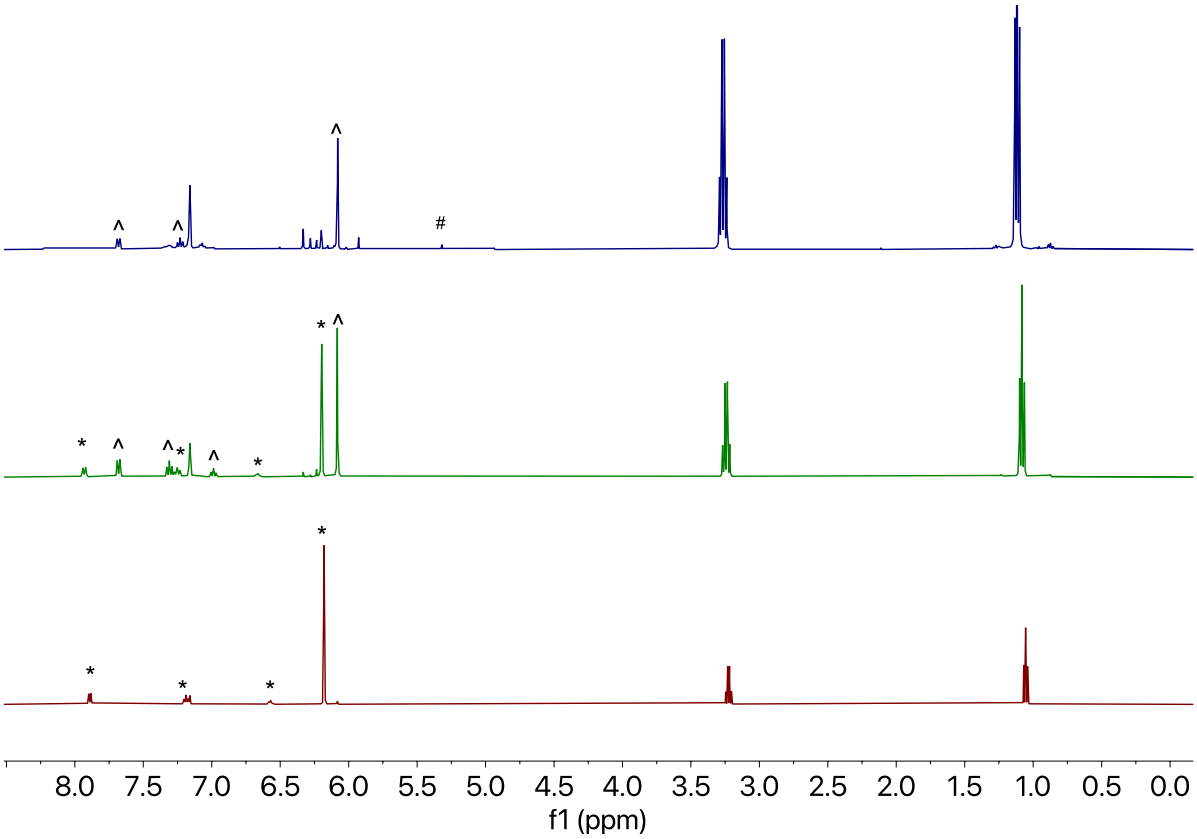

Figure 7.25. (a). ^{1}H NMR spectrum of [Li(Et$_2$O)$_2$][**7.1**] in benzene-d_6 at room temperature. (b) ^{1}H NMR spectrum of [Li(Et$_2$O)$_2$][**7.1**] in benzene-d_6 after standing for 1 d in solution at room temperature. (c) ^{1}H NMR spectrum of [Li(Et$_2$O)$_2$][**7.1**] in benzene-d_6 after standing for 2 d in solution at room temperature. (*) indicates the presence of [Li(Et$_2$O)$_2$][**7.1**] and (^) indicates the presence of 2, and (#) indicated the presence of LiCp.[57]

Experimental Details: Dissolution of [Li(Et$_2$O)$_2$][**7.1**] (15 mg, 0.019 mmol) in benzene-d_6 (0.7 mL) at room temperature resulted in bright red solution. This solution was transferred to an NMR tube equipped with a J-Young valve. After standing for 1 d in solution at room temperature 61% conversion of [Li(Et$_2$O)$_2$][**7.1**] to **7.2**, calculated based of the normalized relative integrations.

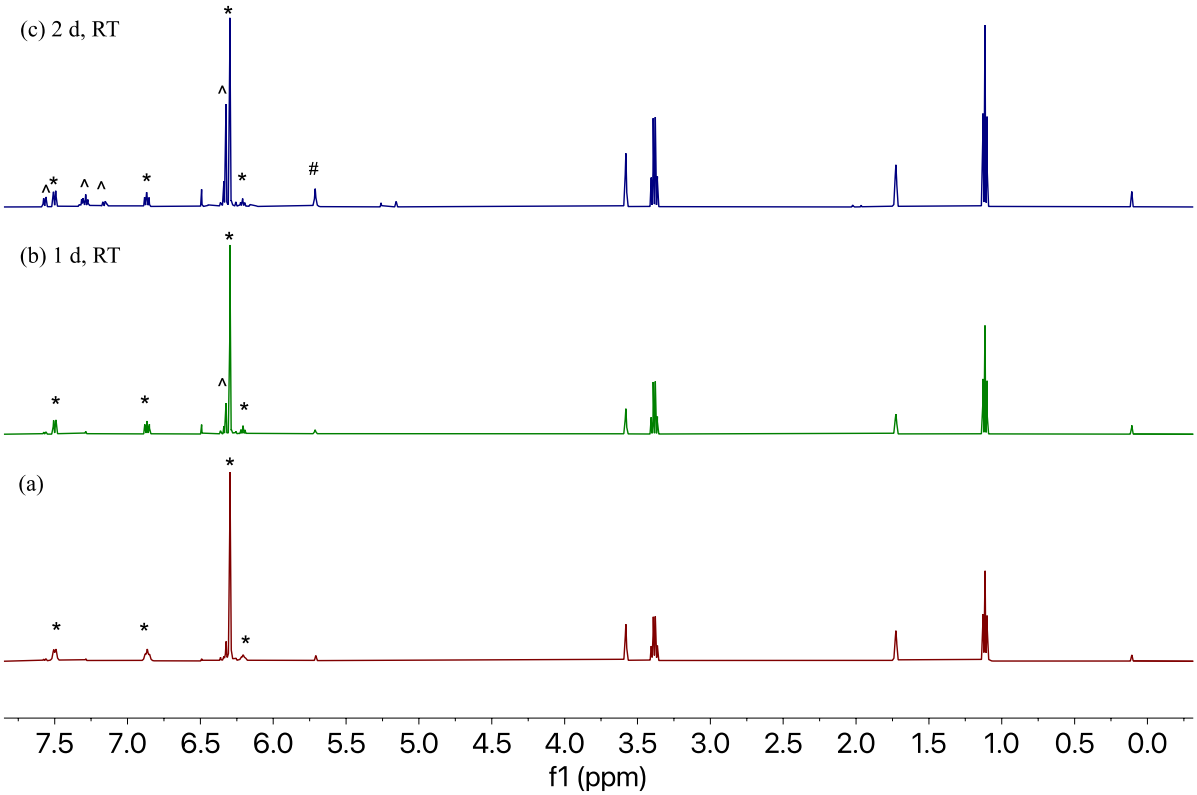

Figure 7.26. (a) ^{1}H NMR spectrum of [Li(Et$_2$O)$_2$][**7.1**] in THF-d_8 at room temperature. (b) ^{1}H NMR spectrum of [[Li(Et$_2$O)$_2$][**7.1**] in THF-d_8 after standing for 1 d in solution at room temperature. (c) ^{1}H NMR spectrum of [Li(Et$_2$O)$_2$][**7.1**] in THF-d_8 after standing for 2 d in solution at room temperature. (*) indicates the presence of [Li(Et$_2$O)$_2$][**7.1**], (^) indicates the presence of 2, (#) indicated the presence of LiCp.

Experimental Details: Dissolution of [Li(Et$_2$O)$_2$][7.1] (13 mg, 0.017 mmol) in THF-d_8 (0.7 mL) at room temperature resulted in dark red solution. This solution was transferred to an NMR tube equipped with a J-Young valve, brought out of the glovebox and monitored for 1d. After standing for 1 d in solution at room temperature 18% conversion of [Li(Et$_2$O)$_2$][7.1] to 7.2, calculated based of the normalized relative integrations.

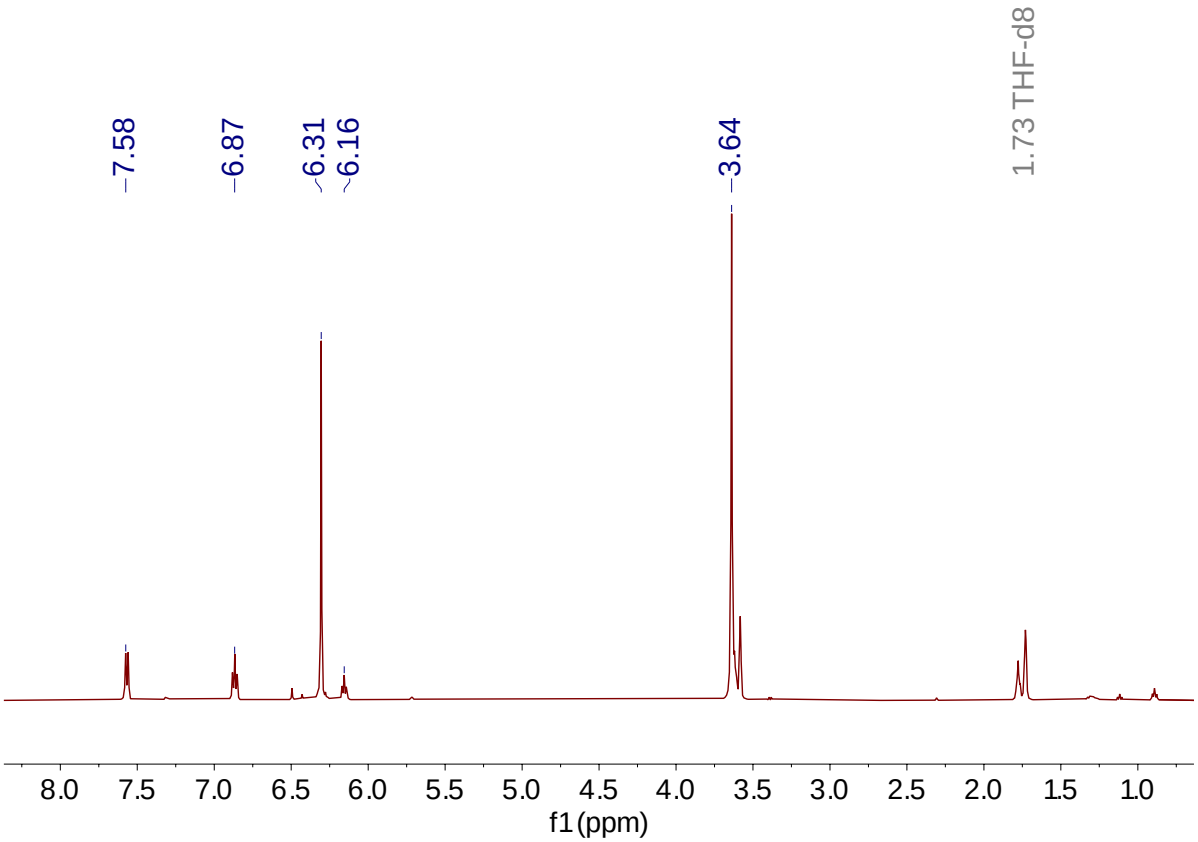

Figure 7.27. ^{1}H NMR spectrum of [Li(12-crown-4)(THF)][**7.1**] in THF-d_8 at room temperature.

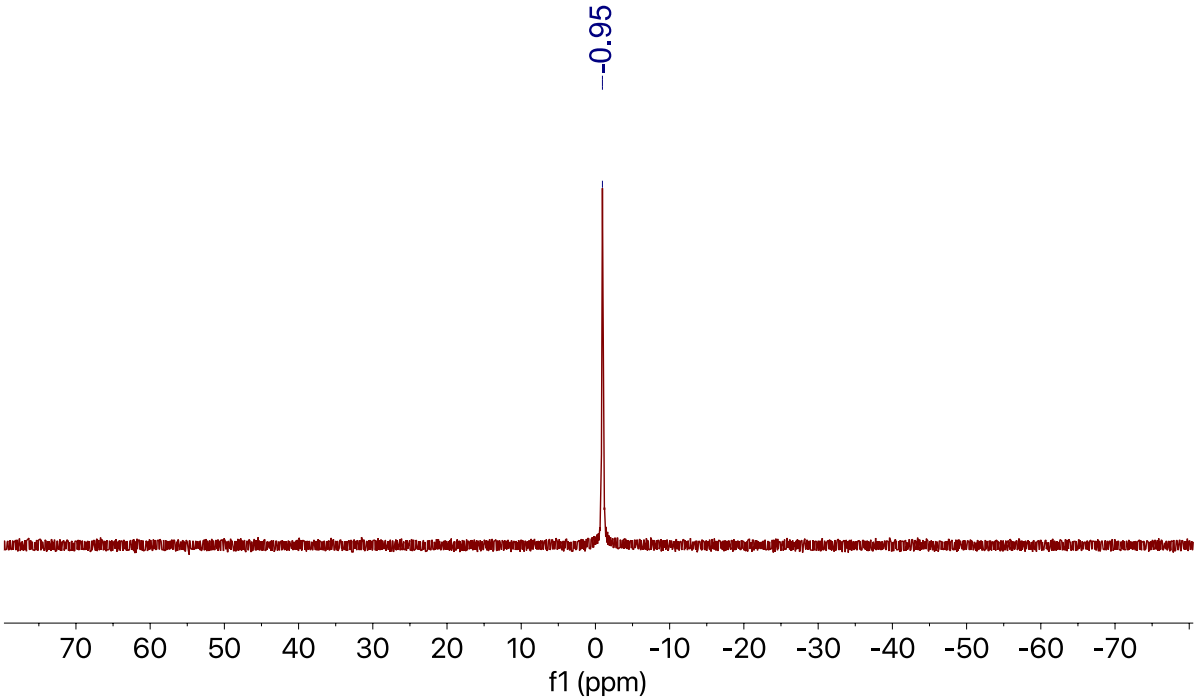

Figure 7.28. $^{7}Li\{^{1}H\}$ NMR spectrum of [Li(12-crown-4)(THF)][**7.1**] in THF-d_8 at room temperature.

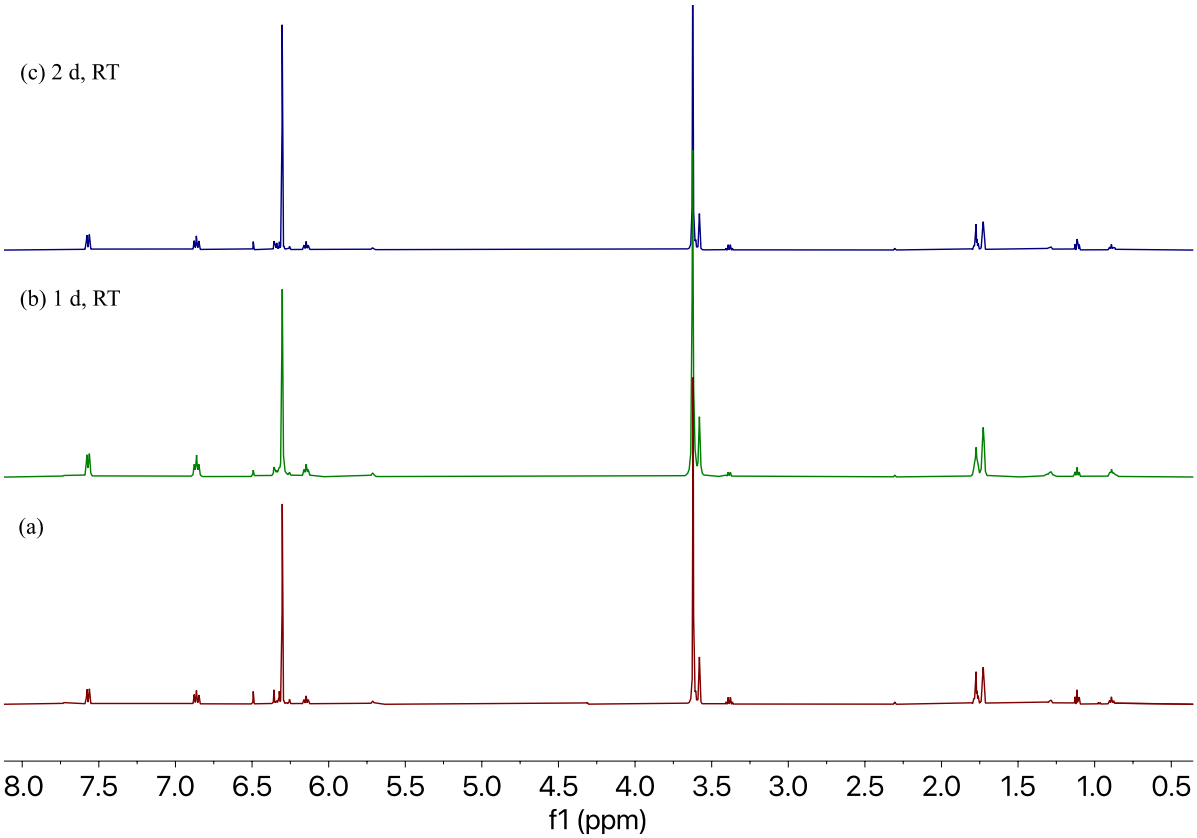

Figure 7.29. (a) ^{1}H NMR spectrum of [Li(12-crown-4)(THF)][**7.1**] in THF-d_8 at room temperature. (b) ^{1}H NMR spectrum of [Li(12-crown-4)(THF)][**7.1**] in THF-d_8 after standing for 1 d in solution at room temperature. (c) ^{1}H NMR spectrum of [Li(12-crown-4)(THF)][**7.1**] in THF-d_8 after standing for 2 d in solution at room temperature.

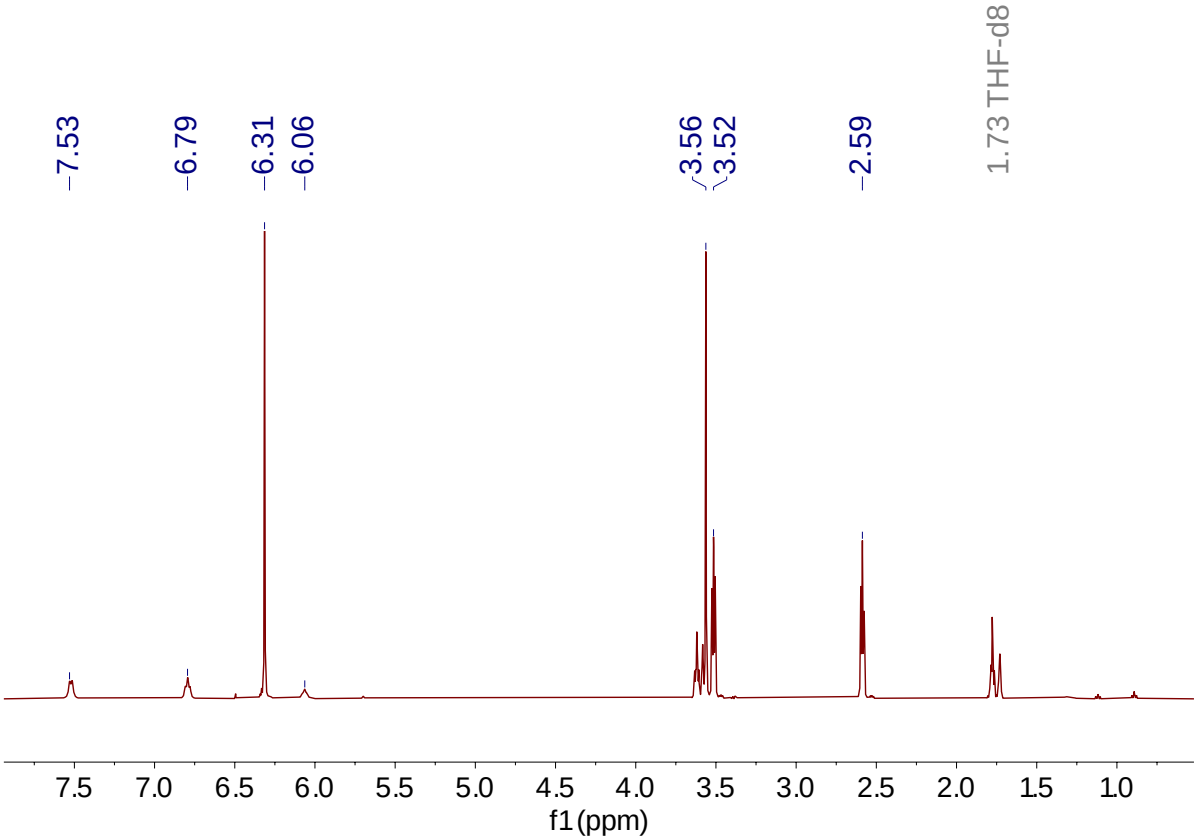

Figure 7.30. ^{1}H NMR spectrum of [Li(2.2.2-cryptand)][**7.1**] in THF-d_8 at room temperature.

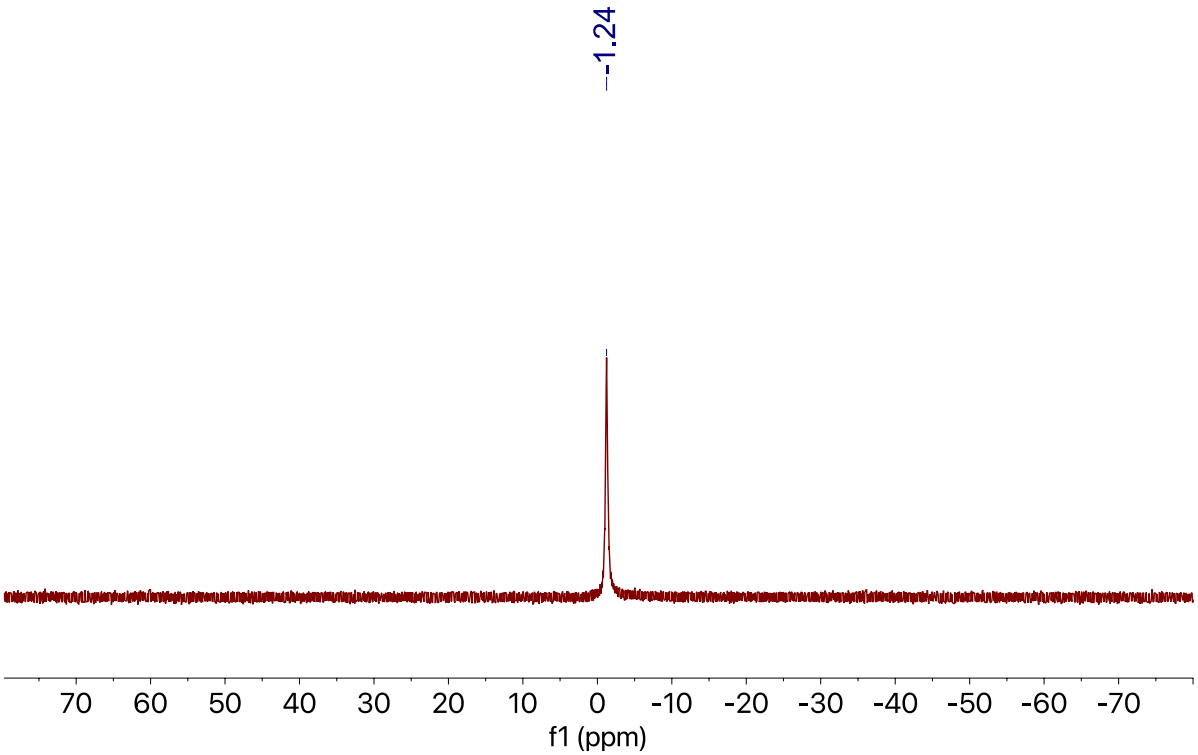

Figure 7.31. $^{7}Li\{^{1}H\}$ NMR spectrum of [Li(2.2.2-cryptand)][**7.1**] in THF-d_8 at room temperature.

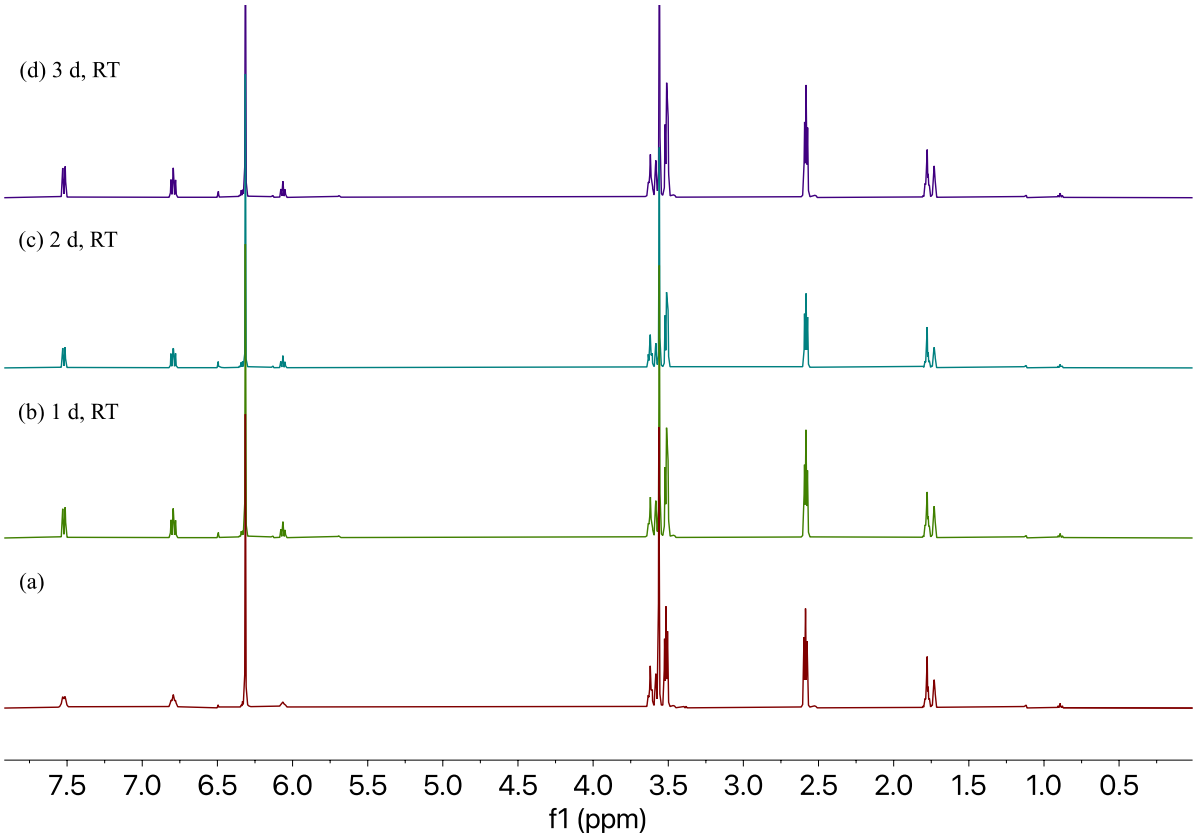

Figure 7.32. (a) ^{1}H NMR spectrum of [Li(2.2.2-cryptand)][**7.1**] in THF-d_8 at room temperature. (b) ^{1}H NMR spectrum of [Li(2.2.2-cryptand)][**7.1**] in THF-d_8 after standing for 1 d in solution at room temperature. (c) ^{1}H NMR spectrum of [Li(2.2.2-cryptand)][**7.1**] in THF-d_8 after standing for 2 d in solution at room temperature. (d) ^{1}H NMR spectrum of [Li(2.2.2-cryptand)][7.1] in THF-d_8 after standing for 3 d in solution at room temperature.

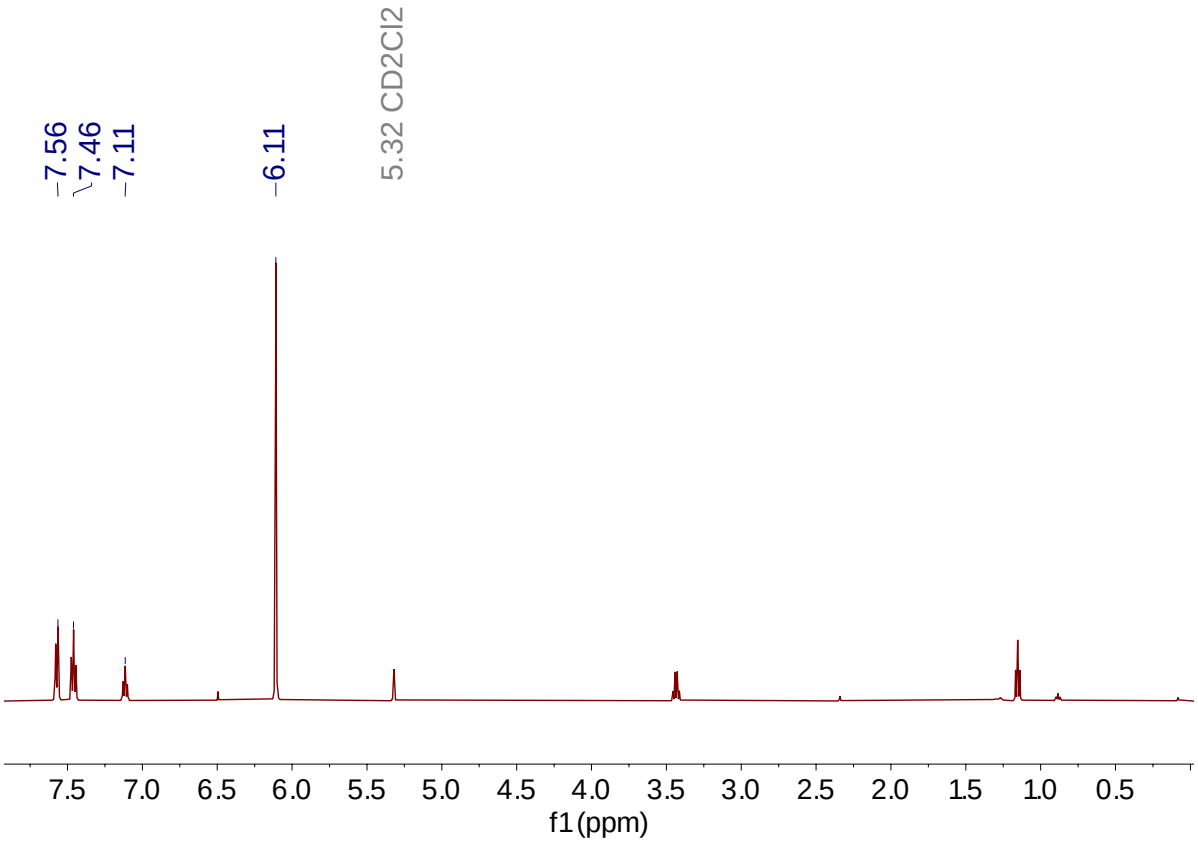

Figure 7.33. ^{1}H NMR spectrum of **7.2** in dichloromethane-d_2 at room temperature.

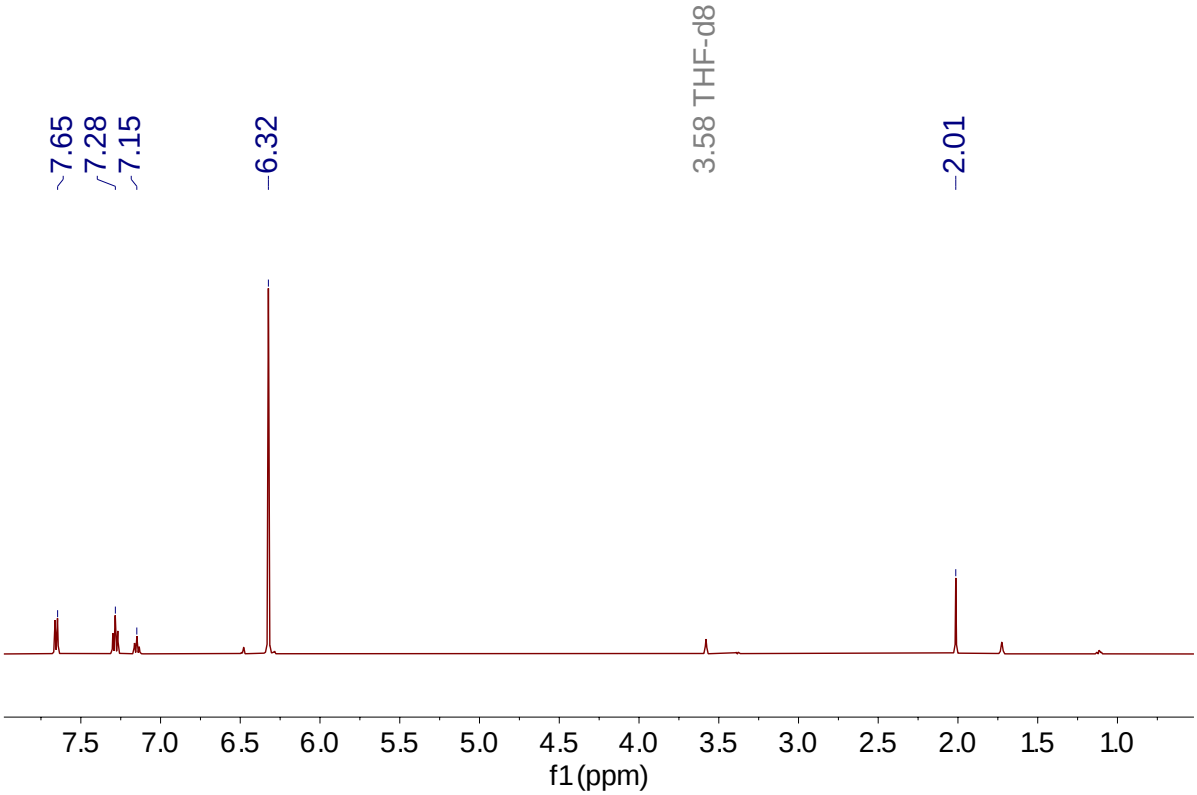

Figure 7.34. ^{1}H NMR spectrum of **7.3** in THF-d_8 at room temperature.

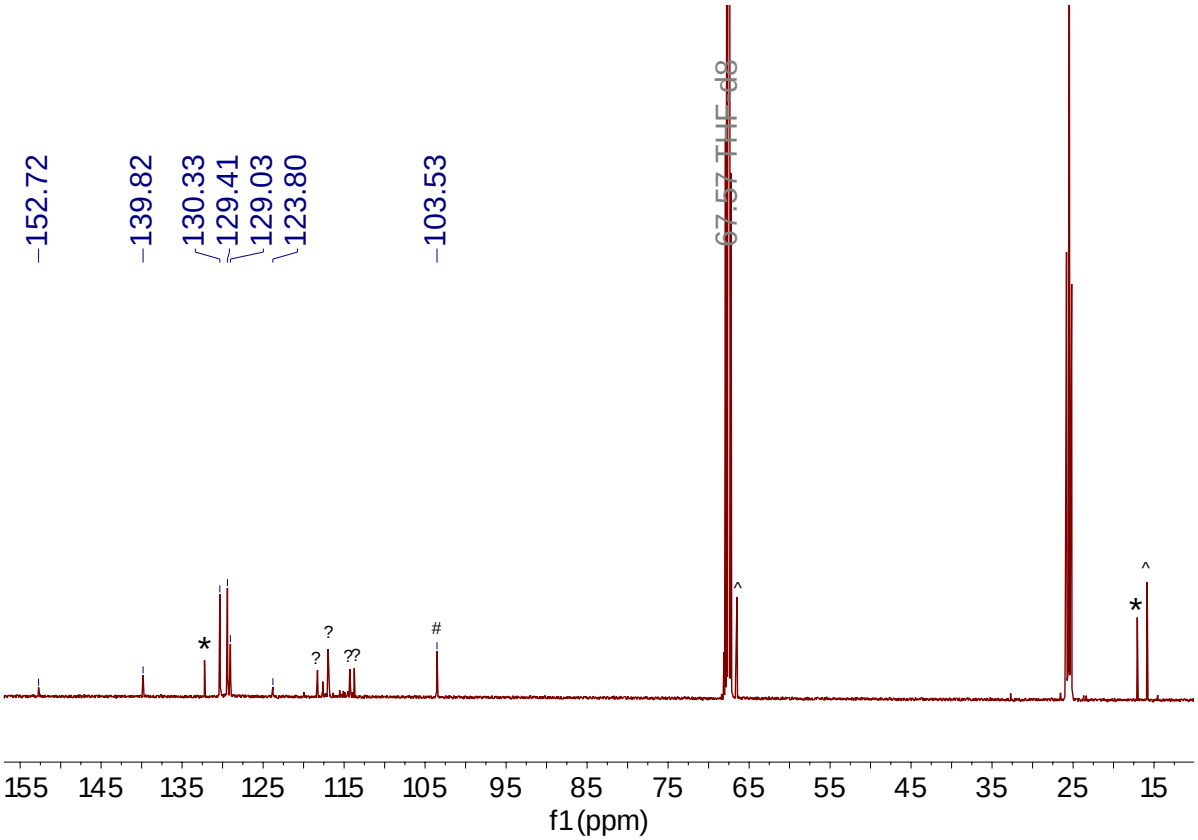

Figure 7.35. $^{13}C\{^{1}H\}$ NMR spectrum of *in situ* reaction of $[Li(Et_2O)_2]$[**7.1**] with 1 equiv of Ph_2CO in THF-d_8 at room temperature. (*) indicates the presence of hexamethylbenzene, (#) indicates the presence of LiCp, (^) indicates the presence of Et_2O, and (?) indicates the presence of unidentified Cp-containing products.

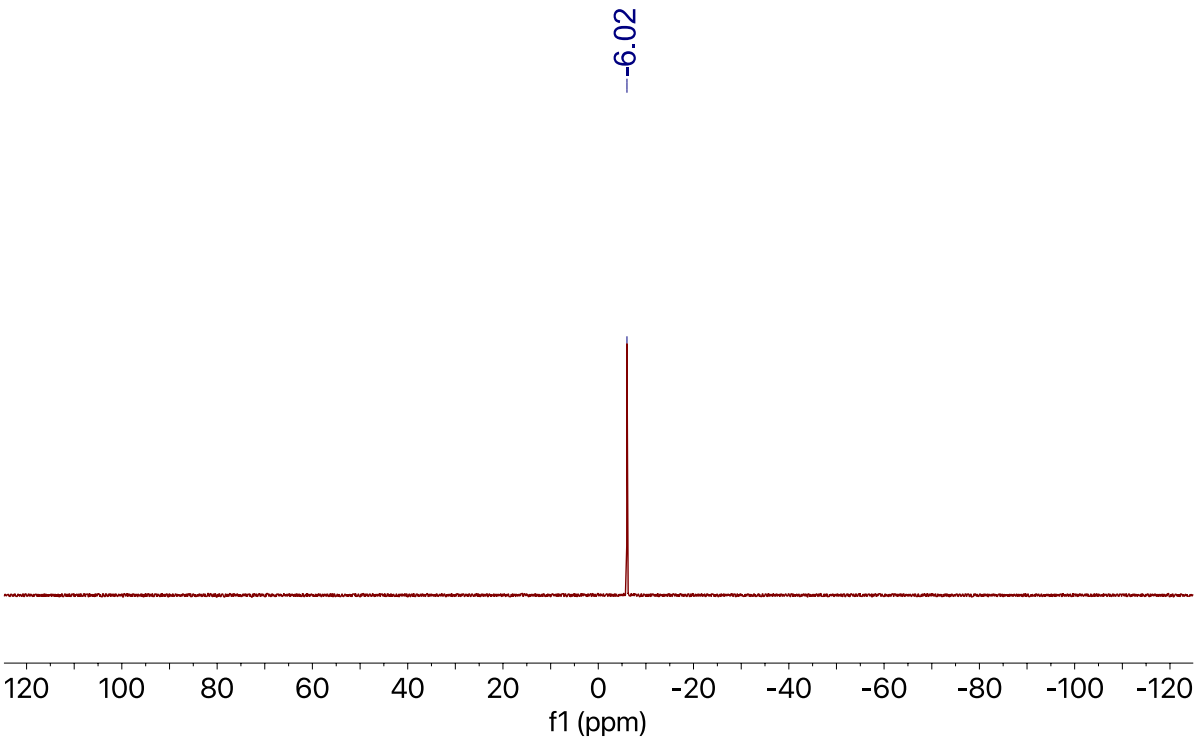

Figure 7.36. $^{7}Li\{^{1}H\}$ NMR spectrum of *in situ* reaction of $[Li(Et_2O)_2]$[**7.1**] with 1 equiv of Ph_2CO in THF-d_8 at room temperature.

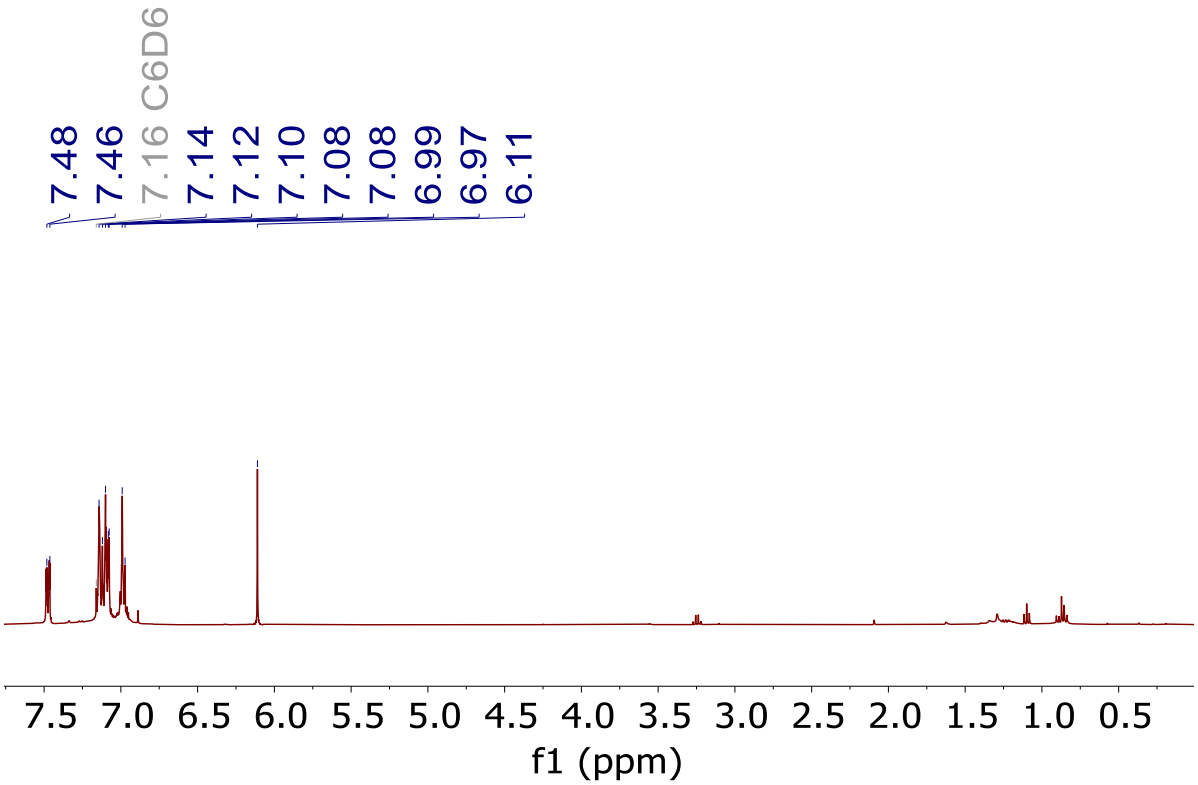

Figure 7.37. ^{1}H NMR spectrum of **7.7** in benzene-d_6 at room temperature.

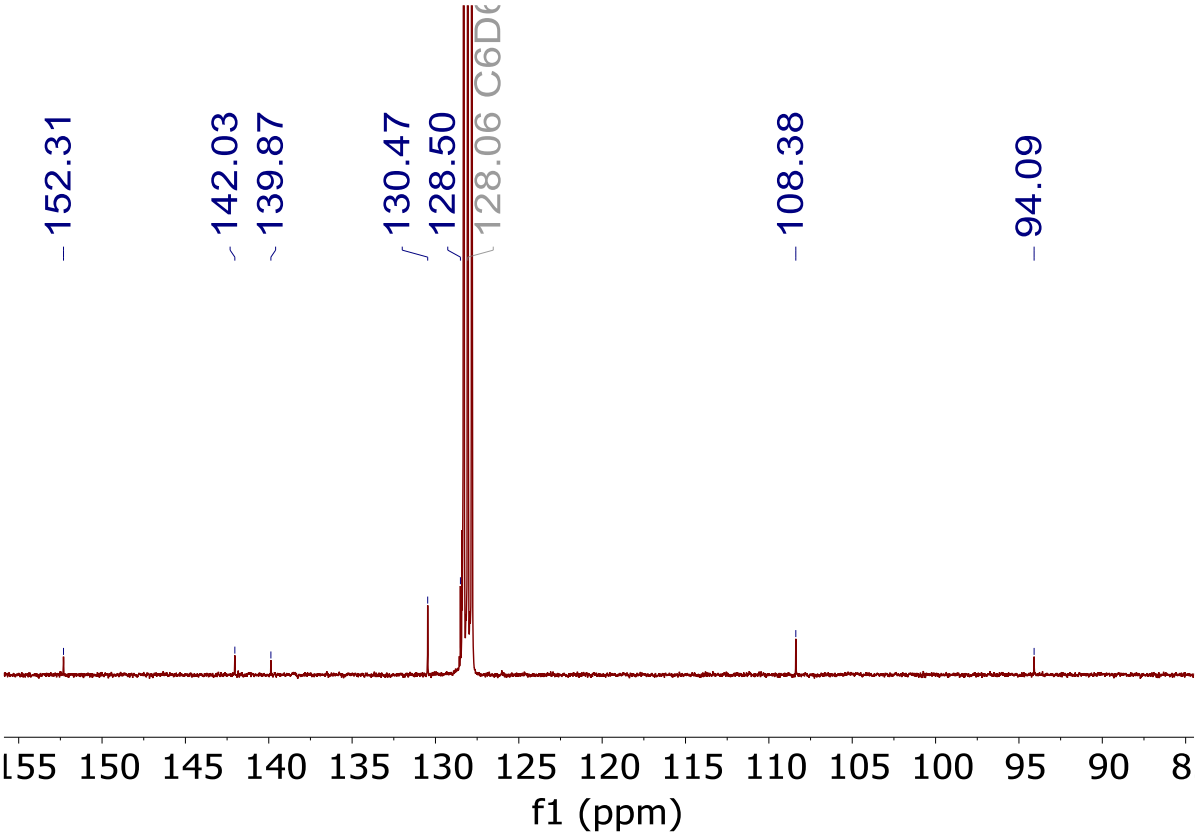

Figure 7.38. $^{13}C\{^{1}H\}$ NMR spectrum of **7.7** in benzene-d_6 at room temperature.

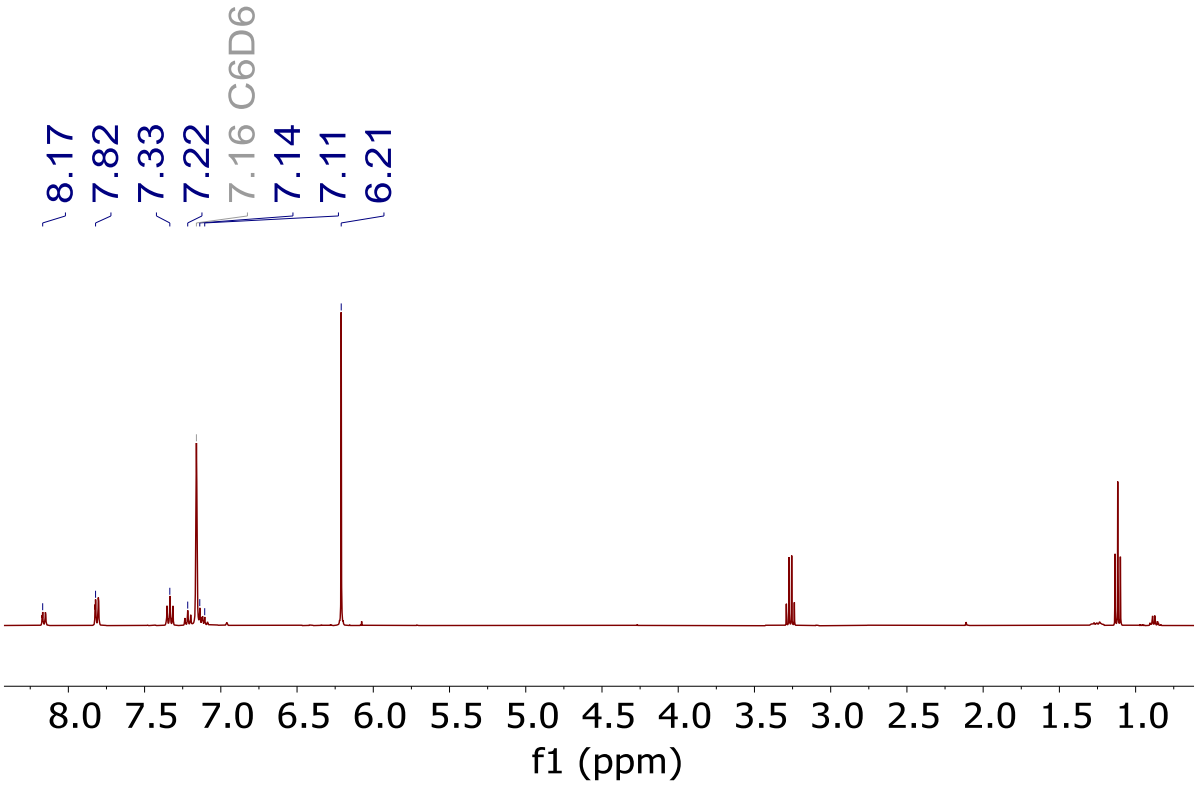

Figure 7.39. ^{1}H NMR spectrum of **7.6** in benzene-d_6 at room temperature.

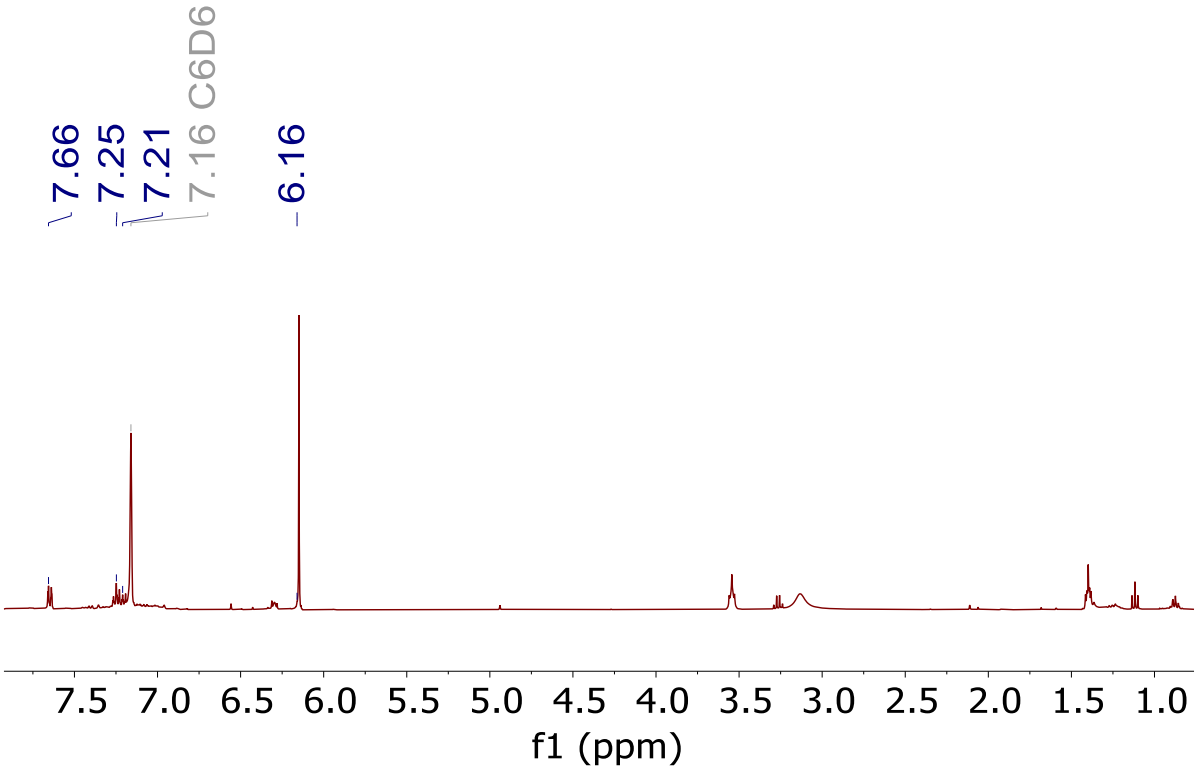

Figure 7.40. ^{1}H NMR spectrum of crude reaction mixture of [Li(12-crown-4)(THF)][**7.1**] with 1 equiv of Ph_2CNH in benzene-d_6 at room temperature.

7.5.2 IR Spectra

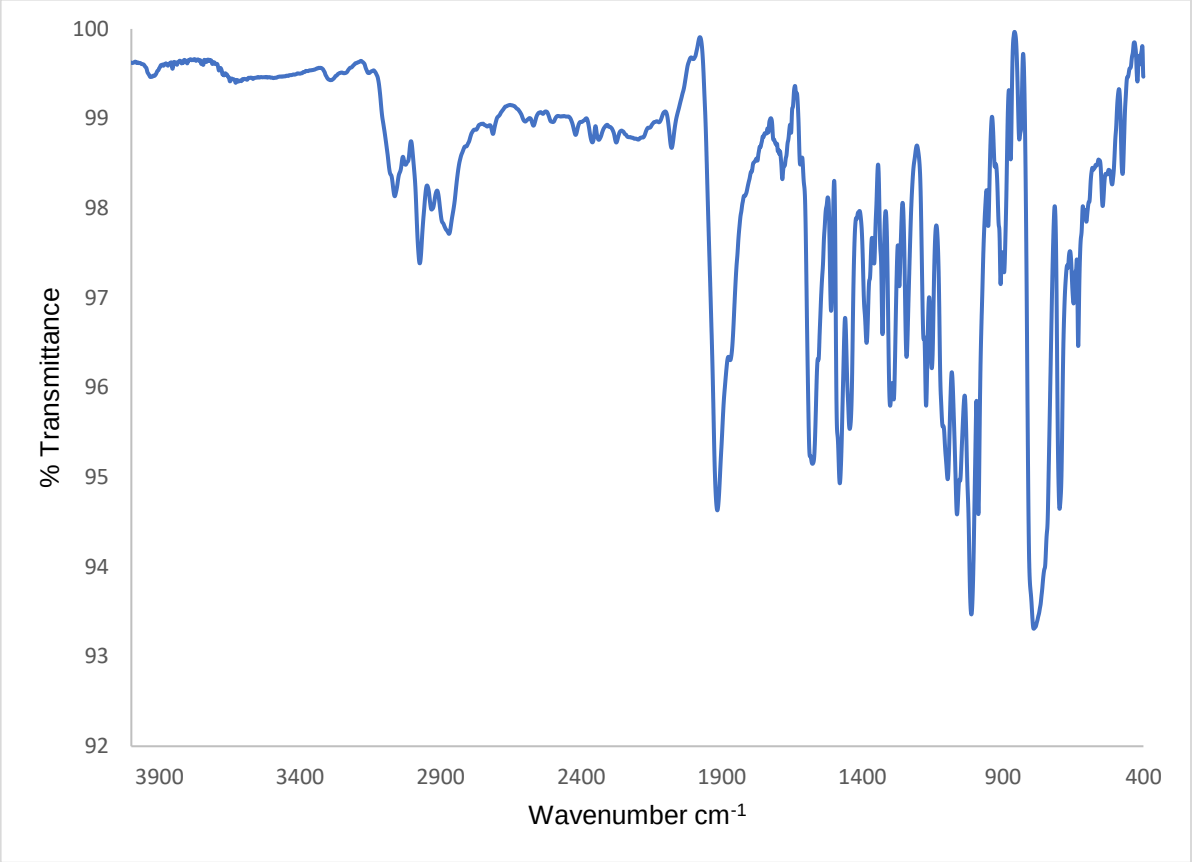

Figure 7.41. IR spectrum of $[Li(Et_2O)_2]$[**7.1**] (KBr Pellet).

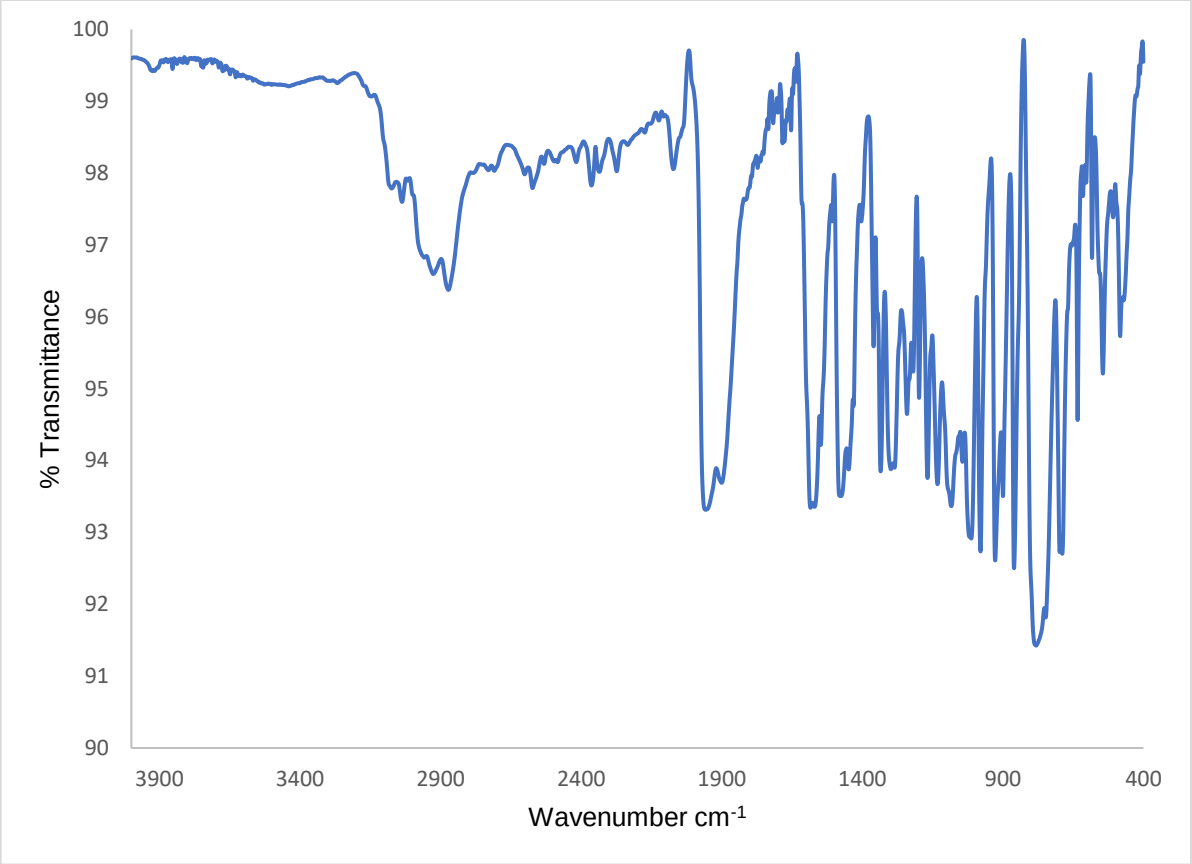

Figure 7.42. IR spectrum of [Li(12-crown-4)(THF)][**7.1**] (KBr Pellet).

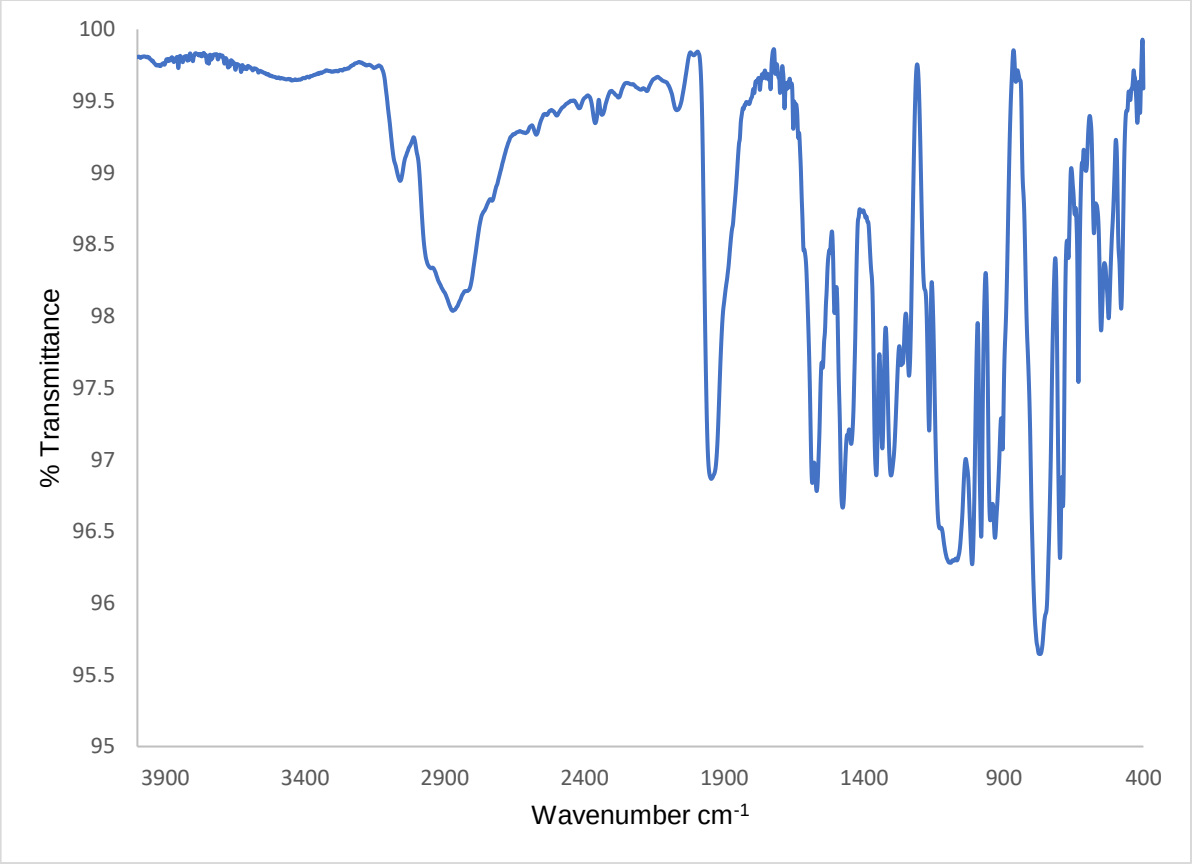

Figure 7.43. IR spectrum of [Li(2.2.2-cryptand)][**7.1**] (KBr Pellet).

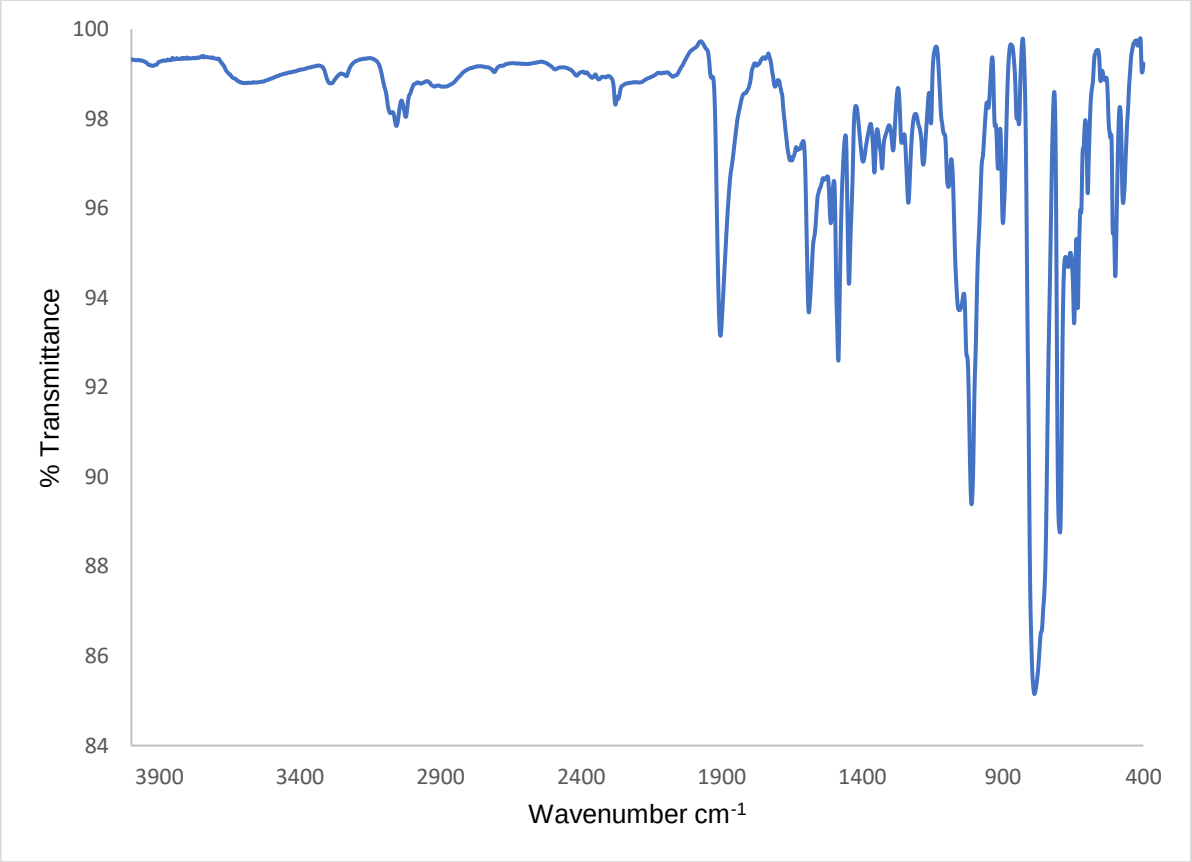

Figure 7.44. IR spectrum of **7.2** (KBr Pellet).

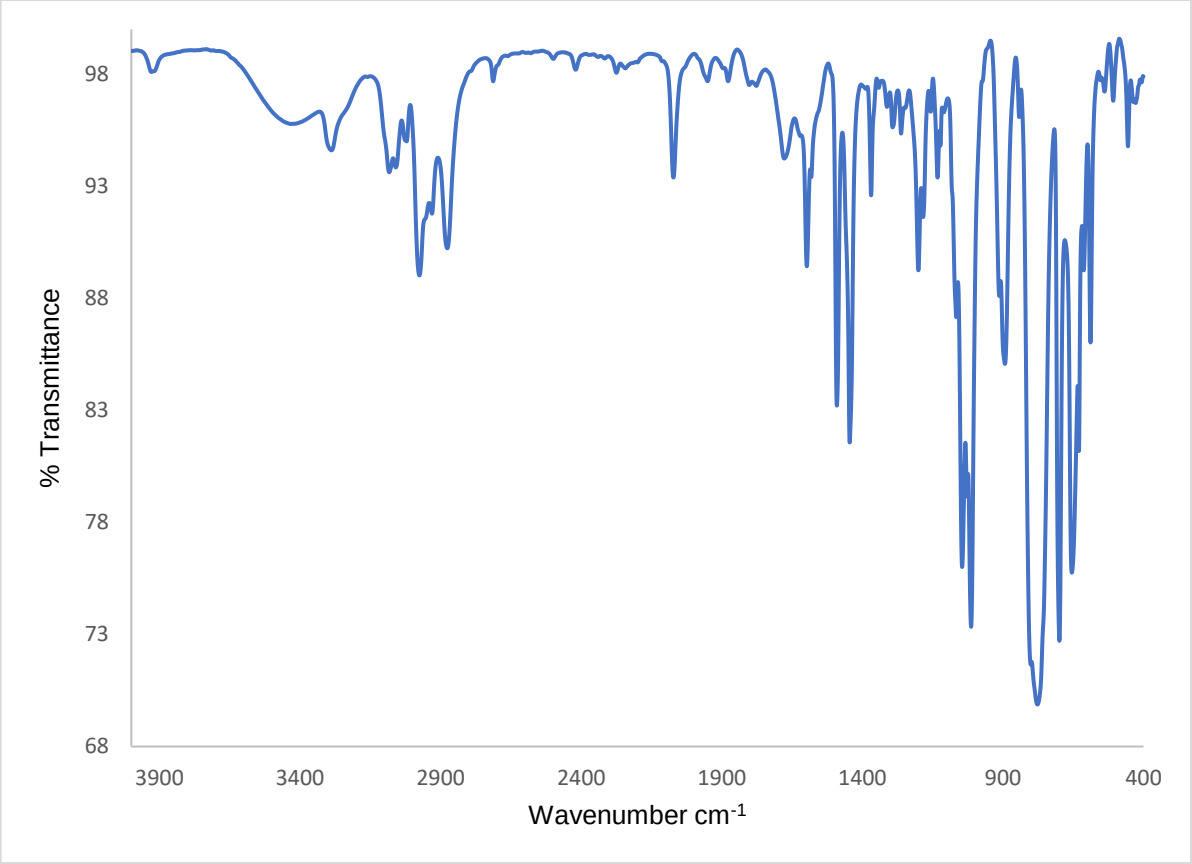

Figure 7.45. IR spectrum of **7.3** (KBr Pellet).

7.5.3 References

(1) Fischer, E. O.; Kalder, H.-J.; Frank, A.; Köhler, F. H.; Huttner, G. 3-Dimethylamino-3-phenylallenylidene, A Novel Ligand at the Pentacarbonyl-chromium and -tungsten Skeleton. *Angew. Chem., Int. Ed.* **1976**, *15*, 623-624.
(2) Berke, H. Simple Synthesis of Dicarbonyl(η-cyclopentadienyl)-(3,3-di-tert-butylallenylidene)managanese. *Angew. Chem., Int. Ed.* **1976**, *15*, 624-624.
(3) Touchard, D.; Dixneuf, P. H. A new class of carbon-rich organometallics. The C_3, C_4 and C_5 metallacumulenes $Ru=(C=)_nCR_2$. *Coord. Chem. Rev.* **1998**, *178-180*, 409-429.
(4) Bruce, M. I. Transition Metal Complexes Containing Allenylidene, Cumulenylidene, and Related Ligands. *Chem. Rev.* **1998**, *98*, 2797-2858.
(5) Rigaut, S.; Touchard, D.; Dixneuf, P. H. Ruthenium-allenylidene complexes and their specific behaviour. *Coord. Chem. Rev.* **2004**, *248*, 1585-1601.
(6) Bruce, M. I. Organometallic chemistry of vinylidene and related unsaturated carbenes. *Chem. Rev.* **1991**, *91*, 197-257.
(7) Cadierno, V.; Gimeno, J. Allenylidene and Higher Cumulenylidene Complexes. *Chem. Rev.* **2009**, *109*, 3512-3560.
(8) Bruneau, C.; Dixneuf, P. H. Metal Vinylidenes and Allenylidenes in Catalysis: Applications in Anti-Markovnikov Additions to Terminal Alkynes and Alkene Metathesis. *Angew. Chem., Int. Ed.* **2006**, *45*, 2176-2203.
(9) Dragutan, V.; Dragutan, B. I. Ruthenium Allenylidene Complexes. *Platin. Met. Rev.* **2006**, *50*, 81-94.
(10) Trost, B. M.; Frederiksen, M. U.; Rudd, M. T. Ruthenium-Catalyzed Reactions—A Treasure Trove of Atom-Economic Transformations. *Angew. Chem., Int. Ed.* **2005**, *44*, 6630-6666.
(11) Cadierno, V.; Gamasa, M. P.; Gimeno, J. Recent Developments in the Reactivity of Allenylidene and Cumulenylidene Complexes. *Eur. J. Inorg. Chem.* **2001**, *2001*, 571-591.
(12) Bruneau, C. Ruthenium Vinylidenes and Allenylidenes in Catalysis. In *Ruthenium Catalysts and Fine Chemistry*, Bruneau, C., Dixneuf, P. H. Eds.; Springer Berlin Heidelberg, 2004; pp 125-153.
(13) Datta, S.; Chang, C.-L.; Yeh, K.-L.; Liu, R.-S. A New Ruthenium-Catalyzed Cleavage of a Carbon−Carbon Triple Bond: Efficient Transformation of Ethynyl Alcohol into Alkene and Carbon Monoxide. *J. Am. Chem. Soc.* **2003**, *125*, 9294-9295.
(14) El Amouri, H.; Gruselle, M. New Bonding Modes, Fluxional Behavior, and Reactivity in Dinuclear Complexes Bridged by Four-Electron Donor Unsaturated Hydrocarbons. *Chem. Rev.* **1996**, *96*, 1077-1104.
(15) Werner, H. Allenylidenes: their multifaceted chemistry at rhodium. *Chem. Commun.* **1997**, 903-904.
(16) Cadierno, V.; Gamasa, M. P.; Gimeno, J. Synthesis and reactivity of α,β-unsaturated alkylidene and cumulenylidene Group 8 half-sandwich complexes. *Coord. Chem. Rev.* **2004**, *248*, 1627-1657.
(17) Coletti, C.; Marrone, A.; Re, N. Metal Complexes Containing Allenylidene and Higher Cumulenylidene Ligands: A Theoretical Perspective. *Acc. Chem. Res.* **2012**, *45*, 139-149.
(18) Esteruelas, M. A.; Gómez, A. V.; López, A. M.; Modrego, J.; Oñate, E. Addition of Carbon Nucleophiles to the Allenylidene Ligand of $[Ru(\eta^5\text{-}C_5H_5)(CCCPh_2)(CO)(PiPr_3)]BF_4$:

Synthesis of New Organic Ligands by Formal C−C Coupling between Mutually Inert Fragments. *Organometallics* **1997**, *16*, 5826-5835.
(19) Akita, M.; Kato, S.-i.; Terada, M.; Masaki, Y.; Tanaka, M.; Moro-oka, Y. Synthesis of Diiron Bridging Allenylidene Complexes $Cp^*_2Fe_2(\mu\text{-}CCCR_1R_2)(\mu\text{-}CO)(CO)_2$ ($Cp^* = \eta^5\text{-}C^5Me^5$) via Nucleophilic Addition to the Diiron Ethynediyl Complex $(\mu\text{-}C{:}C)[FeCp^*(CO)_2]_2$ and Their Conversion to Cationic μ-Vinylcarbyne and μ-Vinylidene Complexes. *Organometallics* **1997**, *16*, 2392-2412.
(20) Re, N.; Sgamellotti, A.; Floriani, C. Density Functional Study of Metallacumulene Complexes. *Organometallics* **2000**, *19*, 1115-1122.
(21) Baya, M.; Crochet, P.; Esteruelas, M. A.; Gutiérrez-Puebla, E.; López, A. M.; Modrego, J.; Oñate, E.; Vela, N. Synthesis and Characterization of Hydride−Alkynyl, Allenylidene, Carbyne, and Functionalized-Alkynyl Complexes Containing the [Os(η5-C5H5)(PiPr3)2]+ Fragment: The Complex [Os(η5-C5H5)(CCCPh2)(PiPr3)2]PF6, a New Type of Allenylidene Derivative from the Reactivity Point of View. *Organometallics* **2000**, *19*, 2585-2596.
(22) García de la Arada, I.; Díez, J.; Gamasa, M. P.; Lastra, E. Nucleophilic Additions to Allenylidene Ruthenium Complexes. *Organometallics* **2015**, *34*, 1345-1353.
(23) Bolaño, T.; Castarlenas, R.; Esteruelas, M. A.; Oñate, E. Sequential and Selective Hydrogenation of the Cα−Cβ and M−Cα Double Bonds of an Allenylidene Ligand Coordinated to Osmium: New Reaction Patterns between an Allenylidene Complex and Alcohols. *J. Am. Chem. Soc.* **2007**, *129*, 8850-8859.
(24) Nishibayashi, Y.; Milton, M. D.; Inada, Y.; Yoshikawa, M.; Wakiji, I.; Hidai, M.; Uemura, S. Ruthenium-Catalyzed Propargylic Substitution Reactions of Propargylic Alcohols with Oxygen-, Nitrogen-, and Phosphorus-Centered Nucleophiles. *Chem. Eur. J.* **2005**, *11*, 1433-1451.
(25) Nishibayashi, Y.; Wakiji, I.; Hidai, M. Novel Propargylic Substitution Reactions Catalyzed by Thiolate-Bridged Diruthenium Complexes via Allenylidene Intermediates. *J. Am. Chem. Soc.* **2000**, *122*, 11019-11020.
(26) Nishibayashi, Y.; Imajima, H.; Onodera, G.; Hidai, M.; Uemura, S. Preparation of a Series of Chalcogenolate-Bridged Diruthenium Complexes and Their Catalytic Activities toward Propargylic Substitution Reactions. *Organometallics* **2004**, *23*, 26-30.
(27) Nishibayashi, Y.; Inada, Y.; Hidai, M.; Uemura, S. Ruthenium-Catalyzed Cycloaddition of Propargylic Alcohols with Phenol Derivatives via Allenylidene Intermediates: Catalytic Use of the Allenylidene Ligand as the C_3 Unit. *J. Am. Chem. Soc.* **2002**, *124*, 7900-7901.
(28) Inada, Y.; Nishibayashi, Y.; Hidai, M.; Uemura, S. Ruthenium-Catalyzed Propargylic Substitution Reaction of Propargylic Alcohols with Thiols: A General Synthetic Route to Propargylic Sulfides. *J. Am. Chem. Soc.* **2002**, *124*, 15172-15173.
(29) Nishibayashi, Y.; Wakiji, I.; Ishii, Y.; Uemura, S.; Hidai, M. Ruthenium-Catalyzed Propargylic Alkylation of Propargylic Alcohols with Ketones: Straightforward Synthesis of γ-Keto Acetylenes. *J. Am. Chem. Soc.* **2001**, *123*, 3393-3394.
(30) Nishibayashi, Y.; Onodera, G.; Inada, Y.; Hidai, M.; Uemura, S. Synthesis of Diruthenium Complexes Containing Chiral Thiolate-Bridged Ligands and Their Application to Catalytic Propargylic Alkylation of Propargylic Alcohols with Acetone. *Organometallics* **2003**, *22*, 873-876.
(31) Nishibayashi, Y.; Yoshikawa, M.; Inada, Y.; Milton, M. D.; Hidai, M.; Uemura, S. Novel Ruthenium- and Platinum-Catalyzed Sequential Reactions: Synthesis of Tri- and

Tetrasubstituted Furans and Pyrroles from Propargylic Alcohols and Ketones. *Angew. Chem., Int. Ed.* **2003**, *42*, 2681-2684.
(32) Nishibayashi, Y.; Yoshikawa, M.; Inada, Y.; Hidai, M.; Uemura, S. Ruthenium-Catalyzed Cycloaddition between Propargylic Alcohols and Cyclic 1,3-Dicarbonyl Compounds via an Allenylidene Intermediate. *J. Org. Chem.* **2004**, *69*, 3408-3412.
(33) Nishibayashi, Y.; Imajima, H.; Onodera, G.; Inada, Y.; Hidai, M.; Uemura, S. Preparation of Alkanechalcogenolate- and Benzenechalcogenolate-Bridged Diruthenium Complexes and Their Catalytic Activity toward Propargylation of Acetone with Propargylic Alcohol. *Organometallics* **2004**, *23*, 5100-5103.
(34) Nishibayashi, Y.; Yoshikawa, M.; Inada, Y.; Hidai, M.; Uemura, S. Ruthenium-Catalyzed Propargylation of Aromatic Compounds with Propargylic Alcohols. *J. Am. Chem. Soc.* **2002**, *124*, 11846-11847.
(35) Nishibayashi, Y.; Inada, Y.; Hidai, M.; Uemura, S. Ruthenium-Catalyzed Carbon−Carbon Bond Formation between Propargylic Alcohols and Alkenes via the Allenylidene-Ene Reaction. *J. Am. Chem. Soc.* **2003**, *125*, 6060-6061.
(36) Gamasa, M. P.; Gimeno, J.; González-Bernardo, C.; Borge, J.; García-Granda, S. Synthesis of Ruthenium(II) 1,2,3-Trimethylindenyl Complexes: X-ray Crystal Structure of [Ru(CCCPh2)(η5-1,2,3-Me3C9H4)(CO)(PPh3)][BF4]. *Organometallics* **1997**, *16*, 2483-2485.
(37) Etienne, M.; Talarmin, J.; Toupet, L. Syntheses and physicochemical properties of polycyano-substituted buta-1,3-dienylidene- and allenylidene-bridged diiron complexes. *Organometallics* **1992**, *11*, 2058-2068.
(38) Castarlenas, R.; Dixneuf, P. H. Highly Active Catalysts in Alkene Metathesis: First Observed Transformation of Allenylidene into Indenylidene via Alkenylcarbyne—Ruthenium Species. *Angew. Chem., Int. Ed.* **2003**, *42*, 4524-4527.
(39) Crochet, P.; Esteruelas, M. A.; López, A. M.; Ruiz, N.; Tolosa, J. I. New Cyclopentadienylosmium Compounds Containing Unsaturated Carbon Donor Coligands: Synthesis, Structure, and Reactivity of $Os(\eta^5\text{-}C^5H^5)Cl(CCCPh_2)(PiPr_3)$. *Organometallics* **1998**, *17*, 3479-3486.
(40) Selegue, J. P. Synthesis and structure of $[Ru(C_3Ph_2)(PMe_3)_2(Cp)][PF_6]$, a cationic diphenylallenylidene complex. *Organometallics* **1982**, *1*, 217-218.
(41) Binger, P.; Müller, P.; Wenz, R.; Mynott, R. (3,3-Diphenylallenylidene)trimethylphosphanetitanocene: The First Titanocene Carbene Complex with Three Cumulative Double Bonds. *Angew. Chem., Int. Ed.* **1990**, *29*, 1037-1038.
(42) Binger, P.; Langhauser, F.; Gabor, B.; Mynott, R.; Herrmann, A. T.; Krüger, C. Dimethylallenediyl as an η^1,η^2-bridging ligand in a dizirconocene complex. *J. Chem. Soc., Chem. Commun.* **1992**, 505-506.
(43) Kent, G. T.; Yu, X. J.; Wu, G.; Autschbach, J.; Hayton, T. W. Synthesis and electronic structure analysis of the actinide allenylidenes, $[\{(NR_2)_3\}An(CCCPh_2)]^-$ (An = U, Th; R = $SiMe_3$). *Chem. Sci.* **2021**, *12*, 14383-14388.
(44) Kent, G. T.; Yu, X. J.; Wu, G.; Autschbach, J.; Hayton, T. W. Ring-opening of a thorium cyclopropenyl complex generates a transient thorium-bound carbene. *Chem. Commun.* **2022**, *58*, 6805-6808.
(45) Chang, K.-H.; Lin, Y.-C.; Liu, Y.-H.; Wang, Y. Reactions of ruthenium cyclopropenyl complexes with trimethylsilyl azide. *J. Chem. Soc., Dalton Trans.* **2001**, 3154-3159.

(46) Lo, Y.-H.; Lin, Y.-C.; Lee, G.-H.; Wang, Y. Synthesis and Reactivity of the Ruthenium Cyclopropenyl Complex with a Tp Ligand. *Organometallics* **1999**, *18*, 982-988.
(47) Sung, H.-L.; Hsu, H.-L. The reactivity of $TMSN_3$ with ruthenium cyclopropenyl complexes containing different ligands and different substituent at Cγ. *J. Organomet. Chem.* **2011**, *696*, 1280-1288.
(48) Chang, K.-H.; Lin, Y.-C. Reactions of ruthenium cyclopropenyl complexes with trimethylsilyl azide. *Chem. Commun.* **1998**, 1441-1442.
(49) Lin, Y.-C. Cyclopropenation of organometallic vinylidene complexes. *J. Organomet. Chem.* **2001**, *617-618*, 141-147.
(50) Ting, P.-C.; Lin, Y.-C.; Lee, G.-H.; Cheng, M.-C.; Wang, Y. Cyclopropenation and Related Reactions of Ruthenium Vinylidene Complexes. *J. Am. Chem. Soc.* **1996**, *118*, 6433-6444.
(51) Chang, C.-W.; Lin, Y.-C.; Lee, G.-H.; Wang, Y. Reactions of Ruthenium Cyclopropenyl Complexes Containing Pentamethylcyclopentadienyl Ligands. *Organometallics* **2000**, *19*, 3211-3219.
(52) Ting, P.-C.; Lin, Y.-C.; Cheng, M.-C.; Wang, Y. Novel Method for the Preparation of Metal Cyclopropenyl Complexes from Vinylidene Complexes with an Electron-Withdrawing Substituent. *Organometallics* **1994**, *13*, 2150-2152.
(53) Chang, C.-W.; Ting, P.-C.; Lin, Y.-C.; Lee, G.-H.; Wang, Y. Synthesis of ruthenium vinylidene complexes with dppe ligand and their cyclopropenation reaction. *J. Organomet. Chem.* **1998**, *553*, 417-425.
(54) Lo, Y.-H.; Lin, Y.-C.; Lee, G.-H.; Wang, Y. Synthesis of (Vinylidene)- and (Cyclopropenyl)ruthenium Complexes Containing a Tris(pyrazolyl)borato (Tp) Ligand. *Eur. J. Inorg. Chem.* **2004**, *2004*, 4616-4623.
(55) Mulks, F. F.; Antoni, P. W.; Rominger, F.; Hashmi, A. S. K. Cyclopropenylgold(I) Complexes as Aurated Carbenoids or Quasi-Carbenes. *Adv. Synth. Catal.* **2018**, *360*, 1810-1821.
(56) Nguyen, T. H.; Yu, X.; Kent, G. T.; Autschbach, J.; Hayton, T. W. U–C Bond Insertion, Ring-Opening, and C–H Activation in a Uranium Bis(diisopropylamino)cyclopropenylidene (BAC) Adduct. *Organometallics* **2023**, *42*, 1005-1012.
(57) Mazzotta, F.; Zitzer, G.; Speiser, B.; Kunz, D. Electron-Deficient Imidazolium Substituted Cp Ligands and their Ru Complexes. *Chem. Eur. J.* **2020**, *26*, 16291-16305.
(58) Bachmann, S.; Gernert, B.; Stalke, D. Solution structures of alkali metal cyclopentadienides in THF estimated by ECC-DOSY NMR-spectroscopy (incl. software). *Chem. Commun.* **2016**, *52*, 12861-12864.
(59) Buncel, E.; Menon, B. Carbanion mechanisms. 9. Spectrophotometric study of triphenylmethyl alkali metal salts. Contact and solvent-separated ion pairs in ethereal solvents. *J. Org. Chem.* **1979**, *44*, 317-320.
(60) Waack, R.; Doran, M.; Baker, E.; Olah, G. Nuclear Magnetic Resonance Investigation of α-C13-Phenylmethyllithiums. *J. Am. Chem. Soc.* **1966**, *88*, 1272-1275.
(61) Waack, R.; Doran, M. A. Electronic Spectra of Organolithium Compounds. *J. Am. Chem. Soc.* **1963**, *85*, 1651-1654.
(62) Li, X.; Schopf, M.; Stephan, J.; Kippe, J.; Harms, K.; Sundermeyer, J. Simple Synthesis of an Allenylidene Heptavalent Rhenium(d^0) Complex. *J. Am. Chem. Soc.* **2004**, *126*, 8660-8661.

(63) Nguyen, T. H.; Pauly, C.; Kent, G. T.; Wu, G.; Hayton, T. W. Dimerization and ring-opening in bis(diisopropylamino)cyclopropenylidene (BAC) mediated by [$U(NR_2)_3(CCPh)$] (R = $SiMe_3$). *Dalton Trans.* **2023**, *52*, 13868-13871.
(64) Kahlert, S.; Görls, H.; Scholz, J. α-Hydrogen Elimination from (1-Aza-1,3-diene)titanium Complexes: Synthesis of Metallacyclic Titanium–Alkylidene Complexes. *Angew. Chem., Int. Ed.* **1998**, *37*, 1857-1861.
(65) Field, L. D.; Gardiner, M. G.; Messerle, B. A.; Raston, C. L. Structure of dilithio-(E)-1,4-bis(trimethylsilyl)but-2-ene by x-ray crystallography and ^{1}H-^{7}Li HOESY. *Organometallics* **1992**, *11*, 3566-3570.
(66) Bartlett, R. A.; Dias, H. V. R.; Power, P. P. Isolation and X-ray crystal structures of the organolithium etherate complexes, [$Li(Et2O)_2(CPh_3)$] and [{$Li(Et_2O)(2,4,6-(CHMe_2)_3C_6H_2)$}$_2$]. *J. Organomet. Chem.* **1988**, *341*, 1-9.
(67) Schumann, H.; Freckmann, D. M. M.; Dechert, S. Synthesis and Structural Characterization of Some Novel Trialkylsilyl-substituted Lithium Benzyl Complexes [Li(tmeda)][$CHRSiMe_2R'$] (R = Ph, 3,5-$Me_2C_6H_3$; R′ = Me, tBu, Ph). *Z. Anorg. Allg. Chem.* **2008**, *634*, 1334-1338.
(68) Brooks, J. J.; Stucky, G. D. π-Groups in ion pair bonding. Triphenylmethyllithium tetramethylethylenediamine. *J. Am. Chem. Soc.* **1972**, *94*, 7333-7338.
(69) Smiles, D. E.; Wu, G.; Hrobárik, P.; Hayton, T. W. Synthesis, Thermochemistry, Bonding, and ^{13}C NMR Chemical Shift Analysis of a Phosphorano-Stabilized Carbene of Thorium. *Organometallics* **2017**, *36*, 4519-4524.
(70) Rungthanaphatsophon, P.; Bathelier, A.; Castro, L.; Behrle, A. C.; Barnes, C. L.; Maron, L.; Walensky, J. R. Formation of Methane versus Benzene in the Reactions of $(C_5Me_5)_2Th(CH_3)_2$ with $[CH_3PPh_3]X$ (X=Cl, Br, I) Yielding Thorium-Carbene or Thorium-Ylide Complexes. *Angew. Chem., Int. Ed.* **2017**, *56*, 12925-12929.
(71) Lide, D. R. A survey of carbon-carbon bond lengths. *Tetrahedron* **1962**, *17*, 125-134.
(72) Ojo, W.-S.; Pétillon, F. Y.; Schollhammer, P.; Talarmin, J.; Muir, K. W. A Bridging Side-on Allenylidene Dimolybdenum Complex without Carbonyl Stabilization. *Organometallics* **2006**, *25*, 5503-5505.
(73) Froom, S. F. T.; Green, M.; Mercer, R. J.; Nagle, K. R.; Orpen, A. G.; Rodrigues, R. A. Reactions of co-ordinated ligands. Part 53. Synthesis of dimolybdenum and ditungsten μ-σ,η^2-(4e)-vinylidene and -allenylidene complexes; crystal structures of [$N(PPh_3)_2$][Mo_2{μ-σ:η^2-(3e)-C_2Ph}$(CO)_4(\eta^5$-$C_9H_7)_2$], [Mo_2{μ-σ:η^2-(4e)-C=C(Ph)$(CH_2)_4$OMe}$(CO)_4(\eta$-$C_5H_5)_2$] and [Mo_2{μ-σ:η^2-(4e)-C=C=CMe_2}$(CO)_4(\eta$-$C_5H_5)_2$]. *J. Chem. Soc., Dalton Trans.* **1991**, 3171-3183.
(74) Capon, J. F.; Le Berre-Cosquer, N.; Bernier, S.; Pichon, R.; Kergoat, R.; L'Haridon, P. New synthesis of μ-allenylidene complexes from dimolybdenum carbenium ions crystal structure of [{$Mo(\eta^5$-$C_5H_5)(CO)_2$}$_2$(μ, η^2-C=C=C_6H_{10})]. *J. Organomet. Chem.* **1995**, *487*, 201-208.
(75) Froom, S. F. T.; Green, M.; Nagle, K. R.; Williams, D. J. Regioselectivity in the Reactions of Dimolybdenum and Ditungsten σ,η^2(4e)-Allenylidene Complexes with Nucleophilic and Electrophilic Reagents; Crystal Structure and Dynamic Behaviour of the Cationic Complex [$W_2(\eta$-$HC_2CMe_2)(CO)_4(\eta$-$C_5H_5)_2$][BF_4]. *J. Chem. Soc., Chem. Commun.* **1987**, 1305-1307.
(76) Froom, S. F. T.; Green, M.; Mercer, R. J.; Nagle, K. R.; Orpen, A. G.; Schwiegk, S. Evidence for a facile switch in the bonding mode of μ-vinylidene ligands from σ, η^2 to σ,σ;

synthesis and structure of a dinuclear μ-σ,η^2-allenylidene complex. *J. Chem. Soc., Chem. Commun.* **1986**, 1666-1668.
(77) Suvova, M.; O'Brien, K. T. P.; Farnaby, J. H.; Love, J. B.; Kaltsoyannis, N.; Arnold, P. L. Thorium(IV) and Uranium(IV) trans-Calix[2]benzene[2]pyrrolide Alkyl and Alkynyl Complexes: Synthesis, Reactivity, and Electronic Structure. *Organometallics* **2017**, *36*, 4669-4681.
(78) Garner, M. E.; Parker, B. F.; Hohloch, S.; Bergman, R. G.; Arnold, J. Thorium Metallacycle Facilitates Catalytic Alkyne Hydrophosphination. *J. Am. Chem. Soc.* **2017**, *139*, 12935-12938.
(79) Settineri, N. S.; Arnold, J. Insertion, protonolysis and photolysis reactivity of a thorium monoalkyl amidinate complex. *Chem. Sci.* **2018**, *9*, 2831-2841.
(80) Wang, Y.; Zhang, C.; Zi, G.; Ding, W.; Walter, M. D. Preparation of a potassium chloride bridged thorium phosphinidiide complex and its reactivity towards small organic molecules. *Nouv. J. Chim.* **2019**, *43*, 9527-9539.
(81) Kent, G. T.; Yu, X. J.; Pauly, C.; Wu, G.; Autschbach, J.; Hayton, T. W. Synthesis of Parent Acetylide and Dicarbide Complexes of Thorium and Uranium and an Examination of Their Electronic Structures. *Inorg. Chem.* **2021**, *60*, 15413-15420.
(82) Carlson, C. N.; Hanusa, T. P.; Brennessel, W. W. Metal Allyl Complexes with Bulky Ligands: Stabilization of Homoleptic Thorium Compounds, $[(SiMe_3)_nC_3H_{5-n}]_4Th$ (n = 1, 2). *J. Am. Chem. Soc.* **2004**, *126*, 10550-10551.
(83) Ren, W. S.; Deng, X. B.; Zi, G. F.; Fang, D. C. The Th=C double bond: an experimental and computational study of thorium poly-carbene complexes. *Dalton Trans.* **2011**, *40*, 9662-9664.
(84) Gregson, M.; Lu, E.; Tuna, F.; McInnes, E. J. L.; Hennig, C.; Scheinost, A. C.; McMaster, J.; Lewis, W.; Blake, A. J.; Kerridge, A.; Liddle, S. T. Emergence of comparable covalency in isostructural cerium(IV)- and uranium(IV)-carbon multiple bonds. *Chem. Sci.* **2016**, *7*, 3286-3297.
(85) Ma, G. B.; Ferguson, M. J.; McDonald, R.; Cavell, R. G. Actinide Metals with Multiple Bonds to Carbon: Synthesis, Characterization, and Reactivity of U(IV) and Th(IV) Bis(iminophosphorano)methandiide Pincer Carbene Complexes. *Inorg. Chem.* **2011**, *50*, 6500-6508.
(86) Lu, E. L.; Lewis, W.; Blake, A. J.; Liddle, S. T. The Ketimide Ligand is Not Just an Inert Spectator: Heteroallene Insertion Reactivity of an Actinide-Ketimide Linkage in a Thorium Carbene Amide Ketimide Complex. *Angew. Chem., Int. Ed.* **2014**, *53*, 9356-9359.
(87) Mantovani, N.; Marvelli, L.; Rossi, R.; Bianchini, C.; Rios, I. d. l.; Romerosa, A.; Peruzzini, M. Backward synthesis of rhenium(I) γ-hydroxyvinylidene and γ-methoxyvinylidene complexes and their conversion to the allenylidene $[Re\{C=C=CPh_2\}(CO)_2(MeC(CH_2PPh_2)_3)](OSO_2CF_3)$. *J. Chem. Soc., Dalton Trans.* **2001**, 2353-2361.
(88) Kolobova, N. E.; Ivanov, L. L.; Zhvanko, O. S.; Khitrova, O. M.; Batsanov, A. S.; Struchkov, Y. T. Protonation of allenylidene- and vinylidene-manganese complexes. Crystal and molecular structure of $[Cp(CO)_2Mn=C=CH=CPh_2]^+ BF_4^-$. *J. Organomet. Chem.* **1984**, *262*, 39-47.
(89) Lai, Y.; Halder, A.; Kim, J.; Hicks, T. J.; Milner, P. J. Electroreductive Radical Borylation of Unactivated (Hetero)Aryl Chlorides Without Light by Using Cumulene-Based Redox Mediators**. *Angew. Chem., Int. Ed.* **2023**, *62*, e202310246.

(90) Albright, H.; Davis, A. J.; Gomez-Lopez, J. L.; Vonesh, H. L.; Quach, P. K.; Lambert, T. H.; Schindler, C. S. Carbonyl–Olefin Metathesis. *Chem. Rev.* **2021**, *121*, 9359-9406.
(91) Schrock, R. R. Multiple metal-carbon bonds. 5. The reaction of niobium and tantalum neopentylidene complexes with the carbonyl function. *J. Am. Chem. Soc.* **1976**, *98*, 5399-5400.
(92) Solowey, D. P.; Kurogi, T.; Manor, B. C.; Carroll, P. J.; Mindiola, D. J. Metallo-Wittig chemistry of an alkylidene to form a terminal titanium oxo complex. *Dalton Trans.* **2016**, *45*, 15894-15901.
(93) Jantunen, K. C.; Burns, C. J.; Castro-Rodriguez, I.; Da Re, R. E.; Golden, J. T.; Morris, D. E.; Scott, B. L.; Taw, F. L.; Kiplinger, J. L. Thorium(IV) and Uranium(IV) Ketimide Complexes Prepared by Nitrile Insertion into Actinide−Alkyl and −Aryl Bonds. *Organometallics* **2004**, *23*, 4682-4692.
(94) Assefa, M. K.; Sergentu, D.-C.; Seaman, L. A.; Wu, G.; Autschbach, J.; Hayton, T. W. Synthesis, Characterization, and Electrochemistry of the Homoleptic f Element Ketimide Complexes $[Li]_2[M(N{=}CtBuPh)_6]$ (M = Ce, Th). *Inorg. Chem.* **2019**, *58*, 12654-12661.
(95) Fürstner, A.; Liebl, M.; Lehmann, C. W.; Picquet, M.; Kunz, R.; Bruneau, C.; Touchard, D.; Dixneuf, P. H. Cationic Ruthenium Allenylidene Complexes as Catalysts for Ring Closing Olefin Metathesis. *Chem. Eur. J.* **2000**, *6*, 1847-1857.
(96) Séméril, D.; Le Nôtre, J.; Bruneau, C.; Dixneuf, P. H.; Kolomiets, A. F.; Osipov, S. N. Fluorine-containing α-alkynyl amino esters and access to a new family of 3,4-dehydroproline analogues. *Nouv. J. Chim.* **2001**, *25*, 16-18.
(97) Picquet, M.; Bruneau, C.; H. Dixneuf, P. Catalytic synthesis of 3-vinyl-2,5-dihydrofurans from yne-enes promoted by photochemically activated metal–allenylidene LRu=C=C=CR2 complex. *Chem. Commun.* **1998**, 2249-2250.
(98) Osipov, Sergey N.; Artyushin, Oleg I.; Kolomiets, Alexey F.; Bruneau, C.; Picquet, M.; Dixneuf, Pierre H. Synthesis of Fluorine-Containing Cyclic α-Amino Acid and α-Amino Phosphonate Derivatives by Alkene Metathesis. *Eur. J. Org. Chem.* **2001**, *2001*, 3891-3897.
(99) Castarlenas, R.; Séméril, D.; Noels, A. F.; Demonceau, A.; Dixneuf, P. H. Allenylidene-ruthenium-arene precatalyst for ring opening metathesis polymerisation (ROMP). *J. Organomet. Chem.* **2002**, *663*, 235-238.
(100) Hayton, T. W. Recent developments in actinide–ligand multiple bonding. *Chem. Commun.* **2013**, *49*, 2956-2973.
(101) Smiles, D. E.; Wu, G.; Kaltsoyannis, N.; Hayton, T. W. Thorium–ligand multiple bonds via reductive deprotection of a trityl group. *Chem. Sci.* **2015**, *6*, 3891-3899.
(102) Fortier, S.; Walensky, J. R.; Wu, G.; Hayton, T. W. Synthesis of a Phosphorano-Stabilized U(IV)-Carbene via One-Electron Oxidation of a U(III)-Ylide Adduct. *J. Am. Chem. Soc.* **2011**, *133*, 6894-6897.
(103) Cooper, O. J.; Mills, D. P.; McMaster, J.; Moro, F.; Davies, E. S.; Lewis, W.; Blake, A. J.; Liddle, S. T. Uranium–Carbon Multiple Bonding: Facile Access to the Pentavalent Uranium Carbene $[U\{C(PPh_2NSiMe_3)_2\}(Cl)_2(I)]$ and Comparison of U^{V}=C and U^{IV}=C Bonds. *Angew. Chem., Int. Ed.* **2011**, *50*, 2383-2386.
(104) Cooper, O. J.; Mills, D. P.; McMaster, J.; Tuna, F.; McInnes, E. J. L.; Lewis, W.; Blake, A. J.; Liddle, S. T. The Nature of the U=C Double Bond: Pushing the Stability of High-Oxidation-State Uranium Carbenes to the Limit. *Chem. Eur. J.* **2013**, *19*, 7071-7083.

(105) Rungthanaphatsophon, P.; Huang, P.; Walensky, J. R. Phosphorano-Stabilized Carbene Complexes with Short Thorium(IV)– and Uranium(IV)–Carbon Bonds. *Organometallics* **2018**, *37*, 1884-1891.
(106) Liddle, S. T. The Renaissance of Non-Aqueous Uranium Chemistry. *Angew. Chem., Int. Ed.* **2015**, *54*, 8604-8641.
(107) Gregson, M.; Wooles, A. J.; Cooper, O. J.; Liddle, S. T. Covalent Uranium Carbene Chemistry. *Comments Inorg. Chem.* **2015**, *35*, 262-294.
(108) Hayton, T. W. Metal–ligand multiple bonding in uranium: structure and reactivity. *Dalton Trans.* **2010**, *39*, 1145-1158.
(109) Boronski, J. T.; Seed, J. A.; Wooles, A. J.; Liddle, S. T. Fragmentation, catenation, and direct functionalisation of white phosphorus by a uranium(IV)–silyl–phosphino–carbene complex. *Chem. Commun.* **2021**, *57*, 5090-5093.
(110) Seed, J. A.; Sharpe, H. R.; Futcher, H. J.; Wooles, A. J.; Liddle, S. T. Nature of the Arsonium-Ylide $Ph_3As{=}CH_2$ and a Uranium(IV) Arsonium–Carbene Complex. *Angew. Chem., Int. Ed.* **2020**, *59*, 15870-15874.
(111) Lu, E.; Cooper, O. J.; McMaster, J.; Tuna, F.; McInnes, E. J. L.; Lewis, W.; Blake, A. J.; Liddle, S. T. Synthesis, Characterization, and Reactivity of a Uranium(VI) Carbene Imido Oxo Complex. *Angew. Chem., Int. Ed.* **2014**, *53*, 6696-6700.
(112) Cantat, T.; Arliguie, T.; Noël, A.; Thuéry, P.; Ephritikhine, M.; Floch, P. L.; Mézailles, N. The U=C Double Bond: Synthesis and Study of Uranium Nucleophilic Carbene Complexes. *J. Am. Chem. Soc.* **2009**, *131*, 963-972.
(113) Ephritikhine, M. Uranium carbene compounds. *C. R. Chim.* **2013**, *16*, 391-405.
(114) Tourneux, J.-C.; Berthet, J.-C.; Cantat, T.; Thuéry, P.; Mézailles, N.; Ephritikhine, M. Exploring the Uranyl Organometallic Chemistry: From Single to Double Uranium−Carbon Bonds. *J. Am. Chem. Soc.* **2011**, *133*, 6162-6165.
(115) Kent, G. T.; Yu, X. J.; Wu, G.; Autschbach, J.; Hayton, T. W. Synthesis and electronic structure analysis of the actinide allenylidenes, $[\{(NR_2)_3\}An(CCCPh_2)]^-$ (An = U, Th; R = SiMe). *Chem. Sci.* **2021**, *12*, 14383-14388.
(116) Shen, Y.; Yu, X.; Meng, Q.; Yao, Y.-R.; Autschbach, J.; Chen, N. ThC2@C82versus Th@C84: unexpected formation of triangular thorium carbide cluster inside fullerenes. *Chemical Science* **2022**, *13*, 12980-12986.
(117) Brizius, G.; Bunz, U. H. F. Increased Activity of in Situ Catalysts for Alkyne Metathesis. *Organic Letters* **2002**, *4*, 2829-2831.
(118) Grüger, F.; Szeimies, G. 3,3,3′,3′-tetramethyl-2,2′-bistrimethylsilyl-1,1′-bicyclopropenyl: Synthesis and isomerization. *Tetrahedron Lett.* **1986**, *27*, 1563-1564.
(119) Seyam, A. M. Thermal studies of 'dialkyldioxouranium(VI)'. *Inorg. Chim. Acta* **1982**, *58*, 71-74.
(120) Seyam, A. M. Observations on the reaction of uranium tetrachloride and dichlorodioxouranium(VI) with lithium alkyls. *Inorg. Chim. Acta* **1985**, *110*, 123-126.
(121) Staun, S. L.; Stevens, L. M.; Smiles, D. E.; Goodwin, C. A. P.; Billow, B. S.; Scott, B. L.; Wu, G.; Tondreau, A. M.; Gaunt, A. J.; Hayton, T. W. Expanding the Nonaqueous Chemistry of Neptunium: Synthesis and Structural Characterization of $[Np(NR_2)_3Cl]$, $[Np(NR_2)_3Cl]^-$, and $[Np\{N(R)(SiMe_2CH_2)\}_2(NR_2)]^-$ (R = $SiMe_3$). *Inorg. Chem.* **2021**, *60*, 2740-2748.
(122) Shannon, R. Revised effective ionic radii and systematic studies of interatomic distances in halides and chalcogenides. *Acta Cryst. A* **1976**, *32*, 751-767.

(123) Barnett, N. D. R.; Mulvey, R. E.; Clegg, W.; Oneil, P. A. Crystal-Structure of Lithium Diisopropylamide (LDA) - an Infinite Helical Arrangement Composed of near-Linear N-Li-N Units with 4 Units Per Turn of Helix. *J. Am. Chem. Soc.* **1991**, *113*, 8187-8188.
(124) Depenbrock, F.; Limpke, T.; Stammler, A.; Oldengott, J.; Bögge, H.; Glaser, T. Molecular and Electronic Structures of a Series of Dinuclear Co Complexes Varied by Exogeneous Ligands: Influence of π-Bonding on Redox Potentials. *Eur. J. Inorg. Chem.* **2022**, *2022*.
(125) Harris, R. K.; Becker, E. D.; Cabral de Menezes, S. M.; Goodfellow, R.; Granger, P. NMR nomenclature. Nuclear spin properties and conventions for chemical shifts (IUPAC Recommendations 2001). *Pure Appl. Chem.* **2001**, *73*, 1795-1818.
(126) Harris, R. K.; Becker, E. D.; Cabral De Menezes, S. M.; Granger, P.; Hoffman, R. E.; Zilm, K. W. Further conventions for NMR shielding and chemical shifts (IUPAC Recommendations 2008). *Pure Appl. Chem.* **2008**, *80*, 59-84.
(127) SMART Apex II, Version 2.1 ed.; Bruker AXS Inc.: Madison WI, 2005.
(128) SAINT Software User's Guide, Version 7.34a ed.; Bruker AXS Inc.: Madison, WI, 2005.
(129) Sheldrick, G. M. SADABS, the Siemens Area Detector Absorption Correction; University of Göttingen: Göttingen, Germany, 2005.
(130) SHELXTL PC, Version 6.12 ed.; Bruker AXS Inc.:Madison, WI, 2005.
(131) Diamond - Crystal and Molecular Structure Visualization; Crystal Impact: Bonn, Germany, http://www.crystalimpact.com/diamond.
(132) Baerends, E. J. et al. AMS2023.104, Theoretical Chemistry, Vrije Universiteit, Amsterdam, The Netherlands. https://www.scm.com.
(133) Becke, A. D. Densityfunctional thermochemistry. III. the role of exact exchange. *J. Chem. Phys.* **1993**, *98*, 5648–5652.
(134) Becke, A. D. Density-functional exchange-energy approximation with correct asymptotic behavior. *Phys. Rev. A* **1988**, *38*, 3098-3100.
(135) Lee, C.; Yang, W.; Parr, R. G. Development of the Colle-Salvetti correlation-energy formula into a functional of the electron density. *Phys. Rev. B* **1988**, *37*, 785-789.
(136) Lenthe, E. v.; Baerends, E. J.; Snijders, J. G. Relativistic regular two-component Hamiltonians. *J. Chem. Phys.* **1993**, *99*, 4597-4610.
(137) Van Lenthe, E.; Baerends, E. J. Optimized Slater-type basis sets for the elements 1–118. *J. Comput. Chem.* **2003**, *24*, 1142-1156.
(138) Grimme, S.; Ehrlich, S.; Goerigk, L. Effect of the damping function in dispersion corrected density functional theory. *J. Comput. Chem.* **2011**, *32*, 1456-1465.
(139) Glendening, E. D.; Landis, C. R.; Weinhold, F. NBO 6.0: Natural bond orbital analysis program. *J. Comput. Chem.* **2013**, *34*, 1429-1437.
(140) Autschbach, J. The role of the exchange-correlation response kernel and scaling corrections in relativistic density functional nuclear magnetic shielding calculations with the zeroth-order regular approximation. *Mol. Phys.* **2013**, *111*, 2544-2554.
(141) Seaman, L. A.; Hrobárik, P.; Schettini, M. F.; Fortier, S.; Kaupp, M.; Hayton, T. W. A Rare Uranyl(VI)–Alkyl Ate Complex $[Li(DME)_{1.5}]_2[UO_2(CH_2SiMe_3)_4]$ and Its Comparison with a Homoleptic Uranium(VI)–Hexaalkyl. *Angew. Chem. Int. Ed.* **2013**, *52*, 3259-3263.
(142) Hrobárik, P.; Hrobáriková, V.; Greif, A. H.; Kaupp, M. Giant Spin-Orbit Effects on NMR Shifts in Diamagnetic Actinide Complexes: Guiding the Search of Uranium(VI)

Hydride Complexes in the Correct Spectral Range. *Angew. Chem. Int. Ed.* **2012**, *51*, 10884-10888.
(143) Pye, C. C.; Ziegler, T. An implementation of the conductor-like screening model of solvation within the Amsterdam density functional package. *Theor. Chem. Acc.* **1999**, *101*, 396-408.
(144) Frisch, M.; Trucks, G. W.; Schlegel, H. B.; Scuseria, G. E.; Robb, M. A.; Cheeseman, J. R.; Scalmani, G.; Barone, V.; Petersson, G. A.; Nakatsuji, H.; Li, X.; Caricato, M.; Marenich, A. V.; Bloino, J.; Janesko, B. G.; Gomperts, R.; Mennucci, B.; Hratchian, H. P.; Ortiz, J. V.; Izmaylov, A. F.; Sonnenberg, J. L.; Williams-Young, D.; Ding, F.; Lipparini, F.; Egidi, F.; Goings, J.; Peng, B.; Petrone, A.; Henderson, T.; Ranasinghe, D. V.; Zakrzewski, G.; Gao, J.; Rega, N.; Zheng, G.; Liang, W.; Hada, M.; Ehara, M.; Toyota, K.; Fukuda, R.; Hasegawa, J.; Ishida, M.; Nakajima, T.; Honda, Y.; Kitao, O.; Nakai, H.; Vreven, T.; Throssell, K.; Montgomery, Jr., J. A.; Peralta, J. E.; Ogliaro, F.; Bearpark, M. J.; Heyd, J. J.; Brothers, E. N.; Kudin, K. N.; Staroverov, V. N. T.; Keith, A.; Kobayashi, R.; Normand, J.; Raghavachari, K.; Rendell, A. P.; Burant, J. C.; Iyengar, S. S.; Tomasi, J.; Cossi, M.; Millam, J. M.; Klene, M.; Adamo, C.; Cammi, R.; Ochterski, J. W.; Martin, R. L.; Farkas, K. O.; Foresman, J. B.; Fox, D. J., **2016**, Gaussian, Inc. Wallingford, CT.
(145) Cao, X.; Dolg, M. Valence basis sets for relativistic energy-consistent small-core lanthanide pseudopotentials. *J. Chem. Phys.* **2001**, *115*, 7348-7355.
(146) Rassolov, V. A.; Pople, J. A.; Ratner, M. A.; Windus, T. L. 6-31G* basis set for atoms K through Zn. *J. Chem. Phys.* **1998**, *109*, 1223-1229.
(147) Hratchian, H. P.; Schlegel, H. B. Using Hessian Updating To Increase the Efficiency of a Hessian Based Predictor-Corrector Reaction Path Following Method. *J. Chem. Theory Comput.* **2005**, *1*, 61-69.

Chapter 8. Synthesis and Characterization of Homoleptic Tetrakis(1,2-benzenedithiolate) Actinide(IV) Complexes, $[An(1,2\text{-}S_2C_6H_4)_4]^{4-}$

Table of Contents

8.1 Introduction

Homoleptic f element complexes have proved useful in comprehending f and d orbital participation in metal-ligand bonds.[1-10] In particular, optical spectroscopic studies of octahedral f^1 hexahalide complexes has been widely employed to understand f orbital bonding, largely attributed to their simple electron configuration.[11-16] In this regard, Hayton and Lukens evaluated metal-ligand bonding in a series of O_h-symmetric uranium(V) complexes featuring halide, alkyl, alkoxide, amide, and ketamide ligands.[17] Specifically, analysis of their EPR spectroscopy, NIR-visible spectroscopy, and crystal field modelling highlights the role played by the orbital energy in determining the strength and covalency in metal-ligand bonds. However, such analysis of O_h-symmetric uranium(V) complexes featuring soft donor thiolate ligands has not been explored. Importantly, understanding the role of soft donor sulfur ligands in f-elements is crucial for designing effective separation processes of spent nuclear fuel.[9, 18, 19] Specifically, the use of extractants containing soft donor sulfur ligands have demonstrated selectivity between the minor actinide and lanthanides.[20, 21]

Interestingly, a significant number of homoleptic actinide thiolate complexes have proven useful in investigating metal-ligand bonds.[22-37] For example, Ephritikhine and co-workers synthesized and characterized homoleptic tris(dithiolene) and tetrakis(dithiolene) complexes of uranium(IV), namely, $[Na_4(THF)_8U(dddt)_4]$ and $[Na(18\text{-crown-6})(py)_2]_2[U(dddt)_3]\cdot 2py$ (dddt = 5,6-dihydro-1,4-dithiine-2,3-dithiolate).[34] Additionally, Arnold and co-workers used *m*-terphenyldithiocarboxylate ligand to stabilize homoleptic actinide(IV) complexes, $[(TerphCS_2)_4An]$ (An = Th and U) and a homoleptic lanthanum(III) complex, $[(TerphCS_2)_3La]$ ($TerphCS_2$ = 2,6-

(C_6H_4-4-^{t}Bu)$_2C_6H_3CS_2$).[32] Furthermore, Gaunt and co-workers examined bonding difference between 4f and 5f in a series of homoleptic complexes with soft donor ligands, M[N(EPPh_2)$_2$]$_3$ (M = U, Pu, La or Ce; E = S or Se) and M[N(EPiPr_2)$_2$]$_3$ (M = U, Pu, La or Ce; E = S, Se or Te). Despite significant advancements in homoleptic actinide thiolate complexes, isolation of higher oxidation states in uranium, such as 5+, remain elusive. This challenge partly arises due to the strong oxidizing nature of U(V), which enables it to oxidize sulfur donors.

In efforts to isolate an O_h-symmetric uranium(V) thiolate complex, I hypothesized that utilizing a chelating ligand, such as 1,2-benzenedithiolate would stabilize the highly oxidizing uranium(V) center. Interestingly, there are a large number of homoleptic transitional metal 1,2-benzenedithiolate complexes that have been reported,[38-52] yet no reported 1,2-benzenedithiolate complexes are known for the actinides. Herein, I describe the synthesis and characterization of two homoleptic actinide(IV) dithiolate complexes [Li(THF)$_2$]$_4$[Th(1,2-(S_2)C_6H_4)$_4$] (**8.1**) and [Li(TMEDA)]$_4$[U(1,2-(S_2)C_6H_4)$_4$] (**8.2**).

Scheme 8.1. Structure of Uranyl and Reverse Uranyl.

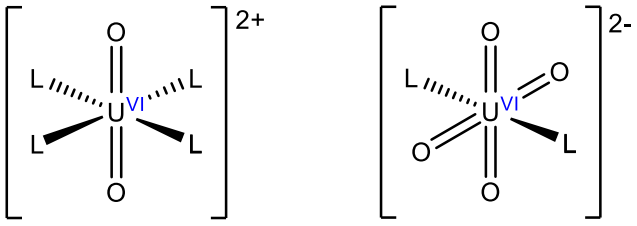

uranyl reverse uranyl

Additionally, in pursuit to deepen our understanding of the electronic structure and chemical bonding, I examined the use of soft donor sulfur ligand with uranyl ion, *trans*-[$U^{VI}O_2$]$^{2+}$, the most studied fragment in uranium chemistry (Scheme 8.1).[53-56]

Interestingly, uranyl features a trans configuration of its oxo ligands (ca 180) with short U═O bond distances (ca. 1.78 Å).[57] Despite substantial progress in uranyl chemistry, understanding the electronic structure in “reverse uranyl” remains limited. It exhibits a square planer $[U^{VI}O_4]^{2-}$ configuration with four short U═O bond distances (ca. 1.90 Å) and two elongated axial U-L bonds (ca. 2.20 Å).[58-60] Only a few example have been reported in the solid-state likely due to the high nucleophilicity of its four oxo ligands results in the formation of bridging interactions that are stronger than the solvation energy. To overcome this challenge of isolating a soluble form, I pursued the synthesis of a mixed-chalcogenide "reverse uranyl" fragment, namely, $[U^{VI}O_2S_2]^{2-}$, to enhance its solubility. The reduced nucleophilicity of the sulfido ligands weaken intermolecular interactions, thereby facilitating solubility and characterization. In this regard, Kim and co-workers reported the reaction of $[PPN][Fe(StBu)_3(NO)]$ with 20 equiv of MMP (methyl-3-mercaptopropionate) at room temperature afford the isolation of a Fe bridging sulfide, $[PPN]_2[Fe_2S_2(MMP)_4]$, along with the generation of thioether MMP ($S(CH_2CH_2C(O)OMe)_2$) (Scheme 8.2).[61, 62]

Scheme 8.2. Synthesis of $[PPN]_2[Fe_2S_2(MMP)_4]$.

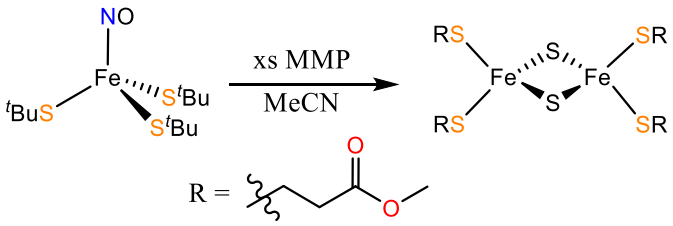

Inspired by this work, I hypothesize that ligating MMP to uranyl, followed by “deprotection” with non-nucleophilic base would afford the formation of $[Na]_2[UO_2S_2(OPCy_3)_2]$ upon elimination of methyl methacrylate (Scheme 8.3). Herein, I

describe the synthesis, characterization, and reactivity of uranyl MMP complexes, namely, $[UO_2(MMP)_2(OPPh_3)_2]$ (**8.3**) and $[UO_2(MMP)_2(OPCy_3)_2]$ (**8.5**).

Scheme 8.3. Proposed deprotection of uranyl MMP, $[UO_2(MMP)_2(OPR_3)_2]$ (R = Ph, Cy).

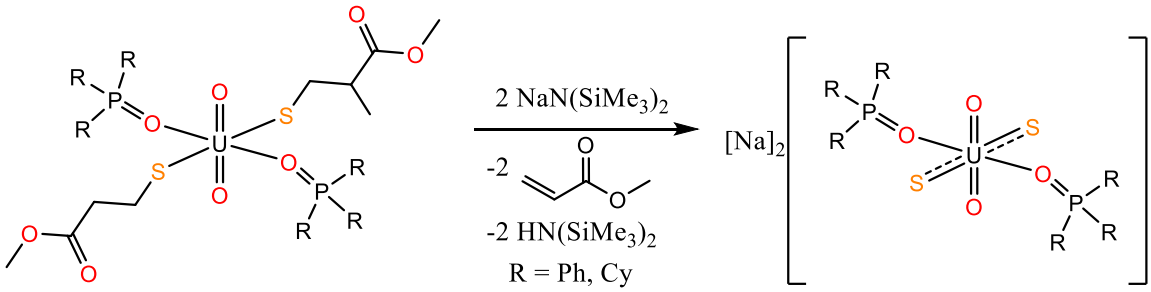

8.2 Results and Discussion

8.2.1 Synthesis and Characterization of Homoleptic Actinide dithiolate Complexes

Addition of cold (-25 °C) THF solution of 4 equiv of $[Li(TMEDA)]_2[1,2\text{-}S_2C_6H_4]$ to cold (-25 °C) THF solution of $ThCl_4(DME)_2$ results in immediate formation of pale yellow solution. Work-up of the reaction mixture, followed by crystallization from THF, affords $[Li(THF)_2]_4[Th(1,2\text{-}S_2C_6H_4)_4]$ (**8.1**), which can be isolated as colorless plates in 35 % (Scheme 8.4). The ^{1}H NMR spectra of **8.1** in benzene-d_6 reveals two distinct resonances at 7.62 ppm and 6.85 ppm, assignable to *ortho* and *meta* positions of the $(1,2\text{-}S_2C_6H_4)^{2-}$ fragment, which are present in a 1:1 ratio (Figure 8.8). Additionally, the $^{13}C\{^1H\}$ NMR spectra of **8.1** in benzene-d_6 reveals three resonances at 151.16 ppm, 133.17 ppm, and 122.08 ppm, attributed to *ipso*, *ortho*, and *meta* of the $(1,2\text{-}S_2C_6H_4)^{2-}$ fragment (Figure 8.9). Finally, the $^7Li\{^1H\}$ NMR spectra displays a single resonance at 1.57 ppm (Figure 8.10). Complex **8.1** is soluble in soluble in Et_2O, THF, and benzene, but is insoluble in hexanes.

Scheme 8.4. $[Li(THF)_2]_4[Th(1,2\text{-}S_2C_6H_4)_4]$ (**8.1**).

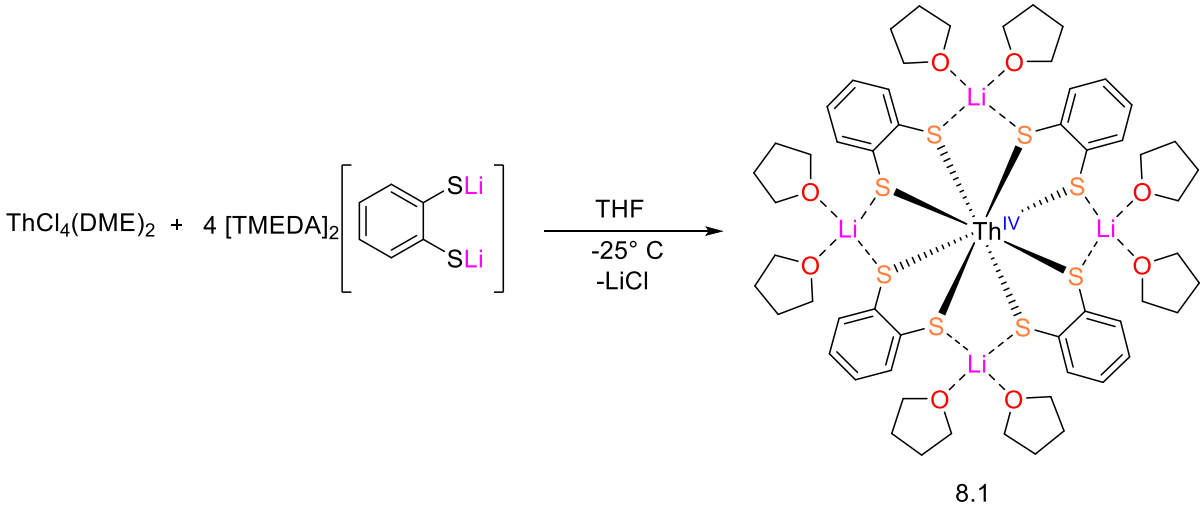

8.1

Similarly, slow addition of cold (-25 °C) THF solution of 4 equiv of $[Li(TMEDA)]_2[1,2\text{-}S_2C_6H_4]$ to cold (-25 °C) Et_2O suspension of UCl_4 results in immediate formation of dark yellow solution. Work-up of the reaction mixture, followed by crystallization from Et_2O, affords $[Li(TMEDA)]_4[U(1,2\text{-}S_2C_6H_4)_4]$ (**8.2**), which can be isolated as yellow plates in 62 % (Scheme 8.5). Interestingly, the ^1H NMR spectra of **8.2** in benzene-d_6 reveals four distinct resonances at 18.09 ppm, 12.10 ppm, 7.67 ppm, and 1.47 ppm, which are assignable to the $(1,2\text{-}S_2C_6H_4)^{2-}$ fragment (Figure 8.11). These resonances are present in a 1:1:1:1 ratio, consistent the S_4 symmetry observed in the solid-state structure. Additionally, the $^7Li\{^1H\}$ NMR spectra displays a single resonance at -5.26 ppm (Figure 8.12). Complex **8.2** is soluble in soluble in Et_2O, THF, and benzene, but is insoluble in hexanes.

Scheme 8.5. Synthesis of $[Li(TMEDA)]_4[U(1,2\text{-}S_2C_6H_4)_4]$ (**8.2**).

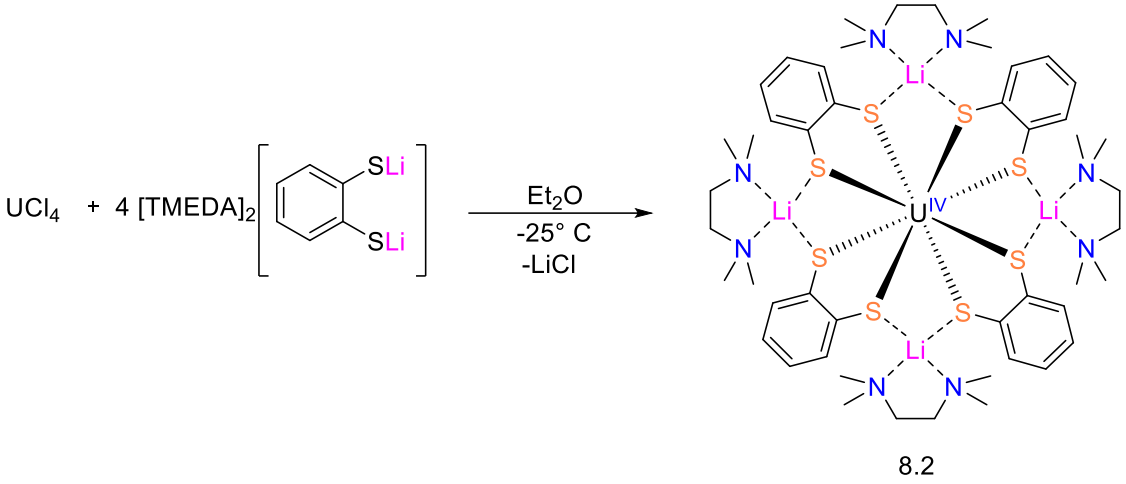

8.2

Complex **8.1** crystallizes in the tetragonal space group $P\bar{4}2_1c$ as the THF solvate, **8.1**·THF (Figure 8.1). Whereas, complex **8.2** crystallizes in the orthorhombic space group $P2_12_12$ (Figure 8.1). According to the continuous shape measure,[63] both **8.1** and **8.2** feature 8-coordinate An centers that are best described as a D_{2d}-symmetric triangular dodecahedra. The eight-coordinate actinide center in both **8.1** and **8.2** features eight Th-S σ-bonds atoms of four $(1,2\text{-}S_2C_6H_4)^{2-}$ ligands. Additionally, each Li^+ cation in **8.1** is coordinated by two sulfur atoms of adjacent $C_6H_4S_2^{2-}$ ligands and two oxygen atoms of THF solvates. Similarly, **8.2** features Li^+ cations coordinated by two sulfur atoms of adjacent $(1,2\text{-}S_2C_6H_4)^{2-}$ ligands and two nitrogen atoms of TMEDA. The average Th-S distance in **8.1** is 2.889 Å (range = 2.887(3) – 2.890(3) Å), which is longer than that observed in other Th-S single bonds likely due to the high charge on the Th center.[64, 65] For examples the Th-S bond distance in $[Cp^*_2Th(SPh)_2]$ (2.7488(11) and 2.7451(10) Å),[66] $[Th(SCPh_3)(NR_2)_3]$ (R = $SiMe_3$) (2.718(3) Å).[67] The average U-S distance in **8.2** is 2.806 Å (range = 2.783(2) – 2.822(2) Å), which is shorter than that found in **8.1** consistent with the smaller ionic radius of the U(IV) ion.[68] The average U-S

bond distance in **8.1** is similar to those found in previous reported U-S bond lengths for U(IV) dithiolene complexes.[69] For instance, the average U-S bond distance in a tetrakis(dithiolene) uranium complex, $[Na_4(THF)_8U(dddt)_4]$ (dddt = 5,6-dihydro-1,4-dithiine-2,3-dithiolate) is 2.83(3) Å with range of 2.790(2) to 2.865(2) Å.[34] However, the average U-S bond distance is longer than those found in $[U(SPh)_4(Py)_3]$ (range = 2.717(2) – 2.764(2) Å).[35] The average Th-S-C angle in **8.1** is 108.4° and in **8.2** is 110.5°, which are both consistent with previous reported U(IV) dithiolene complexes. For examples the average Th-S-C angle in $[Na_4(THF)_8U(dddt)_4]$ is 110.1°.[34] Additionally, the average Li-S bond distances found in in **8.1** is 2.48 Å and in **8.2** is 2.47 Å, which are consistent with previously reported for similar Li-S bonds. For example, the average Li-S bond distances in $[Li_2(THF)_4\{SCH(SiMe_3)_2\}_2]$ is 2.45 Å,[70] $[Li(THF)_3S\text{-}2,4,6\text{-}^tBu_3C_6H_2]$ is 2.45 Å,[71] and $[Li(DME)]_4[U(SCH_2CH_2S)_4]$ is 2.42 Å.[72]

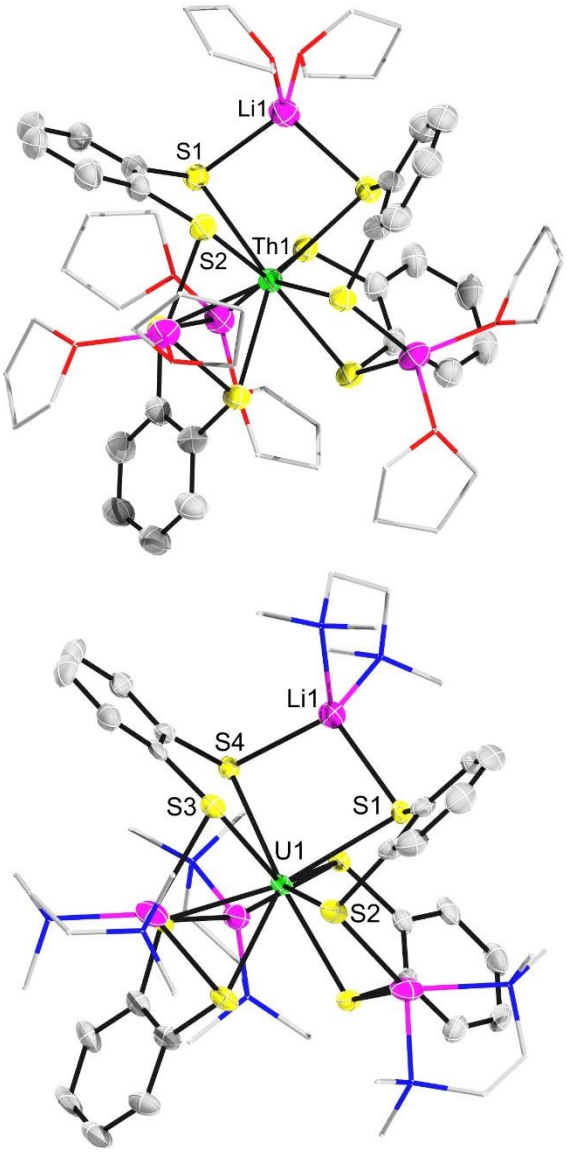

Figure 8.1. Solid-state molecular structure of **8.1** shown with 50% probability ellipsoids (top). Solid-state molecular structure of **8.2** shown with 50% probability ellipsoids (bottom). The THF and TMEDA ligands are shown in wireframe style and hydrogen atoms are omitted for clarity.

In pursuing the isolation of a homoleptic U(V) dithiolate complex in an octahedral geometry, I hypothesized that it could be facilitated through $1e^-$ oxidation. However, reaction

of **8.2** with 0.5 equiv of I_2 or 1 equiv of $AgPF_6$ in THF show no reaction based on analysis of ^1H NMR spectra. Interestingly, a slow addition of cold (-25 °C) dichloromethane solution of 1 equiv of $[(4\text{-}BrC_6H_4)_3N][SbCl_6]$ to a cold (-25 °C) yellow solution of **8.2** results in immediate formation of red solution, concomitant with the deposition of dark blue precipitates. However, workup of the reaction, followed by crystallization from DCM in the presence of 2,2,2-cryptand, affords [Li(2,2,2-cryptand)][Sb((1,2-$(S_2)C_6H_4$)$_3$], which can be isolated as red plates and formulation confirmed by X-ray crystallography (Scheme 8.6).[46] Thus, I hypothesize that the reaction of $[(4\text{-}BrC_6H_4)_3N][SbCl_6]$ with **8.2** results in ligand scrambling, which render this oxidant unsuitable for oxidation. Going forward, further examination of the redox properties and reactivity of complex **8.2** is required to understand electrochemical properties.

Scheme 8.6. Oxidation of **8.2** with $[(4\text{-}BrC_6H_4)_3N][SbCl_6]$.

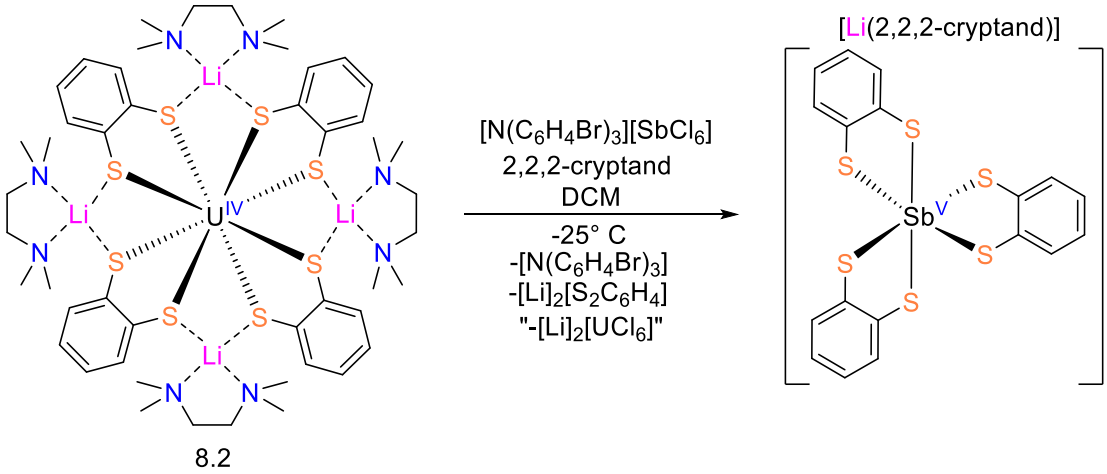

8.2.2 Synthesis and Characterization of Uranyl MMP Complexes

Additionally, in efforts to isolate a soluble mixed-chalcogenide "reverse uranyl" complex I explored the reactivity of methyl-3-mercaptopropionate with uranyl. Thus, addition

of cold (-25 °C) THF solution of 2 equiv of KMMP (MMP = methyl-3-mercaptopropionate) to cold (-25 °C) solution of $[UO_2Cl_2(OPPh_3)_2]$[73] results in immediate formation of dark red solution. After 1 h stirring at room temperature, workup of the reaction mixture, followed by crystallization from THF, affords $[UO_2(MMP)_2(OPPh_3)_2]$ (**8.3**), which can be isolated as red plates in 30% yield (Scheme 8.7). However, the $^{31}P\{^1H\}$ NMR spectra of the isolated red plates of **8.3** in benzene-d_6 reveals two resonances at 46.58 ppm and 45.78 ppm, indicating the presence of a mixture of $OPPh_3$ containing uranyl complexes in solution (Figure 8.13). Evidently, the ^1H NMR spectra of **8.3** in benzene-d_6 shows two different MMP environments (Figure 8.14). Attempts to isolate analytical pure material of **8.3** were unsuccessful. Additionally, in multiple instances the $^{31}P\{^1H\}$ NMR spectra of reveals formation of free $OPPh_3$, which also hindered my ability to isolate **8.3**. On one occasion, a crude red benzene-d_6 solution of **8.3** upon standing at room temperature for 2d resulted in the deposition of a few orange plates, namely, $[UO_2(SH)(MMP)(OPPh_3)_2]$ (**8.4**). The $^{31}P\{^1H\}$ NMR spectra of **8.4** in THF-d_8 shows a resonance at 45.83 ppm that is tentatively assigned to **8.4** and a resonance at 23.58 ppm assigned to free $OPPh_3$ ligand (Figure 8.15). Yet, attempts to isolate analytical pure material of **8.4** were unsuccessful and yield was not recorded. I hypothesized that **8.4** forms of as a result of 1,3 proton shift and loss of methyl acrylate upon standing in solution at room temperature.

Scheme 8.7. Synthesis of $[UO_2(MMP)_2(OPPh_3)_2]$(8.3) and $[UO_2(SH)(MMP)(OPPh_3)_2]$ (**8.4**).

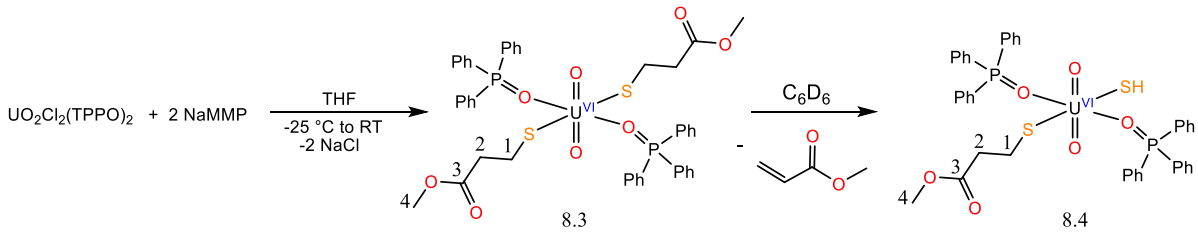

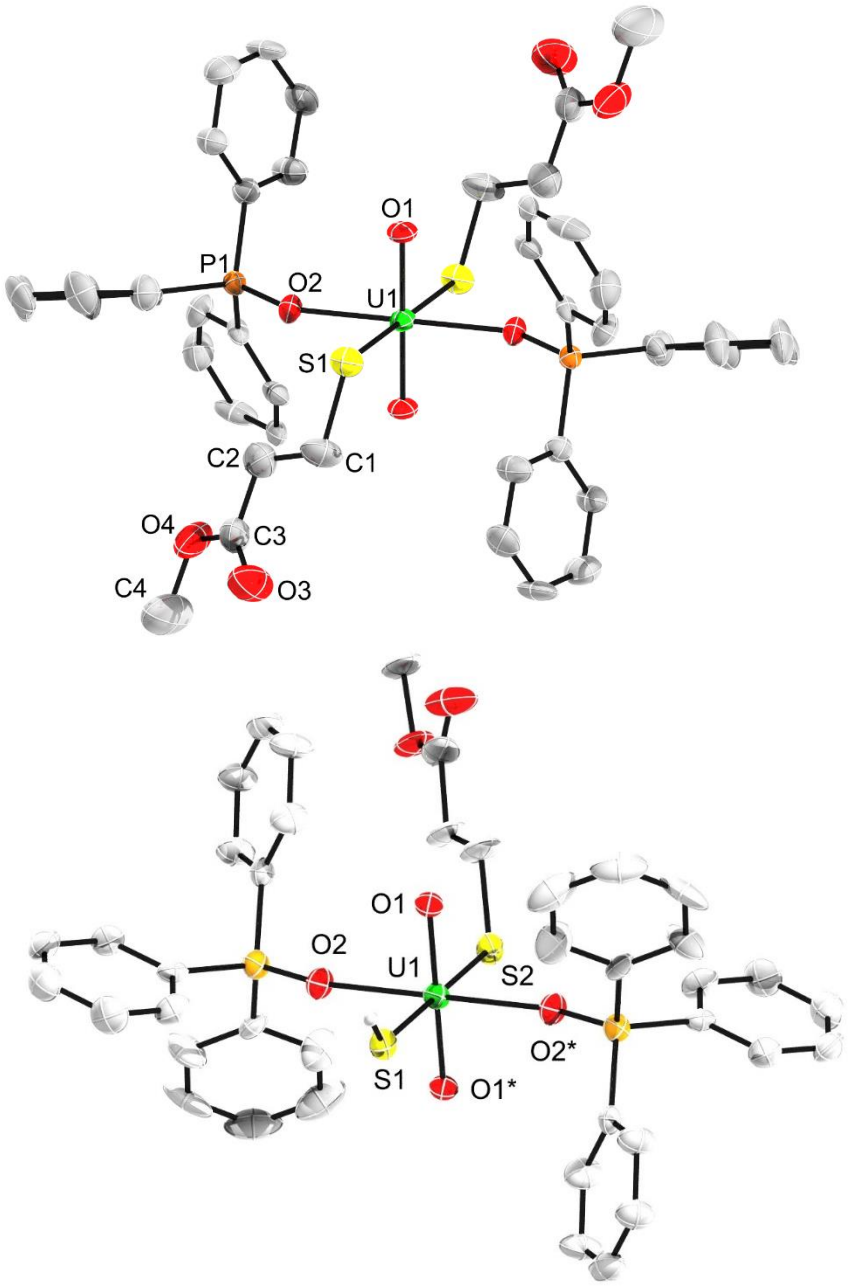

Figure 8.2. Solid-state molecular structure of **8.3** shown with 50% probability ellipsoids (top). Solid-state molecular structure of **8.4** shown with 50% probability ellipsoids (bottom). Hydrogen atoms are omitted for clarity.

Complex **8.3** crystallizes in the monoclinic space group $P2_1/n$. Whereas, complex **8.4** crystallizes in the triclinic space group $P\bar{1}$ (Figure 8.2). The solid-state molecular structure of

8.3 reveal octahedral uranium centers coordinated by two oxygen atoms of the uranyl fragment, two oxygen atoms of the $OPPh_3$ co-ligands, and two sulfur atoms of the MMP ligands. The solid-state molecular structure of **8.4** reveals similar geometric around the uranium center, however, contains one MMP ligand and hydrosulfido ligand. The linear O_{yl}-U-O_{yl} angles observed in **8.3** (180.0°) and **8.4** (180.0°) are typical of the uranyl fragment.[53, 54] The U-O_{yl} in **8.3** (1.787(6) Å) and **8.4** (1.786(5) Å) are similar to those previous reported for uranyl U-O_{yl} bond distances. (range = 1.76-1.79 Å).[7, 74, 75] The U-O_{OPPh3} distance in **8.3** (2.303(6) Å) and **8.4** (2.325(5) Å), are consistent with other complexes of the type $[UO_2X_2(OPPh_3)_n]$ complexes that range from 2.297(2) Å to 2.334(16) Å.[76-80] Additionally, the U-S_{MMP} bond distances in **8.3** is 2.689(3) Å and in **8.4** is 2.68(6) Å, whereas the U-S_{SH} bond distance in **8.4** is 2.67(6) Å. The U-S bond distance in **8.3** and **8.4** are comparable to those found in a uranyl thiolate complex, $[UO_2(S\text{-}2,6\text{-}Cl_2C_6H_3)_2L_2]$ (L = *N*,*N*-diisobutylisopropylamide) (2.7143(7) Å and 2.7325(8) Å).[81] The U-S-C bond angles observed in both **8.3** (107.7(4)°) and **8.4** (109(3)°) are similar to those found in $[UO_2(S\text{-}2,6\text{-}Cl_2C_6H_3)_2L_2]$ (106.1(1)° 111.2(1)°).[81] The angles observed in both **8.3** and **8.4** around the sulfur atom are typical of metal thiolate complexes.[82, 83] In contrast, larger angles are typically found in alkoxide complexes, reflect the difference in bonding between thiolate and alkoxide ligands.[84] Remarkably, isolation of **8.3** and **8.4** represent rare examples of crystallographically authenticated uranyl thiolates with only a handful previously reported.[81, 85-88]

I hypothesized using $OPCy_3$ (Cy = cyclohexyl) as a supporting co-ligand would further enhance the stability of the uranyl fragment due the stronger α donating charactreristic.[89] Thus, addition of cold (-25 °C) THF solution of 2 equiv of NaMMP to cold (-25 °C) solution of $[UO_2Cl_2(OPCy_3)_2]$ results in immediate formation of dark red solution. After 1 h stirring at

room temperature, workup of the reaction mixture, followed by crystallization from THF, affords $[UO_2(MMP)_2(OPCy_3)_2]$ (**8.5**), which can be isolated as red plates in 60 % yield (Scheme 8.8). The ^{1}H NMR spectrum of **8.5** in benzene-d_6 reveals three resonances at 6.28, 3.38, and 3.30 ppm, which are assignable to the C1, C4, and C2 carbon atoms of the MMP ligand (Figure 8.3). The C1, C2, and C4 resonances are present in a 2:2:3 ratio, respectively. Additionally, ^{1}H NMR spectrum of **8.5** features resonance at 2.17 ppm, 1.72 ppm, 1.54 ppm, and 1.17 ppm, assignable to the cyclohexyl substituents. The ^{13}C{^{1}H} NMR spectra of **8.5** in benzene-d_6 reveals resonances at 173.84, 50.85, 45.24, and 32.52 ppm attributed to C3, C1, C2, C4 carbon atoms of the MMP ligand, respectively (Figure 8.17). Additionally, ^{31}P{^{1}H} NMR spectra of **8.5** in benzene-d_6 displays a single resonance at 69.50 ppm, attributed to the $OPCy_3$ ligand (Figure 8.18).

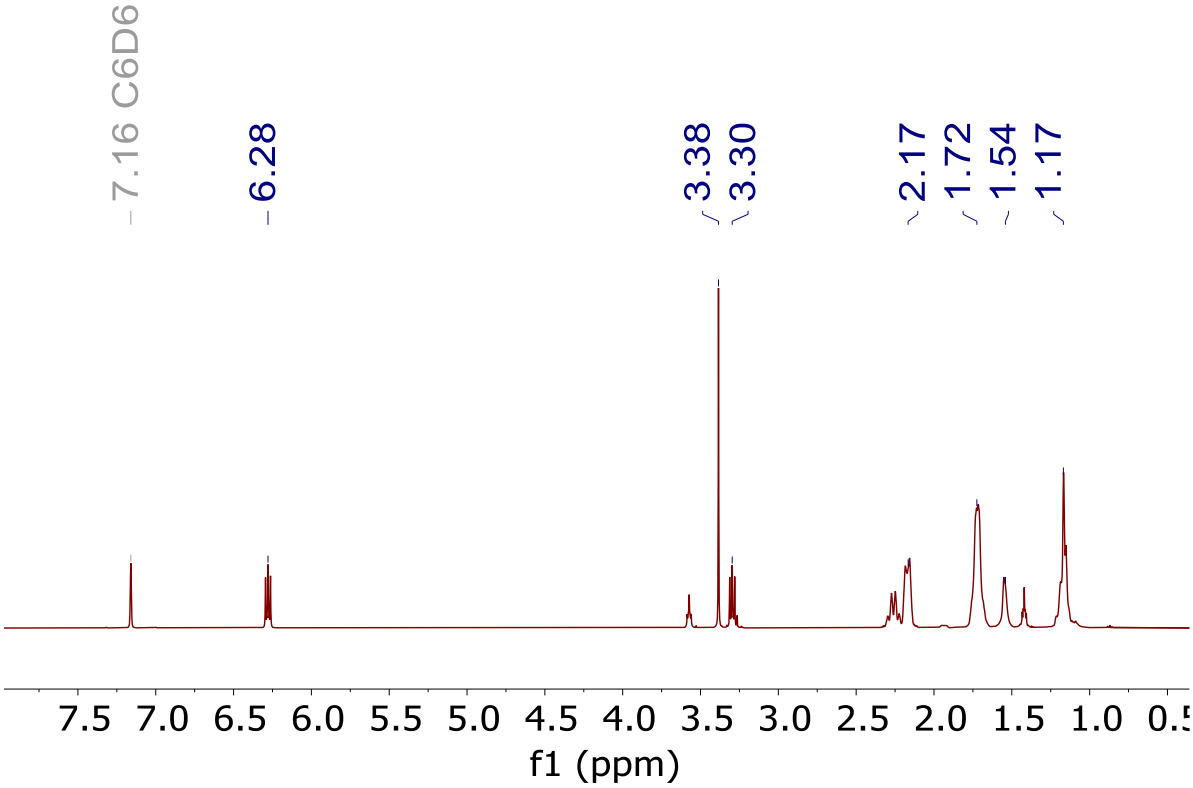

Figure 8.3. ^{1}H NMR spectrum of **8.5** in benzene-d_6 at room temperature.

Scheme 8.8. Synthesis of $[UO_2(MMP)_2(OPCy_3)_2]$ (**8.5**) and $[Na(OPCy_3)_4]_2[UO_2(MMP)_4]$ (**8.6**).

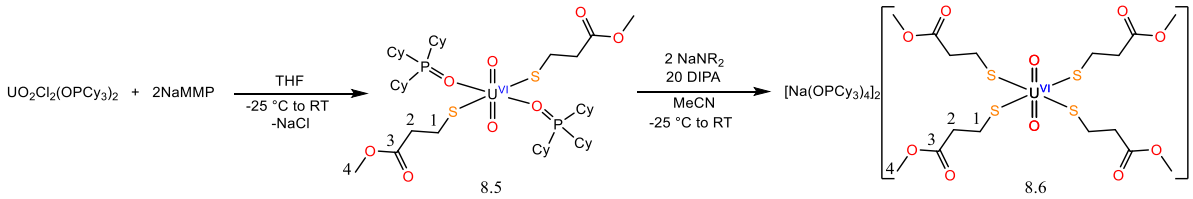

Interestingly, complex **8.5** displays better thermal sensitivity in solution than that observed in **8.3**. For example, thermolysis of a red toluene-d_8 solution of **8.5** in an NMR tube equipped with a J-Young valve, for 4 h at 110 °C reveals minimal decomposition. For example, the ^{31}P NMR spectrum of this toluene-d_8 solution features a resonance 74.16 ppm

corresponding to the $OPCy_3$ ligand in **8.5** and the appearance of a new resonance at 49.85 ppm, assignable to free $OPCy_3$ ligand (Figure 8.19). These resonances are present in a 4.3:1 ratio, respectively. With the isolation of **8.5**, I hypothesized that deprotonation of the C_β carbon on the MMP ligand using an exogenous non-nucleophilic base would result in extrusion of methyl acrylate and formation of $[Na]_2[UO_2S_2(OPCy_3)_2]$. Thus, I investigated the reactivity of **8.5** with a variety of strong bases. Efforts to deprotect **8.5** using 1 equiv of $NaNR_2$ (R = $SiMe_3$) in THF the presence of 2,2,2-cryptand yielded orange reaction mixtures and substantial amounts of insoluble dark brown solids. Presumably the presence of dark brown solids indicated the reduction of $[U^{VI}O_2]^{2+}$ to afford $U^{IV}O_2$. Interestingly, a crude ^1H NMR spectrum of reaction mixture revealed resonances at 3.66, 3.51, and 2.54 ppm, which are assignable to the formation thioether MMP ($S(CH_2CH_2C(O)OMe)_2$) (Figure 8.22 and Scheme 8.9).[90] I hypothesized upon addition of $NaNR_2$ results in extrusion of methyl acrylate, which further reacts with MMP to form undesired thioether MMP. Additionally, the crude ^{31}P NMR spectrum features a single resonance at 45.38 ppm corresponding to the presence of free $OPCy_3$ ligand (Figure 8.23). Similarly, reaction of **8.5** with 2 equiv of $NaNR_2$ (R = $SiMe_3$) in THF the presence of 2,2,2-cryptand yield identical outcomes. Further attempts using various bases, namely, $NaNH_2$ and ^{n}BuLi, also lead to formation of thioether MMP and free $OPCy_3$ ligand.

Scheme 8.9. Deprotection of **8.5.**

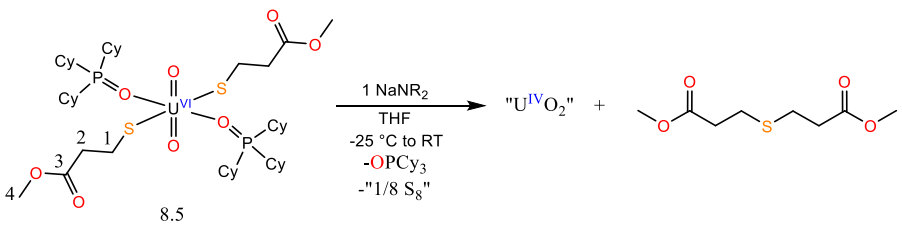

With this in mind, I postulated that the presence of nucleophilic DIPA (DIPA = diisopropylamine) could potentially react with the electrophilic methyl acrylate to afford methyl-(3-diisopropylamino)-propionate in attempts to mitigate undesired side reactions.[91] On one instance, addition of cold (-25 °C) acetonitrile solution of 2 equiv of $NaNR_2$ (R = $SiMe_3$) to a cold (-25 °C) solution of **8.5** in acetonitrile (2 mL) in the presence of 20 equiv DIPA (76 µL, 0.54 mmol) results in immediate formation of dark red solution.. After 1 h stirring at room temperature, workup of the reaction mixture, followed by crystallization from acetonitrile, affords $[Na(OPCy_3)_4]_2[UO_2(MMP)_4]$ (**8.6**), however yield was not recorded (Scheme 8.8). The crude ^{31}P NMR spectrum of **8.6** in acetonitrile-d_3 features a single resonance at 48.55 ppm (Figure 8.20). Additionally, the crude ^{1}H NMR spectrum of **8.6** in acetonitrile-d_3 features three distinct resonances at 5.02 ppm, 3.58 ppm, and 2.81 ppm, which are assignable to the C1, C4, and C2 MMP ligand, respectively (Figure 8.21). These resonances are present in a 2:3:2 ratio, respectively. I hypothesized that formation of **8.6** occurs through ligand scrambling of the MMP and Cy_3PO ligands around the uranyl fragment. Specifically, I propose that $NaNR_2$ (R = $SiMe_3$) reacts with **8.5** to form $[UO_2(NR_2)_2]$ type complex as a byproduct, that induces the MMP and $OPPh_3$ ligands to scramble due to steric effects, leading maximum yield of 50%.

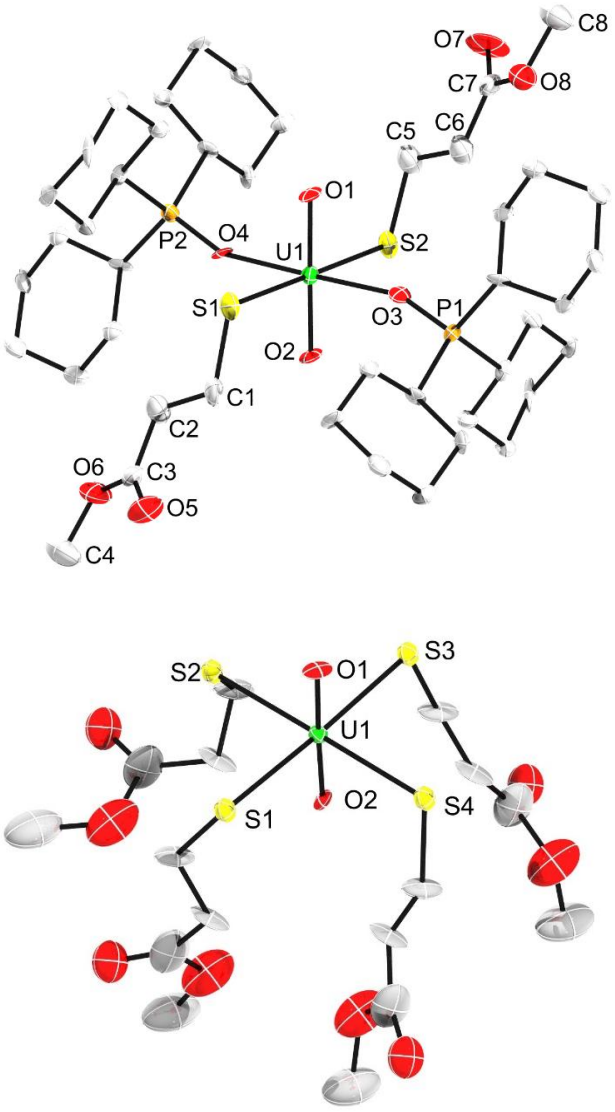

Figure 8.4. Solid-state molecular structure of **8.5** shown with 50% probability ellipsoids (Top). Solid-state molecular structure of **8.6** shown with 50% probability ellipsoids (Bottom). Hydrogen atoms and two $[Na(OPCy_3)_4]^+$ counterions are omitted for clarity.

Complex **8.5** crystallizes in the orthorhombic space group $P2_12_12_1$. Whereas, complex **8.6** crystallizes in the triclinic space group $P\bar{1}$ (Figure 8.4). The solid-state molecular structure of **8.5** reveals an octahedral uranium center coordinated by two oxygen atoms of the uranyl

fragment, two sulfur atoms of the MMP ligands, and two oxygen atoms of the $OPCy_3$ ligands. The solid-state molecular structure of **8.6** reveals an octahedral uranium center that is formed by the two oxygen atoms of the uranyl fragment and four sulfur atoms of the MMP ligands. Additionally, complex **8.6** is a discrete cation-anion pair that features two $[Na(OPCy_3)_4]^+$ counterions in the asymmetric unit cell. The O_{yl}- U-O_{yl} angle in **8.5** is 179.2° and in **8.6** is 177.9°, and is similar to those observed in complex **8.3** and **8.4**, which is also typical of the uranyl fragment.[53, 54] The average U-O_{yl} in **8.5** is 1.783 Å and in **8.6** is 1.826 Å, similar to the uranyl fragment in **8.3** and **8.4**. Additionally, the U-O_{OPCy3} distances in **8.3** are 2.295(12) Å and 2.321(12) Å, are consistent with those observed **8.3** and **8.4**. The U-S bond lengths in **8.5** are 2.706(4) Å and 2.715(5), which are similar to those found in uranyl thiolate complexes.[81] Similarly, the average U-S bond lengths in **8.6** are 2.766 Å with a range of 2.763(6) Å to 2.777(6) Å. Finally, the average U-S-C angles found in **8.5** is 106.2° and in **8.6** is 103.7°, which comparable to those found in **8.3** and **8.4**.

8.2.3 Synthesis and Characterization of Uranyl Py_5Me_2 Complexes

In efforts to synthesize a *cis*-uranyl complex, I explored the reaction of uranyl towards a pentapyridine ligand, 2,6-bis(1,1-bis(2-pyridyl)ethyl)pyridine (Py_5Me_2). The Py_5Me_2 was provided and synthesized in collaboration with Prof. Lena Daumann at Ludwig Maximillian University of Munich. Thus, addition of dichloromethane solution of 0.5 equiv of Py_5Me_2 to a DCM solution of $[UO_2(OTf)_2(THF)_3]$ results in immediate formation of pale-yellow solution. Workup of the reaction mixture, followed by crystallization from DCM, affords $[\{UO_2(OTf)_2(THF)\}_2\{Py_5Me_2\}]$ (**8.7**), which can be isolated as pale-yellow plates in a 60% yield (Scheme 8.10). Complex **8.7** was characterized via X-ray crystallography, however NMR and UV-vis spectra were not recorded. Complex **8.7** crystallizes in the monoclinic space

group $P2_1/c$ as the DCM solvate, **8.7**·2DCM (Figure 8.5). The O-U-O angles in **8.7** are 176.0(4)° and 176.6(4)°, which are typical of the uranyl fragment.[53, 54] The average U-O_{yl} bond lengths in **8.7** is 1.75 Å (range = 1.725(9) – 1.778(11) Å) consistent with typical uranyl U-O_{yl} distances.[53, 54] The coordination of Py_5Me_2 to the uranyl fragment does not result in any significant perturbation of the O-U-O angle likely due to its ability to coordinate two uranyl moieties. I hypothesize that achieving the desired isolation of a *cis*-uranyl complex requires a more rigid chelator.

Scheme 8.10. Synthesis of [{$UO_2(OTf)_2(THF)$}$_2${Py_5Me_2}] (**8.7**).

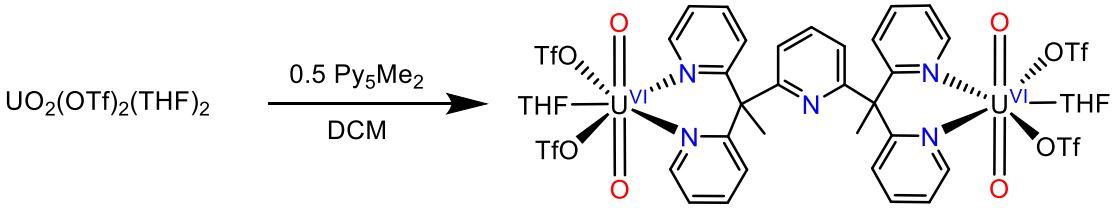

8.7

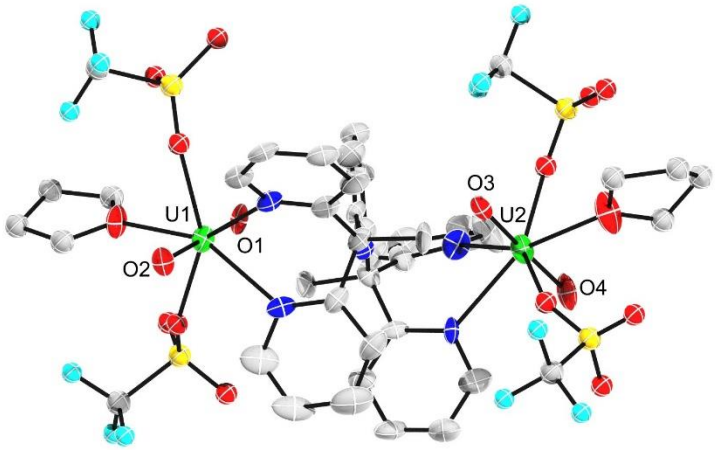

Figure 8.5. Solid-state molecular structure of **8.7** shown with 50% probability ellipsoids. Hydrogen atoms are omitted for clarity.

8.3 Summary

In summary, I have prepared and characterized two homoleptic actinide dithiolato complexes, namely, $[Li(THF)_2]_4[Th(S_2C_6H_4)_4]$ and $[Li(TMEDA)]_4[U(S_2C_6H_4)_4]$, with their formulation confirmed by X-ray crystallography. Remarkably, the isolation of these complexes represents the first examples of 1,2- benzenedithiolate actinide complexes. Efforts to access an O_h-symmetric U(V) complex remained inaccessible despite using various oxidants, namely, I_2 and $AgPF_6$. The difficulty likely arises due to the limited donating ability of the $S_2C_6H_4$ ligand, thereby requiring the use of a very strong oxidant. However, the use of $[(4\text{-}BrC_6H_4)_3N][SbCl_6]$ as a strong oxidant resulted in unexpected ligand scrambling. Moving forward, a thorough investigation including electrochemical analysis of complex **8.2** is required to understand its redox properties, crucial for to accessing an O_h-symmetric U(V) complex the redox properties and reactivity. Additionally, I have prepared and characterized several rare uranyl thiolate complexes, $[UO_2(MMP)_2(OPPh_3)_2]$, $[UO_2(SH)(MMP)(OPPh_3)_2]$, $[UO_2(MMP)_2(OPCy_3)_2]$, and $[Na(OPCy_3)_4]_2[UO_2(MMP)_4]$. However, multiple attempts to make "reverse" uranyl prove unsuccessful likely due to the high reactivity of methyl acrylate resulting in unwanted side reactions. Going forward, exploring the use NaSH through salt metathesis could offer a promising avenue of investigation to overcome the synthetic challenges encountered in attempts to isolate a soluble mixed-chalcogenide "reverse uranyl" complex.

8.4 Experimental

8.4.1 General Procedures

All reactions and subsequent manipulations were performed under anaerobic and anhydrous conditions under an atmosphere of dinitrogen. Hexanes, diethyl ether (Et_2O), and toluene were dried using a Vacuum Atmospheres DRI-SOLV Solvent Purification system and stored over 3Å sieves for 24 h prior to use. Tetrahydrofuran (THF) was distilled over Na/benzophenone and stored over activated 3 Å molecular sieves for 24 h prior to use. Benzene-d_6 and thf-d_8 were dried over 3Å molecular sieves for 24 h prior to use. $[Li(TMEDA)_2][C_6H_4S_2]$,[92] UCl_4,[93] and $ThCl_4(DME)_2$[94] were synthesized according to the previously reported procedures. All other reagents were purchased from commercial suppliers and used as received.

^1H, $^{13}C\{^1H\}$, $^7Li\{^1H\}$, and $^{31}P\{^1H\}$ NMR spectra were recorded on an Agilent Technologies 400-MR DD2 400 MHz spectrometer or a Bruker AVANCE NEO 500 MHz spectrometer. ^1H and $^{13}C\{^1H\}$ NMR spectra were referenced to external tetramethylsilane (TMS) using the residual protio solvent peaks as internal standards. $^7Li\{^1H\}$ NMR spectra are referenced indirectly with the ^1H chemical shift of TMS at 0 ppm, according to IUPAC standard.[95, 96] IR spectra were recorded on a Nicolet 6700 FT-IR spectrometer. Elemental analyses were performed by the Microanalytical Laboratory at the University of California (Berkeley, CA).

Caution! *Depleted uranium (isotope ^{238}U) and naturally-abundant thorium are weak alpha emitters with a half-life of 4.47×10^9 years and 1.41×10^{10} years, respectively. Manipulations and reactions should be carried out in a fume hood or inert atmosphere glovebox in a laboratory equipped with α- and β-counting equipment.*

8.4.2 Synthesis of $[Li(TMEDA)]_2[1,2\text{-}S_2C_6H_4]$.

The synthesis of $[Li(TMEDA)]_2[1,2\text{-}S_2C_6H_4]$ was done according to the literature procedure with slight modifications.[92] A cold (–25 °C) solution of C_6H_5SH (o.5 mL, 4.9 mmol) in hexanes was added dropwise to a cold solution (–25 °C) of *n*-BuLi (4.31 mL, 0.011 mol, 2.5 M) and TMEDA (0.80 mL, 5.5 mmol) in hexanes. After 1d of stirring at room temperature, the pale yellow cloudy solution was cooled (–25 °C) and S_8 (157 mg, 4.9 mmol) was added as a yellow solid in small portions over the course of 5 min. After 2d of stirring at room temperature, the pale pink solid was collected on fritted glass filter and washed with cold hexanes (3 × 3 mL). The solid was isolated and dried *in vacuo* (930 mg, 49 %). ^{1}H NMR (500 MHz, 25 °C, THF-d_8): δ 7.25 (m, 8H, *o*-H)), 6.32 (m, 8H, *m*-H)), 2.30 (s, 16H, $(CH_3)_2NCH_2$), 2.15 (s, 48H, $(CH_3)_2NCH_2$). ^{7}Li{^{1}H} NMR (500 MHz, 25 °C, THF-d_8): δ 0.88 (s).

8.4.3 Synthesis of $[Li(THF)_2]_4[Th(C_6H_4S_2)_4]$ (8.1).

A cold (-25 °C) THF (2 mL) solution of $[Li(TMEDA)]_2[1,2\text{-}S_2C_6H_4]$ (76.8 mg, 0.20 mmol) was added dropwise to a cold (-25 °C), colorless stirring solution of $ThCl_4(DME)_2$ (27.5 mg, 0.05 mmol) in THF (2 mL). This resulted in an immediate color change to pale yellow. After 1 h of stirring, the reaction mixture was filtered through a Celite column (0.5 cm × 5 cm) supported on glass wool to afford a clear, pale-yellow filtrate and the volatiles were removed from the filtrate *in vacuo*. The pale-yellow solid was then extracted into THF (2 mL) and filtered through a Celite column (0.5 cm × 2 cm) supported on glass wool to afford a clear, pale-yellow filtrate. This pale-yellow solution was then layered with hexanes (5 mL). Storage of this vial at –25 ºC for 24 h resulted in the deposition of colorless plates, which were isolated by decanting the supernatant, rinsing the crystals with cold (-25 °C) pentane (2 mL),

and drying *in vacuo* (24.2 mg, 35 % yield). ^{1}H NMR (500 MHz, 25 °C, benzene-d_6): δ 7.62 (m, 8H, *o*-H), 6.85 (m, 8H, *m*-H), 3.61 (s, 32H, OCH_2CH$_2$), 1.38 (s, 32H, OCH$_2$CH_2). ^{13}C{^{1}H} NMR (500 MHz, 25 °C, benzene-d_6): δ 151.16 (*i*-C), 133.17 (*o*-C), 122.08 (*m*-C), 68.20 (O*C*H$_2$CH$_2$), 25.70 (OCH$_2$*C*H$_2$). ^{7}Li{^{1}H} NMR (500 MHz, 25 °C, benzene-d_6): δ 1.57 (s). An IR spectrum was not recorded.

8.4.4 Synthesis of [Li(TMEDA)]$_4$[U(C$_6$H$_4$S$_2$)$_4$] (8.2).

A cold (-25 °C) Et$_2$O (2 mL) solution of [Li(TMEDA)]$_2$[1,2-S$_2$C$_6$H$_4$] (403.0 mg, 1.04 mmol) was added dropwise to a cold (-25 °C), stirring suspension of UCl$_4$ (99.0 mg, 0.26 mmol) in Et2O (2 mL). This resulted in an immediate color change to dark yellow. After 1 h of stirring, the reaction mixture was filtered through a Celite column (0.5 cm × 5 cm) supported on glass wool to afford a clear, dark yellow filtrate and the volatiles were removed from the filtrate *in vacuo*. The dark yellow solid was then extracted into Et$_2$O (2 mL) and filtered through a Celite column (0.5 cm × 2 cm) supported on glass wool to afford a clear, dark yellow filtrate. This pale-yellow solution was then layered with hexanes (5 mL). Storage of this vial at –25 ºC for 24 h resulted in the deposition of colorless plates, which were isolated by decanting the supernatant, rinsing the crystals with cold (-25 °C) pentane (2 mL), and drying *in vacuo* (208 mg, 62 % yield). ^{1}H NMR (500 MHz, 25 °C, benzene-d_6): δ 18.09 (s, 4H, *o*-H), 12.10 (s, 4H, *o*-H), 7.67 (s, 4H, *m*-H), 2.11 (s, 16H, CH$_3$NCH_2), 1.47 (s, 4H, *m*-H), 0.37 (s, 48H, CH_3NCH$_2$), 1.38 (s, 32H, OCH$_2$CH_2). ^{7}Li{^{1}H} NMR (500 MHz, 25 °C, benzene-d_6): δ -5.26 (s). An IR spectrum was not recorded.

8.4.5 Synthesis of $[UO_2(MMP)_2(OPPh_3)_2]$ (8.3).

A cold (-25 °C) suspension of KMMP (55.7 mg, 0.35 mmol) in THF (1 mL) was added dropwise to a cold (-25 °C), stirring solution of $[UO_2Cl_2(OPPh_3)_2]$ (158 mg, 0.17 mmol) in THF (2 mL). This resulted in an immediate color change to dark red solution. After 10 min stirring, the reaction mixture was filtered through a Celite column (0.5 cm × 5 cm) supported on glass to afford a clear red filtrate. The volume of the filtrate was reduced to 2 mL *in vacuo*. Storage of this vial at –25 ºC for 24 h resulted in the deposition of red plates, which were isolated by decanting the supernatant, rinsing the crystals with cold (-25 °C) pentane (2 mL), and drying *in vacuo* (55.6 mg, 30 % yield). ^{31}P NMR (500 MHz, 25 °C, benzene-d_6): δ 46.58 (s), 45.78 (s). ^{1}H NMR (500 MHz, 25 °C, benzene-d_6): δ 8.05 (br s, 12H, *o*-C), 7.80 (br s,12H, *p*-C), 7.06 (br s, 12H, *m*-C), 7.02 (br s), 6.25 (t, MMP, CH_2), 6.16 (t, MMP, CH_2), 3.27 (s, MMP, OCH_3), 3.26 (s, MMP, OCH_3), 2.94 (t, MMP, CH_2), 2.92 (t, MMP, CH_2). ^{13}C NMR and IR spectra of **8.3** were not recorded.

8.4.6 Synthesis of $[UO_2(SH)(MMP)(OPPh_3)_2]$ (8.4).

A cold (-25 °C) suspension of KMMP (60.0 mg, 0.38 mmol) in THF (1 mL) was added dropwise to a cold (-25 °C), stirring solution of $[UO_2Cl_2(OPPh_3)_2]$ (171 mg, 0.19 mmol) in THF (2 mL). This resulted in an immediate color change to dark red solution. After 30 min, an aliquot of reaction mixture was extracted and volatiles were removed *in vacuo*, affording a dark red solid. Subsequent dissolution of red solid in benzene-d_6 (0.7 mL) upon standing at room temperature for 2d resulted in the deposition of a few orange plates. The orange plates were isolated by decanting the supernatant, rinsing the crystals with cold (-25 °C) pentane (2 mL), and drying *in vacuo*, however the yield was not recorded. ^{31}P NMR (500 MHz, 25 °C, THF-d_8): δ 45.83 (s), 23.58 (s). ^{1}H NMR (500 MHz, 25 °C, THF-d_8): δ 7.80 (br s, 12H, *o*-C),

7.54 (br s, 6H, *p*-C), 7.48 (br s, 12H, *m*-C), 3.26 (s, 3H, MMP, OCH_3), 2.70 (t, 2H, MMP, CH_2), 2.59 (t, 2H, MMP, CH_2).

8.4.7 Synthesis of $[UO_2(MMP)_2(OPCy_3)_2]$ (8.5).

A cold (-25 °C) suspension of NaMMP (107.3 mg, 0.75 mmol) in THF (1 mL) was added dropwise to a cold (-25 °C), stirring solution of $[UO_2Cl_2(OPCy_3)_2]$ (333.3 mg, 0.36 mmol) in THF (2 mL). This resulted in an immediate color change to dark red solution. After 1 h stirring, the reaction mixture was filtered through a Celite column (0.5 cm × 5 cm) supported on glass to afford a clear red filtrate. The volume of the filtrate was reduced to 2 mL *in vacuo* and layered with hexanes (5 mL). Storage of this vial at –25 ºC for 24 h resulted in the deposition of red plates, which were isolated by decanting the supernatant, rinsing the crystals with cold (-25 °C) pentane (2 mL), and drying *in vacuo* (236 mg, 60 % yield). ^{1}H NMR (500 MHz, 25 °C, benzene-d_6): δ 6.28 (t, 4H, CH_2), 3.38 (s, 6H, CH_3), 3.30 (t, 4H, CH_2), 2.17 (m, 4H), 1.72 (m, 8H), 1.54 (br s, 2H), 1.17 (m, 8H). ^{13}C NMR (500 MHz, 25 °C, benzene-d_6): δ 173.84 (*C*=O), 50.85 (MMP, *C*H$_2$), 45.24 (MMP, *C*H$_2$), 33.53 (Cy, *C*H) 31.52 (MMP, CH$_3$), 26.96 (Cy, *C*H$_2$), 26.33 (Cy, *C*H$_2$), 26.19 (Cy, *C*H$_2$). ^{31}P{^{1}H} NMR (500 MHz, 25 °C, benzene-d_6): δ 69.50 (s).

8.4.8 Synthesis of $[Na(OPCy_3)_4]_2[UO_2(MMP)_4]$ (8.6).

A cold (-25 °C) solution of $NaNR_2$ (R = $SiMe_3$) (10.0 mg, 0.054 mmol) in MeCN (1 mL) was added dropwise to a cold (-25 °C), stirring solution of $[UO_2(MMP)_2(OPCy_3)_2]$ (30.1 mg, 0.027 mmol) in MeCN (2 mL) in the presence of DIPA (DIPA = diisopropylamine) (76 µL, 0.54 mmol). This resulted in an immediate color change to red solution. After 1 h stirring, the reaction mixture was filtered through a Celite column (0.5 cm × 5 cm) supported on glass to

afford a clear red filtrate. The volume of the filtrate was reduced to 1 mL *in vacuo*. Storage of this vial at –25 ºC for 24 h resulted in the deposition of a few red plates, however the yield was not recorded. $^{31}P\{^{1}H\}$ NMR (500 MHz, 25 °C, benzene-d_6): δ 48.55 (s). ^{1}H NMR (500 MHz, 25 °C, benzene-d_6): δ 5.02 (t, 8H, MMP, CH_2), 3.38 (s, 12H, MMP, CH_3), 2.81 (t, 8H, MMP, CH_2), 1.92 -1.23 (Cy). The NMR spectra were obtained of crude sample of 8.6, however no NMR spectra were recorded for analytical pure material.

8.4.9 Synthesis of [{$UO_2(OTf)_2(THF)$}$_2${Py_5Me_2}] (8.7).

A solution of Py_5Me_2 (22 mg, 0.049 mmol) in DCM (1 mL) was added dropwise to a stirring solution of [$UO_2(OTf)_2(THF)_3$] (77.8 mg, 0.099 mmol) in DCM (2 mL). This resulted in an immediate color change to pale yellow solution. After 24 h stirring, the reaction mixture was filtered through a Celite column (0.5 cm × 5 cm) supported on glass to afford a clear pale-yellow filtrate. The volume of the filtrate was reduced to 1 mL *in vacuo* and was then layered with hexanes (3 mL). Storage of this vial at –25 ºC for 24 h resulted in the deposition of pale-yellow plates, which were isolated by decanting the supernatant and drying *in vacuo* (52 mg, 60 % yield). Complex **8.7** was characterized via X-ray crystallography, however NMR and UV-vis spectra were not recorded.

8.4.10 X-Ray Crystallography

Data for all complexes were collected on a Bruker KAPPA APEX II diffractometer equipped with an APEX II CCD detector using a TRIUMPH monochromator with a Mo Kα X-ray source (α = 0.71073 Å). The crystals were mounted on a cryoloop under Paratone-N oil, and all data were collected at 100(2) K using an Oxford nitrogen gas cryostream. Data were collected using ω scans with 0.5° frame widths. Frame exposures of 15 s were used for

8.1·0.5THF, **8.2**, **8.3**, **8.4**, **8.5, 8.6**. Frame exposure of 20 s was used for **8.7**. Data collection and cell parameter determinations were conducted using the SMART program.[97] Integration of the data frames and final cell parameter refinement were performed using SAINT software.[98] Absorption correction of the data was carried out using the multi-scan method SADABS.[99] Subsequent calculations were carried out using SHELXTL.[100] Structure determination was done using direct or Patterson methods and difference Fourier techniques. All hydrogen atom positions were idealized and rode on the atom of attachment. Structure solution and refinement were performed using SHELXTL.[100] Graphics, and creation of publication materials were performed using Diamond.[101]

Table 8.1. X-ray Crystallographic Data for Complexes **8.1**·THF, **8.2**, **8.3**.

	8.1·0.5THF	**8.2**	**8.3**
Formula	$C_{56}H_{80}O_8S_8Th$	$C_{48}H_{80}N_8S_8U$	$UO_8S_2P_2C_{44}H_{44}$
Crystal Habit, Color	Plate, Colorless	Plate, Yellow	Plate, Red
Crystal Size (mm)	0.2 × 0.2 × 0.1	0.2 × 0.2 × 0.1	0.2 × 0.15 × 0.1
MW (g/mol)	1369.78	1263.75	1064.92
crystal system	Tetragonal	Orthorhombic	monoclinic
space group	P -4 21 c	P 21 21 2	P 21/n
a (Å)	17.899(13)	15.2863(15)	9.4888(19)
b (Å)	17.899(13)	16.4301(16)	14.422(3)
c (Å)	11.011(8)	11.8419(11)	16.352(3)
α (°)	90.00	90.00	90
β (°)	90.00	90.00	98.89(2)
γ (°)	90.00	90.00	90
V ($Å^3$)	3528(6)	2974.2(5)	2210.8(8)
Z	8	2	2
T (K)	100(2)	100(2)	100(2)
λ (Å)	0.71073	0.71073	0.71073
GOF	0.927	1.087	
Density (calcd) (Mg/m^3)	2.046	1.442	1.486
Absorption coefficient (mm^{-1})	8.579	3.048	3.880
F_{000}	1960	1312	934
Total no Reflections	52722	15332	22516
Unique Reflections	3784	7447	4549
Final R indices*	R_1 = 0.0477, wR_2 = 0.1197	R_1 = 0.0436, wR_2 = 0.0568	R_1 = 0.0568, wR_2 = 0.25
Largest Diff. peak and hole ($e^- A^{-3}$)	2.498, -1.664	2.498, -1.664	2.704, -2.611

*For [I>2σ(I)]

Table 8.2. X-ray Crystallographic Data for Complexes **8.4, 8.5,** and **8.6**.

	8.4·$3C_6D_6$	**8.5**	**8.6**	**8.7**·2DCM
Formula	$UO_6S_2P_2C_{40}H_{38}$	$UO_8S_2P_2C_{44}H_{80}$	$UO_{18}S_4P_8Na_2C_{160}H_{292}$	$U_2O_{18}N_5F_{12}S_4C_{41}H_{41}$
Crystal Habit, Color	Plate, Orange	Plate, Red	Plate, Red	Plates, Yellow
Crystal Size (mm)	0.2 × 0.2 × 0.1	0.2 × 0.1 × 0.05	0.2 × 0.2× 0.1	0.2 × 0.1 × 0.05
MW (g/mol)	978.83	1263.75	3164.07	1654.05
crystal system	Triclinic	Orthorhombic	Triclinic	Monoclinic
space group	P -1	P 21 21 2	P -1	P 21/c
a (Å)	10.814(7)	9.0982(10)	18.406(2)	17.686(5)
b (Å)	10.916(7)	19.4973(19)	19.191(3)	17.686(5)
c (Å)	13.192(9)	26.859(3)	30.061(4)	18.456(5)
α (°)	68.795(12)	90.00	72.153(8)	90
β (°)	81.686(13)	90.00	74.797(7)	101.680(5)
γ (°)	84.073(12)	90.00	66.225(8)	90
V ($Å^3$)	1434.3(16)	4764.5(8)	9132(2)	5974(3)
Z	1	4	2	6
T (K)	100(2)	100(2)	100(2)	100(2)
λ (Å)	0.71073	0.71073	0.71073	0.71073
GOF	0.980	1.035	1.117	1.548
Density (calcd) (Mg/m^3)	1.495	1.535	1.132	2.462
Absorption coefficient (mm^{-1})	3.009	3.610	1.061	8.508
F_{000}	648	2248	3348	4080
Total no Reflections	11366	16732	65445	13370
Unique Reflections	4968	8339	30949	8609
Final R indices*	R_1 = 0.0591, wR_2 = 0.1047	R_1 = 0.0667, wR_2 = 0.0951	R_1 = 0.1087, wR_2 = 0.2504	R_1 = 0.0900, wR_2 = 0.2386
Largest Diff. peak and hole ($e^- A^{-3}$)	1.160, -1.633	1.477, -1.390	1.296, -3.100	7.975, -2.622

*For [I>2σ(I)]

8.5 Appendix

8.5.1 NMR Spectra

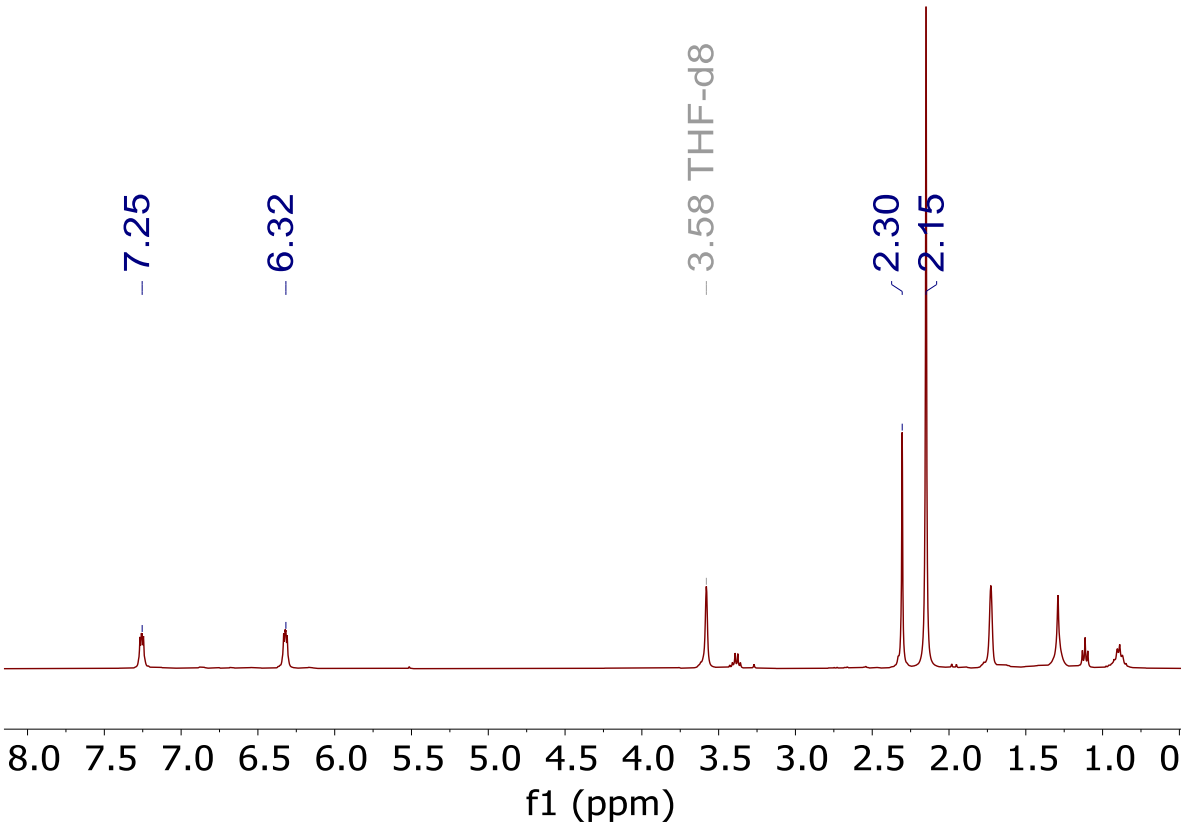

Figure 8.6. ^{1}H NMR spectrum of [Li(TMEDA)]$_2$[1,2-$S_2C_6H_4$] in THF-d_8 at room temperature.

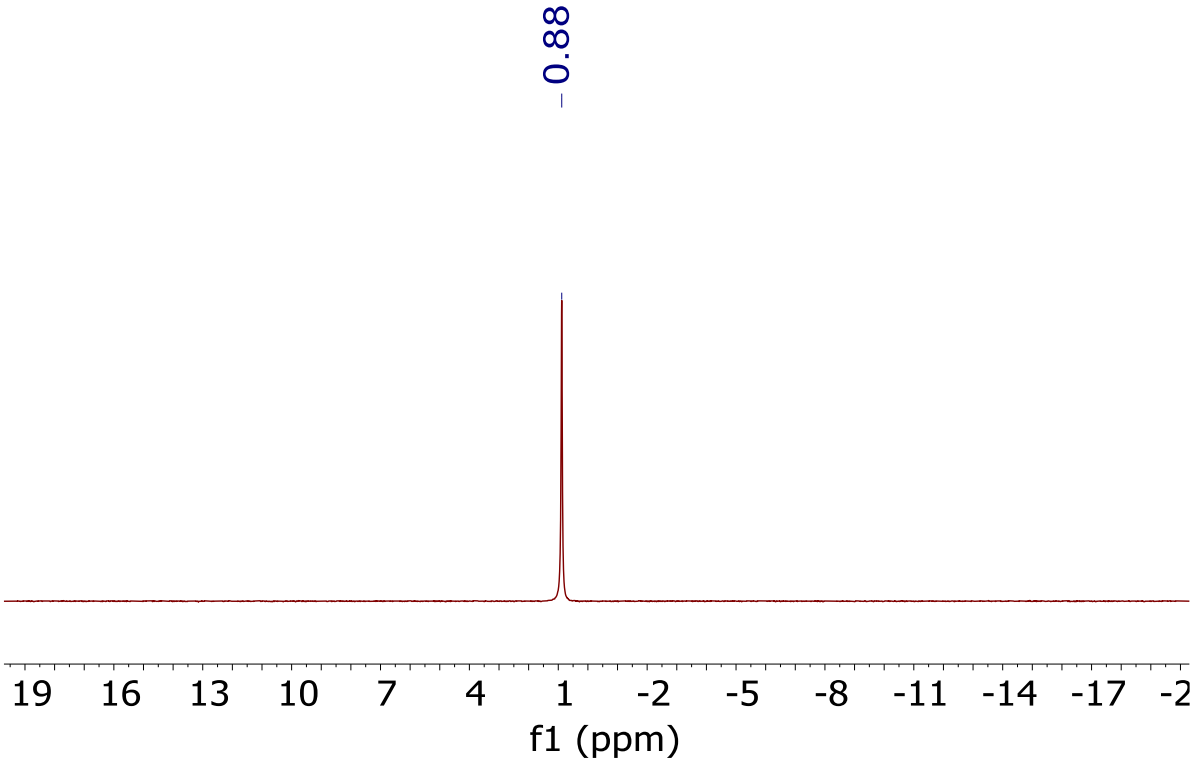

Figure 8.7. $^{7}Li\{^{1}H\}$ NMR spectrum of $[Li(TMEDA)]_2[1,2\text{-}S_2C_6H_4]$ in THF-d_8 at room temperature.

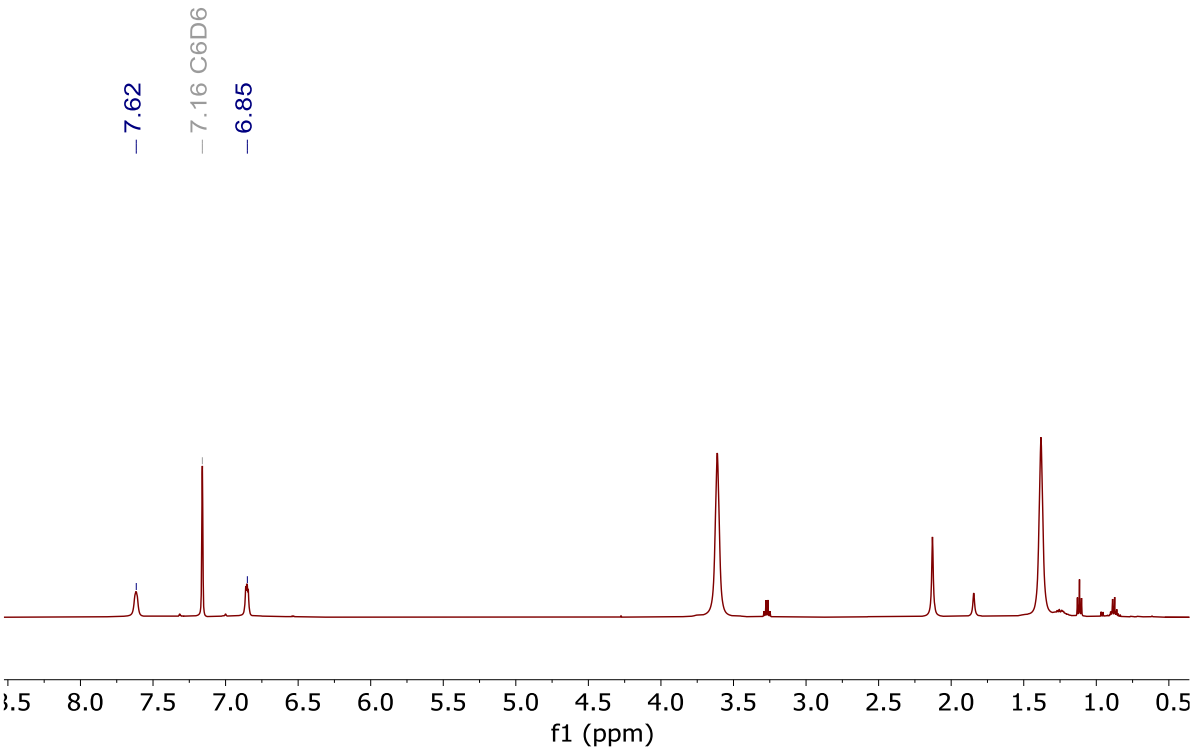

Figure 8.8. ^{1}H NMR spectrum of **8.1** in benzene-d_6 at room temperature.

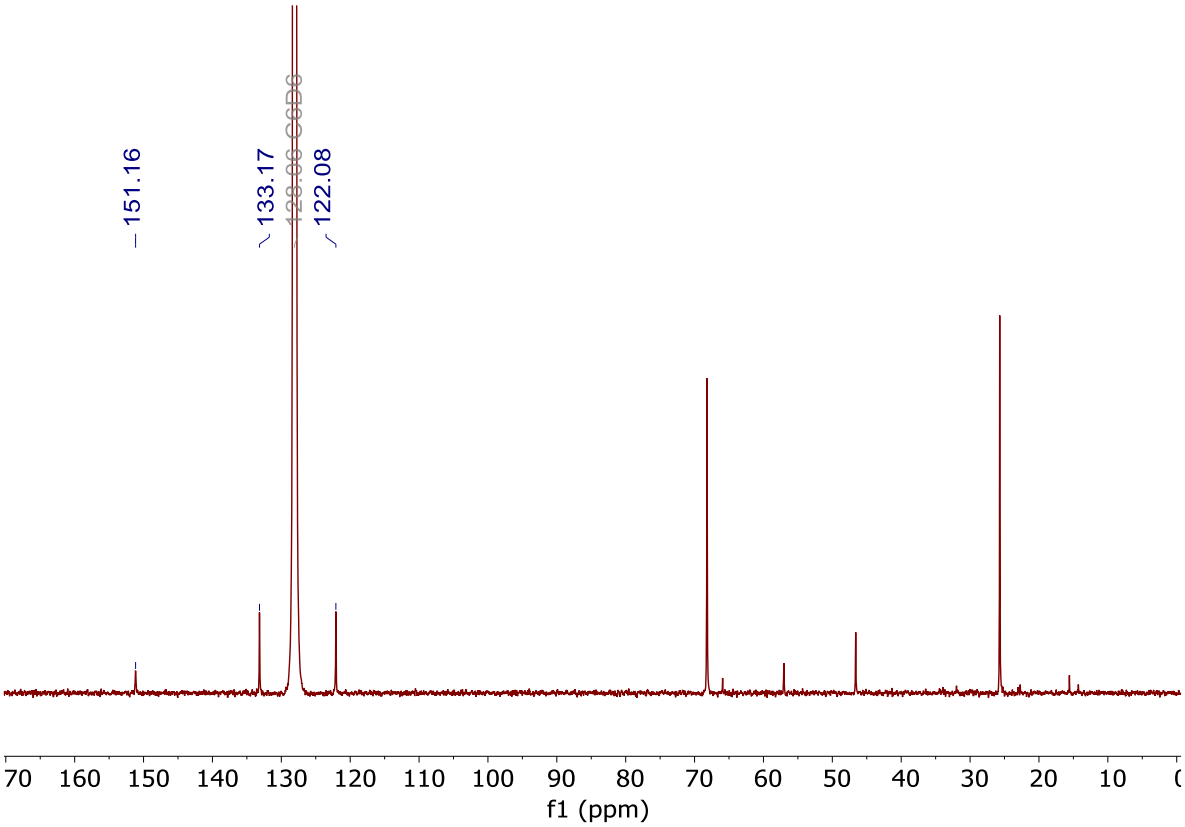

Figure 8.9. $^{13}C\{^{1}H\}$ NMR spectrum of **8.1** in benzene-d_6 at room temperature.

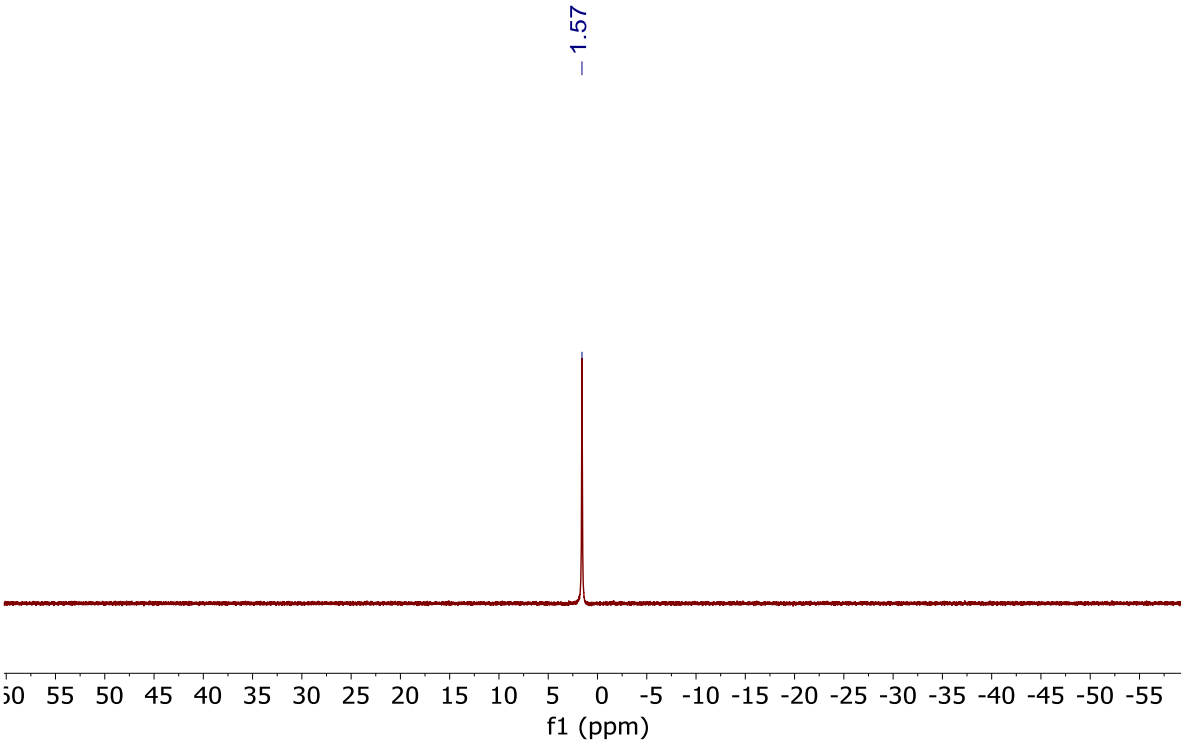

Figure 8.10. $^{7}Li\{^{1}H\}$ NMR spectrum of **8.1** in benzene-d_6 at room temperature.

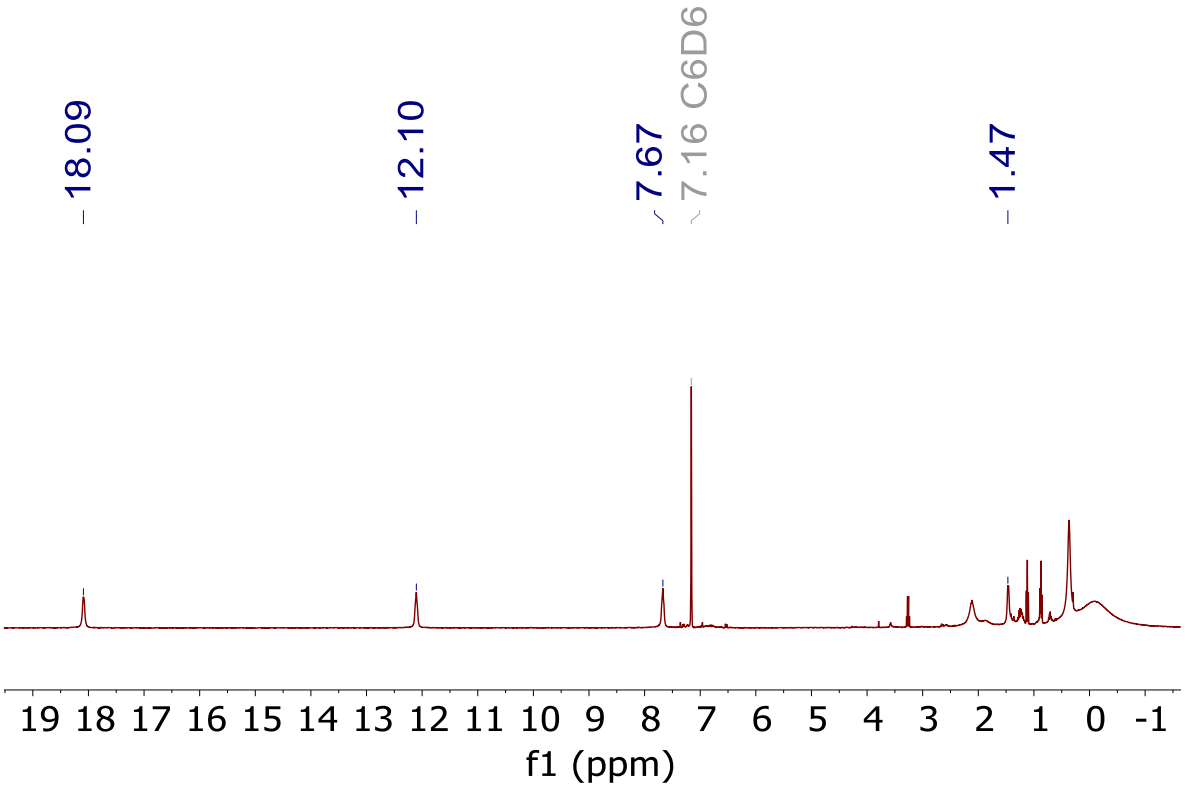

Figure 8.11. ^{1}H NMR spectrum of **8.2** in benzene-d_6 at room temperature.

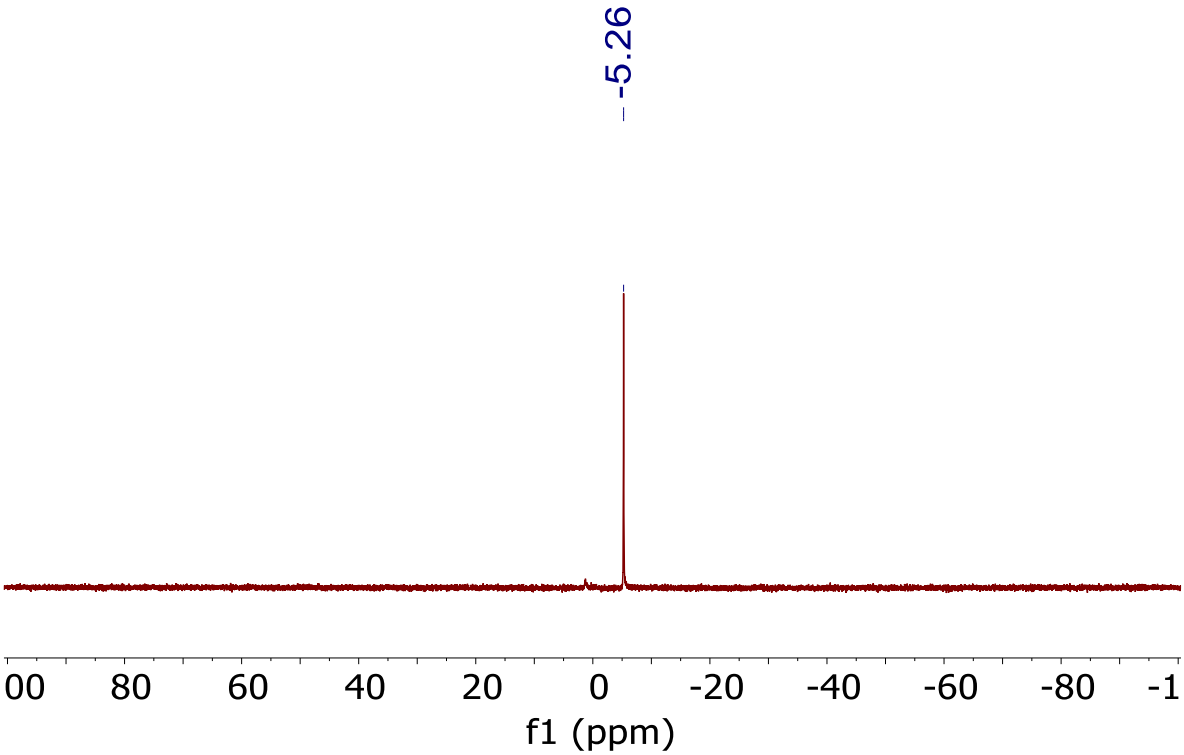

Figure 8.12. $^{7}Li\{^{1}H\}$ NMR spectrum of **8.2** in benzene-d_6 at room temperature.

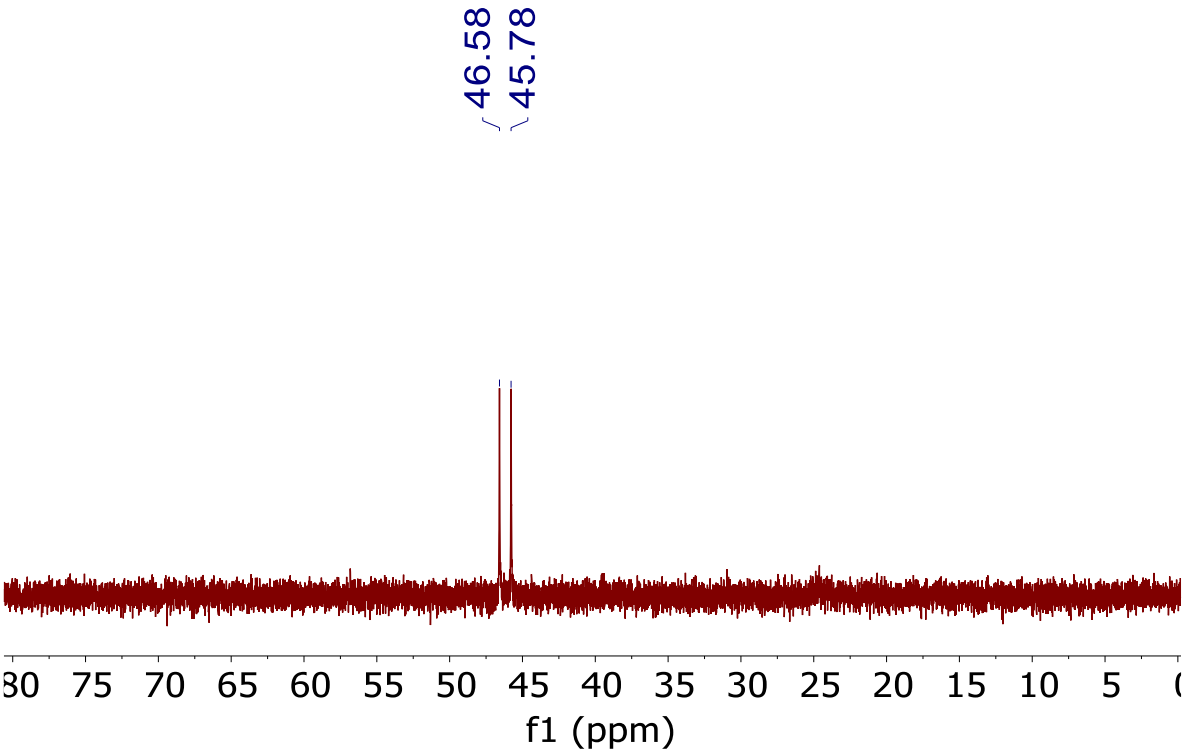

Figure 8.13. $^{31}P\{^{1}H\}$ NMR spectrum of **8.3** in benzene-d_6 at room temperature.

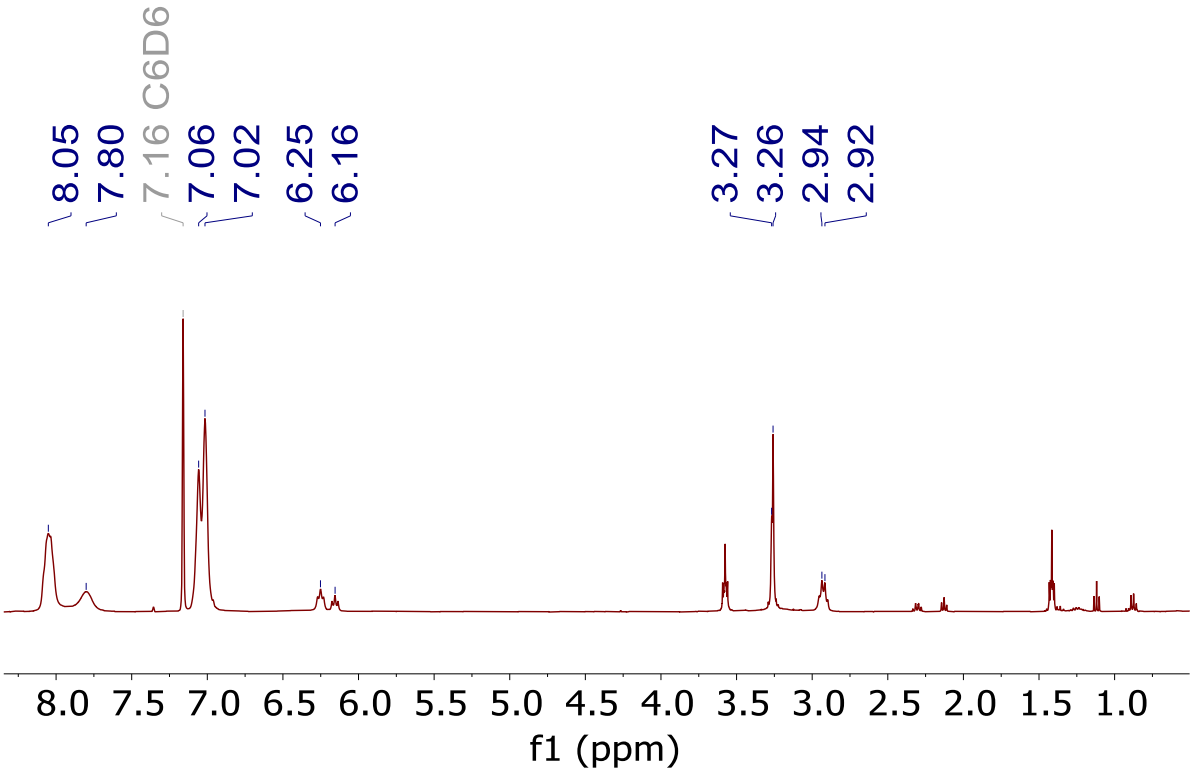

Figure 8.14. ^{1}H NMR spectrum of **8.3** in benzene-d_6 at room temperature.

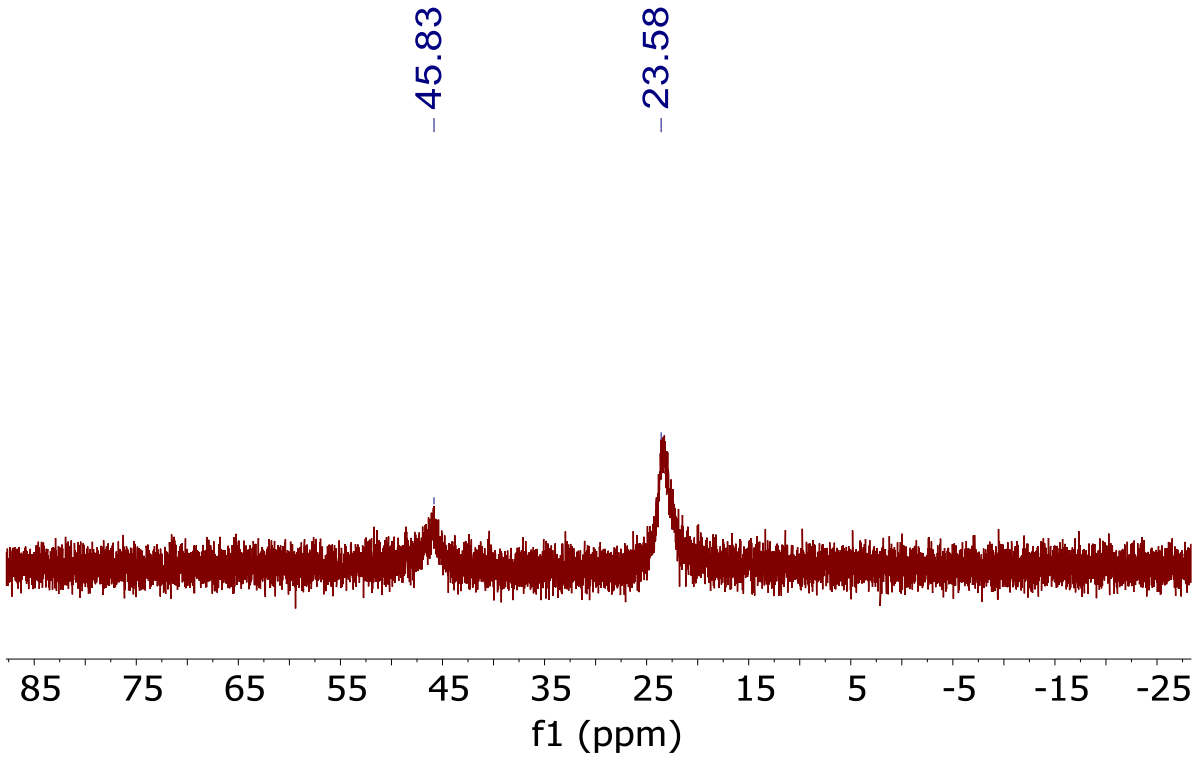

Figure 8.15. $^{31}P\{^{1}H\}$ NMR spectrum of **8.4** in THF-d_8 at room temperature.

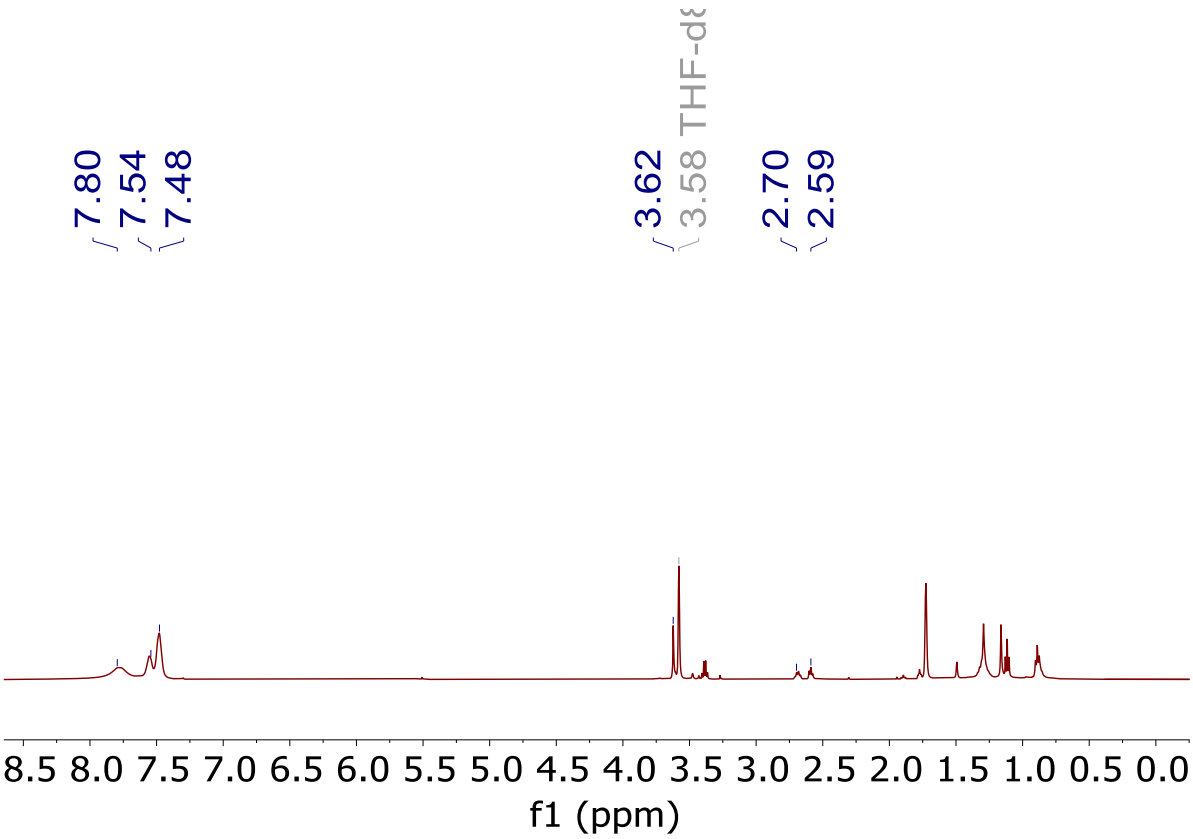

Figure 8.16. ^{1}H NMR spectrum of **8.4** in THF-d_8 at room temperature.

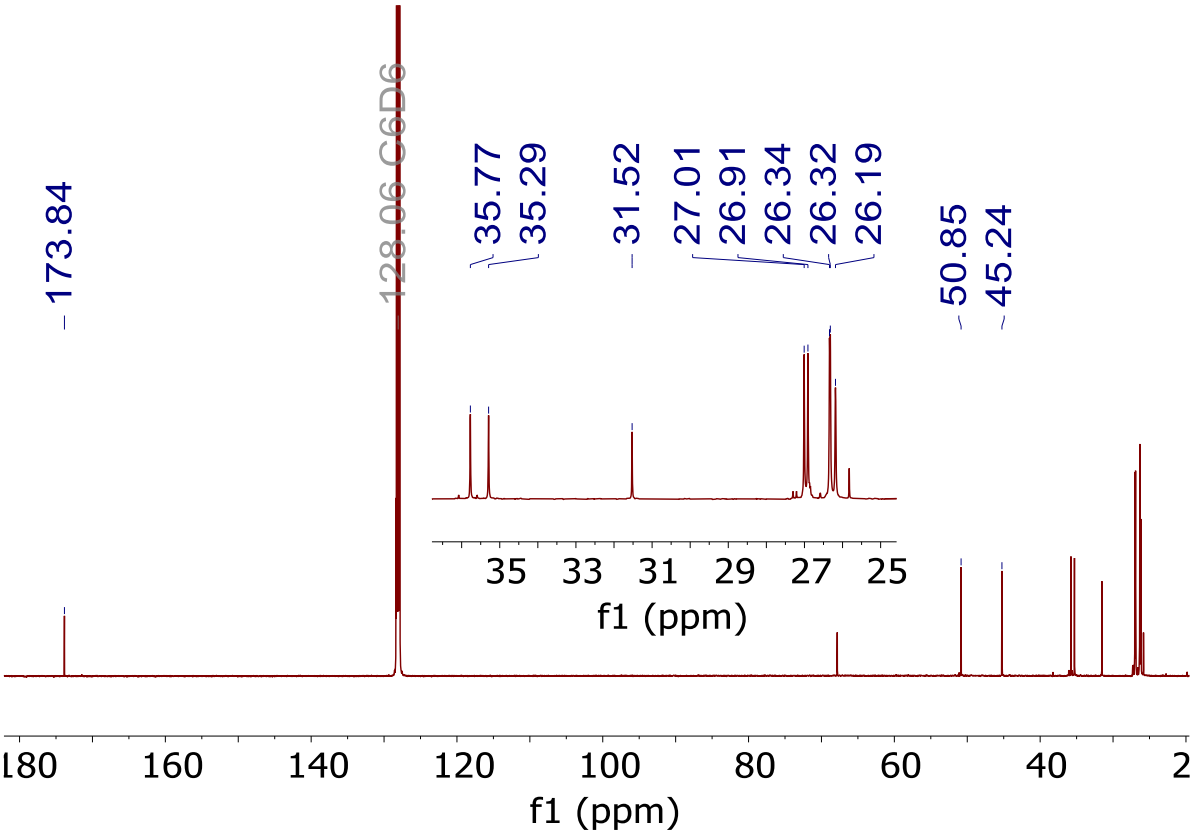

Figure 8.17. $^{13}C\{^{1}H\}$ NMR spectrum of **8.5** in benzene-d_6 at room temperature.

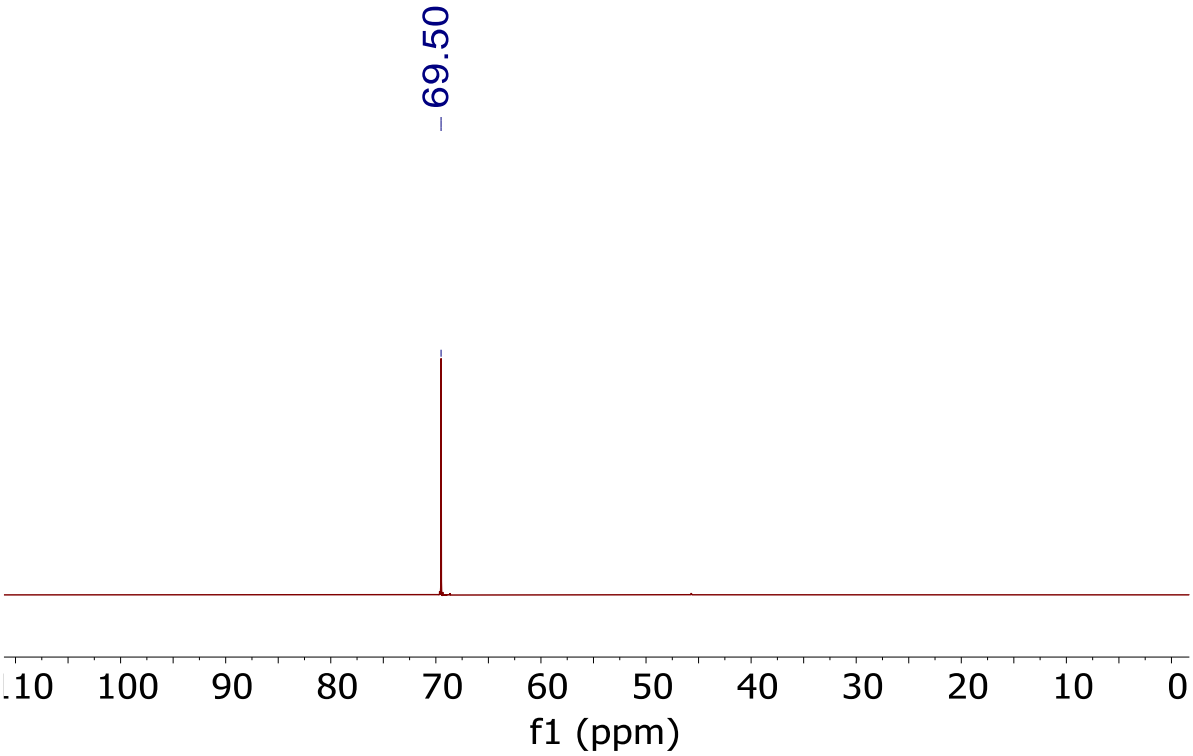

Figure 8.18. $^{31}P\{^{1}H\}$ NMR spectrum of **8.5** in benzene-d_6 at room temperature.

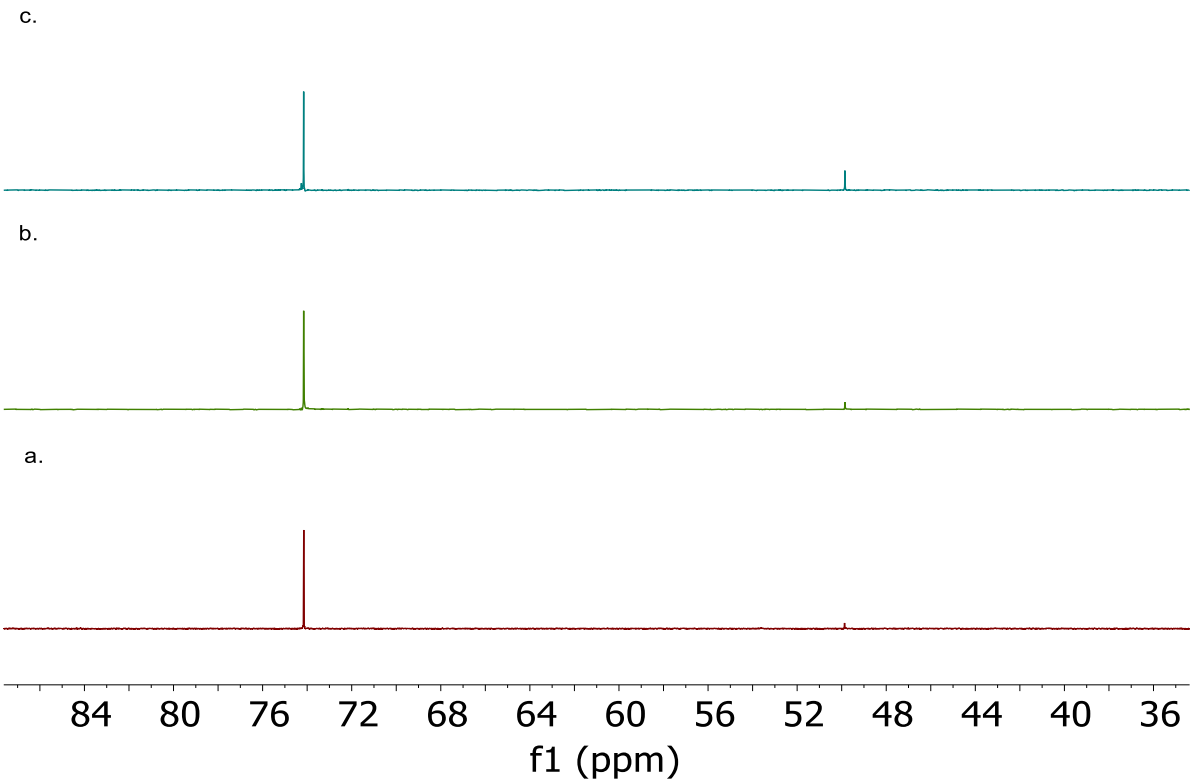

Figure 8.19. a. $^{31}P\{^{1}H\}$ NMR spectrum of **8.5** in benzene-d_6 at room temperature. b. $^{31}P\{^{1}H\}$ NMR spectrum of **8.5** in benzene-d_6 at room temperature after thermolysis for 1 h at 80 °C. c. $^{31}P\{^{1}H\}$ NMR spectrum of **8.5** in benzene-d_6 at room temperature after thermolysis for 4 h at 80 °C.

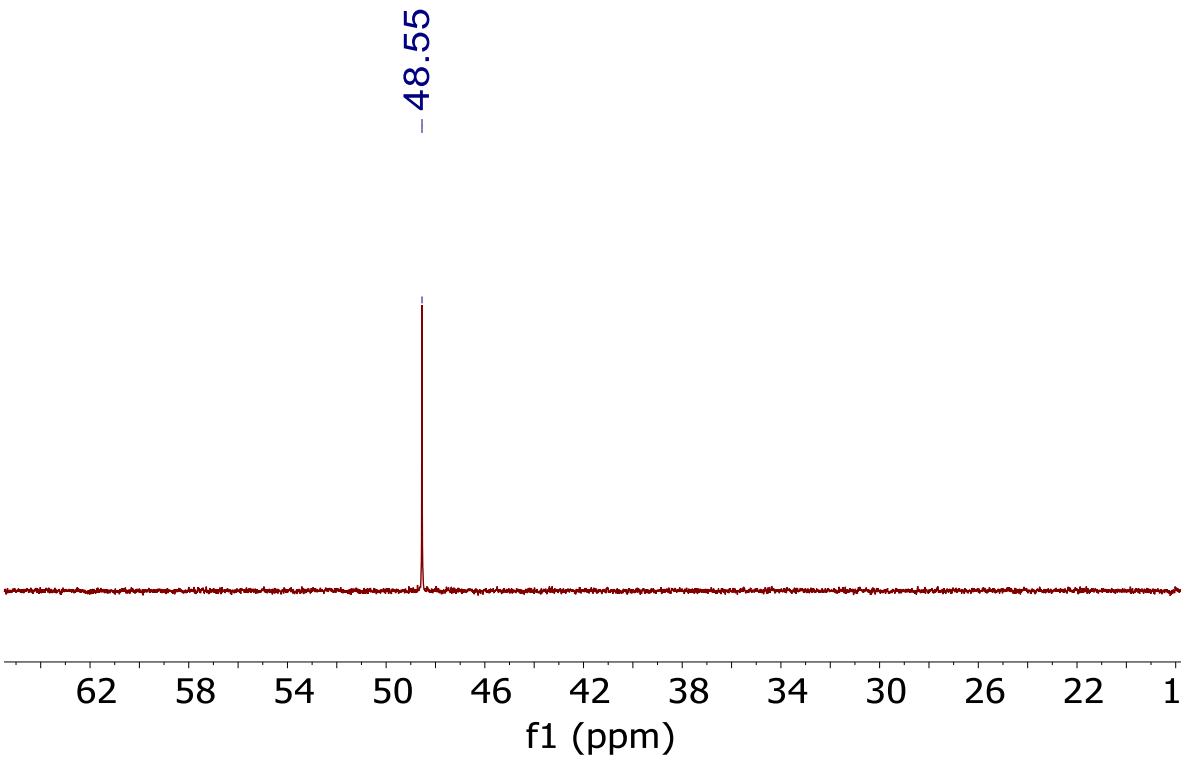

Figure 8.20. $^{31}P\{^{1}H\}$ NMR spectrum of crude **8.6** in acetonitrile-d_3 at room temperature.

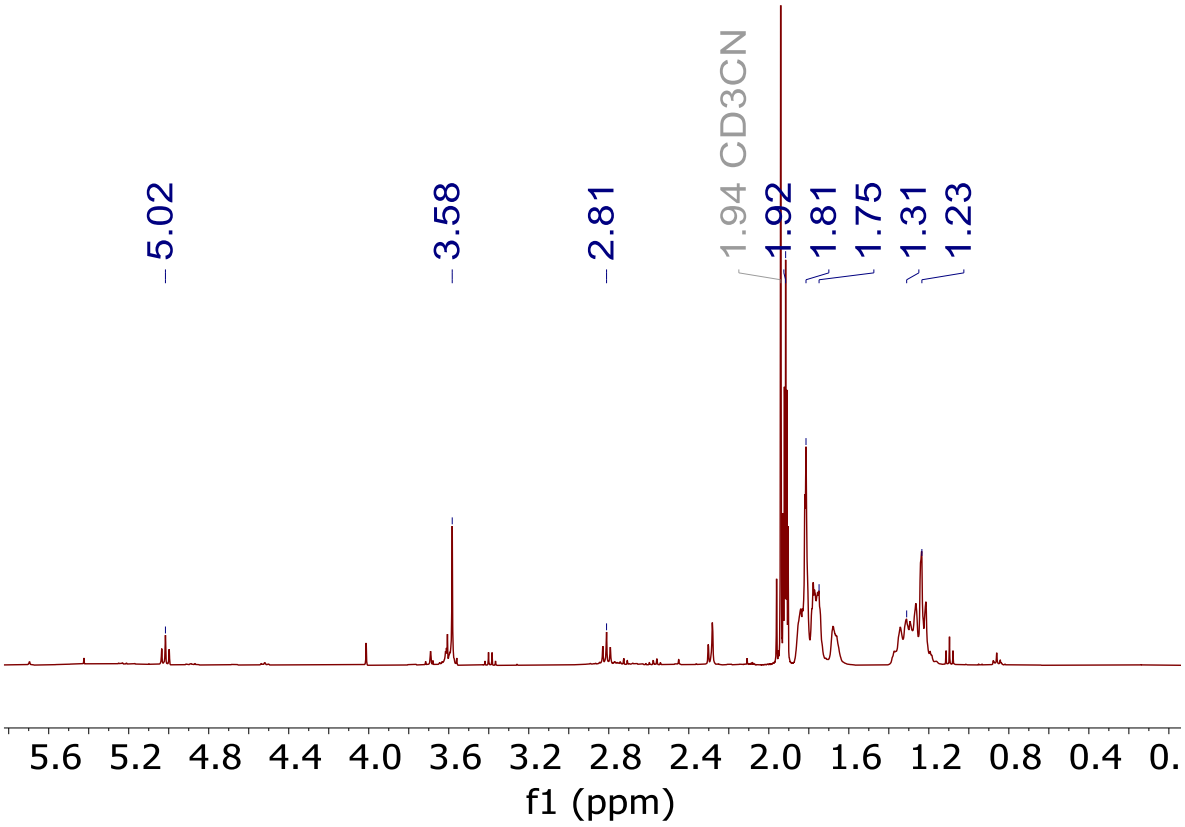

Figure 8.21. ^{1}H NMR spectrum of crude **8.6** in acetonitrile-d_3 at room temperature.

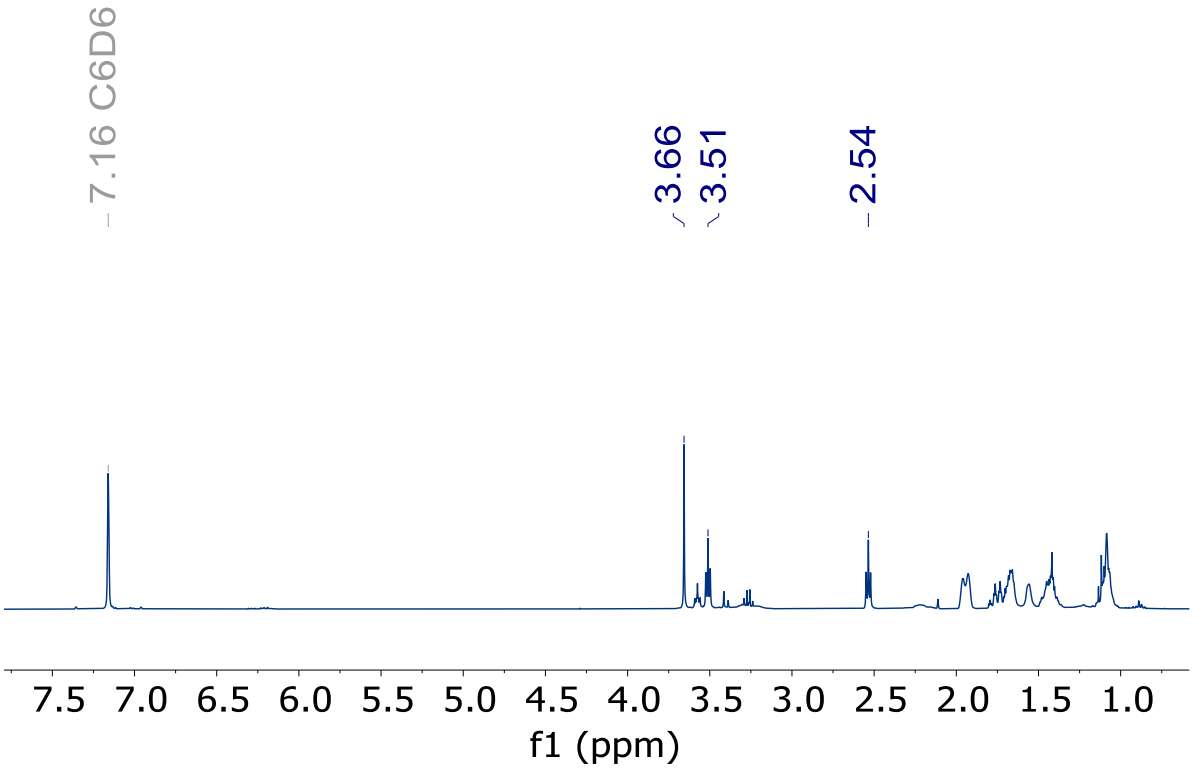

Figure 8.22. ^{1}H NMR spectrum of crude reaction mixture of **8.5** with 1 equiv of $NaNR_2$ (R = $SiMe_3$) in THF the presence of 2,2,2-cryptand in benzene-d_6 at room temperature.

Experimental details: A cold (-25 °C) solution of $NaNR_2$ (R = $SiMe_3$) (8.4 mg, 0.046 mmol) in THE (1 mL) was added dropwise to a cold (-25 °C), stirring red solution of $[UO_2(MMP)_2(OPCy_3)_2]$ (50.5 mg, 0.046 mmol) in THF (2 mL) in the presence of 2,2,2-cryptand. This resulted in an immediate color change to orange solution and substantial formation of dark brown solids. After stirring for 1 h at room temperature, the volatiles were removed *in vacuo* of reaction mixture aliquot (0.5 mL), followed by dissolution in benzene-d_6 (0.7 mL) and transferred to an NMR tube. The ^{1}H NMR spectrum was recorded.

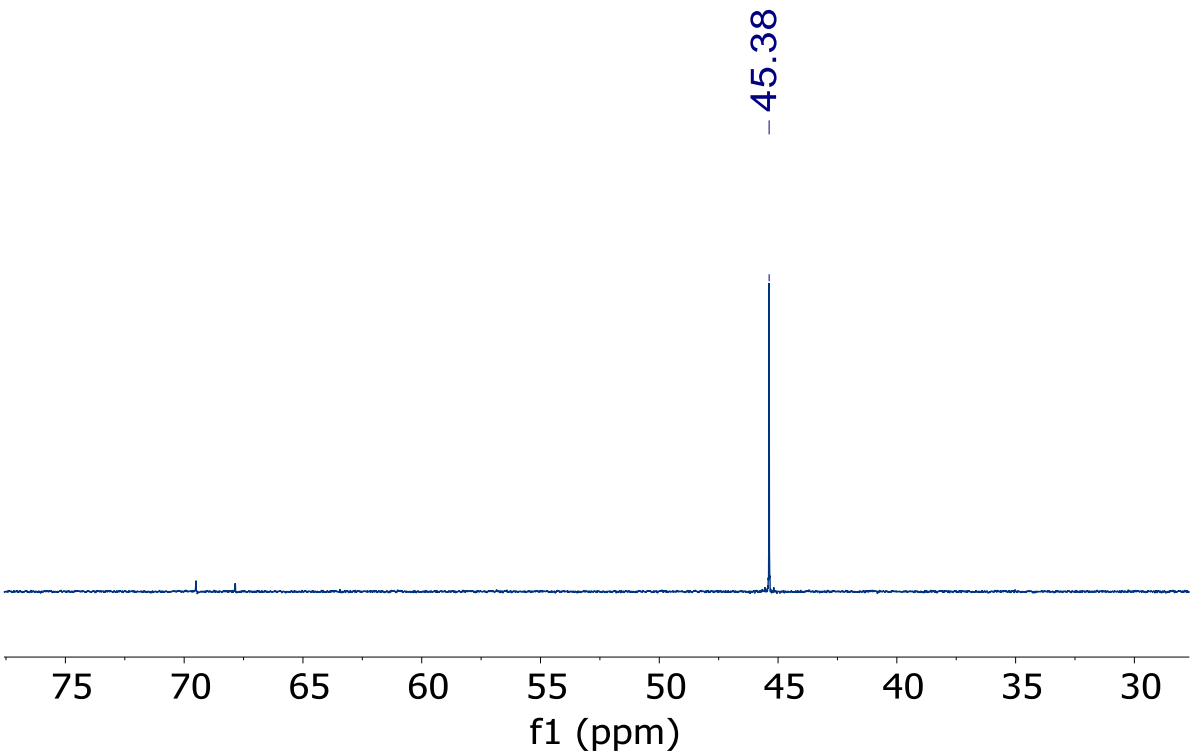

Figure 8.23. ^{31}P NMR spectrum of crude reaction mixture of **8.5** with 1 equiv of $NaNR_2$ (R = $SiMe_3$) in THF the presence of 2,2,2-cryptand in benzene-d_6 at room temperature.

Experimental details: A cold (-25 °C) solution of $NaNR_2$ (R = $SiMe_3$) (8.4 mg, 0.046 mmol) in THE (1 mL) was added dropwise to a cold (-25 °C), stirring red solution of $[UO_2(MMP)_2(OPCy_3)_2]$ (50.5 mg, 0.046 mmol) in THF (2 mL) in the presence of 2,2,2-cryptand. This resulted in an immediate color change to orange solution and substantial formation of dark brown solids. After stirring for 1 h at room temperature, the volatiles were removed *in vacuo* of reaction mixture aliquot (0.5 mL), followed by dissolution in benzene-d_6 (0.7 mL) and transferred to an NMR tube. The ^{31}P NMR spectrum was recorded.

8.6 References

(1) Seaman, L. A.; Walensky, J. R.; Wu, G.; Hayton, T. W. In Pursuit of Homoleptic Actinide Alkyl Complexes. *Inorg. Chem.* **2013**, *52*, 3556-3564.
(2) Marks, T. J.; Seyam, A. M. Observations on the thermal decomposition of some uranium(IV) tetraalkyls. *J. Organomet. Chem.* **1974**, *67*, 61-66.
(3) Cernia, E.; Mazzei, A. Advances in the organometallic chemistry of uranium(IV). *Inorg. Chim. Acta* **1974**, *10*, 239-252.
(4) Assefa, M. K.; Sergentu, D.-C.; Seaman, L. A.; Wu, G.; Autschbach, J.; Hayton, T. W. Synthesis, Characterization, and Electrochemistry of the Homoleptic f Element Ketimide Complexes $[Li]_2[M(N{=}C^tBuPh)_6]$ (M = Ce, Th). *Inorg. Chem.* **2019**, *58*, 12654-12661.
(5) Ordoñez, O.; Yu, X.; Wu, G.; Autschbach, J.; Hayton, T. W. Homoleptic Perchlorophenyl "Ate" Complexes of Thorium(IV) and Uranium(IV). *Inorg. Chem.* **2021**, *60*, 12436-12444.
(6) Ordoñez, O.; Yu, X.; Wu, G.; Autschbach, J.; Hayton, T. W. Assessing the 4f Orbital Participation in the Ln–C Bonds of $[Li(THF)_4][Ln(C_6Cl_5)_4]$ (Ln = La, Ce). *Inorg. Chem.* **2022**, *61*, 15138-15143.
(7) Seaman, L. A.; Hrobárik, P.; Schettini, M. F.; Fortier, S.; Kaupp, M.; Hayton, T. W. A Rare Uranyl(VI)–Alkyl Ate Complex $[Li(DME)_{1.5}]_2[UO_2(CH_2SiMe_3)_4]$ and Its Comparison with a Homoleptic Uranium(VI)–Hexaalkyl. *Angew. Chem. Int. Ed.* **2013**, *52*, 3259-3263.
(8) Su, J.; Batista, E. R.; Boland, K. S.; Bone, S. E.; Bradley, J. A.; Cary, S. K.; Clark, D. L.; Conradson, S. D.; Ditter, A. S.; Kaltsoyannis, N.; et al. Energy-Degeneracy-Driven Covalency in Actinide Bonding. *J. Am. Chem. Soc.* **2018**, *140*, 17977-17984.
(9) Neidig, M. L.; Clark, D. L.; Martin, R. L. Covalency in f-element complexes. *Coord. Chem. Rev.* **2013**, *257*, 394-406.
(10) Löble, M. W.; Keith, J. M.; Altman, A. B.; Stieber, S. C. E.; Batista, E. R.; Boland, K. S.; Conradson, S. D.; Clark, D. L.; Lezama Pacheco, J.; Kozimor, S. A.; et al. Covalency in Lanthanides. An X-ray Absorption Spectroscopy and Density Functional Theory Study of $LnCl_6^{x-}$ (x = 3, 2). *J. Am. Chem. Soc.* **2015**, *137*, 2506-2523.
(11) Edelstein, N.; Brown, D.; Whittaker, B. Covalency effects on the ligand field splittings of octahedral $5f^7$ compounds. *Inorg. Chem.* **1974**, *13*, 563-567.
(12) Eichberger, K.; Lux, F. Die konsistente ligandenfeldtheoretische Interpretation des spektroskopischen und magnetischen Verhaltens des 5-Elektronensystems in oktaedrischen Halogenokomplexen. *Ber. Bunsenges. Phys. Chem.* **1980**, *84*, 800-807.
(13) Notter, F.-P.; Bolvin, H. Optical and magnetic properties of the $5f^1AnX_6^{q-}$ series: A theoretical study. *J. Chem. Phys.* **2009**, *130*, 184310.
(14) Arratia-Pérez, R.; Malli, G. L. Relativistic molecular orbital study of the optical and magnetic properties of hexachloro protactinate (IV): $PaCl_6^{2-}$. *J. Chem. Phys.* **2006**, *124*, 074321.
(15) Arratia-Pérez, R.; Hernandez-Acevedo, L.; Malli, G. L. Calculated optical and magnetic properties of hexafluorouranate (V) anion: UF_6^-. *J. Chem. Phys.* **2004**, *121*, 7743-7747.
(16) Edelstein, N. M. *Covalency in Octahedrally Coordinated $5f^1$ Ccomplexes*; Lawrence Berkeley National Laboratory, 1976.
(17) Lukens, W. W.; Edelstein, N. M.; Magnani, N.; Hayton, T. W.; Fortier, S.; Seaman, L. A. Quantifying the σ and π Interactions between U(V) f Orbitals and Halide, Alkyl, Alkoxide, Amide and Ketimide Ligands. *J. Am. Chem. Soc.* **2013**, *135*, 10742-10754.

(18) Yu, X.; Sergentu, D.-C.; Feng, R.; Autschbach, J. Covalency of Trivalent Actinide Ions with Different Donor Ligands: Do Density Functional and Multiconfigurational Wavefunction Calculations Corroborate the Observed "Breaks"? *Inorg. Chem.* **2021**, *60*, 17744-17757.
(19) Pu, N.; Archer, E.; He, X.; Chen, J.; Rao, L.; Shafer, J. C.; Yang, P.; Xu, C. Tuning Selectivity to f-Elements through Bonding and Solvation Effects of a Sulfur Donor Ligand. *Inorg. Chem.* **2024**, *63*, 6845-6853.
(20) Lewis, F. W.; Hudson, M. J.; Harwood, L. M. Development of Highly Selective Ligands for Separations of Actinides from Lanthanides in the Nuclear Fuel Cycle. *Synlett* **2011**, *2011*, 2609-2632.
(21) Dam, H. H.; Reinhoudt, D. N.; Verboom, W. Multicoordinate ligands for actinide/lanthanide separations. *Chem. Soc. Rev.* **2007**, *36*, 367-377.
(22) Behrle, A. C.; Kerridge, A.; Walensky, J. R. Dithio- and Diselenophosphinate Thorium(IV) and Uranium(IV) Complexes: Molecular and Electronic Structures, Spectroscopy, and Transmetalation Reactivity. *Inorg. Chem.* **2015**, *54*, 11625-11636.
(23) Leverd, P. C.; Lance, M.; Nierlich, M.; Vigner, J.; Ephritikhine, M. Synthesis and crystal structure of homoleptic uranium hexathiolates: $[NEt_2H_2]_2[U(SPh)_6]$ and $[(Ph_3P)Cu(\mu\text{-}SPh)_3\text{-}U(\mu\text{-}SPh)_3Cu(PPh_3)]$. *J. Chem. Soc., Dalton Trans.* **1994**, 3563-3567.
(24) Macor, J. A.; Brown, J. L.; Cross, J. N.; Daly, S. R.; Gaunt, A. J.; Girolami, G. S.; Janicke, M. T.; Kozimor, S. A.; Neu, M. P.; Olson, A. C.; et al. Coordination chemistry of 2,2′-biphenylenedithiophosphinate and diphenyldithiophosphinate with U, Np, and Pu. *Dalton Trans.* **2015**, *44*, 18923-18936.
(25) Roger, M.; Barros, N.; Arliguie, T.; Thuéry, P.; Maron, L.; Ephritikhine, M. U(SMes*)n, (n = 3, 4) and Ln(SMes*)3 (Ln = La, Ce, Pr, Nd): Lanthanide(III)/Actinide(III) Differentiation in Agostic Interactions and an Unprecedented η3 Ligation Mode of the Arylthiolate Ligand, from X-ray Diffraction and DFT Analysis. *J. Am. Chem. Soc.* **2006**, *128*, 8790-8802.
(26) Brown, D.; Holah, D. G.; Rickard, C. E. F. Structure of thorium(IV) tetrakis-(NN-diethyldithiocarbamate). *J. Chem. Soc. A* **1970**, 423-425.
(27) Behrle, A. C.; Myers, A. J.; Kerridge, A.; Walensky, J. R. Coordination Chemistry and QTAIM Analysis of Homoleptic Dithiocarbamate Complexes, $M(S_2CN^iPr_2)_4$ (M = Ti, Zr, Hf, Th, U, Np). *Inorg. Chem.* **2018**, *57*, 10518-10524.
(28) Gaunt, A. J.; Reilly, S. D.; Enriquez, A. E.; Scott, B. L.; Ibers, J. A.; Sekar, P.; Ingram, K. I. M.; Kaltsoyannis, N.; Neu, M. P. Experimental and Theoretical Comparison of Actinide and Lanthanide Bonding in $M[N(EPR_2)_2]_3$ Complexes (M = U, Pu, La, Ce; E = S, Se, Te; R = Ph, ^{i}Pr, H). *Inorg. Chem.* **2008**, *47*, 29-41.
(29) Rehe, D.; Kornienko, A. Y.; Emge, T. J.; Brennan, J. G. Thorium Compounds with Bonds to Sulfur or Selenium: Synthesis, Structure, and Thermolysis. *Inorg. Chem.* **2016**, *55*, 6961-6967.
(30) Brown, D.; Holah, D. G.; Rickard, C. E. F. NN-diethyldithiocarbamate complexes of trivalent lanthanide and actinide elements and the crystal structure of tetraethylammonium neptunium(III) tetrakis-(NN-diethyldithiocarbamate). *J. Chem. Soc. A* **1970**, 786-790.
(31) Pinkerton, A. A.; Storey, A. E.; Zellweger, J.-M. Dithiophosphinate complexes of the actinides. Part 1. Preparation and characterisation of complexes of thorium(IV) and the crystal structures of $[Th(S_2PR_2)_4]$, R = Me or C_6H_{11}. *J. Chem. Soc., Dalton Trans.* **1981**, 1475-1480.

(32) Boreen, M. A.; Parker, B. F.; Hohloch, S.; Skeel, B. A.; Arnold, J. f-Block complexes of a m-terphenyl dithiocarboxylate ligand. *Dalton Trans.* **2018**, *47*, 96-104.
(33) Cary, S. K.; Su, J.; Galley, S. S.; Albrecht-Schmitt, T. E.; Batista, E. R.; Ferrier, M. G.; Kozimor, S. A.; Mocko, V.; Scott, B. L.; Van Alstine, C. E.; et al. A series of dithiocarbamates for americium, curium, and californium. *Dalton Trans.* **2018**, *47*, 14452-14461.
(34) Roger, M.; Arliguie, T.; Thuéry, P.; Fourmigué, M.; Ephritikhine, M. Homoleptic Tris(dithiolene) and Tetrakis(dithiolene) Complexes of Uranium(IV). *Inorg. Chem.* **2005**, *44*, 594-600.
(35) Gaunt, A. J.; Scott, B. L.; Neu, M. P. U(IV) Chalcogenolates Synthesized via Oxidation of Uranium Metal by Dichalcogenides. *Inorg. Chem.* **2006**, *45*, 7401-7407.
(36) Cross, J. N.; Macor, J. A.; Bertke, J. A.; Ferrier, M. G.; Girolami, G. S.; Kozimor, S. A.; Maassen, J. R.; Scott, B. L.; Shuh, D. K.; Stein, B. W.; Stieber, S. C. E. Comparing the 2,2′-Biphenylenedithiophosphinate Binding of Americium with Neodymium and Europium. *Angew. Chem. Int. Ed.* **2016**, *55*, 12755-12759.
(37) Myers, A. J.; Tarlton, M. L.; Kelley, S. P.; Lukens, W. W.; Walensky, J. R. Synthesis and Utility of Neptunium(III) Hydrocarbyl Complex. *Angew. Chem. Int. Ed.* **2019**, *58*, 14891-14895.
(38) Kondo, M.; Minakoshi, S.; Iwata, K.; Shimizu, T.; Matsuzaka, H.; Kamigata, N.; Kitagawa, S. Crystal Structure of a Tris(dithiolene) Vanadium(IV) Complex Having Unprecedented D_{3h} Symmetry. *Chem. Lett.* **1996**, *25*, 489-490.
(39) Melen, R. L.; McPartlin, M.; Wright, D. S. An unexpected dependence on the SnII base; reactions of $Sn(NR_2)_2$ with aromatic dithiols. *Dalton Trans.* **2011**, *40*, 1649-1651.
(40) Martin, J. L.; Takats, J. Crystal and molecular structure of tetraphenylarsonium tris(benzenedithiolato)tantalate(V). *Inorg. Chem.* **1975**, *14*, 1358-1364.
(41) Sellmann, D.; Hennige, A. C.; Heinemann, F. W. Synthesis, Structure, and Properties of Osmium Complexes Containing [Os(′S_4′)] and [Os(′S_2′)$_2$] Fragments (′S_4′$^{2-}$ = 1,2-Bis(2-mercaptophenylthio)ethane(2−), ′S_2′$^{2-}$ = 1,2-Benzenedithiolate). *Eur. J. Inorg. Chem.* **1998**, *1998*, 819-826.
(42) Fataftah, M. S.; Krzyaniak, M. D.; Vlaisavljevich, B.; Wasielewski, M. R.; Zadrozny, J. M.; Freedman, D. E. Metal–ligand covalency enables room temperature molecular qubit candidates. *Chem. Sci.* **2019**, *10*, 6707-6714.
(43) Lin, C.-H.; Chen, C.-G.; Tsai, M.-L.; Lee, G.-H.; Liaw, W.-F. Monoanionic $\{Mn(NO)\}_5$ and Dianionic $\{Mn(NO)\}_6$ Thiolatonitrosylmanganese Complexes: $[(NO)Mn(L)_2]^-$ and $[(NO)Mn(L)_2]^{2-}$ (LH_2 = 1,2-Benzenedithiol and Toluene-3,4-dithiol). *Inorg. Chem.* **2008**, *47*, 11435-11443.
(44) Könemann, M.; Stüer, W.; Kirschbaum, K.; Giolando, D. M. Synthesis, crystal structure and electrochemistry of bis(N,N-dimethylammonium) tris(1,2-benzenedithiolato)titanate(IV). *Polyhedron* **1994**, *13*, 1415-1425.
(45) Huynh, H.; Lügger, T.; Hahn, F. E. Synthesis and X-ray Molecular Structure of $[W^{VI}(C_6H_4S_2\text{-}1,2)_3]$ Completing the Structural Characterization of the Series $[W(C_6H_4S_2\text{-}1,2)_3]^{n-}$ (n = 0, 1, 2): Trigonal-Prismatic versus Octahedral Coordination in Tris(benzene-1,2-dithiolato) Complexes. *Eur. J. Inorg. Chem.* **2002**, *2002*, 3007-3009.
(46) Wegener, J.; Kirschbaum, K.; Giolando, D. M. Synthesis, properties and crystal structures of benzene-1,2-dithiolato complexes of antimony-(III) and -(V). *J. Chem. Soc., Dalton Trans.* **1994**, 1213-1218.

(47) Lorber, C.; Donahue, J. P.; Goddard, C. A.; Nordlander, E.; Holm, R. H. Synthesis, Structures, and Oxo Transfer Reactivity of Bis(dithiolene)tungsten(IV,VI) Complexes Related to the Active Sites of Tungstoenzymes. *J. Am. Chem. Soc.* **1998**, *120*, 8102-8112.
(48) Colmanet, S. F.; Williams, G. A.; Mackay, M. F. Preparation and crystal structures of bis(tetraphenylarsonium) tris(oxalato)technetate(IV), and tetraphenylarsonium tris(benzene-1,2-dithiolato)technetate(V): octahedral versus trigonal-prismatic geometry for tris-bidentate complexes of technetium. *J. Chem. Soc., Dalton Trans.* **1987**, 2305-2310.
(49) Cowie, M.; Bennett, M. J. Trigonal-prismatic vs. octahedral coordination in a series of tris(benzene-1,2-dithiolato) complexes. 3. Crystal and molecular structure of bis(tetramethylammonium) tris(benzene-1,2-dithiolato) zirconate(IV), $[CH_3)_4N]_2[Zr(S_2C_6H_4)_3]$. *Inorg. Chem.* **1976**, *15*, 1595-1603.
(50) Sellmann, D.; Hein, K.; Heinemann, F. W. Synthesis, structure and reactivity of complexes containing $[M(S_2)_2]$ fragments (M=Ru, Os; $(S_2)^{2-}$=1,2-benzenedithiolate (2−)). *Inorg. Chim. Acta* **2004**, *357*, 3739-3745.
(51) Mrkvová, K.; Kameníček, J.; Šindelář, Z.; Kvítek, L.; Mrozinski, J.; Nahorska, M.; Žák, Z. Synthesis, properties and crystal structures of $R[M^{III}(bdt)_2]$ complexes (M = Ni, Co, Cu). *Transition Met. Chem.* **2004**, *29*, 238-244.
(52) Cervilla, A.; Llopis, E.; Marco, D.; Pérez, F. X-ray Structure of $(Bu^{n4}N)$[Mo(1,2-Benzenedithiolate)$_3$]. Trigonal-Prismatic versus Octahedral Coordination in Tris(1,2-Benzenedithiolate) Complexes. *Inorg. Chem.* **2001**, *40*, 6525-6528.
(53) Fortier, S.; Hayton, T. W. Oxo ligand functionalization in the uranyl ion (UO_2^{2+}). *Coord. Chem. Rev.* **2010**, *254*, 197-214.
(54) Morss, L. R.; Edelstein, N. M.; Fuger, J. *The Chemistry of the Actinide and Transactinide Elements (Set Vol. 1-6): Volumes 1-6*; Springer, 2011.
(55) Baker, R. J. New Reactivity of the Uranyl(VI) Ion. *Chem. Eur. J.* **2012**, *18*, 16258-16271.
(56) Jones, M. B.; Gaunt, A. J. Recent Developments in Synthesis and Structural Chemistry of Nonaqueous Actinide Complexes. *Chem. Rev.* **2013**, *113*, 1137-1198.
(57) Denning, R. G. Electronic Structure and Bonding in Actinyl Ions and their Analogs. *J. Phys. Chem. A* **2007**, *111*, 4125-4143.
(58) Wolf, R.; Hoppe, R. R. Ein neues Oxouranat(VI): $K_2Li_4[UO_6]$. Mit einer Bemerkung über $Rb_2Li_4[UO_6]$ und $Cs_2Li_4UO_6$. *Z. Anorg. Allg. Chem.* **1987**, *554*, 34-42.
(59) Juillerat, C. A.; Klepov, V. V.; Morrison, G.; Pace, K. A.; zur Loye, H.-C. Flux crystal growth: a versatile technique to reveal the crystal chemistry of complex uranium oxides. *Dalton Trans.* **2019**, *48*, 3162-3181.
(60) King, R. B. Some Aspects of Structure and Bonding in Binary and Ternary Uranium(VI) Oxides. *Chem. Mater.* **2002**, *14*, 3628-3635.
(61) Fitzpatrick, J.; Kim, E. Synthetic Modeling Chemistry of Iron–Sulfur Clusters in Nitric Oxide Signaling. *Acc. Chem. Res.* **2015**, *48*, 2453-2461.
(62) Fitzpatrick, J.; Kalyvas, H.; Filipovic, M. R.; Ivanović-Burmazović, I.; MacDonald, J. C.; Shearer, J.; Kim, E. Transformation of a Mononitrosyl Iron Complex to a [2Fe-2S] Cluster by a Cysteine Analogue. *J. Am. Chem. Soc.* **2014**, *136*, 7229-7232.
(63) Cirera, J.; Ruiz, E.; Alvarez, S. Continuous Shape Measures as a Stereochemical Tool in Organometallic Chemistry. *Organometallics* **2005**, *24*, 1556-1562.
(64) Ringgold, M.; Wu, W.; Stuber, M.; Kornienko, A. Y.; Emge, T. J.; Brennan, J. G. Monomeric thorium chalcogenolates with bipyridine and terpyridine ligands. *Dalton Trans.* **2018**, *47*, 14652-14661.

(65) Settineri, N. S.; Garner, M. E.; Arnold, J. A Thorium Chalcogenolate Series Generated by Atom Insertion into Thorium–Carbon Bonds. *J. Am. Chem. Soc.* **2017**, *139*, 6261-6269.
(66) Evans, W. J.; Miller, K. A.; Kozimor, S. A.; Ziller, J. W.; DiPasquale, A. G.; Rheingold, A. L. Actinide Hydride Complexes as Multielectron Reductants: Analogous Reduction Chemistry from $[(C_5Me_5)_2UH]_2$, $[(C_5Me_5)_2UH_2]_2$, and $[(C_5Me_5)_2ThH_2]_2$. *Organometallics* **2007**, *26*, 3568-3576.
(67) Smiles, D. E.; Wu, G.; Kaltsoyannis, N.; Hayton, T. W. Thorium–ligand multiple bonds via reductive deprotection of a trityl group. *Chem. Sci.* **2015**, *6*, 3891-3899.
(68) Shannon, R. D. Revised effective ionic radii and systematic studies of interatomic distances in halides and chalcogenides. *Acta Cryst. A* **1976**, *32*, 751-767.
(69) Arliguie, T.; Thuéry, P.; Fourmigué, M.; Ephritikhine, M. Reduction of Dithiocarbonates as a Novel Route to Dithiolene Compounds of Uranium. Crystal Structure of the First Bimetallic Dithiolene Complex of an f-Element. *Organometallics* **2003**, *22*, 3000-3003.
(70) Aslam, M.; Bartlett, R. A.; Block, E.; Olmstead, M. M.; Power, P. P.; Sigel, G. E. The first X-ray crystal structural characterizations of alkali metal alkyl thiolates: X-ray crystal structures of $[Li_2(thf)_4\{SCH(SiMe_3)_2\}_2]$ and $[Li_2(thf)_{3.5}\{SC(SiMe_3)_3\}_2]$(thf = tetrahydrofuran). *J. Chem. Soc., Chem. Commun.* **1985**, 1674-1675.
(71) Sigel, G. A.; Power, P. P. Synthesis and characterization of the bulky thiolate complexes $[Li(OEt_2)_3][Ti\{S\text{-}2,4,6\text{-}iso\text{-}Pr_3C_6H_2\}_4]$ and $Li(THF)_3(S\text{-}2,4,6\text{-}tert\text{-}Bu_3C_6H_2)]$. Comparisons of M-SR and M-OR bonding. *Inorg. Chem.* **1987**, *26*, 2819-2822.
(72) Tatsumi, K.; Matsubara, I.; Inoue, Y.; Nakamura, A.; Cramer, R. E.; Tagoshi, G. J.; Golen, J. A.; Gilje, J. W. A homoleptic uranium thiolate: synthesis, structure, and fluxional behavior of $[Li(dme)]_4[U(SCH_2CH_2S)_4]$ and reaction with carbon disulfide. *Inorg. Chem.* **1990**, *29*, 4928-4938.
(73) Bombieri, G.; Forsellini, E.; Day, J. P.; Azeez, W. I. Crystal and molecular structure of dichlorodioxobis(triphenylphosphine oxide)uranium(VI). *J. Chem. Soc., Dalton Trans.* **1978**, 677-680.
(74) Ordoñez, O.; Yu, X.; Wu, G.; Autschbach, J.; Hayton, T. W. Synthesis and Characterization of Two Uranyl-Aryl "Ate" Complexes. *Chem. Eur. J.* **2021**, *27*, 5885-5889.
(75) Ordoñez, O.; Yu, X.; Wu, G.; Autschbach, J.; Hayton, T. W. Quantifying Actinide–Carbon Bond Covalency in a Uranyl–Aryl Complex Utilizing Solution ^{13}C NMR Spectroscopy. *Inorg. Chem.* **2023**.
(76) Akona, S. B.; Fawcett, J.; Holloway, J. H.; Russell, D. R.; Leban, I. Structures of cis- and trans-dichlorodioxobis(triphenylphosphine oxide)uranium(VI). *Acta Cryst. C* **1991**, *47*, 45-48.
(77) Alcock, N. W.; Roberts, M. M.; Brown, D. Actinide structural studies. Part 1. Crystal and molecular structures of dinitratodioxobis(triphenylphosphine oxide)neptunium(VI), dinitratodioxobis(triphenylphosphine oxide)uranium(VI), and dichlorodioxo-(triphenylphosphine oxide)neptunium(VI). *J. Chem. Soc., Dalton Trans.* **1982**, 25-31.
(78) Arnáiz, F. J.; Miranda, M. J.; Aguado, R.; Mahía, J.; Maestro, M. A. Uranyl polyhalides. Molecular structure of $[UO_2(OAsPh_3)_4](Br_3)_2$ and $[UO_2(OPPh_3)_4](I_3)_2$. *Polyhedron* **2002**, *21*, 2755-2760.
(79) Berthet, J.-C.; Nierlich, M.; Ephritikhine, M. Isolation of a Uranyl $[UO_2]^+$ Species: Crystallographic Comparison of the Dioxouranium(V) and (VI) Compounds $[UO_2(OPPh_3)_4](OTf)_n$ (n=1, 2). *Angew. Chem. Int. Ed.* **2003**, *42*, 1952-1954.

(80) Bombieri, G.; Brown, D.; Graziani, R. Crystal and molecular structure of tetrachlorobis(triphenylphosphine oxide)uranium(IV). *J. Chem. Soc., Dalton Trans.* **1975**, 1873-1876.
(81) Kannan, S.; Barnes, C. L.; Duval, P. B. Synthesis and Structural Characterization of a Uranyl(VI) Complex Possessing Unsupported Unidentate Thiolate Ligands. *Inorg. Chem.* **2005**, *44*, 9137-9139.
(82) Ashby, M. T. Concerning the Spatial Nature of Metal-Thiolate π Bonding. *Comments Inorg. Chem.* **1990**, *10*, 297-313.
(83) Fox, D. C.; Fiedler, A. T.; Halfen, H. L.; Brunold, T. C.; Halfen, J. A. Electronic Structure Control of the Nucleophilicity of Transition Metal−Thiolate Complexes: An Experimental and Theoretical Study. *J. Am. Chem. Soc.* **2004**, *126*, 7627-7638.
(84) Wilkerson, M. P.; Burns, C. J.; Morris, D. E.; Paine, R. T.; Scott, B. L. Steric Control of Substituted Phenoxide Ligands on Product Structures of Uranyl Aryloxide Complexes. *Inorg. Chem.* **2002**, *41*, 3110-3120.
(85) Rose, D.; Chang, Y.-D.; Chen, Q.; Zubieta, J. Reactions of Uranyl Thiolate Complexes with Molecular Oxygen: Syntheses and Crystal and Molecular Structures of the Uranyl Thiolate Peroxo Species $(HNEt_3)_2[(UO_2)_2(O_2)(SC_4N_2H_3)_4]$ and $(HNEt_3)[H(UO_2)_2(O_2)(SC_4N_2H_2Me)_4]\cdot Me_2CO\cdot 0.5Et_3N$ and of the Uranyl Thiolate Oxo Cluster $(HNEt_3)_2[(UO_2)_4(O)_2(SC_5NH_4)_6]\cdot Me_2CO$. *Inorg. Chem.* **1994**, *33*, 5167-5168.
(86) Rose, D. J.; Chen, Q.; Zubieta, J. Synthesis and characterization of uranyl thiolate complexes. Crystal and molecular structures of $[Me_4N][UO_2(NO_3)_2(C_5H_4NS)]$ and $[C_{16}H_{25}N_2S_2Si_2][UO_2(NO_3)_2(C_8H_{12}NSSi)]$. *Inorg. Chim. Acta* **1998**, *268*, 163-167.
(87) Seaman, L. A.; Schnaars, D. D.; Wu, G.; Hayton, T. W. Isolation of a uranyl amide by "ate" complex formation. *Dalton Trans.* **2010**, *39*, 6635-6637.
(88) Alcock, N. W.; Pennington, M. Actinide structural studies. Part 17. The crystal and molecular structures of four uranyl(VI) complexes with N,N-dialkyldithiocarbamate ligands. *J. Chem. Soc., Dalton Trans.* **1989**, 471-479.
(89) Windorff, C. J.; Goodwin, C. A. P.; Sperling, J. M.; Albrecht-Schönzart, T. E.; Bai, Z.; Evans, W. J.; Huffman, Z. K.; Jeannin, R.; Long, B. N.; Mills, D. P.; et al. Stabilization of Pu(IV) in $PuBr_4(OPCy_3)_2$ and Comparisons with Structurally Similar $ThX_4(OPR_3)_2$ (R = Cy, Ph) Molecules. *Inorg. Chem.* **2023**, *62*, 18136-18149.
(90) Sasano, Y.; Kogure, N.; Nagasawa, S.; Kasabata, K.; Iwabuchi, Y. 2-Azaadamantane N-oxyl (AZADO)/Cu Catalysis Enables Chemoselective Aerobic Oxidation of Alcohols Containing Electron-Rich Divalent Sulfur Functionalities. *Org. Lett.* **2018**, *20*, 6104-6107.
(91) Ranu, B. C.; Banerjee, S. Significant rate acceleration of the aza-Michael reaction in water. *Tetrahedron Lett.* **2007**, *48*, 141-143.
(92) Giolando, D. M.; Kirschbaum, K. An Efficient One-Pot Synthesis of 1,2-Benzenedithiol from Benzenethiol. *Synthesis* **1992**, *1992*, 451-452.
(93) Kiplinger, J. L.; Morris, D. E.; Scott, B. L.; Burns, C. J. Convenient Synthesis, Structure, and Reactivity of $(C_5Me_5)U(CH_2C_6H_5)_3$: A Simple Strategy for the Preparation of Monopentamethylcyclopentadienyl Uranium(IV) Complexes. *Organometallics* **2002**, *21*, 5978-5982.
(94) Cantat, T.; Scott, B. L.; Kiplinger, J. L. Convenient access to the anhydrous thorium tetrachloride complexes $ThCl_4(DME)_2$, $ThCl_4(1,4\text{-dioxane})_2$ and $ThCl_4(THF)_{3.5}$ using commercially available and inexpensive starting materials. *Chem. Commun.* **2010**, *46*, 919-921.

(95) Harris, R. K.; Becker, E. D.; Cabral de Menezes, S. M.; Goodfellow, R.; Granger, P. NMR nomenclature. Nuclear spin properties and conventions for chemical shifts(IUPAC Recommendations 2001). **2001**, *73*, 1795-1818.
(96) Harris, R. K.; Becker, E. D.; Cabral de Menezes, S. M.; Granger, P.; Hoffman, R. E.; Zilm, K. W. Further conventions for NMR shielding and chemical shifts (IUPAC Recommendations 2008). **2008**, *80*, 59-84.
(97) SMART Apex II, Version 2.1; Bruker AXS Inc.: Madison, WI; 2005.
(98) SAINT Software User's Guide, Version 7.34a; Bruker AXS Inc.: Madison, WI; 2005.
(99) Sheldrick, G. M. SADABS, University of Gottingen, Germany; 2005.
(100) SHELXTL PC, Version 6.12; Bruker AXS Inc.: Madison, WI; 2005.
(101) Diamond - Crystal and Molecular Structure Visualization. Crystal Impact - Dr. H. Putz & Dr. K. Brandenburg GbR, Kreuzherrenstr. 102, 53227 Bonn, Germany. http://www.crystalimpact.com/diamond.